LA-13262-MS

Summary and Synthesis Report on Radionuclide Retardation for the Yucca Mountain Site Characterization Project

Yucca Mountain Site Characterization Program
Milestone 3784M

Los Alamos
NATIONAL LABORATORY

Los Alamos National Laboratory is operated by the University of California for the United States Department of Energy under contract W-7405-ENG-36.

This work was supported by the Yucca Mountain Site Characterization Project Office as part of the Civilian Radioactive Waste Management Program of the U.S. Department of Energy. The Los Alamos data tracking numbers for this record package are LAIT831341AQ96.001 and LADT831351DQ96.001.

Edited by Roger C. Eckhardt

An Affirmative Action/Equal Opportunity Employer

LA-13262-MS

UC-903 and UC-940
Issued: October 1997

Summary and Synthesis Report on Radionuclide Retardation for the Yucca Mountain Site Characterization Project

Yucca Mountain Site Characterization Program
Milestone 3784M

Inés R. Triay
*Arend Meijer**
James L. Conca†
K. Stephen Kung
Robert S. Rundberg
Betty A. Strietelmeier
C. Drew Tait
David L. Clark
Mary P. Neu
David E. Hobart§

**GCX, 3821 Anderson Ave. SE, Albuquerque, NM 87108*
†WSU Tri-Cities, 100 Sprout Road, Richland, WA 99352
§G. T. Seaborg Institute for Transactinium Science, Livermore, CA 94551

TABLE OF CONTENTS

LIST OF FIGURES

LIST OF TABLES

SUMMARY AND SYNTHESIS REPORT ON RADIONUCLIDE RETARDATION FOR THE YUCCA MOUNTAIN SITE CHARACTERIZATION PROJECT

Yucca Mountain Site Characterization Program Milestone 3784M

by

Inés R. Triay, Arend Meijer, James L. Conca, K. Stephen Kung, Robert S. Rundberg, Betty A. Strietelmeier, C. Drew Tait, David L. Clark, Mary P. Neu, and David E. Hobart

edited by Roger C. Eckhardt

ABSTRACT

This report is a detailed summary of laboratory and modeling studies performed by or for Los Alamos National Laboratory in support of the Yucca Mountain Site Characterization Project (YMP) on the mechanisms by which radionuclide transport from the proposed repository for high-level nuclear waste at Yucca Mountain, Nevada, is retarded or enhanced by sorption, diffusion, solubility limits, and colloid transport. As direct input into these studies, the report also includes a summary of what has been accomplished in the development of a model for groundwater chemistry at Yucca Mountain. Chapter I introduces background material, including discussions of the site of the potential repository, the overall approach to this aspect of site characterization, the chemical nature of the on-site waters, and the types and variability of minerals in the rock matrix and on fracture surfaces. Chapter II discusses the groundwater chemistry of the saturated and unsaturated zones and the different types of processes that influence that chemistry. The first line of defense against radionuclide transport, the limits on solubilities, is discussed in Chapter III along with studies of specific-ion interaction theory for actinide complexes. The second line of defense, the sorption of radionuclides onto the surrounding tuffs, is discussed in Chapter IV. A summary of what is known for the sorption of all the key radionuclides and a presentation of extensive batch-sorption measurements for uranium, plutonium, and neptunium are included. The effect that organic coatings on mineral surfaces has on the sorption of actinides is also covered. Cation-exchange and surface-complexation models that can explain the sorption data are discussed. Chapter V covers dynamic-transport studies that complement and extend the batch-sorption work. These studies include experiments with crushed-rock columns, solid-rock columns, and fractured columns, as well as work on colloid-facilitated transport of radionuclides. Chapter VI summarizes both the work using rock beakers and diffusion cells to study diffusion in saturated tuff and the work using centrifuge-induced flow to study diffusion through unsaturated tuff. The main conclusions of all of this work are presented in Chapter VII, which also includes a summary of research performed as part of the Biological Sorption and Transport Task on how microorganisms affect radionuclide transport at Yucca Mountain.

I. GEOCHEMICAL SETTING

A. THE POTENTIAL REPOSITORY SITE

Yucca Mountain, in southern Nevada, is the potential site for a repository for high-level radioactive waste from commercial power and nuclear defense industries. Yucca Mountain is composed of a thick (greater than 1.5 km) sequence of ash-flow tuff units and subordinate lavas (Fig. 1). Most units retained enough heat after deposition to develop densely welded, devitrified interiors in which the original glass particles consolidated and crystallized to a high-temperature assemblage of feldspars and silica minerals (Levy 1992). Levy reports that the upper and lower margins of the units remain vitric; thinner, bedded tuffs between the main ash flows are also vitric and nonwelded. In the middle and lower units, most glassy tuffs have diagenetically altered to hydrous assemblages dominated by zeolites.

The location of the proposed repository is approximately 300 m below the surface of the mountain and 200 to 400 m above the static water level (Levy 1992). The presence of the thick zeolitic tuffs in continuous zones throughout the region was a major consideration for choosing Yucca Mountain as a potential repository site (Johnstone and Wolfsberg 1980); the zeolites could sorb important radionuclides from groundwaters and thus retard the movement of radioactivity from the repository site. The potential repository at Yucca Mountain would be located within the densely welded devitrified tuff of the Topopah Spring Member of Paintbrush Tuff with a vitrophyre underlying this location.

Because the proposed location is in the unsaturated zone, conditions are oxidizing. The Yucca Mountain region is in the shadow of the Sierra Nevada range and receives little rainfall. Estimates of groundwater flux are extremely low, and the site is remote, located at the western edge of the Nevada Test Site, approximately 100 miles northwest of Las Vegas, Nevada.

One major aspect of characterizing the site and assessing its suitability as a repository is to determine the extent to which the natural geochemical barriers will prevent the release of radionuclides from the underground repository. The retardation of radionuclides by sorption onto tuffs is of major importance, and one of the main goals of our research at the Los Alamos National Laboratory is to obtain data and to develop models for the sorption behavior of key radionuclides under the physical and chemical conditions anticipated at the proposed repository. Such work involves detailed investigation and modeling of the interactions between solid-rock materials and radionuclides in aqueous solutions.

Several related studies support and complement the main sorption research. The characterization and modeling of the chemistry of Yucca Mountain groundwaters is vital. Other studies include the role of diffusion in Yucca Mountain tuff, the limits imposed by the solubilities of the radionuclides, the potential transport of radionuclides by colloids, the effects of organic compounds on sorption, and radionuclide transport through fractures in the tuff. The validation of the results of static batch-sorption studies with dynamic transport studies is also extremely important.

This report summarizes the laboratory and modeling studies carried out or directed by scientists at Los Alamos for this effort. Specifically, we report on investigations of the mechanisms by which radionuclide transport is retarded or enhanced by sorption, diffusion, solubility limits, and colloid transport.

The role of microbial activity on the transport of radionuclides is described in a Los Alamos report on Yucca Mountain Site Characterization Project (YMP) milestone 3663 (Hersman 1996).

An assessment of the potential for radionuclide retardation at Yucca Mountain must be based on an understanding of the petrology and mineralogy of

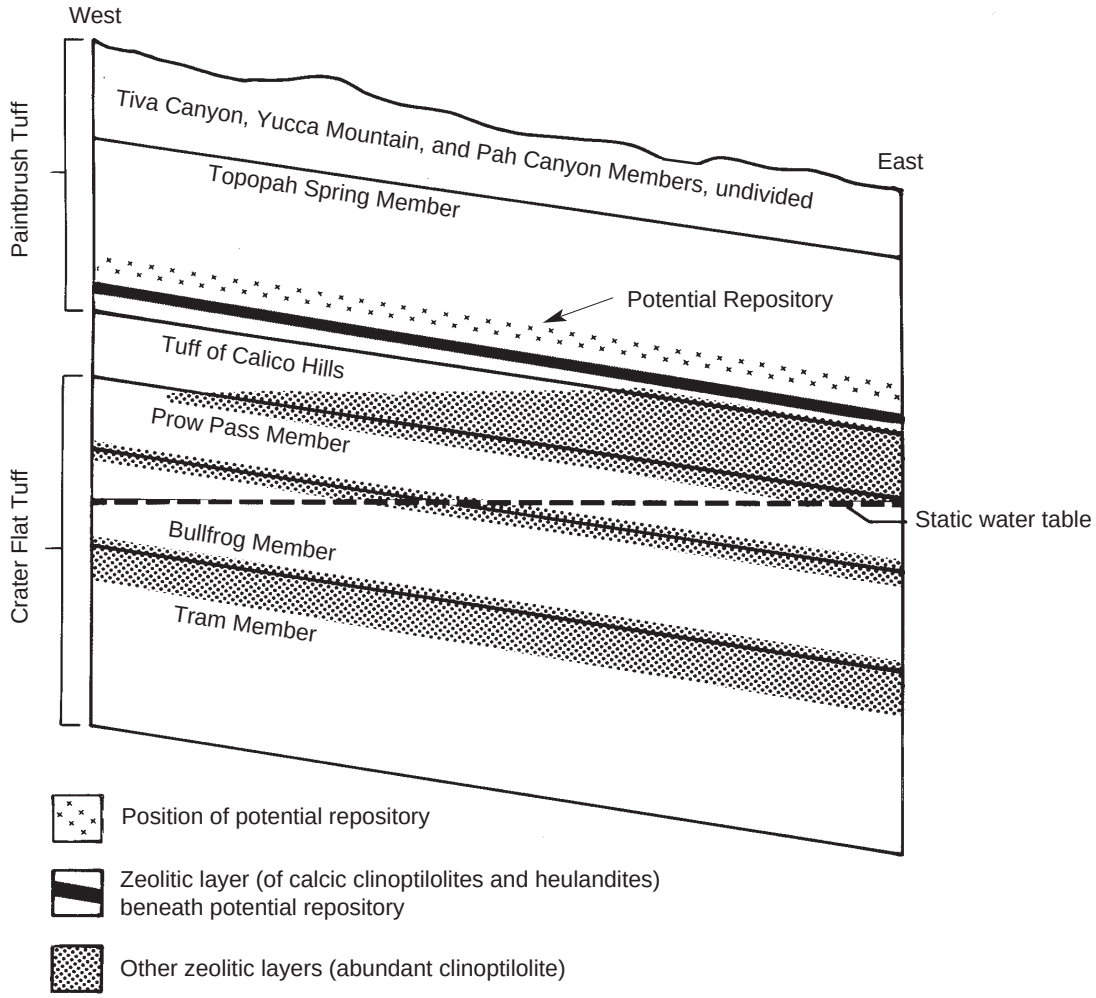

Figure 1. Cross Section of Yucca Mountain. This schematic of an east-west cross section of Yucca Mountain shows the vertical position of the potential repository in relation to the static water table and the principal layers of zeolitic tuffs (from Broxton et al. 1986).

the proposed repository horizon and the underlying strata. This work is summarized in a series of Yucca Mountain Site Characterization milestone reports (Bish et al. 1996a; Levy et al. 1996; Carey et al. 1996).

Regulatory Limits for the Release of Radionuclides

The types of radioactive waste that may be emplaced in the proposed high-level nuclear waste repository include spent fuel, high-level (reprocessing) waste, and high-level defense waste. Oversby (1987) has evaluated compositions and likely inventories of spent fuel and has provided lists of those radionuclides for which the performance of a geological repository site will be critical with respect to meeting the regulatory release limits. Oversby compared the maximum annual release rates from an engineered-barrier system allowed by the Nuclear Regulatory Commission (NRC) regulations of 10 CFR 60 (NRC 1983) with integrated release limits to the accessible environment allowed by the Environmental Protection Agency (EPA) regulations of 40 CFR 191 (EPA 1982). In effect, Oversby assumed the boundary to

the accessible environment and the boundary to the engineered barrier to be one and the same. The "important radionuclides" were identified as those for which the allowed NRC annual release rates from the engineered barrier system resulted in integrated release rates to the accessible environment that exceeded the EPA release limits.

Table 1 lists the "important radionuclides" resulting from this evaluation in order of the degree to which they exceed the EPA release limits. Note that this listing is independent of the characteristics of the engineered-barrier system and of the site—it is a direct result of the composition of any quantity of the emplaced waste and the combined NRC and EPA regulations.

Unless the engineered-barrier system itself is designed to provide compliance with the EPA regulations, site characteristics between the boundary of the engineered barrier and the boundary of the accessible environment must be called on for such compliance. The site characteristics that could ultimately determine the rate at which radionuclides are released to the environment (Fig. 2) include: 1) the solubilities of compounds of the important radionuclides that are stable in groundwaters located between the repository horizon and the accessible environment, 2) the rate and volume of water and air movement through the repository to the accessible environment, 3) the dispersion rates for radionuclides in the groundwater and air-flow systems associated with the site, 4) the sorption of radionuclides to immobile and mobile (for example, colloidal) surfaces present in the groundwater and air-flow systems associated with the site, and 5) the decay of the radionuclides during transport.

Table 1. Important Radionuclides and the Reduction Factor Required to Meet Maximum Allowed Releases

Element	Reduction factor*
Americium	18,300
Plutonium	12,300
Thorium	457
Uranium	52
Curium	46
Carbon	46
Neptunium	46
Radium	38
Nickel	13
Iodine	9
Cesium	5
Tin	5
Selenium	5
Zirconium	5
Niobium	5
Technetium	3
Palladium	3

*Assuming each radionuclide accounts for not more than 0.035 of total U.S. EPA limit and assuming no precipitation.

Stratigraphy of Yucca Mountain

Figure 1 gives the names of the main layers of Yucca Mountain tuff and shows their relationship to the static water table and the intervals of zeolites. Figure 3 is a more detailed, scaled view of Yucca Mountain that also shows the positions of the drill holes used to develop the stratigraphic picture. Samples from the cores of a number of these drill holes were used throughout the research reported on here.

The stratigraphic units in Yucca Mountain include partially welded to densely welded devitrified tuff, moderately welded to densely welded vitrophyre, and nonwelded vitric tuff that in places has been extensively altered to zeolite minerals (Scott et al. 1983; Carr et al. 1986). As we've pointed out, the potential repository is located in a layer of densely welded devitrified tuff. Between the repository and the water table, several stratigraphic intervals containing zeolitic tuffs (containing primarily the zeolites clinoptilolite and mordenite) provide probable barriers to downward radionuclide migration in the unsaturated zone. Additional zeolitic tuffs below the water table provide potential barriers to lateral

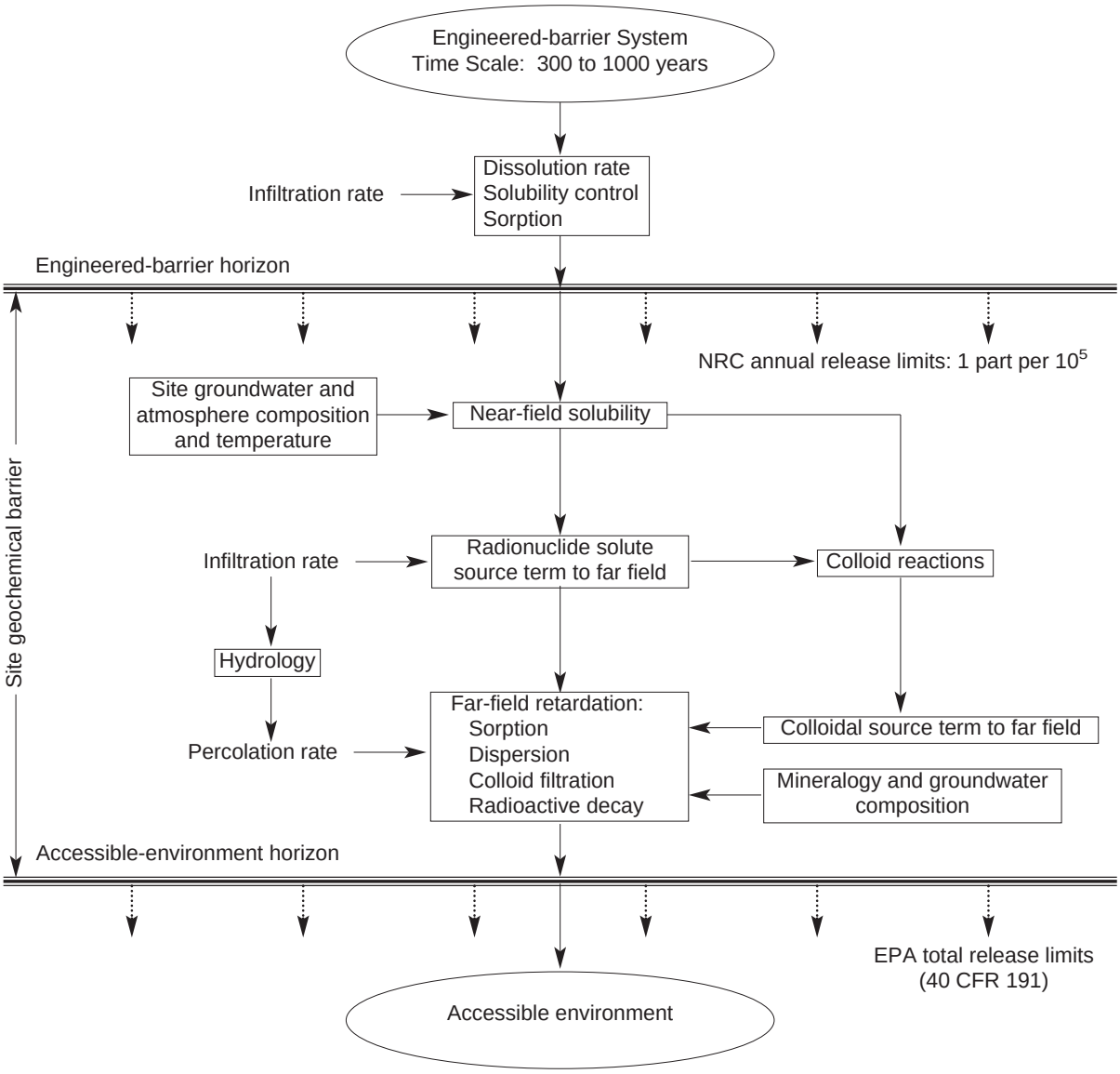

Figure 2. Multiple Natural Geochemical Barriers. This schematic diagram of the potential nuclear-waste repository system illustrates the processes important to retardation of radionuclides between the horizon of the engineered-barrier system, where the release limits are stipulated by the NRC, and the horizon of the accessible environment, where release limits are governed by the EPA. For our purposes, the engineered-barrier system is considered independent of the natural site surrounding that system. Taking the NRC limits as the upper bound for releases across the horizon into the natural site, the various processes (sorption, dispersion, colloid reactions, and so forth) are then examined to see if retardation is adequate to meet the EPA release limits to the accessible environment.

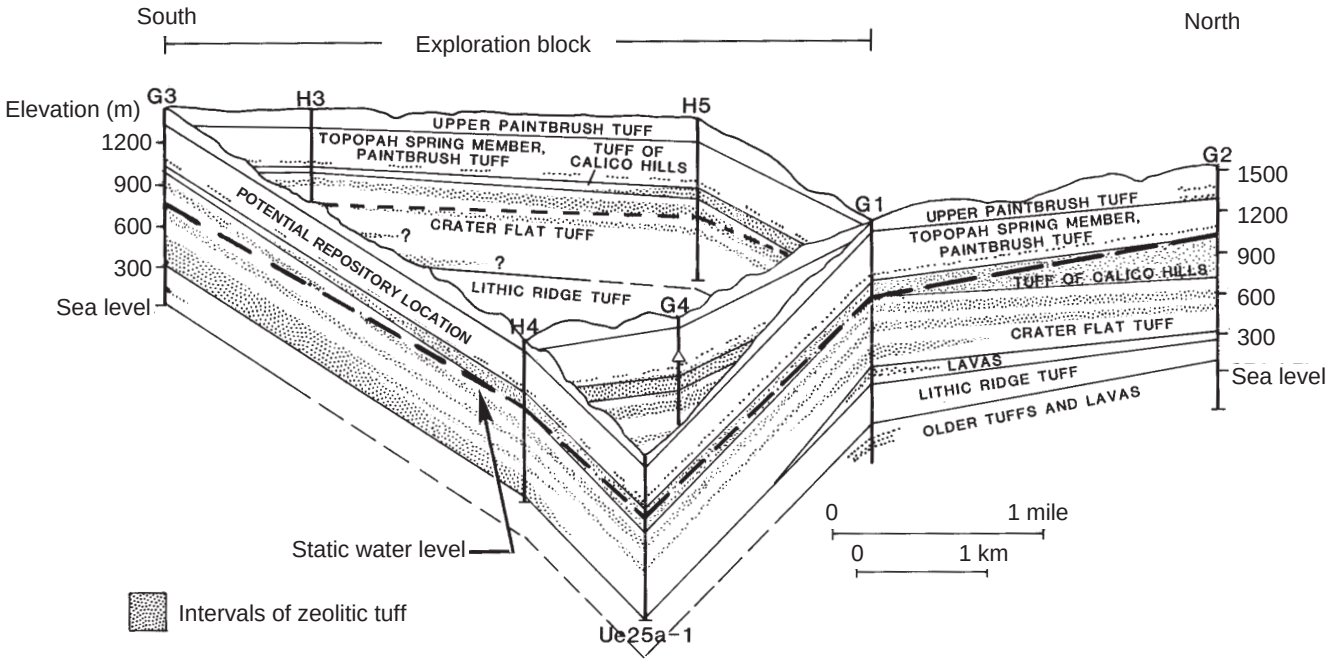

Figure 3. Zeolitic Tuffs at Yucca Mountain. The above fence diagram of the stratigraphy at Yucca Mountain shows the distribution of the principal zeolitic tuffs (tuff containing more than 10% clinoptilolite and mordenite) as shaded areas. The potential repository location is in the lower half of the Topopah Spring member of Paintbrush Tuff. Each "fence post" (for example, G3) represents a USW drill hole. Most of the tuff samples used in the research described in this report were portions of core taken from USW drill holes G-1, G-2, G-4, and GU-3 (located at the G3 site). The figure was taken from Broxton et al. (1986); stratigraphic contacts were from Spengler et al. (1979, 1981), Maldonado and Koether (1983), and Scott and Castellanos (1984); preliminary stratigraphic contacts for drill holes USW H-3, H-4, H-5, and G-4 were provided by R. W. Spengler (personal communication, 1983); and static water-level data were from the USGS Nuclear Hydrology Group.

radionuclide migration through the saturated zone.

The suite of minerals found in the deeper-lying host rock for the potential site includes all four categories of sorptive minerals described by Kent et al. (1988) in the context of a surface-complexation model for radionuclide sorption. These categories are 1) oxide minerals (including iron oxides and silica minerals), 2) multiple-site-type minerals (including the feldspars), 3) fixed-charge minerals (including micas, clays, manganese oxides, and zeolites), and 4) salt-type minerals (including calcite). Chemical speciation and water chemistry may strongly affect the interaction between selected radionuclides and each of these mineral categories, but the mineral variability and presence of all four mineralogic categories of Kent et al. suggest mineralogic robustness for sorption at Yucca Mountain.

Beneath the potential host rock, the stratified layers of devitrified (mostly quartz plus feldspar) and nonwelded (mostly glass or zeolite) tuffs provide significant mineral variability along both unsaturated and saturated transport pathways. The effectiveness of the individual mineral types in sorbing will depend on the geometry, accessibility, fluid environment, duration of contact, and cumulative abundance along the transport pathway.

B. AN INTEGRATED APPROACH TO SITE CHARACTERIZATION

The natural system at Yucca Mountain defines the site-specific conditions under which we must determine to what extent the natural geochemical barrier will prevent the migration of radionuclides away from the repository. The mineralogy, petrology, and water chemistry at Yucca Mountain define the conditions a radionuclide will encounter if the waste package corrodes and dissolved radionuclides are released across the horizon of the engineered-barrier system into the site environment. There may be many scenarios that could affect the near-field environment, creating chemical conditions more aggressive than conditions presented by the unperturbed system (such as pH changes beyond the range of 6.9 to 8.9 or significant changes in the ionic strength of near-field waters). Without clear near-field condition bounds at this time, we assume that at some distance away from the waste package, conditions are dominated by the large rock-mass buffer. In the far field, the near-neutral, oxidizing, low-ionic-strength conditions of the normal site environment control the radionuclide solubility limits and the sorption capacity of the tuff.

Our testing strategy (Canepa et al. 1994) thus shows the need for characterization of the natural system, which defines the experimental conditions for solubility and sorption determination. Such characterization requires data on groundwater composition, including natural colloids, on the mineralogy and petrology of the rock, and on mineral stability. Modeling of the groundwater chemistry is designed to lead to an understanding of solubility and speciation of the important radionuclides as well as the possible formation of radiocolloids. Laboratory experiments attempt to characterize sorption and diffusion of the radionuclides in light of this information. Finally, validation of chemical processes in a dynamic system is crucial before laboratory data are applied to the field tests or natural analogs. In this report, we focus on summarizing the research that has been accomplished in the areas described below.

Modeling of Groundwater Chemistry

The purpose of the groundwater-chemistry modeling task is to develop models that describe compositional variations in groundwaters in the unsaturated and saturated zones beneath Yucca Mountain. These models are used to establish bounds on the water compositions to be expected in the ambient Yucca Mountain flow system. They are also used to bound the composition of waters in the far field of the potential repository at Yucca Mountain in the post-closure period.

We can also derive estimates of the possible range of water compositions to be expected in the Yucca Mountain flow system on the basis of the compositional variations observed in present-day groundwaters in volcanic units over a large area such as the Nevada Test Site. The programs to measure transport parameters, such as sorption coefficients and solubilities, incorporate the compositions of these waters as part of the experimental design.

Radionuclide Solubility Studies

The potentially limited solubility of radionuclides in groundwater can be thought of as the geochemical first line of defense against migration. Evaluation of this effect first requires a knowledge of the groundwater chemistry at the site and the expected spatial and temporal ranges of its variability. Second, quantitative determinations of radionuclide solubility in groundwater within this range of chemistry must be made. Speciation and molecular complexation must be ascertained to interpret and apply solubility results. The solubilities thus determined can be used to assess the effectiveness of solubility in limiting radionuclide migration. We can also use these solubilities to evaluate the effectiveness of other retardation processes expected to operate once any dissolution and migration begin.

The short-term goals of the radionuclide solubility task have been to provide solubilities from bulk experiments that attempt to bracket our current estimate of groundwater conditions that might

exist. Intermediate goals have been to develop the thermodynamic database for solution speciation and solid-state determination as a prerequisite to modeling the results. Once the model is self-consistent and performs well against known solubilities, our long-term goal is to use the model over a continuous, weighted distribution range of potential groundwaters to generate a weighted distribution of solubilities that could be used for performance assessment of the site.

Sorption Studies

A geochemical second line of defense against groundwater transport of radionuclides is "sorption," which comprises several physiochemical processes, including ion exchange, adsorption, and chemisorption. Determining whether sorption will occur requires knowledge of the likely flow paths of the groundwater and the spatial and temporal distribution of sorbing minerals along these paths. Evaluating the retardation effectiveness of sorption for repository design and licensing requires theoretical and quantitative understanding of sorption.

Batch-sorption experiments are useful for bounding more detailed and mechanistic sorption studies. We determined batch-sorption distribution coefficients, defined as

$$K_d = \frac{\text{moles of radionuclide per g of solid phase}}{\text{moles of radionuclide per ml of solution}}\ , \quad (1)$$

as a function of variables representing conditions expected beyond the region disturbed by waste emplacement. The variables included mineralogy, groundwater chemistry, sorbing element concentration, atmospheric conditions, and temperature.

Batch-sorption results are very sample specific and, therefore, difficult to generalize and apply throughout the mountain. Deconvolution of sorption isotherms provides much greater detail about sorption sites (kind, number, specificity, and so forth). Such information can be correlated with crystallographic data and related to specific sorption sites in the crystal structure. All sites are not equally selective for all sorbing species. Examining the sorption behavior of individual pure minerals, such as the zeolites and manganese or iron oxyhydroxides found in Yucca Mountain tuffs, could help predict sorption coefficients along flow paths of known mineral content.

One factor that can have an effect on the sorption of radionuclides is organic materials. Naturally occurring organic compounds generated during the transformation of plant and animal debris over time and as a result of the synthetic activities of microorganisms are ubiquitous in surface and subsurface environments. Sorption of organic material onto mineral surfaces can affect the properties of those surfaces, such as charge and hydrophobicity, thereby altering the reactivity of the mineral toward metal ions. A clear understanding of the effects of the organics that frequently coat mineral surfaces in natural environments will lead to improvements in the sorption models used to predict the mobility of radionuclides in natural aquatic environments.

A better understanding of the sorption of radionuclides onto tuff will be possible if we can relate the data to mechanistic models. Two general mechanisms are important: ion exchange reactions that are primarily electrostatic in nature and surface complexation in which a relatively covalent chemical bond forms with the mineral surface. Ion exchange does not have the same degree of selectivity between aqueous ions of like charge as does surface complexation. The adsorption of metal ions via cation exchange will only occur on surfaces of opposite charge and so is affected by such common components of groundwater as sodium. Surface complexation, on the other hand, can occur even when the mineral surface charge is the same as the aqueous ion. Both of these processes can, in principle, be modeled using a triple-layer surface-complexation model. However, there are significant differences between the cation exchange in zeolites and clays and the formation of surface complexes on metal oxides, so we have treated cation exchange and surface complexation separately.

Physiochemical processes that might accelerate radionuclide migration relative to groundwater flow rates, such as anion exclusion, must also be quantified. These depend largely on the molecular complexation or speciation that occurs in solution. Accordingly, detailed assessment of this possibility is needed to fully evaluate the potential for transport retardation by geochemical processes.

Diffusion Studies

Additional geochemical lines of defense beyond solubility limits and sorption are possible. The lateral diffusion of radionuclide species in porous media may retard longitudinal migration by bringing dissolved radionuclides into contact with sorbing minerals. Also, when the fluid flow is through fractures in highly impermeable rock and there is an absence of sorbing minerals on the fracture surfaces, diffusion may be the only effective retardation mechanism. Most rock (even dense rock such as granite) has small fissures between the crystals that interconnect the pore system containing water. Small molecules of radioactive materials can diffuse in and out of this pore system. The inner surfaces in the rock matrix are much larger than the surfaces in the fractures on which the water flows, and the volume of water in the microfissures is much larger than the volume in fractures. Therefore, over a long time scale, diffusion can play an important role in radionuclide retardation.

Diffusion experiments can provide diffusion information on nonsorbing neutral molecules and anions and on sorbing radionuclides. And because diffusion experiments measure the uptake of radionuclides by tuff as a function of time, information is gained on the kinetics of sorption. The work described here is of two types. In rock-beaker experiments, we placed a radionuclide solution inside the rock beaker and measured the decrease in radionuclide concentration as a function of time. In diffusion-cell experiments, a slab of tuff separates two chambers of groundwater, and we measured the concentration of radionuclide diffusing across the slab from one chamber to the other as a function of time.

Dynamic Transport Studies

Sorption results also must be interpretable and applicable to dynamic and heterogeneous systems, so we developed diffusion and dynamic transport experiments to complement and extend the batch-sorption results to such systems. Three types of dynamic transport experiments were conducted: crushed-rock column experiments, whole-rock column experiments, and transport through fractures.

We used crushed-rock experiments to study kinetic phenomena affecting sorption, including ionic and molecular diffusion. Whole-rock experiments additionally illustrate advective dispersion effects. Fractured-rock experiments represent the closest laboratory approach to the actual environment in which fluid flow and radionuclide migration might occur in an unanticipated scenario.

Studies are also necessary to determine the transport of radionuclides along fractures passing through the site. In the candidate host rock, the fractures contain a complex development of cristobalite, zeolites (mostly clinoptilolite and mordenite), manganese minerals, and calcite (Kent et al. 1988). This composition is in marked contrast to the rock matrix, composed predominantly of feldspars and silica minerals (quartz, cristobalite, and tridymite). Thus, different mechanisms are likely for retardation of radionuclides in flow along fractures and flow through bulk rock, and we have studied these mechanisms using fractured-rock columns.

The fracture-column studies also afforded us an opportunity to investigate colloidal radionuclide migration. Colloidal species may escape sorption and be too large to diffuse, that is, simple filtration may operate to retard movement. On the other hand, fracture flow may afford an easy transport path for colloids to the accessible environment. The dynamic transport experiment is a difficult but powerful method for elucidating separate and coupled processes affecting radionuclide migration.

We also evaluated the likelihood of particle or col-

loid formation by analyzing a typical Yucca Mountain groundwater for the presence of natural colloids and by conducting laboratory experiments to determine the possibility of radiocolloid formation. We estimated the rate of particle aggregation for various colloids using autocorrelation photon spectroscopy.

The use of batch-sorption experiments to identify sorption mechanisms and to obtain sorption distribution coefficients is fast, easy, and inexpensive compared to other types of sorption experiments. However, measurements made under flowing conditions must be carried out to verify the results of the static batch-sorption experiments. We performed such verification using crushed-tuff and solid-rock column experiments in which mass-transfer kinetics were investigated by measuring radionuclide migration as a function of water velocity. The differences between the column and the batch-sorption experiments should be sensitive to multiple-species formation, colloid formation, and other geochemical reactions not adequately described by batch-sorption coefficients.

Quality Approved Detailed Procedures

All work performed to collect data and test, analyze, model, or describe the natural system under study has been done under the Yucca Mountain Project Quality Assurance program at Los Alamos. In particular, all experimental procedures were carried out in conformance with quality-approved procedures that are described in the *Yucca Mountain Project Detailed Procedures* at Los Alamos. The various procedures for each experimental area and the corresponding reference for the current version of that procedure are listed in Table 2.

The Reference Information Base

The stratigraphy referenced in this report is consistent with the Yucca Mountain Project Reference Information Base Section 1.12(a), "Stratigraphy: Geologic/Lithologic Stratigraphy" and with the Prototype Three-Dimensional Framework Model of September 1995.

Table 2. Los Alamos Yucca Mountain Project Detailed Procedures

Research area	Procedure	Reference number
General	pH measurement	LANL-CST-DP-35
	Rock sample preparation (crushing and sieving)	LANL-CST-DP-63
	Neptunium, plutonium, and americium solution preparation	LANL-CST-DP-78
	Liquid-scintillation counting	LANL-CST-DP-79
	Eh measurement	LANL-CST-DP-102
Diffusion	Saturated diffusion-cell experiments	LANL-CST-DP-66
	Rock beaker experiments	LANL-CST-DP-67
Sorption	Batch sorption under atmospheric conditions	LANL-CST-DP-86
	Batch sorption within controlled atmosphere of a glove box	LANL-CST-DP-100
Colloids	Particle size distribution (autocorrelation photon spectroscopy)	LANL-CST-DP-75
	Colloid sampling	LANL-CST-DP-101
Dynamic transport	Crushed-rock column studies	LANL-INC-DP-15
	Solid-rock column experiments	LANL-INC-DP-61
	Fracture core experiments	LANL-INC-DP-68

C. YUCCA MOUNTAIN WATERS

A strategy for determining the retardation of radionuclides must be compatible with the hydrology of the site. A generalized conceptual model of unsaturated-zone water flow in Yucca Mountain is shown in Fig. 4 (Montazer and Wilson 1984). According to Montazer and Wilson, water in the unsaturated portion of this system will flow dominantly in the matrix and intermittently in the fractures. Given the low infiltration rate at Yucca Mountain, the rate of water movement in the matrix should be slow (Sinnock et al. 1984), but according to the modeling efforts of Nitao and Buscheck (1989), the rate of water movement in the fractures may actually be fairly rapid. The question of whether or not there will be significant water flow in the fractures beneath the potential repository horizon after waste has been stored there is unresolved at the present time.

Saturated-zone Groundwater Chemistry

The chemical compositions of groundwaters in the present and future groundwater flow systems are important parameters with regard to the sorption behavior of important radionuclides in this system. Our chemistry and transport studies used water from the Yucca Mountain region, particularly from Well J-13, which accesses the water table several miles east of Yucca Mountain. The uplifted block of tuff units that make up Yucca Mountain dips to the east, and at the J-13 location, the water table and the Topopah Spring Member intersect. Water from Well J-13, although not exactly representative of Yucca Mountain unsaturated pore water, has been in contact with the same unit proposed for the repository and can be used as a reference water.

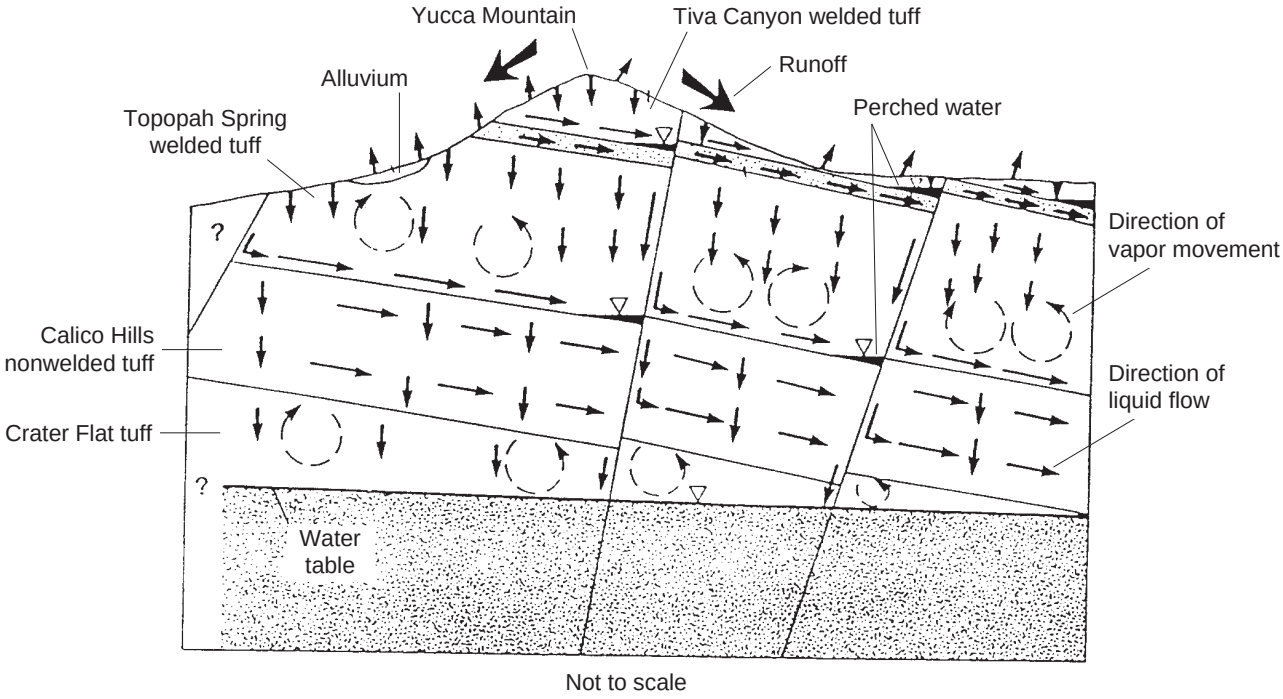

Figure 4. Unsaturated-zone Hydrology Model. This generalized east-west section across Yucca Mountain shows the flow regime under baseline conditions. Dashed arrows indicate movement of water vapor; solid arrows indicate movement of liquid water; and the lengths of the arrows indicate relative magnitude of the fluxes (from Montazer and Wilson 1984).

Well J-13 construction

Details of the construction and penetration levels of Well J-13, located in Fortymile Wash, are presented in Fig. 5. The total depth of the well is 3,500 feet, and it has been producing since its completion in 1963. Inspection of the construction diagram reveals perforations from a long section below the Topopah Spring Member starting at 2,690 feet. However, because of a discrepancy in the records concerning the well configuration (Harrar et al. 1990), it is not clear whether the entire length of the 5.5-inch liner below 1,499 feet is slotted or whether only the interval shown in the figure below 2,690 ft. is open. Resolving this discrepancy is not very important because there is no cement behind the liner, thus providing access to the well to any fluids entering the borehole below about 1,550 feet. However, hydraulic tests performed on the well yielded transmissivities that indicated that only about 20% of the flow may come from other formations, such as the tuffaceous beds of Tuff of Calico Hills, the three Crater Flat Tuff members, and Tuff of Lithic Ridge.

Well UE-25 p#1

Another well, Well UE-25 p#1, is located roughly midway between Yucca Mountain and Well J-13 at a ground-level elevation about 100 meters higher than Well J-13. Water from this well is drawn from the deep paleocarbonates underlying the tuff sequences. It has been the only other water available from the Yucca Mountain region with a chemistry different from J-13 water.

The data available in 1984 on the chemistry of saturated-zone groundwaters were reviewed by Ogard and Kerrisk (1984). In the volcanic units, the groundwaters are basically dilute sodium-bicarbonate waters (Table 3). Listed in order of decreasing concentration in J-13 water, the other major cations are calcium, potassium, and magnesium and the other anions are sulfate, nitrate, chloride, and fluoride. The only other major constituent is silica. The water from the Paleozoic aquifer (Well UE-25 p#l) has higher concentrations of almost all these constituents. Thus, the ionic strength of Well UE-25 p#1 water is higher than that of J-13 water, although both are relatively low in ionic strength.

The chemistry of groundwaters from Wells J-13 and UE-25 p#1 seems to bound that of the Yucca Mountain groundwaters (Meijer 1992), and thus, these two groundwaters serve as standards for the experimental work. However, certain changes (Fig. 6) take place in the chemistry of the waters between their removal at the well and their use in the laboratory. The J-13 and UE-25 p#1 reference data plotted in Fig. 6 were obtained on site by Ogard and Kerrisk (1984). This on-site chemistry is compared with the chemistry of aliquots of J-13 and UE-25 p#1 waters that were collected at later dates, sent to Los Alamos, and filtered. On site, the pH of the two groundwaters is ~7. However, at Los Alamos, the waters equilibrate in the higher-elevation atmosphere with subsequent evolution of carbon dioxide, which causes the pH of J-13 water to increase to 8.5 and the pH of UE-25 p#1 water to increase to ~9. The data of Fig. 6 indicate that

Table 3. Chemistry of Waters from Wells J-13 and UE-25 p#1 and the Unsaturated Zone (UZ) at the Yucca Mountain Site

Element	J-13* (mg/l)	UZ† (mg/l)	UE-25 p#1* (mg/l)
Sodium	45	26–70	171
Bicarbonate	143	—	698
Calcium	11.5	27–127	87.8
Potassium	5.3	5–16	13.4
Magnesium	1.8	5–21	31.9
Sulfate	18.1	39–174	129
Nitrate	10.1	—	< 01
Chloride	6.4	34–106	37.0
Fluoride	2.1	—	3.5
Silicon	30.0	72–100	30.0
pH	6.9	6.5–7.5	6.7
Eh (mV)	340	—	360

*Ogard and Kerrisk 1984; †Yang et al. 1990.

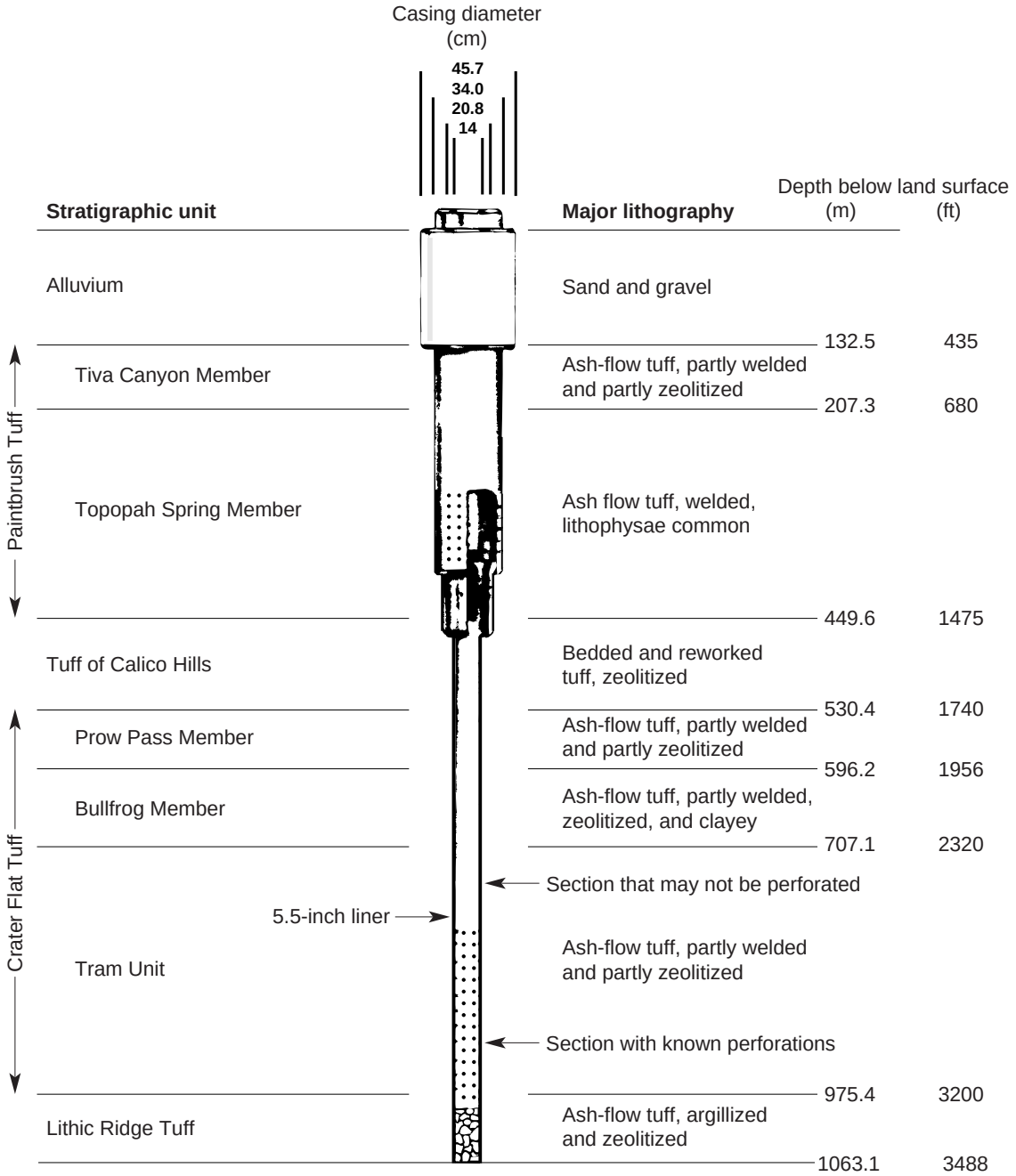

Figure 5. Well J-13. The construction diagram and lithologic units penetrated for Well J-13 (from Harrar et al. 1990) are shown above. Hydraulic tests performed on the well indicate that about 80% of the water flow may come from the Topopah Spring Member of Paintbrush Tuff, which is the same stratigraphic unit as the one proposed for the repository, and only about 20% may come from other formations.

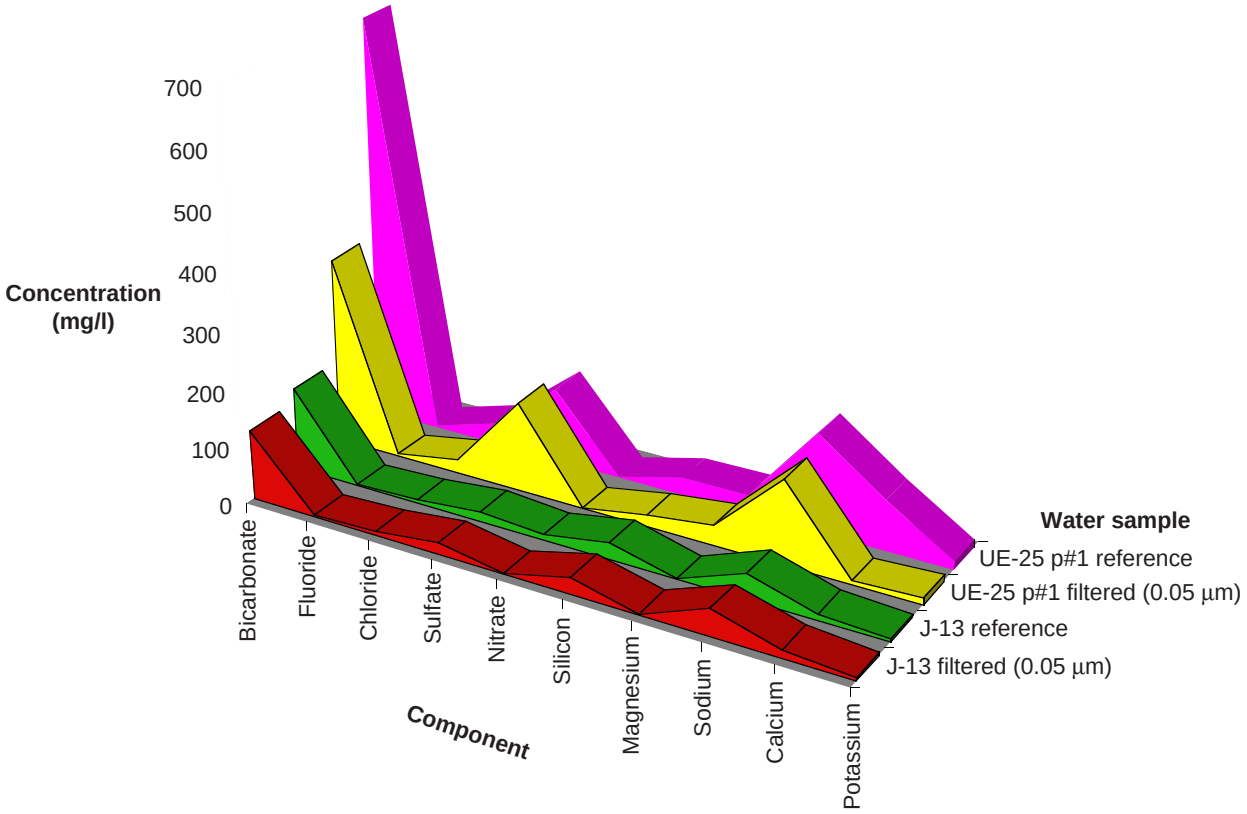

Figure 6. Chemistry of Two Groundwaters. The two reference samples above are water analyzed on-site in Nevada at the J-13 and UE-25 p#1 well sites (Ogard and Kerrisk 1984). The filtered samples are water analyzed at Los Alamos, NM, after being passed through a 0.05-μm filter (data recorded in binder TWS-INC-11-93-32, pages E24–E25, for J-13 water and in binder TWS-INC-03-93-02, page C8, for UE-25 p#1 water). The figure demonstrates the higher ionic strength of UE-25 p#1 water, the stability of J-13 water, and the apparent calcite precipitation in UE-25 p#1 water caused by CO_2 evolution.

carbon-dioxide evolution and filtration does not otherwise change the chemistry of J-13 water but causes calcite precipitation in UE-25 p#1 water. Consequently, the concentrations of bicarbonate and calcium in any UE-25 p#1 water used in the sorption experiments were lower than that of on-site UE-25 p#1 water. Because both waters are oxidizing, all the sorption experiments were performed under oxidizing conditions.

Chemical stability of Well J-13 water

Figure 7 shows a chemical analysis of water from Well J-13 from 1963 to 1993. The front curve represents the average of the chemical analysis of 19 water samples collected between 1963 and 1987 by five different organizations (Los Alamos National Laboratory, U. S. Geological Survey, Lawrence Livermore National Laboratory, Argonne National Laboratory, and Westinghouse-Hanford Company). Analysis of these results led Harrar et al. (1990) to conclude that the water chemistry of Well J-13 did not change between 1963 and 1987. Comparison of the results of Harrar for that period with similar analyses of water collected in 1992 and 1993 (the other curves shown in Fig. 7) indicates that the chemistry of the water in Well J-13 has been stable for thirty years.

We analyzed aliquots of both groundwaters before and after filtration (Figs. 6 and 7). Comparison of

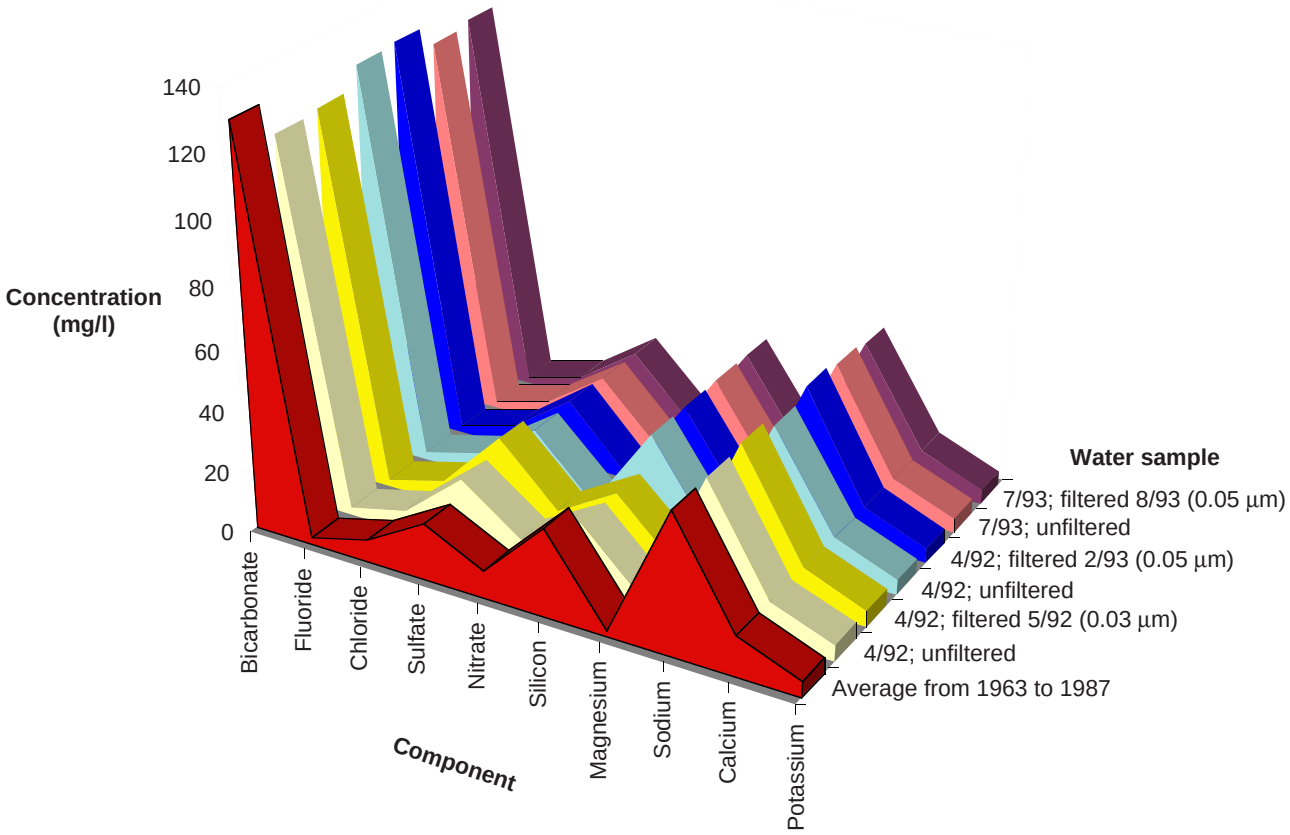

Figure 7. Stability of the Chemistry of Well J-13 Water. The curves above show minimal compositional changes as a function of collection date, filtering, and filter size, indicating that the chemistry of the water in Well J-13 has been stable for 30 years.

these results indicates that filtration does not cause compositional changes (except for the previously noted calcite precipitation in the UE-25 p#1 water that is caused by pH changes).

Unsaturated-zone Water Chemistry

The compositions of waters from the unsaturated zone are not well known. Yang et al. (1990) have reported partial analyses of unsaturated-zone waters from Wells UZ-4 and UZ-5 obtained by triaxial compression and centrifugation methods. Core samples of the wells from which waters were obtained came from the nonwelded portion of the Yucca Mountain and Pah Canyon members of Paintbrush Tuff. The major cation and anion concentrations in these waters are intermediate between the saturated-zone tuffaceous waters and waters from the carbonate aquifer (Table 3). Water samples from UZ-4 cores tend to be closer in composition to the tuffaceous waters, whereas waters from UZ-5 cores appear to be closer in composition to water from the carbonate aquifer, although this statement is not intended to imply genetic associations of the waters with these aquifers.

The pH and the oxidizing potential, Eh, of the groundwaters in Yucca Mountain are particularly important with respect to the solubilities and sorption behavior of a number of the important ele-

ments (such as, actinides and technetium). The available data suggest that most of the waters within Yucca Mountain site are oxidizing (for example, Ogard and Kerrisk 1984). Because the spatial and temporal variability in the Eh parameter will be difficult to quantify, the conservative approach would be to assume all the groundwaters between the potential repository and the accessible environment are in equilibrium with atmospheric oxygen. This assumption is conservative because all the important (radionuclide) elements have either higher or equal solubilities in oxidizing waters compared with reducing waters. Available data on the pH of waters in Yucca Mountain show a range from 6.5 to 9.4 (Ogard and Kerrisk 1984; Yang et al. 1990). In this case, no single value can be chosen as being conservative.

The future compositional variations of groundwaters in Yucca Mountain must also be considered in the development of a sorption strategy. To a first approximation, the variations are likely to be similar to the present-day variations as a result of buffering reactions by the country rock.

Pore Water versus Saturated Groundwaters

We must recognize that there are likely more than one type of water in the Yucca Mountain area. Differences in chemistry may exist between waters in saturated zones (at or below the true water table), waters in tuff pores in the hydrologic units of the unsaturated zone, and perched waters, that is, groundwater separated from the underlying water table by an unsaturated zone.

Unsaturated-zone waters may be strongly influenced by soil-zone processes, including evapotranspiration and the precipitation of pedogenic minerals such as calcite, gypsum, and silica. Chemical properties, such as ionic strength, may be a function of the time interval between infiltration events. Other properties, such as pH and oxidation potential, will depend on the partial pressures in the unsaturated zone of such gases as carbon dioxide and oxygen. Whether or not a particular unit of rock is closed or open to the gas phases of the unsaturated zone is thus important. Also, the various waters may be influenced by hydrolysis reactions, for instance, with aluminosilicates, or by ion exchange reactions with zeolites.

Evaluation of the database on water compositions in volcanic units at the Nevada Test Site indicates that the variability in major constituents is well-bounded by waters from Wells J-13 and UE-25 p#1. The main parameters not bounded by these water compositions are pH, Eh, and chloride concentration. Our experimental programs to measure transport parameters, such as sorption coefficients and solubilities, have incorporated these water compositions as part of the experimental design, and we have carried out the experiments as a function of pH. Therefore, the primary uncertainties are in the effects of variations in Eh and chloride concentrations.

Synthetic Groundwaters

We used both groundwaters (filtered by a 0.05-μm filter) in the batch-sorption experiments, but in the column-transport and the diffusion experiments, we used filtered J-13 water and, because of the unavailability of water at that time from Well UE-25 p#1, a sodium-bicarbonate buffer that simulated this groundwater. In the fracture studies, filtered J-13 water and sodium-bicarbonate waters simulating both J-13 and UE-25 p#1 waters were used. One reason for using synthetic waters for the fracture studies was the prevention of microbial activity in the fracture columns.

Synthetic UE-25 p#1 water was prepared by dissolving 0.39 g of Na_2CO_3 and 8.90 g of $NaHCO_3$ in 10 liters of deionized water, which duplicates the larger amount of bicarbonate in reference, or on-site, UE-25 p#1 water. Synthetic J-13 water was prepared by dissolving 0.03 g of Na_2CO_3 and 1.92 g of $NaHCO_3$ in 10 liters of deionized water.

D. YUCCA MOUNTAIN TUFFS

The stratigraphy of Yucca Mountain considered from the repository horizon to the accessible environment (and including the repository containers themselves) is outlined in Table 4, which shows the rock type for each of the various strata. We have assumed that, for the purposes of sorption measurements, all strata of the same rock type can be grouped. This assumption reduces the number of sorption coefficient distributions needed to four per radionuclide: iron oxides, devitrified tuff, vitric tuff, and zeolitic tuff. The basis for this grouping is the fact that sorption of radionuclides is the result of a chemical reaction between the radionuclide in the groundwater and the minerals in the tuff. The mineralogy of the different strata of the same type of rock is very similar. Thus, the sorption coefficients can be grouped in terms of these rock types (Thomas 1987).

The repository containers are included on the list because the corrosion by-products of the massive multipurpose containers could become a substrate for sorption. In particular, actinides are sorbed strongly by iron oxides, so iron oxides are given as one of the four "rock" types.

Table 4. Stratigraphy versus Rock Type

Stratum name	Rock type
Repository Container	Iron oxides
Repository: Topopah Spring (welded)	Devitrified
Vitrophyre below repository: Topopah Spring (welded, vitrophyre)	Vitric
Calico Hills (nonwelded, vitrophyre)	Vitric
Calico Hills (nonwelded, zeolitized)	Zeolitic
Prow Pass (welded)	Devitrified
Bullfrog (nonwelded)	Zeolitic
Bullfrog (welded)	Devitrified

Mineralogy Variability

The mineralogy and textures of Yucca Mountain tuffs are important to the sorption behavior of the important radionuclides because they determine 1) the types (that is, structure and composition) of mineral surfaces available in the tuffs and 2) the areas of the different mineral surfaces (internal and external) available for sorption of radionuclides.

The mineral species that have been identified in the matrix of Yucca Mountain tuffs are listed in Table 5 in order of overall abundance. Feldspar and quartz are by far the most common matrix minerals (Bish and Vaniman 1985). They are most abundant in the devitrified tuffs, such as those found in the Topopah Spring Member of Paintbrush Tuff, Prow Pass and Tram Members of Crater Flat Tuff, and the older tuffs.

The zeolites clinoptilolite and mordenite are abundant in parts of some nonwelded units (for example, Calico Hills) but are limited to sparse fracture-lining minerals in most of the devitrified tuffs (see below). In the nonwelded units, the zeolitic zones are thickest in the northern and eastern portions of Yucca Mountain but thin out to the south and west (Bish and Vaniman 1985).

Clays are locally abundant in the matrix of some tuffs (for example, in some parts of the vitrophyres in drill hole G2 and in the bottom of drill hole G1) but are a minor component (1–3%) in most of the tuffs beneath the potential repository (Chipera and Bish 1989).

Calcite is generally a minor component in the tuffs with a bimodal distribution. In most holes, it is a minor to abundant constituent at depths less than 300 m and at depths greater than 900 m but is sparse or absent at intermediate depths. Hematite is widely distributed as a trace mineral, particularly in the matrix of the devitrified units.

Tuff sample identification

The tuff samples we used in the batch-sorption and column-transport experiments were obtained from drill holes at Yucca Mountain and labeled with the drill-hole code and drill depth in feet. For example, G4-270 refers to a tuff sample taken from drill hole USW G-4 at a depth of 270 feet. The locations of the drill holes has previously been reported by Bish and Chipera (1989).

The mineralogy of the tuffs that we used in the sorption, diffusion, and transport experiments was determined by x-ray-diffraction (XRD) analysis (Fig. 8), the details of which were previously reported (Bish and Chipera 1989; Chipera and Bish 1989, 1994). Prior to their use in the sorption and the crushed-rock column experiments, all tuff samples were crushed and wet-sieved (with the groundwater being used in the experiment) to obtain particle sizes ranging from 75 to 500 μm. As previously discussed by Triay et al. (1996a), such crushing and sieving does not cause significant differences in the mineralogy of the tuff samples. In several cases, it appears that sieving to eliminate particles smaller that 75 μm reduces the smectite content. Because smectite is a good sorber for most radionuclides, the sieved tuff samples should yield conservative results for the sorption measurements.

Table 5. Minerals in Matrices of Yucca Mountain Rocks

Major phases	Minor and trace phases
Quartz	Hematite
Alkali feldspar	Dolomite
Clinoptilolite	Chlorite
Cristobalite	Illite
Plagioclase	Fluorite
Tridymite	Hornblende
Opal-CT	Pyroxene
Smectite	Fe-Ti Oxides
Mica	Ilmenite
Mordenite	Zircon
Analcime	Allanite
Calcite	Sphene
(Glass)	Rutile

For our experiments, we always used several examples of each of three major rock types for tuff: zeolitic, vitric, and devitrified. Each of these are now briefly described.

Zeolitic tuff

The zeolitic tuffs are represented in Fig. 8 by samples G4-1506 and G4-1510. The major component of these tuffs is clinoptilolite. Other components usually include opal-CT, quartz, and feldspar.

Vitric tuff

The vitric tuffs are represented in Fig. 8 by samples GU3-1405 and GU3-1407. The major component of the vitric tuffs is glass. Another component is usually feldspar. Sample G2-723 is another vitric tuff, but this sample also has a significant component of calcite.

Devitrified tuff

The devitrified tuffs are represented in Fig. 8 by samples G4-268 and G4-270. The major component of the devitrified tuffs is alkali feldspar. Another component of the devitrified tuffs is usually tridymite.

Minerals

In some of the sorption experiments, we used natural and synthetic minerals. The intent was to identify those minerals responsible for dominating radionuclide sorption onto tuff by measuring sorption with single mineral phases. The natural minerals we used were calcite, montmorillonite, bentonite, clinoptilolite (purified with sodium exchange), quartz, and albite. The synthetic minerals we used were calcite and hematite, which were commercially available $CaCO_3$ and Fe_2O_3, respectively.

Surface area of tuffs and minerals

Originally, the available data on total surface area of tuff samples from Yucca Mountain were rather

limited. Wolfsberg et al. (1979) reported surface areas (via the BET method using nitrogen as the adsorbate) for three samples with a range of values from 2.6 to 10.0 m^2/g. Data on the specific surface areas of the various mineral phases in Yucca Mountain tuffs were not available. Wolfsberg and Vaniman (1984) presented a summary of "cation exchange capacities" for Yucca Mountain tuffs. The zeolite and the clay-rich tuffs had cation exchange capacities in the range from 10 to 175 meq/l00 g, and the capacities of devitrified and vitric tuffs were in the range from 0.1 to 10 meq/l00 g.

We performed further surface-area measurements on the tuff samples and the minerals using the BET analysis method. Typical values are shown in Fig. 9.

Fracture Minerals

The Yucca Mountain region has undergone significant deformation due to tectonic and volcanic activity. As a result, many faults and fractures were produced within the tuffaceous units as well as the entire region. In addition, volcanic tuffs are often fractured as a result of cooling. The numerous fractures present at Yucca Mountain potentially represent a breach in the natural barrier by providing a fast pathway for contaminant migration.

Radionuclide transport calculations often assume

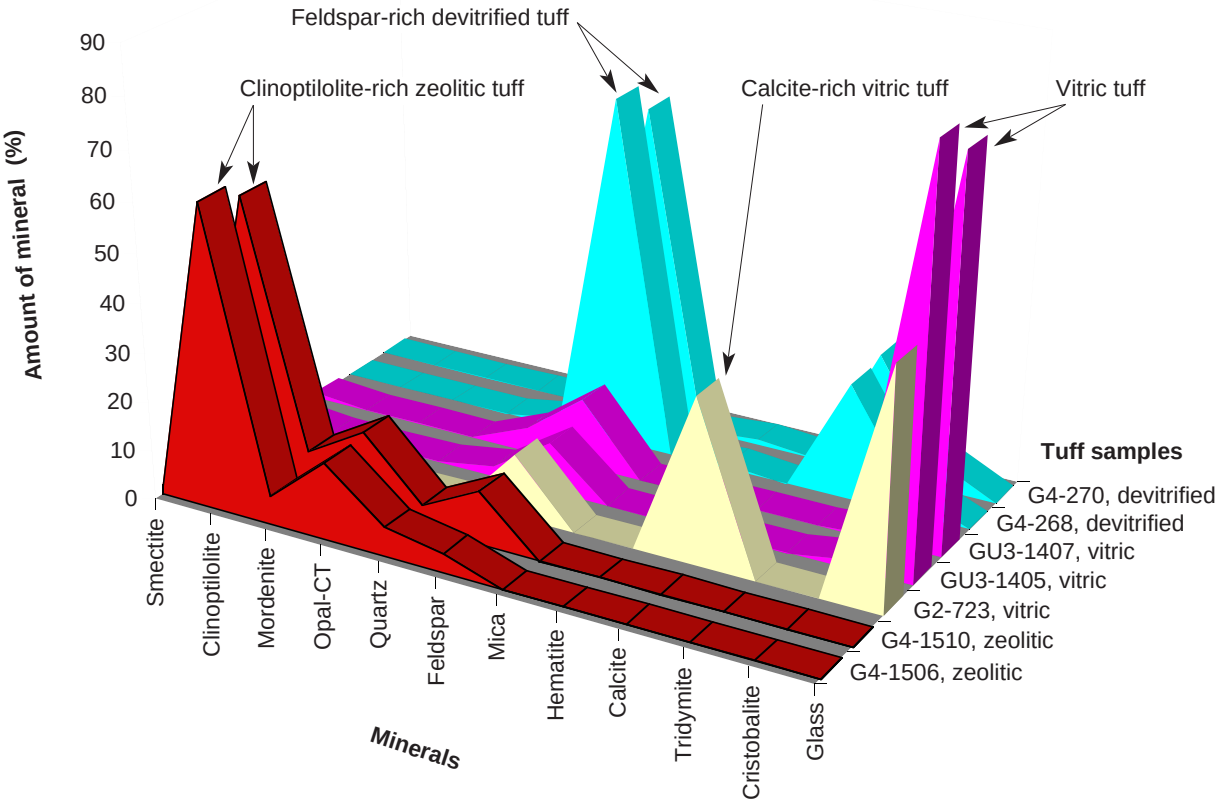

Figure 8. X-ray Diffraction Results. Mineral percentages determined by x-ray diffraction for tuffs used in the experiments are shown. Each tuff, except GU3-1405, was wet-sieved with J-13 well water to particle sizes ranging from 75 to 500 μm.

that radionuclides can travel through fractures unimpeded. This assumption is too simplistic and leads to overconservative predictions of radionuclide releases to the accessible environment. The assumption ignores two of the main retardation mechanisms: diffusion of the radionuclides from the fractures into the rock matrix and sorption of radionuclides onto the minerals coating those fractures.

Minerals coating the fracture walls are generally different from the host-rock mineralogy due to a variety of factors, such as precipitation of hydrothermal waters or alteration of the pre-existing minerals. The minerals lining the fractures found at the Yucca Mountain site (Carlos 1985, 1987, 1989, 1990, 1994; Carlos et al. 1993) are given in Table 6.

Although a relatively large number of fracture minerals have been identified, the overall abundance of these minerals is very small. Manganese minerals are found in fractures throughout most of the holes for which data are available, except in one drill hole where they are restricted to the upper few hundred feet. In most of the holes for which data are available, calcite is common in fractures within a few hundred feet from the surface, is minor or absent in the middle sections of the holes, and is again common in fractures in the lower parts of the holes, which is consistent with the abundance variations of calcite in the matrix. Clays and zeolites generally increase in abundance in fractures with depth and are the dominant secondary minerals in the lower parts of some holes. Silica and iron-oxide/oxyhydroxide phases are somewhat unevenly distributed in fractures but are nonetheless important fracture-lining phases.

Data on the concentrations of elements on surface sites on minerals in Yucca Mountain tuffs are very limited at present. The minerals for which the greatest number of data are available are the zeolites and clays. This emphasis exists because measurement of the bulk cation abundances (that is, calcium, magnesium, sodium, and potassium) in these minerals reflects the cation populations on intracrystalline exchange sites accessible to aqueous species.

Broxton et. al. (1986) have tabulated chemical data for zeolites and clays from various volcanic units

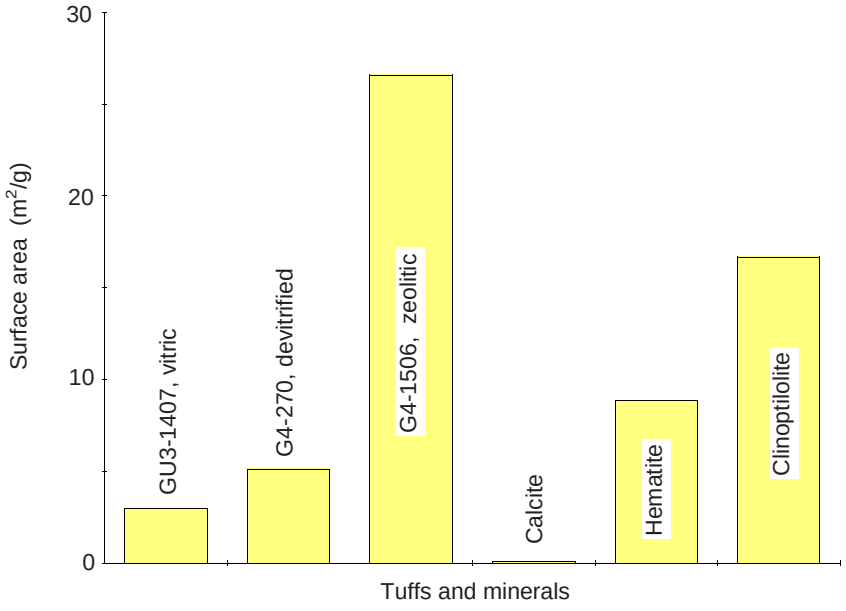

Figure 9. Surface Areas of Tuffs and Minerals. BET analysis was used to determine the surface areas of the tuffs and minerals used in the sorption experiments. The tuffs and the calcite (natural) were wet-sieved with J-13 well water to obtain particle sizes ranging from 75 to 500 µm. The hematite (synthetic) and clinoptilolite were not sieved.

Table 6. Minerals Coating Fracture Walls in Yucca Mountain Tuffs

Zeolites	
Heulandite	Chabazite
Clinoptilolite	Phillipsite
Mordenite	Erionite
Analcime	Stellerite
Silica	
Quartz	Feldspars
Tridymite	Plagioclase-albite
Cristobalite	K-feldspar-sanidine
Opal	
Clays	
Smectites	Sepiolite
Montmorillonite	Palygorskite
Saponite	Illite
Manganese-oxides/hydroxides	
Aurorite	Rancietite
Cryptomelane	Romanechite
Hollandite	Todorokite
Coronadite	Pyrolusite
Lithiophorite	
Iron-oxides/hydroxides	
Hematite	Magnetite
Carbonates and halides	
Calcite	Fluorite

in Yucca Mountain. In general, samples from the west side of the potential repository block are sodium and potassium rich, whereas the eastern samples are enriched in calcium and magnesium (Broxton et al. 1986, Fig. 1). Carlos (1985, 1989) and Carlos et al. (1990) have provided chemical data on zeolites and clays found in fractures. In general, the zeolites found there are similar in composition to zeolites present in the matrix adjacent to a given fracture sample, although exceptions have been noted. Analytical data on the surface compositions of most of the other mineral phases listed in Table 6 are essentially nonexistent. The actual surface structures (for example, defects and pits) of minerals in Yucca Mountain tuffs are also essentially unknown.

II. GROUNDWATER CHEMISTRY MODEL

A. INTRODUCTION

Variations in the chemistry of groundwater can have a significant impact on the transport behavior of radionuclides. For example, the solubility and sorption behavior of the various radionuclides of interest are a function of groundwater chemistry. To derive bounds on transport parameter values pertaining to the post-closure period of the potential repository, experiments must be carried out as a function of groundwater chemistry.

A groundwater chemistry "model" has been developed that can be used to bound the potential variations in groundwater chemistry to be expected in the post-closure period. This model consists of a set of conceptual submodels that describe the chemical processes that control the chemical evolution of pore waters, perched waters, and groundwaters in Yucca Mountain.

Experiments are used to quantify the submodels, and the results of the experiments can be used to link the submodels using variations in water chemistry observed in the site-characterization phase of this project to calibrate the resulting linked models. Unfortunately, the experimentation phase of the project was not carried to completion as a result of budget constraints. As a result, the linking of the conceptual models remains incomplete.

Purpose and Scope

The purpose of the Groundwater Chemistry Modeling Task is to develop models that describe compositional variations in groundwaters in the unsaturated and saturated zones beneath Yucca Mountain. These models will be used to establish bounds on the water compositions to be expected in the ambient Yucca Mountain flow system. They will also be used to bound the composition of waters in the far field of the potential repository at Yucca Mountain in the post-closure period. This information will be used by various other tasks in the project.

In this chapter, we will review the currently available data on the chemistry of waters in Yucca Mountain and develop and discuss models that explain the observed variations. We will combine 1) analytical data for precipitation (rain and snow), for pore waters and perched waters from the unsaturated zone at Yucca Mountain, and for groundwaters from the saturated zone at Yucca Mountain, 2) experimental and theoretical data and models for soil-water and rock-water interactions, and 3) computer modeling to identify both the controls on unsaturated-zone and saturated-zone water compositions in Yucca Mountain and the ranges in chemical compositions to be expected in these waters over the lifetime of the proposed repository.

Computer modeling with the code EQ3/6 was used as a tool to formulate and test conceptual models. However, its use in the prediction of future variations in water compositions is severely restricted because appropriate data on the identity of secondary (alteration) phases and data on the kinetics of formation of these phases (nucleation and crystallization) are lacking. For this reason, only preliminary work has been accomplished, and our discussion in this report does not include extensive reference to EQ3/6 modeling results.

B. GROUNDWATER CHEMISTRY

Sources of Data

The main sources of data for this chapter are the publications on precipitation compositions by McKinley and Oliver (1994, 1995) and publications on groundwater chemistry by Ogard and Kerrisk (1984) and Yang et al. (1988, 1996). It is important to state that the groundwater chemistry data of Ogard and Kerrisk and of Yang et al. represent samples from a very limited number of sites and may not be fully representative of waters in the overall Yucca Mountain flow system.

Precipitation Compositions

Precipitation compositions are important for modeling the compositions of waters at Yucca Mountain because they represent the starting point in the evolution of groundwater chemistry. Precipitation compositions are commonly separated into wet-fall and dry-fall. The composition of wet-fall reflects those solutes in falling rain or snow. The composition of dry-fall reflects the dust composition deposited on the land surface. The composition of wet-fall varies with geographic position due to numerous factors, such as the distance of the sampling site from the ocean (Wagner and Steele 1989). An approximation of wet-fall compositions at a given site can best be obtained by sampling while rain or snow is falling. Dry-fall compositions can be obtained by sampling dust.

A common approach to measuring precipitation compositions is to sample rain gauges and rain collectors either on a regular basis or after significant precipitation events. The precipitation compositions obtained with this approach reflect wet-fall, soluble dry-fall, and evaporation that occurred prior to removal of the sample from the collector. These compositions will here be called integrated precipitation compositions, or simply, precipitation compositions.

Dust (dry-fall) compositions were reported for southern Nevada and the Yucca Mountain area by Reheis (1995). Separate analyses of wet-fall are not available for the Yucca Mountain area, and only a limited number of analyses of integrated precipitation samples is available (Stezenbach 1992). Fortunately, an excellent database of integrated precipitation compositions for the Nevada Test Site area has been provided by a sampling network established by the U.S. Geological Survey in the Kawich Range just north of the Nevada Test Site (McKinley and Oliver 1994, 1995). This database will be used extensively in this report.

Average concentrations for the major constituents in integrated precipitation samples from the Kawich Range site are given in Table 7.

As an example of the variability in precipitation compositions, data for sulfate and chloride concentrations in integrated precipitation samples from the Kawich Range sites are plotted in Fig. 10. The observed scatter reflects variations in wet- and dry-fall compositions between sampling events, variations in the relative contributions from wet-fall and dry-fall in any given sample, evaporation, and ana-

Table 7. Average Integrated Precipitation Composition at Kawich Range Sites*

Component	Concentration (mg/l)
SiO_2	0.17
Calcium	0.96
Magnesium	0.11
Sodium	0.64
Potassium	0.24
Manganese	0.0084
Strontium	0.0058
Chloride	0.55
Fluoride	0.02
Sulfate	1.18
Nitrate	0.42
Alkalinity	2.7
pH	6.1

*from McKinley and Oliver (1994, 1995)

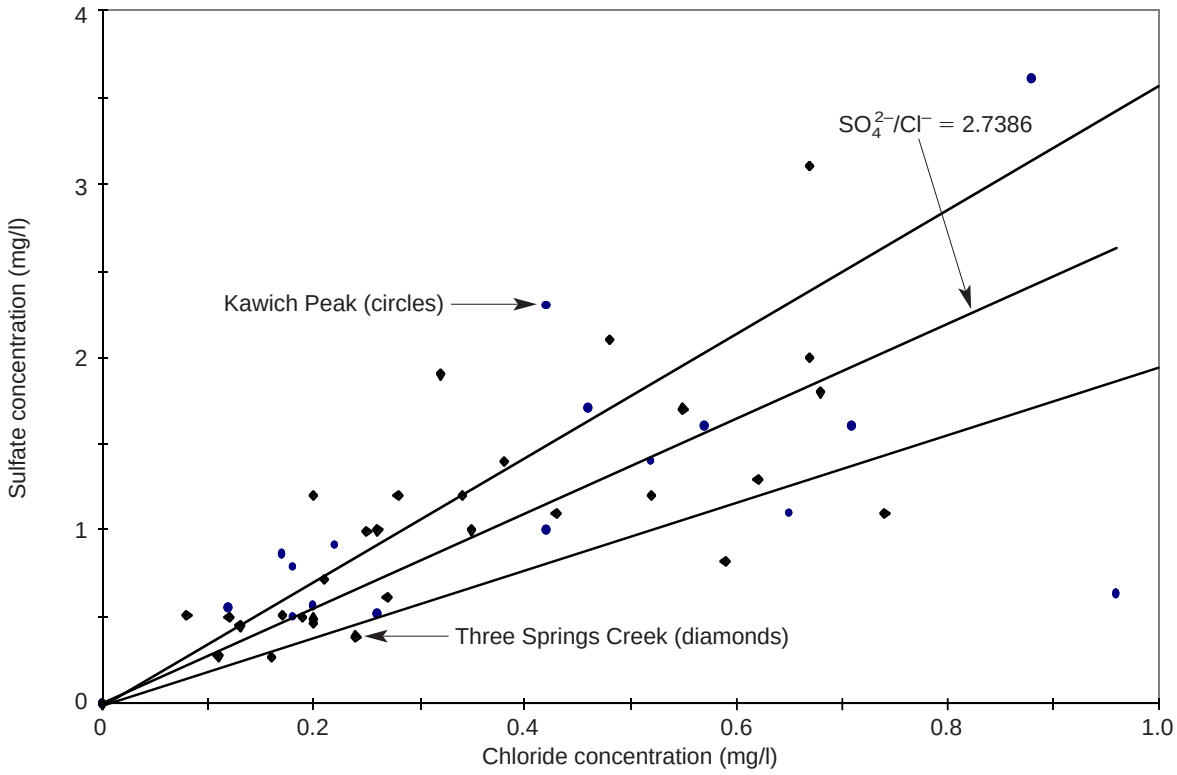

Figure 10. Sulfate versus Chloride in Precipitation. Concentrations of sulfate are plotted against concentrations of chloride for integrated precipitation samples from the Kawich Range sites (from McKinley and Oliver 1994, 1995). The slope of the inner line (a regression fit) gives the SO_4^{2-}/Cl^- ratio of the points plotted. The two outer lines represent a standard deviation of one sigma from the regression line.

lytical errors. Only samples with less than 1.0 mg/l were plotted. Samples with higher chloride concentrations showed significantly greater variability in chloride-to-sulfate ratios, suggestive of unusually high dust inputs. Many of the diagrams in this chapter will show a regression line representing a least-squares fit to the precipitation data and error lines reflecting the variability in the data.

Soil-zone Processes that Influence Water Compositions

In arid regions, such as southern Nevada, the average net infiltration rate is generally very low (Flint and Flint 1994). As a result, dust (dry-fall) and solids dissolved in precipitation (wet-fall) accumulate in the near-surface environment. Over time, this accumulation process can result in the formation of pedogenic horizons enriched in clays, calcite, silica, gypsum, and, in some cases, highly soluble salts (Watson 1992). The formation of these accumulations or horizons can have major impacts on the chemistry of waters that percolate into the unsaturated zone in these environments.

Recharge water to the unsaturated zone within Yucca Mountain passes through the upper surfaces of the mountain, whereas waters in the saturated zone beneath the mountain appear to represent recharge that infiltrated through soils located at higher elevations within and north of the area of Pahute Mesa that are hydrologically upgradient of Yucca Mountain (Winograd and Thordarson 1975). The soils on Yucca Mountain and Pahute Mesa are

not the same. Soils on Yucca Mountain locally contain abundant caliche and silica horizons (Taylor 1986) and support only limited vegetation. Pahute Mesa soils have little or no caliche and support a greater abundance and variety of vegetation (Spaulding 1985). Soil processes in both of these areas need to be considered in terms of potential impacts on groundwater chemistry. The two soil-zone processes that appear to have the greatest influence on the composition of infiltrating waters are evapotranspiration and dissolution/precipitation of solid phases in the soil.

Evapotranspiration

The term evapotranspiration refers to the loss of water from the soil zone as a result of simple evaporation and transpiration by plants (Freeze and Cherry 1980). Evapotranspiration causes the dissolved-solids content of soil waters to increase. A convenient measure of the amount of evapotranspiration and, by inference, the net infiltration rate associated with a given water sample is its chloride-ion concentration (Scalon 1991). Chloride salts of the major cations have high solubilities, and because Yucca Mountain bedrock is not a significant source of chloride to present-day groundwaters (Fabryka-Martin et al. 1996), the concentration of chloride in these waters can be used to estimate net infiltration rates. The following equation is used to derive this estimate.

$$R = \frac{[Cl^-]_{precip}}{[Cl^-]_{water}} P \,, \qquad (2)$$

where R is the infiltration rate, $[Cl^-]_{precip}$ is the average chloride concentration in precipitation, $[Cl^-]_{water}$ is the chloride concentration in the water samples, and P is the rate of precipitation. According to Hevesi et al. (1992), the average annual precipitation rate at Yucca Mountain is currently 170 mm/yr. If we assume an average chloride concentration in precipitation of 0.55 mg/l (Table 7), the concentration of chloride in water samples from Yucca Mountain can be used to calculate net infiltration rates.

The highest measured chloride concentration (245 mg/l) occurs in one of the shallowest and presumably youngest pore-water samples from the Yucca Mountain Member of Paintbrush Tuff (Fig. 11). The infiltration rate calculated for this sample is 0.4 mm/yr. Pore waters from other Paintbrush Tuff nonwelded units have significantly lower chloride concentrations (30–100 mg/l) and are associated with net infiltration rates of 0.9 to 3 mm/yr. The chloride concentrations in pore-water samples from the Topopah Spring nonwelded units are at the high end of the range observed in the nonwelded vitric units of Paintbrush Tuff. This suggests net infiltration rates were lower when the Topopah Spring pore waters were infiltrated compared to the waters in the overlying Paintbrush Tuff, excluding the Yucca Mountain Member. Presumably, this reflects a drier climate at the time the Topopah Spring pore waters were infiltrated.

The Calico Hills pore-water samples show a range in chloride concentrations from 15 to 82 mg/l. This range overlaps with the Paintbrush Tuff pore-water samples (excluding the Yucca Mountain Member sample) but is lower than the Topopah Spring pore waters. This result could reflect higher net infiltration rates for the Tuff of Calico Hills samples compared to the Topopah Spring samples, or it could simply reflect dilution as discussed further below. Water samples from Prow Pass Member are interesting in that *groundwaters* at the 528-m level have low chloride concentrations whereas *pore waters* from this level are at the high end of the distribution of chloride concentrations found in Tuff of Calico Hills pore waters. This observation indicates that equilibration of saturated-zone groundwaters with pore waters must be a very slow process.

Measured chloride concentrations in perched waters are similar to concentrations observed in saturated-zone groundwaters (Fig. 12). The calculated infiltration rates for these samples range from 2.5 mm/yr for UE-25 p#1 groundwater to 22.8 mm/yr for perched water from SD-7. Clearly, perched waters and saturated-zone groundwaters reflect much higher infiltration rates than do the

unsaturated-zone pore waters. Whether the higher infiltration rates for perched waters reflect a previous wet climate at Yucca Mountain or simply unusually wet years in the modern-day climate cannot be discerned from the water-composition data alone. However, the large difference (factor of 10) in chloride concentrations between pore waters and perched waters in samples from the same depth (for example, UZ-16 at 528 m) support a young age for the perched waters, as diffusion processes would tend to equalize these concentrations over time. It is interesting that similar differences in chloride concentrations between pore waters and fracture waters have been observed at Rainier Mesa (White et al. 1980).

It must be emphasized that the calculated infiltration rates cited in this section are only as good as the assumptions on which they are based. These assumptions include a constancy of the annual precipitation rate, a constancy of chloride concentrations in precipitation, the representativeness of the average chloride concentration in precipitation used in the calculations, and the lack of chloride leaching from rocks in contact with the water. The fact that the calculated infiltration rates are in the same range as those based on field measurements, as reported by Flint and Flint (1994), does lend support to this approach.

Dissolution/precipitation of solid phases in the soil zone

If concentration (that is, enrichment) of dissolved constituents by evapotranspiration were the only

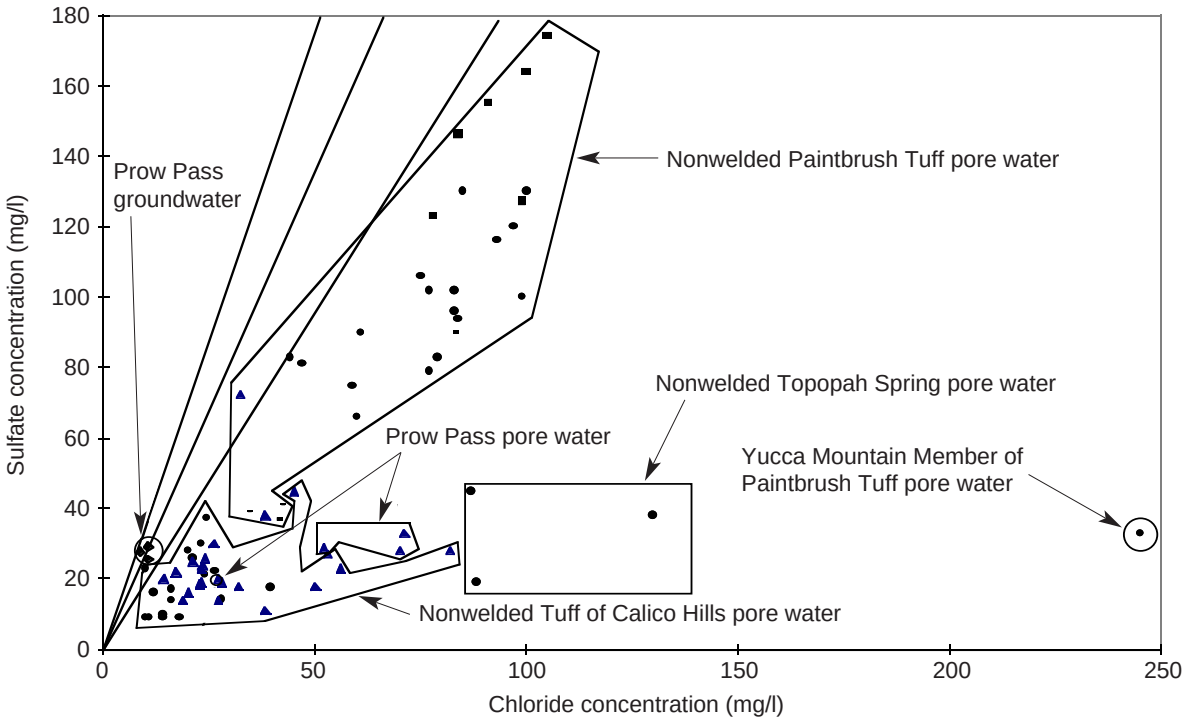

Figure 11. Sulfate versus Chloride in Pore Water. This plot shows sulfate versus chloride concentrations for unsaturated-zone pore-water samples and for three saturated-zone groundwater samples from Prow Pass (all data from Yang et al. 1988, 1996). The central line represents the best-fit line through composition data for precipitation at the Kawich Range sites (see Fig. 10), and the two outer lines reflect one-sigma variability in those precipitation compositions. (Drill-hole designations for the unsaturated-zone data points: circles: UZ-14; triangles: UZ-16; squares: UZ-4; and horizontal bars: UZ-5.)

soil-zone process to impact the composition of infiltrating waters, the concentrations of other major constituents in these waters could be obtained from the net infiltration rate (that is, the chloride concentration) and the ratio of the concentration of the constituent of interest relative to the concentration of chloride in precipitation. However, the presence of soil horizons on Yucca Mountain that are enriched in calcite, silica, and other components (Taylor 1986) suggests the situation is more complicated. These soil horizons indicate that pedogenic processes involving precipitation and dissolution of these phases have occurred in the soils over time. An important question is: "To what extent did these precipitation/dissolution processes influence the unsaturated-zone water compositions analyzed by Yang et al. (1988, 1996), and to what extent are they likely to influence unsaturated-zone water compositions in the future?"

Because age dates obtained for the calcite-rich and silica-rich soil horizons tend to be much older (Paces et al. 1995) than those obtained for pore waters, perched waters, and groundwaters at Yucca Mountain (Yang et al. 1996; Waddell et al. 1984), the relationship between the compositions of these horizons and the compositions of various waters presently in Yucca Mountain is uncertain. To establish a connection, evidence for chemical reactions that are unique to the soil zone must be identified in the unsaturated-zone water compositions.

Sulfate and chloride ions are generally conservative constituents in dilute oxidizing waters such as the unsaturated-zone pore waters in Yucca Mountain. Therefore, we would expect a plot of sulfate and chloride concentrations to show sulfate-to-chloride ratios similar to those observed in precipitation. However, as shown in Fig. 11, unsatu-

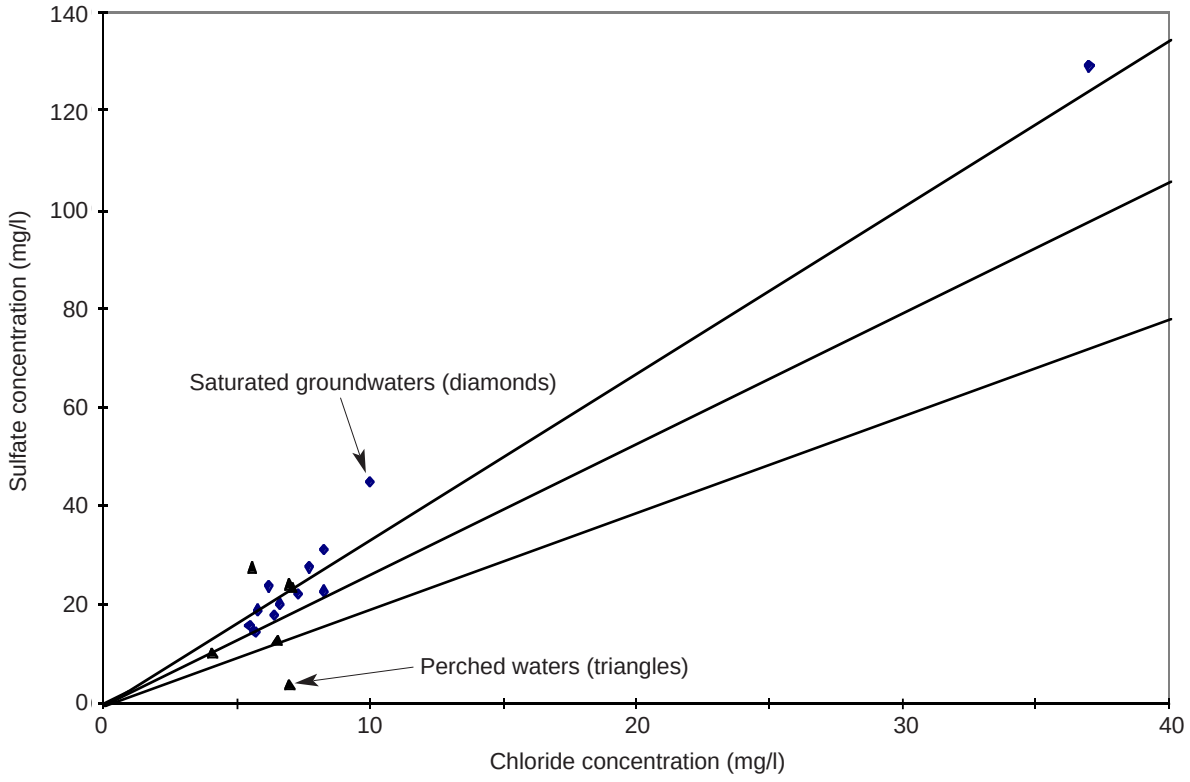

Figure 12. Sulfate versus Chloride in Perched Waters and Groundwaters. This plot shows sulfate versus chloride concentrations for perched waters and saturated-zone groundwaters. The lines are the same precipitation and variation lines as those plotted in Fig. 11.

rated-zone pore waters analyzed by Yang et al. (1988, 1996) show sulfate-to-chloride ratios consistently lower than the ratios observed in recent precipitation. Because all the unsaturated-zone pore-water analyses are grossly undersaturated with chloride phases and with gypsum and other possible sulfate phases involving the major cations, it is unlikely that solid chloride or sulfate phases are precipitated in the unsaturated zone.

Drever and Smith (1978) presented a model that offers one potential explanation for the low sulfate-to-chloride ratios in the unsaturated-zone pore waters. Their model involves drying and wetting cycles in the soil zone. During the drying phase, the concentrations of dissolved solutes are increased in the soil waters by evapotranspiration to the degree that phases such as calcite, gypsum, silica, and the more soluble salts precipitate. During "occasional heavy rains," the phases precipitated during the drying phase are partially redissolved. Because the dissolution rates for highly soluble salts, such as sodium chloride, are higher than the rates for less soluble salts, such as calcite, gypsum, and silica, a portion of the less soluble salts may remain undissolved after the "occasional heavy rains" infiltrate through the soil zone. In terms of sulfate and chloride concentrations, this process could lead to soil waters with lower sulfate-to-chloride ratios than those observed in precipitation. The actual concentrations of sulfate and chloride in these waters would depend on the details of the processes involved, including the dissolution kinetics of the sulfate and chloride phases, the residence time of the waters in the soil zone, and the original masses of sulfate and chloride in the soil zone.

Although differences in the dissolution kinetics of sulfate and chloride salts may be part of the explanation for the low sulfate-to-chloride ratios in pore waters from the unsaturated zone at Yucca Mountain, these differences are likely augmented, and perhaps even dominated, by crystallization-sequence effects. For example, it is possible that minerals, such as calcite and gypsum, that precipitate from evaporating pore waters early in a crystallization sequence are partially or completely sequestered by minerals that precipitate later in the sequence (such as being coated by opal-A and halite). Alternatively, early-crystallized phases may completely fill smaller pores in the rocks and, therefore, be less accessible to infiltrating waters than minerals crystallized later in the sequence in larger pores (for example, Chadwick et al. 1987). During subsequent infiltration events, the latest-formed phases in pores accessible to infiltrating waters would preferentially dissolve, leading to soil solutions enriched in the more soluble salts relative to the less soluble salts.

When viewed from the perspective of this model, chloride and sulfate concentrations for the pore-water sample from the Yucca Mountain Member tuff (Fig. 11) suggest this sample reflects an infiltration event that followed an extended "dry" period of lower than average precipitation. In fact, the chloride concentration of this sample would represent approximately 450 liters of precipitation (rain and snow), assuming an average chloride concentration of 0.55 mg/l for precipitation (Table 7). During the "dry" period, the sulfate concentration in the soil water must have increased to the point where sulfate minerals such as gypsum crystallized from the soil solution. Chloride minerals may also have crystallized at this time. For some extended period, net infiltration into the soil zone was insufficient to wash these pedogenic minerals out of the zone. During this time, these minerals may have been repeatedly dissolved and recrystallized. Eventually, a large precipitation event caused sufficient water to infiltrate the soil zone so that water percolated out of that zone into the unsaturated zone, carrying most of the accumulated chloride and lesser amounts of the accumulated sulfate.

We can estimate the amounts of gypsum and calcite precipitated from the Yucca Mountain Member sample by 1) assuming that soil-zone waters originally had the composition of recent precipitation, 2) assuming that sufficient soil water evaporated so that the chloride concentration in the remaining liq-

uid equals that measured in the Yucca Mountain Member sample, 3) calculating the amount of precipitated gypsum as the difference in the measured sulfate concentration and that inferred from the evaporated precipitation, 4) subtracting enough calcium from the evaporated precipitation to produce the gypsum, 5) assuming that enough calcite precipitated with the remaining calcium so that the concentration measured in the sample is the remainder, and 6) assuming that chloride minerals were totally dissolved by the large infiltration event. The resulting calculated amounts are approximately 700 mg of gypsum and 200 mg of calcite per liter of the Yucca Mountain Member sample.

Pore waters from Paintbrush Tuff, Topopah Spring, Prow Pass, and Tuff of Calico Hills have lower chloride concentrations and lower sulfate-to-chloride ratios than the Yucca Mountain Member sample. According to the model, these would reflect infiltration events that followed shorter "dry" periods. However, there is an additional complication in the sulfate and chloride data for these waters—there is a range of sulfate-to-chloride ratios at a given chloride concentration. If the precipitation of sulfate in the soil zone is the explanation for the deviation of these compositions from evapotranspirated precipitation, it is discomforting that this process appears to produce such a large range of sulfate-to-chloride ratios.

One possible explanation is that the range simply reflects the variability in the infiltration process. For example, if the pore sizes in the sulfate-mineral accumulation horizon are much smaller in one location than another, infiltrating waters may be denied access to a large fraction of the pores in the former case as a result of plugging by early-formed phases (Taylor 1986; Levy 1984). Alternatively, a mixing process could be involved. The rather narrow range of sulfate concentrations (10–40 mg/l) observed for the Calico Hills, Topopah Spring, and Prow Pass samples and the fact that this range includes most perched and saturated-zone samples is suggestive of such a process. The mixing could involve perched or saturated-zone waters with low sulfate and chloride concentrations and pore waters with low sulfate and high chloride concentrations, such as the Yucca Mountain Member sample. Unfortunately, the lack of certainty in the explanation for the variations in sulfate-to-chloride ratios precludes the development of a quantitative model for this process. More information on the detailed hydrology of Yucca Mountain soils is required.

The conceptual model and the calculations described above imply that sulfate minerals will accumulate in the soil zone on Yucca Mountain. However, analyses of Yucca Mountain soils only occasionally show significant amounts of gypsum, although small amounts (1–2%) are routinely detected (Taylor 1986; Vaniman et al. 1995). The fact that gypsum is not more common in Yucca Mountain soils could be due to a variety of factors including: 1) sulfate minerals were not accumulated in soil profiles prior to the last few thousand years as the climate became drier (Spaulding 1985), 2) sulfate minerals occur deeper in the soil profile than the depths covered by the analyses, 3) sulfate minerals were more abundant in soil profiles previously but were leached out during extended wet periods, or 4) some other process such as microbial reduction of sulfate is causing the decrease in sulfate concentrations.

The last factor is unlikely given the oxidizing nature of the unsaturated-zone pore waters. The third factor is a possibility but is difficult to evaluate with existing data. If this factor was responsible, unsaturated-zone waters would have had sulfate-to-chloride ratios in excess of precipitation for some period of time. There is no clear evidence for this process in analyses of the unsaturated zone (Fig. 11), although it is possible that waters of this type were present in the system but were flushed through to the saturated zone. Factor two is unlikely because significant amounts of gypsum were, in fact, found in some of the profiles described by Taylor (1986). The interpretation favored in this report is that sulfate minerals were more abundant in soil profiles in earlier times but

were subsequently leached out, and the amounts found in soils at the present time only reflect the most recent ("dry") climatic regime.

Another important constituent in soil waters is silica. Silica is important because it is by far the most abundant constituent in the volcanic rocks of Yucca Mountain and its concentration in solution has a major impact on the ability of the solution to dissolve additional mineral components. Silica-rich horizons are often interbedded with calcite-rich horizons on Yucca Mountain (Taylor 1986). A model for the origin of silica-rich horizons in soils derived from volcanic rocks was developed by Chadwick et al. (1987). This model involves the reversible adsorption of silica onto surfaces of other soil constituents (for example, clays, sesquioxides, and weathered primary minerals) and the formation of opaline silica sols and coatings as soils dry out. Silica in these types of soils is apparently quite easily solubilized. Chadwick et al. (1987) found that up to 152 mg/l of monomeric silica could be extracted from the soils in 16 hours. These results are consistent with other reports (for example, Gifford and Frugoli 1964) and suggest that waters percolating from the soil zone into the unsaturated zone at Yucca Mountain will be close to saturation with amorphous silica.

The soil zone is also important to carbon-dioxide partial pressures in the unsaturated zone. The partial pressure of CO_2 in soil atmospheres is commonly elevated over the partial pressure of CO_2 in the Earth's atmosphere (Greenland and Hayes 1978). Measurements of the partial pressure of CO_2 at a depth of 10 feet in the unsaturated-zone drill hole UZ-1 in Yucca Mountain indicate that it is approximately four times the atmospheric value (Yang et al. 1996). This fact suggests that soil-zone processes at the surface of Yucca Mountain could influence the partial pressure of CO_2 in the unsaturated zone. However, the fact that CO_2 partial pressures are quite variable with depth in drill hole UZ-1 suggests there may be additional sources of CO_2 in the unsaturated zone. Interestingly, the isotopic composition of CO_2 in various wells on Yucca Mountain suggests it has been strongly influenced by biologic activity (Thorstenson et al. 1989; Yang et al. 1996).

Pore-water Compositions above the Potential Repository Horizon

The types of chemical reactions that could affect unsaturated-zone water compositions include: 1) dissolution/precipitation reactions, 2) ion-exchange reactions, and 3) gas-phase reactions (Meijer 1995). Because the absolute abundance of ion-exchanging minerals is generally low in units above the zeolitized Tuff of Calico Hills (Bish and Chipera 1989), dissolution/precipitation reactions and gas-phase reactions are likely dominant in this zone and will, therefore, be the focus of this section.

Sulfate-to-chloride ratios in waters from the unsaturated zone suggest there are at least two types of waters in the unsaturated zone above Tuff of Calico Hills (Figs. 11 and 12). These are relatively dilute perched waters and pore waters of higher ionic strength. Because perched-water compositions are very similar to saturated-zone water compositions (Fig. 12), they will be discussed in the next section ("Perched-water Compositions below the Potential Repository Horizon").

As discussed in Meijer (1995), dissolution reactions in devitrified and vitric silicic tuffs will involve the hydrolysis of feldspar and glass, respectively. These hydrolysis reactions generally leach sodium ($\pm$ calcium, magnesium, and potassium) in exchange for hydrogen ions (White et al. 1980). Therefore, relative to a conservative solute such as chloride, sodium concentrations should increase in the pore waters relative to the original precipitation compositions if hydrolysis reactions are of importance. As shown in Fig. 13, this is contrary to what is observed. In the pore waters from units above Calico Hills (that is, Yucca Mountain Member, nonwelded Paintbrush Tuff, and nonwelded Topopah Spring), sodium-to-chloride ratios are generally lower than those observed in modern-day precipitation. This

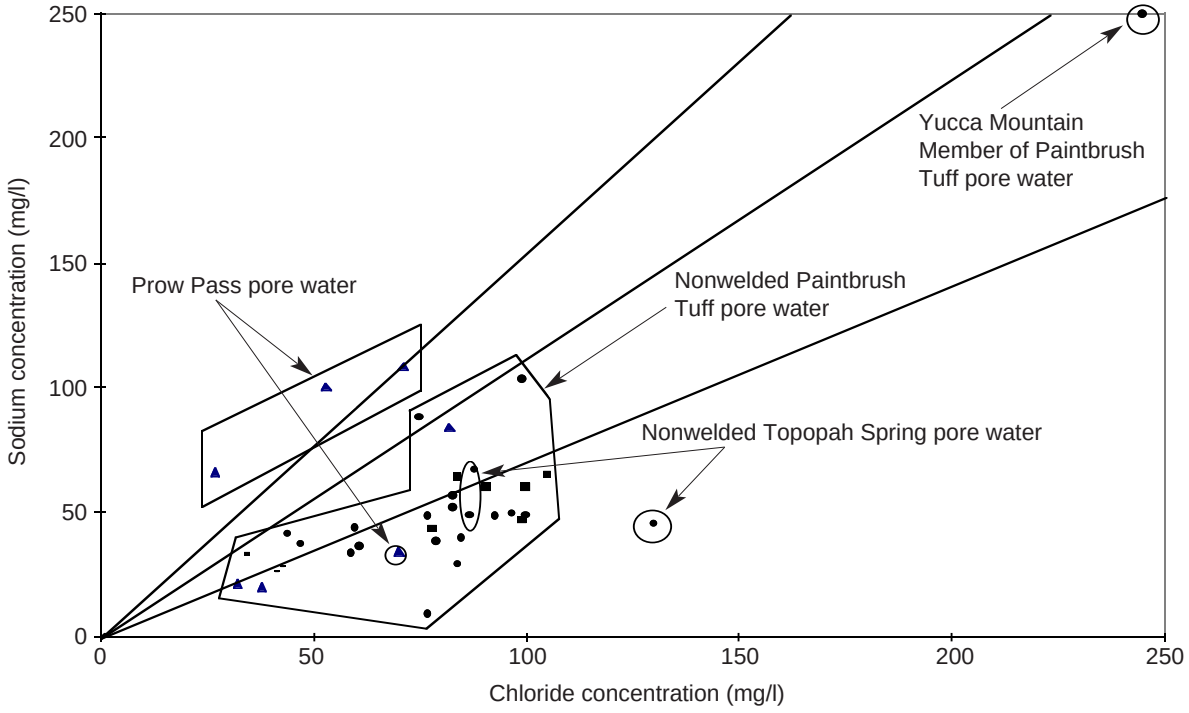

Figure 13. Sodium versus Chloride. This plot shows the sodium (rather than sulfate) concentration versus the chloride concentration of unsaturated-zone pore-water samples from Yucca Mountain. Here, the central line represents a regression fit of sodium-versus-chloride precipitation data, and the outer lines represent one standard deviation for the scatter of those data. (Drill-hole designations for data points: circles: UZ-14; triangles: UZ-16; squares: UZ-4; and horizontal bars: UZ-5.)

observation implies that hydrolysis reactions have not significantly impacted the chemistry of these waters.

Why sodium-to-chloride ratios in these pore waters are lower than those observed in recent precipitation is not entirely clear. Potential explanations include the possibility that nonchloride sodium salts (for example, sodium sulfate) crystallized in the soil zone prior to chloride-salt crystallization and were sequestered, that precipitation (wet-fall plus dry-fall) had lower sodium-to-chloride ratios in the past, or that ion-exchange reactions (for example, with clays) removed sodium ions from solution. The latter explanation appears unlikely given that clay analyses from units at this level are enriched in calcium and magnesium, not sodium (Levy 1984). Resolution of this question will require additional investigations of the soil-zone processes at Yucca Mountain.

The lack of evidence in the sodium-versus-chloride concentration data for hydrolysis reactions in units above Calico Hills is not unexpected and is, in fact, corroborated by other observations. These observations include the persistence of abundant 10-to-12-million-year-old volcanic glass in the unsaturated zone within Yucca Mountain and the fact that, with some exceptions, only limited amounts of secondary minerals are found in the glassy and devitrified tuffs (Bish and Chipera 1989). The exceptions are the localized clay-rich horizons in parts of the nonwelded Paintbrush Tuff. The origin of these horizons is uncertain at the present time. They may reflect alteration of glass in high-flow (water) zones (Levy 1984), or they may have

formed during weathering reactions that occurred while the tuffs were exposed at the surface.

The lack of evidence for hydrolysis reactions in the sodium-versus-chloride concentration data for pore waters in units above Calico Hills likely reflects the fact that concentration of cations (for example, sodium) by evapotranspiration combined with the saturation of infiltrating waters with amorphous silica in the soil zone has lowered the reactivity of these waters with respect to dissolution of the aluminosilicate solids (such as feldspar and glass). For feldspars, this can be quantified by calculating the saturation state of the pore waters with respect to feldspar minerals. Aluminum and potassium concentrations were not reported for pore waters by Yang et al. (1988, 1996), precluding direct calculation of feldspar saturation states. However, the high sodium and silica concentrations in the pore waters ensure that they will be saturated with albite when in contact with a solid source of aluminum (such as feldspar or glass). This effect implies that the feldspars in the devitrified tuffs will not be significantly altered by the waters percolating out of the soil zone. The observed lack of secondary minerals in the devitrified zones (Bish and Chipera 1989) corroborates this conclusion.

In the case of volcanic glass, the situation is less straightforward because glass is thermodynamically unstable with respect to secondary minerals at ambient temperatures and pressures. In fact, many studies have been carried out in recent years to gain an understanding of glass alteration behavior, mainly to provide a basis for predictions of the alteration behavior of nuclear waste glasses. An important result of these studies is that the glass dissolution rate has been shown to be quite sensitive to the silica concentration in solution. As this concentration reaches saturation with amorphous silica, the dissolution reaction slows down dramatically (Grambow 1992). Apparently, for glass alteration to proceed, the "gel reaction zone" that forms on the glass surface needs to dissolve. If the solution phase is saturated with amorphous silica, the dissolution of this material is inhibited because the affinity of the dissolution reaction is low. Conceivably, other silica polymorphs with lower solubilities (for example, opal C-T, cristobalite, and quartz) could nucleate and crystallize, thereby causing the silica concentration in solution to be maintained at a lower level. This effect, in turn, could enhance the glass dissolution rate. However, the nucleation rates of these other polymorphs appear to be inhibited for some reason that remains to be determined.

The concentrations of silica in unsaturated-zone pore waters are generally high (Fig. 14). Although essentially all of the pore-water samples analyzed by Yang et al. (1988, 1996) are saturated with α-cristobalite, many are saturated with opal-CT and some are even saturated with opal-A at 25°C (Fig. 14). The concentrations tend to be higher in pore-water samples from Paintbrush Tuff and Tuffs of Calico Hills compared to samples from Topopah Spring and Prow Pass. Temperature does not appear to be a controlling parameter. Also, there do not appear to be consistent trends in silica concentration with depth in a given unit. The high silica concentrations in the Paintbrush Tuff pore waters presumably reflect the presence of abundant glass in this unit. The slightly lower silica concentrations in Tuff of Calico Hills pore waters may reflect the fact that the mineralogy of the host rock consists of zeolites and opal-CT (Bish et al. 1996b). The mineralogy of the Topopah Spring and Prow Pass tuff samples in drill holes UZ-14 and UZ-16 was not available at the time this report was being written.

Part of the scatter in the silica data plotted in Fig. 14 may reflect analytical techniques. The pore-water samples were not filtered prior to analysis, and the analyses were carried out by inductively coupled plasma-emission spectroscopy, which does not discriminate monomeric silica from other forms of silica in solution. This is likely the explanation for the high silica concentrations ($>$ 80 mg/l) measured in some of the Calico Hills pore-water samples. The analyses of these samples also showed some relatively high alumina concentra-

tions, which are an indication of the presence of particulate matter (for example, colloids), as aluminum is very insoluble in near-neutral solutions. At this point, it is difficult to quantify the controls on pore-water silica concentrations at ambient temperatures other than to say that as long as volcanic glass remains in the unsaturated zone, these concentrations will be in a range between saturation with α-cristobalite and saturation with opal-A.

The concentration of bicarbonate in Yucca Mountain waters is an important parameter with respect to the solubility and sorption of many of the radionuclides in high-level radioactive waste (GCX 1994). The data presented by Yang et al. (1996) show that pore waters in the units above Tuff of Calico Hills tend to have bicarbonate-to-chloride ratios that are equal to or below the average observed in recent precipitation (Fig. 15). This trend likely reflects the crystallization of calcite in the soil zone prior to percolation of the waters into the unsaturated zone. If hydrolysis reactions were important in the evolution of these waters, bicarbonate-to-chloride ratios would exceed those observed in precipitation. This result is, in fact, observed in the analyses of perched waters, saturated-zone groundwaters, and pore waters from Tuff of Calico Hills, as discussed in more detail in the next section on perched-water compositions.

Calcite dissolution and precipitation is also likely to exert a major influence on the calcium concentration in pore waters in units above the zeolitized tuff in Calico Hills. Unfortunately, quantitative modeling of calcite dissolution/precipitation behavior in the unsaturated zone at Yucca Moun-

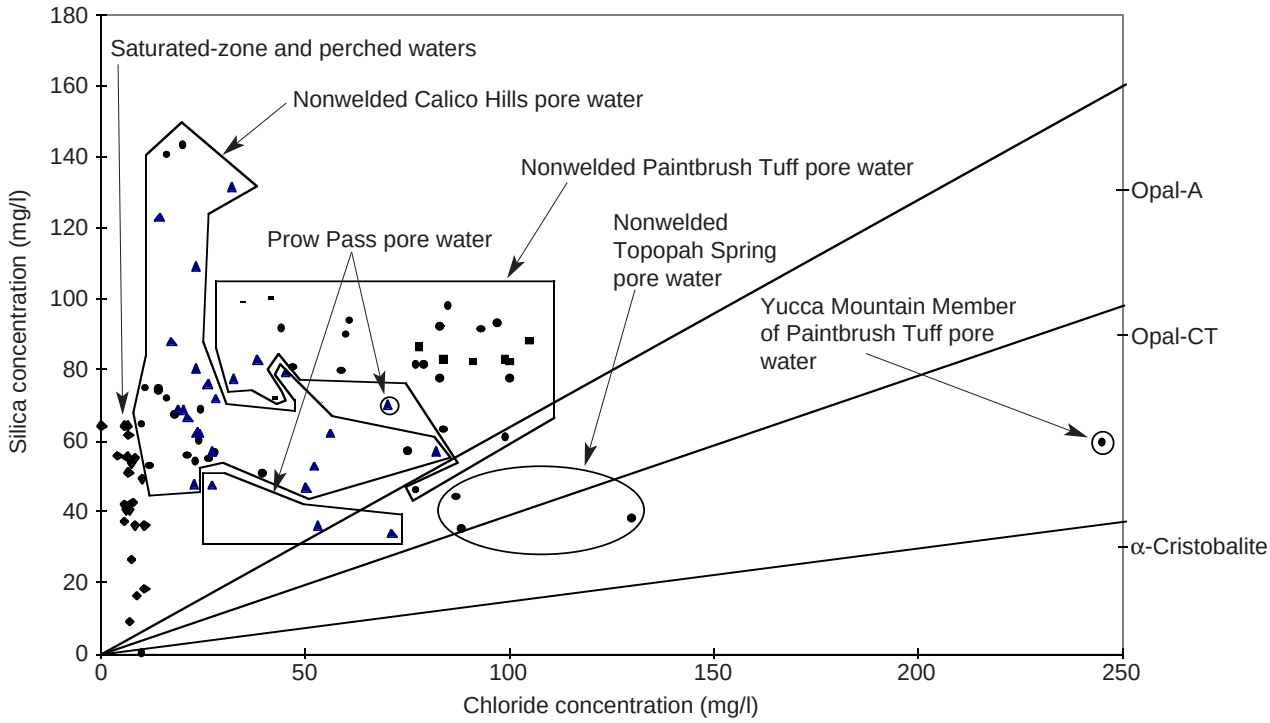

Figure 14. Silica versus Chloride. This plot shows silica versus chloride concentrations in pore waters, perched waters, and saturated-zone groundwaters (perched and saturated-zone data are not differentiated). The silica concentrations at which the waters would be saturated with opal-A, opal-CT and α-cristobalite at 25°C are given on the right. The straight lines are the regression fit to silica-versus-chloride concentrations in precipitation and the one-sigma deviations. (Drill-hole designations: circles: UZ-14; triangles: UZ-16; squares: UZ-4; horizontal bars: UZ-5; and diamonds: perched and saturated-zone waters.)

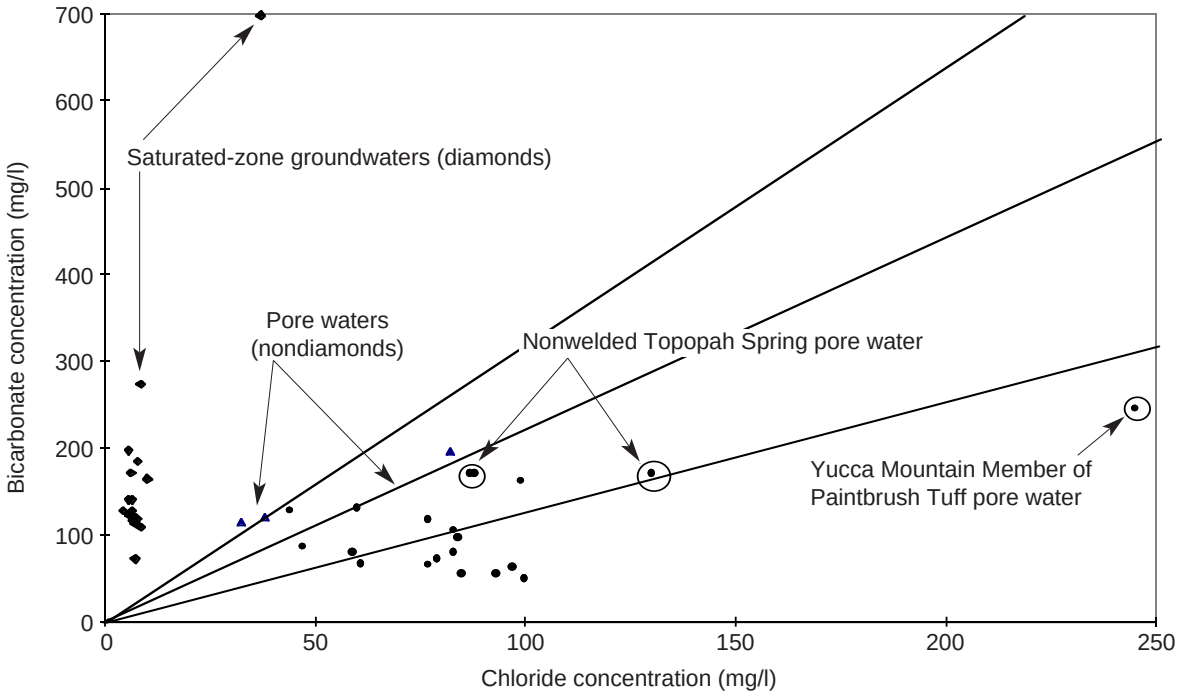

Figure 15. Bicarbonate versus Chloride. This plot shows bicarbonate versus chloride concentrations in pore waters from units above Tuff of Calico Hills and in saturated-zone groundwaters. The central line shows bicarbonate versus chloride concentrations in precipitation; the outer lines are the one-sigma deviations. (Drill-hole designations: circles: UZ-14; triangles: UZ-16; diamonds: saturated-zone waters.)

tain is complicated by the fact that the partial pressure of carbon dioxide in the gas phase present in the unsaturated zone appears to be quite variable (Yang et al. 1996). Detailed gas-composition data have been collected from borehole UZ-1 for over ten years. These data show that, for some as yet undetermined reason, the partial pressure of carbon dioxide in the unsaturated zone exceeds the atmospheric value (0.00032 atmospheres) at nearly all depths sampled. The pressure is approximately 0.01 atmospheres in the alluvium and decreases to approximately 0.0003 atmospheres in the middle tuff of Topopah Spring. Below this depth, it increases to values in excess of 0.003 atmospheres in the lower portion of Topopah Spring where the borehole bottoms out. Data for the partial pressure of carbon dioxide in the gas phase in units below the lower tuff of Topopah Spring are not available.

By combining pore-water compositions from borehole UZ-14 with carbon-dioxide partial pressures reported for borehole UZ-1 (Yang et al. 1996), located in close proximity to UZ-14, the saturation state of calcite in the pore waters can be calculated (Table 8). The values of the calcite saturation index presented in that table reflect the degree to which the water is saturated with calcite. Positive numbers reflect oversaturation and negative numbers reflect undersaturation. It is of interest that only the sample from the Yucca Mountain Member (UZ14-45, which is from borehole UZ-14 at 45 feet) shows a positive value. The sample at 135 feet is close to saturation, whereas the other samples are undersaturated and, therefore, could dissolve calcite if it were present. Because data on the partial pressure of carbon dioxide are not available for pore-water samples from other boreholes, calcite saturation cannot be realistically evaluated for these.

Table 8. Calculated Calcite Saturation Indices

Sample ID	Saturation index*
UZ14-45	0.0153
UZ14-85	–0.1835
UZ14-91	–0.2485
UZ14-95	–0.5756
UZ14-96	–0.5503
UZ14-100	–0.6820
UZ14-114	–0.7885
UZ14-135	–0.0158
UZ14-144	–0.2219
UZ14-147	–0.6269
UZ14-177	–0.8767
UZ14-178	–0.1829
UZ14-215	–0.8890
UZ14-225	–0.7191
UZ14-235	–0.4746
UZ14-240	–0.4952
UZ14-245	–0.7692
UZ14-1258	–0.0389

*$\log(IAP/K_T)$, where $IAP = [Ca^{2+}][CO_3^{2-}]$ is the measured ion association product for the water and K_T is the equilibrium product for the solubility of calcite at the temperature of interest.

The fact that most of the UZ-14 pore-water samples are undersaturated with calcite is not surprising given the spotty distribution of calcite in Yucca Mountain (Vaniman and Chipera 1996). Calcite is more likely to be precipitated in fractures for which the partial pressure of carbon dioxide is lower as a result of more direct access to the atmosphere. Because the total amount of calcite in fractures is small relative to the total mass of solute in pore waters, precipitation/dissolution reactions involving fracture calcite are unlikely to control pore-water calcium concentrations.

The elevated partial pressure of carbon dioxide will tend to keep the pH in the pore waters in the range from 7 to 8. If carbon-dioxide partial pressures in the unsaturated-zone gas phase decrease with time due to venting associated with operations at the potential repository, the pH of pore waters could increase to values above 8, depending on the extent of degassing. Because the total volume of the excavations are small relative to the total volume of the rock mass surrounding the potential repository, it is unlikely this effect will be very significant overall.

The concentrations of the major cations in pore waters are of interest with respect to the solubility and sorption behavior of the radionuclides in high-level radioactive waste. As noted above, the generally low abundances of ion-exchanging minerals in the units above the zeolitized Tuff of Calico Hills suggest that cation proportions in pore waters from this portion of Yucca Mountain will reflect primarily soil-zone precipitation/dissolution processes. As shown in Fig. 16, the calcium-to-chloride ratios in pore waters from units above Tuff of Calico Hills are either on the precipitation line or below it. Sodium-to-chloride ratios in these samples also plot below the precipitation line (Fig. 13). If ion-exchange reactions were controlling the relative concentrations of calcium and sodium, there would be an antithetic relationship in their concentrations. This relationship is not evident in the data, which suggests that ion-exchange reactions are of secondary importance relative to other reactions that involve these elements, such as the precipitation of calcite, gypsum, and other salts in the soil zone.

The oxidation-reduction potential (Eh) of waters in the unsaturated zone should reflect the fact that the gas phase in the unsaturated zone has an oxygen partial pressure equal to that in the atmosphere (Thorstenson et al. 1989; Yang et al. 1996). This condition will cause the Eh to be in the range from 400 to 600 mV.

The pH of pore waters in the unsaturated zone will reflect the partial pressure of carbon dioxide in the gas phase. Because this partial pressure is variable with depth (Yang et al. 1996) and above atmospheric levels, the pH of the pore waters will vary in a range from approximately 7 to 8.

Bounds on future variations in the composition of

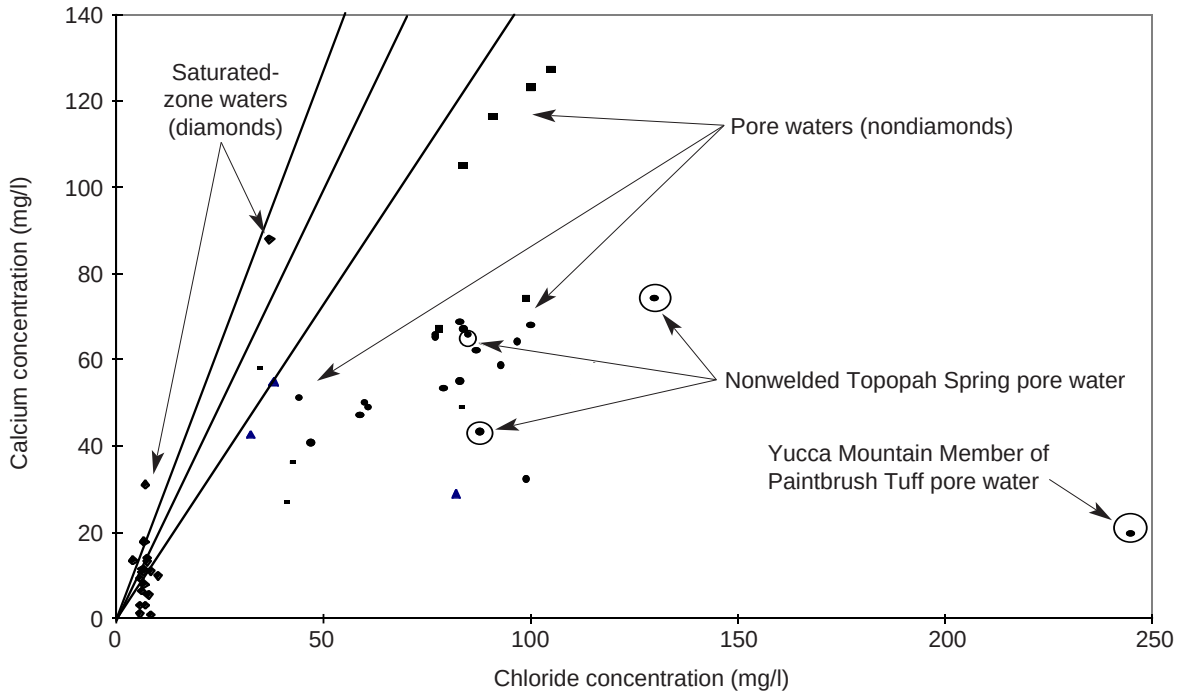

Figure 16. Calcium versus Chloride. This plot shows calcium versus chloride concentrations of unsaturated-zone pore waters from units above Tuff of Calico Hills and of saturated-zone groundwaters. The straight lines are the regression fit of precipitation data for calcium versus chloride and the one-sigma deviations from that fit. (Drill-hole designations: circles: UZ-14; triangles: UZ-16; squares: UZ-4; horizontal bars: UZ-5; diamonds: saturated-zone waters.)

pore waters in units above and within the repository horizon are difficult to determine solely on the basis of chemical arguments. The main controls on these compositions are the amount of evapotranspiration that occurs in the soil zone and precipitation reactions in the soil zone. High amounts of evapotranspiration will lead to pore waters with high ionic strength. Such waters will tend to precipitate calcite, gypsum, silica, and possible other soluble salts. Fortunately, the higher the evapotranspiration, the less infiltration there will be. In other words, pore waters of high ionic strength will be of limited volume and may not percolate to the level of the potential repository over its useful lifetime. Because the detailed soil hydrology can have a significant impact on the chemical evolution of soil waters, a coupled flow-chemistry model is required to properly model the evolution of these waters.

Perched-water Compositions below the Potential Repository Horizon

Sulfate-to-chloride ratios in perched and saturated-zone waters show little evidence of soil-zone precipitation reactions involving gypsum and other soluble sulfate salts. In fact, they show sulfate-to-chloride ratios that are somewhat higher than those observed in precipitation (Fig. 12). This result may reflect somewhat higher sulfate-to-chloride ratios in the precipitation when these waters were infiltrated, or the waters may be dissolving small amounts of sulfate as they infiltrate through the soil zone and the unsaturated zone.

An important characteristic of perched waters, saturated-zone groundwaters, *and* many of the pore waters in Tuff of Calico Hills is that these waters all have elevated bicarbonate-to-chloride and sodi-

um-to-chloride ratios relative to the ratios observed in recent precipitation (Figs. 17 and 18). This observation suggests that these waters have been subject to hydrolysis reactions (White et al. 1980). In these reactions, hydrogen ions resulting from the dissociation of carbonic acid exchange with cations in the solid phase. An example of such a reaction involving sodium is

$$\text{Solid–Na} + H_2CO_3 \leftrightarrow \text{Solid–H} + Na^+ + HCO_3^- .$$

Elevated bicarbonate-to-chloride ratios provide the most definitive evidence of hydrolysis reactions because elevated sodium-to-chloride ratios could also reflect ion-exchange processes.

The fact that pore waters in the Topopah Spring Member overlying Tuff of Calico Hills do not show evidence of significant hydrolysis reactions suggests that either hydrolysis reactions are currently operative in Tuff of Calico Hills or that the Calico Hills pore waters contain water from another source. Pore waters from Prow Pass Member, which underlies Tuff of Calico Hills, have bicarbonate-to-chloride ratios similar to those observed in tuff from Topopah Spring Member. Therefore, the high bicarbonate-to-chloride ratios in pore waters from Calico Hills are sandwiched between units with low bicarbonate-to-chloride pore waters. Interestingly, *groundwater* pumped from Prow Pass Member in borehole UZ-16 has bicarbonate-to-chloride ratios that are much higher than those observed in recent precipitation and that are similar to those observed in the pore waters of Calico Hills. This fact suggests that the higher bicarbonate-to-chloride ratios in the pore waters of Calico Hills are not simply the result of in-situ hydrolysis reactions. If they were, similar bicarbonate-to-chloride ratios would be observed in Prow Pass pore waters. The important point is that pore waters in Tuff of Calico Hills and groundwaters from below the water table have compositions that are distinct from the compositions of pore waters in the units above and below Tuff of Calico Hills.

The relative importance of hydrolysis and ion-exchange reactions in these waters can be approximated as follows. Assume that the "excess" bicarbonate (the amount in excess of that indicated by the precipitation ratio at the given chloride concentration) in these waters reflects only hydrolysis reactions and also that the amount of sodium released to solution during the reaction is approximately 0.6 equivalents of sodium per equivalent of bicarbonate (White et al. 1980). The amount of sodium in the water analysis in excess of that originally in the water (from the sodium-to-chloride ratio in precipitation) plus the sodium released through hydrolysis reactions is assumed to be the amount contributed to the solution by ion-exchange reactions. This calculation suggests that up to 95% of the "excess" sodium in solution (relative to precipitation) appears to be contributed by hydrolysis reactions. The relatively small proportions that appear to be contributed by ion-exchange reactions in pore waters from Tuff of Calico Hills are more or less consistent with the amounts of calcium and magnesium lost from these waters (relative to precipitation) (Figs. 19 and 20).

The Calico Hills pore waters are interesting in that, in addition to showing evidence of hydrolysis reactions in their bicarbonate-to-chloride and sodium-to-chloride ratios (Figs. 17 and 18), they show evidence of soil-zone processes in their sulfate-to-chloride ratios (Fig. 11). That is, these latter ratios are well below those observed in recent precipitation. As discussed above, the sulfate-to-chloride ratios in these pore waters could reflect mixing of perched or saturated-zone waters with pore waters percolating into Tuff of Calico Hills from Topopah Spring Member. If this is true, the high bicarbonate-to-chloride ratios in these pore waters would also be a result of the mixing of these waters. The proportions of perched/saturated-zone water and Topopah Spring pore water in the hypothetical mixtures can be estimated on the basis of chloride concentration of the Topopah Spring samples and the perched/saturated-zone samples at a given bicarbonate concentration. These estimates fall in the range of from 60 to 90% perched/saturated-zone water and from 10 to 40% pore water.

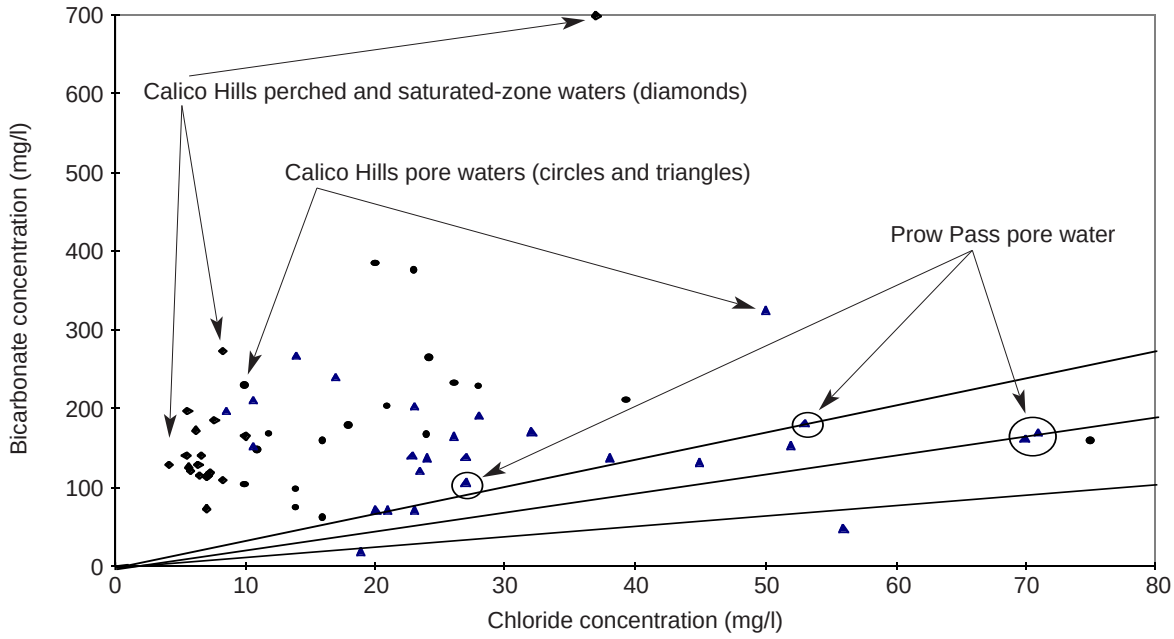

Figure 17. Calico Hills Bicarbonate. This plot shows bicarbonate versus chloride concentrations in Calico Hills pore waters, perched waters, and saturated-zone groundwaters. The straight lines are the regression fit of precipitation data for bicarbonate versus chloride and the one-sigma deviations from that fit. (Drill-hole designations: circles: UZ-14; triangles: UZ-16; diamonds: saturated-zone waters.)

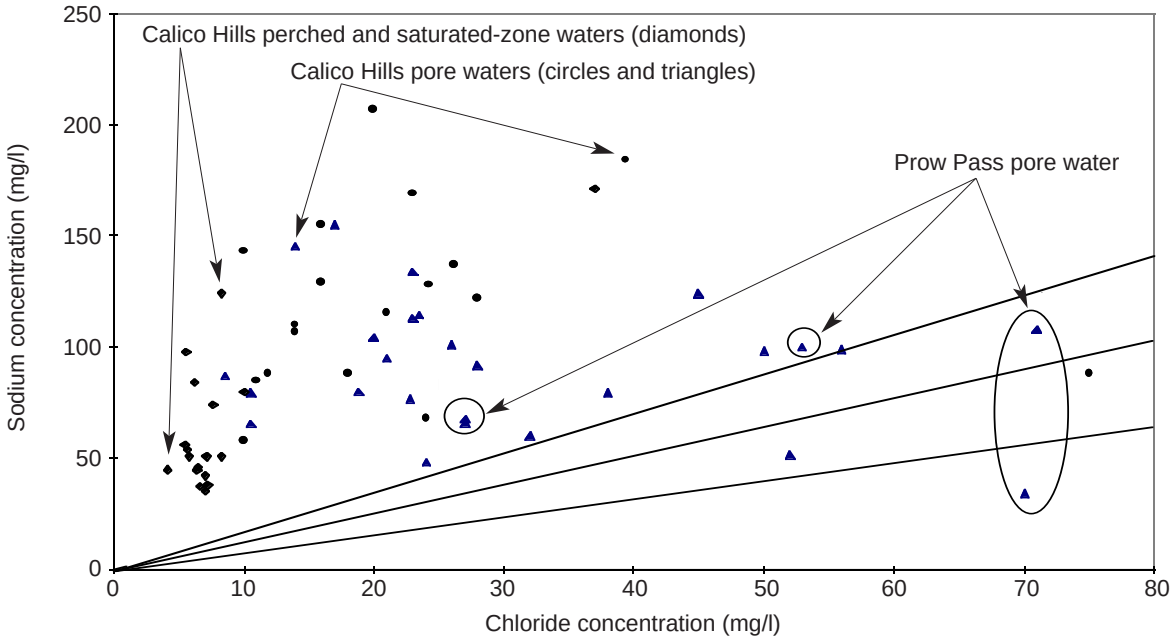

Figure 18. Calico Hills Sodium. This plot shows sodium versus chloride concentrations in Tuff of Calico Hills pore waters, perched waters, and saturated-zone groundwaters. The straight lines are the regression fit and one-sigma deviations for sodium-versus-chloride precipitation data. (Drill-hole designations: circles: UZ-14; triangles: UZ-16; diamonds: saturated-zone waters.)

Whether or not these estimates are representative of waters in Tuff of Calico Hills in other parts of Yucca Mountain cannot be established without additional sampling and detailed flow modeling. The fact that Calico Hills pore waters from depths as much as 100 m above the water table show evidence of hydrolysis reactions does suggest that perched waters are likely the dilute component.

Establishing bounds on the present and future compositions of perched waters and saturated-zone waters requires bounding the impact of the ion-exchange and hydrolysis reactions. Because zeolites in Yucca Mountain have relatively large selectivity coefficients for calcium and magnesium (Pabalan 1994; Viani and Bruto 1992), waters that percolate through the zeolitized Tuff of Calico Hills will lose nearly all their calcium and magnesium before they reach the water table. This loss is evident in pore-water samples obtained from the lower part of Tuff of Calico Hills in drill holes UZ-14 and UZ-16 (Figs. 19 and 20).

As noted above, hydrolysis reactions that involve feldspar are limited by reaction affinity. That is, as the solution reaches saturation with a particular feldspar, the affinity for further reaction is progressively reduced until the solution is saturated with the feldspar, at which point the affinity for dissolution is zero. Therefore, the composition of waters in the devitrified units (such as the potential repository horizon) will be primarily constrained by saturation with feldspar and α-cristobalite. Pore waters percolating into the devitrified zones from nonwelded units will already be supersaturated with feldspar and α-cristobalite as a result of glass dissolution reactions. Therefore, little additional dissolution is anticipated in the devitrified zones over-

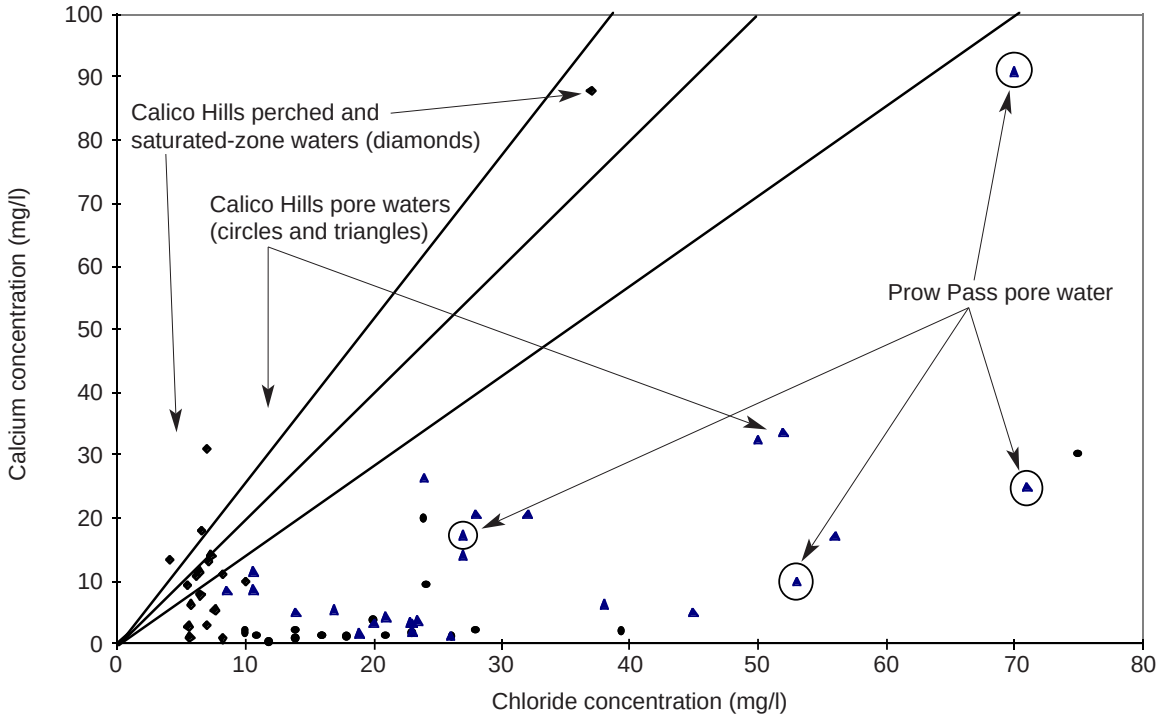

Figure 19. Calico Hills Calcium. The plot shows calcium versus chloride concentrations in Calico Hills pore waters, perched waters, and saturated-zone groundwaters. The straight lines are the regression fit and one-sigma deviations for calcium-versus-chloride precipitation data. (Drill-hole designations: circles: UZ-14; triangles: UZ-16; diamonds: saturated-zone waters.)

lain by nonwelded tuffs. In fact, soluble silica in pore waters from the nonwelded units may be crystallized onto existing α-cristobalite grains in the upper portion of the devitrified units, leading to reductions in porosity.

For vitric units, the situation is less straightforward because volcanic glasses cannot achieve thermodynamic equilibrium with an aqueous solution at ambient temperatures and pressures. That is, all volcanic glass would crystallize if it were not for the slow kinetics of nucleation and crystallization of the secondary phases that can form at ambient temperatures and pressures. Although the recrystallization of volcanic glass may be kinetically inhibited, glasses do dissolve at appreciable rates at ambient temperature and pressure when the dissolving waters are far from equilibrium with potential secondary phases. Many studies have been carried out in recent years to gain an understanding of glass-alteration behavior, mainly to provide a basis for predictions of the alteration behavior of nuclear waste glasses. An important result of these short-term experimental studies is the finding that the glass dissolution rate is quite sensitive to the silica concentration in solution. As the silica concentration in solution approaches saturation with amorphous silica, the dissolution reaction slows down dramatically (Grambow 1992). Apparently, in order for glass alteration to proceed, the "gel reaction zone" that forms on the glass surface needs to dissolve. If the solution phase is near saturation with amorphous silica, the dissolution of this material is inhibited, presumably because the affinity of the dissolution reaction is low.

High silica activities in solution cannot be maintained very long (days to months) in the presence

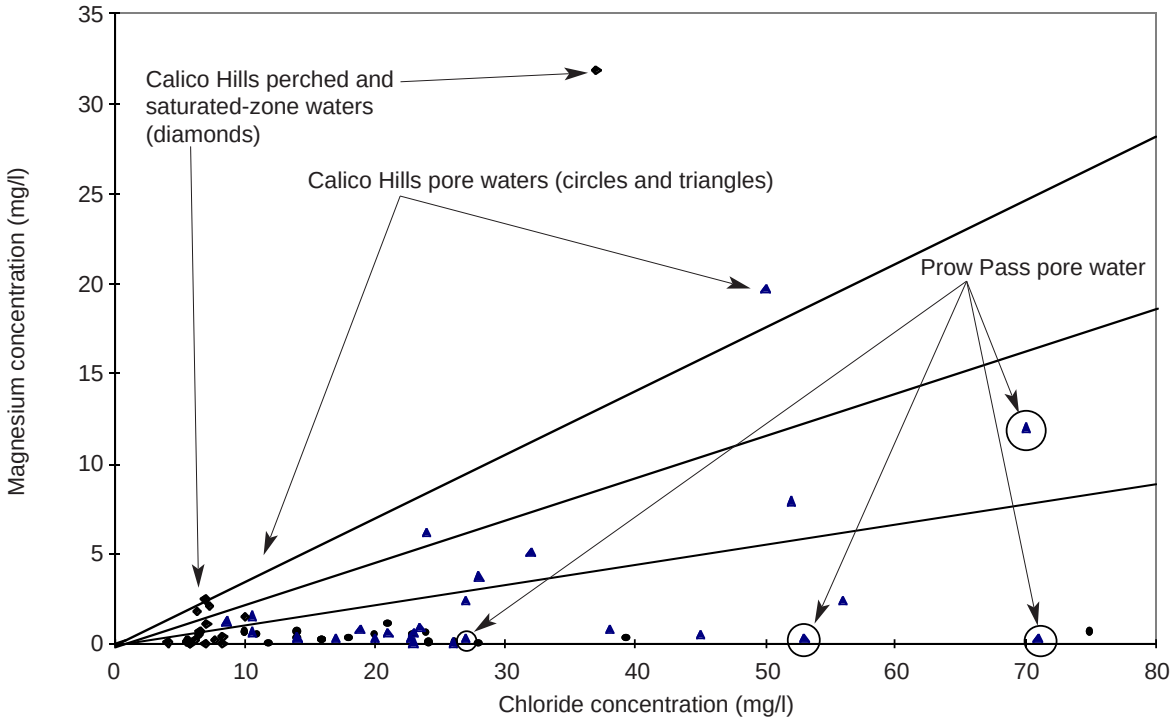

Figure 20. Calico Hills Magnesium. The plot shows magnesium versus chloride concentrations in Calico Hills pore waters, perched waters, and saturated-zone groundwaters. The straight lines are the regression fit and one-sigma deviations for magnesium-versus-chloride precipitation data. (Drill-hole designations: circles: UZ-14; triangles: UZ-16; diamonds: saturated-zone waters.)

of seed crystals of α-cristobalite and quartz (Rimstidt and Barnes 1980). This fact implies that Yucca Mountain waters with high silica activities lack sufficient surface areas of α-cristobalite or quartz seed crystals, in the units from which these waters were obtained, to control silica activities. This situation appears to be the case in nonwelded units within Yucca Mountain (Bish and Chipera 1989). The lack of adequate seed-crystal surface area most likely reflects the slow nucleation kinetics of these minerals at ambient temperature and pressure conditions (Nielsen 1964).

An important point is that most Yucca Mountain waters do not appear to be saturated with amorphous silica at ambient temperatures (Fig. 14). This observation suggests amorphous silica could not nucleate spontaneously, even in waters that contact volcanic glass. Interestingly, this does not mean that amorphous silica is not present in glassy samples. Iler (1973) has shown that the adsorption of ions such as Al^{3+} and Mg^{2+} onto the surface of amorphous silica greatly reduces the "equilibrium" solubility of this phase. Thus, amorphous silica could be a metastable phase in the vitric units, even though the silica concentrations measured in the waters of these units are below saturation levels with regard to amorphous silica. If adsorption of aluminum onto amorphous silica can lower the silica activity in solution, perhaps hydration and hydrolysis of (amorphous) silicic volcanic glass may produce the same result. The volcanic glass in the tuffs is initially 75 to 80 weight per cent SiO_2 and 12 to 13 weight per cent Al_2O_3 (Broxton et al. 1986). After hydration and hydrolysis ($Na^+ \leftrightarrow H^+$), the glass composition and structure likely approximate those of amorphous silica combined with some alumina and minor amounts of cations.

Whether or not such amorphous aluminosilicate material could maintain (metastable) equilibrium with an aqueous solution over time in the same manner that amorphous silica can is uncertain. The fact that volcanic glass remains abundant in many of the vitric units of Yucca Mountain (Bish et al. 1996b) after 11 to 13 million years in a hydrous environment suggests that it can. However, this conclusion must be tempered by the observation that clay minerals are found in many, if not most, of these vitric units. The problem is that these clay minerals could have formed almost anytime in the 11- to-13-million-year interval since these units were deposited. Further, because the distribution of clays is not homogeneous in any given vitric unit, their origin must involve more than simply in-situ alteration in a hydrous environment; otherwise, all glasses in a given unit would show similar evidence of alteration. Open-system alteration may be a determinant of whether or not clays are formed (Gislason and Eugster 1987). For example, clays may be preferentially formed along pathways with higher than average water fluxes (Levy 1984). To model the long-term alteration behavior of silicic volcanic glass, particularly as a function of temperature, data on the kinetics of conversion of the glass to an amorphous aluminosilicate or clay would be required. Such data are unavailable at the present time.

However, data are available on the dissolution rates of silicic volcanic glasses. White et al. (1980) have presented rate constants for the dissolution of vitric silicic tuffs in distilled water at various pH values. The dissolution rate constants for individual elements indicate that the dissolution reactions are incongruent; that is, the dissolution rates of the individual elements were not directly a function of the concentration of the elements in the original glass. This fact suggests that an alteration layer was formed on the glass surface, which was enriched in silica, alumina, and potash relative to the original glass. This layer would presumably control the chemistry of waters in contact with it. It could be an amorphous aluminosilicate or an incipient clay. An important question is what would happen to this layer if temperatures were raised in the glassy units.

Knauss and Peifer (1986) reacted volcanic glass with J-13 water at 90ºC for more than 2 months and found that no secondary minerals were produced and only minor etching was observed. This result suggests

the rate at which the water reacts with glass is very slow, even at somewhat elevated temperatures. Unfortunately, without additional data on the nucleation and crystallization kinetics of the glass surface layer produced during alteration, reliable predictions of glass alteration behavior and the effect of glass alteration on water chemistry cannot be derived.

Hydrolysis reactions can have significant impacts on the pH of waters. The pH of waters in contact with the gas phase in pores in the unsaturated zone in Yucca Mountain will be buffered in the range from 6.8 to 8.0 depending on the actual partial pressure of carbon dioxide. The pH of groundwaters that become isolated from the carbon-dioxide reservoir in the unsaturated zone may increase as hydrolysis reactions consume hydrogen ions. The extent of such increases will be limited if the partial pressure of carbon dioxide in the saturated zone is buffered by some reservoir (for example, diffusion of gas from Paleozoic units). In any case, the potential increases in pH will be limited to values around 10, at which point silicic acid starts to dissociate, buffering the pH.

The oxidation-reduction potential, or Eh, of waters in contact with the unsaturated-zone gas phase will be oxidizing because this gas phase contains the same concentration of oxygen as the atmosphere (Yang et al. 1996). The range of Eh values to be expected in waters in the saturated zone is difficult to define because the identity of the dominant oxidation-reduction reaction is unknown at the present time. It could be reducing or oxidizing depending on the degree to which the waters have access to atmospheric oxygen or to reducing agents (for example, methane). The measurements reported by Ogard and Kerrisk (1984) suggest that reducing conditions exist at depth in some wells in the Yucca Mountain area. Why conditions are reducing in these wells is uncertain. Perhaps the wells access a volume of rock that is isolated from contact with the atmosphere and that contains sulfides or reduced organic compounds. Further measurements are required to develop a more complete understanding of oxidation-reduction potentials in the saturated zone at Yucca Mountain.

In the absence of adequate glass-alteration models, some estimates of upper bounds on the concentrations of cations and bicarbonate species in perched waters, saturated-zone groundwaters, and Calico Hills pore waters can also be derived on the basis of data currently available for analyzed waters from aquifers in a variety of volcanic rock types at the the Nevada Test Site (Ogard and Kerrisk 1984; Yang et al. 1988, 1996; McKinley et al. 1991). On the basis of the compilation by McKinley et al., the concentrations of major cationic constituents and bicarbonate in groundwater from Well UE-25 p#1 are at the high end of the range of concentrations reported for all waters (60 in all) sampled from volcanic units at the Nevada Test Site. In terms of the other anions, water from Well UE-25 p#1 is also at the high end of the range of chloride and fluoride concentrations. Sulfate, nitrate, and silica are exceptions. Sulfate is higher (449 mg/l) than UE-25 p#1 water only in Well J-11 in Jackass Flats. The elevated sulfate in this well may reflect the oxidation of sulfide minerals in the Wahmonie area to the east of the well. Nitrate is higher (up to 12 mg/l) in a number of wells, and silica is higher (up to 81 mg/l) in various wells. Well J-13 has nitrate and silica concentrations at the high end of the range of Nevada Test Site waters. In general, waters from Wells J-13 and UE-25 p#1 bound the range in concentrations of most of the major constituents found in waters from volcanic units over the entire Nevada Test Site.

Importantly, the Eh and pH of J-13 and UE-25 p#1 waters do not bound the ranges for these parameters observed in waters from the Nevada Test Site. Both waters have a relatively oxidizing Eh (360–450 mV) and a low pH (6.7–7.2). The pH values observed in Nevada Test Site waters from volcanic units range from 6.7 to 9.0 (McKinley et al. 1991). The range of Eh values in these waters is unknown as values for this parameter were not reported by McKinley et al. (1991). Ogard and Kerrisk (1984) report a range of –143 to +402 mV for groundwaters from the Yucca Mountain area.

C. SUMMARY AND CONCLUSIONS

The available data on the chemistry of pore waters, perched waters, and saturated-zone groundwaters at Yucca Mountain suggest there are essentially two types of waters at Yucca Mountain. Type-1 waters are found as pore water above Tuff of Calico Hills and from portions of Prow Pass member. Type-2 waters are found as perched water and saturated-zone groundwaters. The pore waters in Tuff of Calico Hills appear to be mixtures of these two water types.

Type-1 Waters

The chemistry of type-1 waters (mainly pore waters above Tuff of Calico Hills) will be controlled primarily by soil-zone processes, including evapotranspiration and the precipitation/dissolution of pedogenic minerals such as calcite, gypsum, and amorphous silica. The primary constraints on these processes are largely nonchemical and include evapotranspiration and the detailed soil-zone hydrology. These waters are generally saturated with opal-CT and do not appear to be influenced by hydrolysis reactions involving aluminosilicates.

Evapotranspiration is important in concentrating solutes in the soil zone that were originally in precipitation as wet-fall and dry-fall. Soil-zone hydrology controls the ionic strength and the chemical composition of waters infiltrating the unsaturated zone. Both the ionic-strength control and the compositional control reflect the flux and residence time of infiltrating waters in the soil zone prior to percolation into the unsaturated zone. The soil hydrology also impacts the water compositions through the crystallization sequence in which small pores are filled with early-formed phases, whereas the later-crystallizing phases preferentially form in the space available in the larger pores.

Because our understanding of soil-zone hydrology at Yucca Mountain is not fully developed, the impact of hydrology on the composition of unsaturated-zone pore waters can best be bounded by analyses of unsaturated-zone pore waters. Fortunately, there is a trade-off between ionic strength and water volume. That is, the higher the ionic strength of the water (for example, more corrosive), the less of it there will be.

The pH and Eh of type-1 unsaturated-zone pore waters will be regulated by the composition of the gas phase in the pores. The Eh will be oxidizing (400–600 mV) because this gas phase has an oxygen partial pressure equal to that observed in the atmosphere (Thorstenson et al. 1989; Yang et al. 1996). The pH should remain in the range of 7 to 8 supported by carbon-dioxide partial pressures that are greater than atmospheric.

Type-2 Waters

The compositions of type-2 waters (perched and saturated-zone waters) are dominated by hydrolysis reactions. These reactions involve the exchange of cations (dominantly sodium) with hydrogen ions on the surfaces of aluminosilicate phases in the rocks (such as feldspar and volcanic glass). Hydrogen ions are supplied by the dissociation of carbonic acid. Therefore, the partial pressure of carbon dioxide is a critical parameter that controls hydrolysis reactions. It also has a major influence on the pH of the waters.

As we stated for type-1 waters, in systems open to the unsaturated-zone gas phase, the pH of the water will remain in the range of 7 to 8. Systems that become closed for some reason may have lower or higher pH values, depending on whether or not there are additional sources of carbon dioxide in the system. The upper bound on pH is approximately 10, the value at which silicic acid dissociation buffers the pH.

The Eh of type-2 water ranges from oxidizing to reducing, depending on whether the waters have access to atmospheric oxygen or to reducing agents, respectively.

Prediction of the future compositional variations in type-2 perched and saturated-zone groundwaters requires that the hydrolysis reactions be modeled. Such modeling requires knowledge of the secondary phases involved in the reactions.

For devitrified tuffs, these phases are likely dominated by alkali feldspar and α-cristobalite. Therefore, the future variations in the composition of waters in devitrified tuffs can be modeled by assuming saturation with alkali feldspar and α-cristobalite. The main unknowns in such modeling would be the pH and Eh of the system. The carbon-dioxide partial pressure must be known to calculate pH. Field measurements are required to constrain the Eh.

For glassy units, the modeling is more difficult because the identity of the secondary phases are not known with certainty. More importantly, the rates at which these phases form are unknown. There is information available on the rate of dissolution of silicic glasses. This information allows one to derive the initial chemistry of waters in vitric units, but it does not provide a basis for predictions of the long-term variations in water chemistry.

A Survey Approach

As a surrogate for the modeling approach, a survey of water chemistries in silicic volcanic rocks can be used to estimate bounds on the future variations of water chemistry in Yucca Mountain. A survey of water compositions from volcanic units indicates that waters from Wells J-13 and UE-25 p#1 have compositions that bound the observed range of variability for most major constituents. The main exceptions are pH, Eh, and chloride concentrations. Laboratory experiments designed to derive transport parameters, such as sorption coefficients and solubilities, have used these two water compositions and a range of pH values.

The variability in chloride concentrations is not a serious issue for the derivation of these parameters because chloride is not a strong complexing agent for most radionuclides of interest. However, chloride concentrations in unsaturated-zone waters are important to the longevity of the waste package, as high chloride concentrations enhance corrosion rates.

Measurements of Eh in the saturated zone beneath Yucca Mountain suggest that reducing conditions exist locally. If redox conditions are generally reducing at depth in the saturated zone, the migration potential of radionuclides of elements such as neptunium and technetium would be greatly diminished. Additional field measurements at the site are required to test the variability in Eh and the redox state of saturated-zone groundwaters.

III. RADIONUCLIDE SOLUBILITY STUDIES

A. SPECIFIC-ION INTERACTION THEORY STUDIES

Introduction

The principle transport mechanism for migration of radioactive transuranic elements away from a potential nuclear waste repository is expected to be by action of water, and therefore, the chemistry of transuranic elements under natural aquatic conditions has received considerable attention in the Yucca Mountain Site Characterization Project. To understand the chemical behavior of transuranic elements in natural aquatic systems, one must consider a wide variety of complex geochemical processes such as sorption (Allard et al. 1983; Combes et al. 1992; Hirose and Tanoue 1994; Meece and Benninger 1993; Sanchez et al. 1985), precipitation/dissolution and redox equilibria (Meece & Benninger 1993), solubility (Nitsche 1987; Nitsche 1991a; Nitsche 1991b; Nitsche 1992; Nitsche and Edelstein 1985; Nitsche et al. 1992b), radiolysis (Giffaut and Vitorge 1993), hydrolysis (Baes and Mesmer 1976; Fuger 1992), colloid generation (Hobart et al. 1989; Kim et al. 1989; Moulin et al. 1992; Newton et al. 1986; Ramsay 1988; Rundberg et al. 1988; Thiyagarajan et al. 1990; Triay et al. 1991a), and the effects of other metal ions and other potential ligands on actinide speciation (Clark et al. 1995; Dozol and Hagemann 1993; Hobart 1990; Kim 1993). The highest potential chelators for actinide ions in groundwaters measured from Yucca Mountain sites are hydroxide and carbonate. Therefore, the thermodynamic formation constants for hydroxo, carbonato, and mixed hydroxo-carbonato complexes must be assessed for use by the Yucca Mountain Site Characterization Project (YMP). In this chapter, we document efforts to determine the technical correctness of thermodynamic data as applied to Tier-I radionuclides as defined by the YMP Solubility Working Group and which include thorium, uranium, neptunium, plutonium, and americium.

Of the fourteen 5-*f* elements following actinium in the periodic table, thorium, protactinium, uranium, and trace amounts of plutonium occur naturally (Seaborg and Loveland 1990). Based on nuclear properties, availability, and distribution, only six of the fourteen actinide elements (thorium, uranium, neptunium, plutonium, americium, and curium) are of potential long-term environmental concern (Hobart 1990). For the Yucca Mountain Site Characterization Project, only the first five are considered. The known oxidation states of these elements are listed in Table 9 (Hobart 1990) with the most stable oxidation state in aqueous solution listed in boldface and with environmentally important oxidation states underlined. The variety of accessible oxidation states for these actinides in aqueous solutions makes this chemistry rather complex. Furthermore, multiple oxidation states of the same element may exist simultaneously; plutonium, for example, may exist, under particular solution conditions, in five oxidation states: Pu(III), Pu(IV), Pu(V), Pu(VI), and Pu(VII) (Katz et al. 1986). A number of the known oxidation states exist only under unusual conditions, such as extreme redox potentials, radiolysis, elevated temperatures, and so forth.

To gain an understanding of the complex geochemical behavior of these materials, we must begin with a fundamental knowledge of actinide

Table 9. Oxidation States of Actinide Tier-I Elements*

Th	U	Np	Pu	Am
				II
III	III	III	III	**III**
IV	IV	IV	**IV**	IV
	V	**V**	V	V
	VI	VI	VI	VI
		VII	VII	

*The most prevalent oxidation states are in boldface; environmentally important states are underlined.

carbonate chemistry. Here we present a critical overview of aqueous processes basic to understanding actinide carbonate chemistry, and some associated aspects of actinide chemistry such as hydrolysis and complexation equilibria. Comparisons between the work of different laboratories throughout the world are therefore required. To accomplish this comparison objectively, several criteria can be employed. The first involves a careful examination of experimental sections in published reports and literature sources to determine whether the method was sound and carried out carefully. A second method involves comparison to other actinide formation constants with the same oxidation state. This oxidation-state analogy is merely a guide; differences certainly exist between actinides of the same oxidation state, but they do show family resemblances. Finally, the use of specific-ion interaction theory (SIT) allows for the detection of stray data points as well as standard-state values of thermodynamic formation constants. At least three points are required to use a linear fit as any kind of test for an outlying data point, and the availability of at least three data points was taken as our threshold for doing the SIT analysis for each particular system. In practice, however, we found that in most cases in which only three data points were available, estimates based on known data for neighboring elements proved more reliable.

The need for accurate thermodynamic data has prompted the Organization for Economic Cooperation and Development, Nuclear Energy Agency (OECD NEA) to initiate a series of detailed expert reviews of the chemical thermodynamics of key elements in nuclear technology and waste management. The first two volumes on the chemical thermodynamics of uranium (Grenthe et al. 1992) and americium (Silva et al. 1995) have been published, and both rely heavily on the SIT approach. We include here an up-to-date review of thermodynamic data for Tier-I radionuclides, more detailed fits of SIT data that can be compared with all the relevant literature, and recommendations for neptunium and plutonium formation constants for cases in which the NEA reviews are not yet available.

Complexation equilibria

Complexation is a dominant factor influencing actinide speciation in natural waters. By altering the charge and composition of actinide ions in solution, complexation may significantly increase actinide solubility and largely affect actinide sorption. The complexation strength is a measure of how effectively a ligand can compete with water in the coordination sphere of an actinide ion. Actinide ions are “hard” acids and, consequently, form strong complexes with highly ionic “hard” ligands such as carbonate and hydroxide (Katz et al. 1986). The relative tendency of actinides to form complexes generally follows the trend: $An(IV) > An(III) \approx AnO_2^{2+} > AnO_2^{+}$ (Katz et al. 1986).

Complexation equilibria can be expressed in a variety of ways. When referencing equilibrium constants, it is very important to refer to the primary literature to find out how the original authors defined their equilibrium constants. Because measurement of the activities of complex ions is not possible for many systems, most equilibrium constants are determined in terms of concentrations. In this review, we will refer to equilibrium constants (K) defined for specific reactions as written, and formation constants (β or $^*\beta$). There are two widely used formalisms applied to the notation of formation constants, and these formalisms need further elaboration. The functional form of the formation constant $^*\beta_{mqn}$ for any compound $M_mL_q(OH)_n$ can be written in the following general form (charges left out for clarity):

$$m\,M + q\,L + n\,H_2O(l) \leftrightarrow M_mL_q(OH)_n + n\,H$$

$$^*\beta_{mqn} = \frac{(M_mL_q(OH)_n)(H)^n}{(M)^m(L)^q\,a_w} \quad , \qquad (3)$$

where parentheses signify activity and a_w is the activity of water.

Alternatively, the formation constant β_{mqn} for any

compound may be written in a slightly different form:

$$mM + qL + nH \leftrightarrow M_mL_qH_n$$
$$\beta_{mqn} = \frac{(M_mL_qH_n)}{(M)^m(L)^q(H)^n} \quad . \qquad (4)$$

The main difference between the notation $*\beta$ and β is in the treatment of the hydrolysis of water. Because both expressions are commonly encountered in the current literature, care must be exercised when formation constants are quoted, and it is desirable to write out the chemical reaction that accompanies the formation constant.

Equilibria involving ionic species are affected by the presence of all ions in solution, which taken together make up the ionic strength. Thermodynamic data are generally referenced to a standard state, and for solution measurements, the standard state of 25°C and zero ionic strength is generally used (Grenthe et al. 1992). Log formation constants ($\log\beta$) can be extrapolated to zero ionic strength using an extended Debye-Hückel approach known as the specific-ion interaction theory (SIT). For more detailed information regarding ionic-strength corrections, the reader is referred to Appendix B of the recent review on the chemical thermodynamics of uranium and the references therein (Grenthe et al. 1992). A limited background discussion of SIT necessary for our data treatment is given in the following section.

Specific-ion interaction theory

An important variable in assessing equilibrium constants is the ionic strength I, where $I_M = 1/2\sum M_i z_i^2$ or $I_m = 1/2\sum m_i z_i^2$ and M_i is the concentration in molarity for species i, m_i is the concentration in molality for species i, and z_i is the charge on species i. The variation of a thermodynamic equilibrium constant with ionic strength forms the basis of all the different approaches toward making ionic-strength corrections. Specific-ion interaction theory is an extended Debye-Hückel method for extrapolating equilibrium-constant data to standard-state condition (zero ionic strength and all activity coefficients $\gamma = 1$). Several steps are involved, as outlined below.

The first step in the analysis of the literature data was to change the ionic strength from the volumetric molar units (M; moles solute/liter solution) to the gravimetric molal units (m; moles solute/kg solvent). Many of the literature data on thermodynamic formation constants were collected in noncomplexing $NaClO_4$ electrolyte solutions, and we shall restrict most of our discussion to the perchlorate medium. From the work of Baes and Mesmer (1976), the ratios $R = I_m/I_M$ have been tabulated for $NaClO_4$ solutions. Because the Baes and Mesmer data are not listed for 5.0 m $NaClO_4$ solutions (Table 10), a plot of the I_m versus I_M data for $NaClO_4$ solutions has been fit to a second-order polynomial to derive a simple conversion formula for evaluating the ratio R for general cases (Fig. 21). Note that such a fit is not exact, as $I_M = I_m$ and

Table 10. Useful Conversion Data for $NaClO_4$ Solutions*

Ionic strength			Debye-Huckel term	
Molar I_M	Molal I_m	$\log R = \log I_m/I_M$	D	$\log a_w$
0.03	0.03	0.00	0.0750	0.000
0.05	0.05	0.00	0.0884	0.000
0.1	0.10	0.003	0.1092	−0.001
0.2	0.20	0.005	0.1363	−0.003
0.3	0.30	0.007	0.1535	−0.004
0.4	0.41	0.009	0.1657	−0.006
0.5	0.51	0.011	0.1755	−0.007
0.7	0.72	0.017	0.1899	−0.010
1.0	1.05	0.021	0.2056	−0.015
1.5	1.61	0.032	0.2225	−0.022
2.0	2.21	0.043	0.2343	−0.034
3.0	3.50	0.066	0.2502	−0.060
4.0	4.95	0.092	0.2612	−0.093

*Data from Baes and Mesmer (1976) and Grenthe et al. (1992).

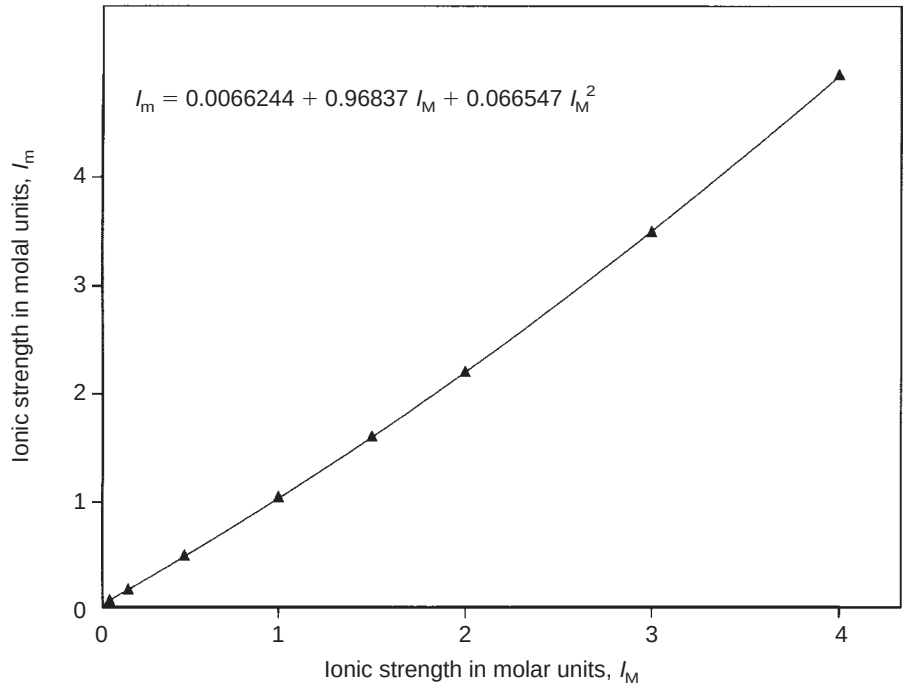

Figure 21. Ionic Strength Molar to Molal Conversion. Using the data of Baes and Mesmer (1976, p. 439) given in Table 10, a plot of I_m versus I_M can be fit to a second-order polynomial and the resulting equation used to calculate values of log$R$ outside the range of the original data.

$R = 1.000$ at zero ionic strength, whereas the fit shows $I_m = 0.0066$ and $R = 1.002$ at $I_M = 0.0$.

Once I_M was determined for general cases in $NaClO_4$ solution, the log*β values from literature sources must be converted from molar to molal units as described in the NEA database for uranium (Grenthe et al. 1992, equation II.27, p. 23):

$$\log^*\beta_m = \log^*\beta_M + \sum\nu \log R \ , \qquad (5)$$

where $\sum\nu$ is the sum of the stoichiometric coefficients of the reaction ($\sum_{products} a_p - \sum_{reactants} a_r$) and a_r and a_p are the stoichiometric coefficients of the reactants and products. The values of R for the calculation of log$R$ are taken from Baes and Mesmer (1976).

For the Debye-Hückel term D, the suggested values from Appendix B (p. 683) of the uranium NEA database (Grenthe et al. 1992) were used, and D at 25ºC is given by

$$D = \frac{0.5091\ (I_m)^{0.5}}{1 + 1.5(I_m)^{0.5}} \ . \qquad (6)$$

The overall SIT equation for the general chemical formula:

$$m\ M + q\ L + n\ H_2O(l) \leftrightarrow M_mL_q(OH)_n + n\ H \qquad (7)$$

is given by

$$\log^*\beta = \log^*\beta^0 + \Delta z^2 D - \Delta\epsilon I_m + n \log a_w \ , \qquad (8)$$

where log*β represents the measured equilibrium constant at ionic strength I_m, log*β^0 is the standard-state thermodynamic equilibrium constant at zero ionic strength, $\Delta\epsilon$ is the change in ionic interaction constants in the reaction, Δz^2 is the change in the squares of the charge for the reaction (products – reactants), which can be calculated using

$$\Delta z^2 = \{(m\ z_M - q\ z_L - n)^2 + n\} - \{m\ z_M{}^2 + q\ z_L{}^2\} \ , \qquad (9)$$

where z_x is the charge of species x (and we used the

facts that H_2O is neutral, OH has a charge of -1, and H has a charge of $+1$). The activity of water in an electrolyte mixture can be calculated from

$$\log a_w = \frac{-\Phi \sum m_k}{55.51 \ln(10)} , \qquad (10)$$

where Φ is the osmotic coefficient for the solution and $\sum m_k$ is the sum of the molalities of the charged species. For this report, we used tabulated values of $\log a_w$ found in Robinson and Stokes (1955). Because $NaClO_4$ electrolyte is not listed, values for NaCl electrolyte are used. Note that a_w is almost always equal to one, so $\log a_w$ tends toward zero and the difference in electrolyte values is negligible. Furthermore, unless hydrolysis is involved, $n = 0$, and the water activity term in Eqn. 8 is exactly 0.

It has been noted by Neck et al. (1994) and others that simple SIT isn't strictly valid for $I_M > 3.5$ M. To account for this weakness in SIT, Ciavatta has proposed the use of a nonconstant $\Delta\epsilon$ (Ciavatta et al. 1979, 1981). Specifically, the following formula was proposed:

$$\Delta\epsilon = \Delta\epsilon_1 + \Delta\epsilon_2 \log I_m . \qquad (11)$$

This approach is examined and plotted in some figures in the section on neptunium, where data at very high ionic strength have been determined. When the extended SIT formalism is used in the neptunium studies, none of the data points are more than 0.4 log units from the SIT fit.

Hydrolysis

Hydrolysis leads to the formation of ionic species or precipitates by the action of water as illustrated (in $\log^*\beta$ form) for a tetravalent actinide ion (Baes and Mesmer 1976; Fuger 1992). Although hydrolysis reactions are often written as

$$An^{4+} + H_2O \leftrightarrow An(OH)^{3+} + H^+ , \qquad (12)$$

for comparison of equilibrium constants of the majority of ligands, it is convenient to express hydrolysis as a complex formation, consistent with the $\log\beta$ notation, described by the following equation:

$$An^{4+} + OH^- \leftrightarrow An(OH)^{3+} . \qquad (13)$$

The formation constants for these two reactions will differ by a factor of $\log K_w$, and thus, it is extremely important to always explicitly show which reaction one is referring to when discussing hydrolysis reactions.

Actinide hydrolysis yields soluble hydroxide or oxide complexes, as well as precipitates of hydroxides, oxides, or basic salts. In fact, the formation of the dioxo "yl" moiety for the $+5$ and $+6$ actinide metals is a manifestation of strong hydrolysis caused by the electric field of these metals in aqueous solutions. Hydrolysis reactions are significant for all of the actinide ions at pH values found in natural waters, with the exception of further hydrolysis of pentavalent ions. The actinide(IV) ions have high charge-to-radius ratios and form hydrolysis products even in acidic solutions as low as a pH of 0 (Katz et al. 1986). Pentavalent actinyl ions, AnO_2^+, do not further hydrolyze until a pH of 9, and the trivalent ions, An^{3+}, and hexavalent actinyl ions, AnO_2^{2+}, do not hydrolyze appreciably below a pH of 4 at room temperature. For a recent summary of actinide hydrolysis constants the reader is referred to Fuger (1992) who notes that "the study of the hydrolysis of highly charged ions poses probably one of the most formidable challenges to the solution chemist due to the multiplicity of species that may form simultaneously and which also are a function of the other ions present in the solution."

The carbonate-bicarbonate ligand system

The aqueous carbonate system is important in the environment because of the high abundance of carbon dioxide and carbonate-containing minerals, such as calcite ($CaCO_3$) and dolomite ($CaMg(CO_3)_2$) (which are estimated to contain more than 80% of the carbon on earth) (Stumm and Morgan 1981). The fundamental equilibrium reactions of the aqueous carbonate system and their equilibrium constants at 25ºC and zero ionic strength are given by (Palmer and Van Eldik 1983; Perrin 1982):

$$CO_2(g) \leftrightarrow CO_2(aq) \quad \log K^0_H = -1.47 \tag{14}$$

$$CO_2(aq) + H_2O \leftrightarrow H_2CO_3 \quad \log K_{eq} = -2.70 \tag{15}$$

$$H_2CO_3 \leftrightarrow H^+ + HCO_3^- \quad \log K^0_1 = -6.35 \tag{16}$$

$$HCO_3^- \leftrightarrow H^+ + CO_3^{2-} \quad \log K^0_2 = -10.33 \tag{17}$$

$$CO_2(g) + H_2O \leftrightarrow 2\,H^+ + CO_3^{2-} \quad \log K^0 = -18.15 \tag{18}$$

$$CO_2(g) + H_2O \leftrightarrow H^+ + HCO_3^- \quad \log K^0 = -7.82 \tag{19}$$

Dissolution of carbon-dioxide gas in water will result in some hydrolyses to form carbonic acid, H_2CO_3, as indicated in Eqns. 14 and 15. The carbonic-acid equilibrium shown in Eqn. 15 lies far to the left, as indicated by the magnitude of $\log K_{eq}$.

Experimentally, it can be extremely difficult to distinguish between CO_2(aq) and H_2CO_3, and hence, it is a common practice to define carbonic acid as the sum of H_2CO_3 and CO_2(aq) and to use CO_2(aq) to symbolize the sum. In closed aqueous-carbonate systems, such as the depths of the oceans and deep groundwaters, the exchange of CO_2 with the surrounding environment is very slow, so the total carbonate concentration can be expressed as $(CO_2(aq)) + (HCO_3^-) + (CO_3^{2-})$. In an open system in which the carbonate solution is in contact with the atmosphere, the total carbonate concentration will vary with the amount of atmospheric CO_2 that dissolves into solution. With a constant CO_2 pressure (P_{CO_2}), the equilibrium in Eqn. 14 is maintained (Henry's Law), where K_H is the Henry's Law constant. Thus, the concentrations of HCO_3^- and CO_3^{2-} in natural waters depend on the ambient P_{CO_2} to which the solutions are exposed. In studying carbonate systems, it is necessary to control the carbon source and the partial pressure of CO_2(g). Hence, equations expressed in terms of gaseous CO_2 are more useful. We obtain such equations, with the relevant equilibrium constants at 25ºC and zero ionic strength, by rearranging the equations given above to yield:

An additional complication of the carbonate-ligand system is that hydroxide ion is also present, and there are always three possible ligands available in carbonate solutions: OH^-, HCO_3^-, and CO_3^{2-}. None of these individual ligand concentrations can be varied independently. Because hydrolysis and carbonate equilibria are intimately connected, one cannot study carbonate complexation without a fundamental understanding of the metal-ion hydrolysis chemistry. Consideration of the above factors has lead some authors to formally consider the actinide-carbonate system as a three-component system of metal, hydroxide, and carbonate.

Actinide Complexes

Thorium

Thorium exists in solution as Th(IV) (see Table 9), and Th(IV) is the largest tetravalent actinide cation, with an ionic radius of 0.99Å (versus 0.93 and 0.90 Å for U(IV) and Pu(IV) respectively) (Shannon 1976).

Thorium hydrolysis.

Thorium(IV) is the tetravalent actinide ion most resistant to hydrolysis. Thorium(IV) hydrolysis has been studied by a number of researchers, and many of these studies indicated stepwise hydrolysis to yield monomeric products of formula $Th(OH)_n^{4-n}$ with $n = 1$, 2, 3, and 4, in addition to a number of polymeric species (Baes and Mesmer 1976; Brown et al. 1983; Bruno et al. 1987; Davydov and Toropov 1992; Engkvist and Albinsson 1992; Grenthe and Lagerman 1991b; Lieser and Hill 1992; Milic and Suranji 1982; Moon 1989; Ryan and Rai 1987). The recent emf study by Grenthe and Lagerman indicates that only two of these monomeric species, $Th(OH)^{3+}$ and $Th(OH)_4$ are of any real importance in dilute solutions ($\leq 10^{-3}$ M Th); the corresponding hydrolysis

constants are: $\log^*\beta_{11} = -4.35$ ($\pm$ 0.09) and $\log^*\beta_{14} = -16.65$ ($\pm$ 0.04) in 3.0 M $NaClO_4$ (Grenthe and Lagerman 1991b). However, in a recent ThO_2 solubility study in 0.5 M $NaClO_4$, the best fit to the experimental data required inclusion of the additional species, $Th(OH)_3^+$ with $\log^*\beta_{13} = -11.22$ (Östhols et al. 1994).

In more concentrated solutions ($\geq 10^{-3}$ M), polynuclear species have been shown to exist. For example the most recent model of Grenthe and Lagerman includes the dimers, $Th_2(OH)_2^{6+}$ and $Th_2(OH)_3^{5+}$, the tetramers, $Th_4(OH)_8^{8+}$ and $Th_4(OH)_{12}^{4+}$, and two hexamers, $Th_6(OH)_{14}^{10+}$ or $Th_6(OH)_{16}^{8+}$ (Grenthe and Lagerman 1991b). These polynuclear complexes are common in chloride and nitrate solutions (Baes and Mesmer 1976; Brown et al. 1983; Bruno et al. 1987; Davydov and Toropov 1992; Engkvist and Albinsson 1992; Grenthe and Lagerman 1991b; Lieser and Hill 1992; Milic and Suranji 1982; Moon 1989; Ryan and Rai 1987). It is noteworthy that these polynuclear hydrolysis products have only been well-defined for thorium and not for other tetravalent actinide ions. For more detailed information on the hydrolysis of Th(IV), the reader is referred to the works of Moon (1989), Lieser and Hill (1992), Engkvist and Albinsson (1992), Davydov and Toropov (1992), Milic and Suranji (1982), Brown et al. (1983), Bruno et al. (1987), Ryan and Rai (1987), Grenthe and Lagerman (1991b), and references therein.

Table 11 lists the major hydrolysis reactions and formation constants taken from the two most recent studies (Grenthe and Lagerman 1991b; Östhols et al. 1994). The most recent data by Östhols et al. and by Grenthe and Lagerman appear to be a result of the most complete and thorough study to date, and these values are recommended for use by the Yucca Mountain Project.

Thorium-carbonato complexes.

Whereas there is a great deal of qualitative information regarding anionic-carbonato complexes of the tetravalent actinides, reliable quantitative data are rare. The most recent solution studies for thorium have been reported by Bruno et al. (1987), Grenthe and Lagerman (1991b), Joâo et al. (1987), and Östhols et al. (1994). In the study by Östhols et al., the solubility of microcrystalline ThO_2 was examined as a function of pH and CO_2 partial pressure.

Table 11. Comparison of Thermodynamic Formation Constants for Th(IV)-hydroxo Complexes as a Function of Ionic Strength

Reaction	I_M	log$K$
$Th^{4+} + H_2O \leftrightarrow Th(OH)^{3+} + H^+$	3.0	–4.35 ($\pm$ 0.9)*
	0.5	–4.16†
$Th^{4+} + 3\ H_2O \leftrightarrow Th(OH)_3^+ + 3\ H^+$	3.0	–12.3 ($\pm$ 0.2)*
	0.5	–11.22†
$Th^{4+} + 4\ H_2O \leftrightarrow Th(OH)_4 + 4\ H^+$	3.0	–16.65 ($\pm$ 0.4)*
	0.5	–15.95†
$2\ Th^{4+} + 2\ H_2O \leftrightarrow Th_2(OH)_2^{6+} + 2\ H^+$	3.0	–5.10 ($\pm$ 0.17)*
	0.5	–6.71†
$2\ Th^{4+} + 3\ H_2O \leftrightarrow Th_2(OH)_3^{5+} + 3\ H^+$	3.0	–7.87 ($\pm$ 0.05)*
	0.5	–8.22†
$4\ Th^{4+} + 8\ H_2O \leftrightarrow Th_4(OH)_8^{8+} + 8\ H^+$	3.0	–19.6 ($\pm$ 0.2)*
$4\ Th^{4+} + 12\ H_2O \leftrightarrow Th_4(OH)_{12}^{4+} + 12\ H^+$	3.0	–38.86 ($\pm$ 0.05)*
$6\ Th^{4+} + 14\ H_2O \leftrightarrow Th_6(OH)_{14}^{10+} + 14\ H^+$	3.0	–33.67 ($\pm$ 0.05)*
$6\ Th^{4+} + 16\ H_2O \leftrightarrow Th_6(OH)_{16}^{8+} + 16\ H^+$	3.0	–42.90 ($\pm$ 0.4)*

*Grenthe and Lagerman (1991b) †Östhols et al. (1994).

The results were consistent with the presence of a thorium mixed hydroxo-carbonato complex of formula $Th(OH)_3(CO_3)^-$ and the pentacarbonato complex $Th(CO_3)_5^{6-}$, and formation constants were determined for both species (Östhols et al. 1994). The observation of a mixed hydroxo-carbonato complex of the readily hydrolyzable tetravalent cation is not unreasonable, because complexes of this type have been found for other ions (Bruno 1990). These formation constants are listed in Table 12.

Table 12. Comparison of Thermodynamic Formation Constants for Th(IV)-carbonato Complexes as a Function of Ionic Strength

Reaction	I_M	log$K$
$Th^{4+} + 5\ CO_3^{2-} \leftrightarrow Th(CO_3)_5^{6-}$	1.0	26.2 (± 0.2)†
	2.5	26.3 (± 0.2)†
	3.0	32.3*
$ThO_2(s) + 4\ H^+ + 5\ CO_3^{2-} \leftrightarrow Th(CO_3)_5^{6-} + 2\ H_2O$	3.0	39.64 (± 0.4)*
$ThO_2(s) + H^+ + H_2O + CO_3^{2-} \leftrightarrow Th(OH)_3(CO_3)^-$	3.0	6.78 (± 0.3)*

*Östhols et al. 1994 †Joâo et al. 1987

The limited data from Table 11 was used to perform a SIT analysis for the reaction:

$$Th^{4+} + 5\ CO_3^{2-} \leftrightarrow Th(CO_3)_5^{6-}$$
$$\Sigma\nu = -5 \qquad (20)$$
$$\Delta z^2 = 36 - (16 + 5 \times 4) = 0\ .$$

The data conversion is indicated in Table 13, and the results of the SIT fit are shown in Fig. 22.

The extrapolation procedure provides a rather crude estimate for $\log^*\beta^0_m = 23.5$ and $\Delta\epsilon = -1.8$. This last value is a tremendously large $\Delta\epsilon$, and the fit to all the data is not very good ($R^2 = 0.47$), so some caution should be exercised in using this number.

Uranium

Uranium hydrolysis.

U(IV) and U(VI) are the oxidation states of uranium expected under environmental conditions. Qualitatively, the hydrolysis of U(IV) is similar to that of Th(IV), although conclusive identification of individual species is lacking (Grenthe et al. 1992). Hydrolysis of U(IV) has been studied extensively in acidic solutions and begins at acid concentrations less than 0.1 M. Uranium concentrations in solution over the relatively insoluble U(IV) dioxide or hydroxide is extremely low, and this fact has most certainly limited the number of reliable studies of U(IV) hydrolysis products (Grenthe et al. 1992). There is reasonably good experimental evidence for the formation of $U(OH)^{3+}$ with $\log^*\beta^0_{11} = -0.54$ (± 0.06) (Grenthe et al. 1992). There is no direct evidence for other intermediate hydrolysis products such as $U(OH)_2^{2+}$ or $U(OH)_3^+$. However, there is a substantial amount of data, particularly from solubility

Table 13. Calculation of Thermodynamic Formation Constants for $Th(CO_3)_5^{6-}$ as a Function of Ionic Strength.

I_M	$\log^*\beta_M$	I_m	R	log$R$	$\Sigma\nu$ log$R$	$\log^*\beta_m$
1.0	26.2	1.05	1.049	0.021	−0.10	26.1
2.5	26.3	2.84	1.136	0.055	−0.28	26.0
3.0	32.3	3.50	1.165	0.066	−0.33	32.0

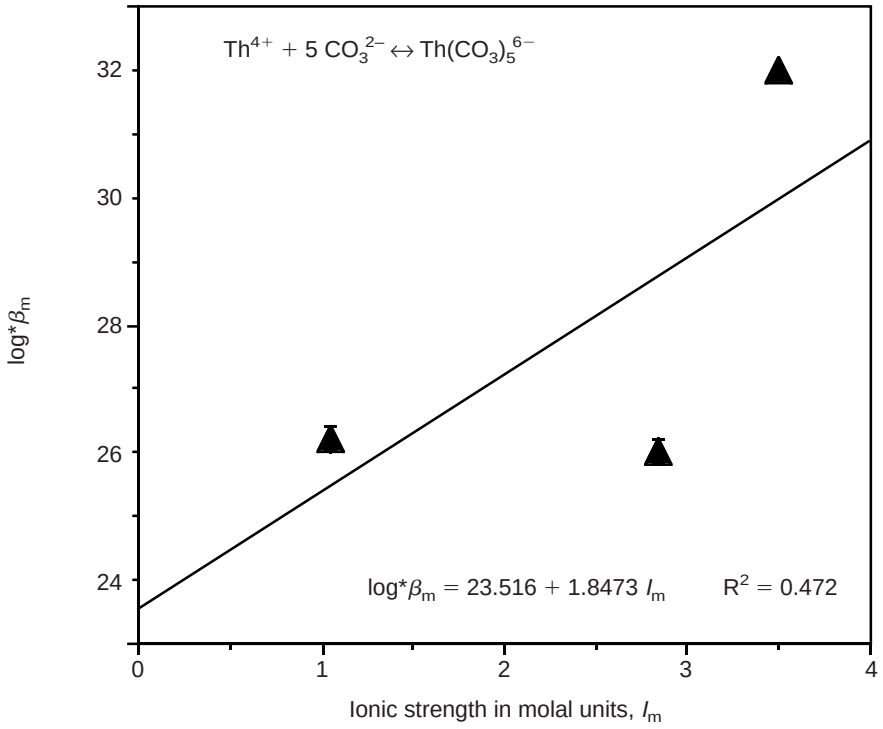

Figure 22. Formation of $Th(CO_3)_5^{6-}$. This graph shows the extrapolation to $I = 0$ of experimental data for the formation of $Th(CO_3)_5^{6-}$ using specific-ion interaction theory.

experiments, that is consistent with the neutral species $U(OH)_4$ (Grenthe et al. 1992). It is unknown whether this species is mono- or polymeric. Solubility studies by Rai et al. indicate that the anionic species $U(OH)_5^-$, if it exists, is only of minor importance (Rai et al. 1990). There is limited evidence for polymeric species such as $U_6(OH)_{15}^{9+}$ (Grenthe et al. 1992). The NEA analysis of uranium data could only provide an $I = 0$ value for the formation of $U(OH)^{3+}$. We revisited the SIT analysis of the first U(IV) hydrolysis constant:

$$U^{4+} + H_2O \leftrightarrow U(OH)^{3+} + H^+ \qquad \Sigma\nu = 0,\ \Delta z^2 = -6\ , \tag{21}$$

studied in $NaClO_4/HClO_4$ solutions. Table 14 lists the necessary conversions to undertake the SIT analysis on the data tabulated in the NEA review, and Fig. 23 provides a least-squares fit to the observed data.

From our analysis, the SIT estimate for $\log^*\beta^0_m = -0.47$ and $\Delta\epsilon = -0.06$. The NEA reviewers arrived at a similar value of $\log^*\beta^0_m = -0.54$. This difference is negligible, and the NEA spent several years analyzing the data and recalculating some values. Therefore, the NEA-recommended value should be accepted for use in the Yucca Mountain Site Characterization Project.

The hydrolysis of uranium(VI) has been studied extensively and begins at a pH value of about 3. The data presented in this section for U(VI) hydrolysis are quoted from Table V.5 of the NEA uranium volume. In solutions containing less than 10^{-4} M uranium, the first hydrolysis product is believed to be $UO_2(OH)^+$ (Grenthe et al. 1992). At higher uranium concentrations, it is accepted that polymeric U(VI) species are predominant in solution. At uranium concentrations above 10^{-4} M, it is generally agreed that the dimer, $(UO_2)_2(OH)_2^{2+}$, is the first hydrolysis product

Table 14. Calculation of Thermodynamic Formation Constants for $U(OH)^{3+}$ as a Function of Ionic Strength.

I_M	$\log^*\beta_M$	I_m	$\Sigma\nu \log R$	$\log^*\beta_m$	$\Delta z^2 D = -6D$	$\log a_w$	$\log^*\beta_m + 6D - \log a_w$
0.017	−0.92	0.017	0	−0.92	−0.22	−0.00	−0.70
0.033	−1.07	0.033	0	−1.07	−0.45	−0.00	−0.62
0.035	−1.00	0.035	0	−1.00	−0.45	−0.00	−0.55
0.045	−1.10	0.045	0	−1.10	−0.53	−0.00	−0.57
0.063	−1.14	0.063	0	−1.14	−0.53	−0.00	−0.61
0.11	−1.28	0.11	0	−1.28	−0.66	−0.00	−0.62
0.11	−1.22	0.11	0	−1.22	−0.66	−0.00	−0.56
0.12	−1.29	0.12	0	−1.29	−0.66	−0.00	−0.63
0.12	−1.23	0.12	0	−1.23	−0.66	−0.00	−0.57
0.19	−1.4	0.19	0	−1.4	−0.82	−0.00	−0.58
0.19	−1.2	0.19	0	−1.2	−0.82	−0.00	−0.38
0.19	−1.1	0.19	0	−1.1	−0.82	−0.00	−0.28
0.25	−1.44	0.25	0	−1.44	−0.87	−0.00	−0.57
0.27	−1.36	0.27	0	−1.36	−0.90	−0.00	−0.46
0.36	−1.59	0.36	0	−1.59	−0.95	−0.01	−0.43
0.36	−1.00	0.36	0	−1.00	−0.95	−0.01	−0.04
0.48	−1.70	0.49	0	−1.70	−1.06	−0.01	−0.63
0.48	−1.07	0.49	0	−1.07	−1.06	−0.01	0.00
0.50	−1.90	0.51	0	−1.90	−1.05	−0.01	−0.84
0.50	−1.00	0.51	0	−1.00	−1.05	−0.01	0.06
0.50	−1.74	0.51	0	−1.74	−1.06	−0.01	−0.67
0.50	−1.54	0.51	0	−1.54	−1.06	−0.01	−0.47
0.51	−1.21	0.52	0	−1.21	−1.06	−0.01	−0.14
0.52	−1.51	0.53	0	−1.51	−1.06	−0.01	−0.44
0.52	−1.50	0.53	0	−1.50	−1.06	−0.01	−0.43
0.55	−1.45	0.56	0	−1.45	−1.06	−0.01	−0.38
0.65	−1.31	0.66	0	−1.31	−1.12	−0.01	−0.18
0.75	−1.44	0.77	0	−1.44	−1.14	−0.01	−0.29
0.86	−1.54	0.89	0	−1.54	−1.17	−0.01	−0.36
0.99	−1.68	1.04	0	−1.68	−1.23	−0.02	−0.45
1.00	−1.57	1.05	0	−1.57	−1.23	−0.02	−0.32
1.01	−1.56	1.06	0	−1.56	−1.20	−0.02	−0.34
1.09	−1.72	1.14	0	−1.72	−1.24	−0.02	−0.46
2.0	−1.63	2.21	0	−1.63	−1.44	−0.03	−0.16
2.0	−1.68	2.21	0	−1.68	−1.40	−0.03	−0.25
3.0	−2.0	3.51	0	−2.0	−1.50	−0.06	−0.44
3.0	−1.95	3.51	0	−1.95	−1.50	−0.06	−0.39
3.0	−2.0	3.51	0	−2.0	−1.50	−0.06	−0.44
3.0	−1.65	3.51	0	−1.65	−1.50	−0.06	−0.09

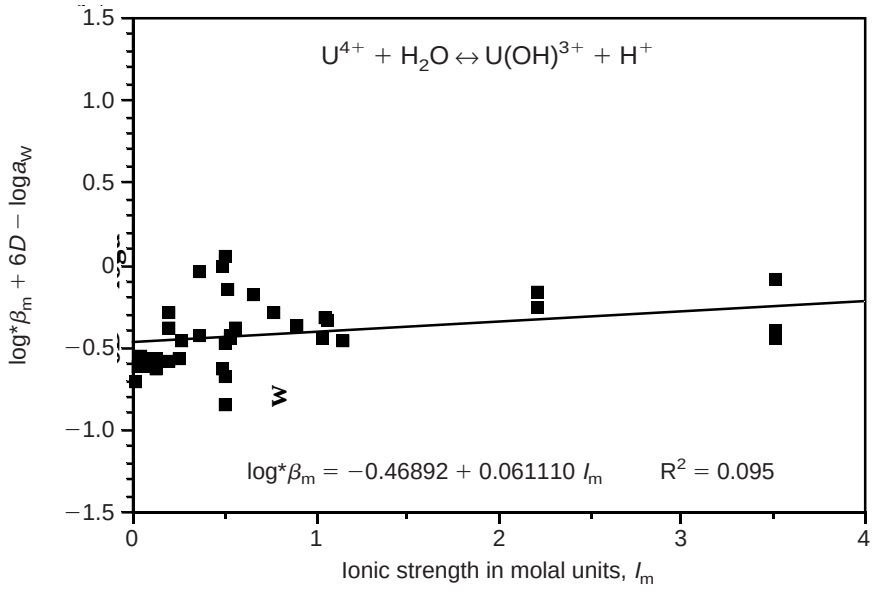

Figure 23. Formation of $U(OH)^{3+}$. This graph shows the extrapolation to $I = 0$ of experimental data for the formation of $U(OH)^{3+}$ using specific-ion interaction theory.

(Grenthe et al. 1992). Trimeric uranyl-hydroxide complexes $(UO_2)_3(OH)_5^+$ and $(UO_2)_3(OH)_4^{2+}$ are also well established (Grenthe et al. 1992). At higher pH, hydrous uranyl-hydroxide precipitate is the stable species (Baes and Mesmer 1976). For a more detailed discussion and critical review of the hydrolysis literature of uranium, the reader is referred to the NEA review of the thermodynamics of uranium. The SIT analysis for the important U(VI) hydrolysis species are characterized by $^*\beta_{11}$, $^*\beta_{22}$, $^*\beta_{34}$, and $^*\beta_{35}$ in $NaClO_4$ solutions. For consistency, we converted the literature data for UO_2OH^+ (tabulated from Grenthe et al. 1992) into a form suitable for the SIT analysis, and the data for the reaction

$$UO_2^{2+} + H_2O \leftrightarrow UO_2OH^+ + H^+ \qquad (22)$$
$$\Sigma\nu = 0,\ \Delta z^2 = -2\ ,$$

are shown in Table 15, and the least squares extrapolation is shown in Fig. 24.

From Fig. 24, we note that the data segregate into two lines, one with $\log^*\beta_m + 2D - \log a_w$ between -5.5 to -6.0 and one between -4.0 and -5.0. As will be seen below for the dimeric $(UO_2)_2(OH)_2^{2+}$ species, the bottom row of points in Fig. 24 correspond closely to the data from the 2:2 hydrolysis plot (Fig. 25), leading to the conclusion that the 2:2 complex was not accounted for in some of the experiments purporting to determine the 1:1 hydrolysis constants. This conclusion was also reached by the NEA (Grenthe et al. 1992), and by taking these factors into consideration, they concluded that $\log^*\beta^0_m = -5.2 \pm 0.3$ and $\Delta\epsilon = -0.4$ for $NaClO_4$ solutions of the monomer. By ignoring the bottom line of data plotted in Fig. 24, we find that $\log^*\beta^0_m \cong -4.5$. We conclude that the NEA recommendation for this constant be adopted, but with some caution.

Table 16 lists the necessary conversions to undertake the SIT analysis on the data tabulated in the NEA review for the formation of $(UO_2)_2(OH)_2^{2+}$ according to

$$2\ UO_2^{2+} + 2\ H_2O \leftrightarrow (UO_2)_2(OH)_2^{2+} + 2\ H^+ \qquad (23)$$
$$\Sigma\nu = -1,\ \Delta z^2 = -2\ ,$$

and Fig. 25 provides a least-squares extrapolation to the observed data.

Table 15. Calculation of Thermodynamic Formation Constants for $UO_2(OH)^+$ as a Function of Ionic Strength

I_M	$\log^*\beta_M$	I_m	$\Sigma\nu \log R$	$\log^*\beta_m$	$\Delta z^2 D = -2D$	$\log a_w$	$\log^*\beta_m + 2D - \log a_w$
~0	−4.5	0.0	0.00	−4.5	0.0	0.00	−4.5
~0	−4.14	0.0	0.00	−4.14	0.0	0.00	−4.14
~0	−4.19	0.0	0.00	−4.19	0.0	0.00	−4.19
~0	−5.08	0.0	0.00	−5.08	0.0	0.00	−5.08
~0	−4.03	0.0	0.00	−4.03	0.0	0.00	−4.03
~0	−5.2	0.0	0.00	−5.2	0.0	0.00	−5.2
~0	−5.1	0.0	0.00	−5.1	0.0	0.00	−5.1
0.05	−6.04	0.05	0.00	−6.04	−0.17	0.00	−5.87
0.1	−6.09	0.10	0.00	−6.09	−0.22	0.00	−5.87
0.1	−5.0	0.10	0.00	−5.0	−0.22	0.00	−4.78
0.1	−4.20	0.10	0.00	−4.20	−0.22	0.00	−3.98
0.1	−4.39	0.10	0.00	−4.39	−0.22	0.00	−4.17
0.4	−6.20	0.405	0.00	−6.20	−0.33	−0.01	−5.86
0.5	−4.00	0.51	0.00	−4.00	−0.35	−0.01	−3.64
0.7	−6.09	0.72	0.00	−6.09	−0.38	−0.01	−5.70
1.0	−6.03	1.05	0.00	−6.03	−0.41	−0.02	−5.60
1.0	−4.77	1.05	0.00	−4.77	−0.41	−0.02	−4.34

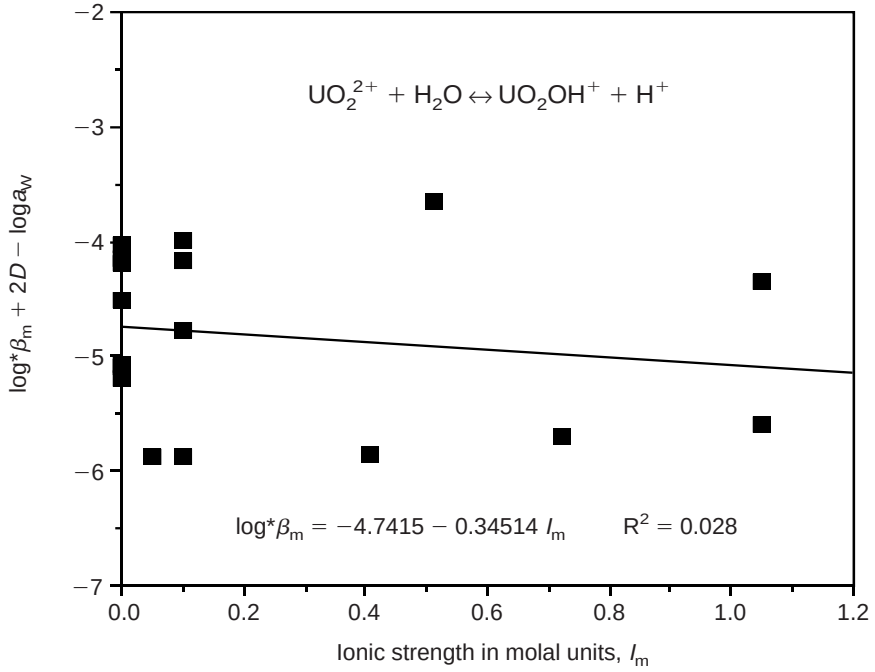

Figure 24. Formation of $UO_2(OH)^+$. Extrapolation of experimental data to $I = 0$ for the formation of $UO_2(OH)^+$ using specific-ion interaction theory.

Table 16. Calculation of Thermodynamic Formation Constants for $(UO_2)_2(OH)_2^{2+}$ as a Function of Ionic Strength.

I_M	$\log^*\beta_M$	I_m	$\Sigma\nu \log R$	$\log^*\beta_m$	$\Delta z^2 D = -2D$	$2 \log a_w$	$\log^*\beta_m + 2D - 2 \log a_w$
~0	−4.95	0	0.00	−4.95	0.0	0.00	−4.95
~0	−5.87	0	0.00	−5.87	0.0	0.00	−5.87
~0	−5.73	0	0.00	−5.73	0.0	0.00	−5.73
0.024	−5.64	0.024	0.00	−5.64	−0.14	0.00	−5.50
0.03	−5.99	0.03	0.00	−5.99	−0.15	0.00	−5.84
0.03	−5.94	0.03	0.00	−5.94	−0.15	0.00	−5.89
0.10	−6.2	0.10	0.00	−6.2	−0.22	0.00	−5.98
0.10	−6.28	0.10	0.00	−6.28	−0.22	0.00	−6.06
0.10	−6.09	0.10	0.00	−6.09	−0.22	0.00	−5.87
0.10	−6.09	0.10	0.00	−6.09	−0.22	0.00	−5.87
0.10	−5.89	0.10	0.00	−5.89	−0.22	0.00	−5.67
0.105	−5.85	0.105	0.00	−5.85	−0.22	0.00	−5.63
0.20	−5.92	0.20	0.00	−5.92	−0.27	0.00	−5.65
0.254	−5.89	0.256	−0.01	−5.90	−0.28	0.00	−5.62
0.50	−6.03	0.51	−0.01	−6.04	−0.35	−0.01	−5.68
0.50	−6.03	0.51	−0.01	−6.04	−0.35	−0.01	−5.68
0.506	−5.97	0.516	−0.01	−5.98	−0.35	−0.02	−5.62
1.0	−6.10	1.05	−0.02	−6.12	−0.41	−0.03	−5.68
1.0	−6.02	1.05	−0.02	−6.04	−0.41	−0.03	−5.60
1.0	−5.91	1.05	−0.02	−5.93	−0.41	−0.03	−5.49
1.005	−6.06	1.055	−0.02	−6.08	−0.41	−0.03	−5.64
2.003	−6.16	2.213	−0.04	−6.20	−0.47	−0.06	−5.67
3.0	−6.31	3.51	−0.07	−6.38	−0.50	−0.12	−5.76
3.0	−6.02	3.51	−0.07	−6.09	−0.50	−0.12	−5.47
3.0	−6.02	3.51	−0.07	−6.09	−0.50	−0.12	−5.47
3.0	−6.17	3.51	−0.07	−6.24	−0.50	−0.12	−5.62
3.0	−6.02	3.51	−0.07	−6.09	−0.50	−0.12	−5.47

This analysis concludes that $\log^*\beta^0_m = -5.71$ and that $\Delta\epsilon = -0.05$ for the formation of the dimeric $(UO_2)_2(OH)_2^{2+}$ complex in $NaClO_4$, as compared to $\log^*\beta^0_m = -5.62$ and $\Delta\epsilon = -0.07$ from the NEA. Points to consider excluding from the analysis are obvious from the plot and include the value of −4.95 from Guiter (1947). The NEA-recommended value should be adopted for use by the Yucca Mountain Site Characterization Project.

There are two trimeric complexes of formula $(UO_2)_3(OH)_4^{2+}$ and $(UO_2)_3(OH)_5^{+}$ that have been discussed in the literature, and the hydrolysis constants for these are expected to be highly correlated. There are also potential problems with the formulation of these clusters, because the cluster $(UO_2)_3(OH)_5^{+}$ has essentially the same stoichiometry as $(UO_2)_3O(OH)_3^{+}$. Clusters of the latter type have been observed in the solid state by Åberg (1978). The NEA review on uranium discussed this problem in some detail. Table 17 lists the necessary conversions to undertake the SIT analysis

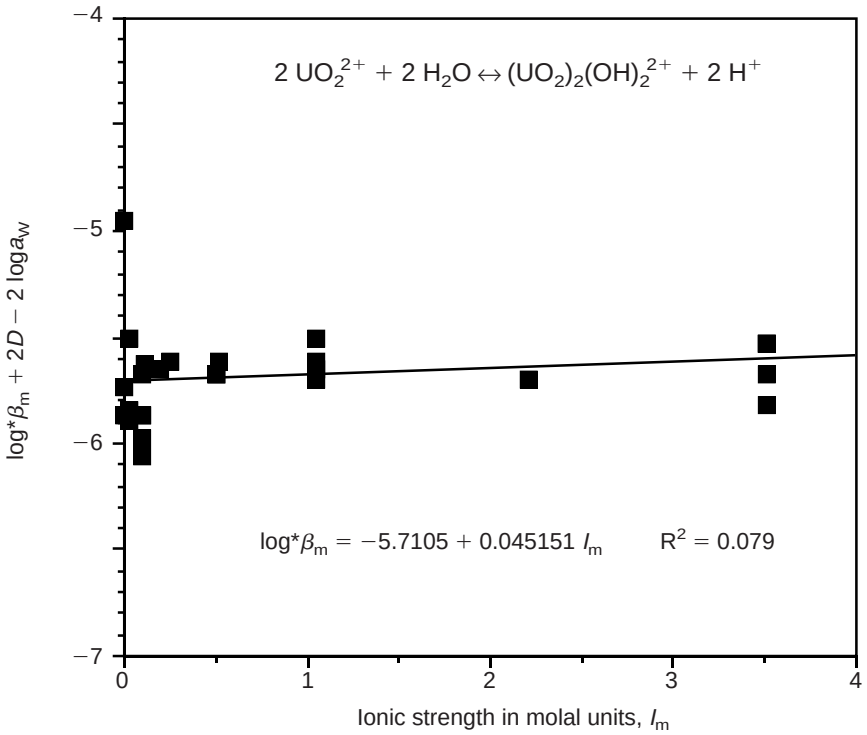

Figure 25. Formation of $(UO_2)_2(OH)_2^{2+}$. This graph shows the extrapolation to $I = 0$ of experimental data for the formation of $(UO_2)_2(OH)_2^{2+}$ using specific-ion interaction theory.

on the data tabulated in the NEA review for the formation of $(UO_2)_3(OH)_4^{2+}$ according to the following reaction:

$$3\ UO_2^{2+} + 4\ H_2O \leftrightarrow (UO_2)_3(OH)_4^{2+} + 4\ H^+ \quad (24)$$
$$\Sigma\nu = -2,\ \Delta z^2 = -4\ ,$$

and Fig. 26 provides a least-squares extrapolation to the observed data.

This analysis would conclude that $\log^*\beta^0_m = -12.53$ and that $\Delta\epsilon = -0.12$ for the formation of the trimeric $(UO_2)_3(OH)_4^{2+}$ complex in $NaClO_4$, as compared to $\log^*\beta^0_m = -11.9$ from the NEA. Owing to the lack of data and the uncertainty of the structure of this complex, the NEA-recommended value should be adopted but used with some caution.

Table 18 lists the necessary conversions to undertake the SIT analysis on the data tabulated in the NEA review for the formation of $(UO_2)_3(OH)_5^+$

Table 17. Calculation of Thermodynamic Formation Constants for $(UO_2)_3(OH)_4^{2+}$ as a Function of Ionic Strength.

I_M	$\log^*\beta_{11}$	I_m	$\Sigma\nu \log R$	$\log^*\beta_m$	$\Delta z^2 D = -4D$	$4 \log a_w$	$\log^*\beta_m + 4D - 4 \log a_w$
0.5	−13.17	0.51	−0.02	−13.19	−0.68	−0.04	−12.47
3.0	−12.60	3.51	−0.13	−12.73	−1.00	−0.24	−11.49
3.0	−13.83	3.51	−0.13	−13.96	−1.00	−0.24	−12.72

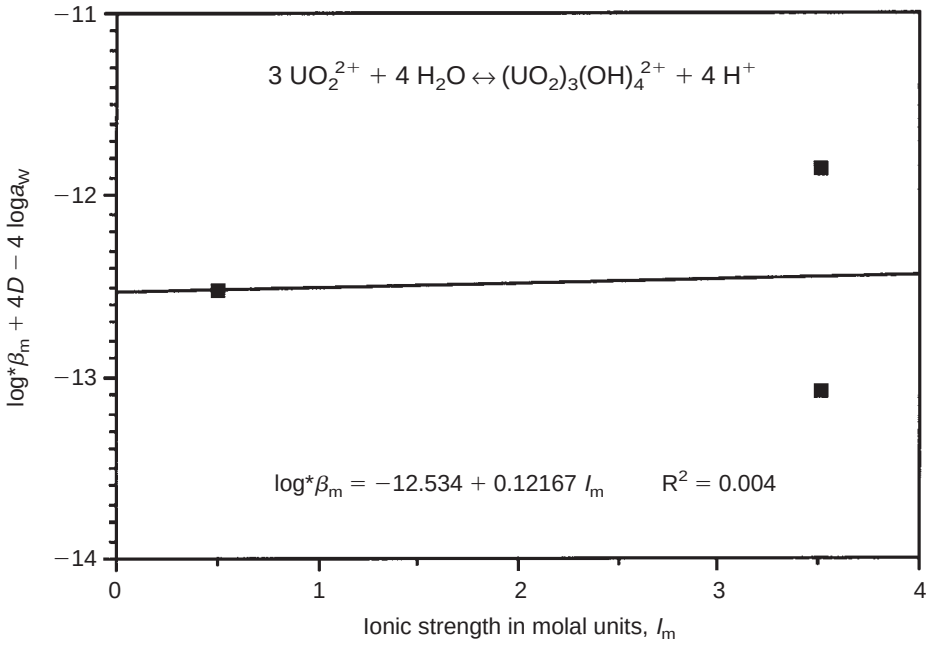

Figure 26. Formation of $(UO_2)_3(OH)_4^{2+}$. Extrapolation of experimental data to $I = 0$ for the formation of $(UO_2)_3(OH)_4^{2+}$ using specific-ion interaction theory.

according to the following reaction:

$$3\ UO_2^{2+} + 5\ H_2O \leftrightarrow (UO_2)_3(OH)_5^{+} + 5\ H^{+}$$
$$\Sigma\nu = -2,\ \Delta z^2 = -6\ , \qquad (25)$$

and Fig. 27 provides a least-squares extrapolation to the observed data.

Therefore, for the formation of the 3:5 complex using all the points available, we obtain $\log^*\beta^0_m = -15.57$ with $\Delta\epsilon = -0.14$ for $NaClO_4$ solutions, as compared to the values of $\log^*\beta^0_m = -15.55$ and $\Delta\epsilon = -0.23$ from the NEA volume (Grenthe et al. 1992) in which only selected values were used. The NEA-recommended value should be adopted for use by YMP.

Uranium-carbonato complexes.
In the case of U(IV), there is quantitative data only for $U(CO_3)_5^{6-}$ and $U(CO_3)_4^{4-}$ (Bruno et al. 1989; Ciavatta et al. 1983). Ciavatta et al. studied the redox equilibrium:

$$UO_2(CO_3)_3^{4-} + 2e^- + 2CO_2 \leftrightarrow U(CO_3)_5^{6-}, \qquad (26)$$

by both potentiometric and spectrophotometric techniques (Ciavatta et al. 1983). The standard potential for the U(IV)-U(VI) redox couple was then used to estimate the value of $\log\beta_{15}$ for the formation of the limiting complex $U(CO_3)_5^{6-}$ given by the reaction

$$U^{4+} + 5\ CO_3^{2-} \leftrightarrow U(CO_3)_5^{6-}\ . \qquad (27)$$

A representative set of U(IV) carbonate equilibria and their formation constants at selected ionic strengths are given in Table 19.

Pratopo et al. analyzed previous solubility data for uranium in a Swedish groundwater by assuming the presence of a mixed hydroxy carbonate of formula $U(OH)_2(CO_3)_2^{2-}$ and proposed a value for the formation constant (Pratopo et al. 1990), but more quantitative data are needed. In the latest NEA report (for americium), it is stated in Appendix D ("Corrections to the Uranium NEA-TDB Review") that mixed hydroxo-carbonato U(IV) compounds must be considered (Silva et al. 1995).

Table 18. Calculation of Thermodynamic Formation Constants for $(UO_2)_3(OH)_5^+$ as a Function of Ionic Strength

I_M	$\log^*\beta_M$	I_m	$\Sigma\nu \log R$	$\log^*\beta_m$	$\Delta z^2 D = -6D$	$5 \log a_w$	$\log^*\beta_m + 6D - 5 \log a_w$
0.024	−15.94	0.024	0.00	−15.94	−0.42	0.00	−15.52
0.03	−16.8	0.03	0.00	−16.8	−0.45	0.00	−16.35
0.03	−16.4	0.03	0.00	−16.4	−0.45	0.00	−15.95
0.1	−15.64	0.10	0.00	−15.64	−0.66	0.00	−14.98
0.1	−16.19	0.10	0.00	−16.19	−0.66	0.00	−15.53
0.105	−16.32	0.105	0.00	−16.32	−0.66	0.00	−15.66
0.2	−16.16	0.20	−0.01	−16.17	−0.82	−0.01	−15.34
0.254	−16.46	0.254	−0.01	−16.47	−0.87	−0.02	−15.58
0.5	−16.78	0.51	−0.02	−16.80	−1.05	−0.04	−15.71
0.5	−16.54	0.51	−0.02	−16.56	−1.05	−0.04	−15.47
0.5	−16.37	0.51	−0.02	−16.39	−1.05	−0.04	−15.30
0.506	−16.51	0.516	−0.02	−16.53	−1.05	−0.04	−15.44
1.0	−16.41	1.05	−0.04	−16.45	−1.24	−0.09	−15.12
1.0	−16.43	1.05	−0.04	−16.47	−1.24	−0.09	−15.14
1.0	−16.74	1.05	−0.04	−16.78	−1.24	−0.09	−15.45
1.005	−16.67	1.055	−0.04	−16.71	−1.24	−0.09	−15.38
2.003	−16.79	2.213	−0.08	−16.87	−1.41	−0.14	−15.32
3.0	−16.54	3.51	−0.13	−16.67	−1.50	−0.24	−14.93
3.0	−17.04	3.51	−0.13	−17.17	−1.50	−0.24	−15.43
3.0	−16.8	3.51	−0.13	−16.9	−1.50	−0.24	−15.16
3.0	−16.54	3.51	−0.13	−16.67	−1.50	−0.24	−14.93

There is only one uranyl(V) species for which quantitative thermodynamic information is available, namely $UO_2(CO_3)_3^{5-}$. With this number of carbonate ligands around the U(V), there is probably no room left for any OH^- ligands, and hence, the data are unambiguous enough to be interpreted quantitatively. The formation constant for this species was determined based on the formation constant of $UO_2(CO_3)_3^{4-}$ and the reduction potential of the following equilibrium (Ferri et al. 1983):

$$UO_2(CO_3)_3^{4-} + e^- \leftrightarrow UO_2(CO_3)_3^{5-} \quad . \quad (28)$$

Representative values of the equilibrium constants for carbonate complexes of U(V) at selected ionic strengths are given in Table 20.

Table 19. Equilibrium Constants of the Carbonate Complexes of Tetravalent Uranium at Room Temperature

Reaction	I_M	$\log K$
$U^{4+} + 5\ CO_3^{2-} \leftrightarrow U(CO_3)_5^{6-}$	0	34.0 ± 0.9*
	3.0	36.86 ± 0.55†
$U(CO_3)_4^{4-} + CO_3^{2-} \leftrightarrow U(CO_3)_5^{6-}$	0	–1.12 ± 0.22§

*Grenthe et al. 1992 †Ciavatta et al. 1983 §Bruno et al. 1989

The aqueous U(VI)-carbonate system has been very thoroughly studied, and there is little doubt about the compositions of the three monomeric

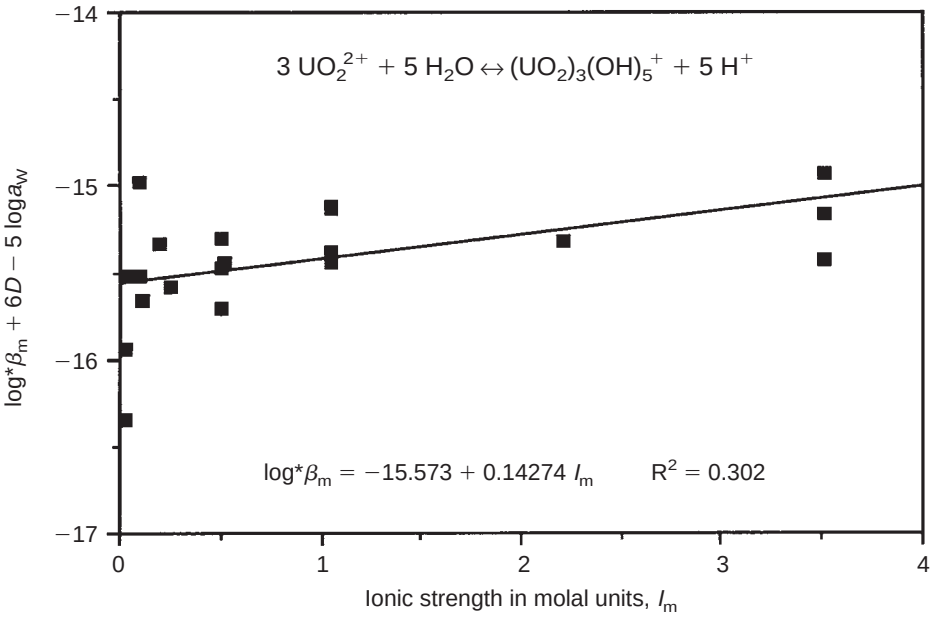

Figure 27. Formation of $(UO_2)_3(OH)_5^+$. Extrapolation of experimental data to $I = 0$ for the formation of $(UO_2)_3(OH)_5^+$ using specific-ion interaction theory.

complexes of general formula $UO_2(CO_3)$, $UO_2(CO_3)_2^{2-}$, and $UO_2(CO_3)_3^{4-}$ (structure I, page 64) present under the appropriate conditions (Grenthe et al. 1992). Solution raman spectroscopic data are consistent with the maintenance of a linear O=An=O unit and bidentate carbonate ligands for $AnO_2(CO_3)_3^{4-}$ complexes in aqueous carbonate solutions of U(VI) (as well as of Np(VI), Pu(VI), and Am(VI) complexes) (Basile et al. 1978; Madic et al. 1983; Nguyen-Trung et al. 1992). Bicarbonate monomeric complexes of AnO_2^{2+} have not been demonstrated to exist even in the pH ranges at which bicarbonate ions are present at higher concentrations than carbonate (Maya 1982b). There is a great deal of evidence from emf, solubility, and spectroscopic data supporting the existence of polymeric solution species of formulas $(UO_2)_3(CO_3)_6^{6-}$, $(UO_2)_2(CO_3)(OH)_3^-$, $(UO_2)_3O(OH)_2(HCO_3)^+$, and $(UO_2)_{11}(CO_3)_6(OH)_{12}^{2-}$, which form only under conditions of high metal-ion concentration or high ionic strength (Grenthe et al. 1992; Grenthe and Lagerman 1991b). Determining the formation constant for the triscarbonato-uranyl monomer, $UO_2(CO_3)_3^{4-}$, is complicated because this species is in equilibrium with the hexakiscarbonato-uranyl trimer, $(UO_2)_3(CO_3)_6^{6-}$. Recently, Bidoglio et al. used thermal-lensing spectroscopy (which is sensitive enough to allow the study of relatively dilute solutions in which the trimer is not favored) to determine the equilibrium constant for the addition of one carbonate to $UO_2(CO_3)_2^{2-}$ to form $UO_2(CO_3)_3^{4-}$ and used this value to calculate the formation constant, β_{13} (Bidoglio et al. 1991). The formation constants for the principal complexes have been determined by a

Table 20. Equilibrium Constants of the Carbonate Complexes of Pentavalent Uranium at Room Temperature

Equilibrium	I_M	log$K$
$UO_2^+ + 3\ CO_3^{2-} \leftrightarrow UO_2(CO_3)_3^{5-}$	0	7.41 ± 0.27*
	3.0	6.54 ± 0.49†

*Grenthe et al. 1992 †Ferri et al. 1983

large number of investigators using a wide variety of techniques and have been critically reviewed by Grenthe et al. (1992).

The trimetallic uranyl cluster $(UO_2)_3(CO_3)_6^{6-}$ has been the subject of a good deal of study, including ^{13}C and ^{17}O NMR spectroscopy (Åberg et al. 1983a; Allen et al. 1995; Bányai et al. 1995; Clark and Palmer 1994; Ferri et al. 1988; Clark et al. 1995c), solution x-ray diffraction (Åberg et al. 1983b), potentiometric titration (Ciavatta et al. 1979; Grenthe et al. 1984; Grenthe and Lagerman 1991b), single-crystal x-ray diffraction (Allen et al. 1995), and EXAFS spectroscopy in both the solid and solution states (Allen et al. 1995). The data in this area have consistently led to the proposal of a triangular cluster in solution as shown qualitatively below as structure II. This structural motif was proposed by Åberg as a result of fits to solution x-ray diffraction data (Åberg et al. 1983b). It was based on the hexagonal $AnO_2(CO_3)$ layers in the solid state structures of $KAnO_2(CO_3)$ (where An = Pu or Am) (Ellinger and Zachariasen 1954), which is a simple structural modification of the rutherfordine structure (Christ et al. 1955).

Ciavatta et al. were the first to propose the $(UO_2)_3(CO_3)_6^{6-}$ cluster based on potentiometric (emf) titration studies (Ciavatta et al. 1979). Åberg et al. reported ^{13}C NMR data for a sample at a pH of 5.7 (25ºC and 0ºC) that showed two ^{13}C NMR resonances consistent with the structure proposed in II (Åberg et al. 1983b). Several years later, Ferri et al. reported an ^{17}O NMR spectrum of a similar sample that displayed five ^{17}O NMR signals between δ = 1130 to 1095 ppm in the expected 2:2:2:1:1 ratio (Ferri et al. 1988), and it was argued that this ^{17}O NMR spectrum confirmed the solution structure of $(UO_2)_3(CO_3)_6^{6-}$ as that shown in II. However, all five ^{17}O resonances appear in the uranyl (O=U=O) chemical-shift region of the ^{17}O NMR spectrum and are more consistent with five different uranyl-oxygen environments. Subsequent ^{17}O NMR studies revealed a single uranyl-^{17}O resonance at δ = 1105 ppm that is consistent with the proposed trimer structure (Allen et al. 1995; Bányai et al. 1995), and the earlier assignment has been corrected. EXAFS measurements performed at the uranium L_{III} edge for solid $[C(NH_2)_3]_6[(UO_2)_3(CO_3)_6]$, solid $K_4[UO_2(CO_3)_3]$, and a solution of $(UO_2)_3(CO_3)_6^{6-}$ gave further support of a trimeric structure for the $(UO_2)_3(CO_3)_6^{6-}$ ion (Allen et al. 1995).

Representative values of the thermodynamic equilibrium constants for U(VI)-carbonato complexes are listed in Table 21. Under solutions conditions expected for Yucca Mountain, only the monomeric complexes $UO_2(CO_3)$, $UO_2(CO_3)_2^{2-}$, and $UO_2(CO_3)_3^{4-}$ are anticipated. Data conversions necessary for a SIT analysis for these monomeric complexes are given in Tables 22, 23 and 24 for

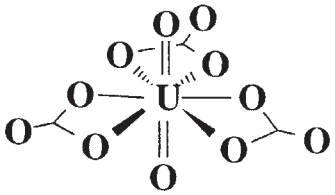

I (monomer)

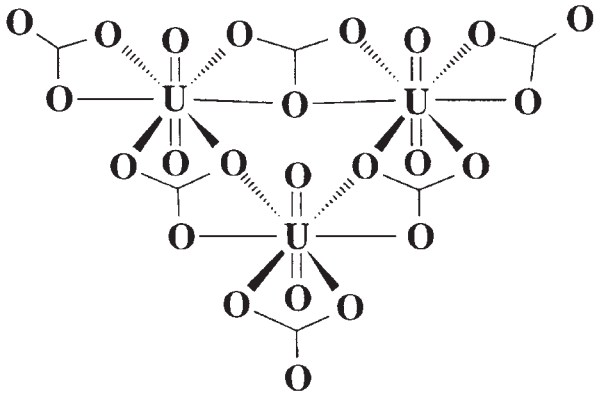

II (trimer)

Table 21. Equilibrium Constants of the Carbonate Complexes of Hexavalent Uranium at Room Temperature

Reaction	I_M	log$K$
$UO_2^{2+} + CO_3^{2-} \leftrightarrow UO_2(CO_3)$	0	9.68 ± 0.04*
	0.5	8.54 ± 0.05†
	3.0	8.89 ± 0.01†
$UO_2^{2+} + 2\ CO_3^{2-} \leftrightarrow UO_2(CO_3)_2^{2-}$	0	16.94 ± 0.12*
	0.1	16.15 ± 0.29§
	0.5	14.93 ± 0.30‡
	3.0	16.20 ± 0.15†
$UO_2^{2+} + 3\ CO_3^{2-} \leftrightarrow UO_2(CO_3)_3^{4-}$	0	21.60 ± 0.05*
	0.1	21.80 ± 0.10§
	0.5	22.30 ± 0.11‡
	3.0	22.61 ± 0.15†
$3\ UO_2(CO_3)_3^{4-} \leftrightarrow (UO_2)_3(CO_3)_6^{6-} + 3\ CO_3^{2-}$	3.0	−11.3 ± 0.01¥
$3\ UO_2^{+} + 6\ CO_3^{2-} \leftrightarrow (UO_2)_3(CO_3)_6^{6-}$	0	54.00 ± 1.0*
	0.5	53.82 ± 0.17‡
	2.5	55.6 ± 0.5**
	3.0	56.23 ± 0.3*
$UO_2(CO_3)_2^{2-} + CO_3^{2-} \leftrightarrow (UO_2)(CO_3)_3^{4-}$	0.5	6.35 ± 0.05††
$2\ UO_2^{2+} + CO_2(g) + 4\ H_2O(l) \leftrightarrow (UO_2)_2CO_3(OH)_3^{-} + 5\ H^{+}$	0	−19.01 ± 0.50§§
	0.1	−18.63 ± 0.08*
	0.5	−19.40 ± 0.11*
$11\ UO_2^{2+} + 6\ CO_2(g) + 18\ H_2O(l) \leftrightarrow (UO_2)_{11}(CO_3)_6(OH)_{12}^{2-} + 24\ H^{+}$	0	−72.5 ± 2.0*
	0.5	−72.48 ± 0.3§§
$3\ UO_2^{2+} + CO_2(g) + 4\ H_2O(l) \leftrightarrow (UO_2)_3O(OH)_2HCO_3^{+} + 5\ H^{+}$	0	−17.5 ± 0.5‡
	3.0	−16.6 ± 0.2‡

*Grenthe et al. 1992 †Grenthe et al. 1984 §Maya 1982b ‡Grenthe and Lagerman 1991b ¥Grenthe et al. 1986a
**Allen et al. 1995 ††Bidoglio et al. 1991 §§Grenthe and Lagerman 1991a

the following reactions:

$$UO_2^{2+} + CO_3^{2-} \leftrightarrow UO_2CO_3(aq) \quad \Sigma\nu = -1,\ \Delta z^2 = -8\ , \tag{29}$$

$$UO_2^{2+} + 2\ CO_3^{2-} \leftrightarrow UO_2(CO_3)_2^{2-} \quad \Sigma\nu = -2,\ \Delta z^2 = -8\ , \tag{30}$$

$$UO_2^{2+} + 3\ CO_3^{2-} \leftrightarrow UO_2(CO_3)_3^{4-} \quad \Sigma\nu = -3,\ \Delta z^2 = 0\ , \tag{31}$$

respectively. The extrapolation to $I = 0$ for these complexes are all shown in Fig. 28.

From the above analyses, we obtain $\log^*\beta^0_{11} = 9.90$ with $\Delta\epsilon = -0.27$, $\log^*\beta^0_{12} = 16.87$ with $\Delta\epsilon = -0.30$, and $\log^*\beta^0_{13} = 21.76$ with $\Delta\epsilon = -0.19$. These can be compared to the recommended NEA values of $\log^*\beta^0_{11} = 9.68$, $\log^*\beta^0_{12} = 16.94$, and $\log^*\beta^0_{13} = 21.60$. The NEA-recom-

Table 22. Calculation of Thermodynamic Formation Constants for $UO_2(CO_3)$ as a Function of Ionic Strength

I_M	$\log\beta_{11}$	I_m	R	$\Sigma\nu \log R$	$\log\beta_{11m}$	$\Delta z^2 D$	$\log\beta_{11m} - \Delta z^2 D$
0.03	9.44	0.03	1.000	0.00	9.44	−0.56	10.00
0.1	9.30	0.10	1.007	0.00	9.30	−0.87	10.17
0.5	8.39	0.51	1.050	−0.02	8.37	−1.40	9.77
0.5	8.56	0.51	1.050	−0.02	8.54	−1.40	9.94
3.0	8.89	3.50	1.165	−0.07	8.82	−2.00	10.82
3.0	9.01	3.50	1.165	−0.07	8.94	−2.00	10.94

Table 23. Calculation of Thermodynamic Formation Constants for $UO_2(CO_3)_2^{2-}$ as a Function of Ionic Strength

I_M	$\log\beta_{12}$	I_m	R	$\Sigma\nu \log R$	$\log\beta_{12m}$	$\Delta z^2 D$	$\log\beta_{12m} - \Delta z^2 D$
0.03	16.7	0.03	1.000	0.00	16.7	−0.56	17.3
0.1	16.2	0.10	1.007	0.00	16.2	−0.87	17.1
0.1	16.15	0.10	1.007	0.00	16.15	−0.87	17.02
0.5	15.56	0.51	1.050	−0.04	15.52	−1.40	16.92
0.5	14.93	0.51	1.050	−0.04	14.89	−1.40	16.29
3.0	16.20	3.50	1.165	−0.14	16.06	−2.00	18.06

Table 24. Calculation of Thermodynamic Formation Constants for $UO_2(CO_3)_3^{4-}$ as a Function of Ionic Strength

I_M	$\log\beta_{13}$	I_m	R	$\Sigma\nu \log R$	$\log\beta_{13m}$	$\Delta z^2 D$	$\log\beta_{13m} - \Delta z^2 D$
0.1	21.8	0.10	1.007	0.00	21.8	0.00	21.8
0.1	21.5	0.10	1.007	0.00	21.5	0.00	21.5
0.5	21.76	0.51	1.050	−0.06	21.70	0.00	21.7
0.5	22.36	0.51	1.050	−0.06	22.30	0.00	22.30
3.0	22.61	3.50	1.165	−0.21	22.40	0.00	22.40

mended values should be adopted for use by the Yucca Mountain Site Characterization Project.

Neptunium

Neptunium hydrolysis.

Np(IV) is expected to be the dominant oxidation state under reducing conditions in natural groundwaters (Katz et al. 1986). Sullivan and Hindman studied the hydrolysis of Np(IV) spectrophotometrically (Sullivan and Hindman 1959). They reported the hydrolysis constant of the first hydrolysis product, $Np(OH)^{3+}$, to be $\log^*\beta_{11} = -2.30$ ($\pm$ 0.03) at room temperature in 2 M $NaClO_4$ solution. Note that this corresponds to $\log\beta_{11} = 11.30$ ($\pm$ 0.03) using a value of $\log K_w = 14.0$. Other Np(IV) hydrolysis products are unknown, but Rai

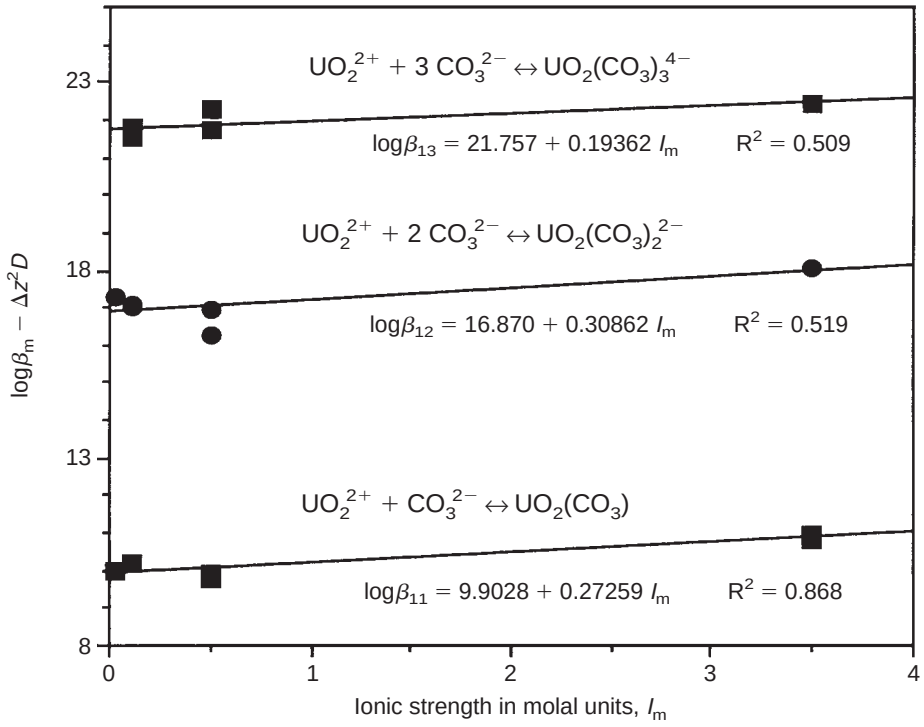

Figure 28. SIT Analysis for Uranyl Carbonates. These plots show the extrapolation of experimental data to $I = 0$ for the formation of $UO_2(CO_3)$ (bottom), $UO_2(CO_3)_2^{2-}$ (middle), and $UO_2(CO_3)_3^{4-}$ (top) using specific-ion interaction theory.

and Ryan (1985) have established an upper limit for $\log\beta_{15}$ of 45.3 for the formation of $Np(OH)_5^-$.

Neptunium(V), in the form NpO_2^+, is the most common oxidation state in oxygen-rich natural waters, and it does not hydrolyze readily below a pH of 9. For recent studies concerning the hydrolysis of Np(V) to form $NpO_2(OH)$ and $NpO_2(OH)_2^-$, the reader is referred to the recent works of Itagaki et al. (1992) and Neck et al. (1992). Despite a number of publications, the hydrolysis data for NpO_2^+ are not consistent but vary over four orders of magnitude. As discussed by Neck et al., most of these values have been determined at ionic-strength values below 1.0 M. Thus, the wide spread in values cannot be due to ionic-strength effects (Neck et al. 1992). Because hydrolysis is generally studied in basic solutions, contamination by carbonate is the most likely source of error. A summary of the first and second hydrolysis constants taken from the literature for Np(V) is given in Table 25 (Bidoglio et al. 1985; Itagaki et al. 1992; Kraus and Nelson 1948; Lierse et al. 1985; Maya 1983; Moskvin 1971a; Nagasaki et al. 1988; Nakayama et al. 1988; Neck et al. 1992; Rösch et al. 1987; Schmidt et al. 1980; Sevost'yanova and Khalturin 1976). The first hydrolysis constant measured at 25ºC is seen to vary by four orders of magnitude.

We converted the literature data for NpO_2OH into a form suitable for the SIT analysis, and the data for the reaction:

$$NpO_2^+ + OH^- \leftrightarrow NpO_2OH \qquad \Sigma\nu = -1,\ \Delta z^2 = -2\ , \tag{32}$$

are shown in Table 26. Note that because the data are tabulated in $\log\beta$ form, we have written Eqn. 32 as a formation, and we will convert the $I = 0$ value to $\log^*\beta$ form following the SIT analy-

Table 25. Equilibrium Constants of the Hydrolyzed Complexes of Pentavalent Neptunium at Room Temperature

Reaction	I_M	logβ
$NpO_2^+ + OH^- \leftrightarrow NpO_2(OH)$	0.001	5.2*
	0.002	5.1†
	0.005	5.7§
	0.02	5.1†
	0.02	3.92‡
	0.01	5.7¥
	0.1	6.0§
	0.1	4.9#
	0.1	2.44**
	0.1	3.33††
	0.1	3.40§§
	0.2	4.16‡‡
	1.0	2.11**
	1.0	2.33¥¥
	1.0	2.67**
	1.0	4.68##
	3.0	3.18**
$NpO_2^+ + 2\ OH^- \leftrightarrow NpO_2(OH)_2^-$	0.005	9.2§
	0.01	8.6¥
	0.1	9.9§
	0.1	4.10**
	0.1	5.61††
	1.0	4.45**
	1.0	4.89¥¥
	1.0	4.41**
	3.0	5.15**

*Schmidt et al. 1980 †Sevost'yanova et al. 1976 §Nagasaki et al. 1988
‡Moskvin 1971b ¥Nakayama et al. 1988 #Kraus and Nelson 1948
**Neck et al. 1992 ††Rösch et al. 1987 §§Tait et al. 1995b
‡‡Bidoglio et al. 1985 ¥¥Lierse et al. 1985 ##Maya 1983

sis. A plot of these data is shown in Fig. 29. Obviously, the spread in the data makes it impossible to perform the extrapolation. A further examination of the experimental details of the publications leads us to exclude all values with log$\beta > 4.0$ because of improper calibration of electrodes, likely contamination by carbonate, or precipitation.

Neck et al. report an internally self-consistent study where the value of logβ_1 was determined at 0.1, 1.0, and 3.0 M ionic strength to be 2.44 ($\pm$ 0.16), 2.67 ($\pm$ 0.20), and 3.18 ($\pm$ 0.33), respectively, and this work appears to be of very high quality (Neck, et al. 1992). Tait et al. determined log$\beta_1 = 3.40 \pm 0.22$ for the equilibrium in Eqn. 32 in 0.1 M electrolyte (Tait et al. 1995b). Great care was taken to exclude carbonate contamination in both studies.

The introduction of unwanted carbonate or the formation of a precipitate would ultimately consume NpO_2^+ and, hence, would make the first hydrolysis constant appear greater than it actually is. Carbonate was eliminated in the experiment of Tait et al. as it would have resulted in a detectable new spectral absorbance peak at 991 nm, which was not observed. The possibility of precipitation requires closer examination.

From the room temperature data of Tait et al. (1995b), for which comparison can be made, half of the concentration of NpO_2^+ ion would have been converted by a pH of 10.5. The equilibrium solubility at this pH is calculated to be 9.6 μM (from Neck et al. (1992) with log$\beta_1 = 2.50$, log$\beta_2 = 4.16$, and log$K_{sp} = -8.56$) and 6.4 μM (from Itagaki et al. (1992) with log$\beta_1 = 3.49$, log$\beta_2 = 4.70$, and log$K_{sp} = -8.94$). Tait's experiments ranged from total neptunium concentrations of 1.5 to 4 μM and are, hence, well below the solubility limit reported from both literature sources. Furthermore, the temporal approach to equilibrium is shown by the work of Itagaki et al. (1992) in which the concen-

Table 26. Calculation of Thermodynamic Formation Constants for $NpO_2(OH)$ as a Function of Ionic Strength

I_M	$\log\beta_M$	I_m	$\Sigma\nu \log R$	$\log\beta_m$	$\Delta z^2 D = -2D$	$\log\beta_m + 2D$
0.001	5.2	0.001	0.0	5.2	−0.030	5.230
0.002	5.1	0.002	0.0	5.1	−0.042	5.142
0.005	5.7	0.005	0.0	5.7	−0.065	5.765
0.01	5.7	0.01	0.0	5.7	−0.088	5.788
0.02	5.1	0.02	0.0	5.1	−0.119	5.219
0.02	3.92	0.02	0.0	3.92	−0.119	4.039
0.1	6.0	0.1	−0.003	5.997	−0.218	6.215
0.1	3.33	0.1	−0.003	3.327	−0.218	3.545
0.1	2.44	0.1	−0.003	2.437	−0.218	2.655
0.1	4.9	0.1	−0.003	4.897	−0.218	5.115
0.1	3.40	0.1	−0.003	3.40	−0.218	3.68
0.2	4.16	0.2	−0.005	4.16	−0.273	4.428
1.0	2.11	1.05	−0.021	2.089	−0.411	2.500
1.0	2.67	1.05	−0.021	2.649	−0.411	3.060
1.0	2.33	1.05	−0.021	2.309	−0.411	2.720
1.0	4.68	1.05	−0.021	4.659	−0.411	5.070
3.0	3.18	3.50	−0.066	3.114	−0.500	3.614

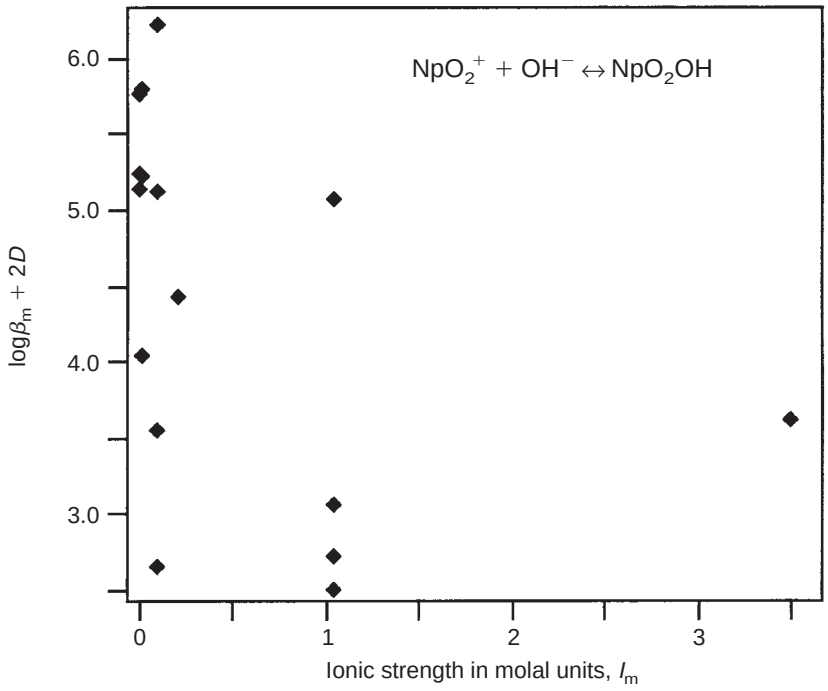

Figure 29. Formation of $NpO_2(OH)$. This plot of experimental data for the formation of $NpO_2(OH)$ using specific-ion interaction theory shows such a spread in the data that extrapolation to $I = 0$ is impossible.

tration remains ≥ 10 μM for several days for 0.1 M ionic-strength solutions even to a pH of 11. Thus we conclude that the value of $\log\beta_1 = 3.40 \pm 0.22$ reported by Tait et al. should be included in the analysis. A plot of only those data for which the room temperature $\log\beta_m < 4$ is shown in Fig. 30. Extrapolation of the data gives $\log\beta^0_1 = 2.82$ with $\Delta\epsilon = -0.16$. A similar SIT extrapolation was presented by Neck et al. that determined $\log\beta^0_1 = 2.7$ (± 0.2), which is in excellent agreement. Finally, using $\log K_w = -14.0$ at $I = 0$, we convert $\log\beta^0_1$ into $\log^*\beta^0_1 = -11.18$ (± 0.5). Therefore, we recommend the use of this last value for the formation of $NpO_2(OH)$.

We converted the literature data for $NpO_2(OH)_2^-$ into a form suitable for the SIT analysis, and the data for the reaction:

$$NpO_2^+ + 2\ OH^- \leftrightarrow NpO_2(OH)_2^- \qquad (33)$$
$$\Sigma\nu = -2,\ \Delta z^2 = -2\ ,$$

are shown in Table 27. A plot of these data is shown in Fig. 31. The same sets of experimental values were omitted as in the case of the first hydrolysis reaction.

From the data in Fig. 31, we find $\log\beta^0_2 = 4.92$ (± 0.5) with $\Delta\epsilon = -0.14$. This value can be compared to the zero ionic strength value of $\log\beta^0_2 = 4.35$ (± 0.15) calculated by Neck et al. Using $\log K_w = -14.0$ at $I = 0$, we convert $\log\beta^0_2$ into $\log^*\beta^0_2 = -23.08$ (± 0.5). This value is recommended for use in the Yucca Mountain Project.

In analogy with U(VI), Cassol et al. (1972) has evidence that the first hydrolysis product for Np(VI) is $NpO_2(OH)^+$ with $\log^*\beta_{11} = -5.17$ (± 0.03) in 1 M $NaClO_4$ solution. In a similar fashion, there is evidence for the formation of a dimer, $(NpO_2)_2(OH)_2^{2+}$, with $\log^*\beta_{22} = -6.68$ (± 0.02), and a trimer, $(NpO_2)_3(OH)_5^+$, with $\log^*\beta_{35} =$

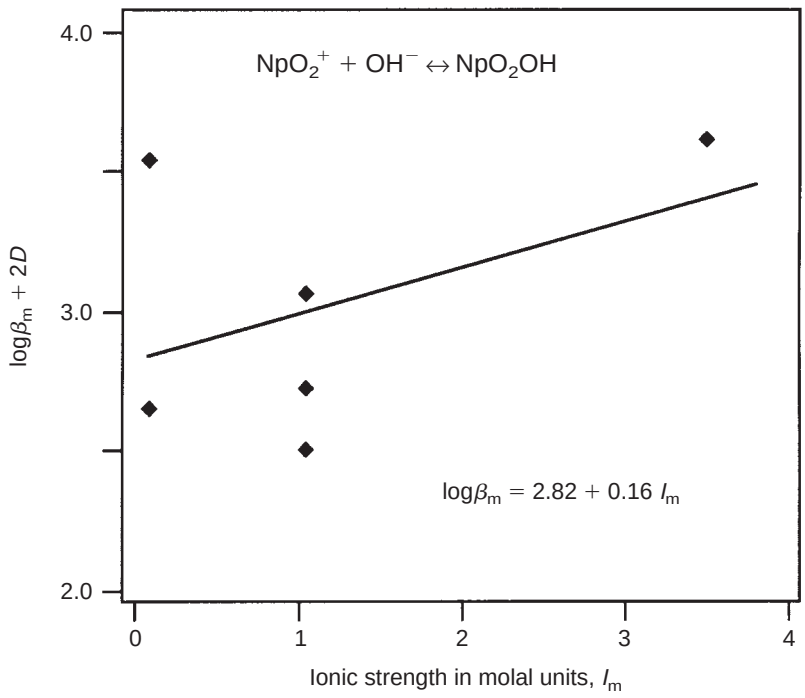

Figure 30. Formation of $NpO_2(OH)$: Refined Data. This plot is the same as that in Fig. 29 except that it uses only those data for which log $\beta_m < 4$, allowing extrapolation to $I = 0$ of formation data for $NpO_2(OH)$ using specific-ion interaction theory.

Table 27. Calculation of Thermodynamic Formation Constants for $NpO_2(OH)_2^-$ as a Function of Ionic Strength

I_M	$\log\beta_M$	I_m	$\Sigma\nu \log R$	$\log\beta_m$	$\Delta z^2 D = -2D$	$\log\beta_m + 2D$
0.1	4.10	0.1	−0.006	4.094	−0.218	4.312
0.1	5.61	0.1	−0.006	5.604	−0.218	5.822
1.0	4.45	1.05	−0.042	4.408	−0.411	4.819
1.0	4.89	1.05	−0.042	4.848	−0.411	5.259
1.0	4.41	1.05	−0.042	4.368	−0.411	4.779
3.0	5.15	3.50	−0.132	5.018	−0.500	5.518

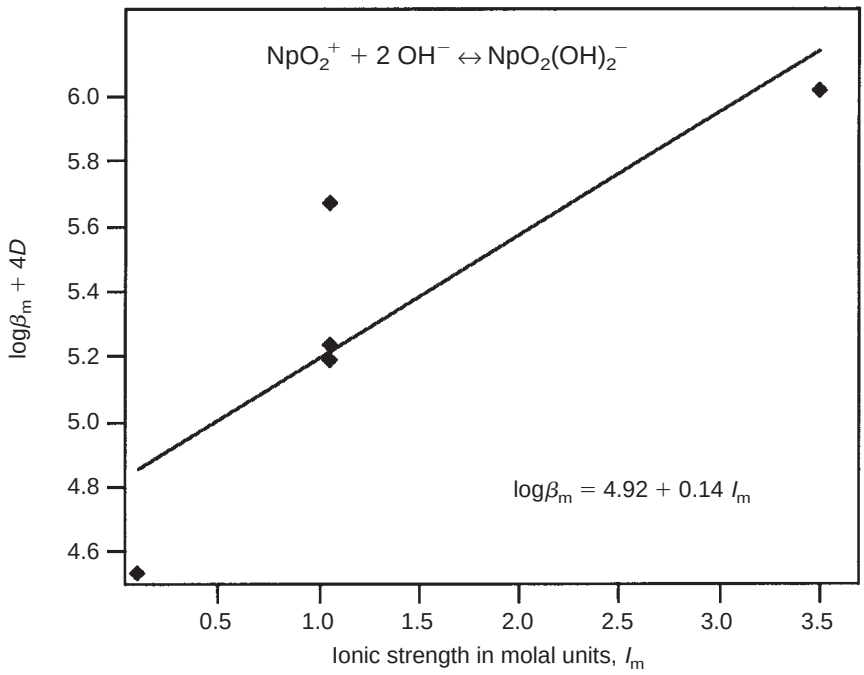

Figure 31. Formation of $NpO_2(OH)_2^-$. This plot shows extrapolation of experimental data to $I = 0$ for the formation of $NpO_2(OH)_2^-$ using specific-ion interaction theory.

−18.25 (± 0.02), both recalculated for a 1 M $NaClO_4$ solution (Cassol et al. 1972). Fuger has calculated the values at zero ionic strength to be $\log^*\beta^0_{11} = -5.0$ (± 0.3), $\log^*\beta^0_{22} = -6.4$ (± 0.3), $\log^*\beta^0_{35} = -19.6$ (± 0.5) (Fuger 1992).

Neptunium-carbonato complexes.
Moriyama and coworkers reported complexation constants of Np(IV) in carbonate solutions based on solubility data and suggested the formation of $Np(CO_3)_3^{2-}$ and $Np(CO_3)_4^{4-}$ in solution (Moriyama et al. 1989). More recently, Pratopo et al. (1990) reported a solubility study of the Np(IV)-carbonate system and concluded that mixed hydroxo-carbonato complexes were required to explain the data. Pratopo et al. proposed the formation of $Np(OH)_4(CO_3)_2^{4-}$ above a pH of 10 and $Np(OH)_2(CO_3)_2^{2-}$ below a pH of 10 (Pratopo et al.

1990). Representative thermodynamic formation constants for Np(IV) taken from the recent literature are listed in Table 28. Vitorge (1995) has reported a bibliography of references collected for the NEA review on neptunium. Although no review has taken place, Vitorge has analyzed much of the available data on Np(IV) and concludes that mixed hydroxo-carbonato complexes are not needed to fit the available data (Vitorge 1995). Vitorge has estimated the zero ionic-strength formation constant at $\log\beta_{15}$ for the formation of $Np(CO_3)_5^{6-}$ by analyzing all the data. These values are somewhat high when compared to uranium, and no recommendation is as yet available. We calculate the unweighted average from the analysis of Vitorge to be $\log^*\beta^0_{15} = 35.9\ (\pm\ 1.0)$. This value can be compared with the uranium value of 34.0 ($\pm$ 1.0).

There have been a variety of studies on the thermodynamic formation constants for neptunyl(V) complexes formed in carbonate media. A representative set of thermodynamic formation constants taken from the recent literature is given in Table 29.

There is ample spectrophotometric and solubility data supporting the formation of the monomeric complex Np(V) anions $NpO_2(CO_3)^-$, $NpO_2(CO_3)_2^{3-}$, and $NpO_2(CO_3)_3^{5-}$ in solution; and these monomers correlate nicely with the known solid-phase salts $MNpO_2(CO_3)$, $M_3NpO_2(CO_3)_2$, and $M_5NpO_2(CO_3)_3$ (where M is a monovalent cation). The formation constants for these species in solutions of ionic strength from 0.1 to 3.5 m have been determined by a number of researchers using a variety of methods. The thermodynamic formation constants for these complex anions are reasonably well understood (Table 29). The most reliable estimates come from Riglet (1990) and Neck et al. (1994), who examined spectrophotometric and solubility data obtained at various ionic strengths.

The first formation constant, $\log\beta_{11}$.
From the ratio values (R), $\log\beta_{11m}$ values were calculated for the first formation constant for molal concentrations, then a SIT analysis was performed for the formation of $NpO_2(CO_3)^-$ via the reaction:

$$NpO_2^+ + CO_3^{2-} \leftrightarrow NpO_2(CO_3)^- \qquad \Sigma\nu = -1,\ \Delta z^2 = -4\ . \tag{34}$$

Extrapolation to $I = 0$ was performed by plotting $\log\beta_{11m} + 4D$ versus I_m.

From the data in Table 30, a linear regression was performed. As expected, the data of Neck et al. (1994) at 5.0 M ionic strength was out of line (because SIT isn't really valid for $I_M > 3$ to 3.5 M). The final regression is shown in Fig. 32, which gives the extrapolated values and interaction terms both with and without the inclusion of the 5.0 M data. Interpolation without the inclusion of the 5.0 M ionic-strength data for the reaction gives the following zero ionic-strength value:

$$\log\beta^0_{11} = 4.81\ (\pm\ 0.5),\ \ \Delta\epsilon = -0.31\ . \tag{35}$$

This value is identical to the zero ionic-strength value of $\log^*\beta^0_{11} = 4.81\ (\pm\ 0.15)$ determined by Neck et al (1994).

Table 28. Equilibrium Constants of the Carbonate Complexes of Tetravalent Neptunium at Room Temperature

Reaction	I_M	log$K$
$Np^{4+} + 3\ CO_3^{2-} \leftrightarrow Np(CO_3)_3^{2-}$	0.3	37.1 ± 1.2*
$Np^{4+} + 4\ CO_3^{2-} \leftrightarrow Np(CO_3)_4^{4-}$	0.3	41.1 ± 1.4*
$Np^{4+} + 4\ OH^- + 2\ CO_3^{2-} \leftrightarrow Np(OH)_4(CO_3)_2^{4-}$	0.1	53.07 ± 0.44†

*Moriyama et al. 1989 †Pratopo et al. 1990 Note: $NaClO_4$ was used to adjust the ionic strength.

Table 29. Equilibrium Constants of the Carbonate Complexes of Pentavalent Neptunium at Room Temperature

Reaction	I_M	log$K$
$NpO_2^+ + CO_3^{2-} \leftrightarrow NpO_2(CO_3)^-$	0	4.69 ± 0.13*
	0.1	4.34 ± 0.11*
	0.1	4.58 ± 0.04†
	0.1	4.38 ± 0.04*
	0.2	4.13 ± 0.03§
	0.5	4.3 ± 0.1‡
	1.0	4.49 ± 0.06¥
	1.0	4.50 ± 0.04†
	1.0	4.14 ± 0.01#
	1.0	4.3 ± 0.2‡
	3.0	5.09**
	3.0	4.76 ± 0.04†
	5.0	5.00 ± 0.05†
$NpO_2^+ + 2\ CO_3^{2-} \leftrightarrow NpO_2(CO_3)_2^{3-}$	0.1	6.4 ± 0.3†
	0.2	7.06 ± 0.05§
	0.5	6.5 ± 0.2‡
	1.0	6.7 ± 0.3‡
	1.0	7.11 ± 0.02¥
	1.0	6.96 ± 0.06†
	1.0	6.78 ± 0.01#
	3.0	7.69± 0.07†
	3.0	8.15**
	5.0	8.29 ± 0.09†
$NpO_2^+ + 3\ CO_3^{2-} \leftrightarrow NpO_2(CO_3)_3^{5-}$	0.5	7.9 ± 0.2‡
	1.0	8.5 ± 0.4‡
	1.0	8.53 ± 0.095¥
	1.0	8.67 ± 0.09†
	3.0	10.46**
	3.0	10.30 ± 0.09†
	5.0	11.47 ± 0.08†

*Nitsche et al. 1990 †Neck et al. 1994 §Bidoglio et al. 1985 ‡Riglet 1990 ¥Maya 1983 #Inoue and Tochiyama 1985
**Grenthe et al. 1986b

As mentioned earlier, to account for the weakness in SIT at high ionic strengths, Ciavatta has proposed the use of a nonconstant $\Delta\epsilon$ (Ciavatta et al. 1981; Ciavatta et al. 1979)—specifically, in the form of Eqn. 11. When this is incorporated into the analysis, we obtain $\log\beta^0_{11} = 4.688$, $\Delta\epsilon_1 = -0.550$, and $\Delta\epsilon_2 = 0.3784$. This approach is plotted in Fig. 33. In this case, none of the data points is more than 0.4 log units from the SIT fit, suggesting that the database for the first carbonate complexation constant for neptunium(V) is in good shape at 25ºC. For consistency, we recommend

Table 30. Calculation of Thermodynamic Formation Constants for $NpO_2(CO_3)^-$ as a Function of Ionic Strength

I_M	I_m	$\log\beta_{11}$	$\log\beta_{11m}$	R	D	$\log\beta_{11m} + 4D$
0.1[c]	0.10076	4.58	4.583	1.0073	0.1095	5.021
0.1[b]	0.10076	4.38	4.383	1.0073	0.1095	4.821
0.1[b]	0.10076	4.34	4.343	1.0073	0.1095	4.781
0.2[a]	0.20236	4.13	4.131	1.0118	0.1367	4.6778
0.5[b]	0.5128	4.3	4.311	1.0256	0.1758	5.0142
1.0[c]	1.0499	4.50	4.521	1.0499	0.2056	5.3434
1.0[c]	1.0499	4.49	4.511	1.0499	0.2056	5.3334
1.0[a]	1.0499	4.14	4.161	1.0499	0.2056	4.9834
1.0[b]	1.0499	4.3	4.321	1.0499	0.2056	5.1434
3.0[c]	3.4956	5.09	5.156	1.1652	0.2502	6.1568
3.0[c]	3.4956	4.76	4.826	1.1652	0.2502	5.8268
5.0[c]	6.5711	5.00	5.119	1.3142	0.2694	6.1966

[a]Solvent extraction [b]Spectroscopy [c]Solubility

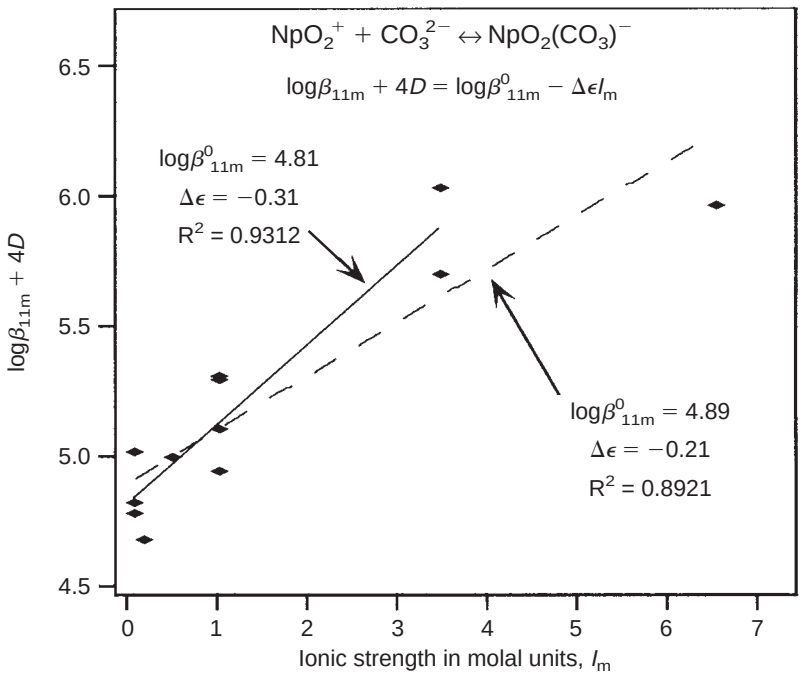

Figure 32. Formation of $NpO_2(CO_3)^-$. This plot shows two extrapolations of experimental data to $I = 0$ for the formation of $NpO_2(CO_3)^-$ using specific-ion interaction theory. The dashed curve uses all the data; the solid curve uses only those data with $I_m \leq 3.5$ m.

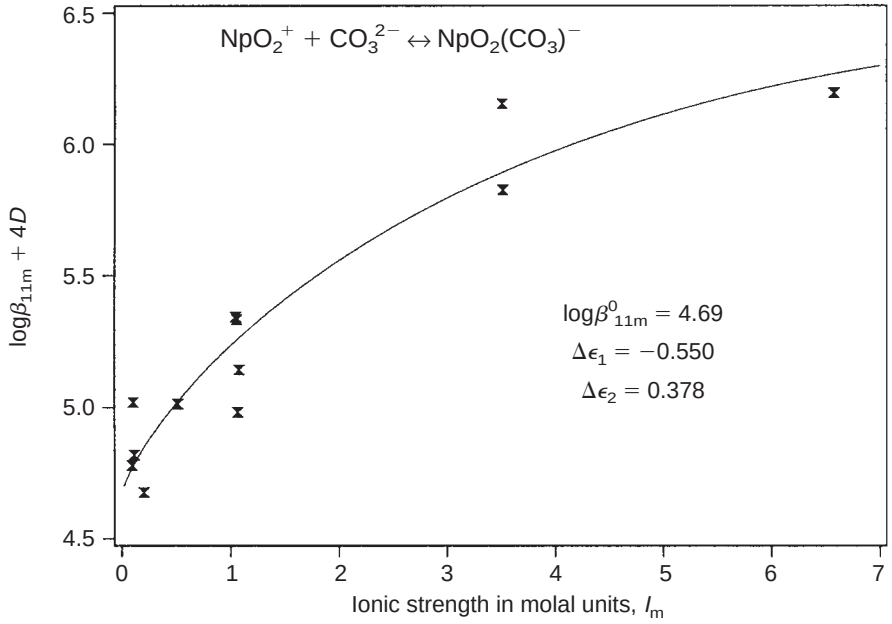

Figure 33. Formation of $NpO_2(CO_3)^-$: Nonconstant $\Delta\epsilon$. This plot shows the extrapolation of experimental data to $I = 0$ for the formation of $NpO_2(CO_3)^-$ using specific-ion interaction theory for nonconstant $\Delta\epsilon$, which may be more suitable for high ionic strengths than the linear approach of Fig. 32.

using the normal SIT extrapolated value of $\log^*\beta^0_{11} = 4.81\ (\pm\ 0.5)$.

The second formation constant, log β_{12}.
For the formation of $NpO_2(CO_3)_2^{3-}$:

$$NpO_2^+ + 2\ CO_3^{2-} \leftrightarrow NpO_2(CO_3)_2^{3-} \qquad \Sigma\nu = -2,\ \Delta z^2 = -0\ . \tag{36}$$

The literature data from Table 29 corrected to molality units and all other necessary terms are given in Table 31. The final regression is shown in Fig. 34, which gives the extrapolated values and interaction terms both with and without the inclusion of the 5.0 M data. Interpolation without the inclusion of the 5.0 M ionic-strength data for the reaction outlined in Eqn. 36 gives the zero ionic-strength value:

$$\log^*\beta^0_{12} = 6.52\ (\pm\ 0.5),\ \Delta\epsilon = -0.35\ . \tag{37}$$

As before, we have also performed the SIT analysis with nonconstant $\Delta\epsilon$, and this fit is shown in Fig. 35. As for the $\log\beta_{11}$ values, the database for $\log\beta_{12}$ values appears to be in good shape, with the data points generally falling within 0.4 log units of the SIT fit. Possible exceptions include the 0.2 M data point of Bidoglio et al. (1985) and the 3.5 m point of Grenthe et al. (1986b). The zero ionic-strength value of $\log^*\beta^0_{12} = 6.52\ (\pm\ 0.5)$ can be compared with the value of $\log^*\beta^0_{12} = 6.55$ $(\pm\ 0.23)$ determined by Neck et al. We recommend that the SIT extrapolated value reported here be used by the Yucca Mountain Project.

The third formation constant, $\log\beta_{13}$.
For the formation of $NpO_2(CO_3)_3^{5-}$:

$$NpO_2^+ + 3\ CO_3^{2-} \leftrightarrow NpO_2(CO_3)_3^{5-}\ , \tag{38}$$

$\Delta z^2 = 12$. The literature data for the reaction is listed in Table 32. Interpolation without the inclusion of the 5.0 M ionic-strength data (Fig. 36) gives the zero ionic-strength value:

$$\log^*\beta^0_{13} = 5.50\ (\pm\ 0.5),\ \Delta\epsilon = -0.52\ . \tag{39}$$

From the linearity of this plot, another analysis with nonconstant $\Delta\epsilon$ is not needed as it was above. Furthermore, all of the data fall within 0.3 log units

Table 31. Calculation of Thermodynamic Formation Constants for $NpO_2(CO_3)_2^{3-}$ as a Function of Ionic Strength

I_M	I_m	$\log\beta_{12}$	$\log\beta_{12m}$	R
0.1[c]	0.10073	6.60	6.594	1.0073
0.1[b]	0.10073	6.4	6.394	1.0073
0.2[a]	0.20236	7.06	7.050	1.0118
0.5[b]	0.5128	6.5	6.478	1.0256
1.0[c]	1.0499	7.11	7.068	1.0499
1.0[c]	1.0499	6.96	6.918	1.0499
1.0[a]	1.0499	6.78	6.738	1.0499
1.0[b]	1.0499	6.7	6.658	1.0499
3.0[c]	3.4956	8.15	8.017	1.1652
3.0[c]	3.4956	7.69	7.557	1.1652
5.0[c]	6.5711	8.29	8.053	1.3142

[a]Solvent extraction [b]Spectroscopy [c]Solubility

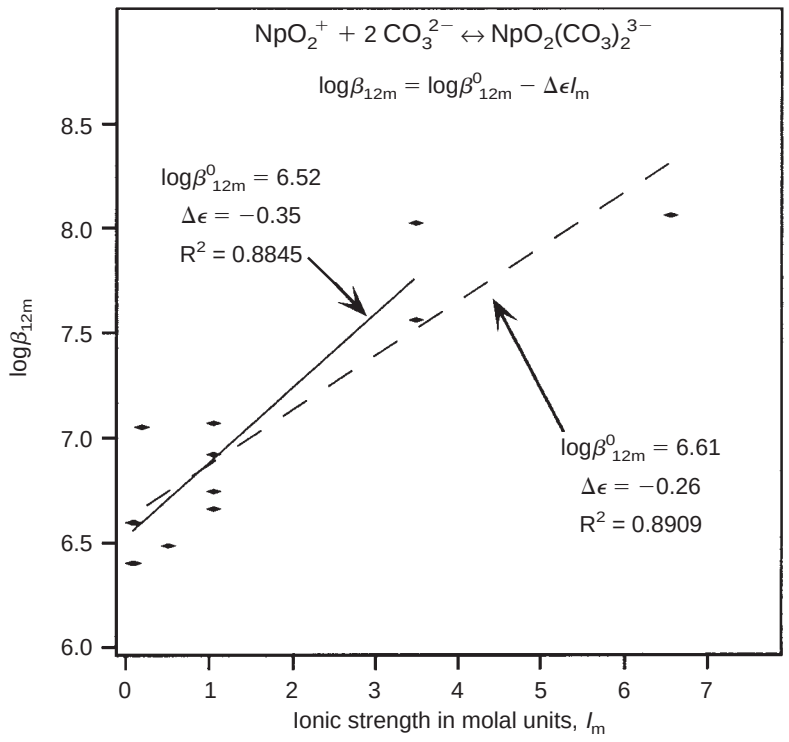

Figure 34. Formation of $NpO_2(CO_3)_2^{3-}$. This plot shows two extrapolations of experimental data to $I = 0$ for the formation of $NpO_2(CO_3)_2^{3-}$ using specific-ion interaction theory and a constant $\Delta\epsilon$. The dashed curve uses all the data; the solid curve uses only those data with $I_m \leq 3.5$ m.

of the SIT line, suggesting that this data set is quite good. The extrapolated value of $\log^*\beta^0_{13} = 5.50$ ($\pm$ 0.5) is in good agreement with the value of $\log^*\beta^0_{13} = 5.54$ ($\pm$ 0.09) determined by Neck et al. All three formation constants derived for Np(V)-carbonato complexes reported here are recommended for use in the Yucca Mountain Project.

The zero ionic-strength values obtained here for the Np(V)-carbonate system using a SIT extrapolation of data with $I_m \leq 3.5$ m (Fig. 36) gives results nearly identical to those obtained by Neck who performed a similar analysis (Neck et al. 1994).

As with other actinyl(VI) systems, the Np(VI) chemistry is quite complicated due to several different complex ions in rapid equilibria with one another and with the aquo ion or hydrolyzed species. Representative examples of the solution equilibria and their thermodynamic formation constants, taken from the recent literature, are listed in Table 33.

All of the relevant data on the neptunyl(VI) complexes point to the limiting monomeric species of general formulas $NpO_2(CO_3)$,

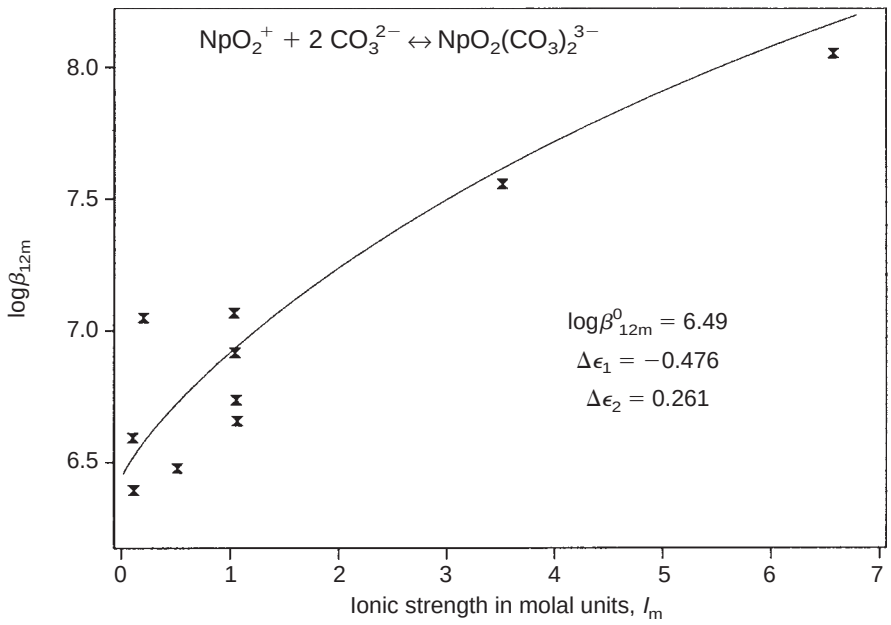

Figure 35. Formation of $NpO_2(CO_3)_2^{3-}$: Nonconstant $\Delta\epsilon$. This plot shows extrapolation of experimental data to $I = 0$ for the formation of $NpO_2(CO_3)_2^{3-}$ using specific-ion interaction theory and a nonconstant $\Delta\epsilon$, which may be more suitable for high ionic strengths than the linear approach of Fig. 34.

Table 32. Calculation of Thermodynamic Formation Constants for $NpO_2(CO_3)_3^{5-}$ as a Function of Ionic Strength

I_M	I_m	$\log\beta_{13}$	$\log\beta_{13m}$	R	D	$\log\beta_{13m} - 12D$
0.5[b]	0.5128	7.8	7.767	1.0256	0.1755	5.661
1.0[c]	1.0499	8.67	8.606	1.0499	0.2036	6.163
1.0[c]	1.0499	8.53	8.466	1.0499	0.2056	5.999
1.0[b]	1.0499	8.5	8.437	1.0499	0.2056	5.970
3.0[c]	3.4956	10.46	10.261	1.1652	0.2451	7.320
3.0[c]	3.4956	10.30	10.101	1.1652	0.2451	7.160
5.0[c]	6.5711	11.47	11.126	1.3024	0.2615	7.945

[a]Solvent extraction [b]Spectroscopy [c]Solubility

$NpO_2(CO_3)_2^{2-}$, and $NpO_2(CO_3)_3^{4-}$ (Grenthe et al. 1986a, 1986b; Maya 1984; Robouch and Vitorge 1987; Ullman and Schreiner 1988) being present under the appropriate conditions. Solution raman spectroscopic data are consistent with the maintenance of a linear O=An=O unit and bidentate carbonate ligands for $AnO_2(CO_3)_3^{4-}$ complexes in aqueous carbonate solutions of U(VI), Np(VI), Pu(VI), and Am(VI) (Basile et al. 1978; Madic et al. 1983; Nguyen-Trung et al. 1992). Bicarbonate complexes of AnO_2^{2+} have not been demonstrated to exist even in the pH ranges at which bicarbonate ions are present at higher concentrations than carbonate (Maya 1982b).

Maya found spectrophotometric evidence for a

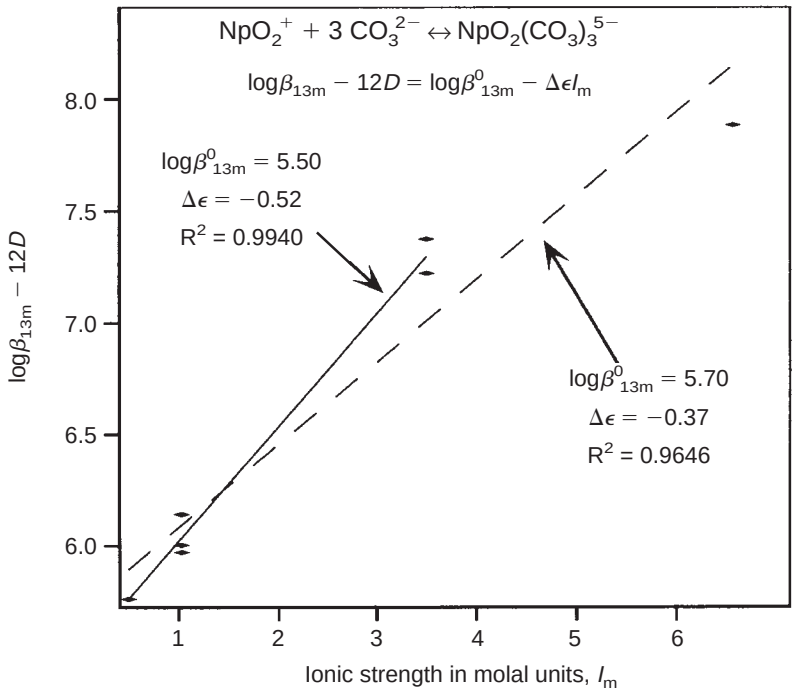

Figure 36. Formation of $NpO_2(CO_3)_3^{5-}$. The plot shows extrapolations of the experimental data to $I = 0$ for the formation of $NpO_2(CO_3)_3^{5-}$ using specific-ion interaction theory and constant $\Delta\epsilon$ and using all the data (dashed line) or only data with $I_m \leq 3.5$ m (solid line).

Table 33. Equilibrium Constants of the Carbonate Complexes of Hexavalent Neptunium at Room Temperature

Reaction	I_M	log$K$
$NpO_2^{2+} + 2\ CO_3^{2-} \leftrightarrow NpO_2(CO_3)_2^{2-}$	1.0	16.51*
	3.0	17.9†
		13.0‡
$NpO_2^{2+} + 3\ CO_3^{2-} \leftrightarrow NpO_2(CO_3)_3^{4-}$	1.0	21.15*
	3.0	22.1†
$3\ NpO_2^{2+} + 6\ CO_3^{2-} \leftrightarrow (NpO_2)_3(CO_3)_6^{6-}$	3.0	56.2†
$3\ NpO_2(CO_3)_3^{4-} \leftrightarrow (NpO_2)_3(CO_3)_6^{6-} + 3\ CO_3^{2-}$	3.0	-10.0 ± 0.1†

*Maya 1984 †Grenthe et al. 1986b ‡Moskvin 1971a

hydroxycarbonate dimer of formula $(NpO_2)_2(CO_3)(OH)_3^-$ in addition to the monomeric $NpO_2(CO_3)_2^{2-}$ (Maya 1984). More recent spectrophotometric and emf studies by Grenthe et al. suggest that the numerical values of the equilibrium constants and the chemical species reported by Maya may be incorrect (Grenthe et al. 1986a). Grenthe's work suggests that the trimeric complex $(NpO_2)_3(CO_3)_6^{6-}$ is the predominant solution species present at high ionic strength and high metal-ion concentration, consistent with the results for uranium (Grenthe et al. 1986a). The existence of both $NpO_2(CO_3)_3^{4-}$ and $(NpO_2)_3(CO_3)_6^{6-}$ species has been confirmed by ^{13}C and ^{17}O NMR spectroscopy within the Yucca Mountain Project (Tait et al 1995b). The monomeric $NpO_2(CO_3)_3^{4-}$ has only one type of carbonate ligand environment, giving rise to a single ^{13}C NMR

resonance ($\delta = 75.5$ ppm) at a pH of 8.0. The proposed trimeric structure for $(NpO_2)_3(CO_3)_6^{6-}$ (structure II on page 64) is expected to show two equal intensity resonances as observed at $\delta = 7.7$ and -88.6 ppm at a pH of 5.7. Variable temperature studies reveal a temperature-dependent chemical shift, and a line broadening in the low-field resonance, consistent with the assignment of the $\delta = 7.7$ resonance to a terminal carbonate ligand (Tait et al 1995b). The higher field resonance at $\delta = -88.6$ ppm does not undergo a line broadening with increasing temperature consistent with the assignment to a bridging carbonate ligand. Thus the ^{13}C NMR data are consistent with Grenthe's interpretation of spectrophotometric and emf data, supporting trimeric $(NpO_2)_3(CO_3)_6^{6-}$ as the dominant solution species at high ionic strength and metal-ion concentration. These data were used to calculate the equilibrium constant, $\log K_{eq} = 19.7$ ($\pm$ 0.8) at 2.5 m ionic strength for the reaction (Tait et al 1995b):

$$3\ NpO_2(CO_3)_3^{4-} + 3\ H^+ \leftrightarrow (NpO_2)_3(CO_3)_6^{6-} + 3\ HCO_3^-. \quad (40)$$

The consistency between the data for U(VI) and Np(VI) is very encouraging. Grenthe et al. have also reported spectroscopic evidence for the formation of $(PuO_2)_3(CO_3)_6^{6-}$ and of mixed metal $(UO_2)_2(AnO_2)(CO_3)_6^{6-}$ clusters, where An is Np or Pu (Grenthe et al. 1986a).

The thermodynamic data sets for Np(VI) carbonates are mostly incomplete. For those cases in which comparisons can be made, they are contradictory. The first set of data to consider are the $\log\beta_{1x}$ values. Clearly, there are very few constants from which to choose; there are no values for $\log\beta_{11}$ and inconsistent values for $\log\beta_{12}$. To judge between the values of $\log\beta_{12}$, we can resort to the oxidation-state analogy in which neighboring actinides of the same oxidation state are expected to have similar equilibrium constants. Care must be taken in using this approach, but it should at least point to the more reliable study in Table 33. To this end, we can compare the SIT analysis on U(VI)-carbonate $\log\beta_{1x}$ values.

Comparison of the Np(VI)-carbonate $\log\beta_{12}$ values with those determined for U(VI) yields the conclusion that the $\log\beta_{12}$ values reported by Maya (1984) and by Grenthe et al. (1986b) are more consistent with the U(VI) data and are, hence, considered more reliable and should be preferred over the value of Moskvin (1971a). Furthermore, the $\log\beta_{13}$ reported by Maya (1984) should also be tentatively used in modeling, as it comes from an apparently reliable study and is also consistent with the U(VI) $\log\beta_{13}$ values. The problem is one of recommending values at $I = 0$. There is simply not enough data on Np(VI)-carbonato complexes to perform the analysis, and no zero ionic-strength values can be recommended at this time.

Plutonium

Plutonium hydrolysis.

Pu(III) hydrolysis is not well known because Pu(III) is readily oxidized to Pu(IV) in anything but strong acid solutions. The first hydrolysis product, $Pu(OH)^{2+}$, was identified by Kraus and Dam who reported $\log\beta_{11} = 6.78$ in 0.07 M $NaClO_4$ (Kraus and Dam 1949).

The hydrolysis of Pu(IV) is extremely complicated. In 0.05 M acid solutions, $Pu(OH)^{3+}$ and $Pu^{4+}(aq)$ are present at about equal concentrations (Newton 1975). At lower acid concentrations, further hydrolysis is reported to give the ions $Pu(OH)_2^{2+}$ and $Pu(OH)_3^+$, and the neutral species $Pu(OH)_4$ (equivalent to $PuO_2{\cdot}2H_2O$) (Kim and Kanellakopulos 1989; Lierse 1986; Pazukhin and Kudryavtsev 1990). Formation constants have been estimated for these species, but the majority of literature references report the first hydrolysis product for the formation of $Pu(OH)^{3+}$. The paucity of data for further hydrolysis products is due to the formation of colloidal $PuO_2{\cdot}2H_2O$ under the solution conditions required for existence of these soluble hydrolyzed species, as discussed in the report on YMP milestone 4026 (Clark 1994). The most recent Pu(IV) hydrolysis experiments have been reported by Lierse (1986), Kim and

Kanellakopulos (1989), and Pazukhin and Kudryavtsev (1990). The hydrolysis constants reported by Lierse (1986) and by Pazukhin and Kudryavtsev (1990) agree reasonably well. Representative values taken from Pazukhin and Kudryavtsev are $\log\beta_{11} = 12.48$, $\log\beta_{12} = 24.28$, $\log\beta_{13} = 35.53$, and $\log\beta_{14} = 46.43$ at an ionic strength of 3.0 M (Pazukhin and Kudryavtsev 1990). Again, this raises the question as to what values can be used for $I = 0$ calculations.

Pu(V) in the form of PuO_2^+ does not hydrolyze below a pH of 9, at which $PuO_2(OH)$ forms with $\log\beta_{11} = 4.05$ ($\pm$ 0.1) in 0.1 M $NaClO_4$ (Bennett et al. 1992). This value would correspond to a $\log^*\beta_{11} = -9.73$ ($\pm$ 0.1), which can be compared to -11.18 ($\pm$ 0.5) calculated here for neptunium, and is the only value available for use in modeling.

Pu(VI) exists mainly as the free PuO_2^{2+} ion at low plutonium concentrations in acidic solutions. At higher pH, $PuO_2(OH)^+$, $PuO_2(OH)_2$, $PuO_2(OH)_3^-$, $(PuO_2)_2(OH)_2^{2-}$ and $(PuO_2)_3(OH)_5^+$ have been proposed with, respectively, $\log\beta_{11} = 8.26$, $\log\beta_{12} = 14.91$, $\log\beta_{13} = 16.90$, $\log\beta_{22} = 21.98$, and $\log\beta_{35} = 56.28$ in 0.1 M $NaClO_4$ (Kim et al. 1984). There are still multiple questions regarding the identity of many of the hydrolyzed plutonium species for the oxidation states of environmental interest. Using $\log K_w = -13.78$ (0.1 M $NaClO_4$), we calculate $\log^*\beta_{11} = -5.52$, $\log^*\beta_{12} = -12.65$, $\log^*\beta_{13} = -24.44$, $\log^*\beta_{22} = -5.58$, and $\log^*\beta_{35} = -12.62$. These can be compared with the corresponding values for uranium, which are $\log^*\beta_{11} = -5.2$, $\log^*\beta_{12} = -10.30$, $\log^*\beta_{13} = -19.20$, $\log^*\beta_{22} = -5.62$, and $\log^*\beta_{35} = -15.55$. It is seen that the hydrolysis constants for the 1:1 and 2:2 complexes, $\log^*\beta_{11} = -5.52$ and $\log^*\beta_{22} = -5.58$, appear quite reasonable when compared with uranium data, whereas $\log^*\beta_{12}$, $\log^*\beta_{13}$, and $\log^*\beta_{35}$ differ by several orders of magnitude and should be used with caution.

Despite the importance of hydrolysis reactions, the literature data for the first Pu(VI) hydrolysis vary by $\sim$ 3 orders of magnitude, even at room temperature (Table 34) (Pashalidis et al. 1995). Even values from the same laboratory have changed with time as the workers refine experimental techniques. As an example, values ranging from $\log\beta_{11} = 8.84$ ($\pm$ 0.30) to 8.10 ($\pm$ 0.15) have been reported from Kim's lab in Germany (Pashalidis et al. 1995; Pashalidis et al. 1993). This spread in data is actually rather small, and the values, again, are very similar to the accepted values for uranium.

To further complicate this situation, Reed's group at Argonne has made a convincing case that what most investigators have actually determined is β_{22} rather than β_{11}, that is, the formation of dimeric $(PuO_2)_2(OH)_2^{2+}$ rather than $(PuO_2)OH^+$ (Okajima and Reed 1993). Therefore, at least some of the scatter is due to the different plutonium concentrations used in the various experiments reported in the literature. Although this dimer has been reported to exist down to at least 69 mM plutonium con-

Table 34. Equilibrium Constants for the First Hydrolysis of Pu(IV) to Form $Pu(OH)^{3+}$ at Room Temperature.

Method	Medium	$\log\beta_{11}$
potentiometric titration	1 M $NaClO_4$	8.07*
solubility	0.01 M $NaClO_4$	10.45[†]
solubility	NH_4ClO_4	10.39[§]
potentiometric titration	1 M $NaClO_4$	7.83[‡]
spectroscopy	0.1 M $NaClO_4$	9.88[¥]
pulse radiolysis	——	7.7[#]
solubility	0.1 M $NaClO_4$	8.26[¥, **]
spectroscopy	0.1 M $NaClO_4$	8.58[††]
spectroscopy	1 M $NaClO_4$	8.69[§§]
spectroscopy	0.1 M $NaClO_4$	8.10[§§]

*Kraus and Dam 1949 [†]Krevinskaia et al. 1959
[§]Moskvin and Zaitseva 1962 [‡]Cassol et al. 1972
[¥]Musante and Porthault 1973 [#]Schmidt et al. 1983
**Lierse and Kim 1986 [††]Okajima and Reed 1993
[§§]Pashalidis et al. 1993

centration, the monomer is still the more environmentally relevant species because of the low concentrations expected in the field (Okajima and Reed 1993). However, the value for $\log\beta_{11}$ reported in YMP letter report 4091 places a limit of $\log\beta_{11} < 8.7$ (Tait et al. 1996). Comparison to Table 34 therefore allows us to eliminate the values of Krevinskaia (1959), Moskvin and Zaitseva (1962), and Musante and Porthault (1973) from further consideration. We conclude that the data are too sparse for a rational decision to be made at this time. If we exclude the above mentioned data for the reasons described, we calculate an unweighted average $\log\beta_{11} = 8.4$ ($\pm$ 0.5), which at $I = 0.1$ M, corresponds to $\log^*\beta_{11} = -5.4$ ($\pm$ 0.5) and is comparable to the uranium value of -5.2 ($\pm$ 0.3) and the neptunium value of -5.0 ($\pm$ 0.3). Until further data can be collected and analyzed, this value could be used.

Plutonium-carbonato complexes.
There is a great deal of scatter in the Pu(IV)-carbonate formation constants reflecting the extreme difficulties encountered when working with aqueous Pu(IV). The Pu(IV) aquo ion is notoriously unstable in aqueous solution, being prone to rapid hydrolysis, and the formation of colloidal Pu(IV) is a pervasive problem in all Pu(IV) complexation studies. Silva described spectrophotometric and complex competition experiments leading to a lower limit for the binding constant for $Pu(CO_3)^{2+}$ of $\log\beta_{11} > 13$ (Silva 1985). Lierse performed solubility studies of Pu(IV) in carbonate solutions and interpreted the results in terms of stepwise formation constants for the series of ions $Pu(CO_3)^{2+}$, $Pu(CO_3)_2$, $Pu(CO_3)_3^{2-}$, $Pu(CO_3)_4^{4-}$, and $Pu(CO_3)_5^{6-}$ in analogy with the reported solid phases. His valves are given in Table 35 (Lierse 1986). Lierse's value for the first complex formation constant of $\log\beta_{11} = 17$ is many orders of magnitude lower than the original values discussed by Newton and Sullivan (1985) and appears to be a much more reasonable value for a mono-ligand complex.

However, it is likely that these constants will be highly correlated, and careful consideration of the mathematical and statistical details is necessary. In fact, it was previously pointed out in the report for YMP milestone 3350 (Tait et al. 1995a) that the fit of the data of Lierse et al. used too many species, thereby casting doubt on the simple $Pu(CO_3)_x$ (with no OH^- ligand) picture. Using a combination of conventional absorption spectroscopy and photoacoustic absorption spectroscopy (PAS) over a broader pH and carbonate concentration range, at least four different plutonium species have been found as characterized by absorption peaks at 485, 492, 500, and 513 nm. The best interpretation of the data for carbonate concentrations greater than 10 mM requires the following simultaneous equations:

$$Pu(OH)_x(CO_3)_y^{4-(x+2y)} + H_2O \leftrightarrow Pu(OH)_{x+1}(CO_3)_y^{4-(x+1+2y)} + H^+ , \quad (41)$$

$$Pu(OH)_x(CO_3)_y^{4-(x+2y)} + CO_2 + H_2O \leftrightarrow Pu(OH)_x(CO_3)_{y+1}^{4-(x+(2y+1))} + 2\,H^+ , \quad (42)$$

Table 35. Equilibrium Constants of the Carbonate Complexes of Tetravalent Plutonium at Room Temperature

Reaction	I_M	log$K$
$Pu^{4+} + CO_3^{2-} \leftrightarrow Pu(CO_3)^{2+}$	0.3	17.0 ± 0.7*
$Pu^{4+} + 2\,CO_3^{2-} \leftrightarrow Pu(CO_3)_2$	0.3	29.9 ± 0.96*
$Pu^{4+} + 3\,CO_3^{2-} \leftrightarrow Pu(CO_3)_3^{2-}$	0.3	39.1 ± 0.82*
$Pu^{4+} + 4\,CO_3^{2-} \leftrightarrow Pu(CO_3)_4^{4-}$	0.3	42.9 ± 0.75*
$Pu^{4+} + 5\,CO_3^{2-} \leftrightarrow Pu(CO_3)_5^{6-}$	0.3	44.5 ± 0.77*
$Pu^{4+} + 2\,CO_3^{2-} + 4\,OH^- \leftrightarrow Pu(OH)_4(CO_3)_2^{4-}$	≈ 0.1	46.4 ± 0.7†

*Lierse 1986 †Yamaguchi et al. 1993
Note: $NaClO_4$ was used to adjust the ionic strength in these studies.

where $\log K = -8.14$ for Eqn. 41 and -15.72 for Eqn. 42.

Comparison with a recent solubility report (Yamaguchi et al. 1994) with low carbonate concentrations suggests $x = 1$ and $y = 2$. They determined that mixed hydroxo-carbonato compounds of general formula $Pu(OH)_x(CO_3)_y$ must be present (Yamaguchi et al. 1994). The equilibria were quite complicated and multiple mixed-ligand complexes were detected. Yamaguchi et al. studied the solubility of Pu(IV) in carbonate solutions and concluded that mixed hydroxy-carbonate complexes were needed to fit the data. They interpreted their results in terms of the formation of $Pu(OH)_2(CO_3)_2^{2-}$ below a pH of 10 and $Pu(OH)_4(CO_3)_2^{4-}$ at pH values greater than 10 (Yamaguchi et al. 1994). Note that the presence of mixed hydroxo-carbonato Pu(IV) compounds is more consistent with the parallel finding of mixed hydroxo-carbonato U(IV) compounds discussed above. This observation should be tempered by the fact that Vitorge (1995) has argued that in the Np(IV) case, mixed hydroxo-carbonato complexes are not needed to fit the Np(IV) data, whereas at the same time, Grenthe notes that mixed hydroxo-carbonato complexes are likely to be important for U(IV) at pH values below 7 (Grenthe et al. 1992). We cannot recommend any thermodynamic formation constants to be used for Pu(IV)-carbonato complexes at this time. Further data will need to be obtained. However, our bias, as derived from our own work for YMP (Clark et al. 1994; Tait et al. 1995a), is to reject the $Pu(CO_3)_x^{4-2x}$ species equilibria in favor of the mixed $Pu(OH)_x(CO_3)_y^{4-x-2y}$ complexes.

For Pu(V)-carbonato complexes, Bennett and coworkers determined the formation constant for $PuO_2(CO_3)^-$ using photoacoustic spectroscopy (PAS), then employed the specific-ion interaction theory to calculate a formation constant at zero ionic strength (Table 36) (Bennett et al. 1992). This value compares favorably with the corresponding $\log^*\beta_{11}$ for the $NpO_2(CO_3)^-$ analog. We recommend that this value of $\log^*\beta_{11} = 5.12\ (\pm\ 0.07)$ be adopted. No evidence for mixed hydroxo-carbonato species was found in this study, in which hydrolysis behavior of the PuO_2^+ ion was also investigated. The formation constant for the triscarbonato species, $PuO_2(CO_3)_3^{5-}$ was determined by Lierse using the formation constant of $PuO_2(CO_3)_3^{4-}$ and the one-electron reduction potential between the two species in analogy to Eqn. 28 (Lierse 1985).

The formation of Pu(VI)-carbonato complexes is less controversial. Unlike the Pu(IV) case described above, mixed hydroxo-carbonato complexes are not required, consistent with U(VI)- and Np(VI)-carbonato complexes. A survey of the literature data on these carbonate complexes is shown in Table 37. The principle values involve the reaction of PuO_2^{2+} with one-, two-, and three-carbonate ligands. The outlier appears to be $\log\beta = 15.1$ for the formation of the bis complex (Ullman and Schreiner 1988). Aside from this value, the progression in complexes from mono to bis and from bis to tris follows a consistent increase of $\sim$5 log units for $\log\beta$, as would be expected from such a progression. Furthermore, these values are $\sim$3 log units less than the corresponding values for Np(VI)-carbonate and U(VI)-carbonate complexes (Clark et al. 1995b), which are themselves quite similar. Finally, the formation of the trimer $(PuO_2)_3(CO_3)_6^{6-}$ has been reported by Grenthe et al (1986a), but direct evidence from EXAFS, NMR, and Raman spectroscopies has not

Table 36. Equilibrium Constants of the Carbonate Complexes of Pentavalent Plutonium at Room Temperature

Reaction	I_M	$\log K$
$PuO_2^+ + CO_3^{2-} \leftrightarrow PuO_2(CO_3)^-$	0	5.12 ± 0.07*
	0.5	4.60 ± 0.04*
$PuO_2^+ + 3\ CO_3^{2-} \leftrightarrow PuO_2(CO_3)_3^{5-}$	1[a]	10.0 ± 2.1*

*Bennett et al. 1992 [a]Na_2CO_3 electrolyte

Table 37. Equilibrium Constants of the Carbonate Complexes of Hexavalent Plutonium at Room Temperature

Reaction	I_M	log$K$
$PuO_2^{2+} + CO_3^{2-} \leftrightarrow PuO_2(CO_3)$	3.5	8.6 ± 0.3*
$PuO_2(OH)_2 + 2\ HCO_3^- \leftrightarrow PuO_2(CO_3)_2^{2-} + 2\ H_2O$	0.1	4.4†
$PuO_2^{2+} + 2\ CO_3^{2-} \leftrightarrow PuO_2(CO_3)_2^{2-}$	0[a]	15.1§
	0.1	13.1 ± 0.1†
	3.5	13.6 ± 0.7*
$PuO_2^{2+} + 3\ CO_3^{2-} \leftrightarrow PuO_2(CO_3)_3^{4-}$	0	18.5§
	3.5	18.2 ± 0.4*
$3\ PuO_2(CO_3)_3^{4-} \leftrightarrow (PuO_2)_3(CO_3)_6^{6-} + 3\ CO_3^{2-}$	3.0	−7.4 ± 0.2‡

*Robouch and Vitorge 1987 †Sullivan et al. 1982 §Ullman et al. 1988 ‡Grenthe et al. 1986a
[a]$NaClO_4/Na_2SO_4$ electrolyte, I_m = 0 data calculated; $NaClO_4$ was used to adjust the ionic strength in all other studies

been found as it has for the uranyl and neptunyl cases (Neu et al. 1995; Clark et al. 1995b; Allen et al. 1995).

Americium

Americium hydrolysis.

Am(III) is expected to be the dominant oxidation state of americium in natural waters. Hydrolysis reactions of Am(III) are not significant even at near-neutral pH values. Stadler and Kim investigated the hydrolysis of Am(III) in aqueous-perchlorate media and in carbonate-free saline solutions using solubility (Stadler and Kim 1988). They were able to derive hydrolysis constants for $Am(OH)^{2+}$, $Am(OH)_2^+$, and $Am(OH)_3$ of $\log\beta_{11} = 6.3\ (\pm\ 0.3)$, $\log\beta_{12} = 12.2\ (\pm\ 0.4)$, and $\log\beta_{13} = 14.4\ (\pm\ 0.5)$ in 0.1 M $NaClO_4$ solution (Stadler and Kim 1988). Using $\log K_w = -13.78$, we calculate $\log^*\beta_{11} = -7.48\ (\pm\ 0.3)$, $\log^*\beta_{12} = -15.36\ (\pm\ 0.4)$, and $\log^*\beta_{13} = -26.94\ (\pm\ 0.5)$. These constants seem very reasonable when compared to those found for Pu(III). An interesting aspect of this work is that in concentrated NaCl solutions ($I_m > 3$, pH > 7), alpha radiolysis generates substantial amounts of oxidized chlorine species, which subsequently oxidize Am(III) to Am(V). These researchers also provide a thorough review of published americium hydrolysis studies (Stadler and Kim 1988; Runde and Kim 1994). Representative hydrolysis constants for Am(III) are presented in Table 38.

The recently published NEA review of americium has discussed the hydrolysis of Am(III) in some detail and re-evaluated published data in cases where discrepancies existed or where results of doubtful interpretation were reported (Silva et al. 1995). The study of Am(III) hydrolysis is very complicated due to experimental difficulties in preventing precipitation and adsorption. The NEA review concluded that there is ample evidence for the existence of $Am(OH)^{2+}$, $Am(OH)_2^+$, and $Am(OH)_3$ but no experimental data for the existence of anionic hydrolysis complexes such as $Am(OH)_4^-$ (Silva et al. 1995). The experimental data for Am(III) hydrolysis spans an extremely wide range, complicating the interpretation by the NEA. For example, data on the first hydrolysis constant, $\log\beta_1$, spans six orders of magnitude! The reviewers were able to discount a reasonable portion of the data, but the data are still widely scattered. This problem is exacerbated by the fact that data from the same investigators using different techniques (solubility versus speciation) can also span half a log unit. Therefore, the NEA reviewers chose to use an unweighted average of the values extrapolated to $I = 0$ and derived values of $\log^*\beta^0_1 = -6.4\ (\pm\ 0.7)$ and $\log^*\beta^0_2 = -14.1\ (\pm\ 0.6)$ for the following reactions:

$$Am^{3+} + H_2O(l) \leftrightarrow Am(OH)^{2+} + H^+ \quad , \quad (43)$$

$$Am^{3+} + 2\ H_2O(l) \leftrightarrow Am(OH)_2^+ + 2\ H^+ \ . \quad (44)$$

Table 38. Formation Constants of the Hydrolysis Complexes of Trivalent Americium at Room Temperature

Reaction	I_M	log$K$
$Am^{3+} + H_2O \leftrightarrow Am(OH)^{2+} + H^+$	0	-6.4 ± 0.7*
	0.1	-5.92 ± 0.11†
	0.1	-7.5 ± 0.3§
	0.1	-7.7 ± 0.3‡
	0.1	-7.5 ± 0.2¥
	1.0	-7.03 ± 0.04#
	3.0	-6.40 ± 0.11**
$Am^{3+} + 2\ H_2O \leftrightarrow Am(OH)_2^+ + 2\ H^+$	0	-14.1 ± 0.6*
	0.1	-16.7 ± 0.7‡
	0.1	-15.4 ± 0.3¥
	3.0	-13.40 ± 0.16**
$Am^{3+} + 3\ H_2O \leftrightarrow Am(OH)_3 + 3\ H^+$	0	-25.7 ± 0.5*
	0.1	-25.0 ± 0.3‡
	0.1	-26.9 ± 0.2¥
	3.0	-20.31 ± 0.17**

*Silva et al. 1995 †Désiré et al. 1969 §Lundqvist 1982 ‡Silva 1982
¥Stadler and Kim 1988 #Nair et al. 1982 **Pazukhin and Kochergin 1989

A recalculation and extrapolation to $I = 0$ using the data of Stadler and Kim (1988) provided $\log{}^*\beta^0_3 = -25.7\ (\pm\ 0.5)$ for the reaction (Silva et al. 1995):

$$Am^{3+} + 3\ H_2O(l) \leftrightarrow Am(OH)_3 + 3\ H^+ \quad . \quad (45)$$

Due to the spread in the data, and complications in the Am(III) hydrolysis system just described, the NEA reviewers have done about as well as can be expected. This area is clearly deserving of more study, particularly when other, more sophisticated techniques become available.

Americium-carbonato complexes. Am(III)-carbonate complexation has been studied by spectrophotometry, solubility, potentiometry, and solvent extraction techniques. However, the number of experimental studies to derive thermodynamic formation constants for the Am(III)-carbonate system are rather limited. Nitsche et al. used absorption spectrophotometry to determine $\log\beta_{11}$ for formation of $Am(CO_3)^+$ in 0.1 M perchlorate solution (Nitsche et al. 1989). Felmy and coworkers studied the solubility of $Am(OH)(CO_3)$ over a wide range of conditions and proposed the formation of $Am(CO_3)^+$, $Am(CO_3)_2^-$, and $Am(CO_3)_3^{3-}$, consistent with the known solids (Felmy et al. 1990). Meinrath and Kim examined the absorption and photoacoustic spectroscopy of Am(III) species under a 1% CO_2 atmosphere. $Am_2(CO_3)_3$ precipitated and was found to be the solubility-controlling solid under those conditions. Parallel solubility and spectroscopic studies were performed for this study, and the data were consistent with the formation of $Am(CO_3)^+$ and $Am(CO_3)_2^-$ (Meinrath and Kim 1991a). Meinrath's and Kim's value for $\log\beta_{11}$ is in good agreement with that reported by Nitsche. Bernkoff and Kim used a model containing mono-, bis-, and tris-carbonato complexes as well as mixed hydroxo-carbonato complexes to fit americium-carbonate solubility data using $Am(CO_3)(OH)$ as the solid phase (Bernkopf and Kim 1984). The NEA review on americium thermodynamics argued that the solid phase in Bernkoff and Kim's work was not characterized and decided not to consider mixed hydroxo-carbonato complexes in the NEA analysis (Silva et al. 1995). For Am(III), this decision seems justified since hydroxo-carbonato complexes are not needed to fit the solubility data, and unlike the tetravalent actinides, there is no spectroscopic data to support the formation of these complexes for Am(III). The NEA provides a thorough review of the data presented by Bernkopf and Kim (1984) and demonstrates a faulty assumption regarding the nature of the solid phase. For this

reason, the data of Bernkopf and Kim should be treated as suspect. Giffaut and Vitorge reported evidence for radiolytic oxidation of $^{241}Am(III)$ to $^{241}Am(V)$ under CO_2 atmospheres and indicated that the slow kinetics of precipitation can induce experimental uncertainties in solubility measurements for these intensely radioactive isotopes (Giffaut and Vitorge 1993). Representative thermodynamic formation constants for Am(III)-carbonate complexes are given in Table 39.

Table 39. Equilibrium Constants of the Carbonate Complexes of Trivalent Americium at Room Temperature

Reaction	I_M	log$K$
$Am^{3+} + CO_3^{2-} \leftrightarrow Am(CO_3)^+$	0	7.8 ± 0.3*
	0	7.6†
	0.1	6.69 ± 0.15§
	0.1	5.08 ± 0.92‡
	0.1[a]	7.7 ± 0.18¥
	0.1[c]	6.48 ± 0.03#
	0.1[b]	5.97 ± 0.15#
	1.0	5.3 ± 0.4**
	1.0	5.81 ± 0.04**
	3.0	5.45 ± 0.12††
	5.0[a]	5.7 ± 0.4§§
$Am^{3+} + 2\ CO_3^{2-} \leftrightarrow Am(CO_3)_2^-$	0	12.3 ± 0.4*
	0	12.3†
	0.1	9.27 ± 2.2‡
	0.1[c]	9.94 ± 0.24#
	0.1[b]	9.58 ± 0.24#
	0.2	11.45 ± 0.08‡‡
	1.0	9.72 ± 0.10**
	3.0	8.92 ± 0.15††
	5.0[a]	9.7 ± 0.5§§
$Am^{3+} + 3\ CO_3^{2-} \leftrightarrow Am(CO_3)_3^{3-}$	0	15.2 ± 0.6*
	0	15.2†
	0.1	12.12 ± 0.85‡
	3.0	11.44 ± 0.12††
	5.0[a]	12.9 ± 0.2§§
$Am^{3+} + CO_3^{2-} + OH^- \leftrightarrow Am(OH)(CO_3)$	0.1	12.15 ± 0.15‡
$Am^{3+} + 2\ CO_3^{2-} + OH^- \leftrightarrow Am(OH)(CO_3)_2^{2-}$	0.1	16.16 ± 0.14‡
$Am^{3+} + CO_3^{2-} + 2\ OH^- \leftrightarrow Am(OH)_2(CO_3)^-$	0.1	18.29 ± 0.17‡

*Silva et al. 1995 †Felmy et al. 1990 §Nitsche et al. 1989 ‡Bernkopf and Kim 1984
¥Giffaut and Vitorge 1993 #Meinrath and Kim 1991b **Lundqvist 1982
††Robouch 1989 §§Runde and Kim 1994 ‡‡Bidoglio 1982
[a]NaCl electrolyte; $NaClO_4$ was used to adjust the ionic strength in all other studies
[b]Solubility [c]Speciation

Americium(IV) is generally very unstable with respect to reduction or disproportionation in non-complexing aqueous solutions, but it can be stabilized in carbonate solutions (Hobart et al. 1982). Tetravalent actinide carbonate solids have only been well studied for thorium and uranium. The aqueous solution chemistry of the tetravalent actinide-carbonate complexes is extremely complex. Bourges and coworkers reported formal potentials for the Am(III)-Am(IV) couple in carbonate solution and concluded that there were two more carbonate ligands bound to the Am(IV) ion than in the Am(III) complex (Bourges et al.1983). This observation prompted Grenthe and coworkers to propose the formation of $Am(CO_3)_5^{6-}$ with $\log\beta_{15} \approx 40$. This value agrees relatively well with that reported for the uranium analog (Grenthe et al. 1986b). The NEA review on americium used the Gibbs energy of formation to

derive $\log\beta^0_{15} = 39.3 (\pm 2.1)$ (Silva et al. 1995).

Ferri, Grenthe, and Salvatore recalculated previous redox data of Bourges et al. (1983) for the AmO_2^{2+}/AmO_2^{+} redox couple in carbonate media (Ferri et al. 1983). This reinterpretation indicates that AmO_2^{+} forms a limiting carbonate complex $AmO_2(CO_3)_3^{5-}$ with approximately the same formation constant as found for the analogous uranyl(V) species. One problem with extrapolation of the formation constants of $AmO_2(CO_3)_3^{5-}$ to zero ionic strength arises from the strong ion pairing between cations such as Na^+ and the penta-anion. Runde and Kim determined the formation constants for the formation of $AmO_2(CO_3)^{-}$, $AmO_2(CO_3)_2^{3-}$, and $AmO_2(CO_3)_3^{5-}$ from solubility data in 3 and 5 M NaCl, and the values collected at $I = 3.0$ are shown in Table 40 (Runde and Kim 1994). These values compare extremely well with the values of $\log\beta_{11} = 4.76 (\pm 0.04)$, $\log\beta_{12} = 7.69 (\pm 0.07)$, and $\log\beta_{13} = 10.30 (\pm 0.09)$ determined at $I = 3.0$ by Neck et al. (1994).

Concluding Remarks

Both carbonate and hydroxide strongly complex actinide ions and will affect the mobility of actinide ions in natural groundwater systems. Therefore, identification of the carbonate complexes and determination of the thermodynamic parameters associated with their formation is a crucial area of study. Advances in the last decade can be attributed, in part, to the application of many new techniques for the study of actinide speciation including photothermal (PAS, PTL) and laser-induced fluorescence (LIF) spectroscopies, extended x-ray absorption fine structure (EXAFS), laser-resonance ionization mass spectroscopy, improved trace analyses, combined extraction methods, and NMR spectroscopy. It is expected that further applications of these new techniques will greatly expand our understanding of these systems in the future.

In general, actinyl(VI)-carbonate systems are quite complicated in that they consist of several complex ions in rapid equilibria with one another and with the aquo ion or hydrolyzed species. In aqueous solution, there is little doubt that the important species are $AnO_2(CO_3)$, $AnO_2(CO_3)_2^{2-}$, $AnO_2(CO_3)_3^{4-}$, and $(AnO_2)_3(CO_3)_6^{6-}$ (for An = U, Np, and possibly Pu). For uranyl there is also a great deal of evidence for the additional polymeric species $(UO_2)_2(CO_3)(OH)_3^{-}$, $(UO_2)_3O(OH)_2(HCO3)^{+}$, and $(UO_2)_{11}(CO_3)_6(OH)_{12}^{2-}$; the corresponding neptunyl, plutonyl, and americyl-carbonate systems need further study. However, quantitative thermodynamic data are still needed for the Np(VI) and Pu(VI) hydrolysis and carbonate systems.

For pentavalent actinide carbonates in solution, the carbonato complexes $AnO_2(CO_3)_n^{(2n-1)-}$ ($n = 1$, 2, or 3, An = Np, Pu, or Am) have been observed. Consistent quantitative data are available for all three monocarbonato complexes and for the bis-carbonato-neptunyl complex.

Table 40. Equilibrium Constants of the Carbonate Complexes of Pentavalent Americium at Room Temperature

Reaction	I_M	log$K$
$AmO_2^{+} + CO_3^{2-} \leftrightarrow AmO_2(CO_3)^{-}$	3	4.74 ± 0.09*
$AmO_2^{+} + 2\ CO_3^{2-} \leftrightarrow AmO_2(CO_3)_2^{3-}$	3	7.42 ± 0.03*
$AmO_2^{+} + 3\ CO_3^{2-} \leftrightarrow AmO_2(CO_3)_3^{5-}$	3	9.54 ± 0.13*

*Runde and Kim 1994 Note: NaCl electrolyte was used in these studies.

From a perusal of the variety of proposed An(IV) hydrolysis and carbonate species and their corresponding thermodynamic formation constants, there is clearly no uniform, accurate model. For example, the major species for Th(IV) and U(IV) are clearly identified as

$Th(CO_3)_5^{6-}$ and $U(CO_3)_5^{6-}$; whereas for Pu(IV), the entire series $Pu(CO_3)_n^{4-2n}$ ($n = 1 - 5$) has been proposed. Clearly, the widely scattered nature of the carbonate formation constants for tetravalent plutonium and the question of whether mixed hydroxy-carbonates $Pu(OH)_n(CO_3)_2^{n-}$ ($n = 2$ or 4) or $Pu(CO_3)_n^{4-2n}$ ($n = 1 - 5$) are the predominant solution species illustrate the difficulty in identifying properly the solution species and determining their thermodynamic stabilities. Most studies of Th, U, Np, and Pu do indicate that mixed hydroxy-carbonate complexes are important in describing the aqueous solution behavior. It is also quite evident from consideration of available thermodynamic data that the Np(IV) and Pu(IV) hydrolysis systems are extremely complicated and the plutonium system is in need of further study.

The compositions of trivalent actinide-carbonate complexes are well established. In aqueous solution, there is evidence for the stepwise formation of $An(CO_3)^+$, $An(CO_3)_2^-$, and $An(CO_3)_3^{3-}$ for An = Am and Cm. In a similar fashion, the hydrolysis complexes for Am(III) are known to be $Am(OH)^{2+}$, $Am(OH)_2^-$, and $Am(OH)_3$.

Clearly, there are many areas of actinide research that require further study to define the nature of contaminants, to predict how actinides may behave in natural systems, to explore alternative methods for industrial processes and effluent treatment, to find acceptable methods for remediation and transuranic waste storage, and to manage responsibly the transuranic elements so their unique properties may be used.

We have demonstrated the utility of using the SIT formalism to compare and judge thermodynamic equilibrium constants required by the YMP for solubility and sorption measurements. A recalculation of relevant values for uranium and americium demonstrate consistency with the two NEA thermodynamic reviews, and it is recommended that the Yucca Mountain Site Characterization Project adopt these values. We have performed SIT analysis on Np and Pu data and provide recommendations for those cases in which enough literature data exist to perform the analysis. In those cases for which there were inadequate data, we provide some limited recommendations on which literature values to use based on comparisons with know parameters for adjacent actinide elements.

We have also shown the use of a $\Delta\epsilon$ that is dependent on I_m. Whether there is physical justification for this or not, the extra degree of freedom allowed all the data to be fit with a single SIT curve over the entire range of experimental I_m and is, therefore, operationally an attractive option. Furthermore, it has been discussed in the NEA uranium volume and is, therefore, a defensible standard. Note that even in the more complicated Pitzer approach to ionic-strength corrections, physical reality is certainly compromised. For instance, the existence of solution species such as $CaCl^+$ and $CaCl_2$ is well known but ignored in the strict Pitzer approach. The approach makes up for this physical simplification by adding tertiary terms to the interaction coefficients, effectively using additional degrees of freedom to obtain good fits, just as we may have done for the simpler SIT formalism.

Finally, Table 41 lists our recommended thermodynamic formation constants for use in the Yucca Mountain Site Characterization Project. In this table, we also denote whether the recommended values were obtained under a QA program. These are the recommended values for use in performance-assessment calculations, and other similar data in the many different databases should be replaced by these values.

Table 41. Recommended Thermodynamic Formation Constants (in log*β_m format) for Use in the Yucca Mountain Site Characterization Project

Reaction	I_M	log*β_m	QA[†]
Thorium			
$Th^{4+} + 5\ CO_3^{2-} \leftrightarrow Th(CO_3)_5^{6-}$	0	23.5	N
$Th^{4+} + H_2O \leftrightarrow Th(OH)^{3+} + H^+$	0.5	−4.16	N
$Th^{4+} + 3\ H_2O \leftrightarrow Th(OH)_3^+ + 3\ H^+$	0.5	−11.22	N
$Th^{4+} + 4\ H_2O \leftrightarrow Th(OH)_4 + 4\ H^+$	0.5	−15.95	N
$2\ Th^{4+} + 2\ H_2O \leftrightarrow Th_2(OH)_2^{6+} + 2\ H^+$	0.5	−6.71	N
$2\ Th^{4+} + 3\ H_2O \leftrightarrow Th_2(OH)_3^{5+} + 3\ H^+$	0.5	−8.22	N
Uranium			
$U^{4+} + H_2O \leftrightarrow U(OH)^{3+} + H^+$	0	−0.54 ± 0.3	Y*
$UO_2^{2+} + H_2O \leftrightarrow UO_2(OH)^+ + H^+$	0	−5.2 ± 0.3	Y*
$2\ UO_2^{2+} + 2\ H_2O \leftrightarrow (UO_2)_2(OH)_2^{2+} + 2\ H^+$	0	−5.2 ± 0.3	Y*
$3\ UO_2^{2+} + 4\ H_2O \leftrightarrow (UO_2)_3(OH)_4^{2+} + 4\ H^+$	0	−11.9 ± 0.3	Y*
$3\ UO_2^{2+} + 5\ H_2O \leftrightarrow (UO_2)_3(OH)_5^+ + 5\ H^+$	0	−15.55 ± 0.12	Y*
$2\ UO_2^{2+} + H_2O \leftrightarrow (UO_2)_2(OH)^{3+} + H^+$	0	−2.7 ± 1.0	Y*
$3\ UO_2^{2+} + 7\ H_2O \leftrightarrow (UO_2)_3(OH)_7^- + 7\ H^+$	0	−31.0 ± 2.0	Y*
$4\ UO_2^{2+} + 7\ H_2O \leftrightarrow (UO_2)_4(OH)_7^+ + 7\ H^+$	0	−21.90 ± 1.0	Y*
$U^{4+} + 5\ CO_3^{2-} \leftrightarrow U(CO_3)_5^{6-}$	0	34.0 ± 0.9	Y*
$UO_2^{2+} + 3\ CO_3^{2-} \leftrightarrow UO_2(CO_3)_3^{5-}$	0	7.41 ± 0.27	Y*
$UO_2^{2+} + CO_3^{2-} \leftrightarrow UO_2(CO_3)$	0	9.68 ± 0.04	Y*
$UO_2^{2+} + 2\ CO_3^{2-} \leftrightarrow UO_2(CO_3)_2^{2-}$	0	16.94 ± 0.12	Y*
$UO_2^{2+} + 3\ CO_3^{2-} \leftrightarrow UO_2(CO_3)_3^{4-}$	0	21.60 ± 0.05	Y*
$3\ UO_2^{2+} + 6\ CO_3^{2-} \leftrightarrow (UO_2)_3(CO_3)_6^{6-}$	0	54.00 ± 1.0	Y*,[‡]
$2\ UO_2^{2+} + CO_2(g) + 4\ H_2O(l) \leftrightarrow (UO_2)_2CO_3(OH)_3^- + 5\ H^+$	0	−19.01 ± 0.50	Y*
$11\ UO_2^{2+} + 6\ CO_2(g) + 18\ H_2O(l) \leftrightarrow (UO_2)_{11}(CO_3)_6(OH)_{12}^{2-} + 24\ H^+$	0	−72.5 ± 2.0	Y*
$3\ UO_2^{2+} + CO_2(g) + 4\ H_2O(l) \leftrightarrow (UO_2)_3O(OH)_2HCO_3^+ + 5\ H^+$	0	−17.5 ± 0.5	Y*
Neptunium			
$NpO_2^+ + H_2O \leftrightarrow NpO_2(OH) + H^+$	0	−11.18 ± 0.5	Y[‡]
$NpO_2^+ + 2\ H_2O \leftrightarrow NpO_2(OH)_2^- + 2\ H^+$	0	−22.81 ± 0.5	N
$NpO_2^{2+} + H_2O \leftrightarrow NpO_2(OH)^+ + H^+$	0	−5.0 ± 0.3	N
$2\ NpO_2^{2+} + 2\ H_2O \leftrightarrow (NpO_2)_2(OH)_2^{2+} + 2\ H^+$	0	−6.4 ± 0.3	N

Table 41 continued. Recommended Thermodynamic Formation Constants (in log*β_m format) for Use in the Yucca Mountain Site Characterization Project

Reaction	I_M	log*β_m	QA[†]
Neptunium continued			
$3\ NpO_2^{2+} + 5\ H_2O \leftrightarrow (NpO_2)_3(OH)_5^{+} + 5\ H^{+}$	0	-17.5 ± 0.5	N
$Np^{4+} + 5\ CO_3^{2-} \leftrightarrow Np(CO_3)_5^{6-}$	0	35.9 ± 1.0	N
$NpO_2^{+} + CO_3^{2-} \leftrightarrow NpO_2(CO_3)^{-}$	0	4.81 ± 0.5	Y[‡]
$NpO_2^{+} + 2\ CO_3^{2-} \leftrightarrow NpO_2(CO_3)_2^{3-}$	0	6.52 ± 0.5	Y[‡]
$NpO_2^{+} + 3\ CO_3^{2-} \leftrightarrow NpO_2(CO_3)_3^{5-}$	0	5.50 ± 0.5	Y[‡]
Plutonium			
$PuO_2^{+} + H_2O \leftrightarrow PuO_2(OH) + H^{+}$	0.1	-9.73 ± 0.5	N
$PuO_2^{2+} + H_2O \leftrightarrow PuO_2(OH)^{+} + H^{+}$	0	-5.4 ± 0.5	Y[‡]
$2\ PuO_2^{2+} + 2\ H_2O \leftrightarrow (PuO_2)_2(OH)_2^{2+} + 2\ H^{+}$	0	-5.54 ± 0.5	N
$3\ PuO_2^{2+} + 5\ H_2O \leftrightarrow (PuO_2)_3(OH)_5^{+} + 5\ H^{+}$	0	-12.5 ± 0.5	N
$PuO_2^{+} + CO_3^{2-} \leftrightarrow PuO_2(CO_3)^{-}$	0	5.12 ± 0.07	N
Americium			
$Am^{3+} + H_2O \leftrightarrow Am(OH)^{2+} + H^{+}$	0	-6.4 ± 0.7	Y*
$Am^{3+} + 2\ H_2O \leftrightarrow Am(OH)_2^{+} + 2\ H^{+}$	0	-14.1 ± 0.6	Y*
$Am^{3+} + 3\ H_2O \leftrightarrow Am(OH)_3 + 3\ H^{+}$	0	-25.7 ± 0.5	Y*
$Am^{3+} + CO_3^{2-} \leftrightarrow Am(CO_3)^{+}$	0	7.8 ± 0.3	Y*
$Am^{3+} + 2\ CO_3^{2-} \leftrightarrow Am(CO_3)_2^{-}$	0	12.3 ± 0.4	Y*
$Am^{3+} + 3\ CO_3^{2-} \leftrightarrow Am(CO_3)_3^{3-}$	0	15.2 ± 0.6	Y*

[†]The recommended values listed in this table are extrapolations to zero ionic strength (Standard Solution Condition) done, when possible, through the SIT formalism. Because Yucca Mountain waters are expected to be low ionic strength, the final computational values are adequately modified in EQ3/6 with the B-dot method for the ionic strength that is actually being contemplated, and subsequently, the corresponding $\Delta\epsilon$ values are not listed. Moreover, because several data points were used to obtain the zero ionic strength numbers, different levels of QA are possible for the recommended values as described below:

Y* = values can be considered to be QA data because of their agreement with published tables from the NEA volumes.

Y[‡] = some (but not all) of the data points in the regression were obtained under YMP QA procedures.

B. SOLUBILITY LIMITS

Radionuclide migration would be mitigated by several barriers in a potential repository. One of the initial barriers is the solubility of the radionuclides in any water that infiltrates the potential repository. The solubility of neptunium, plutonium, and americium will depend on solution speciation (especially with OH^- and CO_3^{2-} ligands) and on the solubility-limiting actinide-bearing solid. Bulk solubility experiments can provide empirical data directly, but since they are long-term experiments, only a limited amount of data can be collected over a limited range of conditions. To determine solubility for general conditions, the system must be modeled thermodynamically. The model can be tested against the solubility found from the bulk experiments prior to being used in the general cases for performance assessment. Therefore, our short-term goal has been to provide solubilities from bulk experiments that attempt to bracket our current estimate of groundwater conditions that might exist. Intermediate goals have been to develop the thermodynamic data for solution speciation and solid-state determination as a prerequisite for modeling the results using the chemical-equilibrium code EQ3/6. Once this model is self-consistent and tests well against known solubilities, the long-term goal will be to use the model over a continuous, weighted-distribution range of potential groundwaters to generate a weighted distribution of solubilities that could be used in the performance assessment. This distribution would have a clear, documented path (using quality-assured protocol) for acquiring solubility numbers for the total-system performance assessment (TSPA) that does not resort to "expert elicitation."

Neptunium

Recent measurements (Efurd et al. 1996) have shown that the bulk solubility of neptunium in J-13 water ranges from 6×10^{-6} to 10^{-3} M (top values in Table 42). This study strived to minimize the ionic strength that, in a previous study (lower values in brackets in Table 42), was induced by controlling pH (Nitsche et al. 1993a). The reduced ionic strength resulted in solubilities up to an order of magnitude lower. Furthermore, the solubility-limiting solid was predominately (but not exclusively) Np_2O_5 rather than the double-carbonate salt $NaNpO_2CO_3 \cdot xH_2O$. For water conditions expected at Yucca Mountain, the data for Np(V) solutions (in the previous section, "Specific-ion Interaction Theory Studies") is consistent, and modeling with the EQ3/6 computer code suggests the dominate species to be a combination of NpO_2^+ and $NpO_2CO_3^-$ (Janecky et al. 1994, 1995). The current state of modeling is to decide on which set of Np(IV) data to use (especially the solid-state formation constants). Recent modeling work at Los Alamos indicates Np(IV) solids may form in Yucca Mountain waters (Janecky et al. 1994, 1995), depending on which solid-state numbers are used. The importance of this observation is that Np(IV) solids may be much less soluble than the Np(V) solids currently considered in the performance-assessment calculations (Efurd et al. 1996).

Plutonium

The same study (Efurd et al. 1996) showed that the bulk solubility of plutonium in J-13 water extends over a relatively narrow range from 4×10^{-9} to 5×10^{-8} M (top values in Table 43). The values

Table 42. Solubility of Neptunium (in M) in J-13 Waters

Top values from Efurd et al. (1996).
Lower values (brackets) from Nitsche et al. (1993a).

T(°C)	pH = 5.9	pH = 7.0	pH = 8.5
25	6.5×10^{-4} [5.3×10^{-3}	3.1×10^{-5} 1.3×10^{-4}	1.5×10^{-5} 4.4×10^{-5}]
60	9.4×10^{-4} [6.4×10^{-3}	1.6×10^{-5} 9.8×10^{-4}	1.7×10^{-5} 1.0×10^{-4}]
90	0.9×10^{-3} [1.2×10^{-3}	7.9×10^{-6} 1.5×10^{-4}	5.5×10^{-6} 8.9×10^{-5}]

are again generally lower than those reported previously by Nitsche et al. (1993a). Both studies agree that the predominate solubility-limiting solid is a Pu(IV) oxide polymer at 25ºC that ages to the more crystalline PuO_2(s) at 90ºC. Controversies involving solution speciation have been noted (in the previous section, "Specific-ion Interaction Theory Studies"), and because of the uncertainties about the solution thermodynamic constants, modeling work is still in the preliminary stages (Janecky et al. 1994, 1995). The model calculates that plutonium speciation is dominated by $Pu(OH)_5^-$ in J-13 water and the solids PuO_2(s) and $Pu(OH)_4$(s) are supersaturated to saturated (Janecky et al. 1994). Some of the current sets of data, such as the alternate composite data set (data0.alt.R1b) provided by Lawrence Livermore National Laboratory, can be dismissed from this early modeling work.

Table 43. Solubility of Plutonium (in M) in J-13 Waters

Top values from Efurd et al. (1996).
Lower values (brackets) from Nitsche et al. (1993a).

T(˚C)	pH = 5.9	pH = 7.0	pH = 8.5
25	4.7×10^{-8} [1.1×10^{-6}	2.4×10^{-8} 2.3×10^{-7}	0.9×10^{-8} 2.9×10^{-7}]
60	0.9×10^{-8} [2.7×10^{-8}	0.8×10^{-8} 3.8×10^{-8}	0.6×10^{-8} 1.2×10^{-7}]
90	4.3×10^{-9} [6.2×10^{-9}	3.6×10^{-9} 8.8×10^{-9}	4.2×10^{-9} 7.3×10^{-9}]

Americium

Because of americium's low solubility (Table 44) and high sorption coefficients (Meijer 1992), less emphasis has been placed on this radionuclide in the Yucca Mountain Project. The bulk solubility experiment of Nitsche et al. (1993a) is summarized in Table 44, and the solubility is observed to range from 3×10^{-10} to 4×10^{-6}, with the latter value possibly a bad datum point as judged by its neighboring values in the table. Note that the 25 and 90ºC experiments were carried out with a mixture of Nd^{3+} and ^{241}Am, whereas the 60ºC experiment was carried out both with the mixture and with pure ^{243}Am (both gave comparable results). The use of Nd^{3+} as a surrogate and carrier for the americium stems from the belief that only Am(III) (and no other oxidation state) is important in solutions (Nitsche et al. 1993a), although such an assumption was challenged in the higher-temperature bulk-solubility study of americium from undersaturation in UE-25 p#1 water by Hobart and co-workers (Becraft et al. 1994). The solubility-limiting solid was reported to be a mixture of hexagonal and orthorhombic forms of $AmOHCO_3$ (Nitsche et al. 1993a), but this assertion is controversial, and more work needs to be done to confirm or reject this statement. Only preliminary modeling of americium has been done in which the predominate solution species was calculated to be $AmCO_3^+$ in J-13 water except at 90ºC and a pH of 8, in which case the dominant species was calculated to be $Am(CO_3)_2^-$ (Janecky et al. 1994). Furthermore, the hydroxo solids $Am(OH)_3$ and amorphous $Am(OH)_3$ were calculated to be significantly below saturation throughout the experimental conditions for the bulk solubility study (Janecky et al. 1994). The only solid to approach saturation in these calculations was $AmOHCO_3$.

Table 44. Solubility of Americium (in M) in J-13 Waters

All values from Nitsche et al. (1993a).

T(˚C)	pH = 5.9	pH = 7.0	pH = 8.5
25	1.8×10^{-9}	1.2×10^{-9}	2.4×10^{-9}
60	3.6×10^{-6}	5.5×10^{-9}	1.6×10^{-8}
90	1.7×10^{-9}	3.1×10^{-10}	3.4×10^{-10}

C. SOLUBILITY-LIMIT VALUES RECOMMENDED FOR PERFORMANCE ASSESSMENT

Assumptions about Groundwater Chemistry

Solubility is a function of groundwater chemistry. The water chemistry at Yucca Mountain is summarized in section C, "Yucca Mountain Waters," of chapter I (for example, Table 3) and was reviewed by Meijer (1992). The concentration of the major cations and anions in unsaturated-zone groundwaters appears to be intermediate between the saturated-zone tuffaceous waters (Well J-13) and waters from the carbonate Paleozoic aquifer (Well UE-25 p#1). Consequently, the first assumption made to recommend values for the performance assessment was that the water from these two wells be taken to bound the chemistry of the groundwaters at Yucca Mountain.

Most of the waters at Yucca Mountain are oxidizing. Two basic container types are being considered for the potential repository: a thin stainless-steel or alloy container and a large container with a thick iron shroud over a thin stainless-steel or alloy liner ("a robust container"). The large amounts of iron in the robust container would result in a reducing environment, although it is not clear how long that reducing environment would last. The conservative approach is to assume that groundwaters that move from the repository to the accessible environment are oxidizing because radionuclides (such as the actinides and technetium) have higher solubilities in oxidizing than in reducing waters. Consequently, the second assumption was to consider solubility under oxidizing conditions only.

The third assumption was that the solubilities would be best determined by the far-field environment. The increased temperature from the repository may cause more aggressive groundwater chemistries and increased solubilities for radionuclides in the near field; however, when the solute is transported out of the near field, the potentially lower solubilities in the far field would cause precipitation and, thus, would be the limiting factor. This assumption is due primarily to the dirth of information about the near-field water chemistry, which made accurate predictions of solubility impossible for this region. It must be noted that the high thermal loads being considered for the potential repository (for example, 114 kilowatts per acre) may cause near-field conditions to extend throughout the unsaturated zone.

Dependence of Solubility on Temperature

The functional dependence of solubility with temperature can be expressed with thermodynamic rigor. However, this approach requires knowing the thermodynamic solubility products (K_{sp}°) of the dominating dissolution reactions. The thermodynamic treatment to obtain the functional dependence of an equilibrium constant (such as K_{sp}°) with temperature, which follows, is only valid when considering the same chemical reaction attaining equilibrium at different temperatures.

The symbols used in this derivation are:

K_{sp}° = solubility product,

G = Gibbs free energy,

$\Delta G = \sum_{\text{products}} G_i - \sum_{\text{reactants}} G_i$,

° refers to reactants and products in their standard state (1 atm, zero ionic strength),

H = enthalpy,

S = entropy,

R = gas constant,

T = temperature,

C_p = heat capacity at constant pressure, and

a, b, c are constants.

First, at constant T, the laws of thermodynamics give

$$\Delta G = \Delta H - T\Delta S \ . \qquad (46)$$

The functional dependence of the heat capacity of a substance with temperature is described by

$$C_p = a + bT + cT^{-2} \quad . \tag{47}$$

Thus, the functional dependence of ΔC_p with temperature, where ΔC_p is the sum of the heat capacities of the products minus the corresponding sum for the reactants (that is, the net change in heat capacity resulting from the reaction), is given by

$$\Delta C_p = \Delta a + \Delta bT + \Delta cT^{-2} \quad . \tag{48}$$

Next, Kirchoff's formula is

$$\Delta C_p = \left[\frac{\partial(\Delta H)}{\partial T} \right]_p \quad . \tag{49}$$

Substituting Eqn. 48 for ΔC_p in Eqn. 49 and then integrating yields

$$\Delta H = \Delta H_i + \Delta aT + \frac{1}{2}\Delta bT^2 - \Delta cT^{-1} \quad , \tag{50}$$

where ΔH_i is an integration constant. We can now take the partial derivative of Eqn. 46 with respect to temperature at constant pressure to get

$$\left[\frac{\partial(\Delta G/T)}{\partial T} \right]_p = -\frac{\Delta H}{T^2} \quad , \text{or}$$

$$\left[\frac{\partial(\Delta G/T)}{\partial(1/T)} \right]_p = \Delta H \quad . \tag{51}$$

Substituting for ΔH using Eqn. 50 and integrating either form of Eqn. 51 yields

$$\Delta G = \Delta H_i - \Delta aT \ln T - \frac{1}{2}bT^2 - \frac{1}{2}\Delta cT^{-1} + iT \quad , \tag{52}$$

where i is another integration constant.

The solubility product is related to Gibbs free energy by

$$\Delta G^o = -RT \ln K_{sp}^{\circ} \quad . \tag{53}$$

Substituting Eqn. 52 for $\Delta G°$ in this equation yields, after algebraic rearrangement,

$$-R \ln K_{sp}^{\circ} = \frac{\Delta H_i^o}{T} - \Delta a \ln T - \frac{1}{2}\Delta bT - \frac{1}{2}cT^{-2} + i \quad , \tag{54}$$

an equation that describes the functional dependence of the solubility product with respect to temperature.

Limitations of Empirical Solubility Data

With regard to the Laboratory's empirical solubility data for actinides (Nitsche et al. 1993a), it is important to make the following observations: 1) Nitsche et al. only report solubility data obtained from oversaturation, 2) the solid phases reported at 25ºC and 60ºC for neptunium do not match the solid phases found at 90ºC, 3) information on the solid phases of plutonium formed is not available, and 4) it is not clear that equilibrium is obtained in the time scale of the experiments. These observations are important for the following reasons: 1) Deriving a K_{sp} from the data of Nitsche et al. requires knowing the dissolution reaction and knowing that the same reaction takes place across the desired temperature range. It is not clear that this is the case for either neptunium or plutonium. 2) If equilibrium is not attained during the solubility experiments, the variability of the solubility data with temperature could be a result of kinetic effects. In particular, the apparent solubility as measured by Nitsche et al. could increase with temperature as a result of faster dissolution rates at higher temperatures. 3) To define a K_{sp}, equilibrium has to be attained from oversaturation and from undersaturation. The same solubility for americium, neptunium, and plutonium must be measured (regardless of whether the experimenter starts from an oversaturated solution or from an undersaturated solution using the solid phases formed during the oversaturation experiments). Data from undersaturation are not available yet, although experiments are in progress (Nitsche et al. 1993a, 1993b). Consequently, the members of the Radionuclide Solubility Working Group (SolWOG) of the Yucca Mountain Site Characterization Project (David Morris, Mike Ebinger, Heino Nitsche, Robert Silva, James Johnson, David Clark, and Drew Tait) decided not to apply a rigorous thermodynamic treatment to extrapolate the empirical solubilities reported by Nitsche et al. (1993a, 1993b) as a function of temperature.

Two potentially important issues were ignored in the solubility data used: the impact of future climate changes as they relate to potential changes in the water chemistry at Yucca Mountain and the impact of colloid formation in facilitating radionuclide transport at Yucca Mountain. A strategy was developed by the Yucca Mountain Site Characterization Project to address the latter issue (Triay et al. 1995b). The results of the work delineated by Triay et al. will be used in the next total-system performance-assessment (TSPA) calculation.

Table 45 shows the parameters for the solubility models that were presented to the members of SolWOG. After reviewing the actinide solubilities, they suggested only two changes: 1) the minimum value for the solubility of neptunium should be 5×10^{-6} M (rather than 10^{-8}) and 2) the minimum value for the solubility of plutonium should be 10^{-8} M (rather than 10^{-10}).

Solubility Distributions

Americium

The minimum and maximum values for the americium solubility distribution in Table 45 are based on the empirical solubility data reported by Nitsche et al. (1993a, 1993b). The SolWOG members thought that any value within the range would be equally likely (a uniform distribution). A uniform distribution over the range implies that approximately 90% of samples from this distribution would lie between 10^{-7} and 10^{-6} M, whereas approximately 0.1% of the samples would lie between 10^{-10} and 10^{-9} M.

Plutonium

Plutonium is more soluble than americium (as the SolWOG members pointed out) based on the data of Nitsche et al. (1993a, 1993b). These experts chose a distribution for plutonium solubility identical to the one chosen for americium. As has been already pointed out, a uniform distribution over the

Table 45. Solubilities Used in TSPA-1993

Element*	Minimum value (M)	Maximum value (M)	Expected value (M)	Coefficient of variation	Distribution
Americium	10^{-10}	10^{-6}			uniform
Plutonium	10^{-10} (10^{-8})†	10^{-6}			uniform
Uranium	10^{-8}	10^{-2}	$10^{-4.5}$	0.20	log beta
Thorium	10^{-10}	10^{-7}			log uniform
Radium	10^{-9}	10^{-5}	10^{-7}	0.10	log beta
Lead	10^{-8}	10^{-5}	$10^{-6.5}$	0.08	log beta
Neptunium	10^{-8} ($10^{-5.3}$)†	10^{-2}	10^{-4}	0.20	log beta
Protactinium	10^{-10}	10^{-5}			log uniform
Actinium	10^{-10}	10^{-6}			uniform
Tin	10^{-11}	10^{-7}			uniform
Nickel	10^{-6}	10^{-1}	$10^{-2.75}$	0.25	log beta
Strontium	10^{-6}	10^{-3}	10^{-4}	0.12	log beta
Samarium	10^{-10}	10^{-6}			uniform
Zirconium	10^{-12}	10^{-7}			log uniform
Niobium	10^{-9}	10^{-7}			log uniform

*Cesium, iodine, technetium, selenium, carbon, and chlorine are very soluble. †Values in parentheses recommended by SolWOG.

range in Table 45 implies that most of the samples from this distribution would lie between 10^{-8} and 10^{-6} M. Kerrisk (1984a) used the computer program EQ3/6 to calculate the solubility of plutonium in Yucca Mountain groundwaters and obtained a value of 1.8×10^{-6} M. The SolWOG members agree that the empirical data were more reliable for the TSPA calculations.

Uranium
No empirical data have been collected by the Yucca Mountain Site Characterization Project for uranium because its high solubility is not expected to be the limiting factor for the uranium source term. The possible solubilities for uranium occur over a wide range, but the data support a central tendency between 10^{-4} and 10^{-5} M with an approximate one-order-of-magnitude spread (Wanner and Forest 1992). The SolWOG members thought that uranium solubility should be represented in terms of logarithmic space; the resulting distribution is skewed log-normal.

Thorium
Thorium is extremely insoluble (less soluble than americium and plutonium). Such low solubilities make this element generally unimportant. As with americium, the SolWOG members believed that the range of values was well defined but that the distribution should favor selection of lower solubilities. They decided on a log-uniform distribution believing that it was equally likely to select the log of any value within the prescribed range.

Radium
Radium solubility is similar to barium solubility. The distribution chosen is based on Kerrisk's calculation with EQ3/6 (Kerrisk 1984a). The solubility of radium depends on the presence of sulfates. The SolWOG members chose a small relative standard deviation for radium solubility because this element forms only one cation and is relatively insensitive to groundwater chemistry.

Lead
The lead solubility distribution is based on the range published by Andersson (1988) and Pei-Lin et al. (1985). This element's solubility depends on the amount of carbonate in the groundwater so that variations in carbonate concentration in the groundwaters cause variations in lead solubility.

Neptunium
The neptunium solubility distributions were based on Nitsche's data (1993a, 1993b). The SolWOG members believed that the data supported a central tendency on log space with a spread of less than an order of magnitude. The neptunium solubilities used in TSPA-1991 (Barnard et al. 1992) were very low (approximately five orders of magnitude below those suggested by the SolWOG members). The TSPA-1991 solubilities were derived from spent fuel tests (conducted by Wilson 1990a, 1990b). The results from the spent-fuel test are not necessarily representative of neptunium solubilities in the groundwaters.

Cesium, iodine, technetium, selenium, carbon, and chlorine
All these elements are very soluble. The source term needs to be determined by leaching tests. A source term of 1 M is a reasonable approximation.

Protactinium
The range for protactinium solubilities was derived from the results of the Swedish Nuclear Power Inspectorate (SKI) (Andersson 1988). The solubility distribution for protactinium is expected to have a large variance, skewed towards smaller values. The SolWOG members believed that this radionuclide was less soluble than the range published by Andersson suggests. Therefore, a log-uniform distribution was chosen for protactinium.

Actinium
The solubility distribution chosen for actinium is identical to the americium solubility distribution.

Tin
Tin is very insoluble. The distribution range was obtained from the results published by SKI (Andersson 1988); any value within this range was

equally probable. A uniform solubility distribution was chosen.

Nickel
Nickel solubility is a function of pH. The SolWOG members chose the same range as the one published by the SKI (Andersson 1988). The mean and standard deviation of the solubility distribution were approximated from data gathered in support of the caisson experiment conducted at Los Alamos (Siegel et al. 1993).

Strontium
The solubility distribution for strontium is based on the results of SKI (Andersson 1988) and those published by Siegel et al. (1993).

Samarium
The solubility distribution chosen for samarium is identical to that for americium

Zirconium
Zirconium is very insoluble. The chosen distribution was based on the SKI results (Andersson 1988). A log-uniform solubility distribution was chosen for this element because the SolWOG members expected to see many values for zirconium solubility in the lower range.

Niobium
The niobium solubility distribution is based on SKI results (Andersson 1988)

IV. SORPTION AND SORPTION MODELING STUDIES

A. BATCH-SORPTION DATA

Introduction

The solubility limits of radionuclides can act as an initial barrier to radionuclide migration from the potential repository at Yucca Mountain. However, once radionuclides have dissolved in water infiltrating the site, sorption of these radionuclides onto the surrounding tuffs becomes a potentially important second barrier. Thus, the study of the retardation of actinides and other key radionuclides is of major importance in assessing the performance of the potential repository.

Sorption actually comprises several physicochemical processes, including ion exchange, adsorption, and chemisorption. Determining whether sorption will occur requires knowledge of the likely flow paths of the groundwater and the spatial and temporal distribution of sorbing minerals along these paths. Evaluating the retardation effectiveness of sorption for repository design and licensing requires theoretical and quantitative understanding of sorption. We thus combined experimental measurements of sorption with modeling of the data in an attempt to identify key sorption mechanisms.

The use of batch-sorption experiments to obtain sorption distribution coefficients and to identify sorption mechanisms is fast, easy, and inexpensive compared to other types of sorption experiments. A disadvantage is the fact that such experiments are static in nature, whereas transport of radionuclides through the site is, obviously, a dynamic process. However, batch-sorption experiments are useful for bounding more detailed and mechanistic sorption studies, and a major part of our experimental effort was devoted to such measurements.

In our experiments, we determined batch-sorption distribution coefficients as a function of variables representing conditions expected beyond the region disturbed by waste emplacement. The variables included mineralogy, groundwater chemistry, sorbing element concentration, atmospheric conditions, and temperature. Batch-sorption results are very sample specific and, therefore, difficult to generalize and apply throughout the mountain. Deconvolution of sorption isotherms provides much greater detail about sorption sites (kind, number, specificity, and so forth), and we did this analysis for a number of the actinides. Such information is correlated with crystallographic data and related to specific sorption sites in the crystal structure. All sites are not equally selective for all sorbing species.

We also examined the sorption behavior of individual pure minerals, such as the zeolites and manganese or iron oxyhydroxides found in Yucca Mountain tuffs. This approach can help predict sorption coefficients along flow paths of known mineral content.

Linear versus nonlinear sorption

The sorption distribution coefficient, K_d, for the species being sorbed, is the ratio of its concentration in the solid phase, F, to its concentration in the solution phase, C, which implies a linear relationship between the concentrations:

$$F = K_d C \ . \qquad (55)$$

Besides linearity, the valid use of sorption distribution coefficients in transport calculations also requires the sorption to be instantaneous and reversible, conditions that may or may not be met for the sorption of radionuclides onto Yucca Mountain tuffs.

Nonlinear adsorption isotherms have been reviewed by de Marsily (1986, p. 258). A useful nonlinear relationship, Freundlich's isotherm, is given by the equation

$$F = KC^{1/n} \ , \qquad (56)$$

where K and n are positive constants (with $n \geq 1$). Another nonlinear relationship is Langmuir's

isotherm, given by

$$F = \frac{K_1 C}{1 + K_2 C} \ , \qquad (57)$$

where K_1 and K_2 are positive constants. Part of our research was an attempt to assess the validity of using the linear distribution coefficients as opposed to other isotherm functional forms to describe retardation by sorption in transport calculations.

Mechanistic models

A better understanding of the sorption of radionuclides onto tuff is possible if we can relate the data to mechanistic models. Two general mechanisms are important: ion-exchange reactions that are primarily electrostatic in nature and surface complexation in which a relatively covalent chemical bond forms with the mineral surface. Ion exchange does not have the same degree of selectivity between aqueous ions of like charge as does surface complexation. The adsorption of metal ions via cation exchange will only occur on surfaces of opposite charge and so is affected by such common components of groundwater as sodium. Surface complexation, on the other hand, can occur even when the mineral surface charge is the same as the aqueous ion. Both of these processes can, in principle, be modeled using a triple-layer surface-complexation model. However, there are significant differences between the cation exchange in zeolites and clays and the formation of surface complexes on metal oxides, so we have treated cation exchange and surface complexation separately.

Physiochemical processes that might accelerate radionuclide migration relative to groundwater flow rates must also be quantified. For example, mineral surfaces in rock pores are predominantly negatively charged, so anions are typically repelled and can actually migrate through the rock faster even than the water. Such acceleration processes depend largely on the molecular complexation or speciation that occurs in solution. Accordingly, detailed assessment of this possibility is needed to fully evaluate the potential for transport retardation by geochemical processes.

Experimental procedures

All batch-sorption experiments were performed at room temperature. The procedure first involved pretreating the solid phase with the groundwater being studied (J-13 or UE-25 p#1 well water or a synthetic bicarbonate groundwater) in the ratio of 1 g of solid to 20 ml of solution. The pretreated solid phase was then separated from the groundwater by centrifugation and equilibrated with 20 ml of a radionuclide solution (in the groundwater being studied). After sorption, the phases were again separated by centrifugation.

The amount of radionuclide in solution initially and then after sorption was either determined with a liquid-scintillation counter (such as for neptunium and plutonium) or with inductively coupled plasma mass spectrometry (such as for uranium). The amount of radionuclide in the solid phase was determined by difference.

The liquid-scintillation counting technique we used can discriminate alpha activity from beta activity. Consequently, no interference from beta emitters (such as ^{233}Pa, the daughter of ^{237}Np) is expected. Because the efficiency of this liquid-scintillation counter is approximately 100%, the counts per minute (cpm) measured are approximately equivalent to disintegrations per minute.

As controls, we used container tubes without solid phases in them to monitor radionuclide precipitation and sorption onto the container walls during the sorption experiment. The difference in the concentration of the radionuclide in the initial solution and in the solution in the control tube generally was only a few percent, and then in either a plus or a minus direction.

Results for the plutonium solution did show a small amount of sorption onto the container walls. Even here, the difference in concentration between the initial plutonium solution and the plutonium solution in the control tube never exceeded 7% for the experiments reported. Nevertheless, in the case of plutonium, we calculated the amount of radionu-

clide sorbed in the solid phase by taking the difference of the final plutonium solution concentration both with the initial solution concentration and with the solution concentration in the control tube. The latter approach is conservative because plutonium may sorb to container walls only in the absence of the geologic material.

We performed batch-sorption experiments under atmospheric conditions and inside glove boxes with a carbon-dioxide overpressure. The pH of the J-13 and UE-25 p#1 waters under atmospheric conditions was approximately 8.5 and 9, respectively, and inside the glove boxes was 7 (the carbon-dioxide overpressure was adjusted to bring the pH of both waters down to 7). Details of the experimental setup and the analytical techniques that we used in the sorption experiments are given in the *Yucca Mountain Project Detailed Procedures* (Table 2, page 10).

The distribution coefficient

The batch-sorption distribution coefficient, K_d, was calculated using

$$K_d = \frac{F}{C} = \frac{\text{moles of radionuclide per g of solid phase}}{\text{moles of radionuclide per ml of solution}} . \quad (58)$$

K_d thus has units of ml/g.

Determination of very small or very large batch-sorption distribution coefficients results in large uncertainties in the K_d values calculated. When very little sorption occurs, calculations can yield negative K_d values; the error results from subtracting two large numbers (the initial radionuclide concentration in solution and the radionuclide concentration after sorption) to obtain a small number (the amount of radionuclide left in the solid phase). Therefore, small K_d values (in the range of ± 1) are not significant. On the other hand, when a great deal of sorption occurs, calculations can yield large uncertainties associated with measuring the small amount of radioactivity left in solution after sorption. Because of these uncertainties, most K_d values are only reported to one significant figure.

Niobium, Thorium, Tin, and Zirconium

The radionuclides of concern represented by these elements have several characteristics in common. First, in groundwater-rock systems of concern in this report, these elements have stable oxidation states. Niobium is present in a $+5$ oxidation state, whereas the others are typically in $+4$ oxidation states (Brookins 1988). Second, in aqueous solutions with compositions typical of groundwaters, these elements tend to occur as sparingly soluble oxides or silicates (Brookins 1988). They may also form solid solutions with other, more common, sparingly soluble oxides, such as titania (TiO_2). Third, the dominant solution species associated with these oxides are hydrolysis products (Baes and Mesmer 1976). Fourth, the hydrolyzed solution species tend to have high affinities for adsorption onto oxide surfaces as discussed further below. The radionuclides represented by these elements are in the "strongly sorbing" group discussed by Meijer (1992).

Niobium

Behavior in solutions representative of Yucca Mountain groundwaters.

According to Baes and Mesmer (1976), at a dissolved niobium concentration of 10^{-6} M, the dominant solution species in pure water are the neutral species $Nb(OH)_5$ and the anionic species $Nb(OH)_6^-$. The anionic species predominates at values of pH above 7, and the neutral species is stable below a pH of 7. At surficial temperatures and pressures, evidence for significant complexation of niobium by nonhydroxide ligands in natural aqueous solutions is lacking. As discussed below, carbonate complexation may occur at higher temperatures and pressures.

The concentrations of niobium in surficial aqueous solutions are extremely low, presumably due to the low solubility of the pentavalent oxide (Baes and Mesmer 1976) and to sorption onto mineral surfaces. In geologic systems, niobium may substitute

as a trace element in the more abundant oxide phases such as micas, titanium oxides (for example, rutile), and clays (Goldschmidt 1958). This effect also leads to low solution concentrations.

Qualitative evidence for behavior in the surficial environment.
The geologic literature contains numerous papers that qualitatively discuss the mobility, or more accurately, the immobility of niobium in rocks during alteration processes (for example, Cann 1970). In various studies of soils or altered, weathered, or metamorphosed rocks, geological, geochemical, and statistical evidence has been presented that supports the conclusion that niobium is essentially immobile in the surficial environment. Although some of these studies deal with rocks that have been altered under conditions of low fluid-to-rock ratios, the general lack of evidence for niobium mobility suggests that this element would also be immobile in systems with higher water-rock ratios, such as the Yucca Mountain flow system. For example, Brookins (1983) notes that 100 per cent of the niobium produced by fission at the natural reactor at Oklo, Gabon, has been retained by the host pitchblende even though the reactor was active in water-bearing sandstones that were subjected to elevated temperatures during and after the critical (that is, nuclear) stage of the reactor.

Grimaldi and Berger (1961) studied the concentrations of niobium in twenty lateritic soils from West Africa and concluded that silica is depleted more rapidly from these soils than is niobium and niobium more rapidly than aluminum. Further, these workers note that there is a strong association of niobium with the clay-sized fraction and also with titanium. They propose that the association of niobium with the clay fraction may be due to the presence of niobium-rich authigenic rutile in the clays. The observation that niobium was mobilized more readily than aluminum in this environment does not necessarily imply niobium was transported out of the system as a dissolved solution species. The tendency of elements such as niobium, titanium, tin, and so forth to form very fine-grained precipitates is well known. Such colloidal-sized particles can be transported by soil solutions and surface waters.

Evidence for niobium mobility during greenschist metamorphism of mafic rocks has been presented by Murphy and Hynes (1986). These workers suggest that carbonate-rich metamorphic solutions can mobilize and transport niobium (as well as titanium, zirconium, phosphorus, and yttrium). Presumably, carbonate can form mobile complexes with niobium under conditions of elevated temperature and pressure. No references were found that address the ability of carbonate to complex niobium under low temperatures and near atmospheric pressures.

Conclusions regarding sorption behavior with respect to expected variations in groundwaters.
On the basis of the geological evidence and because niobium forms primarily hydrolyzed species in groundwaters of the type associated with Yucca Mountain, niobium should be very insoluble in Yucca Mountain groundwaters and strongly sorbed onto mineral phases present in Yucca Mountain tuffs from the whole range of groundwater compositions expected at the site.

Thorium
Behavior in solutions representative of Yucca Mountain groundwaters.
Langmuir and Herman (1980) have compiled and critically reviewed thermodynamic data for thirty-two dissolved thorium species and nine thorium-bearing solid phases. In the groundwater compositions expected within Yucca Mountain, thorium will be fully hydrolyzed ($Th(OH)_4$), and thorium complexing with other inorganic ligands will be insignificant based on the data presented in Langmuir and Herman (1980). Thorium compounds are among the most insoluble in the group of elements considered in this report. Solubilities of the order of 10^{-50} M are common for thorium compounds (for example, thorianite (ThO_2) and thorite ($ThSiO_4$)). Nevertheless, concentrations well above this value have been found in various natural waters and appear to reflect complexation with organic ligands in organic-rich waters. Such

waters are not expected at Yucca Mountain.

Qualitative evidence for behavior in the surficial environment.
Thorium is one of the elements considered to be immobile in most surficial environments (Rose et al. 1979). Studies of the isotopic disequilibrium in the uranium and thorium decay series found in natural aquifers suggest that thorium isotopes are strongly retarded in these flow systems relative to other members of the decay series (Krishnaswami et al. 1982). Studies of the migration of thorium away from thorium ore bodies also indicate that it is "extraordinarily immobile" in these environments (Eisenbud et al. 1984). Brookins (1983) found that thorium was immobile in the Oklo reactor environment. Studies of thorium concentration gradients with depth in seawater also point to high sorption affinities for this element on oceanic particulate matter (Moore and Hunter 1985).

Data from laboratory sorption experiments.
Hunter et al. (1988) carried out thorium sorption experiments on MnO_2 and FeOOH in artificial seawater and in a simple NaCl solution. The primary objective was to determine the effects of major ions (for example, Mg^{2+} and SO_4^{2-}) on the adsorption of thorium by goethite (FeOOH) and MnO_2 relative to sorption in a pure NaCl electrolyte system. The effects of magnesium and calcium ions on thorium adsorption were very small (probably within the margin of experimental error), but the presence of sulfate at seawater concentrations (0.028 M) increased the adsorption edge on FeOOH by one-half of a pH unit. Because the adsorption edge is in the range of pH values from 3 to 5 in all the experiments, this effect is not considered important for thorium sorption behavior at the Yucca Mountain site.

LaFlamme and Murray (1987) evaluated the effects of carbonate on the adsorption characteristics of thorium on goethite. They found that carbonate alkalinity could decrease thorium sorption onto goethite at alkalinity values greater than 100 meq/l. Because the alkalinity values expected in the Yucca Mountain flow system are orders of magnitude lower than this value, carbonate alkalinity is not expected to affect thorium adsorption behavior in this system.

According to Langmuir and Herman (1980), the adsorption of thorium onto clays, oxides, and organic material increases with pH and approaches 100 per cent completion by a pH of about 6.5. As the thorium ion is largely hydrolyzed above a pH of about 3.2, it follows that hydroxy complexes of thorium are primarily involved in adsorption processes (in carbonate-poor systems). Using a mixed quartz-illite soil as a sorbent, Rancon (1973) measured a K_d value of 5 ml/g at a pH of 2, which increased to 5×10^5 ml/g at a pH of 6. With a quartz-illite-calcite-organic-matter soil, Rancon found that the K_d decreased from 10^6 ml/g at a pH of 8 to 100 ml/g at a pH of 10. This change was attributed to the dissolution of soil humic acids and the formation of thorium-organic complexes at this high pH.

Lieser and Hill (1992) reported thorium sorption coefficients for rock-water systems associated with the Gorleben site in Germany. They found that thorium was strongly sorbed in such systems ($K_d = 10^3$–10^5 ml/g). However, they also found that colloidal transport may be of potential significance to the migration of thorium in the surficial environment.

Thorium sorption experiments on Yucca Mountain rock samples in J-13 groundwater were reported by Rundberg et al. (1985) and Thomas (1988). The sorption coefficients obtained in these experiments ranged from 140 to 23,800 ml/g. No correlations were noted between the values obtained for the sorption coefficient and rock type or pH (5.3–7.5). Part of the reason for the large range in sorption coefficients obtained in these experiments may lie in the presence of fine colloidal particles in the solution phase used to obtain the sorption coefficients (for example, Lieser and Hill 1992).

Conclusions regarding sorption behavior with respect to expected variations in groundwaters.
The dominance of hydrolysis reactions in solution, the low solubility of thorium oxides and silicates, the large values measured for thorium sorption coefficients in different water compositions, including seawater, combined with the general lack of evidence for mobility of thorium in the surficial environment suggest that the sorption coefficients for thorium will be large ($>$ 100 ml/g) in all hydrochemical environments associated with Yucca Mountain in the present day or in the future.

Tin

Behavior in solutions representative of Yucca Mountain groundwaters.
The dominant tin solution species in surficial waters appears to be $Sn(OH)_4$. The concentrations of tin in natural groundwaters are extremely low due to the ion solubility of the tetravalent oxides (about 10^{-9} M in pure water; Baes and Mesmer 1976). Cassiterite (SnO_2) should be the solubility-limiting oxide in most groundwaters. Tin could also coprecipitate with other insoluble oxides or silicates such as niobium pentoxide, zirconium and thorium dioxide, and thorium silicate. In natural waters with high sulfide concentrations, tin sulfide minerals could control tin solubility. However, such water compositions are not expected in association with the proposed repository site at Yucca Mountain.

Qualitative evidence for behavior in the surficial environment.
Tin is one of the elements considered to be immobile in most near-surface geologic environments (Rose et al. 1979). This assignment is based on various types of data, including observations on the mobility of tin in and around tin ore deposits. However, De Laeter et al. (1980) note that some tin has migrated out of the pitchblende at the natural reactor at Oklo, Gabon. The cause for this migration has not been established but may reflect the existence of reducing conditions during some phase of the history of the reactor.

Data from laboratory sorption experiments.
Sorption experiments with tin have been carried out on several whole-rock samples from Yucca Mountain in contact with J-13 water, UE-25 p#l water, H-3 water, and several waters separately spiked with sodium sulfate, sodium bicarbonate, and calcium chloride (Knight and Thomas 1987). The measured sorption coefficients ranged from 77 to 35,800 ml/g at pH values in the range of 8.4 to 9.2. Coefficients obtained from desorption experiments were generally larger (300–52,500 ml/g) than those obtained from sorption experiments. The devitrified tuff samples produced the highest sorption and desorption coefficient values ($>$ 2900 ml/g), whereas the vitric and zeolitic tuff samples produced lower values. Sorption coefficients were generally highest in the UE-25 p#l water and the calcium-chloride-spiked J-13 water. Apparently, high calcium concentrations in the solution phase result in high sorption-coefficient values for tin. Alternatively, high calcium concentrations cause the precipitation of some type of tin-bearing compound. As with thorium, the large range in sorption coefficients observed in the experiments may reflect the presence of colloidal-size particles in the solution phase used to obtain the coefficients.

Conclusions regarding sorption behavior with respect to expected variations in groundwaters.
The dominance of hydrolysis reactions in solution, the low solubility of tin oxides, and the large values measured for tin sorption coefficients in different water compositions combined with the general lack of evidence for mobility of tin in the surficial environment suggest that the sorption coefficients for tin will be large ($>$ 100 ml/g) in all hydrochemical environments associated with Yucca Mountain in the present-day or in the future.

Zirconium

Behavior in solutions representative of Yucca Mountain groundwaters.
In near-neutral solutions, the dominant zirconium solution species appear to be hydrolysis products, such as $Zr(OH)_4$. The degree to which zirconium forms complexes with other inorganic ligands pre-

sent in Yucca Mountain groundwaters is insignificant (Sillen and Martell 1964, 1971). The solubility of zirconium in dilute solutions is extremely small (Sillen and Martell 1964, 1971), although the identity of the solubility-controlling solid is uncertain. The solubility-controlling compounds for zirconium in most natural groundwaters are likely zircon ($ZrSiO_4$) or baddeleyite (ZrO_2). Zirconium solubilities in surficial environments may also reflect coprecipitation in other sparingly soluble oxides or silicates. The concentrations of zirconium in natural waters may be dominantly controlled by sorption reactions.

Qualitative evidence for behavior in the surficial environment.
Zirconium is one of the elements considered to be immobile in most near-surface geologic environments (Rose et al. 1979). Studies of zirconium concentrations in altered and unaltered or less-altered rocks from the same original geologic unit (Cann 1970) form part of the basis for this conclusion. Other evidence includes the persistence of zircon ($ZrSiO_4$) in the weathering zone and the low concentrations of zirconium in waters associated with zirconium-rich rocks. Brookins (1983) noted that zirconium was retained within the reactor zones at Oklo, Gabon, although it may have been subject to very local-scale redistribution.

Data from laboratory sorption experiments.
Data on the sorption behavior of zirconium in soil-rock-water systems have been reported by Rhodes (1957), Spitsyn et al. (1958), Prout (1959), Serne and Relyea (1983), and others. Rhodes (1957) has presented data on zirconium sorption coefficients for a soil-water system that show large values ($>$ 1980 ml/g) up to a pH of 8.0 followed by a decrease to 90 ml/g at a pH of 9.6 and a return to high values at a pH of 12. He attributed the decreased sorption for values of pH from 8 to 12 to the stabilization of colloidal components in solution in this pH range. Spitsyn et al. (1958) observed little movement of zirconium through a sandy soil in a field test under both acidic and alkaline conditions. Serne and Relyea (1983) report large values for zirconium sorption coefficients in all media tested.

Conclusions regarding sorption behavior with respect to expected variations in groundwaters.
The dominance of zirconium hydrolysis reactions in solution suggests that pH will be the dominant groundwater compositional parameter controlling zirconium solubility and sorption behavior. The lack of evidence for zirconium transport in field tests under both acidic and alkaline conditions and the general lack of evidence for mobility of zirconium in the surficial environment combined with the large values of the sorption coefficient reported in the literature for zirconium suggest that in all hydrochemical environments associated with Yucca Mountain in the present-day or in the future this element's sorption coefficients will be large ($>$ 100 ml/g).

Actinium, Americium, and Samarium

The radionuclides of concern represented by these elements have the following characteristics in common: 1) In groundwater-rock systems of concern in this report, these elements are all present in the $+3$ oxidation state. 2) In aqueous solutions with compositions typical of groundwaters, the solubility of these elements tends to be controlled by sparingly soluble carbonates, phosphates, fluoride-carbonate complexes, and to a lesser extent, hydroxy-carbonate compounds (Mariano 1989). The elements may also form solid solutions with carbonates, phosphates, fluorides, and oxides of the major cations in groundwaters. 3) The dominant solution species associated with these elements are generally complexes with carbonate, phosphate, and hydroxide ligands (Sillen and Martell 1964, 1971). 4) The solution species tend to have high affinities for adsorption onto oxide surfaces as discussed further below. The radionuclides represented by these elements are all in the "strongly sorbing" group discussed by Meijer (1992).

Because the chemistry of all three of these elements is similar in aqueous solution and sorption

reactions, they will be discussed as a group.

Behavior in solutions representative of Yucca Mountain groundwaters.
The trivalent ions of the rare-earth elements are essentially spherical and form aqueous complexes that are similar to those formed by the alkaline and alkaline-earth elements. Thompson (1979) notes that the partially filled *f* orbital is so effectively shielded from most chemical bonding that the crystal-field effects are about 100 cm^{-1} compared to values of around 30,000 cm^{-1} for many first-row transition elements. Chemical interactions of the rare-earth elements are almost entirely ionic, and the rare-earth elements are not easily polarized owing to their relatively large charge-to-ionic-radius ratio. As noted by Cotton and Wilkinson (1988), the trivalent actinides show many similarities in solution chemistry to the lanthanides. In fact, Nitsche et al. (1994) have used neodymium as a direct analog for americium in solubility studies.

In solution, americium and the rare-earth elements occur as simple (trivalent) cations, carbonate complexes, phosphate complexes, and hydrolysis products (Wood 1990). Complexes with other inorganic ligands (for example, Cl^-, F^-, and SO_4^{2-}) will not be of importance in the water compositions expected in the Yucca Mountain flow system. Therefore, speciation models for the rare-earth elements and trivalent actinides should consider pH, carbonate-ion concentration, and possibly phosphate-ion concentration as key variables. According to Byrne and Kim (1993), phosphate complexes will not be significant unless the ratio of the total phosphate concentration to the total carbonate concentration is greater than 1.3×10^{-3}. This condition makes it unlikely that phosphate rare earths or americium complexes will be important in Yucca Mountain groundwaters. Therefore, carbonate complexes are expected to dominate the solution species for these elements. The solubility-controlling solids in Yucca Mountain groundwaters will likely be carbonates, hydroxycarbonates (Kerrisk 1984b), and possibly phosphates (see the following section).

According to Nitsche et al. (1992a, 1994), the solubilities of americium compounds in solutions representative of water compositions expected within Yucca Mountain are approximately 1 to 2×10^{-9} M in J-13 water and 3 to 30×10^{-7} M in UE-25 p#l water as a function of pH at 25ºC. At 60ºC, the solubilities of americium compounds were 1×10^{-8} to 2.5×10^{-6} M in J-13 water and 7×10^{-10} to 3×10^{-9} M in UE-25 p#l water as a function of pH. The solubility-controlling solids were found to be hexagonal and orthorhombic forms of $AmOHCO_3$. The speciation of americium in these solutions could not be determined due to the low solubilities of americium in these water compositions relative to the detection limits of the available spectroscopic techniques. Preliminary modeling calculations with the speciation code EQ3 suggest that carbonate complexes dominate in both J-13 and UE-25 p#l waters at 25º and 60ºC (Ogard and Kerrisk 1984).

Qualitative evidence for behavior in the surficial environment.
Although the geological community generally regards the rare-earth elements as immobile during most water-rock alteration processes (Taylor and McLennan 1988), detailed studies of weathering profiles suggest that these elements may be redistributed within these profiles during weathering. Duddy (1980) studied a weathering profile formed on a homogeneous sedimentary rock unit in southeastern Australia. This profile was formed in a cool temperate climate with 200 cm/yr precipitation. The profile contained bleached zones and ferruginous zones in which iron was reduced or oxidized, respectively. The rare-earth elements were up to 7 times enriched in the bleached portions of the profile. Based on the sorption data discussed in the following section, this is somewhat puzzling as one might expect these elements to be coprecipitated or adsorbed to the secondary ferric oxides formed in the profile. In fact, the rare-earth elements appeared to be enriched in vermiculite, an expanding magnesium-ferrous iron trioctahedral clay that formed in the weathering profile as a result of the alteration of biotite. Up to 10 weight

per cent of rare-earth elements was reported in vermiculites on the basis of electron-probe analyses. The elements originated from the dissolution of apatite ($Ca_5(PO_4)_3(F,Cl,OH)$) and other minerals present higher in the profile.

Banfield and Eggleton (1989) studied the rare-earth elements in an Australian weathering profile formed on granite. These authors also noted that these elements were mobile in the profile. However, they found that (primary) biotite crystals in the granite contained apatite inclusions rich in rare-earth elements or cavities resulting from the dissolution of apatite. The apatite crystals were apparently dissolved during weathering leaving behind fine-grained (< 10 μm) rare-earth-element phosphate phases including florencite, rhabdophane ($CePO_4 \cdot H_2O$), and an unidentified phosphate-free aluminum-rare-earth-element mineral, possibly a carbonate, hydroxycarbonate, or fluorocarbonate. Vermiculites were also present in this profile, but they were not analyzed for rare-earth-element contents.

These two studies clearly indicate that the rare-earth elements can be mobilized in the surficial environment. However, they also suggest that this mobilization is generally of a local nature resulting in the precipitation of new rare-earth-element phases or the incorporation of these elements in other secondary phases, such as clays. These studies did not address the question of whether adsorption of the rare-earth elements onto the surfaces of other mineral phases is a significant process in controlling the mobility of these elements in surficial environments. Loubet and Allegre (1977) noted that the light rare-earth elements were not mobilized in the reactor zones at Oklo, Gabon.

Data on the behavior of americium in the surficial environment is limited to anthropogenic examples. Americium was found to be very immobile in most of the studies located in the literature (for example, Means et al. 1978; Carpenter et al. 1987). The main uncertainty regarding the surficial behavior of americium appears to be the degree to which it is mobilized through colloidal transport (for example, Penrose et al. 1990).

Data from laboratory sorption experiments. Ion-exchange studies involving the sorption of lanthanide ions on montmorillonitic clays have been reported by Frysinger and Thomas (1960), Aagard (1974), Bruque et al. (1980), and Bonnot-Courtois and Jaffiezic-Renault (1982). These studies conclude that essentially all of the exchange capacity of the clays is available to lanthanide ions and that the exchange reactions are rapid (that is, minutes). Frysinger and Thomas noted that the Cs^+–Y^{3+} binary exchange was not dependent on pH over the range from 3 to 7. At low cesium concentrations, such as are likely to occur in the potential repository horizon, the clay showed a slight preference for the lanthanide ions relative to cesium, and this preference increased with temperature (30–75ºC).

Bruque et al. (1980) only studied the exchange of lanthanide ions with hydrogen-montmorillonite, which is not of interest in this report. However, Bonnot-Courtois and Jaffrezic-Renault (1982) studied the exchange reactions in potassium-, sodium- and calcium-exchanged clays, which are of interest. In the latter study, the rare-earth elements, at initial solution concentrations of 10^{-2} to 10^{-4} M, showed distribution coefficients greater than 1.0 only when the concentrations of the major cations were, in the case of sodium and potassium, below 0.1 M and, in the case of calcium, below 0.01 M. The rare-earth elements were apparently, to a large degree, sorbed irreversibly, as they could not be readily desorbed from the clay.

Koeppenkastrop and De Carlo (1992, 1993) have evaluated the sorption of the rare-earth elements by iron oxides, manganese oxides, and apatite from high ionic-strength aqueous solutions (that is, ultraviolet-irradiated natural seawater). One nanomole of each rare-earth-element radiotracer was equilibrated with approximately 10 mg of the solid phase in 1 kg of seawater. The pH of the system was maintained at 7.8 in all the experiments. The percentage of rare-earth element adsorbed on FeOOH

and MnO_2 was measured in the presence and absence of carbonate. Carbonate appeared to affect the kinetics of the adsorption reactions but not the extent of adsorption at equilibrium. The sorption reactions equilibrated within tens of minutes. Under the conditions of the experiments, the rare-earth elements are shown to have very high affinities for the oxide and phosphate phases ($K_d >>$ 1,000 ml/g). Koeppenkastrop and De Carlo (1993) further state that modeling of sorption data derived from experiments with natural particles indicates that desorption rate constants are much smaller than adsorption rate constants.

The high affinity of the rare-earth elements for iron- and manganese-oxide phases suggests that these phases would act as "getters" for these elements in surficial environments. Yet the data reported by Duddy (1980) suggest that the rare-earth elements in the weathering profile he studied were preferentially incorporated in vermiculite in the "bleached" zones and not adsorbed onto ferric oxides in the ferruginous zones. This effect suggests that there were other constituents in the solution phase of the profile investigated by Duddy (1980) that had higher affinities for the oxide surfaces than the rare-earth elements and that they were present in sufficient quantity to saturate the available surface sites. A possible candidate would be the Al^{3+} ion (for example, see Brown et al. 1956).

Stammose and Dolo (1990) reported on batch-sorption experiments with americium (10^{-8} M) on clay as a function of pH and ionic strength. The clay used in the experiments was a mixed-layer clay consisting of kaolinite and smectite. At ionic strengths of 0.01 and 0.1 M ($NaClO_4$), the americium sorption coefficient was greater than 10^3 ml/g over the entire pH range (3–10) addressed by the experiments. In the higher ionic-strength solutions (1 and 3 M), the sorption coefficients were low (10 ml/g) at a pH of 2 but increased to values in the range of 10^4 to 10^5 ml/g for pH values greater than 6.

Overall, the data presented by these authors suggest: 1) the ion-exchange sites on the clay have a very high selectivity for americium at trace concentrations; 2) sodium ions at sufficiently high concentrations can displace the americium from these sites; 3) americium is also adsorbed in surface-complexation reactions; 4) the surface-complexation reactions define a sorption edge that has minimum values at low pH and reaches a maximum at a pH of approximately 7; 5) americium is adsorbed as an inner-sphere complex, and its adsorption affinity in surface-complexation reactions is therefore not a function of ionic strength; and 6) at trace americium concentrations, carbonate complexation of americium may compete with surface-complexation reactions in the pH range from 8 to 10, leading to a slight decrease in adsorption in this range.

Allard and Beall (1979) have presented americium sorption-coefficient data for a range of mineral types including clays, feldspars, carbonates, phosphates, oxides, oxyhydroxides, and other less common minerals. The sorption coefficients were measured over a range of pH from 4 to 9 in a low ionic-strength (synthetic) groundwater similar in composition to an average Yucca Mountain groundwater. Initial americium solution concentrations were in the range from 1.8 to 5.0×10^{-9} M. Data presented for clay minerals indicate that ion exchange occurred on these minerals in the lower pH range (< 6). Surface recrystallization reactions are evident in the low pH data for apatite (also, see Jonasson et al. 1985) and fluorite. On the remaining silicates and nonsilicates, americium appears to sorb dominantly by surface-complexation reactions. In all cases, the sorption coefficient values are in excess of 10^3 ml/g over the pH range likely to be encountered in the Yucca Mountain groundwaters.

In summary, trivalent actinium, americium, and samarium likely sorb by at least two distinct mechanisms. At pH values less than approximately 6, ion-exchange reactions on clays and other ion-exchanging minerals may dominate the adsorption behavior of these elements in low ionic-strength solutions. These reactions will show dependencies

on ionic strength and ion selectivity. At pH values greater than 6, sorption appears to involve primarily inner-sphere surface-complexation reactions. Although these reactions are independent of ionic strength, they will likely be subject to competition with other sorbing species at sufficiently high sorption densities. In the pH range from 8 to 10, carbonate-complexation reactions in solution may compete with the surface-complexation reactions involving these elements. However, the surface-complexation reactions are expected to dominate over carbonate-complexation reactions in Yucca Mountain groundwaters.

Sorption data obtained on Yucca Mountain samples.
Sorption coefficients for cerium, europium, and americium have been determined for a variety of rock samples from Yucca Mountain and in several groundwater compositions from the site (Thomas 1987; Knight and Thomas 1987). The data are generally consistent with the conclusions stated in the previous section. However, several additional points should be emphasized. First, experiments with rock samples that contained calcite (for example, G1-2901 and G2-723) or groundwater that was saturated with calcite (such as UE-25 p#l) showed very large sorption coefficients for these elements. This result suggests the radionuclides were either coprecipitated with carbonates (for example, calcite) or formed solid solutions on the surfaces of existing carbonates. Because groundwaters in the unsaturated zone at Yucca Mountain are likely near saturation with calcite, this observation suggests the trivalent lanthanides and actinides will not be mobile in the proposed repository horizon.
Second, experiments on samples with more than a few percent clay (for example, G1-3658) also showed high sorption coefficients. For these rock types, the ionic strength of the groundwaters may play a role in determining the magnitude of the sorption coefficients for these elements. Third, experiments with groundwaters containing high carbonate concentrations (such as UE-25 p#l) show large sorption coefficients for these elements, suggesting that carbonate complexation in solution does not lead to significant decreases in the sorption coefficients for these elements in Yucca Mountain groundwaters.

Conclusions regarding sorption behavior with respect to expected variations in groundwaters.
The impact of variations in groundwater compositional parameters within the ranges expected in Yucca Mountain on the sorption behavior of actinium, americium, and samarium should be relatively minor. Over the expected pH range (6–9), the trivalent actinides and lanthanides appear to sorb primarily by inner-sphere surface-complexation mechanisms. These mechanisms are not sensitive to variations in ionic strength. Further, these elements appear to have high affinities for the mineral surfaces typically available in the Yucca Mountain rock units over the entire pH range expected. This result suggests that the trivalent actinide and lanthanide radionuclides will be strongly sorbed ($K_d > 100$ ml/g) over the entire range of expected groundwater compositions.

Plutonium

Behavior in solutions representative of Yucca Mountain groundwaters.
The solution behavior of the element plutonium is the most complicated of all the elements of interest and the least understood, particularly in near-neutral solutions representative of water compositions expected within the Yucca Mountain flow system. Plutonium can have several oxidation states in a given solution, and it can form complexes with a variety of ligands.

According to Nitsche et al. (1992a, 1994), plutonium will be present in the $+3$, $+4$, $+5$, and $+6$ oxidation states in solutions representative of water compositions expected within Yucca Mountain. The $+5$ and $+6$ oxidation states should predominate in solution at redox potentials in the range of 230 to 350 mV. In J-13 and UE-25 p#l waters, the $+5$ oxidation states should be dominant (60–80%) at 25ºC. Most of the remaining plutonium in solution is in the $+6$ oxidation state in J-13 water and

the +4 oxidation state in UE-25 p#l water.

Experimentally determined solubilities range from 3.0×10^{-7} to 1.0×10^{-6} M at 25ºC. The solubility-controlling solids were found to be mixtures of polymeric Pu(IV) and smaller amounts of plutonium carbonates. The solubilities measured at pH values of 6 and 7 are consistent with the data reported by Rai et al. (1980). However, the solubilities measured for a pH of 8.5 exceed those reported by Rai et al. for amorphous $Pu(OH)_4$ in 0.0015 M $CaC1_2$. This result suggests that carbonate complexation of plutonium is significant at a pH of 8.5 in the Yucca Mountain groundwaters.

At 60ºC, the +6 oxidation state was dominant (> 80%) in the UE-25 p#l water at all three pH values. In J-13 water, the +5 and +6 oxidation states were present in nearly equal amounts (50%) at a pH of 7, whereas the +5 state dominated (60%) at a pH of 8.5 and the +6 state dominated (70%) at a pH of 6.

Experimentally determined solubilities at 60ºC in J-13 water ranged from 2.7×10^{-8} M at a pH of 6 to 1.2×10^{-7} M at a pH of 8.5. For UE-25 p#l water, the solubilities ranged from 4.5×10^{-7} M at a pH of 7 to 1.0×10^{-6} M at a pH of 8.5. The solubility-controlling solids at 60ºC were found to be amorphous Pu(IV) polymer and PuO_2.

The speciation of plutonium in these solutions could not be determined due to the low solubilities of plutonium in these water compositions relative to the detection limits of the available spectroscopic techniques. Modeling calculations with the EQ3 speciation computer code suggest that in J-13 water at 25ºC the plutonyl ion and various carbonate complexes are most important at pH values from 6 to 7, whereas carbonate complexes and hydrolysis products are most important at a pH of 8.5 (Nitsche 1991a). Speciation in the UE-25 p#l water has not been modeled.

It is noteworthy that the experimentally determined redox behavior of plutonium in solution was quite distinct from the behavior predicted on the basis of EQ3 calculations (Nitsche 1991a). The causes for the differences in measured and calculated behavior have not been defined. They could involve various types of kinetic effects, including radiolysis effects, as well as the quality of the literature data in the EQ3 database. In any case, the uncertainties in our knowledge of the solution behavior of plutonium will make it difficult to properly interpret the sorption behavior of that element.

Qualitative evidence for behavior in the surficial environment.
Although naturally occurring plutonium has been detected at ultratrace levels in the environment, there is little documentation of the chemical controls on the mobility of this plutonium. However, anthropogenic plutonium has been present in the environment for decades. Data on the environmental behavior of this plutonium provide some indications of the behavior to be anticipated for plutonium emplaced in the proposed repository at Yucca Mountain.

Various papers in the literature discuss the transport of plutonium in the surficial environment around process stream outfalls or burial sites (for example, Means et al. 1978; Price and Ames 1978; Polzer et al. 1983). Unfortunately, the data on plutonium transport discussed in these papers are difficult to apply to the Yucca Mountain site because the waste streams included various types of organic ligands (for example, EDTA) that tend to enhance the transport of plutonium at these sites. In addition, the initial pH of many of these waste streams was in the acid range (2–4). Low pH conditions are not expected in the Yucca Mountain flow system. Organic ligands may be present at trace levels in this flow system, but they are not expected to play a major role in radionuclide transport.

The results of studies of plutonium transport in areas exposed to physical dispersal processes (for example, safety tests of nuclear weapons) are also difficult to interpret because of subsequent disturbances of the surface soils by wind, burrowing ani-

mals, construction activities, and so forth (for example, Essington et al. 1978).

Studies of the fate of global fallout for atmospheric nuclear weapons tests are more appropriate to the prediction of the transport of plutonium from a potential repository at Yucca Mountain. Most of these studies have involved the measurement of plutonium activities in seawater, lake water, and associated sediments (for example, Sholkovitz 1983). In general, these studies find that the bulk of the fallout-derived plutonium is present in the sediments with minor concentrations found in the waters. Interestingly, the plutonium present in the waters is often an oxidized form (that is, $+5$ or $+6$), whereas the fraction in the sediment is thought to be a reduced form (Waters 1983). "Distribution coefficients" have been calculated based on the water and sediment plutonium concentrations even though the water and sediment samples may be from areas that are separated by tens of kilometers. This makes it difficult to evaluate the calculated distribution coefficients in relation to sites such as the potential repository in Yucca Mountain.

More pertinent perhaps are the measurement of plutonium concentrations in oceanic sediments and their associated pore waters (Buesseler and Sholkovitz 1987). Such studies invariably yield sorption coefficients for plutonium in the range of 10^3 to 10^5 ml/g with the lower values observed in the more oxidized sediments. Given the high ionic strength of seawater (that is, the pore waters), these data suggest that ionic-strength effects are not an issue in the plutonium sorption behavior in natural systems. However, complexation of plutonium by carbonate can be significant and appears to be the cause for elevated plutonium activities in several high alkalinity (0.3–3.0 M) lakes in the western United States (Sanchez et al. 1985). Because alkalinity values are expected to be orders of magnitude lower within the Yucca Mountain flow system relative to the levels found in these lakes, carbonate complexation in the solution phase should not be an issue at this site.

An important aspect of all the studies on plutonium sorption behavior is the issue of redox disequilibrium. In seawater and many lake waters, the inorganic species of plutonium in solution appears to be dominated by the $+5$ and $+6$ oxidation states with the $+3$ and $+4$ states present at much lower concentrations (Waters 1983). In the solid phase, the oxidation state is thought to be predominantly $+4$. This aspect of plutonium solution chemistry has been studied in the laboratory for many years and appears to involve various disproportionation reactions that are not fully understood (for example, Newton et al. 1986).

The question of concern to the present study is how groundwater compositional parameters will effect this redox disequilibrium and, in turn, the sorption behavior of plutonium. In the disproportionation experiments reported by Newton et al. (1986) and in the solubility experiments reported by Nitsche et al. (1992a, 1994), plutonium concentrations in the experiments were sufficiently high that radiation effects were evident. An important question is "If plutonium is present at trace levels and not in contact with a 'pure' plutonium compound, are disproportionation reactions still a factor?" If they are not, then the next question would be "What is the stable oxidation state of plutonium when it is present at trace levels in Yucca Mountain groundwaters?" If the $+5$ or $+6$ oxidation states of plutonium are the dominant stable states in groundwaters such as those found within Yucca Mountain, as suggested by the experiments of Nitsche et al. (1992a, 1994), then plutonium might be as mobile as neptunyl in the far-field of the potential repository, assuming it is present as the plutonyl ion or its complexes. On the other hand, if the $+4$ or $+3$ oxidation states are the dominant stable states in these groundwaters, this element would likely behave as other $+3$ and $+4$ actinides and be strongly sorbed with minimal migration potential.

Data from laboratory sorption experiments. Allard (1982) reported results on experiments involving plutonium sorption on quartz, apatite, attapulgite, montmorillonite, and various minerals

rich in ferrous iron in a dilute groundwater containing plutonium at 1.8×10^{-11} M. For all the minerals, the sorption coefficients were greater than 10^3 ml/g over a pH range from 4 to 9. Apatite, attapulgite, biotite, and montmorillonite showed sorption coefficients greater than 10^4 ml/g over this pH range. Torstenfelt et al. (1988) presented data for plutonium sorption on feldspars, clays, and granite in contact with J-13 water. The sorption coefficients reported by them are generally between 100 to 200 ml/g in neutral to alkaline solutions. These authors emphasized the importance of proper experimental technique in the determination of sorption coefficient values for plutonium and noted the potential for colloid formation in these types of experiments. Data indicating high affinity of plutonium for ferric oxyhydroxide, manganese oxide, and carbonate mineral surfaces were presented by Means et al. (1978), Keeney-Kennicutt and Morse (1985), and Sanchez et al. (1985). Means et al. noted that manganese oxides sorb plutonium more strongly than ferric oxyhydroxides in natural environments (presumably as a result of redox reactions on the manganese-oxide surface).

Measurements of plutonium sorption coefficients involving Yucca Mountain rock samples and J-13 groundwater were summarized by Thomas (1987). The following observations are considered the most significant. First, the values measured for the plutonium sorption coefficient range from 20 to greater than 4,500 ml/g with most values lying between 100 to 2,000 ml/g at a pH of from 8.2 to 8.8. Second, the coefficients determined during the desorption experiments were occasionally in the range of the sorption coefficient values, but more typically, they were 10 to 20 times larger, reflecting the irreversibility of the sorption reactions. Third, zeolitic samples typically had lower sorption-coefficient values than vitric or devitrified samples. It appears that rocks that have essentially no reduction capacity remaining (that is, samples lacking ferrous iron or sulfide) show the lowest sorption coefficients for plutonium. Fourth, samples with calcite or clay showed the largest sorption coefficients ($>$ 4,500 ml/g for samples with 30% calcite). Fifth, based on the six to eight experiments for which data are available, there was up to a factor of twelve variation in sorption coefficients as a function of groundwater composition. Water from Well UE-25 p#1 was associated with the largest values (240–540 ml/g, sorption-desorption) with waters from Wells H-3 and J-13 showing the lowest values (20–230 ml/g). The higher values obtained with UE-25 p#l water may reflect calcite precipitation. Sixth, there did not appear to be a dependence of the sorption coefficient on pH over the range from 7 to 9, although the available data are limited on this issue. Seventh, there was less than a factor of four dependence of the sorption coefficient on radionuclide concentration over the range from 10^{-9} to 10^{-12} M.

Conclusions that can be drawn from these data include: 1) the plutonium sorption coefficient will be greater than 100 ml/g for most of the groundwater and rock compositions likely to be encountered within Yucca Mountain; 2) calcite and clay promote plutonium sorption/coprecipitation and may retard plutonium migration in fractures; and 3) the redox state of the groundwaters and of the rock units in which they occur may be critical to the sorption behavior of plutonium.

We studied the sorption of plutonium onto the three main types of tuff in J-13 water (under oxidizing conditions) using a carbon-dioxide overpressure (to obtain a pH of 7). To identify the sorbing minerals in the tuffs, we also studied sorption onto the pure minerals hematite, clinoptilolite, albite, and quartz. The results of the batch-sorption experiments for plutonium are summarized in Fig. 37. Because plutonium sorbs onto nongeologic media, the batch-sorption distribution coefficients reported in Fig. 37 are based on the concentration of plutonium in the control solutions. The affinity of tuffs for plutonium at a pH of 7 in decreasing order is zeolitic $>$ vitric $>$ devitrified. The affinity of minerals for plutonium in decreasing order is hematite $>$ clinoptilolite $>$ albite $>$ quartz. Inspection of Fig. 37 indicates that plutonium sorption is nonlinear in the concentration range

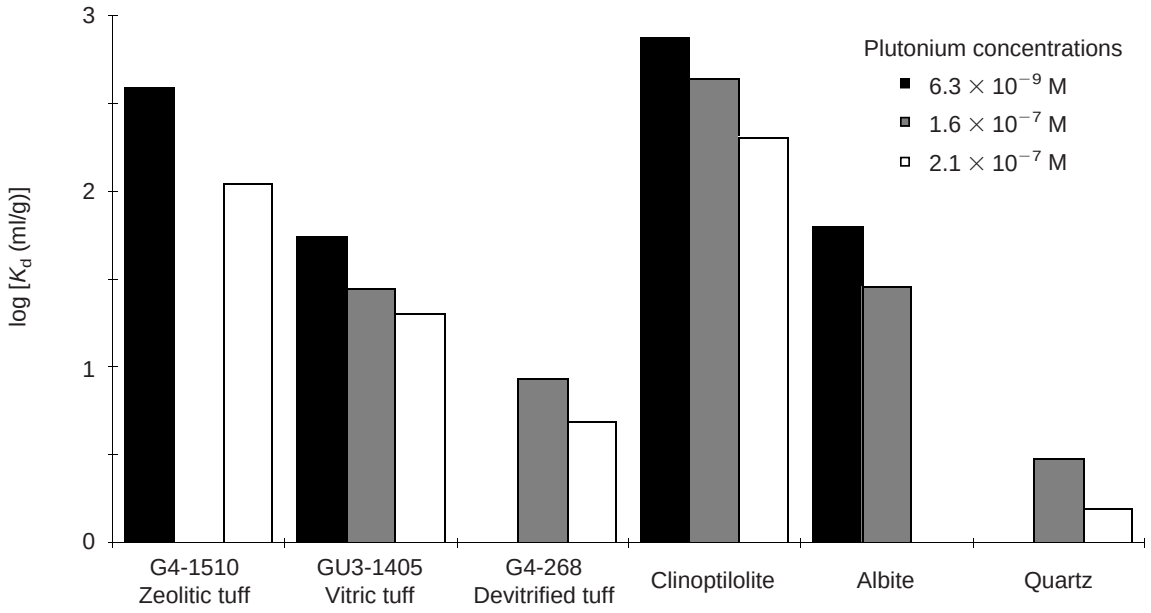

Figure 37. Plutonium Sorption. The logarithm of the batch-sorption distribution coefficient, log K_d, is shown for the sorption of plutonium in J-13 well water at a pH of 7 and the specified initial plutonium concentrations. All solids, except clinoptilolite, were wet-sieved to particle sizes ranging from 75 to 500 μm. The periods of pretreatment and sorption were each 3 days.

---

from 6×10^{-9} to 2×10^{-7} M.

Nitsche et al. (1993a) report that even when a plutonium solution in J-13 or UE-25 p#1 water is prepared starting in the $+4$ oxidation state, the predominant final oxidation state is $+5$, or Pu(V). The solution used for our plutonium sorption experiments was prepared from a well-characterized Pu(V) acidic stock in J-13 well water. Consequently, it would be reasonable to assume that the plutonium would have remained predominantly in the $+5$ oxidation state in the solution used for the sorption studies.

Comparison of the data of Fig. 37 with the results of similar experiments with neptunium and uranium indicates that significant plutonium sorption occurred in tuffs and minerals that exhibit very small sorption of Np(V) and U(VI). This result is very puzzling; if plutonium in J-13 well water is predominantly Pu(V) and Pu(VI), it is expected that its sorption behavior would have been similar to that observed for Np(V) and U(VI). Several possible explanations of the plutonium sorption results are: 1) Nitsche's data for the oxidation states are incorrect, and the predominant plutonium oxidation state in J-13 well water at a pH of 7 is Pu(IV), not Pu(V) and Pu(VI); 2) the Pu(IV) species is what sorbs from J-13 water but a re-equilibration in the solution phase produces more Pu(IV) to maintain equilibrium (which implies that the kinetics of plutonium speciation in solution are fast); and 3) Pu(V) and Pu(VI) reduce to Pu(IV) at solid surfaces (as a result of changes in the solution redox potential in the presence of the solid phases).

The sorption of plutonium onto tuffs and minerals in J-13 and synthetic UE-25 p#1 water under atmospheric conditions was studied as a function of time and initial plutonium solution concentration (Fig. 38 shows an example). Inspection of this figure indicates that plutonium sorption is extremely slow (possibly due to a redox reaction at the solid surface). Even after 32 days of sorption, equilibra-

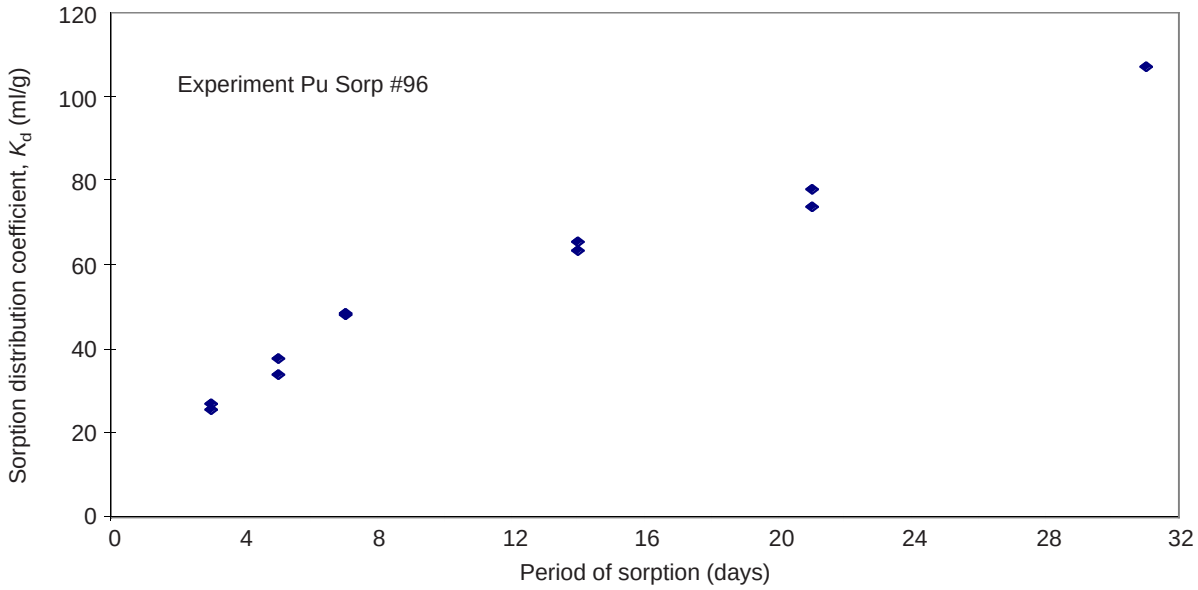

Figure 38. Plutonium Sorption onto Devitrified Tuff in J-13 Water. The plot shows plutonium sorption onto tuff sample G4-272 as a function of time under atmospheric conditions with an original plutonium concentration in J-13 well water of 2.4×10^{-7} M.

Table 46. Plutonium Sorption Distribution Coefficients (under atmospheric conditions)

Solid phase	K_d range in J-13 water (ml/g)	K_d range in synthetic UE-25 p#1 water (ml/g)
Vitric tuff	600 – 2,000	100 – 400
Zeolitic tuff	300 – 500	100 – 400
Devitrified tuff	40 – 100	20 – 70
Synthetic hematite	> 10,000	> 10,000
Montmorillonite	> 10,000	> 10,000
Clinoptilolite	600 – 3,000	2,000 – 5,000
Calcite	200 – 1,000	100 – 800
Gibbsite	0 – 10	10 – 90
Albite	3 – 10	< 10
Quartz	< 10	< 10

tion had not been achieved. The sorption of plutonium onto the tuffs and minerals is very substantial.

Table 46 summarizes the ranges for sorption distribution coefficients in Yucca Mountain groundwaters for plutonium. The sorption isotherms for plutonium (Figs. 39 to 54) indicate that plutonium sorption as a function of radionuclide concentration cannot be expressed using a K_d; the isotherms are generally nonlinear. However, given the high affinity of Yucca Mountain tuffs for plutonium and the other observations made in this study, it

continued on page 121

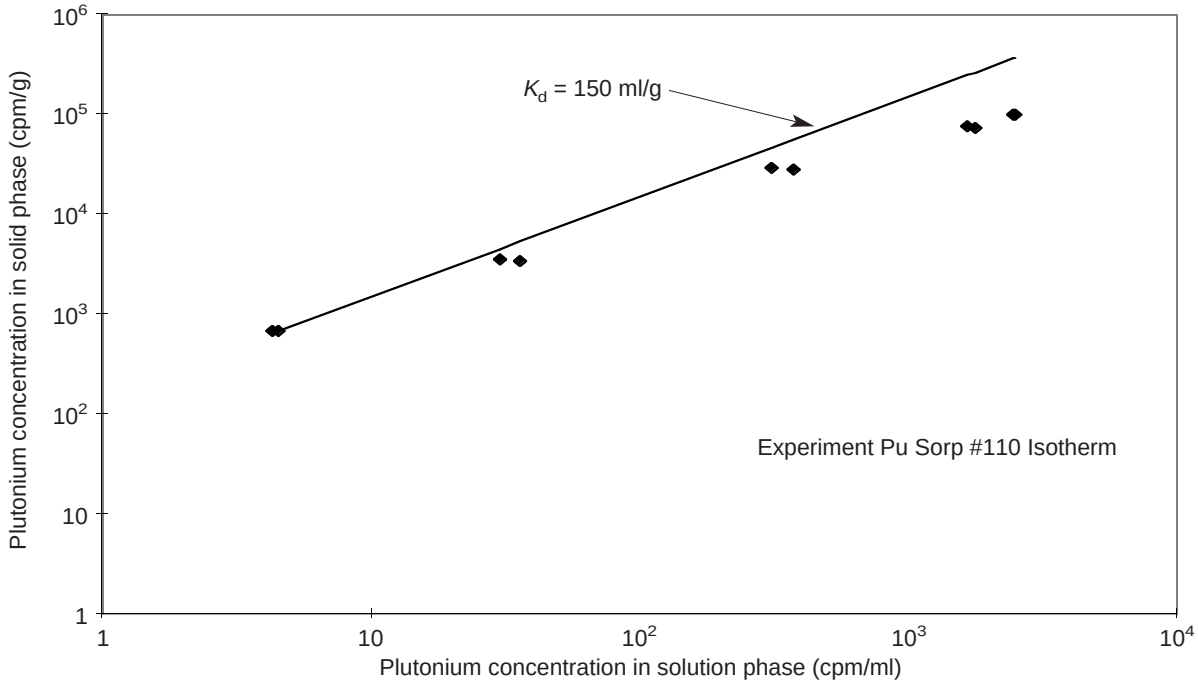

Figure 39. Plutonium Isotherm for Devitrified Tuff in J-13 Water. This plot shows plutonium sorption data (diamonds) and a linear isotherm (line) for sorption onto the tuff sample G4-272 under atmospheric conditions in J-13 well water. The period of sorption was 21 days.

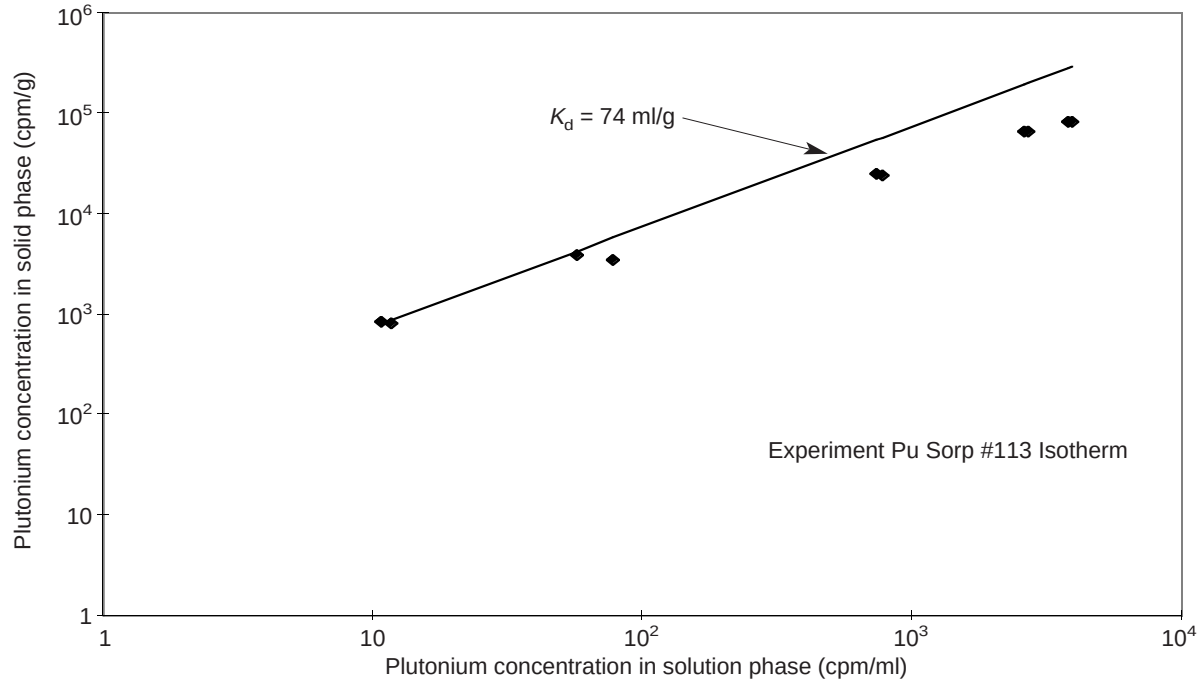

Figure 40. Plutonium Isotherm for Devitrified Tuff in Synthetic UE-25 p#1 Water. This plot shows plutonium sorption data (diamonds) and a linear isotherm (line) for sorption onto the tuff sample G4-272 under atmospheric conditions in synthetic UE-25 p#1 water. The period of sorption was 21 days.

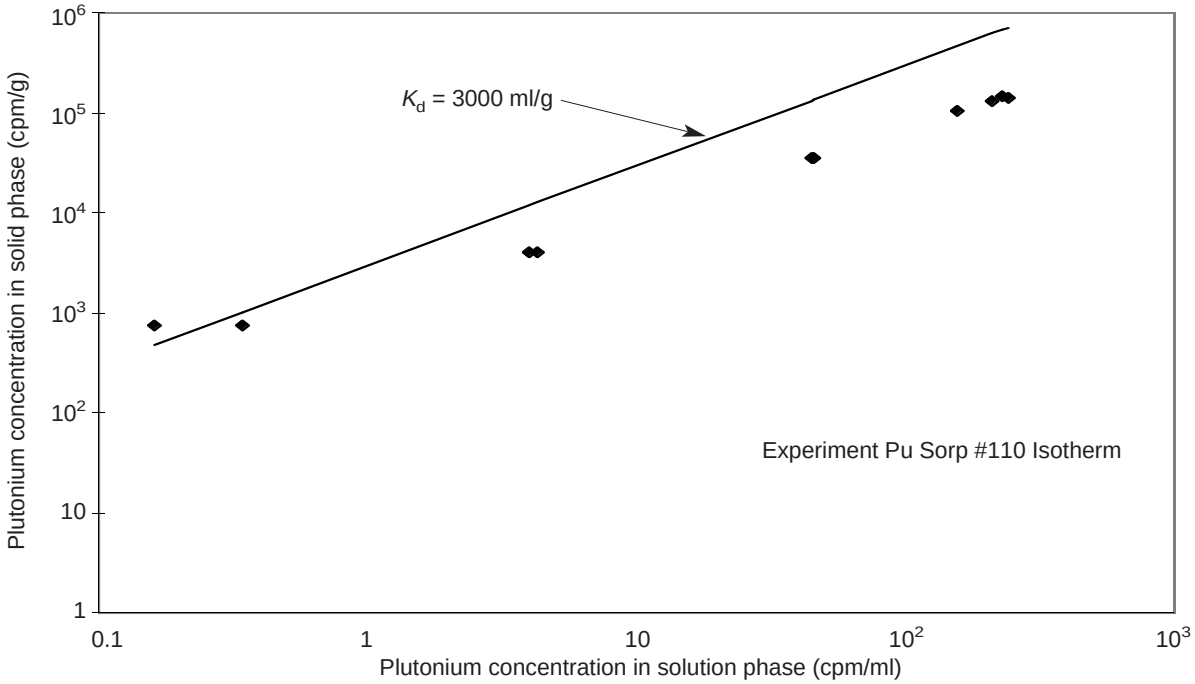

Figure 41. Plutonium Isotherm for Vitric Tuff in J-13 Water. This plot shows plutonium sorption data (diamonds) and a linear isotherm (line) for sorption onto the tuff sample GU3-1414 under atmospheric conditions in J-13 well water. The period of sorption was 21 days.

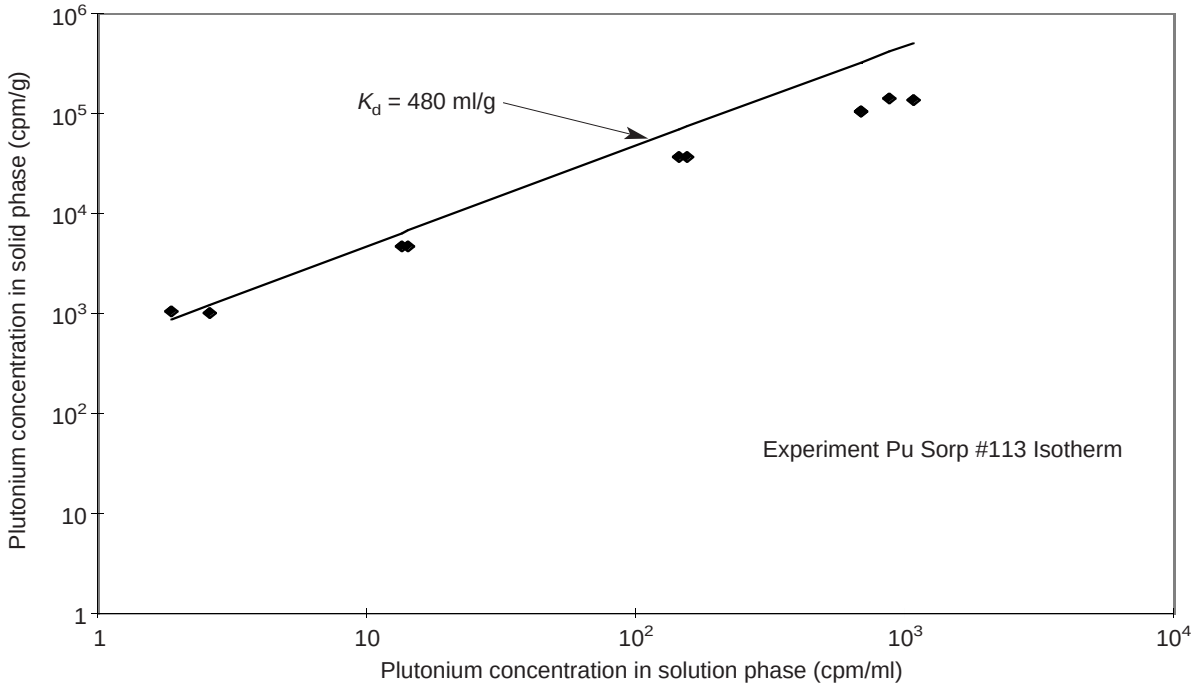

Figure 42. Plutonium Isotherm for Vitric Tuff in Synthetic UE-25 p#1 Water. This plot shows plutonium sorption data (diamonds) and a linear isotherm (line) for sorption onto the tuff sample GU3-1414 under atmospheric conditions in synthetic UE-25 p#1 water. The period of sorption was 21 days.

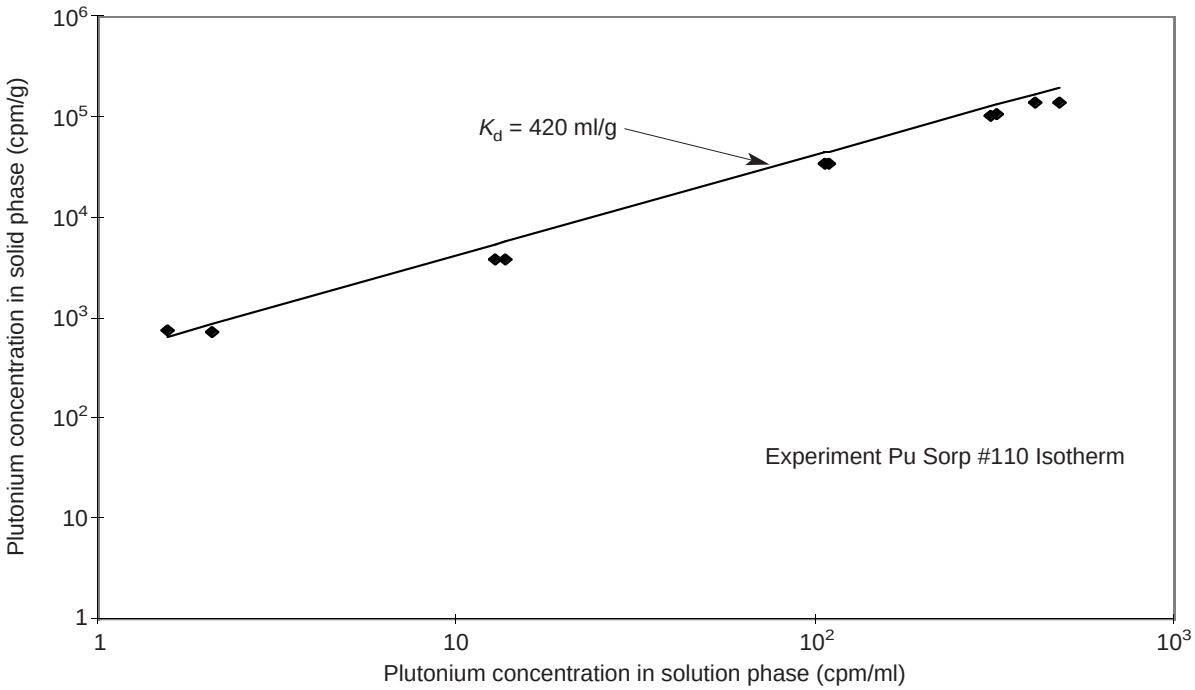

Figure 43. Plutonium Isotherm for Zeolitic Tuff in J-13 Water. This plot shows plutonium sorption data (diamonds) and a linear isotherm (line) for sorption onto the tuff sample G4-1515 under atmospheric conditions in J-13 well water. The period of sorption was 21 days.

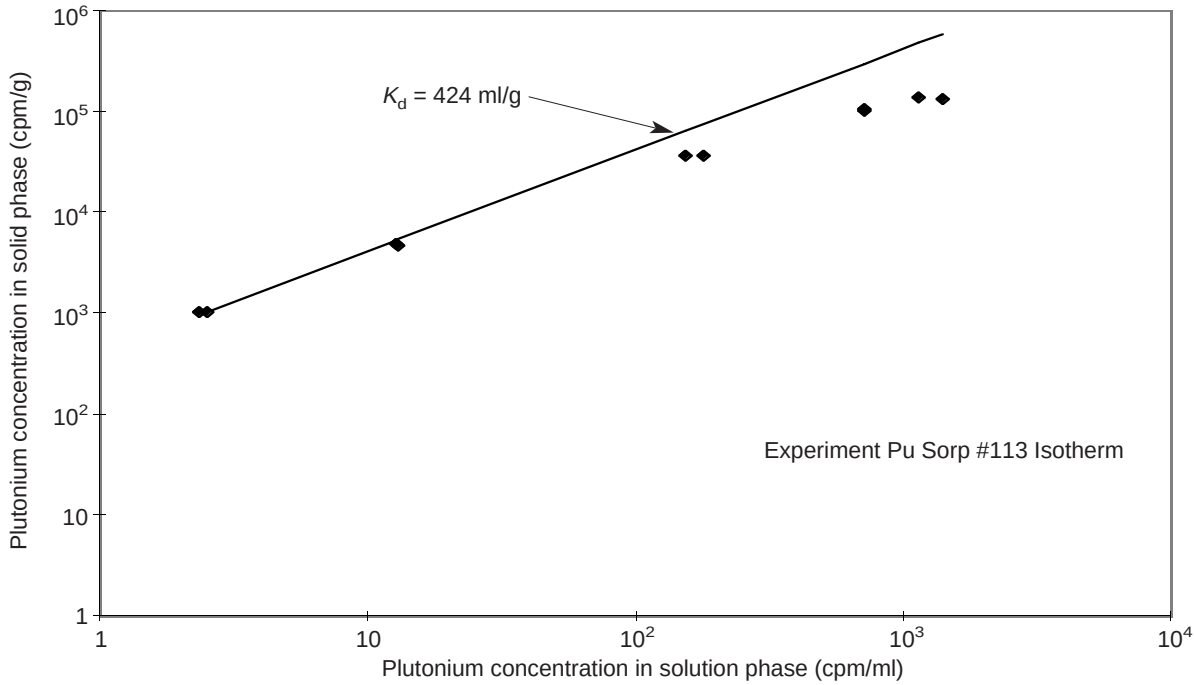

Figure 44. Plutonium Isotherm for Zeolitic Tuff in Synthetic UE-25 p#1 Water. This plot shows plutonium sorption data (diamonds) and a linear isotherm (line) for sorption onto the tuff sample G4-1515 under atmospheric conditions in synthetic UE-25 p#1 water. The period of sorption was 21 days.

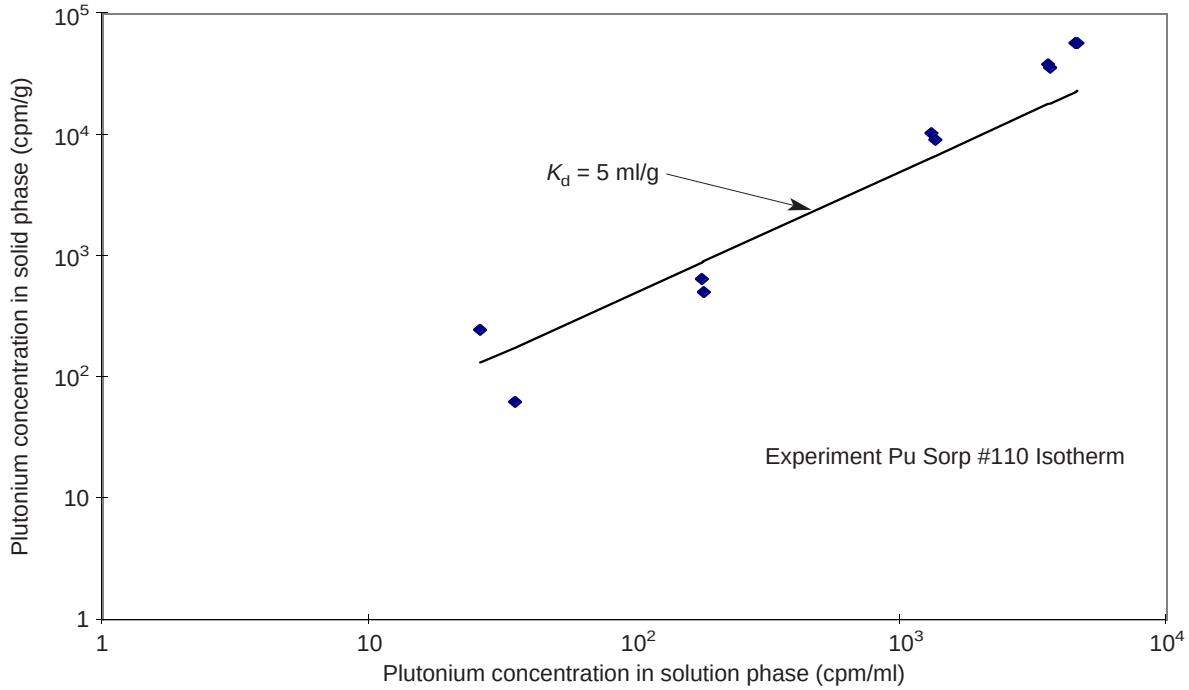

Figure 45. Plutonium Isotherm for Albite in J-13 Water. This plot shows plutonium sorption data (diamonds) and a linear isotherm (line) for sorption onto albite under atmospheric conditions in J-13 well water. The period of sorption was 21 days.

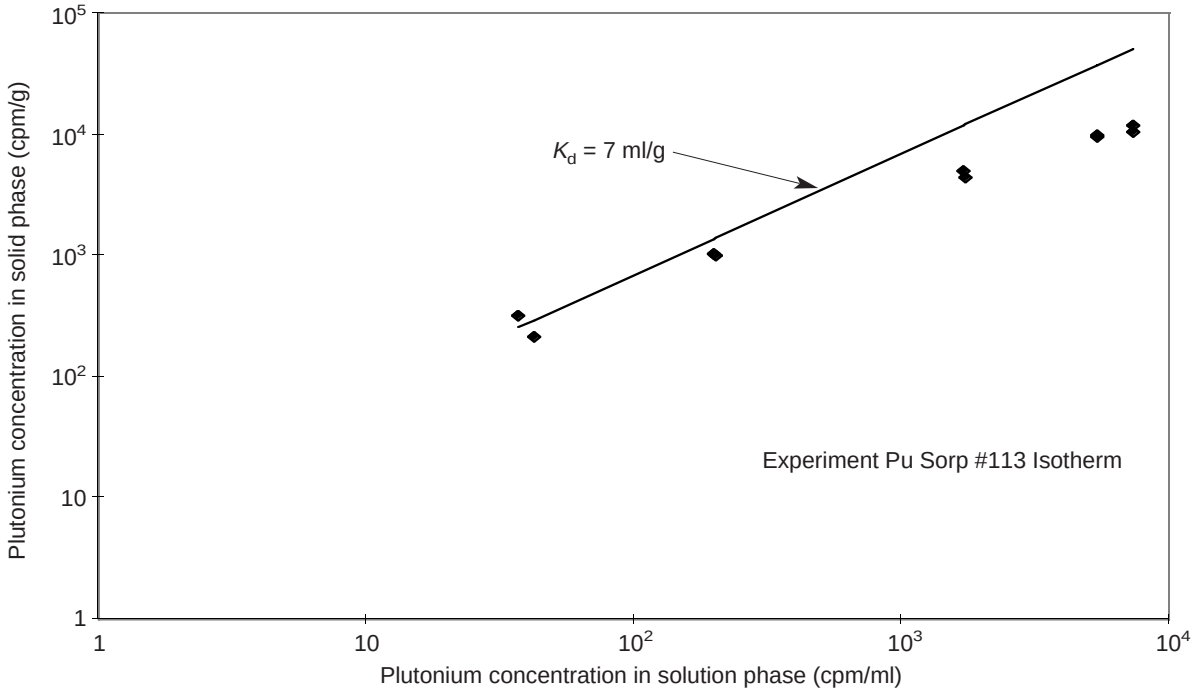

Figure 46. Plutonium Isotherm for Albite in Synthetic UE-25 p#1 Water. This plot shows plutonium sorption data (diamonds) and a linear isotherm (line) for sorption onto albite under atmospheric conditions in synthetic UE-25 p#1 water. The period of sorption was 21 days.

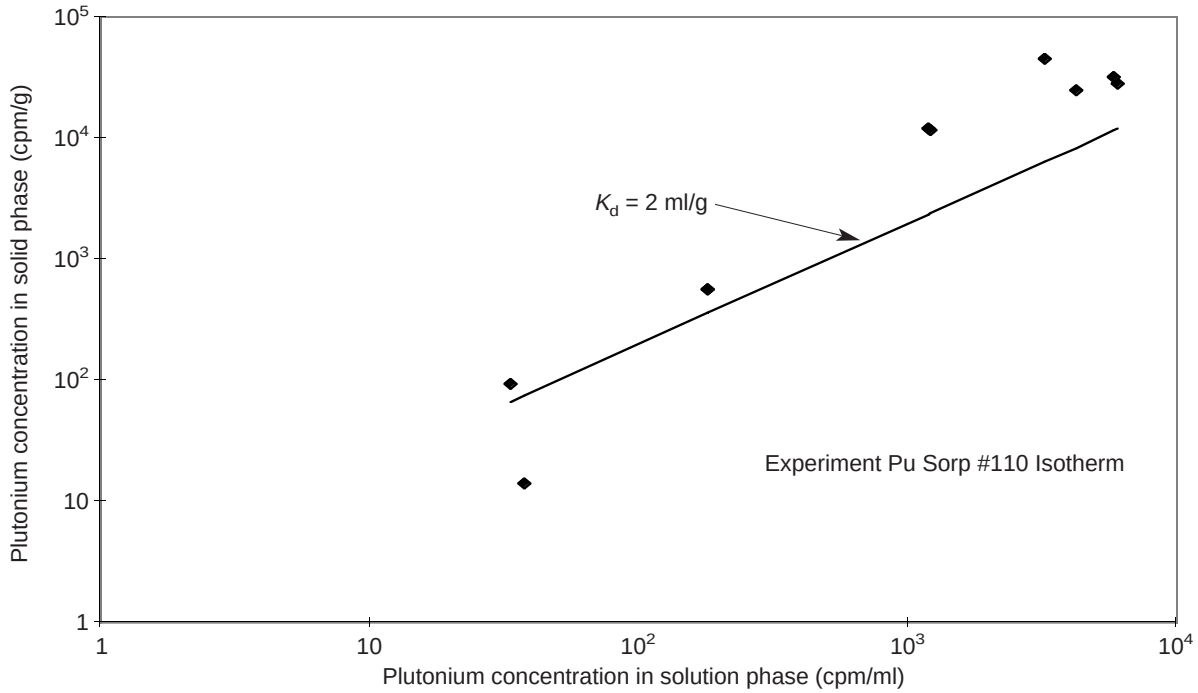

Figure 47. Plutonium Isotherm for Gibbsite in J-13 Water. This plot shows plutonium sorption data (diamonds) and a linear isotherm (line) for sorption onto gibbsite under atmospheric conditions in J-13 well water. The period of sorption was 21 days.

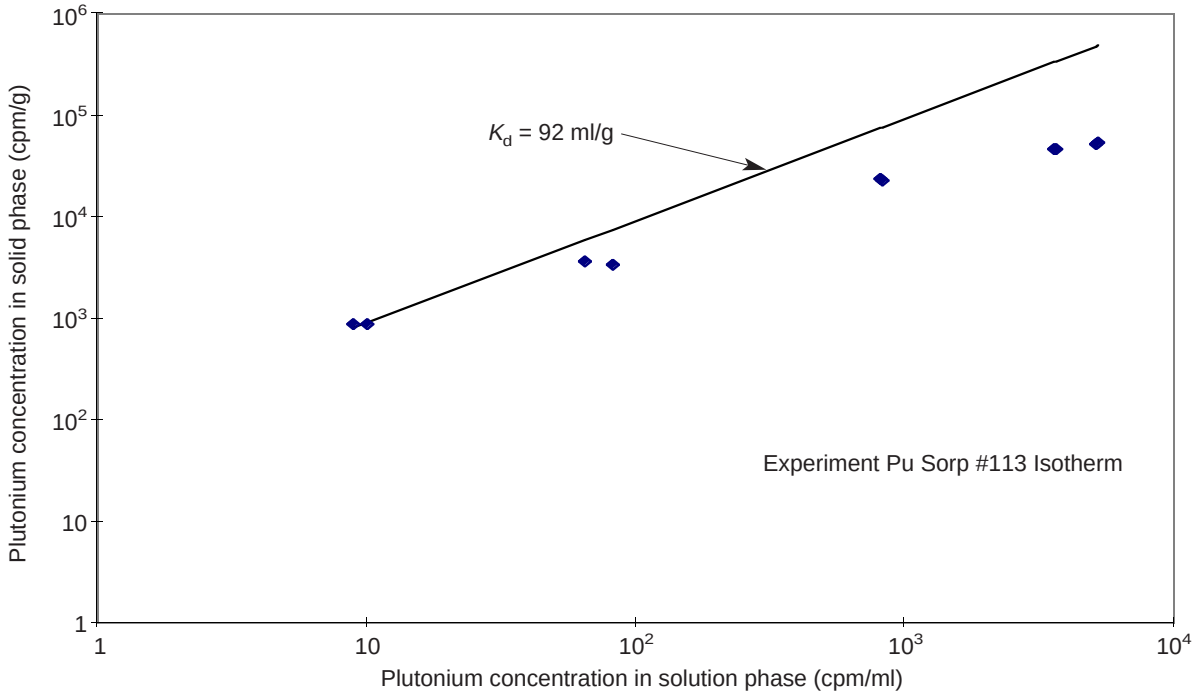

Figure 48. Plutonium Isotherm for Gibbsite in Synthetic UE-25 p#1 Water. This plot shows plutonium sorption data (diamonds) and a linear isotherm (line) for sorption onto gibbsite under atmospheric conditions in synthetic UE-25 p#1 water. The period of sorption was 21 days.

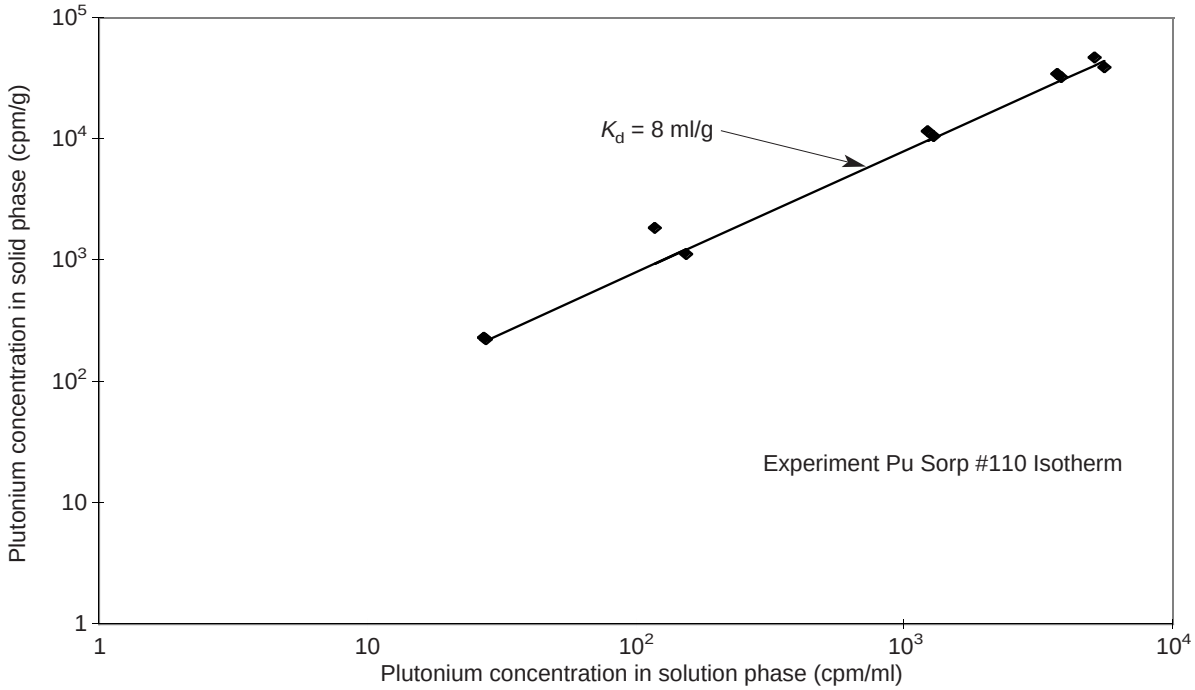

Figure 49. Plutonium Isotherm for Quartz in J-13 Water. This plot shows plutonium sorption data (diamonds) and a linear isotherm (line) for sorption onto quartz under atmospheric conditions in J-13 well water. The period of sorption was 21 days.

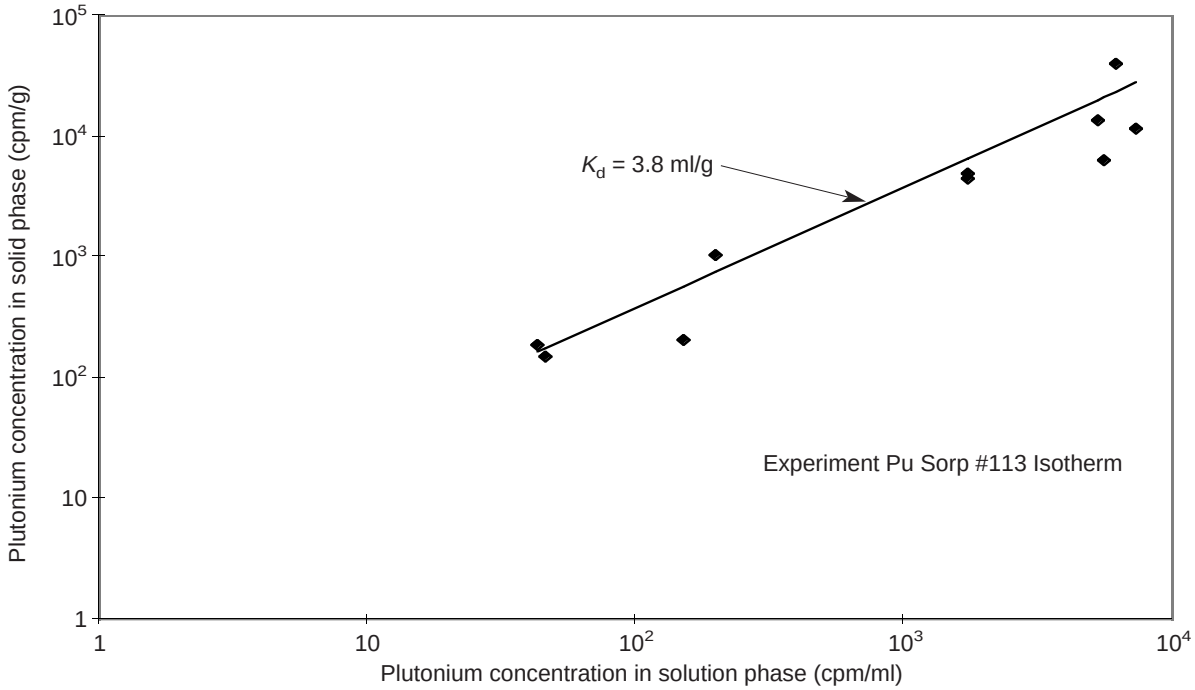

Figure 50. Plutonium Isotherm for Quartz in Synthetic UE-25 p#1 Water. This plot shows plutonium sorption data (diamonds) and a linear isotherm (line) for sorption onto quartz under atmospheric conditions in synthetic UE-25 p#1 water. The period of sorption was 21 days.

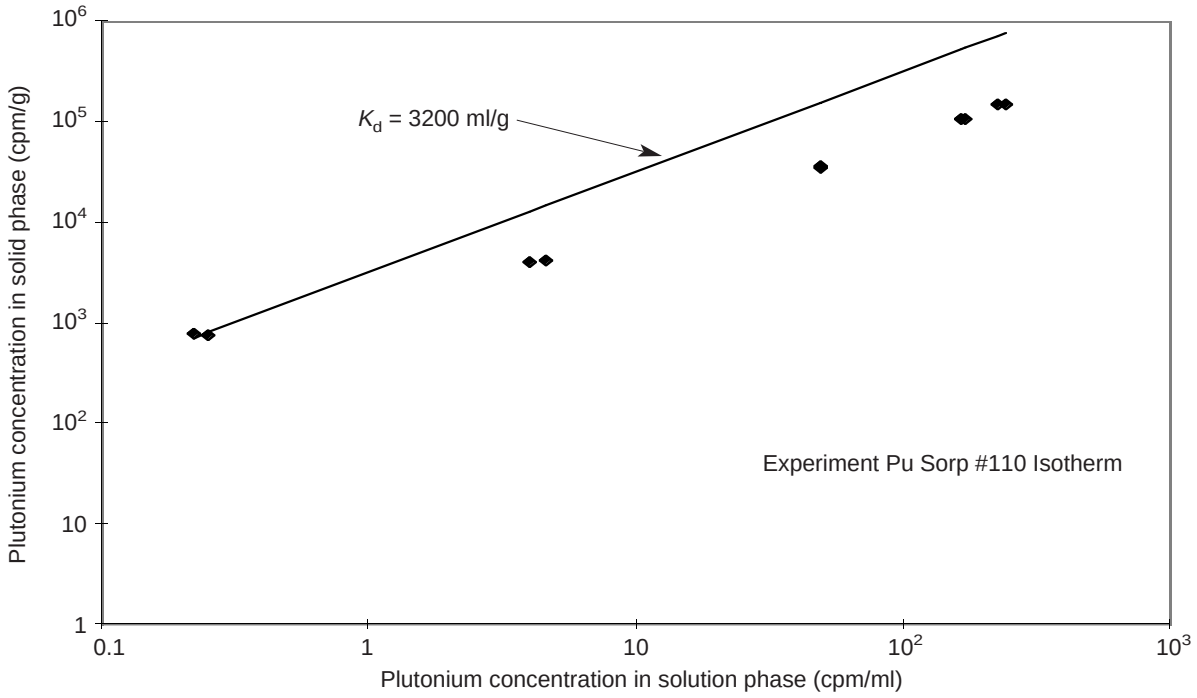

Figure 51. Plutonium Isotherm for Clinoptilolite in J-13 Water. This plot shows plutonium sorption data (diamonds) and a linear isotherm (line) for sorption onto clinoptilolite under atmospheric conditions in J-13 well water. The period of sorption was 21 days.

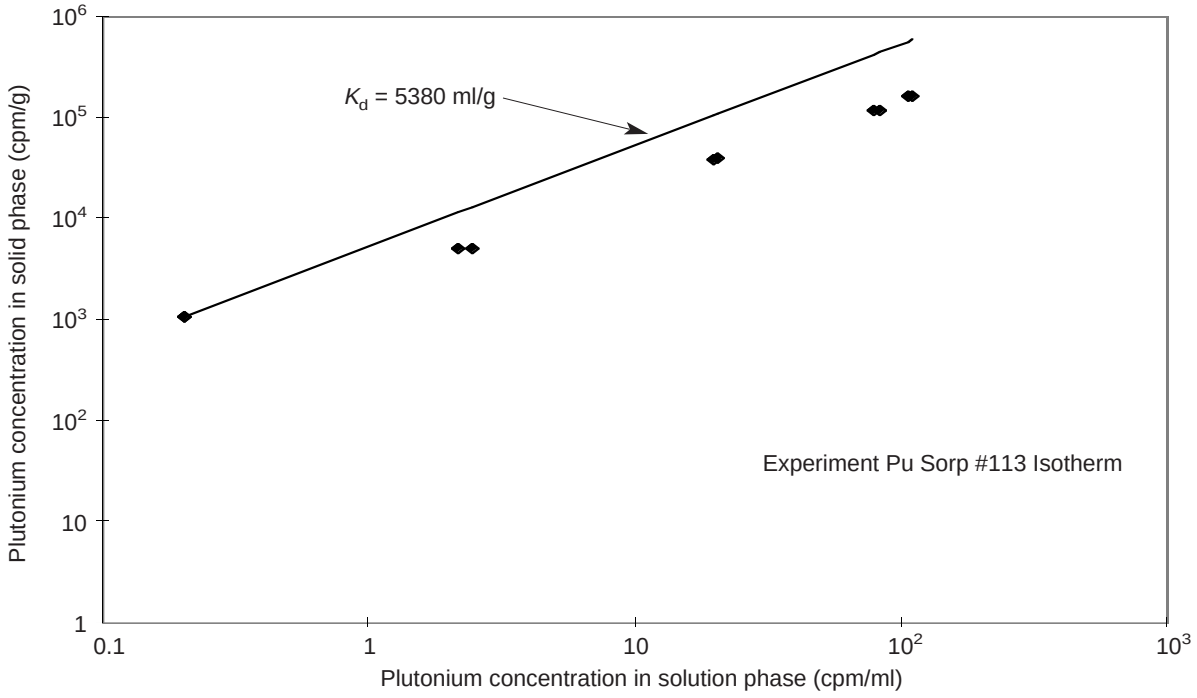

Figure 52. Plutonium Isotherm for Clinoptilolite in Synthetic UE-25 p#1 Water. This plot shows plutonium sorption data (diamonds) and a linear isotherm (line) for sorption onto clinoptilolite under atmospheric conditions in synthetic UE-25 p#1 water. The period of sorption was 21 days.

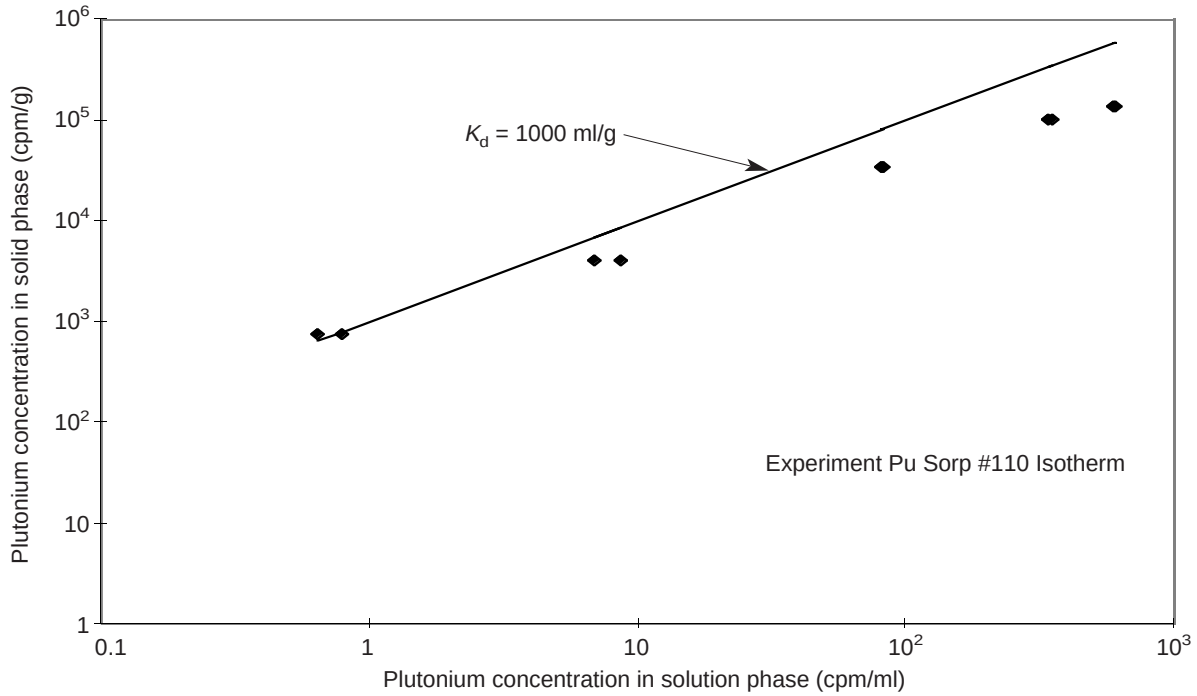

Figure 53. Plutonium Isotherm for Natural Calcite in J-13 Water. This plot shows plutonium sorption data (diamonds) and a linear isotherm (line) for sorption onto natural calcite under atmospheric conditions in J-13 well water. The period of sorption was 21 days.

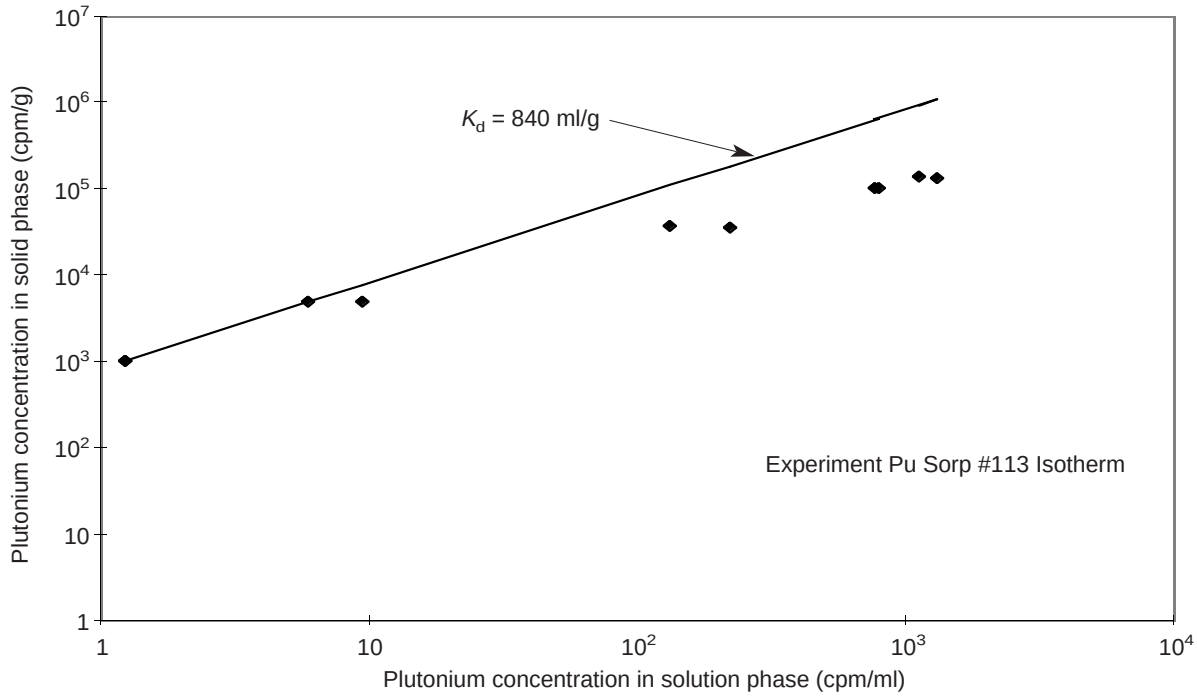

Figure 54. Plutonium Isotherm for Natural Calcite in Synthetic UE-25 p#1 Water. This plot shows plutonium sorption data (diamonds) and a linear isotherm (line) for sorption onto natural calcite under atmospheric conditions in synthetic UE-25 p#1 water. The period of sorption was 21 days.

continued from page 112

appears that using a K_d to predict plutonium radionuclide transport in performance-assessment calculations will provide conservative predictions for the release of radionuclides.

Conclusions regarding sorption behavior with respect to expected variations in groundwaters.
On the basis of the discussion in the previous sections, it appears the most important groundwater compositional parameter in relation to plutonium sorption is the redox potential. Closely related to this parameter is the abundance of ferrous iron in the rock units. Note that redox potentials in groundwaters may not reflect equilibrium with the host rock (Lindberg and Runnells 1984). Complexation reactions with inorganic ligands in solution and variations in solution pH appear to have less significant impacts on the sorption behavior of plutonium in Yucca Mountain rock-water systems.

Cesium, Radium, and Strontium

Behavior in solutions representative of Yucca Mountain groundwaters.
These elements show relatively simple solution behavior in typical groundwaters. They are not subject to changes in oxidation state in the groundwater compositions expected in Yucca Mountain. Radium and cesium are invariably present as the simple Ra^{2+} and Cs^{+} cations in the expected groundwater compositions (Ogard and Kerrisk 1984). Strontium exists primarily as the Sr^{2+} ion in these waters but may also be present as the neutral aqueous species $SrSO_4$ at concentrations of a few per cent of the total strontium solution concentration (Ogard and Kerrisk 1984).

Qualitative evidence for behavior in the surficial environment.
The literature on the behavior of cesium, radium, and strontium in the surficial environment is voluminous and will not be reviewed here. Their sorption behavior is fairly well understood and is largely controlled by ion-exchange reactions (Bolt and Bruggenwert 1976), although surface-complexation reactions involving these elements have also been discussed (for example, Balistrieri and Murray 1982). The dominant controls on the ion-exchange reactions are the cation-exchange capacities of the minerals in the system, the abundances of these ion-exchanging minerals, their selectivity coefficients for the various cations in the solution phase, and the concentrations of the competing cations in the solution phase. The selectivity of most clays and zeolites for cesium, radium, and strontium is greater than the selectivities for the major cations in solution. Further, pH does not have a significant effect on the sorption behavior of these elements over the pH range of interest. Because their sorption behavior is fairly well understood and because this behavior depends strongly on local conditions, data from sites other than Yucca Mountain will not be reviewed here.

Data from laboratory sorption experiments.
Sorption coefficients for cesium, radium, and strontium were reviewed by Daniels et al. (1982), Thomas (1987), and Meijer (1990). For cesium at low concentrations (10^{-8} M), sorption coefficients are greater than 100 ml/g for all water-rock combinations tested except UE-25 p#l water in contact with vitric tuff (Knight and Thomas 1987). Cesium sorption coefficients for the devitrified-tuff/J-13-water system show a clear concentration dependence that has been modeled with a Fruendlich isotherm (Polzer and Fuentes 1988). The coefficients for this particular rock-water system are greater than 100 ml/g for cesium solution concentrations below 5×10^{-5} M. For UE-25 p#l water in contact with this rock type, the coefficient would be 100 ml/g at somewhat lower solution concentrations. In any case, in the higher ionic-strength waters (0.02 eq/l), including unsaturated-zone waters, the sorption coefficients for cesium on devitrified and vitric samples may be less than 100 ml/g if solution concentrations of cesium exceed 10^{-6} M. For zeolitic tuffs, cesium sorption coefficients are greater than 100 ml/g for all water compositions and cesium concentrations anticipated in the potential repository environment.

Radium appears to have a somewhat higher affinity for sorption onto Yucca Mountain tuffs than cesium. In addition, the solubility of $RaSO_4$ limits the concentrations in solution to trace levels (10^{-7}–10^{-8} M; Ogard and Kerrisk 1984). At concentrations below the solubility limit for $RaSO_4$, sorption coefficients for radium are greater than 100 ml/g in essentially all rock-water combinations tested, using barium as an analog for radium (Knight and Thomas 1987). This fact suggests that a minimum sorption coefficient of 100 ml/g can be used for radium in all rock-water systems. For zeolitic samples, minimum values of 1,000 ml/g can be used.

Strontium sorption behavior is more sensitive to mineral and water compositions than the other two elements discussed in this section. For devitrified and vitric tuffs, sorption coefficients for the higher ionic-strength waters (such as UE-25 p#l) are in the range of 10 to 30 ml/g (Knight and Thomas 1987). These sorption coefficients will decrease as the solution concentration of strontium is increased above approximately 10^{-5} M (Thomas 1987). However, this concentration is close to the solubility limit for $SrCO_3$ in these waters so that the 10 to 30 ml/g range is likely appropriate for use in performance-assessment calculations in the devitrified or vitric tuffs. For zeolitic tuffs, a minimum value of 1,000 ml/g would be appropriate (Knight and Thomas 1987).

Conclusions regarding sorption behavior with respect to expected variations in groundwaters.
The existing sorption-coefficient database for cesium, radium, and strontium should be adequate for performance-assessment calculations. The main concern would be the concentration of cesium in the solution phase in contact with devitrified and vitric tuffs. If this concentration is over 10^{-5} M, the appropriate value for the sorption coefficient may be less than the minimum recommended value of 100 ml/g. The sorption coefficients for strontium in devitrified and vitric tuffs will be as low as 10 to 30 ml/g in higher ionic-strength waters. If additional experiments were to be carried out for this group of elements, they should focus on strontium in contact with devitrified and vitric tuffs in the higher ionic-strength waters.

Nickel and Lead

Behavior in solutions representative of Yucca Mountain groundwaters.
The aqueous solution behavior of nickel and lead is relatively simple. Within the range of groundwater compositions expected in the Yucca Mountain flow system, these elements are present in solution primarily as simple divalent cations. Several per cent of the total nickel concentration will be present as the $NiSO_4^+$(aq) complex. Similarly, several per cent of the total lead concentration will be present as the $PbCl^+$ complex.

Qualitative evidence for behavior in the surficial environment.
The behavior of nickel and lead in the surficial environment has been studied in some detail (for example, Snodgrass 1980). These elements are generally quite particle-reactive. The dominant mechanisms that control their sorption behavior are ion exchange on clay minerals (for example, Bowman and O'Conner 1982) and adsorption onto various oxides (for example, Theis and Richter 1980). The selectivities of clay minerals for nickel and lead are large relative to the major cations (such as Mg^{2+}) in typical groundwaters (Decarreau 1985). Solution compositional parameters that can influence this adsorption behavior include pH, ionic strength, concentrations of competing ions, and concentrations of complexing agents (see review by Rai and Zachara 1984).

Data from laboratory sorption experiments.
Data on the sorption behavior of nickel in Yucca Mountain rock-water systems were reported by Knight and Lawrence (1988). Sorption and desorption ratios were determined in several water compositions in the pH range from 8.3 to 9.0 with nickel concentrations in solution of approximately 10^{-8} M. For devitrified and zeolitic samples,

sorption coefficients were in the range of 200 to 400 ml/g. Sorption coefficients obtained in the desorption step were generally a factor of two larger than the sorption coefficients. In the only vitric sample analyzed, sorption coefficients ranged from approximately 30 to 70 ml/g. For the desorption step, the coefficients were in the range of 33 to 72 ml/g for this rock type. We were unable to find references to the adsorption behavior of lead on tuffaceous or even granitic rock samples.

Data on sorption of transition metals on synthetic zeolites suggest that Pb^{2+} has a high affinity for ion exchange compared with Sr^{2+}, whereas Ni^{2+} has a lower affinity relative to Sr^{2+} (Barrer and Townsend 1976; Obeng et al. 1981; Blanchard et al. 1984). This suggests the zeolitic zones within Yucca Mountain could be significant barriers to lead migration.

Conclusions regarding sorption behavior with respect to expected variations in groundwaters.
Based on information in the literature, the sorption behavior of these elements will be determined largely by the free-ion activities in solution and the cation-exchange capacity of the host rock (for example, Bowman and O'Connor 1982; Rai and Zachara 1984). Solution pH and oxide-mineral abundances may be a factor in rocks in which nickel and lead sorb primarily by surface-complexation mechanisms. In any case, lead appears to sorb more strongly than nickel in most surficial environments, and both elements appear to sorb more strongly than strontium (Bowman and O'Connor 1982). The nickel sorption coefficients discussed in the previous section could reasonably be used as default values for lead in performance-assessment calculations. For nickel, a minimum sorption coefficient of 100 ml/g could be used in the devitrified and zeolitic zones. For the vitric zones, the performance-assessment calculations could be done using random sampling and a normal distribution ranging from 0 to 50 ml/g.

Neptunium, Protactinium, Selenium, and Uranium

The main factor that neptunium, protactinium, selenium, and uranium have in common is that they all tend to show small values for sorption coefficients in the rock-water systems expected within Yucca Mountain under oxidizing conditions. Under more reducing conditions, they would all have much lower solubilities and higher sorption affinities in Yucca Mountain groundwaters. As the solution and sorption behavior is somewhat different for each of these elements, they will be discussed separately.

Neptunium

Behavior in solutions representative of Yucca Mountain groundwaters.
In solutions representative of water compositions expected within the Yucca Mountain flow system, neptunium will be predominantly in a $+5$ oxidation state. Unlike pentavalent niobium and protactinium, Np(V) compounds are relatively soluble (Nitsche et al. 1994). This result appears to be due to the formation of the oxocation NpO_2^+ in solution. Pentavalent niobium and protactinium apparently do not form analogous oxocations (that is, NbO_2^+ and PaO_2^+) in near-neutral solutions to an appreciable degree. Instead they hydrolyze and form insoluble precipitates. The NpO_2^+ ion appears to be quite stable in aqueous solutions (Cotton and Wilkinson 1988).

Nitsche et al. (1992a, 1994) studied the solubilities and speciation of neptunyl compounds in solutions representative of water compositions expected within Yucca Mountain. The results at 25ºC and several pH values are summarized in Table 47. The solubility-controlling solids were found to be hydrated sodium neptunyl carbonates, and the primary species for the water compositions expected at Yucca Mountain were NpO_2^+ and $NpO_2(CO_3)^-$. The speciation results of Table 47 for J-13 water are similar, although not identical, to those calculated using the EQ3 speciation code (Nitsche 1991a).

At higher temperatures (60º and 90ºC), neptunium was less complexed by carbonate at pH values of 6 and 7 but more highly complexed with carbonate at a pH of 8.5. The solubilities at 60ºC were similar to those in Table 47, although they were somewhat higher at a pH of 8.5 relative to the 25ºC results.

Qualitative evidence for behavior in the surficial environment.
Although ^{237}Np has been detected in the surficial environment (for example, Sakanoue 1987), essentially no information has been found on its transport behavior in this environment.

Data from laboratory sorption experiments.
Laboratory experiments have been carried out on neptunium sorption with a variety of rock and mineral types and solution compositions. The results of neptunium sorption experiments with pure mineral separates have been reported by Allard (1982), Meijer et al. (1989), Triay et al. (1993b), and others. On the basis of these results, it is evident that neptunium has a high affinity for ferric oxides and oxyhydroxides, apatite, and attapulgite (a magnesium-rich clay). It has a somewhat lower affinity for carbonates (such as calcite), sulfates (for example, anhydrite) and manganese minerals (for example, cryptomelane). It has a low affinity for most silicate minerals. Neptunium also shows high affinities for minerals that contain ferrous iron (such as pyrite, olivine, augite, magnetite, hornblende, epidote, biotite, and chlorite). This affinity is likely due to the reduction of Np^{5+} to Np^{4+} by Fe^{2+} on the surfaces of these minerals. Although ferrous iron-bearing minerals are, at best, minor species in Yucca Mountain tuffs (Bish and Chipera 1989), they could be of considerable significance to neptunium sorption.

In addition to the nature of the available mineral surfaces, it is also evident that pH is a critical parameter. In general, neptunium sorption increases with increasing pH. This effect is particularly evident in the experiments with iron oxyhydroxides (for example, Combes et al. 1992). However, similar behavior is evident in the sorption experiments with silicate minerals. In the latter case, the sorption edge (as a function of pH) is located at a higher pH (8–9) than the edge associated with the ferric oxyhydroxides (a pH of 6–7). Data reported by Combes et al. (1992) suggest neptunium is sorbed as an inner-layer complex on ferric oxyhydroxide.

Table 47. Solubility and Speciation of Neptunium in Groundwaters at 25°C

Water	pH	Solubility (M)	NpO_2^+	$NpO_2CO_3^-$
J-13	6	5×10^{-3}	90%	10%
	7	1×10^{-4}	45%	55%
	8.5	4×10^{-5}	40%	60%
UE-25 p#1	6	3×10^{-3}	100%	0%
	7	5×10^{-4}	60%	40%
	8.5	7×10^{-6}	0%	100%

Neptunium does not appear to have a high affinity for ion-exchange reactions on clays and zeolites (Allard 1982; Triay et al. 1993b). This phenomenon may be due to the small charge-to-radius ratio and the large size of the neptunyl ion.

The results of neptunium sorption experiments involving Yucca Mountain rock and water samples have been reported by Daniels et al. (1982), Thomas (1987, 1988), Triay et al. (1993b), and others. These experiments indicate that neptunium has a low affinity (for example, K_d values of 0–5 ml/g) for the surfaces in Yucca Mountain tuffs over most of the pH range and water compositions expected in the Yucca Mountain flow system. The sorption mechanisms are apparently not entirely reversible as coefficients obtained from desorption experiments are commonly larger than those obtained from sorption experiments even though the isotherms are linear in the concentration range covered by these experiments. There is some indication of increased sorption coefficients (5–40 ml/g) at the highest pH values (8.5–9.0). Torstenfelt et al. (1988) suggest that this result

reflects increased hydrolysis of the neptunyl ion, resulting in an increase in surface-adsorption reactions. However, in Yucca Mountain rock-water systems, it could also reflect increased potential for calcite precipitation at high pH.

In the pH range from 6.5 to 8.5, the small but consistent affinity of neptunium for the tuffs most likely reflects the existence of a limited number of favorable adsorption sites for neptunium. This number apparently does not involve ion-exchange sites because zeolitic rock samples also show low sorption coefficients. For example, Thomas (1988) describes a case in which a zeolitic tuff sample (G4-1608) with a cation-exchange capacity of approximately 1.5 meq/g appears to have essentially the same affinity for neptunium as a devitrified tuff sample (GU3-433) with an exchange capacity of approximately 0.02 meq/g. These sites are apparently not present in the same abundance on all tuff samples. That is, some zeolitic, vitric, and devitrified tuff samples have almost no affinity for neptunium over the pH range from 6.5 to 8.5, whereas other samples with similar proportions of major minerals show sorption coefficients in the range of 5 to 10 ml/g. This result suggests, but does not prove, that the favorable sites are associated with some minor primary or secondary phase that has variable abundance. Hematite and calcite are candidates for this phase based on pure mineral studies. Because ferric oxides are present at trace levels in most of the rock units within Yucca Mountain, they could be the source of the low but consistent values (0.5–2 ml/g) observed in experiments on devitrified and zeolitic tuffs. Alternatively, neptunium may be sorbed (through reduction to Np^{4+}) by the small amounts of ferrous-iron-bearing minerals present in the rock samples used in the sorption experiments.

The increased sorption of neptunium on tuffaceous samples known to contain calcite suggests this mineral is of considerable potential significance to neptunium sorption on Yucca Mountain tuffs. If so, prediction of the adsorption behavior of neptunium will depend on knowledge of the surface areas of calcite in the various hydrologic units or on the saturation state of calcite in groundwaters present in these units.

Because even small amounts of calcite appear to significantly increase neptunium sorption coefficients, current mineral identification techniques may not be adequate for prediction of neptunium sorption behavior. A more viable approach may be to determine the calcite saturation level in the various groundwater compositions expected within Yucca Mountain. If calcite is saturated or oversaturated in a given groundwater, the upper end of the range of experimentally determined sorption coefficients could be used with the assumption that neptunium will either coprecipitate with calcite or adsorb to calcite surfaces. Alternatively, if calcite is undersaturated in a given water, the lower end of the range could be used under the assumption that neptunium is sorbed on oxides, such as ferric or ferrous oxides. For vitric units lacking iron oxides and calcite, neptunium may not be sorbed at all.

We studied the sorption of Np(V) onto samples of the three types of tuff in J-13 water (under oxidizing conditions) at two pH values (7 and 8.5). However, to identify the sorbing minerals in the tuffs, we also studied sorption onto the pure minerals hematite, clinoptilolite, albite, and quartz. We found that neptunium in J-13 water does not sorb onto devitrified and vitric tuffs, albite, and quartz (Table 48).

The initial neptunium concentrations for the data reported in Table 48 ranged from 1×10^{-7} to 3×10^{-5} M. We used wet-sieved tuffs, albite, and quartz samples with particle sizes in the range from 75 to 500 μm. The pretreatment period lasted 2 to 3 days, and the sorption period, 2 to 4 days. The negative values reported in the table are a result of the analytical error for the case of very little sorption (that is, a small number is obtained as the difference of two large numbers).

For the experimental conditions cited earlier, the sorption of neptunium onto zeolitic tuffs and

Table 48. Neptunium Sorption in J-13 Water under Oxidizing Conditions

Solid phase	pH	K_d (ml/g)*
G4-268, devitrified tuff	7	7×10^{-3}
	8.5	-4×10^{-2}
GU3-1405, vitric tuff	7	2×10^{-1}
	8.5	3×10^{-1}
Quartz	7	-1×10^{-1}
	8.5	-2×10^{-1}
Albite	7	-8×10^{-2}
	8.5	-1×10^{-1}

*The uncertainties in the data are ± 0.5

clinoptilolite appears to be linear in the concentration range from 1×10^{-7} to 3×10^{-5} M and can be fitted using a K_d (Figs. 55 and 56). The sorption of neptunium onto zeolites is higher at a pH of 7 than a pH of 8.5, which might be explained by the larger amount of NpO_2^+ relative to $NpO_2CO_3^-$ in J-13 well water at a pH value of 7 than at a pH value of 8.5.

As we've pointed out, one surprise for neptunium is the relatively small amount of sorption (values of K_d ranging from 1.5 to 3 ml/g) compared to the large amount expected for a cation-exchange sorption mechanism in a zeolite with a large cation-exchange capacity (such as clinoptilolite). This result indicates that the sorption mechanism for neptunium onto clinoptilolite is a surface reaction rather than cation exchange within the cages of the zeolite. One possible explanation is steric: the shape and large size of the neptunyl cation prevents cation exchange. This ion likely has a trans-dioxol configuration normal to a puckered equatorial ring containing six bound water molecules.

The experiments with pure clinoptilolite indicate that sorption increases with decreasing pH for Np(V). Because the major constituent of tuff G4-1510 is clinoptilolite, predictions of the K_a (K_d divided by the solid-phase surface area) were made for neptunium sorption onto this tuff by assuming that clinoptilolite is the only sorbing phase. Table 49 shows measured and predicted values of K_a for the clinoptilolite-rich tuff G4-1510 at two different pH values. Because sorption is correlated with surface area, we made similar calculations (Table 50) for a series of tuff samples containing various amounts of clinoptilolite for which the surface area had been measured. The values in the two tables indicate that reasonable predictions can be made based on neptunium sorption data for pure clinoptilolite (assuming clinoptilolite is the only sorptive mineral).

The sorption of neptunium onto pure iron oxides is very large (we measured values of K_d for hematite that range from 100 to 2000). Although the sorption onto the pure iron oxide hematite is very large, neptunium sorption onto devitrified tuffs, which appear to have traces of hematite (1% ± 1), is essentially zero. This result could be due to differences in the surface of pure hematite compared to hematite in tuff. It could also be due to passivation of the hematite surfaces in the tuff by elements (such as the rare earths) that have a higher affinity for hematite than neptunium and, thus, occupy the sorption sites.

We investigated sorption as a function of sieving procedure for devitrified (G4-270) and zeolitic (G4-1506) tuffs in J-13 and UE-25 p#1 well

Table 49. Prediction of Neptunium Sorption on Clinoptilolite-rich G4-1510 Tuff in J-13 Water

Initial concentration (M)	pH	Measured K_a (m)	Predicted K_a (m)*
1×10^{-7} to 3×10^{-5}	7	1×10^{-7}	9×10^{-8}
	8.5	6×10^{-8}	5×10^{-8}

*Assuming clinoptilolite is the only sorbing mineral in the tuff

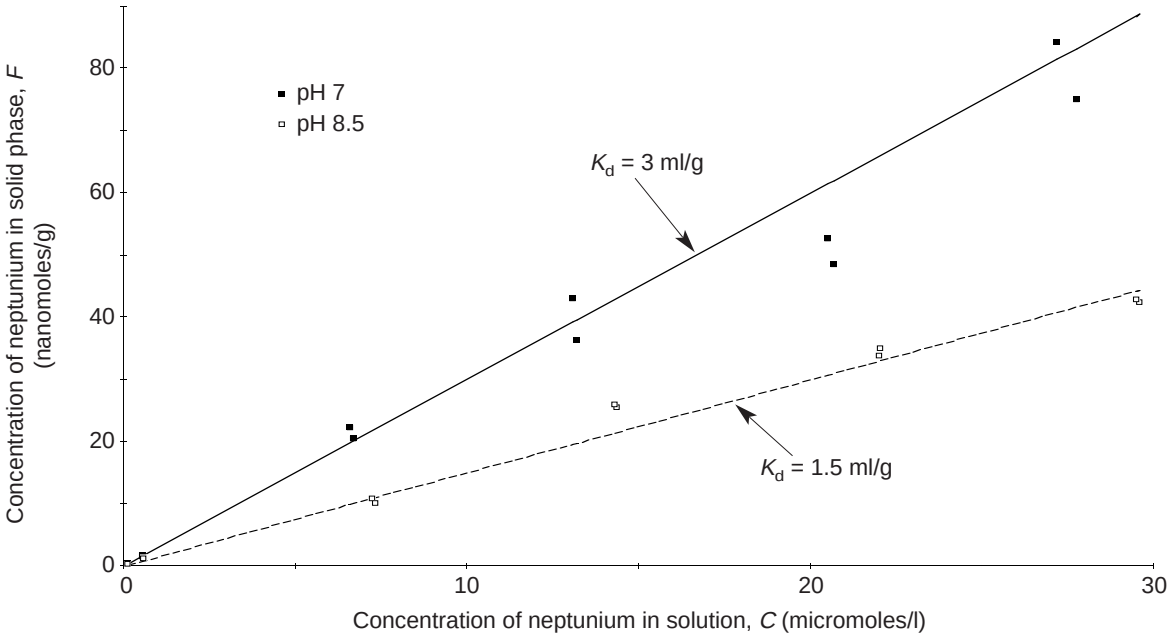

Figure 55. Neptunium Sorption onto Clinoptilolite-rich Tuff. A plot is shown of the concentration, *F*, of neptunium in the solid phase of the clinoptilolite-rich tuff G4-1510 versus the concentration, *C*, of neptunium in the solution phase of J-13 well water and linear (K_d) fits to the data for two values of pH.

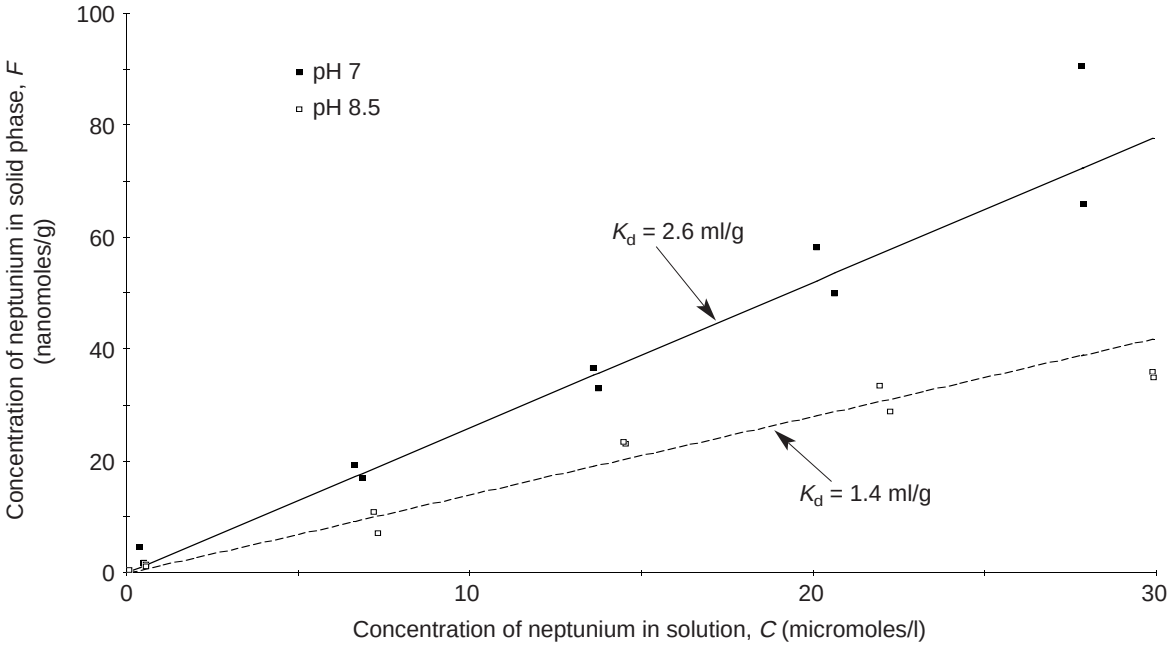

Figure 56. Neptunium Sorption onto Clinoptilolite. A plot is shown of the concentration, *F*, of neptunium in the solid phase of clinoptilolite versus the concentration, *C*, of neptunium in the solution phase of J-13 well water and linear (K_d) fits to the data for two values of pH.

waters. Data presented in Fig. 57 indicate that wet-sieving probably eliminates small particles that cause artificially high K_d values. As previously determined by Rogers and Chipera (1994), the optimal batch-sorption procedure involves wet-sieving the tuff samples to a size of 75 to 500 μm. Figure 58 illustrates the problem that could arise when sorption experiments are performed with pure minerals consisting of very finely divided particles that cannot be wet-sieved. The neptunium batch-sorption coefficients determined vary by more than an order of magnitude between the dry- and the wet-sieved natural calcite. The potential differences in surface area and particle size between a pure mineral and that same mineral in the tuff samples may make predictions of sorption behavior on whole rock impossible when the basis of those predictions is pure mineral work. As illustrated in Fig. 58, the trends in sorption as a function of concentration and groundwater chemistry stay the same regardless of whether dry- or wet-sieved calcite is used.

Table 50. Neptunium Sorption onto Clinoptilolite-rich Tuffs in J-13 Water*

Tuff sample	Measured K_a (m)	Predicted K_a (m)	Clinoptilolite percentage
G1-1405	1×10^{-7}	1×10^{-7}	68 ± 7
G4-1505	9×10^{-8}	1×10^{-7}	74 ± 7
G4-1506	1×10^{-7}	1×10^{-7}	62 ± 7
G4-1510	8×10^{-8}	1×10^{-7}	59 ± 7
G4-1529	7×10^{-8}	1×10^{-7}	59 ± 8
G4-1625	9×10^{-8}	1×10^{-7}	61 ± 7
G4-1772	1×10^{-7}	1×10^{-7}	63 ± 5
G4-2077	5×10^{-8}	8×10^{-8}	51 ± 8

*Atmospheric conditions; initial neptunium concentrations ranged from 6 to 8×10^{-7} M; tuffs were wet-sieved to particle sizes ranging from 75 to 500 μm; the pretreatment period was 2 to 14 days; and the sorption period was 3 to 23 days.

Consequently, the most effective use of pure mineral sorption data is the identification of trends in the sorptive behavior of a mineral. Figures 57 and 58 also illustrate the effect of water chemistry on neptunium sorption; for example, the sorption of neptunium onto zeolitic tuffs decreases considerably with the increasing carbonate content and ionic strength of the UE-25 p#1 water. The reverse trend is observed for calcite samples.

We investigated the kinetics of neptunium sorption onto tuffs and pure minerals and found that the sorption of neptunium onto tuffs and clinoptilolite appears to be fast (Fig. 59). No significant differences are observed in neptunium sorption as a function of time for the tuffs studied and for clinoptilolite. This is not the case for pure minerals that tend to sorb by means of a coprecipitation mechanism (such as calcite) or by surface complexation (such as hematite). Figures 60 and 61 show the sorption dependence with time for calcite and hematite in waters from the Wells J-13 and UE-25 p#1. The dissolution/precipitation reactions that may accompany the coprecipitation of neptunium with calcite may be slow compared with other sorption mechanisms. Future experiments will address this issue by monitoring the chemistry of the groundwater as it is being equilibrated with these minerals.

Figures 62 and 63 give further data from our investigation of the dependence of neptunium sorption on pH in J-13 water. The figures show that for vitric tuffs (such as samples G2-767 and GU3-1407), pH does not seem to make a significant difference in the amount of neptunium sorption measured. Likewise, the sorption of neptunium onto devitrified tuffs (such as sample G4-270) in J-13 is not affected by pH. Samples G2-1813, G2-1951, G2-2000, and G2-2222 are zeolitic tuffs, but until the XRD analyses of these samples become available, it is difficult to know the relative amounts of clinoptilolite versus mordenite in each. However, tuff samples G4-1510 and G4-1395 consist of 59% and 22% clinoptilolite, respectively, and exhibit the same trend as clinoptilolite itself: an increase in

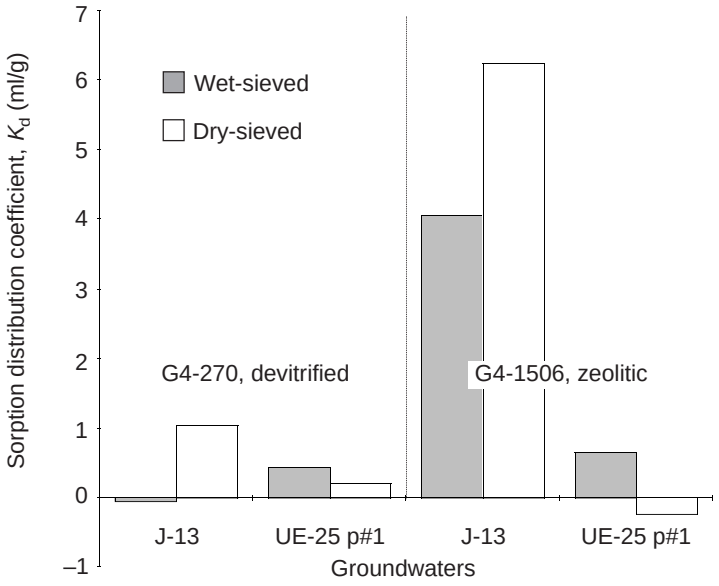

Figure 57. Neptunium Sorption for Wet- and Dry-sieved Tuffs. Experimental values of the batch-sorption distribution coefficient, K_d, are shown for sorption of neptunium onto tuff (under atmospheric conditions) that allow comparisons of both groundwaters (J-13 and UE-25 p#1), two types of tuff (devitrified and zeolitic), and wet- or dry-sieving to particle sizes ranging from 75 to 500 µm. The initial neptunium concentration was 1×10^{-6} M. The pretreatment period with the two groundwaters was 13 to 15 days; the neptunium sorption period was 21 to 22 days.

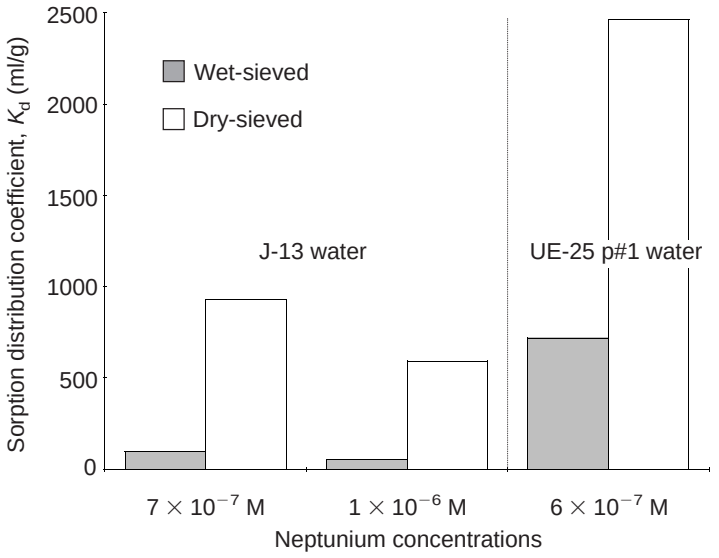

Figure 58. Neptunium Sorption for Wet- and Dry-sieved Calcite. Experimental values of the batch-sorption distribution coefficient, K_d, are given for sorption of neptunium onto calcite (under atmospheric conditions) that allow comparisons of both groundwaters (J-13 and UE-25 p#1), different initial concentrations of neptunium, and wet- or dry-sieving to particle sizes ranging from 75 to 500 µm. The pretreatment period was 14 to 15 days; the sorption period was 17 to 24 days.

sorption as the pH is decreased from 8.5 to 7, probably because of the increase of neptunyl cation concentration. As discussed earlier, these results seem to indicate that neptunium sorption onto clinoptilolite may follow an ion-exchange mechanism, but the fact that neptunium sorption on pure clinoptilolite is so small favors a surface-complexation reaction, even for this zeolite. Again, the reason may be that the hydrated neptunyl cation is too large to fit in the zeolite cages.

We also studied the sorption of neptunium in UE-25 p#1 water and found that, regardless of the conditions, neptunium sorption onto tuffs and zeolites is negligible ($K_d < 1$ ml/g) in this water (Fig. 64). If clinoptilolite is the only mineral affecting neptunium sorption and if ion exchange at the surface is the dominating mechanism, one might conclude that the reason for the lack of neptunium sorption on clinoptilolite is the formation of the neptunium carbonato complex ($NpO_2CO_3^-$) in

continued on page 132

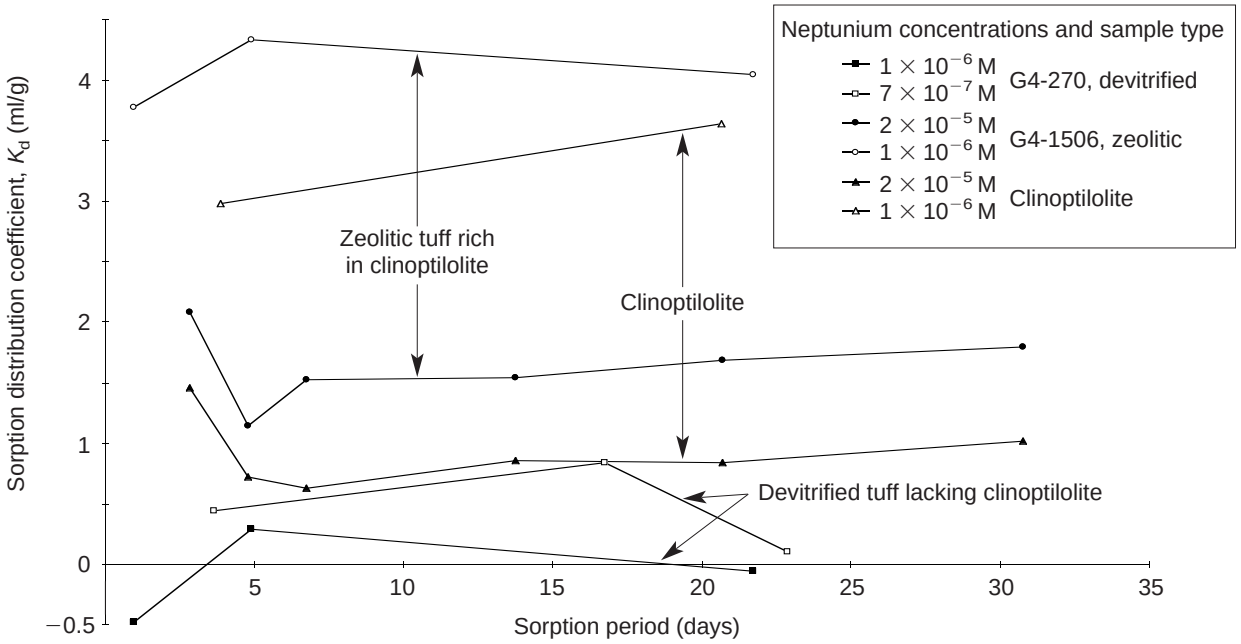

Figure 59. Time Dependence of Neptunium Sorption for Tuffs and Clinoptilolite. Variation with time of K_d for sorption of neptunium onto devitrified tuff (G4-270) lacking clinoptilolite (squares), zeolitic tuff (G4-1506) rich in clinoptilolite (circles), and pure clinoptilolite (triangles) under atmospheric conditions and at the specified initial neptunium concentrations in J-13 well water. Tuffs were wet-sieved to particle sizes from 75 to 500 µm; the clinoptilolite was not sieved. The pretreatment period was 2 to 14 days.

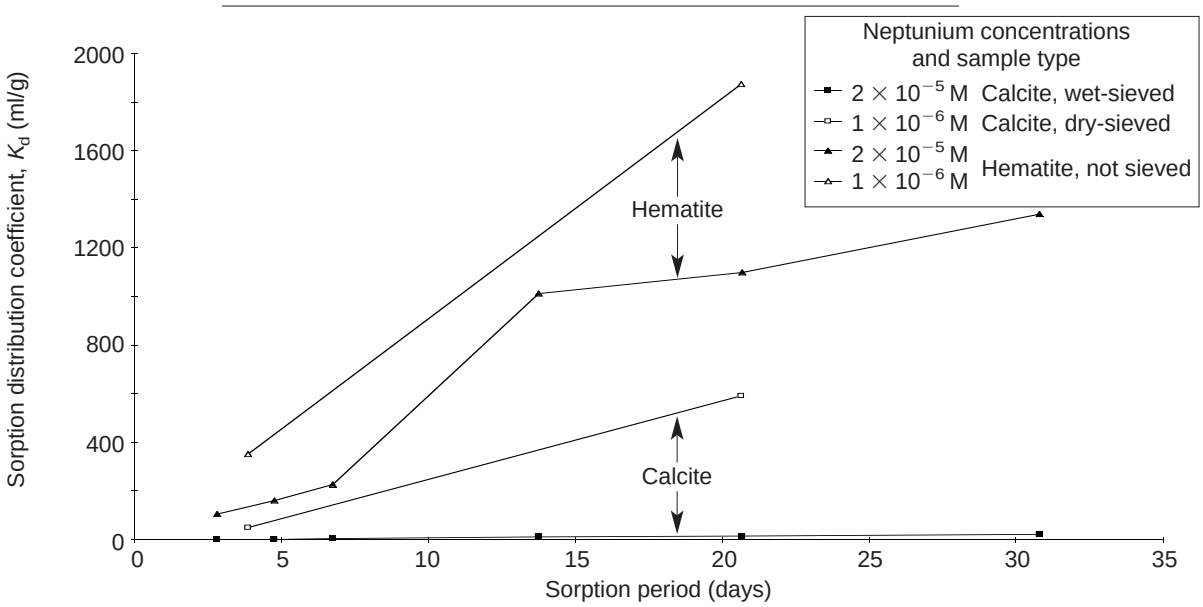

Figure 60. Time Dependence of Neptunium Sorption for Calcite and Hematite in J-13 Water. Variation with time of K_d for sorption of neptunium onto calcite (squares) and hematite (triangles) under atmospheric conditions and at the specified initial neptunium concentrations in J-13 well water. The calcite was either wet- or dry-sieved to particle sizes from 75 to 500 µm; the synthetic hematite was not sieved. The pretreatment period with J-13 water was 2 to 14 days.

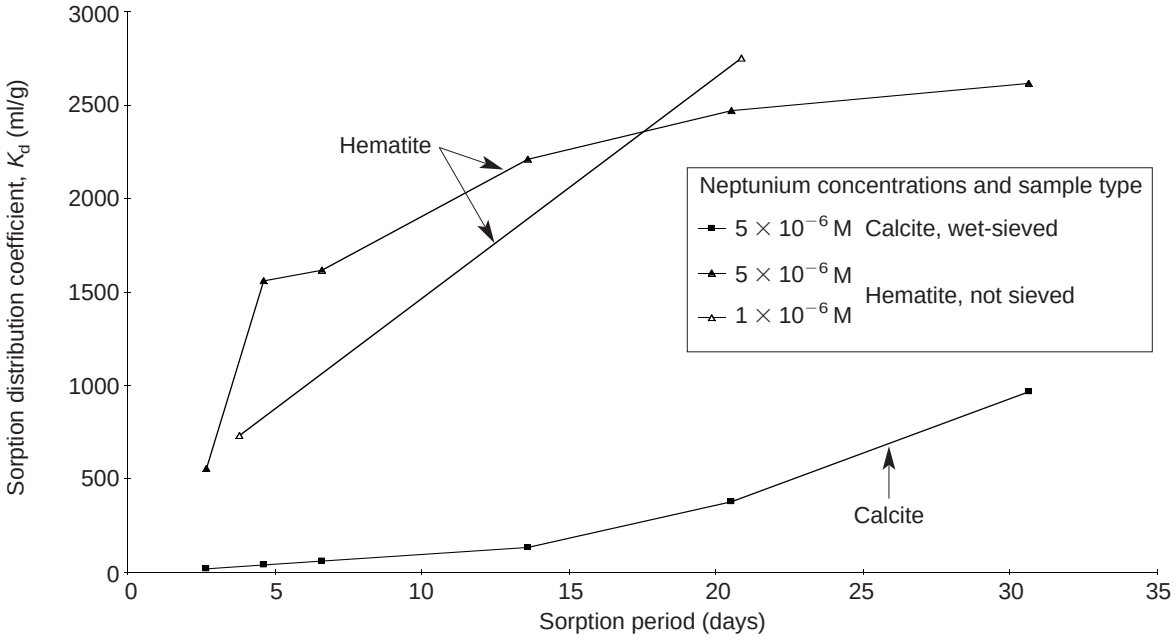

Figure 61. Time Dependence of Neptunium Sorption for Calcite and Hematite in UE-25 p#1 Water. Variation with time of K_d for the sorption of neptunium onto calcite (squares) and hematite (triangles) under atmospheric conditions and at the specified initial neptunium concentrations in UE-25 p#1 well water. The calcite was wet-sieved to particle sizes ranging from 75 to 500 µm; the synthetic hematite was not sieved. The pretreatment period in UE-25 p#1 water was 2 to 13 days.

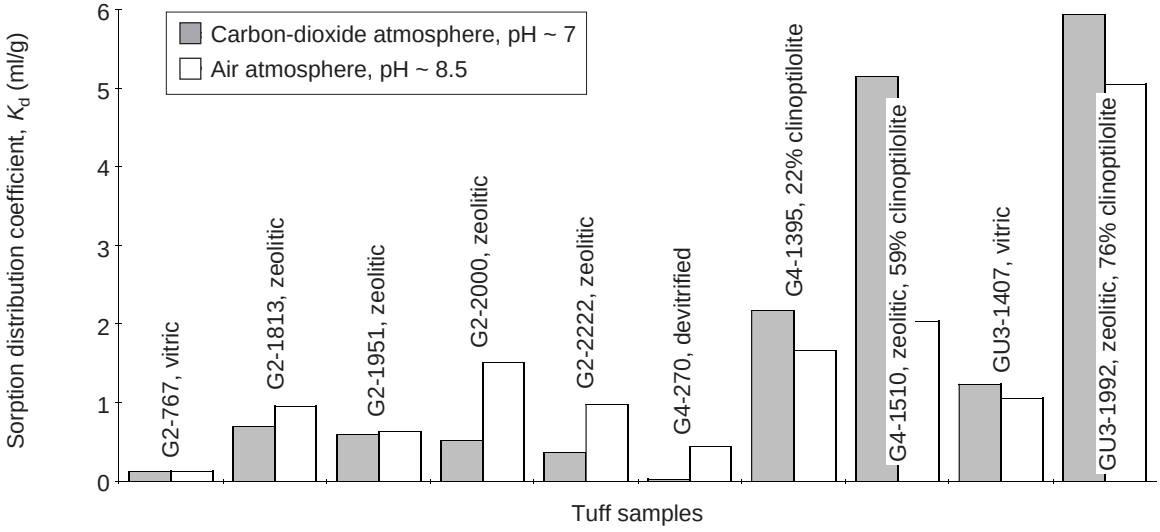

Figure 62. pH Dependence of Neptunium Sorption onto Tuffs at 10^{-7} M. Experimental values of K_d for the sorption of neptunium onto tuffs in J-13 water at initial concentrations of 6 to 7 $\times 10^{-7}$ M are compared for atmospheric conditions (pH $\sim$ 7) and a carbon-dioxide overpressure (pH $\sim$ 8.5). Tuffs were wet-sieved (75 to 500 µm); the pretreatment period was 2 to 3 days; the sorption period was 3 to 5 days.

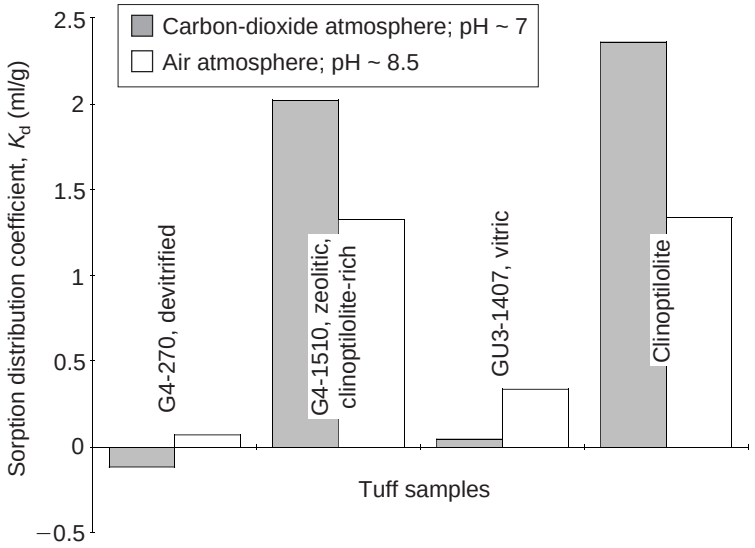

Figure 63. pH Dependence of Neptunium Sorption onto Tuffs at 10^{-5} M. Experimental values of K_d for the sorption of neptunium onto several tuffs and clinoptilolite in J-13 well water at an initial neptunium concentration of 3×10^{-5} M are compared for both atmospheric conditions (pH ~ 8.5) and a carbon-dioxide overpressure (pH ~ 7). Tuffs were wet-sieved (75 to 500 µm); the clinoptilolite was not sieved. The pretreatment period was 2 to 3 days; the sorption period was 3 to 5 days.

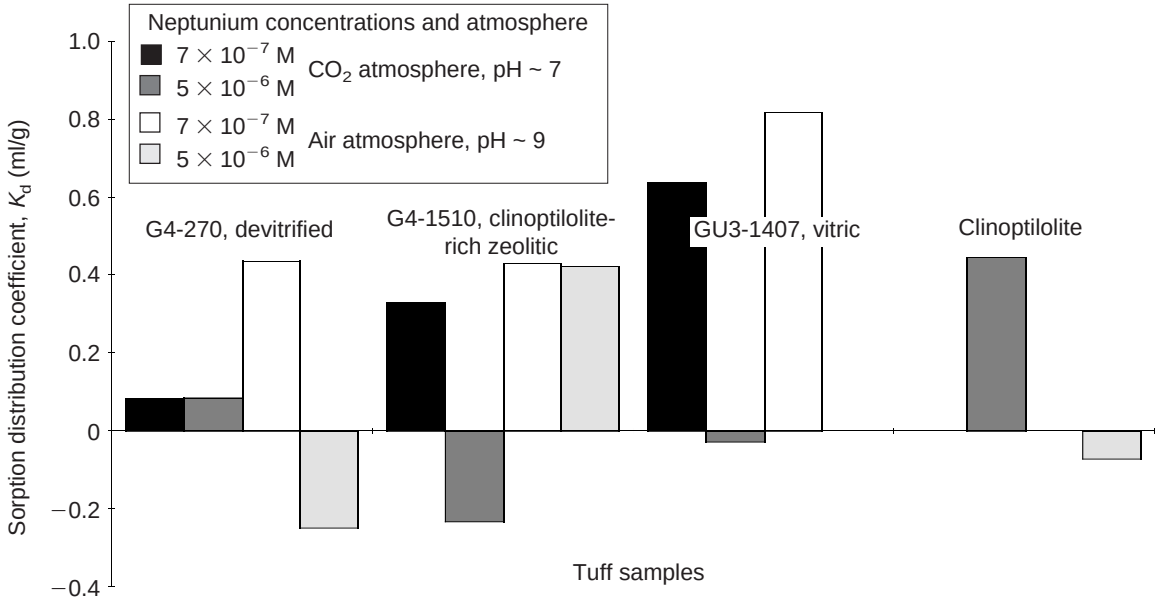

Figure 64. Neptunium Sorption in UE-25 p#1 Well Water. Experimental values of the batch-sorption distribution coefficient, K_d, for neptunium in UE-25 p#1 water show negligible sorption regardless of sample type (devitrified tuff, clinoptilolite-rich zeolitic tuff, vitric tuff, or clinoptilolite), pH (~ 7 or ~ 9), or initial neptunium concentration (5×10^{-6} or 7×10^{-7}).

continued from page 129

UE-25 p#1 water to the exclusion of the neptunyl cation. The data reported by Nitsche et al. (1994) do not support this conclusion (Table 47); the relative amount of neptunyl in UE-25 p#1 water is larger than that in J-13 water at a pH of 7. If the data of Nitsche et al. are correct, another possible reason for the lack of neptunium sorption on clinoptilolite in UE-25 p#1 water is competitive effects due to the larger ionic strength of that water compared with J-13 water, which has a smaller

ionic strength by nearly an order of magnitude.

As we mentioned earlier, iron oxides have a high affinity for neptunium (Combes et al. 1992). Figure 65 shows further data on the sorption of neptunium onto hematite, this time in both J-13 and UE-25 p#1 waters as a function of pH. It is important to note that the trends observed in this figure (sorption increasing with increasing pH and larger sorption in UE-25 p#1 water than in J-13 water) are not followed by the neptunium sorption reported for clinoptilolite-rich tuff samples. Also once again, the neptunium sorption in the rest of the tuff samples is so small (even in the samples that contain traces of hematite) that the iron oxides appear to be passivated in the tuffs.

As illustrated in Fig. 66, regardless of the tuff studied, neptunium sorption onto tuffaceous materials is extremely limited. One exception is tuff sample G2-723 (not shown), which contains a large amount of calcite, a good sorber for neptunium. This sample will be discussed later.

Figure 67 is a plot both of neptunium sorption data in J-13 water and of surface area for tuffs for which BET-surface-area and XRD analyses exist. The surface-area data correspond to the surface area for the tuffs sieved in J-13 water with the following exceptions: the surface area used for sample G4-2077 was for dry-sieved tuff; the surface area used for tuffs G4-268 and G4-272 was the same as that measured for tuff G4-270; the surface area plotted for tuffs G4-1505 and G4-1510 was the same as that measured for tuff G4-1506; and the surface area plotted for tuff GU3-1405 was the same as that measured for tuff GU3-1407. Figure 68 shows a reasonable correlation between sorption and surface area. The surface areas that are larger than 18 m^2/g correspond to clinoptilolite-rich tuffs.

Figures 68 and 69 summarize the sorption of neptunium under atmospheric conditions for tuffs and minerals as a function of water type. Sorption onto zeolitic tuffs decreases considerably with increasing carbonate content and ionic strength of the water. Figure 69 also shows the calcite-rich tuff G2-723 (34% calcite), which exhibits considerable sorptive capacity for neptunium. Assuming that the calcite in the tuff sample has the same surface area as the natural calcite used for these experiments (and that calcite is the only sorptive mineral in the tuff), one would predict from neptunium sorption on pure calcite a logK_d for tuff G2-723 of 1.5. This prediction agrees well with the measured K_d (Fig. 69).

As the neptunium concentration is increased towards the solubility limit for neptunium in the J-13 and UE-25 p#1 groundwaters, the observed sorption decreases, but the general trends remain the same (as seen by comparing Figs. 67 and 70). The extremely low neptunium sorption reported for devitrified tuffs in J-13 and UE-25 p#1 waters is supported by the sorption data plotted for albite

continued on page 136

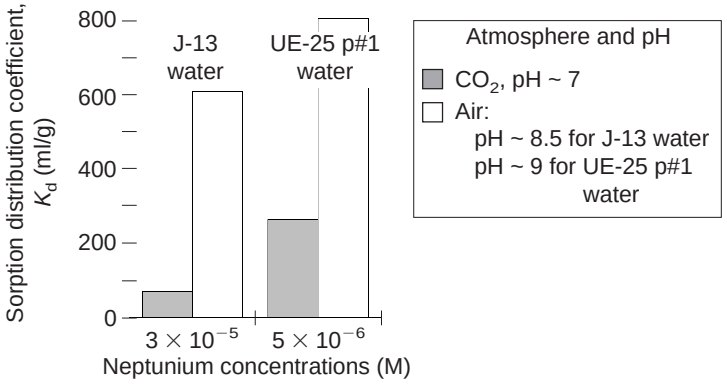

Figure 65. Neptunium Sorption for Hematite. Values of the batch-sorption distribution coefficient, K_d, are given for the sorption of neptunium onto hematite in UE-25 p#1 well water at the specified initial neptunium concentrations and pH values. The pretreatment period was 2 to 3 days, and the sorption period was 3 to 5 days.

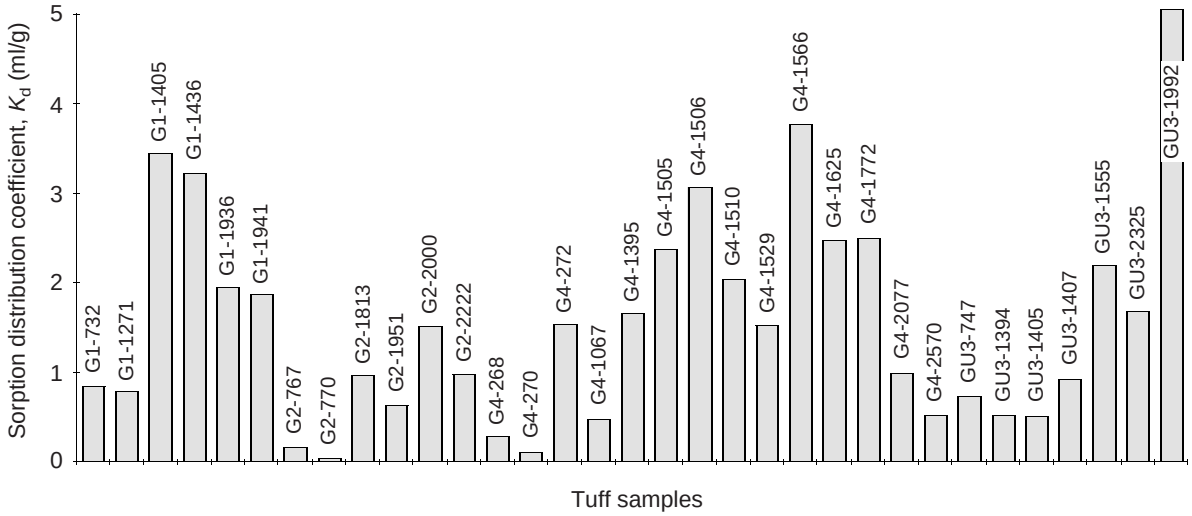

Figure 66. Neptunium Sorption in J-13 Well Water. These values of the batch-sorption distribution coefficient, K_d, illustrate the limited sorption of neptunium onto a large range of Yucca Mountain tuffs in J-13 well water under atmospheric conditions. The initial neptunium concentration ranged from 6 to 8×10^{-7} M. The tuffs were wet-sieved to particle sizes that ranged from 75 to 500 µm. The pretreatment period was 2 to 14 days; the sorption period was 3 to 23 days.

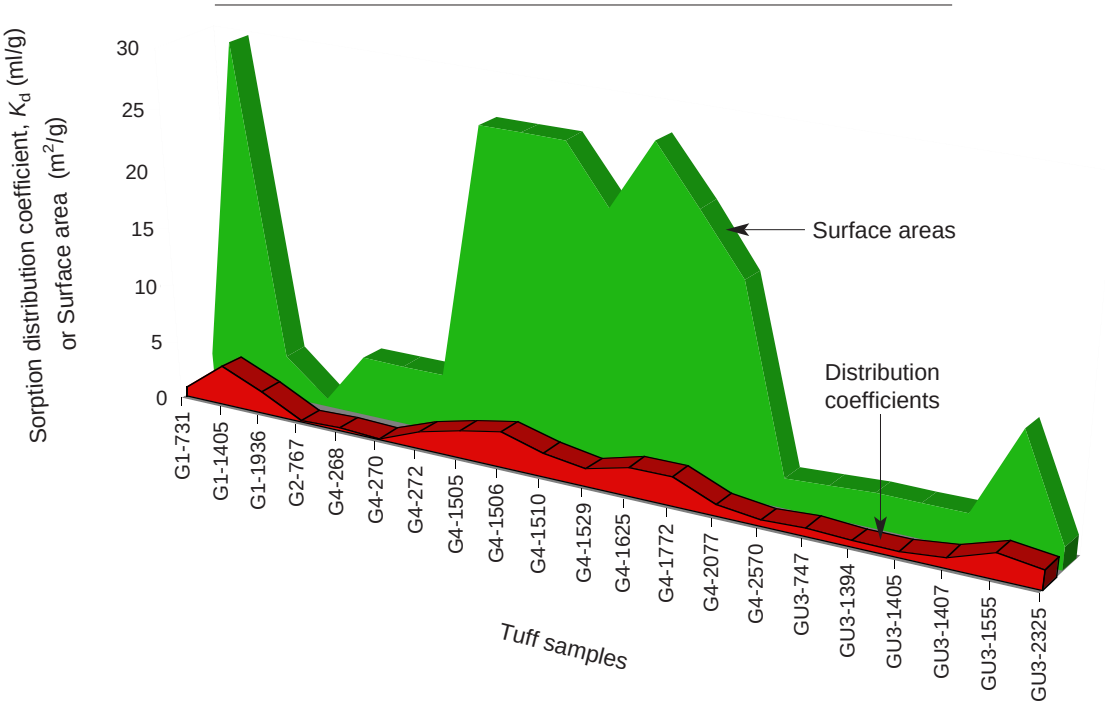

Figure 67. Neptunium Sorption and Surface Area. Values of the batch-sorption distribution coefficient, K_d, for neptunium onto various tuffs are compared to the corresponding surface areas of those tuffs. The sorption is for J-13 well water under atmospheric conditions at an initial neptunium concentration ranging from 6×10^{-7} to 8×10^{-7} M. The tuffs were wet-sieved to particle sizes that ranged from 75 to 500 µm. The pretreatment period was 2 to 14 days; the sorption period was 3 to 23 days.

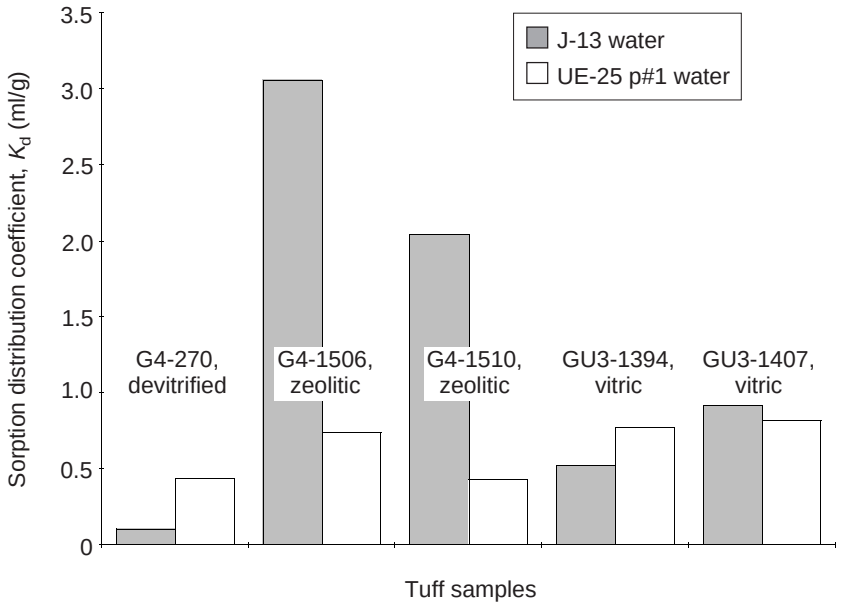

Figure 68. Dependence on Water for Sorption onto Tuffs. Values of K_d for sorption of neptunium onto several tuffs that allow comparison of sorption (under atmospheric conditions) for the two types of groundwaters. The initial neptunium concentration ranged from 6×10^{-7} to 8×10^{-7} M. The tuffs were wet-sieved to particle sizes ranging from 75 to 500 µm. The pretreatment period was 2 to 14 days, and the sorption period was 3 to 23 days.

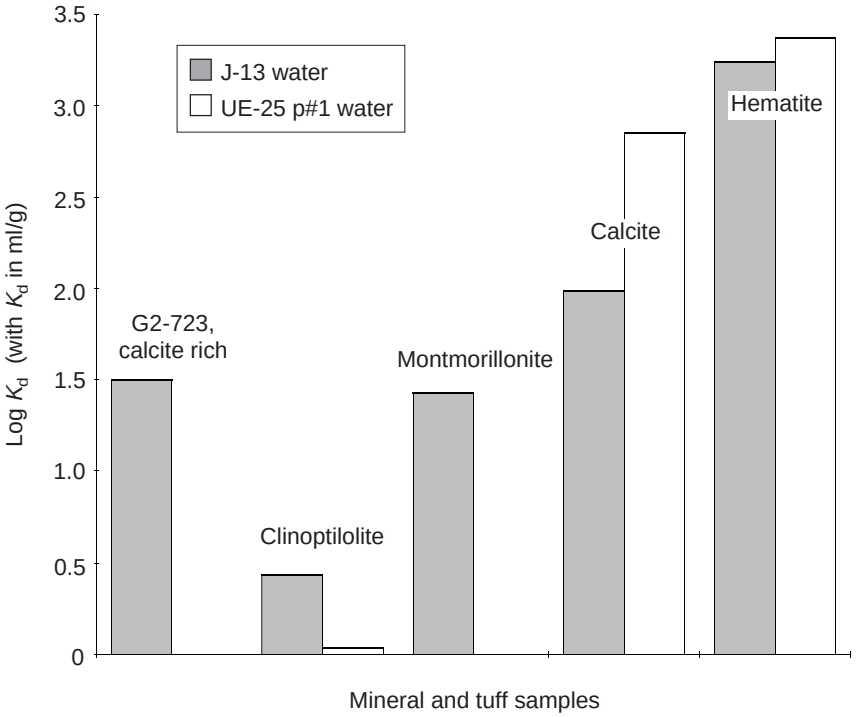

Figure 69. Dependence on Water for Sorption onto Minerals. Values of K_d for neptunium onto several minerals and a calcite-rich tuff that allow comparison of sorption (under atmospheric conditions) for the two groundwaters. The initial neptunium concentration ranged from 6×10^{-7} to 8×10^{-7} M. The tuff and the calcite were wet-sieved to particle sizes ranging from 75 to 500 µm; the montmorillonite was dry-sieved; the clinoptilolite and hematite were not sieved. The sorption period was 17 to 22 days.

continued from page 133

(Fig. 71), which appears to be a very poor sorber for neptunium (in both waters). The nonlinearity of neptunium sorption in the high-concentration region (approaching the solubility limits for neptunium) is further illustrated in Figs. 72 and 73 (for J-13 and UE-25 p#1 waters under a carbon-dioxide atmosphere at a pH of 7).

Conclusions regarding sorption behavior with respect to expected variations in groundwaters.
The mechanisms by which neptunium appears to sorb onto mineral surfaces in the Yucca Mountain flow system appear to be surface complexation on oxide phases and coprecipitation and surface adsorption involving carbonate minerals. The surface-complexation mechanism appears to be relatively insensitive to variations in ionic strength, detailed groundwater composition, and pH over the range from 6.5 to 8.5. This mechanism is likely responsible for the 0.5 to 5.0 ml/g range in sorption-coefficient values consistently measured in many different rock samples. The high end of this range may reflect secondary mechanisms, such as the reduction of Np(V) to Np(IV) on mineral surfaces containing ferrous iron. Regardless of the details of the mechanisms, performance-assessment calculations could use a probability distribution for sorption-coefficient values, as was done for the 1993 total-system performance assessment (Wilson et al. 1994).

For hydrologic units in which calcite is known to be present or in which groundwaters are oversaturated in calcite, higher neptunium sorption coefficients could be used in the calculations if it could be established through laboratory experiments that such coefficients are appropriate. To date, most neptunium sorption coefficients have been obtained using samples from the unsaturated zone, many of which came from levels above the repository horizon. According to the mineralogic studies, calcite is more common at depths below the potential repository horizon than it is at the intermediate depths. Many of the samples used in sorption experiments to date have been obtained from intermediate depths.

Protactinium

Behavior in solutions representative of Yucca Mountain groundwaters.
In aqueous systems, protactinium appears to exist dominantly in the $+5$ oxidation state although the $+4$ state may occur in reducing environments (Brookins 1988). In both oxidation states, protactinium is strongly hydrolyzed and forms highly insoluble compounds (Cotton and Wilkinson 1988). This result implies that the $+5$ solution chemistry of protactinium is more akin to that of Nb(V) than to other actinides in $+5$ oxidation states, such as PuO_2^+ or NpO_2^+. If this interpretation is correct, then the solution parameter of greatest importance to protactinium sorption behavior would be pH.

Qualitative evidence for behavior in the surficial environment.
Information on behavior of protactinium in the surficial environment is sparse. Because protactinium forms such insoluble compounds, it is generally assumed to be immobile in the surficial environment.

Data from laboratory sorption experiments.
Batch-sorption experiments with protactinium have yielded some interesting results. In dilute to intermediate ionic-strength solutions, Allard et al. (1982) report large values (10^4 ml/g) for the protactinium sorption coefficient on alumina and silica at pH values greater than 6 to 7 but much lower values (90–500 ml/g) at pH values less than 7. Rundberg et al. (1985) report protactinium sorption coefficients in the range from 3.7 to 8.2 ml/g for a zeolitic tuff in contact with J-13 water spiked with 10^{-11} to 10^{-14} M protactinium at pH values of 6.3 to 6.7. Together, these data suggest that protactinium sorbs by a surface-complexation mechanism and that there is a rather steep sorption edge for protactinium as a function of pH at a pH value of approximately 7.

Conclusions regarding sorption behavior with respect to expected variations in groundwaters.
Batch-sorption data for protactinium suggest that

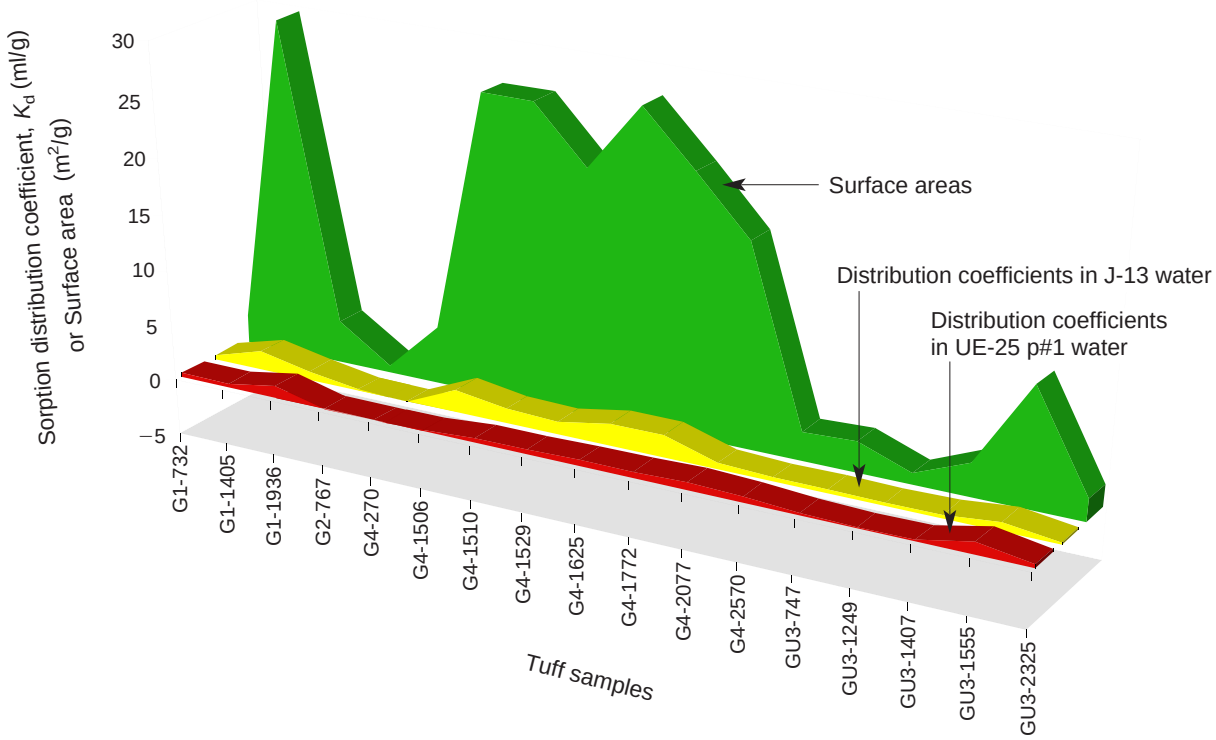

Figure 70. High-concentration Sorption onto Tuffs. Values of K_d for sorption of neptunium onto tuffs under atmospheric conditions and near the solubility limit (initial neptunium concentrations of 2 to 4×10^{-5} M in J-13 water and 5×10^{-6} M in UE-25 p#1 water) are compared with the surface areas of those tuffs. The tuffs were wet-sieved to particle sizes ranging from 75 to 500 µm. The pretreatment period was 2 to 5 days; the sorption period was 2 to 4 days.

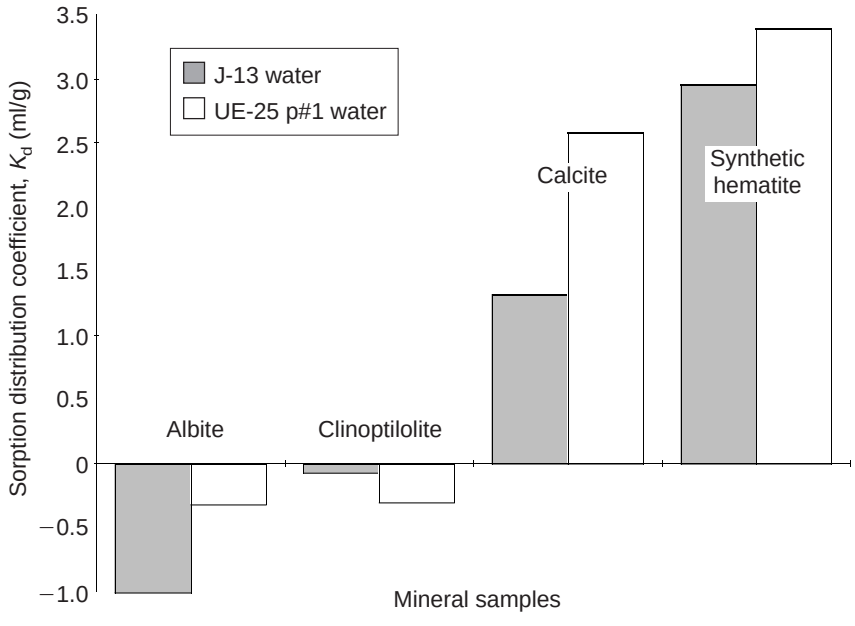

Figure 71. High-concentration Sorption onto Minerals. Values of K_d for sorption of neptunium onto minerals under atmospheric conditions for neptunium concentrations near the solubility limit (initially, 2 to 4×10^{-5} M in J-13 water and 5×10^{-6} M in UE-25 p#1 water). The calcite was wet-sieved to particle sizes ranging from 75 to 500 µm; the others were not sieved. The pretreatment period was 2 to 31 days; the sorption period was 21 days.

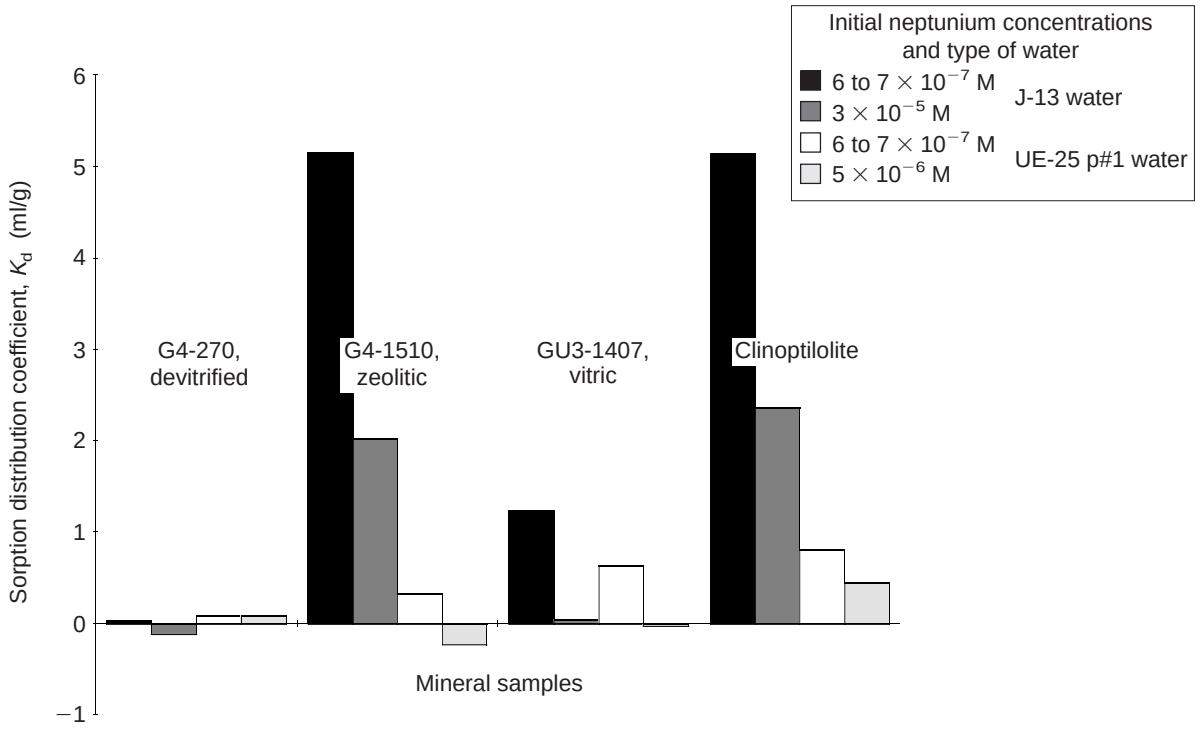

Figure 72. High-concentration Sorption onto Tuffs at pH 7. Values of K_d for sorption of neptunium onto several tuffs and clinoptilolite under a carbon-dioxide overpressure (to obtain a pH of approximately 7) are shown. The tuffs were wet-sieved to particle sizes ranging from 75 to 500 µm; the clinoptilolite was not sieved. The pretreatment period was 2 to 3 days; the sorption period was 3 to 4 days.

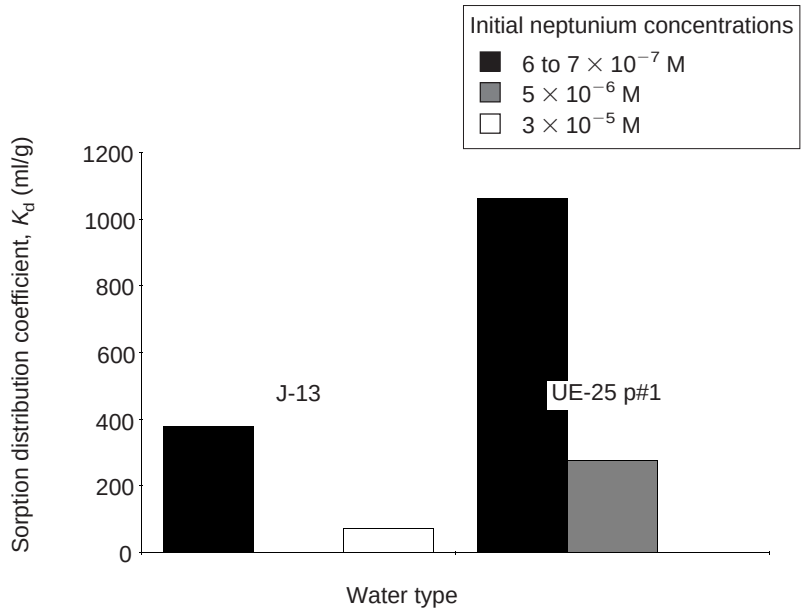

Figure 73. High-concentration Sorption onto Hematite at pH 7. Values of the batch-sorption distribution coefficient, K_d, are shown for sorption of neptunium onto unsieved synthetic hematite under a carbon-dioxide overpressure (to obtain a pH of ~ 7). The pretreatment period was 2 to 3 days; the sorption period was 3 to 4 days.

sorption coefficients for this element will be large ($>$ 1,000 ml/g) at a pH value greater than 7 and small ($<$ 10 ml/g) at lower pH values. Because protactinium sorption experiments on rock samples from Yucca Mountain have only been carried out in the low pH range, it would be prudent to carry out several experiments using a Yucca Mountain water at several pH values from 7 to 9.

Selenium

Behavior in solutions representative of Yucca Mountain groundwaters.

Selenium will occur as anionic species in all water compositions expected at Yucca Mountain. Although the two oxidation states of $+4$ and $+6$ (Howard 1977) are found for selenium in surficial waters in contact with atmospheric oxygen, the $+4$ state predominates under the conditions expected for groundwaters at Yucca Mountain (Howard 1977; White et al. 1991). In that state, selenium is found as the SeO_3^{2-} and $HSeO_3^{-}$ selenite ions. In the $+6$ oxidation state, selenium occurs as the SeO_4^{2+} and $HSeO_4^{-}$ selenate ions.

Qualitative evidence for behavior in the surficial environment.

Selenium behavior in the surficial environment is very closely tied to the redox potential of different parts of the near-surface environment. Under reducing conditions, selenium is immobilized as $FeSe_2$ at low pH ($<$ 5) and as native selenium at higher pH (Howard 1977). The stability range for native selenium extends nearly to surface redox conditions. When in contact with atmospheric oxygen levels, selenium is apparently stabilized as the selenite ion (SeO_3^{2-}). At higher redox potentials, selenium is oxidized to the selenate ion (SeO_4^{2-}), which appears to be more mobile in the surficial environment than the selenite ion (Howard 1977).

Data from laboratory sorption experiments.

Because selenium occurs as anionic species in the surficial environment, its adsorption behavior is controlled primarily by surface-complexation reactions on oxide minerals including iron oxides and oxyhydroxides (Balistrieri and Chao 1987), manganese oxides and oxyhydroxides, clays (Bar-Yosef and Meek 1987), and other minerals with affinities for anionic species. These surface-complexation reactions are quite sensitive to pH. For example, adsorption on iron oxyhydroxides decreases for both selenite and selenate ions with increasing pH (Balistrieri and Chao 1987). Selenate ions appear to sorb dominantly in the outer layer of the electrical double layer present on oxide surfaces, whereas selenite tends to sorb in the inner layer (Hayes et al. 1987). Selenate ions are subject to ionic-strength effects as well as competitive effects with sulfate and other anions in solution, presumably because they sorb in the outer layer. Selenite ions are not subject to ionic-strength effects but may be subject to competition from other anions sorbing on inner-layer sites (Hingston et al. 1971).

Studies of selenite adsorption on soils in the pH range expected for Yucca Mountain groundwaters indicate relatively limited adsorption ($<$ 30%) from 0.05 N chloride solutions containing 0.16 to 0.63 mg/l selenium (Neal et al. 1987). This limited sorption potential will likely be further decreased in natural waters containing high concentrations of competing anions.

Data for selenium sorption coefficients on Yucca Mountain rock samples in contact with J-13 water have been summarized by Thomas (1987). Most measured values are less than 5 ml/g, and they do not appear to correlate with rock type. A puzzling feature of the data is that, for a given rock sample, sorption coefficients are larger in the higher pH experiments (pH of 8.8) compared to the lower pH experiments (pH of 6.0). This result is contrary to the pH dependence predicted on the basis of double-layer theories. Neal et al. (1987) noted a similar effect for selenium sorption on soils for a solution phase enriched in calcium. They suggested the effect may be due to the formation of a calcium-rich surface precipitate or, alternatively, a change in surface charge due to the adsorption of divalent calcium cations. Benjamin (1983) made

similar observations involving other divalent cations. These data suggest that in groundwaters relatively enriched in calcium, and perhaps other divalent cations, selenium adsorption may be somewhat enhanced in the alkaline pH range.

Conclusions regarding sorption behavior with respect to expected variations in groundwaters.
Sorption coefficients for selenium on Yucca Mountain rock samples have only been measured in J-13 water. These experiments do not show the expected decrease in sorption coefficient with pH. Therefore, variations in pH over the range expected in Yucca Mountain groundwaters do not appear to be the most important groundwater compositional parameter in the sorption behavior of this element. Based on the data obtained in other studies, divalent cations may have a significant impact on the sorption behavior of this element in Yucca Mountain rock-water systems. Additional experiments with waters enriched in divalent cations (such as UE-25 p#l water) may be productive and may enlarge the range of selenium sorption-coefficient values appropriate for use in performance-assessment calculations.

Uranium

Behavior in solutions representative of Yucca Mountain groundwaters.
Under the redox potentials expected in Yucca Mountain groundwaters, particularly in the unsaturated zone, uranium should be in the $+6$ oxidation state. In this oxidation state, uranium will be present in solution in a variety of complexes including $(UO_2)_2CO_3(OH)_3^-$, $UO_2(CO_3)_2^{2-}$, $UO_2(CO_3)_3^{4-}$, $UO_2(OH)_2(aq)$, $UO_2(CO_3)(aq)$, and other minor species. Phosphate, fluoride, or sulfate species will not be significant within the concentration ranges for these anions and the pH range expected in Yucca Mountain groundwaters. In the high-silica groundwaters of Yucca Mountain, the solubility-controlling compound for uranium should be haiweeite ($Ca(UO_2)_2(Si_6O_{15})(H_2O)_5$), according to available thermodynamic data (Bruton 1990, 1991). Interestingly, leaching experiments on uranium-oxide pellets (Bates et al. 1990) at 90ºC using J-13 water produced a variety of phases on reacted surfaces that did not include haiweeite.

Qualitative evidence for behavior in the surficial environment.
Data on the behavior of uranium in the surficial environment are available from various sources. Several types of uranium ore deposits have been studied as natural analogs to repository settings. Other sources of data include studies of uranium mill-tailings piles, waste-stream outfalls, and other uranium ore deposits. Only the natural analog studies will be discussed in this section.

The deposits that have been studied as natural analogs include the deposits at Oklo, Gabon, the Alligator Rivers region in Australia, Cigar Lake in Canada, Poças de Caldas in Brazil, and Peña Blanca in Mexico. Each of these deposits has been studied in considerable detail to define the geochemical behavior of uranium and its daughter products in the environments in which the ore deposits are found. Although none of the environments are completely analogous to the Yucca Mountain site, the Peña Blanca deposit is at least situated in Tertiary volcanic tuffs similar to those present at Yucca Mountain.

A critical aspect of any analog to potential uranium migration at the Yucca Mountain site is that the uranium source must be subject to redox potentials similar to those expected at Yucca Mountain, particularly in the unsaturated zone. This fact eliminates from detailed consideration data from the Cigar Lake and probably the Oklo deposits (Goodwin et al. 1989; Cramer and Sargent 1994; Brookins 1983).

The Alligator Rivers deposits are exposed to oxidizing conditions in a surficial environment (Gilbin and Snelling 1983). Uranium isotope-disequilibrium studies at this site indicate that uranium migration has occurred relatively recently (Snelling and Dickson 1979). However, evidence for recent transport does not by itself provide an estimate of the rate of transport and, more importantly, of the

chemical controls on this rate. The latter type of information could be very useful to the Yucca Mountain Program.

At the Koongarra deposit, uranium migration is significantly retarded by the precipitation of uranyl phosphate minerals (Snelling 1980). Although phosphate concentrations in local groundwaters are not high (0.01–0.1 mg/l), significant phosphate concentrations are found in the country rocks in minerals such as apatite. The phosphate in the rocks is apparently redistributed locally by groundwater, resulting in the precipitation of uranyl phosphate minerals within the zone of weathering (Snelling 1980). This retardation mechanism is not expected to be important at Yucca Mountain, given the low phosphate concentrations found in Yucca Mountain rock units (Broxton et al. 1986).

Uranium in the zone of weathering at Alligator Rivers also appears to be associated with and is probably retarded by ferric-iron compounds (Payne et al. 1991 and others). Sorption experiments have been carried out involving uranium sorption on whole-rock samples and on pure mineral samples (Payne et al. 1991). The results of these experiments suggest that ferric hydroxides are strong sorbers of uranium in this system over a pH range of 5 to 9. This result is not particularly new as similar results on ferric oxyhydroxides have been reported by others (for example, Hsi and Langmuir 1985). A potentially important result from these studies would be the derivation of some defensible estimate of the rate of transport of uranium in this system using the experimentally derived chemical constraints on uranium adsorption behavior and a valid groundwater flow model. Unfortunately, hydrologists who are knowledgeable about the site suggest the complicated nature of the flow system may preclude the development of defensible flow models (S. N. Davis, cited in Curtis and Fabryka-Martin 1988).

The Peña Blanca uranium deposits in Mexico provide a potentially more appropriate analog site in relation to Yucca Mountain. The primary uranium deposits at this site are hydrothermal in origin and were emplaced in structural features associated with Tertiary silicic volcanic tuffs that overlie Mesozoic calcareous basement (George-Aniel et al. 1991). In addition to the hydrothermal deposits, which contain sulfide minerals as well as uranium oxides, supergene deposits have formed locally through the leaching of uranium from the volcanic rocks and subsequent precipitation as uranyl silicate minerals, including uranophane (Murphy 1992). The supergene deposits are hosted by kaolinitized and silicified rhyolite and do not appear to contain sulfide minerals. The absence of sulfide minerals is important because sulfides, such as pyrite, oxidize readily in the surficial environment to produce acidic conditions unlike those expected within Yucca Mountain. The supergene deposits are thought to have formed in the surficial environment (George-Aniel et al. 1991), and their study may offer useful insight into the potential for migration of uranium from the proposed repository within Yucca Mountain. No data on the present-day sorption behavior or rate of migration of uranium in these deposits has been reported to date. However, several geochemical studies are currently under way to provide such data (Murphy 1992).

A qualitative study by Rosholt et al. (1971) established that uranium was leached from devitrified tuff samples but not from hydrated glassy samples obtained from a given geologic unit. This and other data presented suggest devitrification makes the uranium in tuffs more mobile in the surficial environment. Zielinski et al. (1986) and Flexser and Wollenberg (1991) observed that uranium in Yucca Mountain devitrified tuffs was commonly associated with manganese oxides. This fact suggests that, although uranium may be mobile in the unsaturated devitrified tuffs in Yucca Mountain, it could be retarded to the extent that there are manganese oxides present along the flow path with sufficient capacity to sorb the potential flux of uranium from the proposed repository horizon. Given the amount of uranium to be emplaced in the potential repository, it would seem the sorption capacity of the manganese oxides present in the

mountain (Bish and Chipera 1989) would be rapidly saturated. Nonetheless, manganese oxides may significantly retard the movement of uranium in some of the fracture-flow scenarios.

Data from laboratory sorption experiments.
Data have been presented on the adsorption of uranium onto a variety of pure mineral phases in simple electrolytes. Among the solid phases investigated are goethite (for example, Hsi and Langmuir 1985), hematite (Ho and Miller 1986), silica gel (Zielinski 1980), clays (Tsunashima et al. 1981), and zeolites (Ames et al. 1983). The results reported are sometimes difficult to reconcile. For example, Hsi and Langmuir report that hematite sorbs very little of the uranium in solutions with 5×10^{-5} M uranium and 10^{-3} M total carbonate, whereas Ho and Miller report that hematite sorbs up to 100 per cent of the uranium in their experiments with similar uranium and bicarbonate solution concentrations. Both sets of experiments had similar hematite surface areas. The main difference was that the solution phase in the Hsi and Langmuir experiments also contained 0.1 M $NaNO_3$. However, $NaNO_3$ is generally considered to be a nonreactive electrolyte, and nitrate does not form complexes with uranium in the pH range addressed in these experiments. Why there is a difference in these results is unclear. One possibility is that the surface characteristics of the solid phases used were not the same in the two sets of experiments.

Silica gel appears to have a clear affinity for uranium as established by the results of laboratory experiments and by observations on the association of uranium with opals in nature (Zielinski 1980). According to Maya (1982a), the uranium is adsorbed to silica gel as the uranyl ion, free of carbonate ligands. Zielinski has shown that sorption of uranium onto silica gel is sensitive to the total carbonate concentration of the solution phase when this concentration is above 0.01 M. Interestingly, experiments carried out at elevated temperatures (65–80ºC) resulted in somewhat higher sorption coefficients. Data regarding competitive effects on silica gel between uranium and other constituents in groundwaters at near-neutral pH have not been found in the literature.

Sorption of uranium by clays has been investigated in some detail. Borovec (1981) has presented data that indicate montmorillonite has a high selectivity for uranyl ions relative to divalent ions of zinc, manganese, calcium, magnesium, cobalt, cadmium, and nickel at a pH of 6 in chloride solutions. However, Tsunashima et al. (1981) found montmorillonite has a greater selectivity for calcium, magnesium, and barium ions than for uranyl ions in nitrate solutions over the pH range from 4.0 to 4.5. Montmorillonite was found to have a greater selectivity for the uranyl ion than for sodium and potassium ions in the same solutions. Ames et al. (1983) found that uranium was strongly sorbed to montmorillonite from 0.01 M NaCl solutions but weakly sorbed from 0.01 M $NaHCO_3$ solutions in the pH range from 8 to 9.

Because groundwaters in Yucca Mountain contain significant concentrations of bicarbonate, calcium, and magnesium ions, these data suggest overall that uranyl ions may not compete favorably for exchange sites on clay minerals in Yucca Mountain, although quantitative prediction of the extent of exchange would require more detailed analysis.

Data available on uranium sorption on zeolitic minerals are very limited. Ames et al. (1983) report that clinoptilolite has a low affinity for trace levels of uranium in the pH range from 8 to 9 in 0.01 M $NaHCO_3$. Doi et al. (1975) found that uranium at concentrations of 10^{-6} g per g of solution was strongly sorbed onto clinoptilolite from perchlorate solutions in the pH range from 4 to 8.5.

Data on uranium sorption coefficients for Yucca Mountain rock-water systems were reported by Thomas (1987) and discussed by Meijer (1990, 1992). The affinity of the devitrified and vitric tuffs for trace levels of uranium is generally small ($K_d < 5$ ml/g) over the pH range from 6 to 9 in J-13 water. For zeolitic tuffs, the K_d is near zero

at a pH of 9 but increases with decreasing pH to values of approximately 25 ml/g at a pH of 6 in J-13 water. This behavior suggests uranyl ions can exchange with the major cations in zeolites.

In UE-25 p#1 water, uranium batch-sorption experiments were only carried out in the pH range from 8.3 to 9.3 with the result that the measured sorption coefficients were small (0–2.7 ml/g; Thomas 1988). The devitrified sample showed the largest sorption coefficient. In the pH range from 6 to 8, it is expected that the sorption coefficients for uranium in UE-25 p#l water will increase with decreasing pH, but they will likely be smaller than the coefficients obtained for the same rock samples in J-13 water over this pH range. In H-3 groundwater, sorption coefficients were also low for zeolitic and devitrified rock types over the pH range from 9.2 to 9.3, presumably reflecting the elevated carbonate content of this water. However, data for a vitric sample showed a value of 6.2 ml/g for the uranium sorption coefficient at a pH of 9. This relatively high value has not been explained.

We studied the sorption of U(VI) onto samples of the three types of tuff in J-13 water (under oxidizing conditions) at the two pH values (7 and 8.5). However, to identify the sorbing minerals in the tuffs, we also studied sorption onto the pure minerals hematite, clinoptilolite, albite, and quartz. We found that uranium in J-13 water does not sorb onto devitrified and vitric tuffs, albite, and quartz (Table 51).

We used wet-sieved tuffs, albite, and quartz samples with particle sizes in the range from 75 to 500 μm. Initial uranium concentrations ranged from 8×10^{-8} to 1×10^{-4} M. The pretreatment period was 2 to 4 days, and the sorption period, 3 to 4 days. The negative values reported in Table 51 are the result of analytical error for the case of very little sorption (that is, a small number obtained as the difference of two large numbers). For the experimental conditions cited, uranium sorption onto zeolitic tuffs and clinoptilolite is nonlinear and can be fitted with Freundlich and Langmuir isotherms (Figs. 74 and 75).

Table 51. Uranium Sorption in J-13 Water under Oxidizing Conditions

Solid phase	pH	K_d (ml/g)*
G4-268, devitrified tuff	7	2×10^{-1}
	8.5	7×10^{-1}
GU3-1405, vitric tuff	7	-5×10^{-1}
	8.5	6×10^{-1}
Quartz	7	1×10^{-1}
	8.5	7×10^{-2}
Albite	7	-5×10^{-2}
	8.5	-1×10^{-1}

*The uncertainties in the data are ± 3

For the clinoptilolite-rich zeolitic tuff sample G4-1510, the scatter in the data makes it impossible to conclude whether there is a significant difference between the experiments performed under a carbon-dioxide overpressure and a pH of 7 or at atmospheric conditions and a pH of 8.5 (Fig. 74). However, the experiments with pure clinoptilolite indicate that sorption increases with decreasing pH for U(VI) (Fig. 75), as is the case for Np(V). Because the major constituent of tuff sample G4-1510 is clinoptilolite, predictions of the K_a (K_d divided by the solid-phase surface area) were made for uranium sorption onto this tuff by assuming that clinoptilolite is the only sorbing phase. Inspection of Table 52 indicates that reasonable predictions are obtained with this assumption for a pH of 7 but not for a pH of 8.5. In all cases, predictions based on clinoptilolite sorption are conservative.

The sorption of uranium onto pure iron oxides (such as hematite) is very large (and large uncertainties in the K_d values result from measuring the small amounts of radionuclide left in solution after sorption). Although the measured sorption of uranium onto pure hematite is very large, sorption

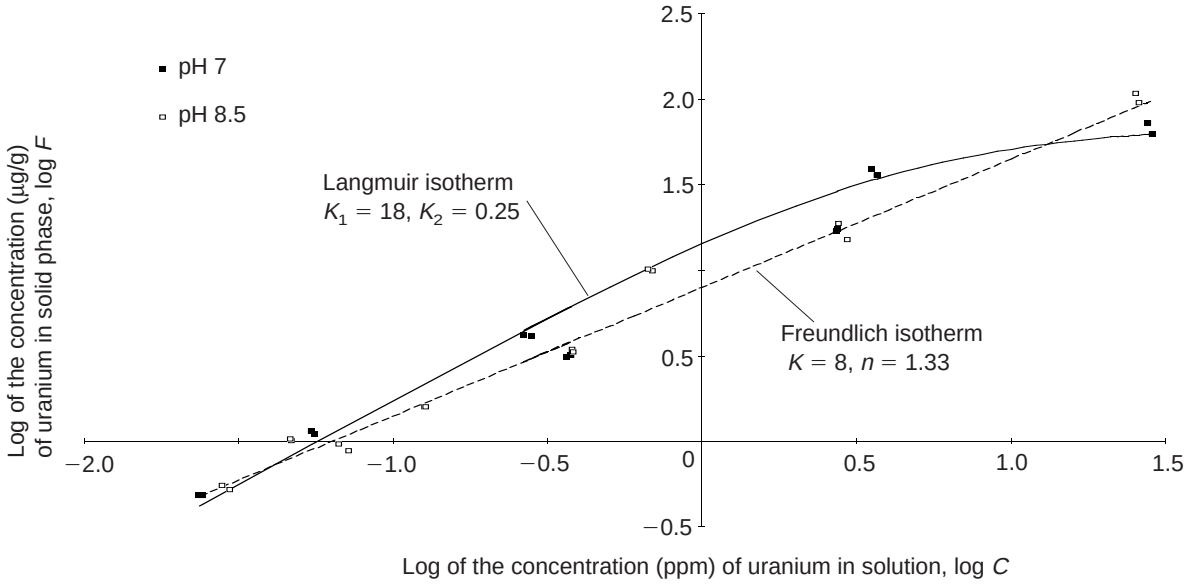

Figure 74. Uranium Sorption onto Clinoptilolite-rich Tuff. A log-log plot of the concentration of uranium in the solid phase, *F*, of the clinoptilolite-rich tuff G4-1510 versus the concentration of uranium in the solution phase, *C*, of J-13 well water. The tuff was wet-sieved to give particles that ranged in size from 75 to 500 μm. The period of pretreatment was 2 to 4 days; the period of sorption was 3 to 4 days. The data for a pH of 7 have been fitted with a Langmuir isotherm; the data for a pH of 8.5 have been fitted with a Freundlich isotherm.

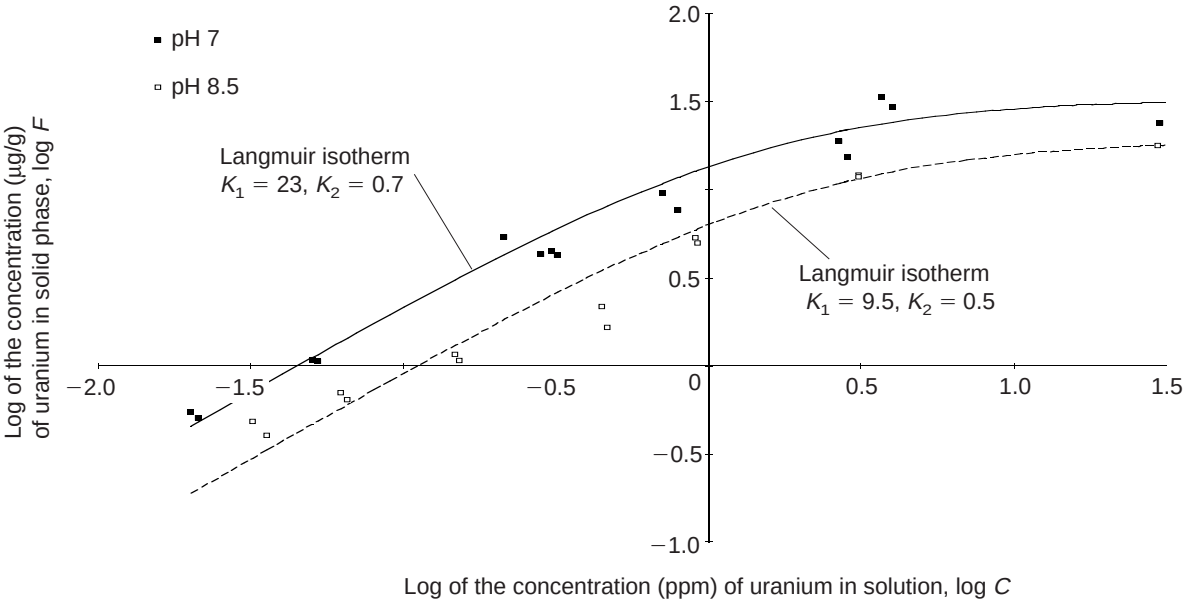

Figure 75. Uranium Sorption onto Clinoptilolite. A log-log plot of the concentration of uranium in the solid phase, *F*, of clinoptilolite versus the concentration of uranium in the solution phase, *C*, of J-13 water. The mineral was unsieved. The period of pretreatment was 2 to 4 days; the period of sorption was 3 to 4 days. The data for each pH (7 and 8.5) have been fitted with a Langmuir isotherm.

onto devitrified tuffs, which appear to have traces of hematite (1% $\pm$ 1), is essentially zero. As with neptunium, this result could be due to differences in the surface of pure hematite compared to hematite in tuff, or it could be due to passivation of the hematite surfaces in the tuff by elements (such as the rare earths) that have a higher affinity for hematite than uranium and, thus, occupy the sorption sites.

Table 52. Prediction of Uranium Sorption on Clinoptilolite-rich G4-1510 Tuff in J-13 Water

Initial concentration (M)	pH	Measured K_a (m)	Predicted K_a (m)*
2×10^{-7} to 4×10^{-7}	7	8×10^{-7}	8×10^{-7}
	8.5	8×10^{-7}	4×10^{-7}

*Assuming clinoptilolite is the only sorbing mineral in the tuff

Conclusions regarding sorption behavior with respect to expected variations in groundwaters. The dominant groundwater compositional controls on the sorption behavior of uranium on Yucca Mountain rock samples will likely be pH, carbonate content, and the concentrations of calcium and magnesium ions in solution. The pH and carbonate contents influence the sorption largely as a result of the decrease in carbonate complexation of uranium with decreasing pH. These two parameters are therefore not entirely independent. However, different water compositions can have different carbonate contents at a given pH. The expectation is that waters with higher carbonate contents will be associated with lower sorption coefficients. This trend would apply to both ion-exchange and surface-complexation sorption mechanisms. However, decreasing pH will have different effects on uranium sorption behavior in zeolitic and clay-rich samples versus devitrified and vitric samples. In the former samples, the uranium sorption coefficient will likely increase with decreasing pH due to the increase in uranyl ion concentrations with decreasing pH. For a given rock-water system, the magnitude of this increase will depend on the concentrations of competing ions such as calcium and magnesium in the water. For high calcium and magnesium waters, the competition effects will be substantial. Because unsaturated-zone waters are relatively enriched in calcium and magnesium, uranium sorption coefficients in the unsaturated zone may be on the low end of the range reported to date (Thomas 1987, 1988) unless the low total carbonate concentrations in these waters balance the effect of the elevated calcium and magnesium concentrations.

It will be important to carry out experiments on representative rock samples using a high-calcium-and-magnesium, low-carbonate, unsaturated-zone water composition with pH controlled over a range from 6 to 9. Similar experiments should be carried out with a high total-carbonate and high calcium-and-magnesium water composition, such as UE-25 p#1 water, over the pH range from 6 to 8.

Carbon, Chlorine, Iodine, and Technetium

Because carbon, chlorine, iodine, and technetium are unlikely to have significant sorption affinity in the rock-water systems expected at Yucca Mountain, their sorption behavior will not be discussed in detail. For carbon, the most robust retardation mechanism will be isotopic exchange with stable carbon isotopes in groundwater and on carbonate mineral surfaces (Meijer 1993).

Chloride and iodide ions will have no significant retardation in Yucca Mountain rock-water systems and may even have slightly enhanced migration rates due to anion-exclusion effects (Ogard and Vaniman 1985). If conditions were to become sufficiently oxidizing to convert iodide to iodate, some retardation of iodine might occur in the flow system. Although such conditions might occur locally, for example, due to radiolysis effects, it is considered unlikely that such conditions would be

present over a significant volume of the flow system for an extended period of time.

Technetium appears to show nonzero, although minimal, retardation in Yucca Mountain rock-water systems (Ogard and Vaniman 1985; Rundberg et al. 1985; Thomas 1988). However, the cause of this retardation has not been identified, and it may simply be an experimental artifact. Because the minimal values obtained for technetium sorption coefficients to date will not result in significant retardation of technetium, it does not seem prudent to expend funds on the detailed investigation of potential sorption mechanisms for this element. More significantly, if sufficiently reducing conditions could be shown to exist in portions of the flow system down-gradient of the proposed repository, retardation of technetium by the precipitation and sorption of Tc^{4+} species might occur.

B. EFFECTS OF ORGANICS ON ACTINIDES

Introduction

Naturally occurring organic compounds generated during the transformation of plant and animal debris over time and as a result of the synthetic activities of microorganisms are ubiquitous in surface and subsurface environments. For example, pore water from a well-developed soil environment usually contains dissolved organic carbon in quantities greater than 20 mg/l in top soils and in quantities of about 5 mg/l in subsoils. Dissolved organic carbon concentrations in groundwaters typically depend on the environment and are usually below 2 mg/l (Drever 1988). The decrease in concentrations of organic materials with increasing depth is attributed to chemical and biological degradation as well as to sorption on mineral surfaces. Sorption of organic materials onto mineral surfaces is considered the dominant contributing factor to the removal of organics from solution during percolation through the subsurface.

The interaction between organic materials and mineral surfaces in the natural environment is important to mineral surface geochemistry. Sorption of organic material onto mineral surfaces affects not only the solubility and charge of the organic materials in solution but also the properties of the mineral surfaces, such as their charge and hydrophobicity, thereby altering the reactivity of the mineral toward metal ions. A clear understanding of the effects of the organic materials that frequently coat mineral surfaces in natural environments will lead to improvements in the sorption models used to predict the mobility of radionuclides in natural aquatic environments (Choppin 1992).

The objective of this section is to summarize the laboratory results for the effect of organic materials on the sorption of plutonium and neptunium on selected mineral oxides and tuff material.

Experimental Procedures

Preparation of tuff and oxide minerals

Three synthetic iron oxides (goethite, hematite, and ferrihydrite), one synthetic aluminum oxide (boehmite), and a natural crushed-tuff material from Yucca Mountain (USW G4-270, a devitrified tuff) served as model sorbents. Methods for preparing the oxides are described in the literature (Kung and McBride 1989a, 1989b, 1991).

In brief, iron oxide was synthesized by reacting ferric chloride with dilute sodium hydroxide under slightly acidic conditions and was then aged at raised temperature for several days. X-ray powder diffraction (XRD) analysis confirmed the oxide to be pure goethite. The surface area of the goethite, calculated from nitrogen adsorption by the three-point BET method, was about 89.5 m^2/g.

The ferrihydrite preparation involved the overnight hydrolysis of ferric salt at low pH followed by raising the pH with dilute sodium hydroxide and, finally, aging the mixture for two weeks at raised temperature. The surface area of the freeze-dried material was 91.5 m^2/g. XRD analysis indicated a poorly crystalline product containing ferrihydrite.

Hematite was prepared by aging ferric nitrate solution at raised temperature for 3 days. The surface area of the freeze-dried material was 39.4 m^2/g. XRD analysis confirmed that this material was well-crystallized hematite.

Boehmite was prepared by fast hydrolysis of aqueous aluminum chloride with sodium hydroxide, followed by mixing and aging. The surface area of the freeze-dried material was 324 m^2/g. XRD analysis confirmed that this aluminum oxide was poorly crystallized boehmite, an aluminum oxyhydroxide.

The metal oxides were stored either in a freeze-dried state or in suspensions containing 0.1 M KCl. For those in suspensions, the solid concentration of these oxide suspensions was less than 20 mg/ml.

XRD analysis of the crushed-tuff material (USW G4-270, a devitrified tuff), obtained from S. Chipera at Los Alamos, indicated that it was about 30% silica and 69% feldspar, the remainder consisting of trace amounts of layer silicates and iron oxide. Part of the tuff material was treated with a 15% hydrogen-peroxide solution to remove any natural organic material from the tuff surface.

Preparation of organics and radionuclides

Catechol, alanine, DOPA, and NAFA were used as model organic materials. Catechol is a phenolic compound that may chelate with metal ions and undergo redox reaction with the metal. Alanine is an amino acid that will complex with the hard-acid type of metal ions in solution. DOPA, a naturally occurring amino acid commonly found in plant seedlings, pods, and broad beans, was chosen because it contains well-defined organic functional groups such as carboxylic acid, amine, and phenols. The catechol, alanine, and DOPA, purchased from Fluca Chemical Company with purity greater than 99%, were used as received. The NAFA, obtained from the International Humic Substances Society (IHSS), is identified by IHSS as a reference fulvic acid with the code number 1R105F and is prepared and homogenized from a designated aquatic source by IHSS.

Neptunium-237 was obtained from Amersham International (product code NGZ-44). The plutonium-239 stock solution was prepared in the Pu(V) oxidation state (this concentrated stock solution was obtained from P. Parmer at Los Alamos). The desired concentrations of neptunium and plutonium were diluted and stored in 0.1 M KCl solutions. Under the experimental conditions used in this work, the plutonium and neptunium are expected to exist as the chemical species PuO_2^+ and NpO_2^+, respectively.

Sorption Measurements

DOPA sorption

Sorption isotherms were obtained by mixing the desired sorbent suspension and sorbate in Teflon or polycarbonate centrifuge tubes. The initial DOPA concentrations ranged from 20 to 100 μM. The pH was adjusted by adding 0.05 M NaOH or HCl immediately after mixing. The tubes were capped and shaken for at least 20 hours at 22 ± 1ºC. The solid phase was separated from suspension by centrifugation. The supernatant was analyzed for unsorbed DOPA by ultraviolet spectrometry (Hewlett-Packard 8450A), and the amount of sorption was calculated by determining the difference between the initial and final concentrations. Potassium chloride was used as a background electrolyte to maintain an essentially constant ionic strength of 0.1 M.

Radionuclide sorption

A similar method was used to obtain plutonium and neptunium sorption isotherms. The amount of radionuclide in solution was determined by liquid scintillation counting (Packard 2550-TR/AB). The metal ions were introduced into the tubes after the pH in each suspension was adjusted. For the multisorbate systems, the organic sorbate was added before the radionuclide sorbate. Solution pH was measured after shaking. The carbon dioxide was not controlled in all the systems studied. For the initial sorption isotherms, about 0.03 to 0.5 μM plutonium solutions and about 0.1 to 4 μM neptunium solutions were used. Standard sorbate solutions (to which no sorbent was added and which were subjected to the same shaking treatment) were used to generate standard curves. No sorbate sorption onto the centrifuge tubes was detected.

Results and Discussion

Neptunium

Sorption as a function of tuff and oxide minerals. The isotherms for neptunium sorption on different iron oxides are shown in Fig. 76. In this experiment, the three iron oxides were used as sorbents. Results show that, on a weight basis, hematite was the most adsorptive, whereas goethite was the least adsorptive. Thus, the sorption of neptunium on model iron oxides follows the order hematite > ferrihydrite > goethite.

Two things should be noted in this study. First, the surface areas of these iron oxides were different, and the sorptivity of neptunium was not compared on a unit surface-area basis. For ferrihydrite and goethite, the surface areas are around 90 m^2/g, whereas the surface area of hematite is about 40 m^2/g. Higher surface areas are expected to have higher sorptions. Secondly, the sorption experiments were not conducted at the same pH. Sorption on ferrihydrite was conducted at a pH of 6.2, whereas sorption on hematite and goethite were conducted at a pH of 6.9. The pH may affect the sorptivity of neptunium on iron oxides. The effect of pH on neptunium sorption will be presented in the next section.

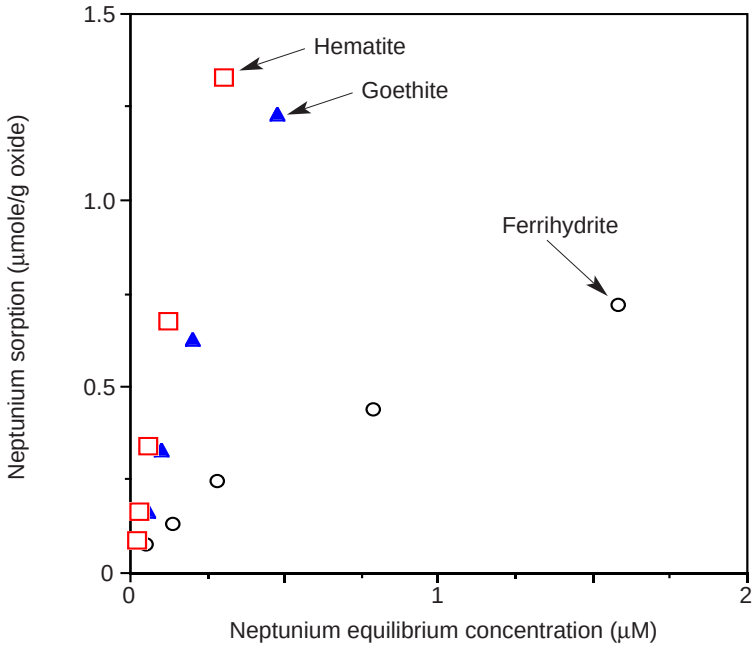

Figure 76. Neptunium Sorption per Unit Mass on Iron Oxides. The plot shows isotherms for the sorption of neptunium on three different iron oxides, calculated on the basis of unit mass.

The effect of oxide surface areas on neptunium sorption was replotted in Fig. 77. In this figure, the amount of neptunium sorption was normalized on a unit surface-area basis (m^2). Results again showed that the sorption of neptunium on iron oxides follows the order hematite > ferrihydrite > goethite. Evidently, hematite has the highest sorptivity for neptunium on the basis of both weight and unit surface area.

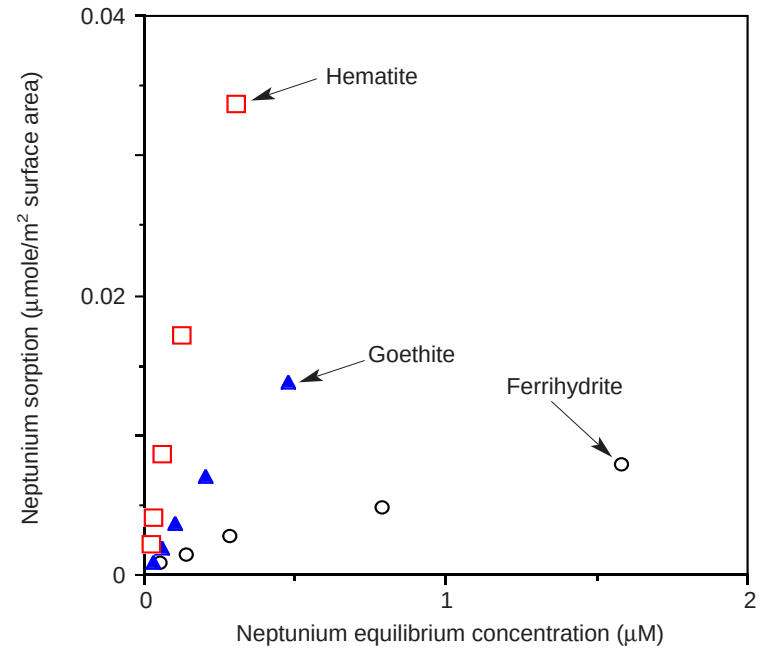

Figure 77. Neptunium Sorption per Unit Area on Iron Oxides. The plot shows isotherms for the sorption of neptunium on three different iron oxides, calculated on the basis of unit surface area.

Effect of pH on sorption.
To quantify organic sorption, it is required that we understand the effect of organics on radionuclide sorption. Experiments were conducted to study organic

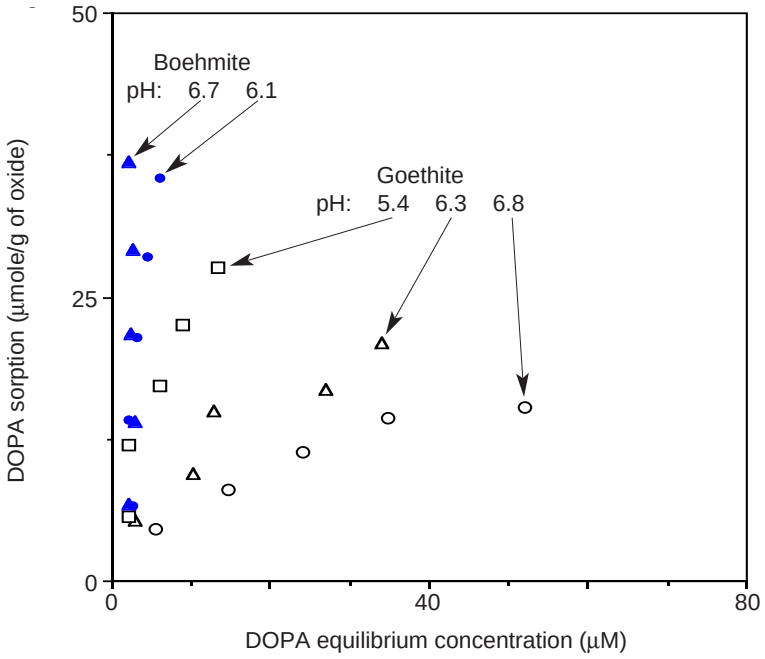

Figure 78. pH Dependence of DOPA Sorption on Oxides. This plot shows isotherms for the sorption of DOPA on goethite and on boehmite at different pH levels in the presence of 0.1 M KCl.

sorption, and the results are presented in this section. The isotherms for DOPA adsorption on goethite and boehmite at different pH levels are shown in Fig. 78. On a weight basis, boehmite was more adsorptive than goethite. The linear sorption curves for these oxides suggest a low degree of coverage of the surface reactive sites by the organic material in the presence of excess potassium chloride. This finding is consistent with the theoretical calculation of coverage, which suggests that the amount of DOPA sorption is much less than a monolayer, based on the BET surface area.

Increasing the solution pH resulted in a higher organic sorptivity for all oxides. Under neutral and slightly acidic conditions (pH values from 5.5 to 7), iron and aluminum oxides were expected to have positive surface charges (Sposito 1989). Although the sorption of DOPA is apparently not dependent on surface charge effects such as electrostatic attraction, it may be controlled by the deprotonation process of the organic material. DOPA is expected to be dominated by neutral species under neutral and slightly acidic conditions, but raising the pH level will increase the concentration of deprotonated DOPA species, which are expected to have a stronger affinity for oxide surfaces in direct surface complexation. Therefore, it is reasonable to assume that DOPA forms direct surface bidentate complexes on the oxide surfaces.

The isotherms for neptunium sorption on goethite at different pH levels are shown in Fig. 79. Increasing the solution pH from 6.2 to 6.9 resulted in a higher neptunium sorptivity.

Effect of model organics on sorptive behavior.

We examined the effect of natural organics on radionuclide sorption onto natural tuff material that may have been precoated with natural organic material. The standard method for removing the natural organic material from mineral samples is to use hydrogen peroxide to oxidize the material (Kunze and Dixon 1986). We used a 15% hydrogen-peroxide solution when we removed organic material from crushed-tuff samples collected from Yucca Mountain. In the sorption experiments conducted to study the effect of the naturally presorbed organics on neptunium sorption, half of the tuff samples were treated with hydrogen peroxide, half were not.

Figure 80 shows the sorption isotherms of neptunium on both types of tuff samples. The results suggest that treatment with hydrogen peroxide had little or no effect on the sorption of neptunium onto the tuff material.

The lack of effect of hydrogen-peroxide treatment on neptunium sorption on tuff materials is attribut-

able to three factors. First, untreated tuff may contain very little or no organic material on its surface. Low organic content on the untreated tuff surface could be expected because crushed tuff material is generated from bedrock that may have little exposure to natural organic materials. New surfaces generated during the crushing process would not contain organic materials, in which case untreated tuff would be expected to behave essentially the same as tuff treated with hydrogen peroxide. Second, neptunium has intrinsically low sorptivity on tuff material. No observable difference in sorption on both treated and untreated tuff is attributed to the low sorption of neptunium on both sorbents. Any minute differences in sorption are likely to occur below the level of detection. Third, the sorption of neptunium may be unaffected by organic material, assuming that organic materials such as DOPA do not influence neptunium sorption on tuff, goethite, or boehmite.

To explore the possibility that the untreated tuff contained little organic material, 4 to 50 µM of DOPA was purposely added to both treated and untreated crushed tuff materials, and the sorption isotherms of neptunium on these systems were compared. As Figs. 81 and 82 illustrate, the addition of DOPA had no effect on neptunium sorption on either treated or untreated crushed-tuff materials. These data thus sup-

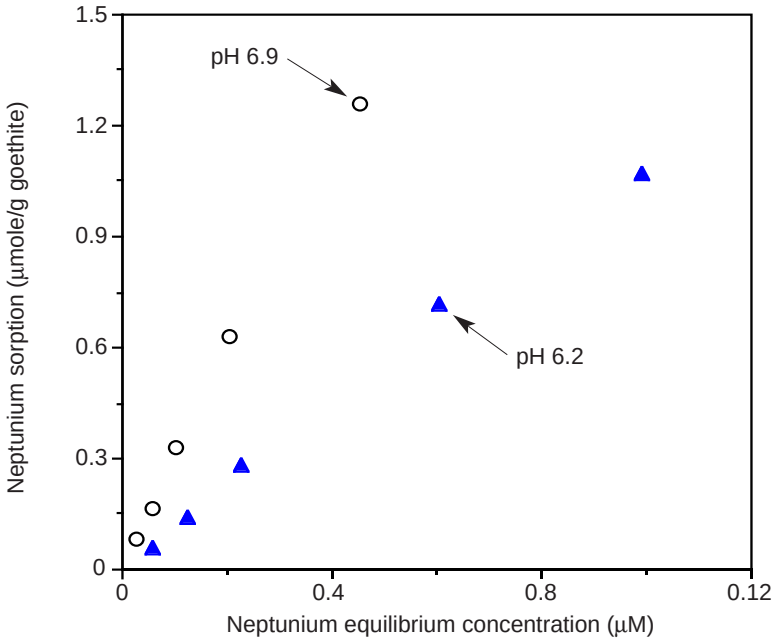

Figure 79. Neptunium Sorption on Goethite. This plot shows isotherms for the sorption of neptunium on goethite at a pH of 6.2 and 6.9.

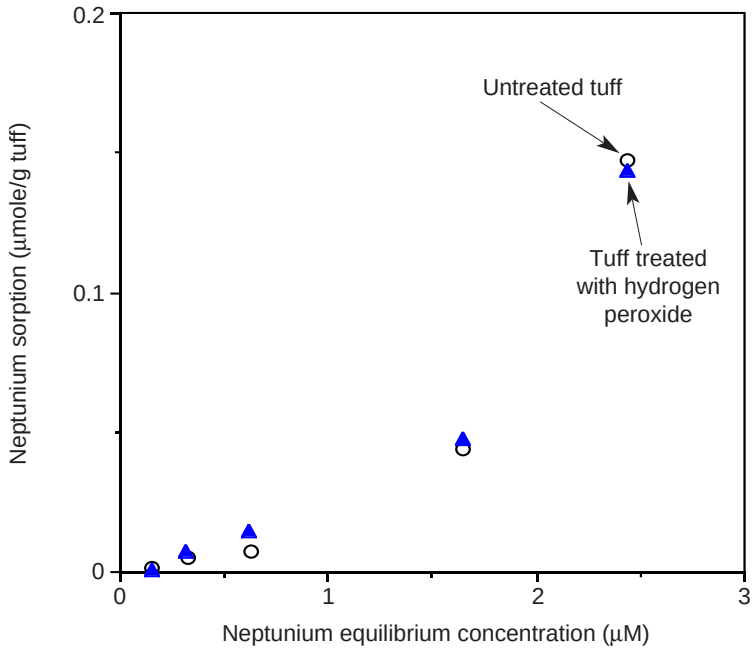

Figure 80. Neptunium Sorption on Treated and Untreated Tuff. This plot shows isotherms for the sorption of neptunium on devitrified tuff (G4-270) treated with hydrogen peroxide and untreated.

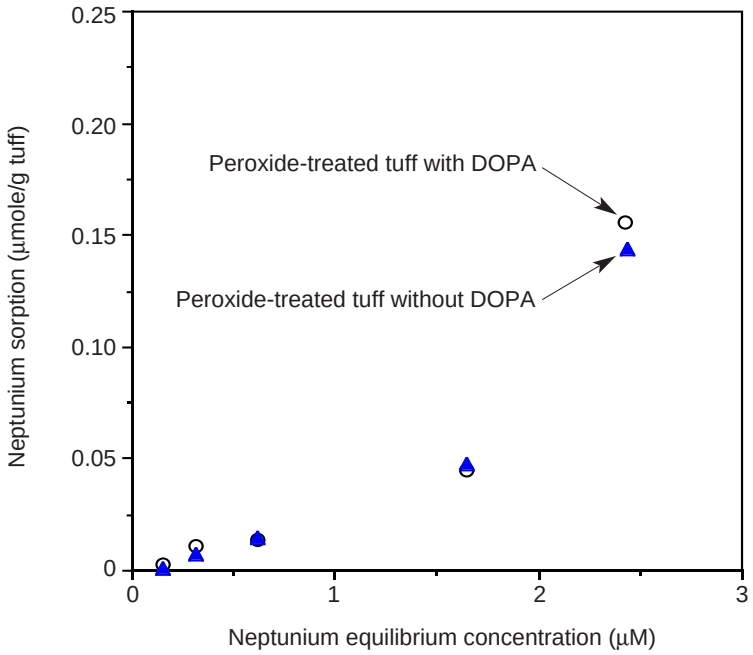

Figure 81. Sorption with and without DOPA on Treated Tuff. This plot shows isotherms for the sorption of neptunium on hydrogen-peroxide-treated tuff materials (G4-270) with and without DOPA.

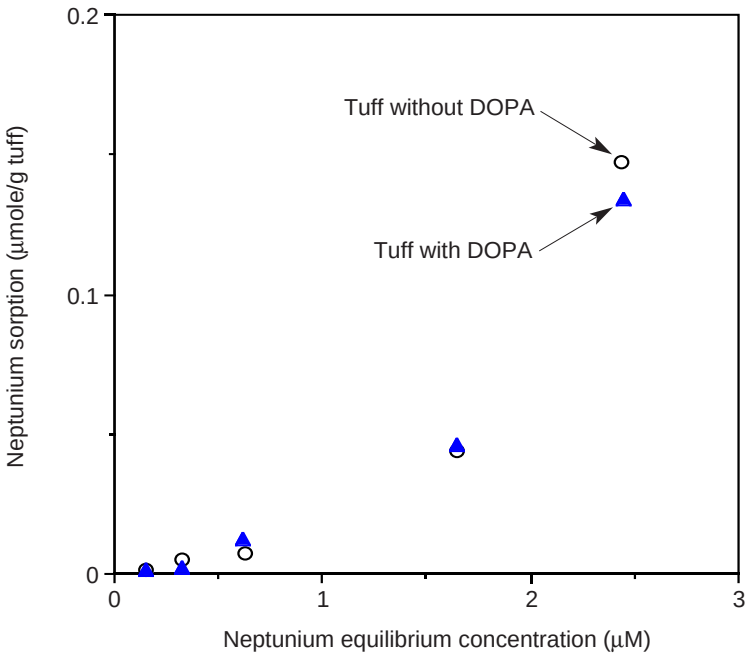

Figure 82. Sorption with and without DOPA on Untreated Tuff. This plot shows isotherms for the sorption of neptunium on untreated tuff samples (G4-270) with and without DOPA.

port the premise that the presence of organic material does not affect neptunium sorption on tuff materials.

Because this experiment did not rule out the possibility that the lack of an observable effect was a result of the intrinsically low sorptivity of tuff materials, the sorption of neptunium on iron and aluminum oxides in the absence and presence of DOPA was examined. The sorption of neptunium is expected to be much higher on iron and aluminum oxides than on tuff material. Thus, any effect of DOPA on neptunium sorption ought to appear in the oxide systems. To verify this assumption, sorption isotherms were measured for neptunium on iron and aluminum oxides and tuff material in the absence of organic materials with 0.1 M KCl at a pH of 6.2. The results (Fig. 83) indicate that the sorptivity of boehmite and goethite is approximately one and two orders of magnitude higher, respectively, than the sorptivity of tuff material. Thus, any effect of DOPA on neptunium sorption should be easily detectable in these oxide systems.

Neptunium sorption isotherms on iron and aluminum oxides in the presence of DOPA are shown in Figs. 84 and 85. In these experiments, 0.1 M KCl was used to maintain an essentially constant ionic strength, and the final pH of the suspensions was adjusted to a value of 6.2. The

initial neptunium concentration ranged from 0.2 to 2 µM, and the initial DOPA concentration ranged from 4 to 50 µM. The sorption isotherms of neptunium on aluminum and iron oxides suggest that DOPA does not significantly affect the sorption of neptunium. The relatively weak complexation of the pentavalent neptunium ion is a result of its relatively low effective charge on the cation (Choppin and Rao 1984). These results imply that there is no significant influence of DOPA on neptunium sorption on aluminum and iron oxides.

The occurrence of surface complexation between DOPA and oxide surfaces is supported by the observed sorption of catechol on metal oxide, which indicates that catechol chemisorbs on metal oxide by forming a bidentate complex with the surface metal atoms. DOPA is an organic with functional groups like catechol (phenols) and alanine (amino acids). Thus, the effect of simple organics such as catechol and alanine on the sorption of neptunium was studied. Both catechol and alanine are expected to complex with metal ions in solution. Besides the formation of metal-organic complexes, catechol readily undergoes redox reactions with some metal and metal oxides (McBride and Wesselink 1988). For example, catechol at high concentrations may undergo electron-transfer reactions with manganese and iron oxides.

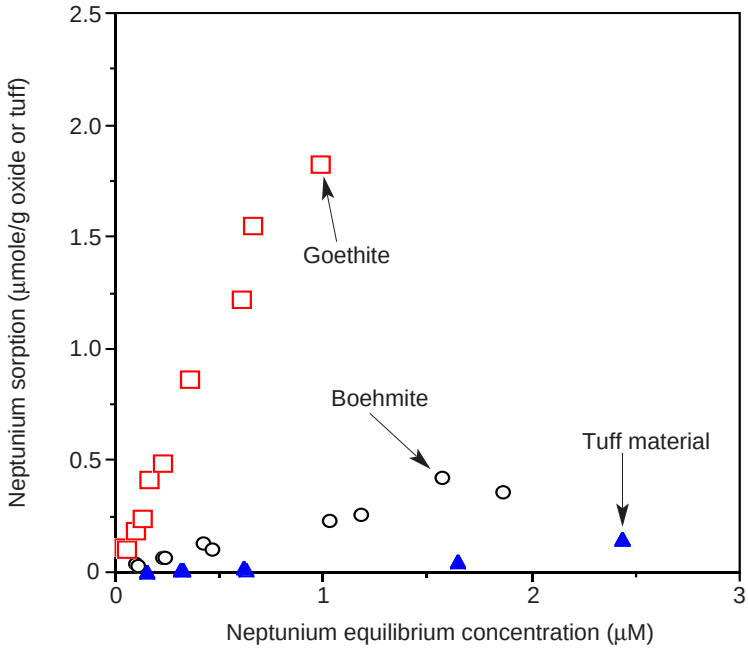

Figure 83. Neptunium Sorption on Oxides and Tuff. This plot shows isotherms for the sorption of neptunium on goethite, boehmite, and tuff material (G4-270).

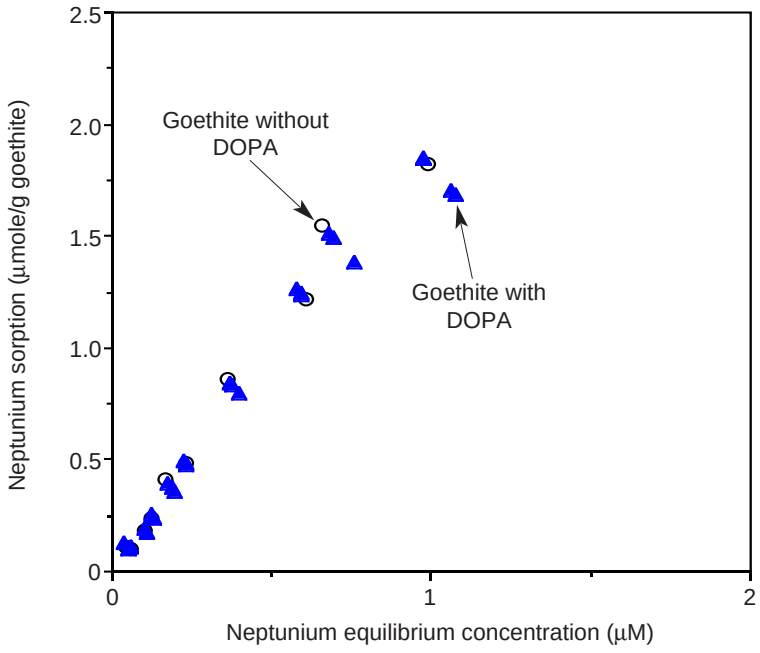

Figure 84. Sorption on Goethite with or without DOPA. This plot show isotherms for the sorption of neptunium on goethite in the presence and absence of DOPA at a pH of 6.2.

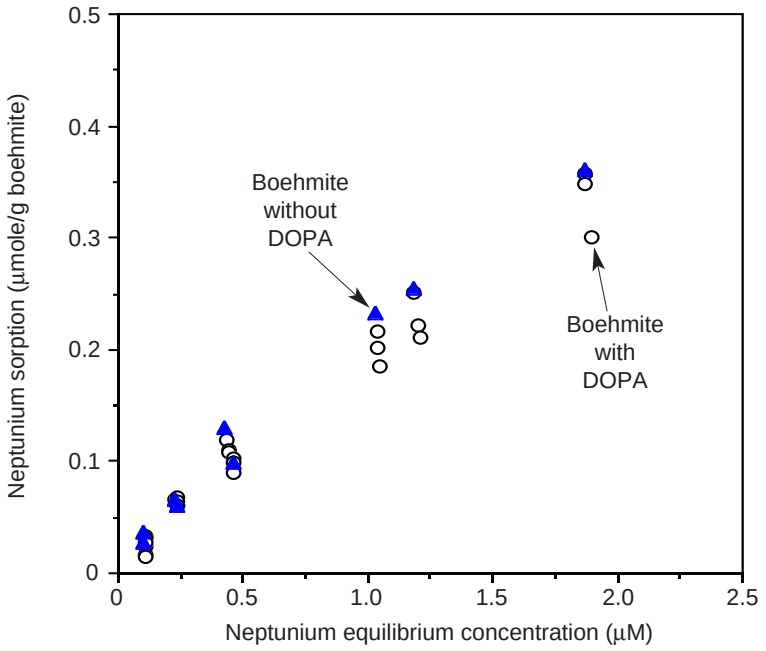

Figure 85. Sorption on Boehmite with or without DOPA. This plot shows isotherms for the sorption of neptunium on boehmite in the presence and absence of DOPA at a pH of 6.2.

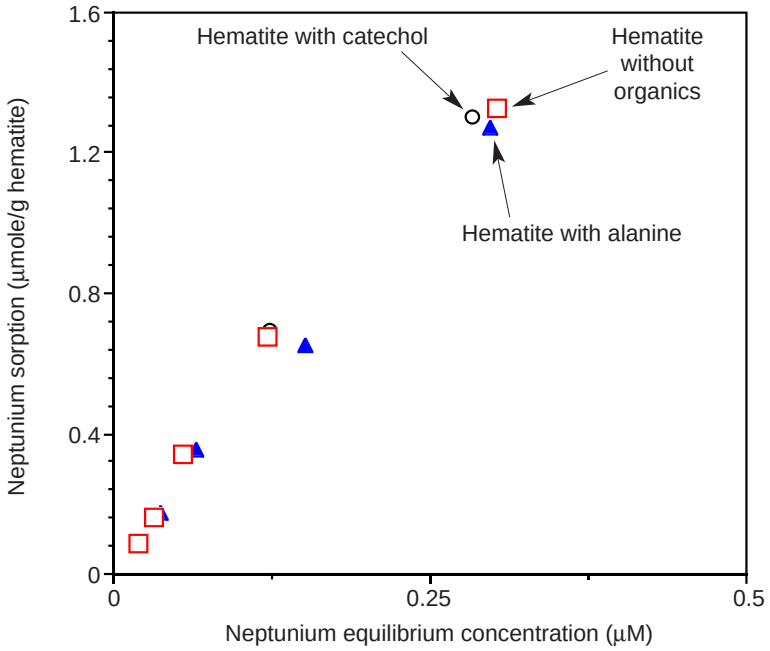

Figure 86. Sorption on Hematite with or without Organics. This plot shows isotherms for neptunium sorption on hematite in the presence and absence of catechol or alanine (1 µM) at a pH of 6.9.

We quantified the effect of catechol and alanine on neptunium sorption by measuring isotherms for sorption on hematite, ferrihydrite, and goethite in the presence and absence of catechol and alanine (Figs. 86 to 88). In these experiments, 0.1 M KCl was used to maintain an essentially constant ionic strength. The final pH of the suspensions was adjusted to 6.2 for ferrihydrite and to 6.9 for goethite and hematite. The initial neptunium concentration ranged from 0.2 to 2 µM, and the initial catechol and alanine concentrations were 1 µM. The sorption isotherms of neptunium on iron oxides suggest that catechol and alanine do not significantly affect the sorption of neptunium. The implication of these results is that there is no significant influence of catechol and alanine on neptunium sorption on different iron oxides.

Although both catechol and alanine may complex with neptunium in solution, the organic-metal complexes are apparently not strong enough to affect the neptunium sorption. These results are consistent with the data of Fig. 84 for the iron oxide, goethite, which indicate that DOPA has no effect on neptunium sorption.

In another set of experiments to study the effect of naturally occurring organic material on neptunium sorption, NAFA served as the model fulvic material. The isotherms for the sorp-

tion of neptunium on boehmite in the presence and the absence of NAFA are shown in Fig. 89 and for the sorption of neptunium on goethite in Fig. 90. Similar isotherms for the sorption of neptunium on treated tuff materials are shown in Fig. 91 and for untreated tuff materials in Fig. 92. In these experiments, 0.1 M KCl was used as the background electrolyte, and the final pH was adjusted to 6.2. Initial neptunium concentrations ranged from 0.2 to 3 µM, and the NAFA concentrations ranged from 0.1 to 0.4 ppm.

As shown in Figs. 89 to 92, the fulvic material NAFA had little effect on neptunium sorption in all systems. Thus, we concluded that organics do not affect the sorption of neptunium both in simple, low-molecular-weight organics and in naturally occurring fulvic organic material. The lack of detectable effects of organics on neptunium sorption is possibly attributable to the stable redox state of Np(V) in solution and to low complexation between neptunium ions and organic chemicals.

Plutonium

Sorption as a function of tuff and oxide minerals.

Plutonium sorption on different iron oxides is shown in Fig. 93. On a weight basis, hematite was the most adsorptive, whereas goethite was the least adsorptive. The sorption of plutonium on model iron oxides follows the order hematite > ferrihydrite >

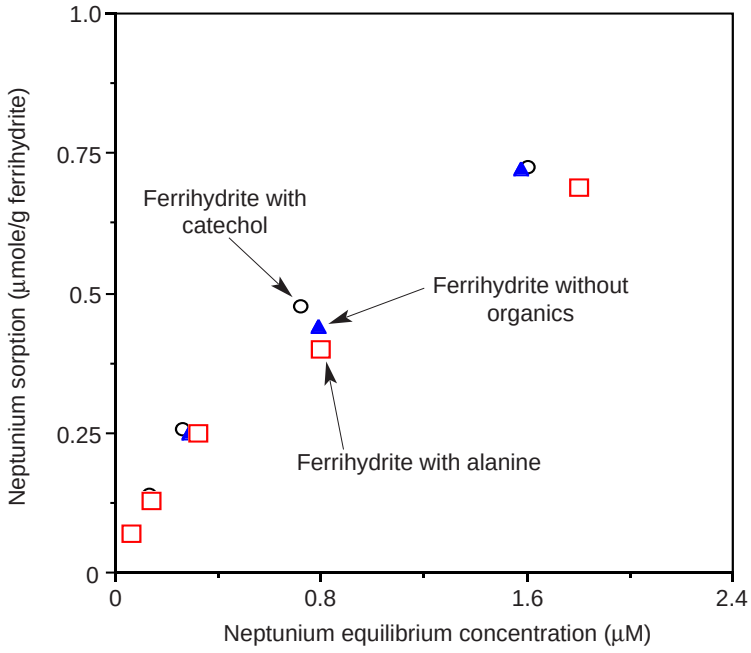

Figure 87. Sorption on Ferrihydrite with or without Organics. The plot shows isotherms for sorption of neptunium on ferrihydrite in the presence and absence of catechol or alanine (1 µM) at pH 6.2.

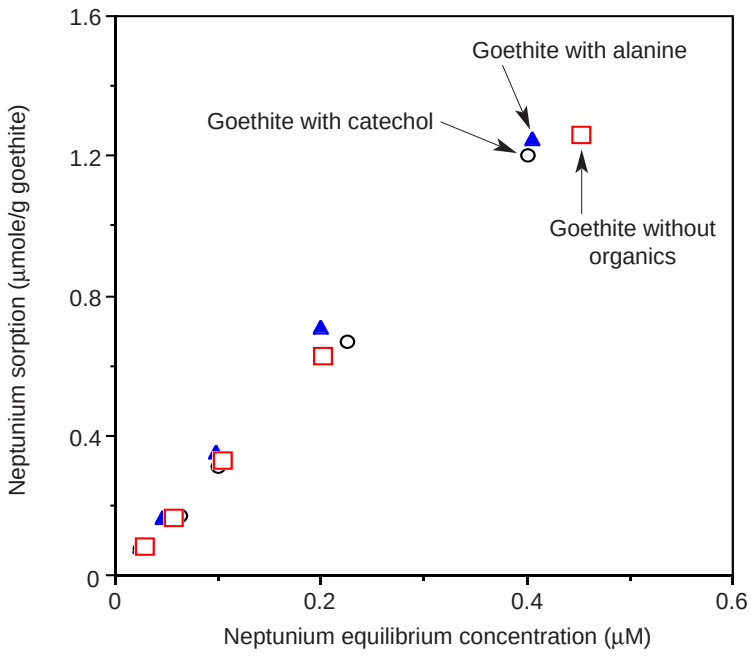

Figure 88. Sorption on Goethite with or without Organics. This plot shows isotherms for the sorption of neptunium on goethite in the presence and absence of catechol or alanine (1 µM) at a pH of 6.9.

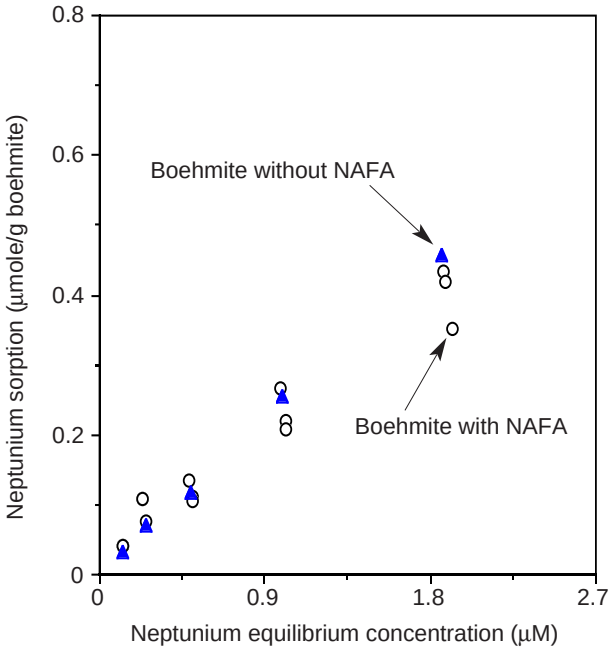

Figure 89. Boehmite with or without NAFA. This plot shows isotherms for the sorption of neptunium on boehmite with and without NAFA.

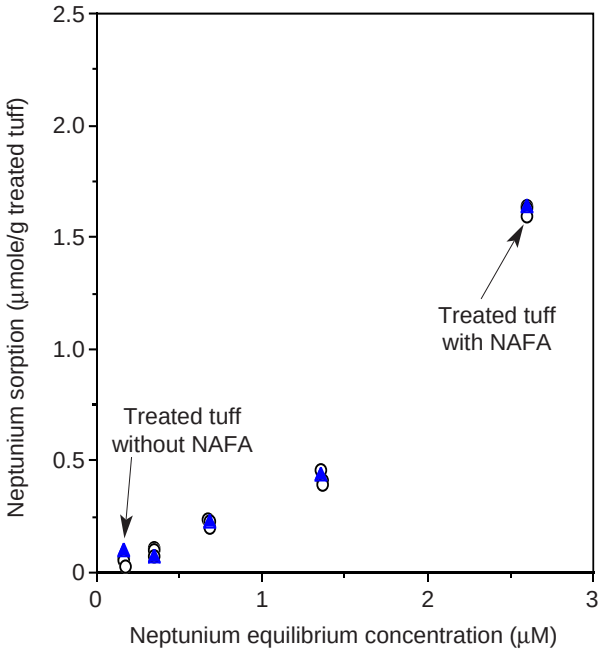

Figure 91. Treated tuff with or without NAFA. This plot shows isotherms for neptunium sorption on treated tuff (G4-270) with and without NAFA.

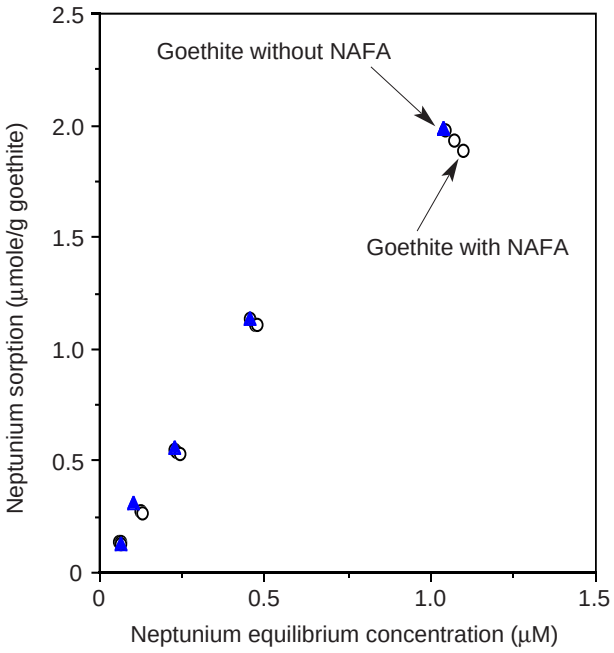

Figure 90. Goethite with or without NAFA. This plot shows isotherms for the sorption of neptunium on goethite with and without NAFA.

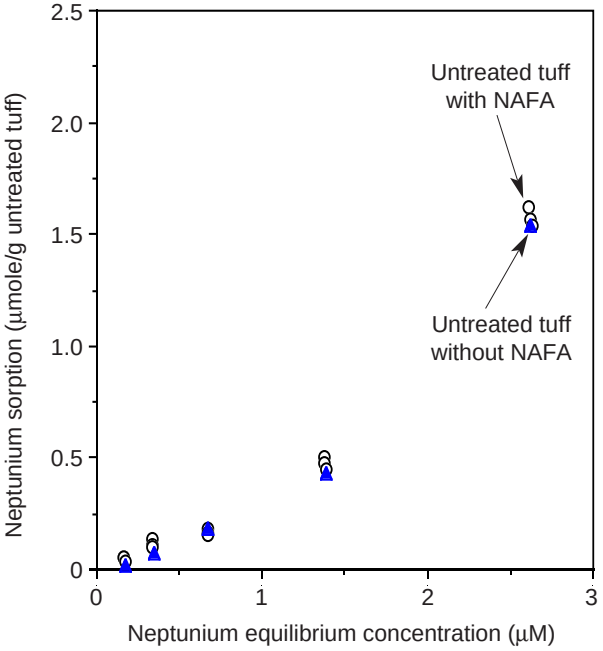

Figure 92. Untreated tuff with or without NAFA. This plot shows isotherms of neptunium sorption on untreated tuff (G4-270) with and without NAFA.

goethite. Thus, for both neptunium and plutonium, hematite is the most adsorptive, but goethite and ferrihydrite reverse order.

As was the case for neptunium, two things should be noted in this result for plutonium. First, the surface area of these iron oxides were not the same. For ferrihydrite and goethite, the surface areas are around 90 m^2/g; for hematite, the surface area is about 40 m^2/g. Second, the sorption experiments were not conducted at the same pH. The sorption on ferrihydrite was conducted at a pH of 6.1; the sorptions on hematite and goethite were conducted at a pH of 6.9.

The effect of oxide surface areas on plutonium sorption was replotted in Fig. 94, with the amount of plutonium sorption normalized to unit surface area (m^2). Results again showed that the sorption of plutonium on model iron oxides follows the order hematite > ferrihydrite > goethite.

Effect of pH on sorption. The isotherms for plutonium sorption on goethite at two different pH levels are shown in Fig. 95. Increasing the solution pH from 6.6 to 6.9 resulted in a higher plutonium sorptivity. It should be noted that the initial plutonium concentration was the same for both isotherms; however, the amount of goethite was different. The linear sorption curves suggest a low degree of coverage of the surface reactive

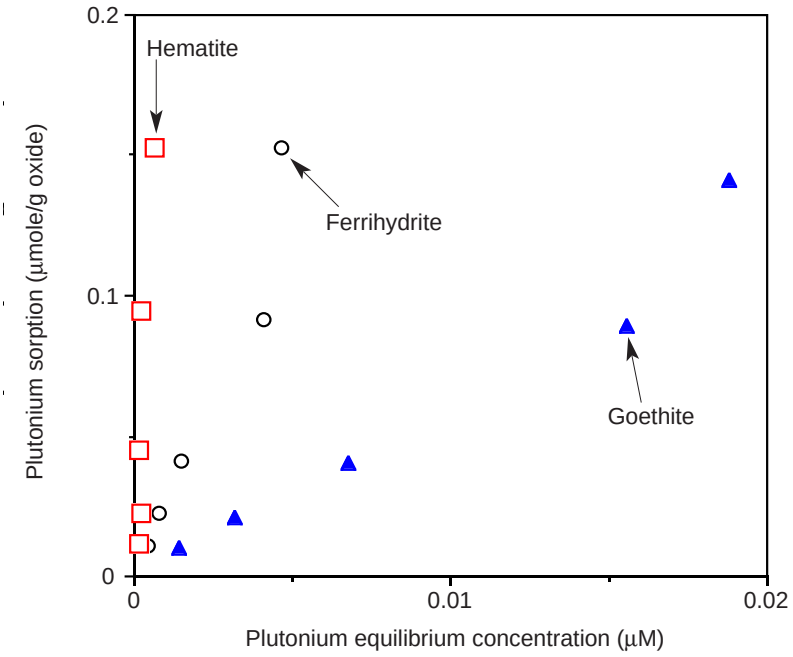

Figure 93. Plutonium Sorption per Unit Mass on Iron Oxides. This plot shows isotherms for the sorption of plutonium on three iron oxides, calculated on the basis of unit mass.

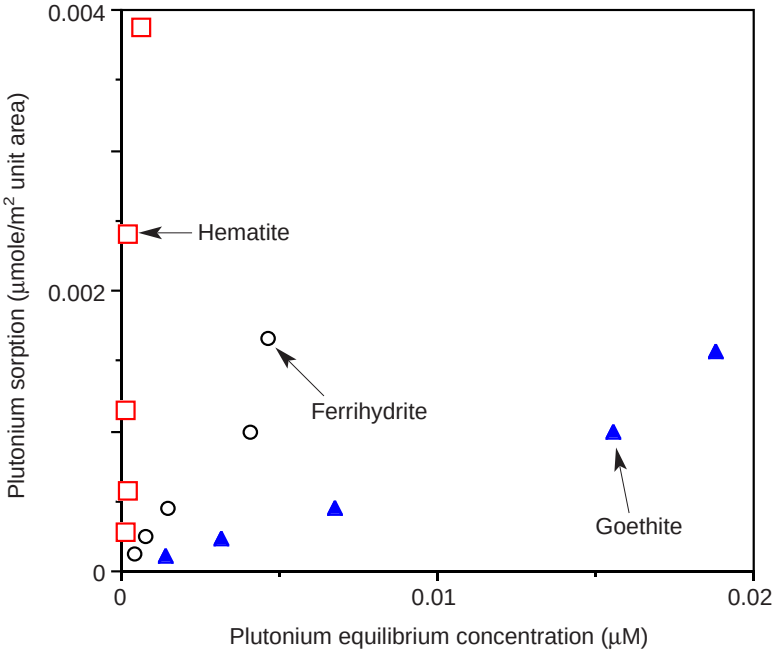

Figure 94. Plutonium Sorption per Unit Area on Iron Oxides. This plot shows isotherms for the sorption of plutonium on three different iron oxides, calculated on the basis of unit surface area.

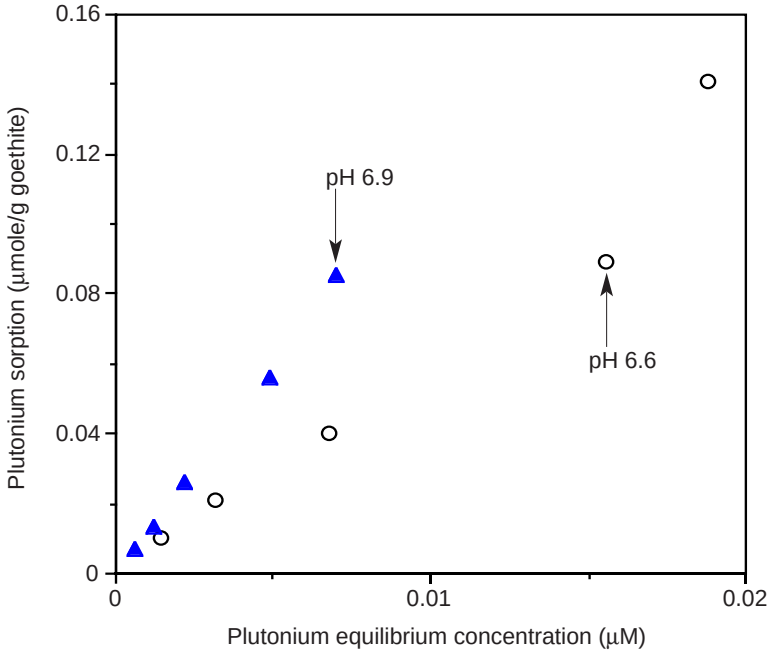

Figure 95. pH Dependence of Plutonium Sorption on Goethite. This plot shows isotherms for the sorption of plutonium on goethite at two different values of pH.

sites by plutonium ions in the presence of excess potassium chloride. This finding is consistent with the theoretical calculation of coverage, which suggests, based on BET surface areas, that the amount of plutonium sorption is much less than a monolayer.

Increasing the solution pH resulted in a higher plutonium sorptivity. Under neutral conditions (a pH of 7), goethite is expected to have positive surface charges. However, the sorption of plutonium on goethite was found to increase as solution pH increased. The sorption of plutonium is apparently not dependent on ion exchange because iron oxide should have no cation-exchange capacity. The sorption is believed to be controlled by a surface-complexation process because plutonium is expected to be dominated by the cationic species PuO_2^+ under neutral and slightly acidic conditions.

Effect of model organics on sorptive behavior. The isotherms for plutonium sorption on ferrihydrite in the presence of catechol and alanine are shown in Fig. 96, and the isotherms for plutonium sorption on goethite and hematite in the presence of catechol and alanine are shown in Fig. 97. The isotherms clearly demonstrate that the sorption of plutonium onto goethite and ferrihydrite was affected by the presence of the organic materials.

The amount of plutonium sorption on goethite and ferrihydrite was lower in systems that contained alanine than in systems that contained no alanine. Apparently, the presence of alanine suppressed the plutonium sorption on the surface of these iron oxides, probably because of a lowering of the free plutonium-ion activity in solution by the formation of an alanine-plutonium complex.

Conversely, the amount of plutonium sorption on goethite and ferrihydrite was higher in the presence of catechol than it was in the absence of catechol. Evidently, catechol enhanced the sorption.

However, the effect of catechol and alanine on plutonium sorption was not found in the hematite system. The presence of these organic materials had little effect on the sorption of plutonium on hematite (Fig. 97). The lack of an observable effect in this case is probably a result of the intrinsically high sorptivity of plutonium on hematite. Any small enhancement or suppression of sorption that might be attributed to catechol and alanine under such a high sorptivity would not be detected.

Overall, the results of our study suggest that the model organic materials catechol and alanine do affect the sorption of plutonium on iron oxides.

The isotherms for sorption of plutonium on ferrihy-

drite and goethite in the absence of DOPA and in its presence at three concentration levels (1, 0.1, and 0.01 µM) clearly demonstrate (Figs. 98 and 99) that such sorption was affected by the presence of the organic material DOPA. Plutonium sorption was higher in systems that contained DOPA than in systems that contained no DOPA. Furthermore, sorptivity increased as the initial DOPA concentration increased from 0.01 to 1 µM. Evidently, the presence of DOPA enhanced the sorption of plutonium on goethite and ferrihydrite. This result is likely attributable to the formation of stable surface DOPA-plutonium ternary complexes and to a redox reaction between DOPA and plutonium. Reduction of Pu(V) to lower oxidation states will enhance the sorption/precipitation of the plutonium.

For neptunium, however, the effect of DOPA on sorption was not found in goethite (Fig. 84), boehmite (Fig. 85), and tuff material (Fig. 82). The presence of DOPA had little effect. It is possible that DOPA does not complex with neptunium in solution or that DOPA cannot reduce Np(V) to lower oxidation states. Such relatively weak complexation is possibly a result of the relatively low effective charge on the cation (Choppin and Rao 1984), consistent with the fact that neptunium complexed weakly with a natural humic material extracted from a groundwater (Kim and Sekine 1991).

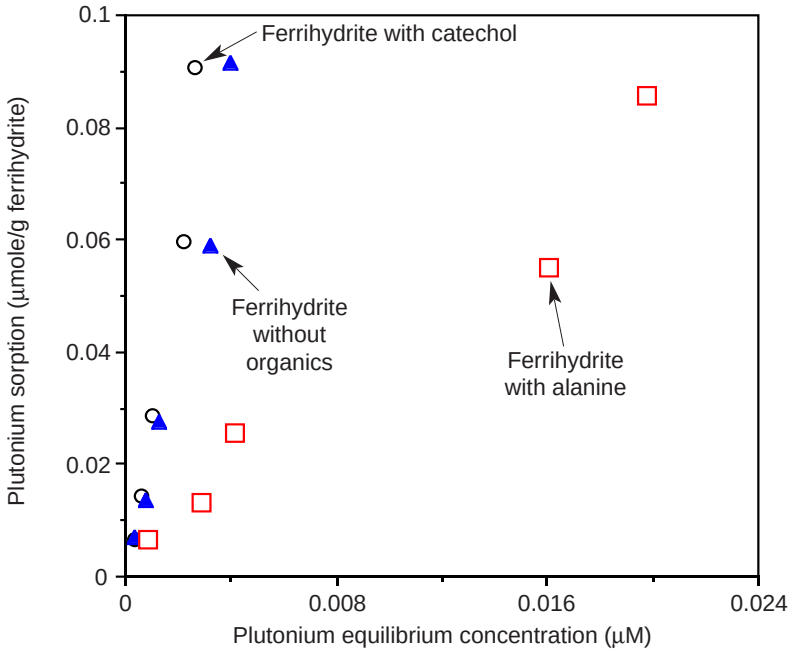

Figure 96. Sorption on Ferrihydrite with and without Organics. This plot shows isotherms for plutonium sorption on ferrihydrite with and without catechol or alanine (1 µM) at a pH of 6.2 in 0.1 M KCl.

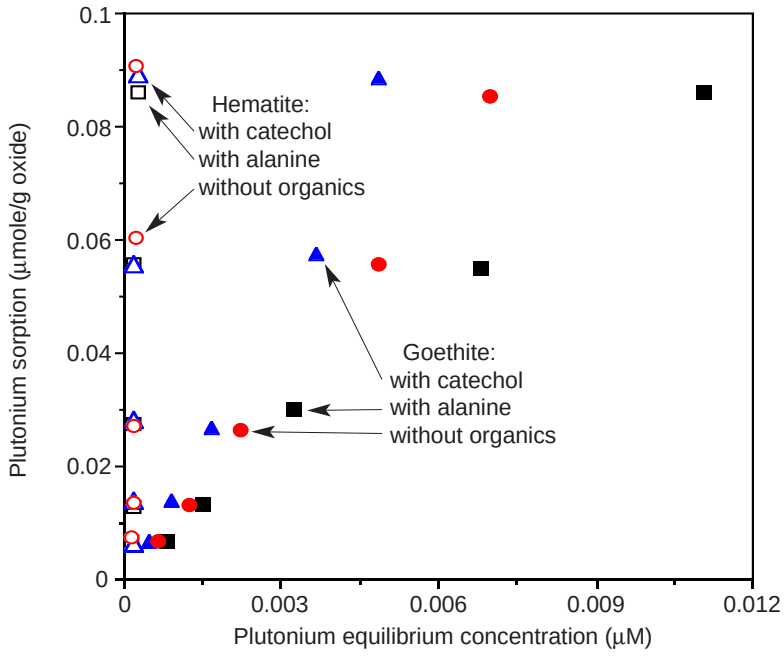

Figure 97. Sorption with and without Organics. This plot shows isotherms for the sorption of plutonium on hematite and goethite with and without catechol or alanine at a pH of 6.9 in 0.1 M KCl.

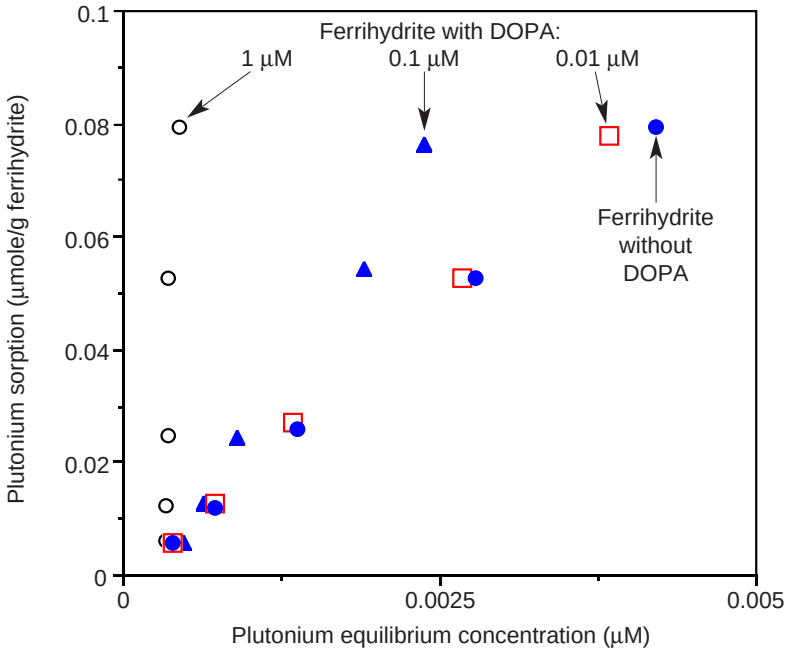

Figure 98. Sorption on Ferrihydrite with and without DOPA. This plot shows isotherms for the sorption of plutonium on ferrihydrite with and without DOPA at a pH of 6.2 in 0.1 M KCl.

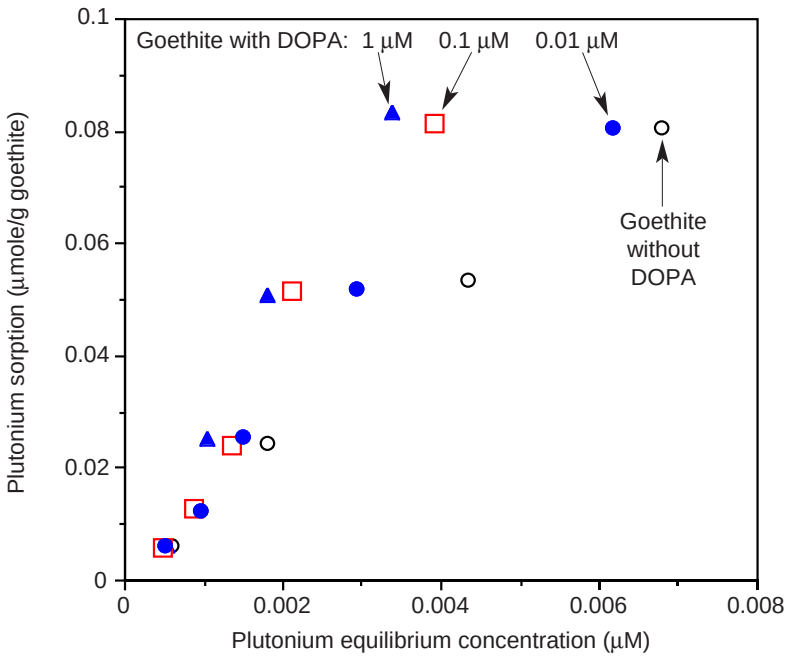

Figure 99. Sorption on Goethite with and without DOPA. This plot shows isotherms for the sorption of plutonium on goethite with and without DOPA at a pH of 6.9 in 0.1 M KCl.

Summary

From the sorption data, the following conclusions can be drawn concerning the effect of natural organic materials on the sorption of neptunium and plutonium by iron and aluminum oxides and by crushed-tuff material:

- The sorption of model organic material DOPA on oxide surfaces follows the order aluminum oxide > iron oxide. For a given sorbent, the higher the pH, the more DOPA is sorbed. Surface complexation is the most likely sorption mechanism.
- The sorption of plutonium on iron oxides generally follows the order hematite > ferrihydrite > goethite. The sorption of neptunium on iron oxide is higher than that on aluminum oxide. The sorption of neptunium on crushed-tuff material was much lower than that on oxide surfaces.
- The sorption of plutonium and neptunium on iron oxides increases as the solution pH is raised. The sorption of plutonium on hematite, goethite, and ferrihydrite is much higher than that of neptunium.
- The amount of neptunium sorption was not affected by any of the organic materials that were studied. The presence of the model organic materials of alanine, catechol,

DOPA, and NAFA did not influence the sorption of neptunium on tuff or on iron and aluminum oxides. This lack of an observable effect is presumably a result of the weak complexation between neptunium and the model organics.

- The sorption of plutonium was influenced by the presence of DOPA on goethite and ferrihydrite. Increasing the amount of DOPA resulted in higher sorption of plutonium on goethite and ferrihydrite. Alanine decreases the sorption of plutonium. However, in the system containing catechol, plutonium sorption was increased. The enhancement of plutonium sorption in the presence of catechol is probably due to the reduction of Pu(V) to Pu(IV) by the organic. The inhibition of plutonium sorption in the presence of alanine is probably caused by the lowering of the free plutonium-ion activity in solution by formation of an alanine-plutonium complex. No observable effect of organics on plutonium sorption was found in the hematite system, which is probably due to a relatively high sorptivity of plutonium on the hematite surface.

C. MODELS THAT CAN EXPLAIN THE SORPTION DATA

Radionuclides are known to be adsorbed by mineral surfaces in rocks and soils. The strongest interactions between aqueous species and mineral surfaces are the formation of electrostatic and covalent bonds. Ion exchange reactions are primarily electrostatic interactions (outer electronic sphere and diffuse layer). Inner-sphere surface complexes form a chemical bond (to the mineral surface) that is more covalent. The electrostatic interaction does not have the same degree of selectivity between aqueous ions of like charge as does the more covalent inner-sphere surface complex. Stable inner-sphere complexes can be formed even when the mineral surface charge is the same as the aqueous ion. On the other hand, the adsorption of metal ions via cation exchange will only occur on surfaces of opposite charge and is affected by such common components of groundwater as sodium. Both of these processes can, in principle, be modeled using a triple-layer surface-complexation model. There are significant differences between the cation exchange in zeolites and clays and the formation of outer-sphere complexes on metal oxides. For this reason, cation exchange and surface complexation will be treated separately.

Cation Exchange

Description of the process

The cation exchange capacity of aluminosilicates is often high. Zeolites, such as clinoptilolite and mordenite, and clays, such as montmorillonite, have enormous surface areas because of their channeled and layered structures, respectively. The surfaces are negatively charged because they are composed of tetrahedrally bound silica and alumina. Aluminum requires an additional electron in order to share electrons equally between four oxygen atoms in a tetrahedral structure. The excess negative charge is balanced by an alkali-metal or alkaline-earth cation. These cations can be exchanged for cationic radionuclides. The extent to which a radionuclide is adsorbed depends on the selectivity for that cation. The equilibrium reaction can be represented, for example, as follows:

$$t\text{-AlO}^{-}\text{Na}^{+} + \text{Cs}^{+} \leftrightarrow t\text{-AlO}^{-}\text{Cs}^{+} + \text{Na}^{+}, \quad (59)$$

where t-AlO^{-} represents a tetrahedrally bound aluminum site. The equilibrium expression for this reaction is

$$K = \frac{[\text{AlO}^{-}\text{Cs}^{+}][\text{Na}^{+}]}{[\text{AlO}^{-}\text{Na}^{+}][\text{Cs}^{+}]} \quad , \quad (60)$$

where K is the selectivity coefficient. For a mineral with one type of cation exchange and a binary aqueous salt, this expression can be rewritten in terms of the solid-phase concentration, q, of one of the cations of interest (here, cesium). The result is

$$q = \frac{KQc}{(K-1)c + c_o} \quad , \quad (61)$$

where, in this case, $q = [\text{AlO}^{-}\text{Cs}^{+}]$, c is the solution-phase concentration of the cation, $[\text{Cs}^{+}]$, c_o is the total solution-phase cation concentration ($[\text{Cs}^{+}] + [\text{Na}^{+}]$), and Q is the cation exchange capacity of the solid phase ($[\text{AlO}^{-}\text{Cs}^{+}] + [\text{AlO}^{-}\text{Na}^{+}]$). Equation 61 is nearly identical to the Langmuir isotherm (derived for the adsorption of gases on solids) and will be referred to as such in the remainder of this report.

Factors affecting cation exchange

There are many factors affecting cation exchange in natural systems, such as competition between multiple cation exchange sites, selectivity between cations in groundwater and the radionuclide of interest, and aqueous speciation of the radionuclide, to name a few. Competition between multiple cation exchange sites leads to nonlinear adsorption isotherms. The selectivity between cations depends on the geometry of the cation exchange site and the relative degree of hydration of the aqueous cations. In clays and zeolites, the selectivity coefficient increases from more- to less-hydrated cations, so that the order for alkali metal cations is lithium $<$ sodium $<$ potassium $<$ rubidium $<$ cesium (see McBride 1994, for example). Aqueous speciation can change the charge and the net size of the ions. In addition, there are sites in minerals,

such as analcime, that can exclude larger ions, like cesium, entirely.

In principle, an equilibrium code, such as EQ3/EQ6 (Wolery 1983), could predict cation exchange if selectivity coefficients for all the significant cationic constituents of groundwater were known for each cation exchange site in each mineral contained in tuff. In practice, few selectivity coefficients are known for single minerals, let alone individual exchange sites.

Experimental methods

The most useful experiment for determining sorption thermodynamic data is the adsorption isotherm. The adsorption isotherm is a measurement of the solid-phase concentration versus the aqueous-phase concentration at constant temperature. If the behavior of the isotherm is ideal, it can be described by a Langmuir isotherm (Eqn. 61), which can be the case only if there is one type of cation exchange site and if outer-sphere surface complexation is not significant.

Pure cation exchange cannot be measured in a system also capable of surface complexation, whether that system is a whole rock or a clay mineral. By varying the pH and electrolyte concentration, either surface complexation or cation exchange can be enhanced, which allows information about both mechanisms to be extracted from the data. The Swiss nuclear waste program has made great progress in developing such methods (Baeyens and Bradbury 1995a, 1995b; Bradbury and Baeyens 1995).

Ion-exchange models

One approach that allows the determination of the free energy of exchange in even nonideal systems is that of Gaines and Thomas (1953). This approach requires that the adsorption isotherm be taken from one end member (for example, sodium saturated) to the other end member. In this case, the free energy of exchange, ΔG^o, is related to the definite integral over the mole ratio of cations from one end member to the other as follows:

$$\Delta G^o = -\frac{RT}{Z_1 Z_2}\left[(Z_2 - Z_1) + \int_0^1 \ln K \, dA\right] , \quad (62)$$

where Z_1 and Z_2 are the charges on the original and incoming cations, respectively, A is the mole ratio of the incoming cation, R is the gas constant, and T is absolute temperature. This approach cannot, in general, be used to calculate distribution coefficients because it cannot describe nonideal solid solutions.

Ion exchange arises from two distinctly different chemical structures on the surfaces of minerals. One is the incorporation of aluminum (with a valence of 3) in a tetrahedrally bonded silicate structure. The other is the amphoteric reaction of metal oxides with acids and bases. The former is a negatively charged surface of a fixed nature with the charge compensated by cations. The latter can be either negatively or positively charged depending on the pH of the aqueous phase. The exchange capacity of the former structure is fixed, whereas the exchange capacity of the latter depends on pH, ionic strength, and the concentration of specific inner-sphere complexing ligands. The adsorption of exchangeable ions on an activated metal-oxide surface is a form of outer-sphere surface complexation.

The selectivity in aluminosilicates for a given radionuclide over another has been shown to be not a simple binary exchange process, even when the solution is a simple binary aqueous solution, because not all positions in aluminosilicate are equivalent with respect to crystallographic structure. For example, there can be differences due to steric crowding. These differences have been studied by deconvolving the ion-exchange isotherm.

The method of deconvolution has been shown to be effective in studying structural effects on ion selectivities in synthetic zeolites (Triay and Rundberg 1989a). In that study, the shape of the ion-exchange isotherm was shown to be due to differences in the crystallographic structure at the ion exchange sites. This interpretation could not be made on the basis of the deconvolution of adsorption isotherms without spectroscopic data. How-

ever, the method of deconvolution does allow a quantitative correlation of the ion-exchange data with the spectroscopic data.

The method of analysis assumes ion exchange. The thermodynamics of ion exchange have been reviewed by Cremers (1977). The selectivity coefficient K for the hypothetical ion-exchange process in the reaction

$$\mathrm{AlO–M_1} + \mathrm{M_2^+} \leftrightarrow \mathrm{M_1^+} + \mathrm{AlO–M_2} \quad (63)$$

is given by

$$K = \frac{q_2 a_1}{q_1 a_2} \ , \quad (64)$$

where a_1 and a_2 are the activities in solution of the cation to be exchanged and the entering cation, respectively, and q_1 and q_2 are the corresponding concentrations of these cations in the solid phase expressed as moles of cation per gram of the exchanger.

As a result of mass-balance considerations, Eqn. 64 can be rewritten as

$$q_2 = \frac{KQ\gamma_2 C_2}{C_o\gamma_1 + (K\gamma_2 - \gamma_1)C_2} \ , \quad (65)$$

where Q is the total moles of exchangeable sites per gram of exchanger ($Q = q_1 + q_2$), C_2 is the concentration of the entering cation in the liquid phase, C_o is the total concentration of cations in the liquid phase ($C_1 + C_2$), and γ_1 and γ_2 are the activity coefficients in the solution phase of the cation to be exchanged and the entering cation, respectively (that is, $a_1 = \gamma_1 C_1$ and $a_2 = \gamma_2 C_2$).

Equation 65 represents the dependence of the solid-phase concentration on the liquid-phase concentration. It has the mathematical form of the Langmuir isotherm. In general, adsorption isotherms do not follow the Langmuir isotherm. Many authors have successfully described cation exchange in terms of multiple sites (Barrer and Klinowksi 1972; Barrer and Munday 1971; Brouwer et al. 1983). The underlying assumption of the deconvolution method is that the nonideality of the adsorption isotherm is due to adsorption at multiple sites. Consequently, one may consider a set of simultaneous equilibria

$$\begin{aligned} \mathrm{A^1–M_1} + \mathrm{M_2^+} &\leftrightarrow \mathrm{A^1–M_2} + \mathrm{M_1^+} \\ \mathrm{A^2–M_1} + \mathrm{M_2^+} &\leftrightarrow \mathrm{A^2–M_2} + \mathrm{M_1^+} \\ &\vdots \\ \mathrm{A^n–M_1} + \mathrm{M_2^+} &\leftrightarrow \mathrm{A^n–M_2} + \mathrm{M_1^+} \ , \end{aligned} \quad (66)$$

where $\mathrm{A^1}, \mathrm{A^2}, \ldots, \mathrm{A^n}$ represent different sites in the ion exchanger.

The solid-phase concentration of the cation $\mathrm{M_2^+}$ in site i is given by

$$q_2^i = \frac{K^i Q^i \gamma_2 C_2}{C_o\gamma_1 + (K^i\gamma_2 - \gamma_1)C_2} \ , \quad (67)$$

and the total solid-phase concentration of $\mathrm{M_2^+}$ is given by the sum

$$q_2 = \sum_{i=1}^{n} q_2^{\,i} = \sum_{i=1}^{n} \frac{K^i Q^i \gamma_2 C_2}{C_o\gamma_1 + (K^i\gamma_2 - \gamma_1)C_2} \ . \quad (68)$$

This approach is further generalized by replacing the sum in Eqn. 68 with the integral equation

$$q_2(C_2) = \int q_2(C_2,K)\, f(K)\, \mathrm{d}K \ , \quad (69)$$

where $f(K)$ is a distribution function for the selectivity coefficient of the exchange.

The idea of expressing the heterogeneity of the exchanger in terms of a distribution function has been previously presented (Brouwer et al. 1983; Adamson 1982; Sposito 1979, 1980, 1984; Kinniburgh et al. 1983). Equation 69 is a Fredholm integral of the First Kind, and the methodology used here to solve for $f(K)$ has been described by the authors (Triay and Rundberg 1987, 1989b) and others (Butler et al. 1981; Britten et al. 1983). The computer code INVPOS has been written (Travis 1996) to solve Eqn. 69. INVPOS uses the method of Butler, Reeds, and Dawson (1981) to find an optimal solution using regularization with a positivity constraint.

Semiempirical adsorption isotherms, such as the Freundlich isotherm, are derived by evaluating the

integral (Eqn. 69) using closed-form approximations and assuming some arbitrary site energy distribution. These approaches are only valid for data interpolation because they do not provide insight into the actual mechanism of adsorption.

Description of cation exchange sites in Yucca Mountain tuff

Detailed adsorption isotherms adequate for the analysis described above have not been done for the Yucca Mountain Project. Measurements of the mineralogy of Yucca Mountain tuff have shown an abundance of minerals known to have both pH-independent cation exchange sites (that is, tetrahedral aluminum sites) and surface complexation sites (for example, clay edge sites) for outer-sphere surface-complex formation. The most abundant minerals found in Yucca Mountain tuff (Bish et al. 1983; Daniels et al. 1982) with a high cation exchange capacity are listed in Table 53.

In addition to the minerals listed in that table, feldspars may be important cation exchangers in the devitrified tuffs. Cation exchange capacity for a feldspar is not an intrinsic property because only the external surfaces are available for exchange. Thus, the number of sites depends on the crystal size and morphology.

State of knowledge of cation exchange with respect to Yucca Mountain tuff

As early as 1983 (Daniels et al. 1982), it was shown that the sorption distribution coefficient, K_d, for the adsorption of cesium onto Yucca Mountain tuff could be predicted to within a factor of three using literature data for the cation exchange on the minerals in Table 53 with the addition of analcime. These predictions only considered competition with sodium. This simplification was made because there were no data for the cation exchange of the other alkali metals and alkaline earths present in J-13 well water. Some of the observed scatter could possibly be reduced with these additional data. Unfortunately, over the years since then, the situation has not changed. Thus, there is no predictive model based on mineralogy for cation exchange for radionuclides other than cesium.

We determined the relative contribution of cation exchange to the adsorption of neptunyl onto the zeolitic tuff sample G4-1506 from a sodium-bicarbonate solution. The experiment was based partly on the method of Baeyens and Bradbury. Crushed tuff G4-1506 was equilibrated with 1 M sodium perchlorate to remove alkali metals and alkaline earths by mass action. Solutions containing 0.0022 M sodium bicarbonate (as a pH buffer) were prepared with sodium perchlorate added to provide sodium concentrations that varied from 0.0022 M to 0.22 M. Distribution coefficients for neptunium were determined using the standard procedure (Fig. 100).

The surface complexation of neptunyl has been shown to be inner sphere and noncharging. Therefore, the surface complexation of neptunium is expected to be largely independent of sodium-ion concentration. The results show a linear decrease in K_d with sodium concentration at low sodium concentrations that is consistent with cation exchange (see Eqn. 64). At high sodium concentrations, the K_d asymptotically approaches 2.5 ml/g, consistent with surface complexation. The ion-exchange component is larger than the surface-complexation component, which corresponds to a K_d of about 10 in 0.0022 M sodium bicarbonate. The relatively low K_d for neptunyl in a zeolitic tuff is likely due to the large ion size and high hydration number. The K_d in pure sodium-bicarbonate solution is larger than

Table 53. Minerals in Yucca Mountain Tuff with High Cation Exchange Capacities

Mineral	Maximum abundance	Capacity (meq/g)
Clinoptilolite	90%	2.3
Mordenite	60%	2.3
Montmorillonite	40%	0.8–1.5
Illite	20%	0.13–0.42

that observed in J-13 water; this effect is due to competition with the additional cations in J-13 water of calcium, magnesium, and potassium. A model that describes these data and predicts neptunium sorption in the zeolitic tuff of Calico Hills will be described in the next section.

Surface Complexation

Description of surface-complexation process

The model that we will use to interpret the results of our experiments is the triple-layer surface-complexation model (Davis et al. 1978). The most important difference between this model and conventional chemical equilibria is the effect of surface charge on the activity of ions in the triple layer. This effect is calculated by multiplying the bulk-solution concentration, $[M^+]_{bulk}$, by a Boltzmann factor

$$[M^+] = [M^+]_{bulk}\, e^{-\left(\frac{e\psi_0}{kT}\right)} , \qquad (70)$$

where k is the boltzmann constant, T is the absolute temperature, e is electronic charge, and ψ_o is the potential of the ion in the inner Helmholtz layer.

The charge on the metal-oxide surface is produced by the amphoteric reaction of the metal-oxide surface with acids and bases. The basic charge-producing reactions are with Brönsted acids and bases:

$$MOH_2^+ + H_2O \leftrightarrow MOH + H_3O^+ \text{ and} \qquad (71)$$

$$MOH + H_2O \leftrightarrow MO^- + H_3O^+ , \qquad (72)$$

for which the equilibrium constants are

$$K_{a_1}^{int} = \frac{[MOH][H_3O^+]}{[MOH_2^+]}\, e^{-\left(\frac{e\psi_0}{kT}\right)} \text{ and} \qquad (73)$$

$$K_{a_2}^{int} = \frac{[MO^-][H_3O^+]}{[MOH]}\, e^{-\left(\frac{e\psi_0}{kT}\right)} . \qquad (74)$$

Cations and anions can interact with the electric field near the metal-oxide surface by forming outer-sphere complexes. Ions can also be repelled from the aqueous phase near the metal-oxide surface, as illustrated by Eqn. 59, which can lead to what appears to be a negative sorption distribution coefficient. This phenomenon is a result of the

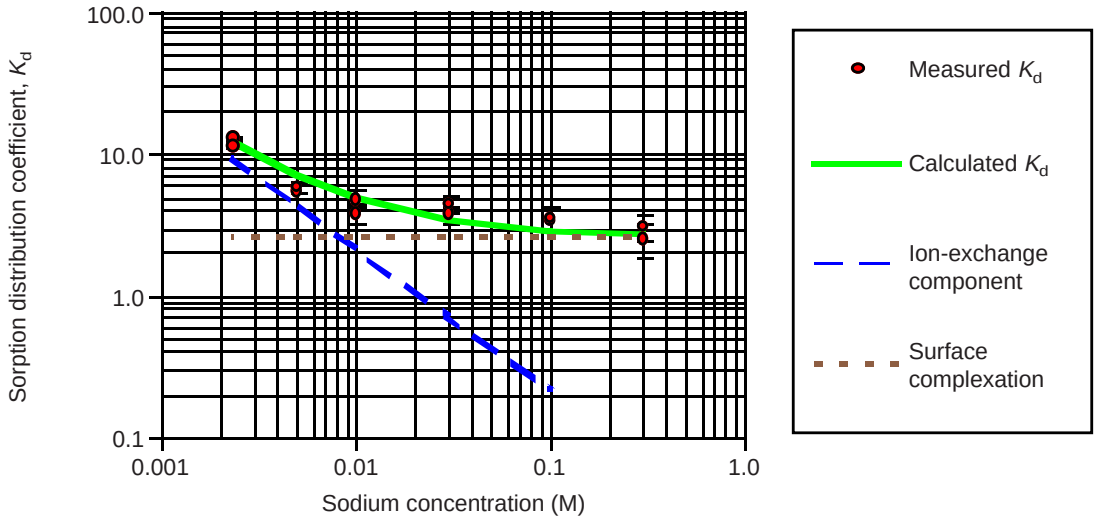

Figure 100. Modeling of Neptunium Sorption. The plot shows data points for the sorption distribution coefficient of neptunium on the zeolitic tuff sample G4-1506 at a pH of 8.4 as a function of sodium-ion concentration. Surface complexation should not vary with sodium concentration, so the horizontal dashed asymptote at high concentrations is a measure of surface complexation and the dashed linear slope at low concentrations is a measure of the ion-exchange component of the sorption.

increase in tracer concentration in the bulk solution due to repulsion of ions from the solution within the double layer. This effect is always small, $K_d > -1$ ml/g. The strict definition of K_d does not allow for negative values because that would imply a negative concentration (which is meaningless). The negative K_d arises because, experimentally, it is impossible to separate the solid phase without including the thin layer of water close to its surface.

Negative K_d values can be used in the same way as positive K_d values and lead to the correct prediction of more rapid migration of excluded tracer with respect to tritiated water, that is, retardation factors less than 1. This phenomenon has been used by van den Hul and Lykelma (1968) to measure the specific surface area of suspended materials. Outer-sphere surface complexation can account for this phenomenon and is represented by the following equations:

$$MOH_2^+ + An^- \leftrightarrow MOH_2^+An^- \text{ and} \quad (75)$$

$$MO^- + Cat^+ \leftrightarrow MO^-Cat^+ , \quad (76)$$

where An^- is the anion and Cat^+ is the cation. The equilibrium constants corresponding to these equations are

$$K_{an}^{int} = \frac{[MOH_2^+An^-]}{[MOH_2^+][An^-]} e^{-\left(\frac{e\psi_\beta}{kT}\right)} \text{ and} \quad (77)$$

$$K_{cat}^{int} = \frac{[MO^-Cat^+]}{[MO^-][Cat^+]} e^{\left(\frac{e\psi_\beta}{kT}\right)} , \quad (78)$$

where ψ_β is the potential of the ion in the outer Helmholtz layer. The ions adsorbed in the outer layer can be exchanged for other ions. The ion-exchange process would be expected to have selectivity differences due to factors such as ion size.

Factors affecting surface complexation

Surface-complexation models are equilibrium models and, therefore, account for speciation reactions explicitly. It is inherently difficult to characterize whole rock, however. This difficulty arises from the very surface nature of the reactions described. The number of available sites depends on the crystal size and morphology. The identity of available sites depends on the availability of mineral surfaces to the pore water and can be changed by weathering. Given these inherent difficulties, we will attempt to develop a simplified model of surface complexation, including cation exchange.

HSAB (hard-soft acid-base) theory

The surface-complexation coefficients for monodentate surface complexes have been shown to be proportional to the first hydrolysis constant of the aqueous metal ion. This relationship is the natural consequence of the Lewis acid-base theory. The Lewis definition of an acid is an electron-pair acceptor and of a base, an electron donor. The hydrolysis of metal ions in aqueous solution proceeds by reacting with a water molecule displacing a hydrogen ion (an Arrhenius acid) yielding a monohydroxide:

$$M^{n+} + H_2O \leftrightarrow MOH^{(n-1)+} + H^+ . \quad (79)$$

This reaction is analogous to the formation of a monodentate surface complex on a metal oxide, for example, alumina:

$$Al_{surf}\text{–}OH + M^{n+} \leftrightarrow Al_{surf}\text{–}OM^{(n-1)+} + H^+. \quad (80)$$

The principal difference between these reactions is that the hydroxide ion is the Lewis base in the aqueous hydrolysis reaction (Eqn. 79) and the surface oxygen is the Lewis base in the surface-complexation reaction (Eqn. 80). The strength of the Lewis acid M^{n+} in both reactions is related to the first hydrolysis constant, K_{11}. The basicity of the surface oxygen is related to the second acid-dissociation constant, K_{a_2}, of the metal oxide. This relationship can be tested by comparing the sum of the logarithms of the surface-complexation constant and the second acid-dissociation constant against the logarithm of the first hydrolysis constant of the metal ion. The log K_a values for the first and second acid-dissociation constants of metal oxides expected to be found in Yucca Mountain tuff are listed in Table 54, along with the point of zero charge (the pH at which surface in equilibrium with that solution has no net charge). The comparison of literature values (Dzombak and Morel

1990; Kinniburgh et al. 1976; Huang and Stumm 1973; Schindler 1985) for surface complexation ($\log K_s + \log K_{a_2}$), of metal ions on alumina, silica, and iron oxide are shown in Fig. 101.

The results of this comparison demonstrate that the surface-complexation constant can be estimated to within an order of magnitude, for most metals, given the first hydrolysis constant. A similar comparison for bidentate attachment has yet to be developed, primarily because of the lack of reliable data for bidentate surface complexes.

Description of surface complexation sites in Yucca Mountain tuff

Although surface complexation has just begun to be studied on Yucca Mountain tuff, there are a number of mineral surfaces having known surface complexation sites. These are hematite and related iron oxides, silica, and the edge sites of clays. The clay edge sites have been studied and found to be most similar to octahedral alumina (Wieland 1988; Stumm 1992). Although there is no supporting data to determine the relative abundance of these sites, the HSAB approach described above allows one to predict the surface-complexation mechanisms in terms both of stoichiometry and of equilibrium constants.

Table 54. Intrinsic Constants for Metal Oxides

Metal oxide	log K_{a_1}	log K_{a_2}	Point of zero charge
SiO_2	−0.5	−8.2	4.3
Al_2O_3	−7.8	−11.3	9.3
FeOOH	−7.6	−11.4	8.5

Modeling of Yucca Mountain tuff

A surface-complexation model for neptunium adsorption onto the zeolitic tuff sample G4-1506 was developed to fit the sodium-concentration

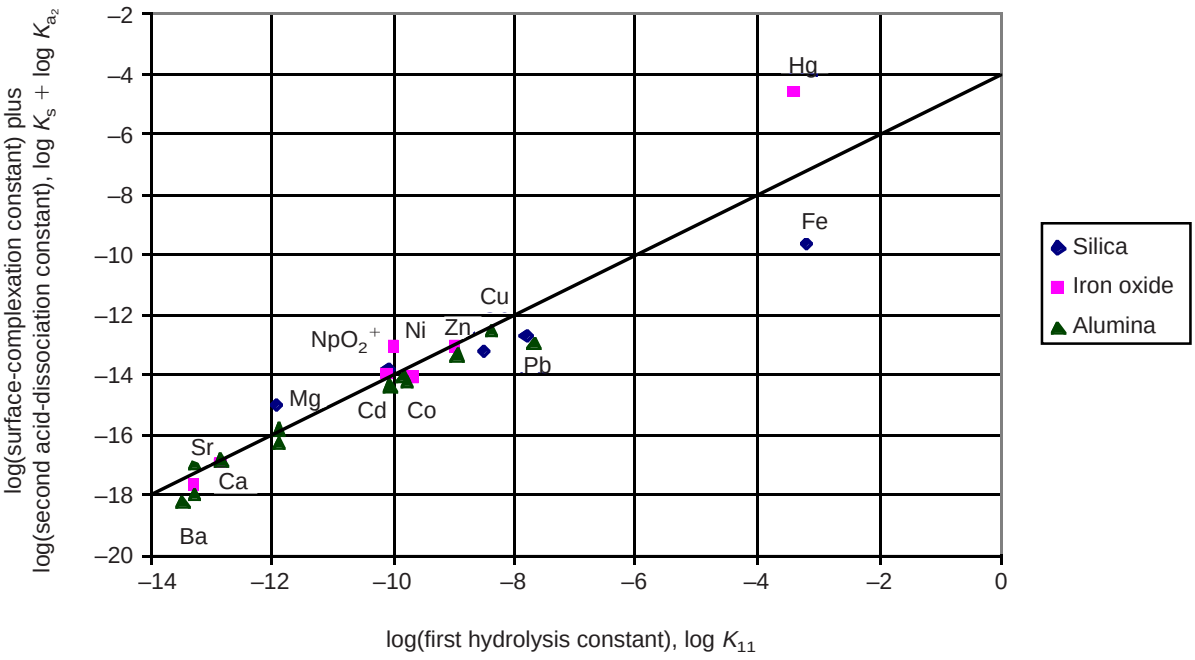

Figure 101. Surface Complexation versus Hydrolysis. This plot compares surface complexation ($\log K_s + \log K_{a_2}$) for monodentate attachment of metal ions with hydrolysis ($\log K_{11}$) based on the HSAB (hard-soft acid-base) theory.

dependence. The model considered a simple ion-exchange mechanism:

$$AlO^{-}Na^{+} + NpO_2^{+} \leftrightarrow AlO^{-}NpO_2^{+} + Na^{+}, \quad (81)$$

and the formation of an inner-sphere surface complex with octahedral alumina (edge sites) or hematite:

$$AlOH + NpO_2^{+} \leftrightarrow AlONpO_2 + H^{+} \quad . \quad (82)$$

The number of cation exchange sites available to neptunium (Table 55) was based on the apparent saturation of sites observed in a neptunium adsorption isotherm measured for tuff sample G4-1608 in a carbon-dioxide atmosphere (Thomas 1987). The neptunium exchange capacity is four orders of magnitude smaller than the cation exchange capacity of clinoptilolite (Table 53). This difference can be explained by the large size of the hydrated neptunyl ion. If no sorption occurs in the intracrystalline channels of the clinoptilolite, the maximum exchange capacity will be on the order of a μmole per gram, assuming a 3-μm crystal diameter. The selectivity for neptunium was used as an adjustable parameter, and the model was fit to the results of the sodium-ion dependence of neptunium adsorption onto tuff sample G4-1506.

The inner-sphere surface complexation of neptunium was modeled assuming that surface complexation occurs primarily on clay edge sites or iron-oxide surfaces. The constant for inner-surface complexation of neptunium onto iron oxide was used because the analogous constant for alumina is expected to be nearly equal on the basis of the HSAB theory shown above. Thus, the second adjustable parameter was the edge-site density.

Table 55. Equations and Parameters Used to Model Neptunium Adsorption onto Zeolitic Tuff

Type of reaction	Equilibrium reactions	log *K*
Aqueous reactions:	$NpO_2^{+} + H_2O \leftrightarrow NpO_2OH(aq) + H^{+}$	−10.8
	$NpO_2^{+} + 2\ H_2O \leftrightarrow NpO_2(OH)_2^{-} + 2\ H^{+}$	−23.5
	$NpO_2^{+} + CO_3^{2-} \leftrightarrow NpO_2CO_3^{-}$	4.13
	$HCO_3^{-} \leftrightarrow CO_3^{2-} + H^{+}$	−10.25
	$CO_2(g) + H_2O \leftrightarrow H_2CO_3 \leftrightarrow HCO_3^{-} + H^{+}$	−7.8
Metal-oxide surface protolysis:	$MOH + H^{+} \leftrightarrow MOH_2^{+}$	7.6
	$MOH_2^{+} + ClO_4^{-} \leftrightarrow MOH_2^{+}ClO_4^{-}$	2.0
	$MOH \leftrightarrow MO^{-} + H^{+}$	−11.4
	$MO^{-} + Na^{+} \leftrightarrow MO^{-}Na^{+}$	1.2
Neptunyl adsorption reactions:	$t\text{-}Al^{-}Na^{+} + NpO_2^{+} \leftrightarrow t\text{-}Al^{-}NpO_2^{+} + Na^{+}$	2.1
	$MOH + NpO_2^{+} \leftrightarrow MONpO_2 + H^{+}$	−2.2
Extension to groundwater:	$2\ t\text{-}Al^{-}Na^{+} + Ca^{2+} \leftrightarrow t\text{-}Al_2^{2-}Ca^{2+} + 2\ Na^{+}$	5.0
	$MOH + Ca^{2+} \leftrightarrow MOCa^{+} + H^{+}$	−5.85
	$MOCa^{+} + Cl^{-} \leftrightarrow MOCa^{+}Cl^{-}$	2.0

Parameters

Type of site	Site density (eq/kg)	Layer	Capacitance (F/m^2)
Tetrahedral(*t*) aluminum	2×10^{-4}	Inner Helmholtz	1.1
Octahedral aluminum (edge)	3×10^{-6}	Outer Helmholtz	0.2

To extend this model to the empirical measurements done under the project's geochemistry program, additional assumptions were made. The competition of cations in groundwater for cation exchange sites was based on the selectivities derived from measurements on the mineral tobermorite (Tsuji and Komarneni 1993). This approach was the result of the argument explaining the reduced cation exchange capacity for neptunium. If exchange occurs only on the exterior of the zeolite crystal, then steric effects must be avoided. Tobermorite offers an open structure that could be expected to have less steric effects than a zeolite. Furthermore, that work showed little difference between magnesium and calcium so that both magnesium and calcium were treated as one competitor. There were no data for potassium, so competition with potassium was not considered.

Table 56. Groundwater Compositions Used for Neptunium Sorption Modeling

Constituent	Concentration (mg/l)		
	J-13 water	UZ water	UE-25 p#1 water
Sodium	45	26–70	171
Potassium	5.3	5–16	13.4
Magnesium	1.8	5–21	31.9
Calcium	11.5	27–127	87.8
Silicon	30	72–100	30
Fluoride	2.1	–	3.5
Chloride	6.4	34–106	37
Sulfate	18.1	39–174	129
Bicarbonate	143	–	698
pH	6.9	6.5–7.5	6.7

The surface-complexation constant for calcium was taken from the HSAB theory. Thus, there were no additional adjustable constants. The concentrations used for J-13 and UE-25 p#1 well water are shown in Table 56. The calculations were made using the FITEQL equilibrium code in the forward mode only, that is, no fitting. The results of the modeling are shown in Figs. 102 and 103. The agreement between the model calculations and the measured results were in general excellent. The correct pH dependence was predicted for the dry-sieved samples; the wet-sieved samples agreed better with a calculation that had no surface complexation sites. The implications of these results are not yet fully understood. Two possibilities are that either the clay particles are washed out, reducing the available edge sites, or that a trace component of J-13 water is forming a strong surface complex that competes with neptunium. The model also predicted the observed reduction in the sorption distribution coefficient, K_d, due to the components of UE-25 p#1 water. In this water, the higher carbonate concentration eliminates the contribution of surface complexation observed in J-13 water at pH values above 7.

A model was also developed for pH dependence of uranium adsorption onto crushed devitrified tuff. This treatment was similar to that used to model neptunium adsorption except that 1) the cation exchange capacity for uranium was not known (that is, there was no adsorption isotherm) and 2) a cation exchange with the monohydroxy-uranyl complex was included. The parameters used are listed in Table 57. The number of sites used to model these data was much greater than for the zeolitic tuff. The possible reason for this is the exposure of fresh surfaces of feldspar and quartz combined with the lack of exposure to a complex groundwater.

The results of this exercise are shown in Fig. 104 and are in excellent agreement with the results of Leckie and his students (Davis et al. 1978). The equilibrium concentration of uranium at pH values of 9 and above are above the solubility limit for uranium hydroxide. The effect of precipitation was evident in the experimental data. The solubility product was not included in this model.

State of knowledge of surface complexation with respect to Yucca Mountain

Surface-complexation reactions with Yucca Mountain tuff have just begun to be studied. The pH

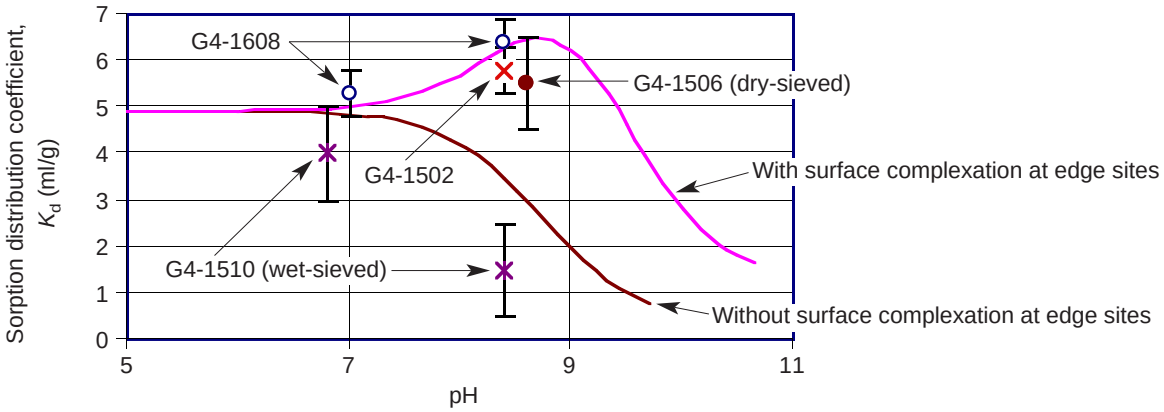

Figure 102. Neptunium Sorption in J-13 Water. This plot compares sorption data (points) with the predictions of the FITEQL code for the pH dependence of neptunium sorption on zeolitic tuff from J-13 water with and without surface complexation at edge sites (curves). The sorption data for samples G4-1608 and G4-1502 are from Thomas (1987).

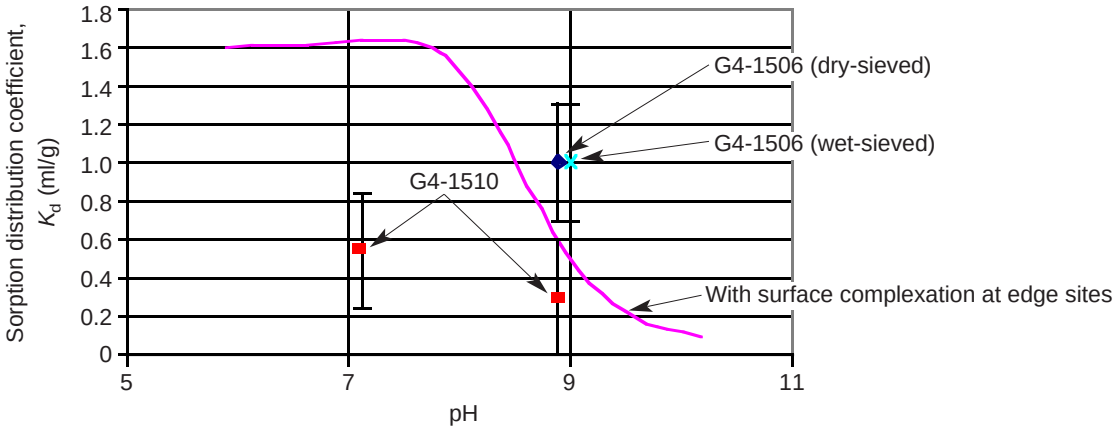

Figure 103. Neptunium Sorption in UE-25 p#1 Water. This plot compares sorption data (points) with the predictions of the FITEQL code for the pH dependence of neptunium sorption on zeolitic tuff from UE-25 p#1 water with surface complexation at edge sites (curve).

dependence of actinide adsorption can be readily explained with a combined surface-complexation and ion-exchange model. The effect of changing groundwater composition on neptunium adsorption has also been successfully modeled using a surface-complexation model. There are significant gaps in the knowledge base, however. From a fundamental standpoint, an HSAB model for bidentate inner-sphere complexes needs to be developed. The consequences of a bidentate attachment mechanism, as was included in the uranium adsorption model, is an increased sensitivity to competition with metal ions favoring monodentate attachment (for example, calcium). From an experimental standpoint, the effects of wet-sieving needs to be better understood. If wet-sieving removes all of the clay minerals, the resulting distribution coefficients may be too low (overly conservative). On the other hand, if a trace component of groundwater is responsible for the decrease in surface com-

Table 57. Additional Equations and Parameters Used to Model Uranium Adsorption onto Devitrified Tuff

Type of reaction	Equilibrium reactions	log *K*
Aqueous reactions:	$UO_2^{2+} + H_2O \leftrightarrow UO_2OH^+ + H^+$	−5.8
	$UO_2^{2+} + 2\ H_2O \leftrightarrow UO_2(OH)_2 + 2\ H^+$	−12.5
	$2\ UO_2^{2+} + 2\ H_2O \leftrightarrow (UO_2)_2(OH)_2^{2+} + 2\ H^+$	−5.62
	$3\ UO_2^{2+} + 5\ H_2O \leftrightarrow (UO_2)_3(OH)_5^+ + 5\ H^+$	−15.63
Uranyl adsorption reactions:	$2\ t\text{-}Al^-Na^+ + UO_2^{2+} \leftrightarrow (t\text{-}Al^-)_2UO_2^{2+} + 2\ Na^+$	1.8
	$t\text{-}Al^-Na^+ + UO_2^{2+} + H_2O \leftrightarrow t\text{-}Al^-UO_2OH^+ + Na^+ + H^+$	−1.5
	$MOH + UO_2^{2+} \leftrightarrow MOUO_2^+ + H^+$	0.60
	$MOH + UO_2^{2+} + Cl^- \leftrightarrow MOUO_2^+Cl^- + H^+$	2.8
	$2\ MOH + UO_2^{2+} \leftrightarrow (MO)_2UO_2 + 2\ H^+$	−2.8

Parameters:	Type of site	Site density (eq/kg)
	Tetrahedral(*t*) aluminum	2×10^{-2}
	Octahedral aluminum (edge)	2×10^{-3}

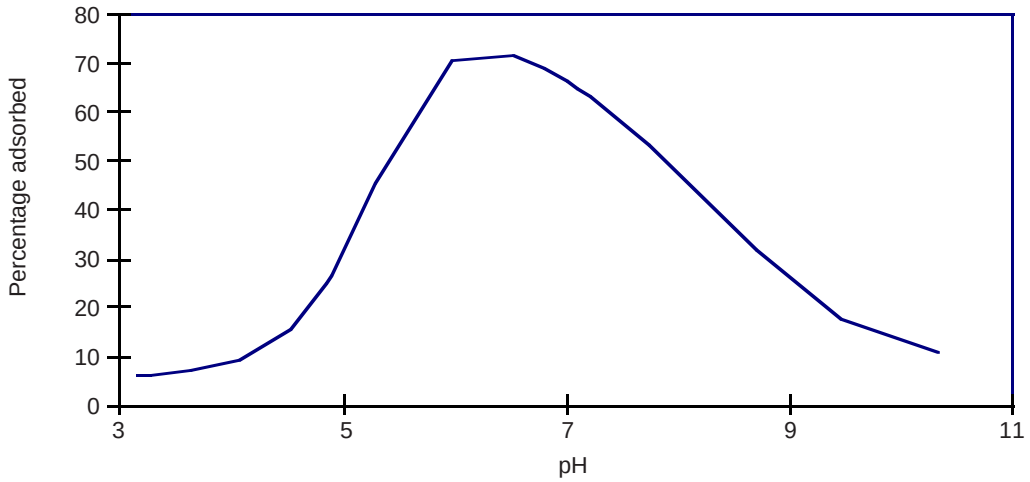

Figure 104. Uranium Adsorption. The curve above shows the predictions of the FITEQL code for the adsorption of uranium onto crushed devitrified tuff from an 0.1 M sodium-chloride solution in a controlled atmosphere with an initial uranium concentration of 1×10^{-6} M.

plexation, it must be identified and measured in groundwaters and in pore waters.

The modeling of actinide sorption shows that high carbonate concentrations will severely reduce the ability to form surface complexes on tuff. The ion exchange of actinides appears to dominate under normal conditions over surface complexation. Furthermore, divalent cations are found to be strong competitors for cation exchange sites found in Yucca Mountain tuff.

D. SORPTION DATA RECOMMENDED FOR PERFORMANCE ASSESSMENT

Sorption is a function of water chemistry and the type of tuff at Yucca Mountain. The water chemistry at Yucca Mountain was reviewed by Meijer (1992) and is discussed in "Yucca Mountain Waters" (Section C of Chapter I) and "Groundwater Chemistry Model" (Chapter II) of this report. The concentration of the major cations and anions in unsaturated-zone (UZ) groundwaters appears to be intermediate between the saturated-zone tuffaceous waters (for example, from Well J-13) and waters from the Paleozoic carbonate aquifer (from Well UE-25 p#1). Consequently, the first assumption made for the performance-assessment recommendations was that the waters from Wells J-13 and UE-25 p#1 bound the chemistry of the groundwaters at Yucca Mountain.

The second assumption made dealt with grouping all strata on the basis of rock type (the stratigraphy considered from the repository horizon to the accessible environment is outlined in Table 4, page 17). This assumption reduced the number of sorption-coefficient distributions elicited to four per radionuclide: iron oxides, devitrified tuff, vitric tuff, and zeolitic tuff. The basis for this grouping is the fact that sorption of radionuclides is the result of a chemical reaction between the radionuclide in the groundwater and the minerals in the tuff. The mineralogy of the different strata of the same rock group is very similar, and the sorption coefficients can be grouped in terms of these rock types (Thomas 1987).

The containers to be used in the repository were added to the list after consideration of whether the corrosion by-products of the massive multipurpose container could become a substrate for sorption. Actinides are sorbed strongly by iron oxides. However, although hematite is found in the tuffs at Yucca Mountain, the iron-oxide minerals in the tuffs appear to be "passivated"—that is, all of the sorption sites could be occupied by other metals (Triay et al. 1993b)—and the sorption of the radionuclides onto tuff (containing iron oxides as trace minerals) is not as large as predicted on the basis of the sorption of radionuclides onto synthetic pure iron oxides. Because the sorption sites on the degraded container material would not necessarily be occupied by other metals, the experts agreed to add iron oxides to the list of "rock" types.

The effect of temperature on sorption coefficients was reviewed by Meijer (1990). Measured sorption coefficients onto tuffs were higher at elevated temperatures for all elements studied: americium, barium, cerium, cesium, europium, plutonium, strontium, and uranium. Consequently, the third assumption made was that sorption coefficients measured at ambient temperatures should be applicable and generally conservative when applied to describing aqueous transport from a hot repository. (This assumption is meaningful provided that the high temperatures that will be sustained for long time periods due to potential high thermal loads do not result in changes in the mineralogy and the water chemistry at Yucca Mountain that are not predictable by short-term laboratory and field experiments.)

Table 58 shows the parameters for the sorption-coefficient probability models recommended for performance assessment for the unsaturated-zone units, and Table 59 shows the same parameters for saturated-zone units. We now discuss the source of these values for each of the elements separately.

Americium

Americium sorbs strongly to most materials (Triay et al. 1991b). The potential mechanisms for actinide sorption onto mineral surfaces has been reviewed by Meijer (1992). The sorption-coefficient distributions for americium in Yucca Mountain tuffs and iron oxides given in Tables 58 and 59 were inferred from the data presented by Thomas (1987), Triay et al. (1991b), and Meijer (1992).

Table 58. Sorption-coefficient Distributions for Unsaturated-zone Units

Element	Rock type	Min K_d (ml/g)	Max K_d (ml/g)	$E[x]$	COV*	Distribution type
Americium	Devitrified	100	2000			Uniform
	Vitric	100	1000	400	0.20	Beta
	Zeolitic	100	1000			Uniform
	Iron oxide	1000	5000			Uniform
Plutonium	Devitrified	20	200	100	0.25	Beta
	Vitric	50	200	100	0.25	Beta
	Zeolitic	30	200	100	0.25	Beta
	Iron oxide	1000	5000			Uniform
Uranium	Devitrified	0	4.0	2.0	0.3	Beta
	Vitric	0	3.0	1.0	0.3	Beta
	Zeolitic	0	30.0	7.0	1.0	Beta(exp)
	Iron oxide	100	1000			Uniform
Neptunium	Devitrified	0	6.0	1.0	0.3	Beta
	Vitric	0	15.0	1.0	1.0	Beta(exp)
	Zeolitic	0	3.0	0.5	0.25	Beta
	Iron oxide	500	1000			Uniform
Radium	Devitrified	100	500			Uniform
	Vitric	50	100			Uniform
	Zeolitic	1000	5000			Uniform
	Iron oxide	0	500	30	1.0	Beta(exp)
Cesium	Devitrified	20	1000			Uniform
	Vitric	10	100			Uniform
	Zeolitic	500	5000			Uniform
	Iron oxide	0	500	30	1.0	Beta(exp)
Strontium	Devitrified	10	50			Uniform
	Vitric	0	20			Uniform
	Zeolitic	500	2000			Uniform
	Iron oxide	0	30	10	0.25	Beta
Nickel	Devitrified	0	500	100	0.33	Beta
	Vitric	0	100	50	0.33	Beta
	Zeolitic	0	500	100	0.33	Beta
	Iron oxide	0	1000			Uniform
Lead	Devitrified	100	500			Uniform
	Vitric	100	500			Uniform
	Zeolitic	100	500			Uniform
	Iron oxide	100	1000			Uniform
Tin	Devitrified	20	200			Uniform
	Vitric	20	200			Uniform
	Zeolitic	100	300			Uniform
	Iron oxide	0	5000			Uniform
Protactinium	Devitrified	0	100			Uniform
	Vitric	0	100			Uniform
	Zeolitic	0	100			Uniform
	Iron oxide	500	1000			Uniform
Selenium	Devitrified	0	30	3	1.0	Beta(exp)
	Vitric	0	20	3	1.0	Beta(exp)
	Zeolitic	0	15	2	1.0	Beta(exp)
	Iron oxide	0	500	30	1.0	Beta(exp)
Carbon	Iron oxide	10	100			Uniform
Actinium, Niobium, Samarium, Thorium, Zirconium: see Americium						
Chlorine, Technetium, Iodine		0	0			

*Coefficient of variation: COV = $\sigma[x]/E[x]$

Table 59. Sorption-coefficient Distributions for Saturated-zone Units

Element	Rock type	Min K_d (ml/g)	Max K_d (ml/g)	$E[x]$	COV*	Distribution type
Americium	Devitrified	100	2000			Uniform
	Vitric	100	1000	400	0.20	Beta
	Zeolitic	100	1000			Uniform
	Iron oxide	1000	5000			Uniform
Plutonium	Devitrified	50	300	100	0.15	Beta
	Vitric	50	300	100	0.15	Beta
	Zeolitic	30	300	100	0.15	Beta
	Iron oxide	1000	5000			Uniform
Uranium	Devitrified	0	5.0	2.0	0.3	Uniform
	Vitric	0	4.0	1.0	0.3	Uniform
	Zeolitic	5	20.0	7.0	0.3	Beta
	Iron oxide	100	1000			Uniform
Neptunium	Devitrified	0	10.0	3.0	0.3	Beta
	Vitric	0	15.0	1.5	1.0	Beta(exp)
	Zeolitic	0	12.0	4.0	0.25	Beta
	Iron oxide	500	1000			Uniform
Radium	Devitrified	100	500			Uniform
	Vitric	100	500			Uniform
	Zeolitic	1000	5000			Uniform
	Iron oxide	0	1500	30	1.0	Beta(exp)
Cesium	Devitrified	20	1000			Uniform
	Vitric	10	100			Uniform
	Zeolitic	500	5000			Uniform
	Iron oxide	0	500	30	1.0	Beta(exp)
Strontium	Devitrified	10	200			Uniform
	Vitric	20	50			Uniform
	Zeolitic	2000	5000			Log uniform
	Iron oxide	0	30	10	0.25	Beta
Nickel	Devitrified	0	500	100	0.33	Beta
	Vitric	0	200	100	0.33	Beta
	Zeolitic	0	500	100	0.33	Beta
	Iron oxide	0	1000			Uniform
Lead	Devitrified	100	500			Uniform
	Vitric	100	500			Uniform
	Zeolitic	100	500			Uniform
	Iron oxide	100	1000			Uniform
Tin	Devitrified	20	200			Uniform
	Vitric	20	200			Uniform
	Zeolitic	100	300			Uniform
	Iron oxide	0	5000			Uniform
Protactinium	Devitrified	0	100			Uniform
	Vitric	0	100			Uniform
	Zeolitic	0	100			Uniform
	Iron oxide	500	1000			Uniform
Selenium	Devitrified	0	30	3	1.0	Beta(exp)
	Vitric	0	20	3	1.0	Beta(exp)
	Zeolitic	0	15	2	1.0	Beta(exp)
	Iron oxide	0	500	30	1.0	Beta(exp)
Carbon	Iron oxide	10	100			Uniform
Actinium, Niobium, Samarium, Thorium, Zirconium: see Americium						
Chlorine, Technetium, Iodine		0	0			

*Coefficient of variation: COV = $\sigma[x]/E[x]$

Plutonium

One of the problems of interpreting sorption data for plutonium is that this element can exist in multiple oxidation states under oxidizing conditions at near-neutral pH values (Nitsche et al. 1993a). Plutonium can also exits as a polymer (Triay et al. 1991a). The lack of information on the speciation of plutonium in the groundwaters at Yucca Mountain makes it difficult to assess the sorption mechanism for this element. However, the empirical data obtained in Yucca Mountain tuffs indicate that plutonium sorbs strongly. The sorption-coefficient distributions for plutonium in Yucca Mountain tuffs given in Tables 58 and 59 were inferred from the data presented by Thomas (1987) and Meijer (1992).

Uranium

No additional data for uranium have been collected for Yucca Mountain tuffs since the 1991 total-system performance-assessment effort (TSPA-1991). Consequently, no change was made for the sorption-coefficient distributions used for this element. As previously discussed (Meijer 1992), uranium sorbs strongly to synthetic iron oxides.

Thorium

The information elicited for americium was also used for thorium. This approach is due both to the lack of sorption information available for thorium and to the similarities exhibited by the sorption behavior of these two elements (Thomas 1987).

Radium

Barium has been used as an analog for radium in the experiments performed at Los Alamos (Thomas 1987). These elements sorb to Yucca Mountain tuffs via an ion-exchange mechanism and surface-adsorption reactions (Meijer 1992). The sorption-coefficient distributions for radium in Yucca Mountain tuffs and iron oxides given in Tables 58 and 59 were inferred from the data presented by Thomas (1987), Meijer (1992), and Triay et al. (1991c).

Lead

Lead tends to complex with fulvics in the groundwaters and sorbs as a complex. The sorption-coefficient distributions for lead in Yucca Mountain tuffs and iron oxides given in Tables 58 and 59 were inferred from the data presented by Meijer (1990).

Neptunium

Sorption-coefficient distributions for neptunium in tuff are the same as those used in TSPA-1991. Recently obtained data (Triay et al. 1993b) agree with previous observations. Neptunium is a poorly sorbing radionuclide in tuff even when the tuffs are known to have iron oxides because the iron oxides in the tuff appear to be passivated. The neptunium sorption-coefficient distribution for sorption onto iron oxides given in Tables 58 and 59 was inferred from data presented by Meijer (1992) and Triay et al. (1993b) for sorption onto synthetic iron oxides.

Protactinium

Very little information exists for protactinium sorption onto tuffs (Thomas 1987), so the experts decided to use for this element the same sorption coefficients elicited for neptunium.

Tin

There is very little information for the sorption of tin onto tuffs (Thomas 1987). Based on the data available, Meijer (1992) suggested that tin exhibited large values of K_d in the devitrified tuffs (larger than 1000 ml/g). The sorption-coefficient distributions given in Tables 58 and 59 were inferred from the work by Andersson (1988); the uniform distributions chosen were the result of the expert's uncertainty about the sorption of tin.

Nickel

For devitrified, vitric, and zeolitic tuffs, the nickel sorption-coefficient distributions given in Tables 58 and 59 were inferred from data presented by Meijer (1992). For iron oxides, the nickel sorption-coefficient distribution was inferred from the data presented by Siegel et al. (1992 and 1993).

Cesium

Cesium sorption-coefficient distributions for tuff and iron oxides were inferred from the data presented by Thomas (1987), Meijer (1992), and Triay et al. (1991c). Cesium has one of the highest selectivity coefficients for zeolites among all chemical elements (Meijer 1992). Cesium sorption onto devitrified and vitric samples could be the result of ion exchange onto clays or feldspars in the tuff samples or surface-adsorption reactions (Meijer 1992).

Strontium

Strontium sorption-coefficient distributions for tuff and iron oxides were inferred from the data presented by Thomas (1987) and Triay et al. (1991c). Strontium sorbs strongly onto zeolites by ion exchange. This element's sorption onto other types of tuff may be dominated by the amount of clay in the tuff units. The values given in Tables 58 and 59 are generally conservative.

Selenium

There are limited data on tuff for selenium sorption (Thomas 1987), so the experts decided to use the same sorption-coefficient distributions for selenium as the ones elicited for uranium. This decision is a conservative one because uranium can be oxidized much more readily than selenium in Yucca Mountain groundwaters.

Carbon

Carbon is a special case because transport is expected to occur primarily in the gaseous phase as carbon dioxide. The major retardation mechanism is exchange of carbon-14 with the carbon in the carbon dioxide dissolved in the groundwater.

Actinium, Samarium, Niobium, and Zirconium

All these elements are strongly sorbing (Meijer 1992). The experts advised using for these elements the same sorption-coefficient distributions as those elicited for americium.

Iodine, Technetium, and Chlorine

Iodine and chlorine have anions that do not sorb onto tuffs. Technetium exists as pertechnetate under oxidizing conditions and does not sorb either (Triay et al. 1993a).

V. DYNAMIC TRANSPORT STUDIES

A. CRUSHED-ROCK COLUMNS

Generally, batch-sorption experiments, which were discussed in the previous chapter, are used to identify sorption mechanisms and to obtain sorption distribution coefficients (Triay et al. 1996a, 1996b). Such experiments are fast, easy, and inexpensive compared to other types of sorption experiments. In this section, we discuss our attempts to verify the results of earlier batch-sorption measurements by performing crushed-tuff column studies under flowing conditions without significantly changing the surface properties of the tuff. By comparing differences with the batch-sorption measurements, such studies would be most sensitive to multiple-species formation, colloid formation, and any other geochemical reactions (such as changes in surface reactivity due to agitation) not adequately described by batch-sorption distribution coefficients. In these crushed-tuff column experiments, we investigated mass-transfer kinetics by studying radionuclide migration as a function of water velocity.

Column elution curves can be characterized by two parameters: the time of arrival of the radionuclide eluted through the column and the broadness (dispersion) of the curve. The arrival time depends on the retardation factor, R_f, which, for soluble radionuclides, depends, in turn, on the sorption distribution coefficient, K_d. Significant deviations (those larger than expected based on sampling variability) in arrival time from that predicted on the basis of the batch-sorption distribution coefficients indicate one of the following problems:

- the presence of more than one chemical species that are not readily exchanged and that have different selectivities in tuff minerals,
- the presence of the radionuclide as a colloid,
- extremely slow sorption kinetics,
- nonreversibility of the sorption process, and
- solubility effects due to the presence of solids.

The broadness, or apparent dispersion, of the curve depends on

- the kinetics and reversibility of sorption and
- the linearity of the isotherm that describes the dependence of sorption on radionuclide concentration.

The main goal of our study was to test the necessary assumptions made in using values of the sorption distribution coefficient, K_d, (determined by batch-sorption measurements) to describe hydrologic transport. These assumptions are:

1. microscopic equilibrium is attained between the solution species and the adsorbate,
2. only one soluble chemical species is present (or if more than one is present, they interchange rapidly),
3. the radionuclides in the solid phase are adsorbed on mineral surfaces (that is, they are not precipitated), and
4. the dependence of sorption on concentration is described by a linear isotherm.

The importance of verifying these assumptions can be demonstrated by the following hypothetical cases. If equilibrium were not attained in the batch experiments (violation of assumption 1), the retardation of radionuclides could be dependent on groundwater velocity. If a radionuclide were present in solution as an anionic and a cationic species and solution equilibrium were not maintained (violation of assumption 2), the batch measurement would predict a single retardation factor, whereas in a flowing system, the anion could move unimpeded (its size

and charge excluding it from the pores of the Yucca Mountain tuff) compared to movement of the cation. If the radionuclide had precipitated in the batch experiments (violation of assumption 3), the value of the K_d thus determined would be meaningless, and depending on the precipitation mechanism, colloid transport could be important. If the isotherm was nonlinear (violation of assumption 4), the migration front of the radionuclides in a column study would usually broaden, appearing as increased dispersion over that observed for nonsorbing tracers.

Experimental Procedures

Groundwaters and solutions

Because the J-13 and UE-25 p#1 well waters that bound the Yucca Mountain groundwaters are both oxidizing (Ogard and Kerrisk 1984), all the batch-sorption and column experiments were performed under oxidizing conditions. In the batch-sorption experiments, both groundwaters (filtered by a 0.05-μm filter) were used, but in the column experiments, we used J-13 water (filtered) and a sodium-bicarbonate buffer that simulated UE-25 p#1 groundwater (because of the unavailability of water from this well). The synthetic UE-25 p#1 water was prepared by dissolving 0.39 g of Na_2CO_3 and 8.90 g of $NaHCO_3$ in 10 liters of deionized water, which duplicates the larger amount of bicarbonate in reference, or on-site, UE-25 p#1 water.

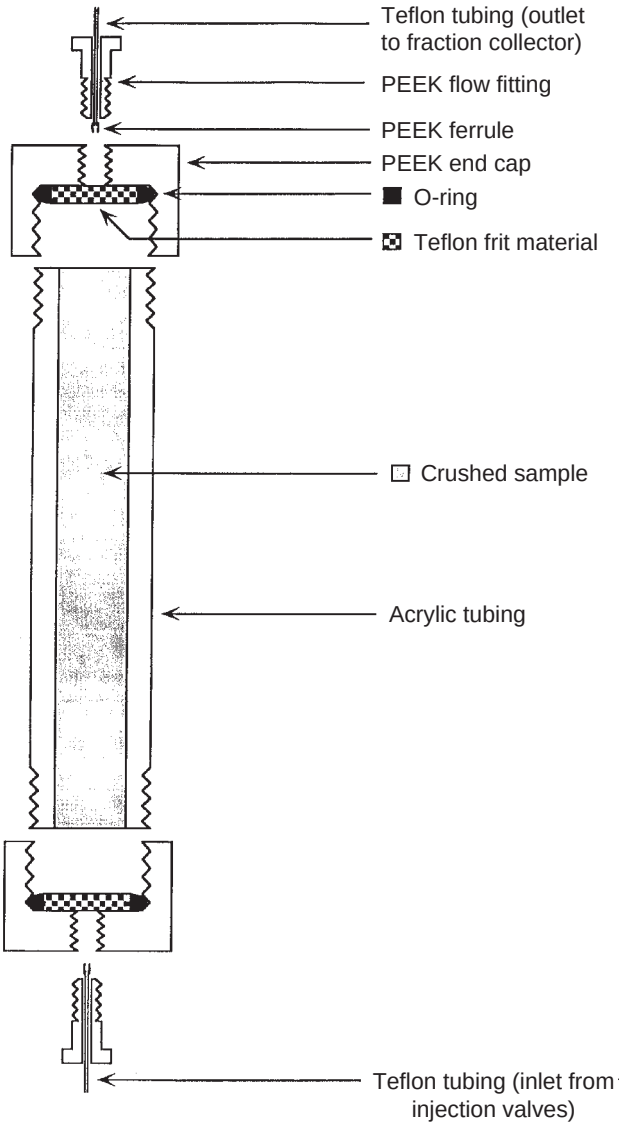

Figure 105. Cross Section of Crushed-rock Columns.

In the column experiments, we used neptunium and plutonium solutions prepared in the same way as for the batch-sorption experiments—by taking an aliquot of a well-characterized $^{237}Np(V)$ or $^{239}Pu(V)$ acidic stock and diluting it in the water being studied. We also used tritium and pertechnetate solutions, which were similarly prepared by adding an aliquot of ^{3}H or ^{95m}Tc acidic stock to the groundwater being studied.

Crushed-rock column procedure

The details of the crushed-rock column experimental setup and procedure are illustrated in Figs. 105 and 106. We packed plexiglas columns with crushed tuff by using a continuously agitated wet slurry, a technique that provides a relatively homogeneous packing nearly free of stratification. As in the batch-sorption experiments, all tuff samples had previously been crushed and wet-sieved (with the groundwater being used in the experiment) to obtain particle sizes ranging from 75 to 500 μm.

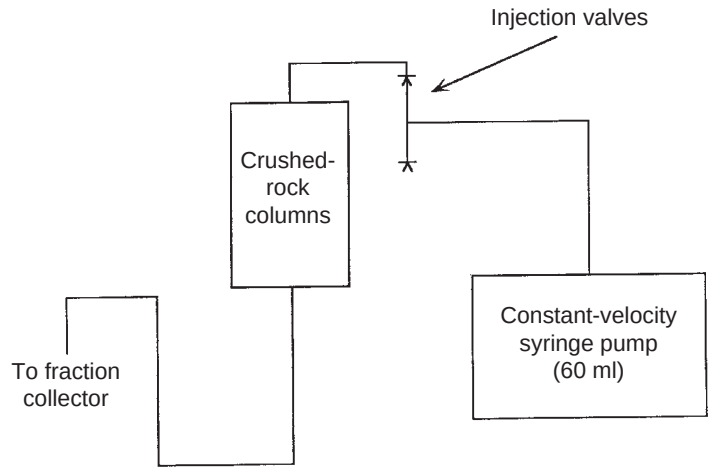

Figure 106. Flow Chart of Crushed-rock Column Experiment.

After establishing the desired flow rate in the tuff column using the desired groundwater, we injected an aliquot of the radionuclide solution and then used a syringe pump to elute the radionuclide through the column. The breakthrough or elution curve was measured. Tritiated water was used to measure the free volume of the column, which excludes dead-end pore volume. The concentration of tritium, pertechnetate, ^{239}Pu, or ^{237}Np in the eluent was measured by liquid-scintillation counting. The crushed-rock column dimensions and flow velocities that we used followed the guidelines provided by Relyea (1982).

Relationship between column and batch experiments

We measured the batch-sorption distribution coefficients under static conditions by equilibrating a solution containing the radionuclides with a sample of crushed tuff. If we assume that equilibrium is achieved between a single aqueous chemical species and the species adsorbed on the solid phase, the rate at which a radionuclide moves through a column can simply be related to the sorption distribution coefficient, K_d. The relationship between the retardation factor, R_f, obtained from column-transport experiments, and the values of K_d, obtained from batch-sorption experiments, is generally given by

$$R_f = 1 + \frac{\rho_b}{\epsilon} K_d \ , \qquad (83)$$

where ρ_b is the dry bulk density (including pores) and ϵ is the porosity of the column. Hiester and Vermeulen (1952) derived this equation and carefully described its underlying assumptions. To test these assumptions, the radionuclide solution used in the batch-sorption measurements was eluted through columns containing tuff samples that came from the same drill hole and depth interval and that had been crushed and sieved to the same size fraction as samples used in the batch-sorption studies.

Results and Discussion

The most comprehensive explanation of the fate of reactive and nonreactive solutes and suspended particles in porous and fractured media has been presented by de Marsily (1986, Chapter 10). The transport of radionuclides in porous media is governed by advection, diffusion, or kinematic dispersion. Advection is the mechanism in which dissolved species are carried along by the movement of fluid. Diffusion causes species to be transferred from zones of high concentration to zones of low concentration. Kinematic dispersion is a mixing phenomenon linked to the heterogeneity of the microscopic velocities inside the porous medium. The migration of a solute in a saturated porous medium is described by the following transport equation

$$\nabla \cdot (\mathbf{D}\, \nabla C - C\mathbf{U}) = \epsilon \frac{\partial C}{\partial t} + Q \ , \qquad (84)$$

where **D** is the dispersion tensor, C is the concentration of solute in the solution phase, **U** is the filtration velocity (Darcy's velocity), ϵ is the porosity, t is time, and Q is a "net source or sink term" that accounts for such things as reactivity or adsorption.

For the case of a sorbing, nonreactive solute, the

equation becomes

$$\nabla \cdot (\mathbf{D}\,\nabla C - C\mathbf{U}) = \epsilon \frac{\partial C}{\partial t} + \rho_b \frac{\partial F}{\partial t} \quad , \quad (85)$$

where ρ_b, again, is the dry bulk density of the medium and F is the mass of solute sorbed per unit mass of solid.

Dispersion has three components: the longitudinal dispersion coefficient in the direction of the flow, D_L, and the transverse dispersion coefficient, D_T, in the two directions at right angles to the velocity of the flow. These components are given by

$$\begin{aligned} D_L &= \epsilon d + \alpha_L |U| \text{ and} \\ D_T &= \epsilon d + \alpha_T |U| \quad , \end{aligned} \quad (86)$$

where d is the effective diffusion coefficient in the medium and α is dispersivity.

The characteristics of the sorption determine the actual relationship between F and C. For the case in which sorption is linear, reversible, and instantaneous, the ratio between F and C is simply equal to the sorption distribution coefficient:

$$\frac{F}{C} = K_d \ . \quad (87)$$

Substitution of Eqn. 87 into Eqn. 85 yields

$$\nabla \cdot (\mathbf{D}\,\nabla C - C\mathbf{U}) = \epsilon \left[1 + \frac{\rho_b}{\epsilon} K_d \right] \frac{\partial C}{\partial t} \ . \quad (88)$$

The expression in brackets in Eqn. 88 corresponds to the retardation factor, R_f, given earlier (Eqn. 83). Thus, we have a way to compare sorption coefficients obtained under advective, diffusive, and dispersive conditions with sorption coefficients obtained from batch-sorption experiments. However, this approach is valid only if sorption is linear, reversible, and instantaneous.

Neptunium results

We measured the elution of Np(V) as a function of water velocity through zeolitic, devitrified, and vitric crushed tuff in columns with J-13 well water and with synthetic UE-25 p#1 water. The elution curves have been previously published (Triay et al. 1996c). We calculated the porosity as the free column volume divided by the total column volume (free volume was defined as the volume of tritium solution that had to be eluted to recover 50% of the injected tritium). We then calculated values of R_f for the column experiments by dividing the free column volume into the volume of neptunium solution that had to be eluted to recover 50% of the injected ^{237}Np. From these values of R_f, we used Eqn. 83 to calculate the column sorption-distribution coefficients listed in Table 60.

How do the earlier results of batch-sorption experiments (Triay et al.1996a, 1996b) compare with the results of the crushed-tuff column experiments? Inspection of Table 60 indicates good agreement between the values of K_d obtained by the two approaches, which means that the arrival time of ^{237}Np can be predicted from a value for K_d. On the other hand, the broad, dispersive shape of the elution curves indicates that sorption of neptunium onto zeolitic and vitric tuffs appears to be nonlinear, nonreversible, or noninstantaneous. Previous work has found that sorption of neptunium onto clinoptilolite-rich tuffs is rapid (Triay et al. 1996a) and can be fit with a linear isotherm (Triay et al. 1996b). Consequently, the degree of reversibility of neptunium sorption onto zeolitic and vitric tuffs may be the most likely reason for the apparent dispersivity in the tuff-column elution curves.

The elution curves also reveal that, regardless of the water being studied, the elution of ^{237}Np does not precede the elution of tritium for any of the tuffs. This observation is extremely important because if charge-exclusion effects were to cause the neptunyl-carbonato complex (an anion) to elute faster than neutral tritiated water molecules, significant neptunium releases could occur at Yucca Mountain. Another important observation that can be drawn from these experiments is that values of K_d can be used to obtain accurate or conservative estimates for the performance-assessment calculations of neptunium transport through Yucca Mountain tuffs.

Table 60. Comparison of Neptunium K_d Values from Batch and Column Measurements

Column number	Tuff sample	Water type	Batch K_d (ml/g)	Column K_d (ml/g)
1	G4-1508, zeolitic	J-13	1.7 ± 0.4 (G4-1510)	1.7
2	G4-1508, zeolitic	J-13	1.7 ± 0.4 (G4-1510)	1.2
3	G4-1505, zeolitic	J-13	2.1 ± 0.4	2.8
4	G4-1505, zeolitic	Syn. UE-25 p#1	0.2 ± 0.3 (G4-1506)	0.4
5	G4-1505, zeolitic	Syn. UE-25 p#1	0.2 ± 0.3 (G4-1506)	0.2
6	G4-1505, zeolitic	Syn. UE-25 p#1	0.2 ± 0.3 (G4-1506)	0.2
7	G4-268, devitrified	J-13	–0.04 ± 0.2	0.07
8	G4-268, devitrified	J-13	–0.04 ± 0.2	0.01
9	G4-268, devitrified	J-13	–0.04 ± 0.2	0.02
10	G4-268, devitrified	J-13	–0.04 ± 0.2	0.01
11	G4-272, devitrified	Syn. UE-25 p#1	0.2 ± 0.3 (G4-270)	0.06
12	G4-268, devitrified	Syn. UE-25 p#1	0.2 ± 0.3 (G4-270)	0.03
13	G4-268, devitrified	Syn. UE-25 p#1	0.2 ± 0.3 (G4-270)	0.03
14	GU3-1407, vitric	J-13	0.1 ± 0.5	0.2
15	GU3-1407, vitric	J-13	0.1 ± 0.5	0.1
16	GU3-1405, vitric	J-13	0.03 ± 0.2	0.1
17	GU3-1405, vitric	Syn. UE-25 p#1	0.2 ± 0.4 (GU3-1407)	0.1
18	GU3-1405, vitric	Syn. UE-25 p#1	0.2 ± 0.4 (GU3-1407)	0.1
19	GU3-1405, vitric	Syn. UE-25 p#1	0.2 ± 0.4 (GU3-1407)	0.1

Neptunium summary

- Using crushed-rock columns, we studied the retardation of ^{237}Np by zeolitic, devitrified, and vitric tuffs in sodium-bicarbonate waters under oxidizing conditions (at room temperature, under atmospheric conditions, and using different water velocities).

- We compared the sorption distribution coefficients obtained from the column experiments under flowing conditions to those obtained from batch-sorption experiments under static conditions.

- The column and batch distribution coefficients agreed well for all tuffs regardless of the groundwater studied and the water velocity used for the column experiments.

- We found that batch-sorption distribution coefficients predict well the arrival time for neptunium eluted through a crushed-rock column.

- The apparent dispersivity of the neptunium elution curves through the zeolitic and vitric tuffs indicates that the sorption is either nonlinear, irreversible, or noninstantaneous, which means the transport cannot be completely described using a sorption distribution coefficient. The reversibility of neptunium sorption onto tuff will be studied as the most likely reason for the apparent dispersivity of the elution curves.

- The use of a batch-sorption distribution coefficient to calculate neptunium transport through Yucca Mountain tuffs would result in conservative values for neptunium release.

- Neptunium never eluted prior to the nonsorb-

ing radionuclide (tritiated water) used in the column experiments. Thus, charge exclusion does not appear to exclude neptunium from the tuff pores.

- Corroborated by these column experiments were the general trends previously observed for neptunium sorption using batch-sorption experiments:
  a) neptunium sorption onto devitrified and vitric tuffs is minimal, and
  b) neptunium sorption onto zeolitic tuffs decreases as the amount of sodium and bicarbonate/carbonate in the groundwaters increases.

Plutonium and technetium results

The elution of Pu(V) through zeolitic, devitrified, and vitric crushed tuff was measured in columns with J-13 well water and with synthetic UE-25 p#1 water. The elution curves for these experiments (Figs. 107 through 109) indicate that vitric and zeolitic tuffs sorb plutonium significantly, which is probably due to their clay content. The shape of the elution curves for plutonium indicates that use of K_d values to predict plutonium transport through Yucca Mountain tuffs will predict plutonium releases conservatively. Results by Triay et al. (1995a) indicate that plutonium sorption onto tuffs is a slow process and probably due to a redox reaction occurring at the tuff surfaces. To verify these batch-sorption results, which suggest that plutonium sorption, even to the lowest sorbing tuff type (devitrified), could be significant, the migration of plutonium as a function of flow velocity was measured in devitrified tuff using J-13 and UE-25 p#1 waters. Inspection of these elution curves (Figs. 110 and 111) confirms the trends observed using batch-sorption techniques; the elution curves observed for

continued on page 186

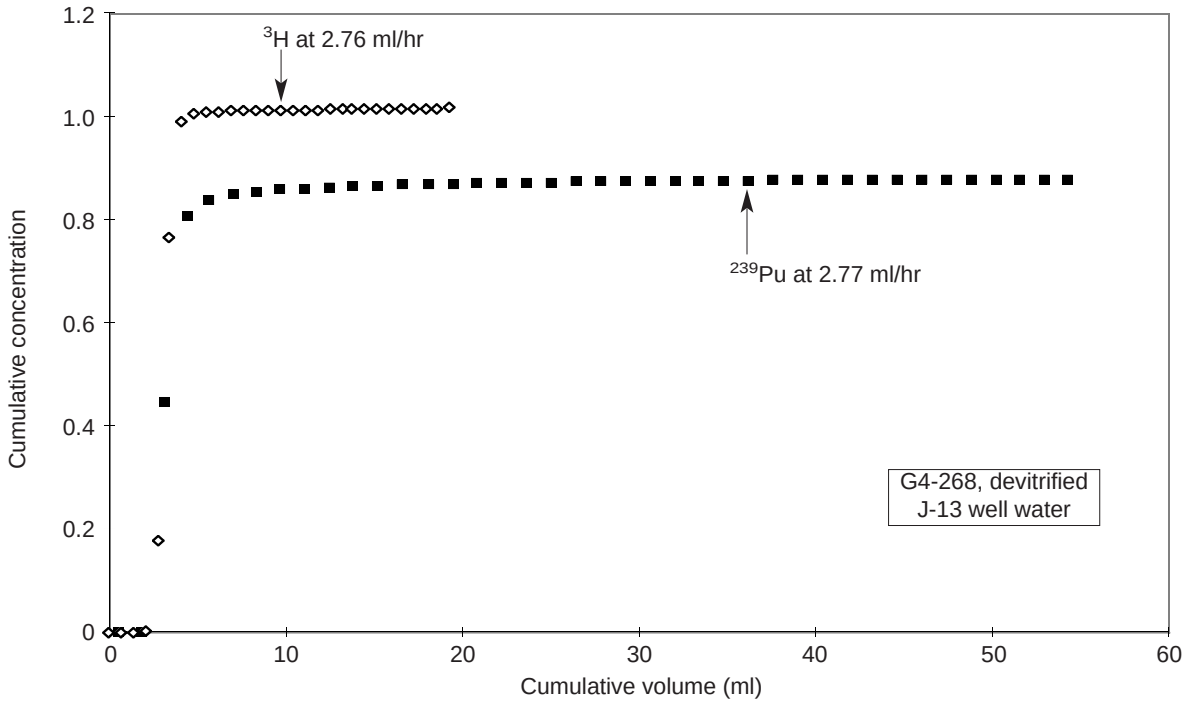

Figure 107. Plutonium through Devitrified Tuff. This plot shows the elution curves for tritium and plutonium-239 through devitrified tuff sample G4-268 with J-13 well water. Cumulative concentration (in Figs. 107 through 114) is the total activity of the recovered tracer divided by the total activity injected initially. As seen by the variation of the final part of the curves, this variable has an experimental error of about ± 20%.

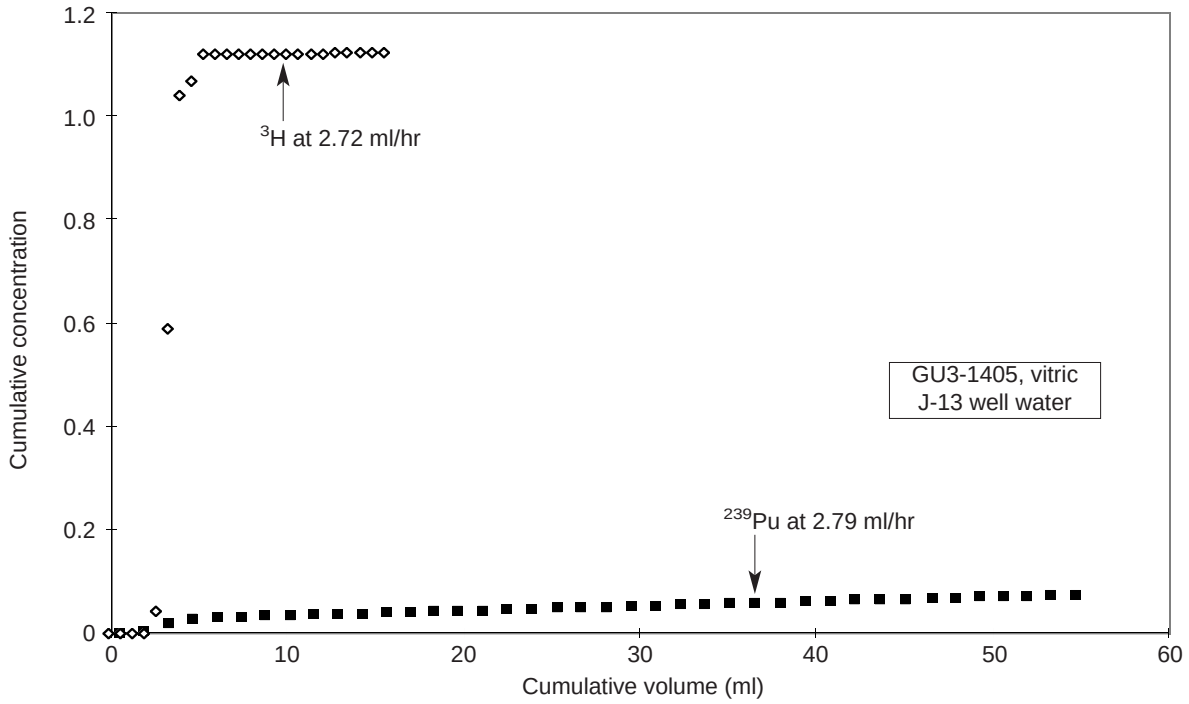

Figure 108. Plutonium through Vitric Tuff. This plot shows the elution curves for tritium and plutonium-239 through vitric tuff sample GU3-1405 with J-13 well water.

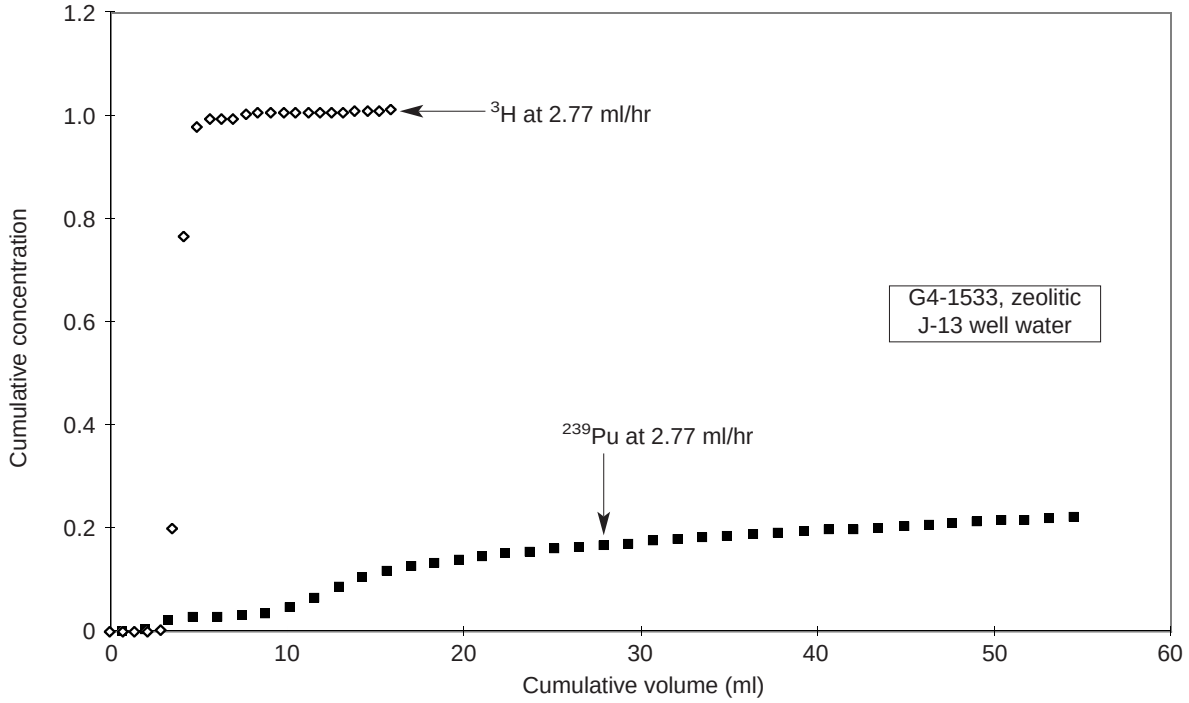

Figure 109. Plutonium through Zeolitic Tuff. This plot shows the elution curves for tritium and plutonium-239 through zeolitic tuff sample G4-1533 with J-13 well water.

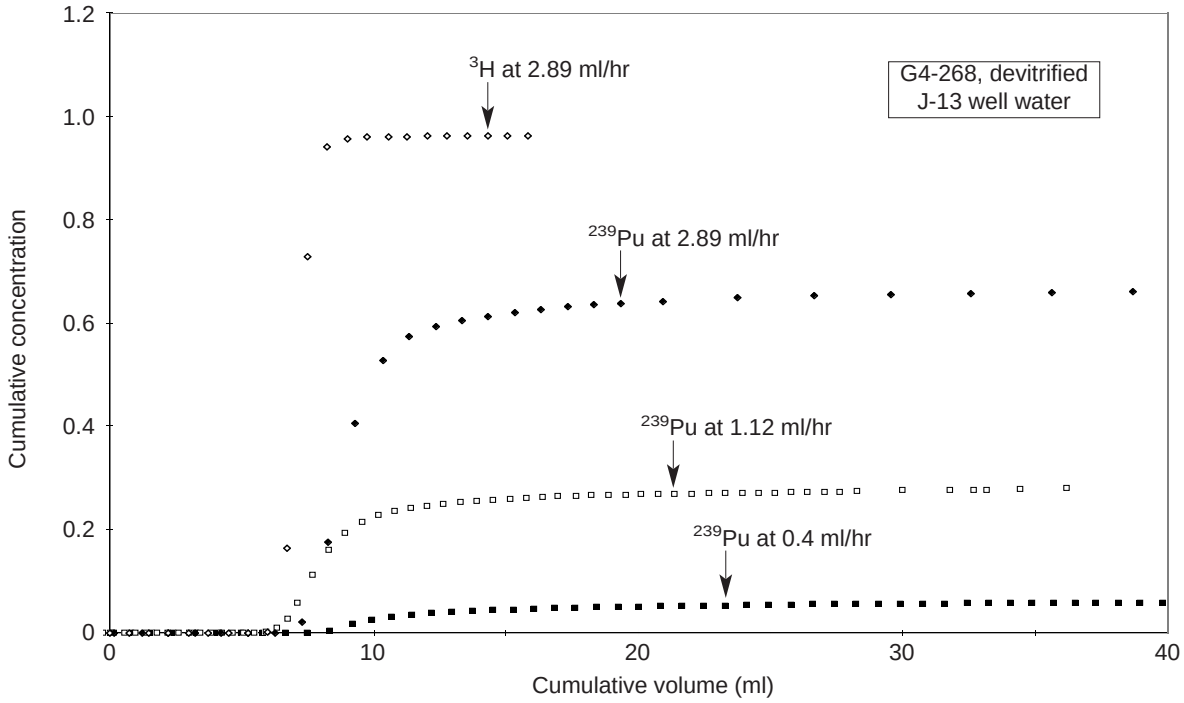

Figure 110. Plutonium in Devitrified Tuff at Various Flow Rates (J-13 Water). This plot shows elution curves for tritium and plutonium-239 at different flow rates with J-13 water through devitrified tuff G4-268.

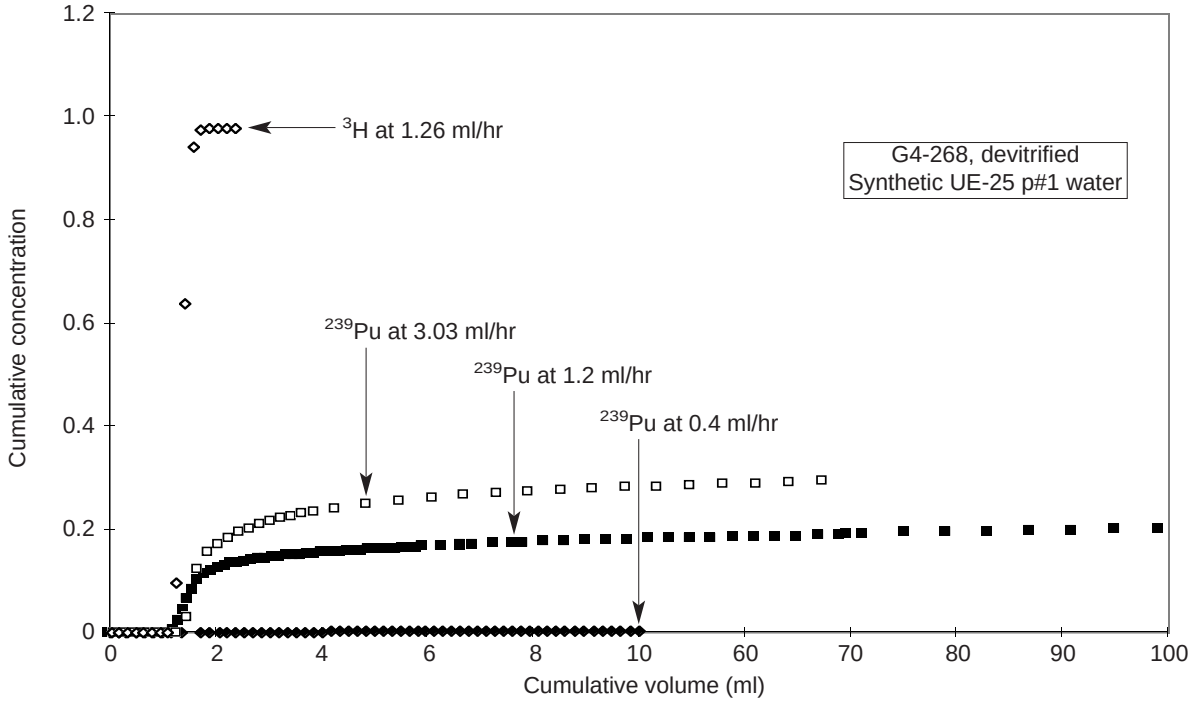

Figure 111. Plutonium in Devitrified Tuff at Various Flow Rates (UE-25 p#1). This plot shows elution curves for tritium and plutonium-239 at different flow rates in synthetic UE-25 p#1 water and tuff G4-268.

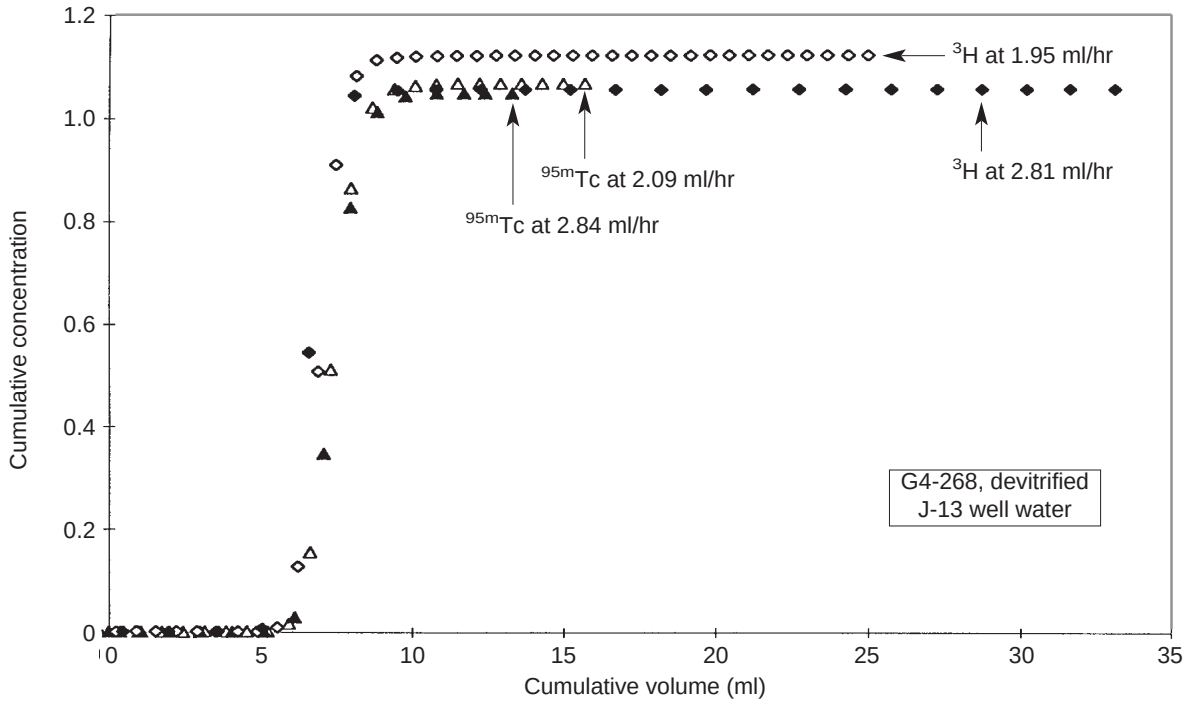

Figure 112. Technetium in Devitrified Tuff. This plot shows the elution curves for tritium and technetium-95m at different flow rates with J-13 well water through devitrified tuff sample G4-268.

continued from page 183

these columns are consistent with slow sorption kinetics.

The elution of pertechnetate was also studied in devitrified, vitric, and zeolitic tuffs in J-13 and synthetic UE-25 p#1 waters as a function of flow velocity. Inspection of the elution curves (Figs. 112 through 114) indicate that anion-exclusion effects for pertechnetate in crushed tuff are essentially negligible except in the case of technetium transport through zeolitic tuff in J-13 well water (Fig. 114). In this case, the anion-exclusion effect is small but measurable.

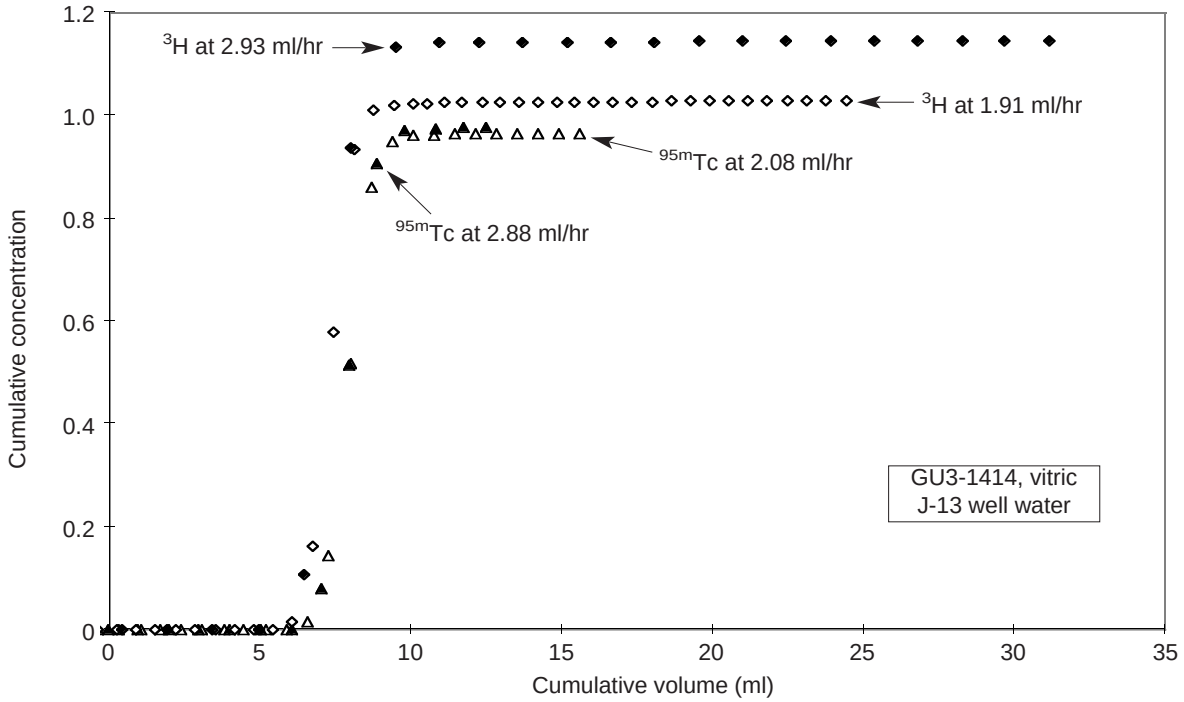

Figure 113. Technetium in Vitric Tuff. This plot shows the elution curves for tritium and technetium-95m at different flow rates with J-13 well water through vitric tuff sample GU3-1414.

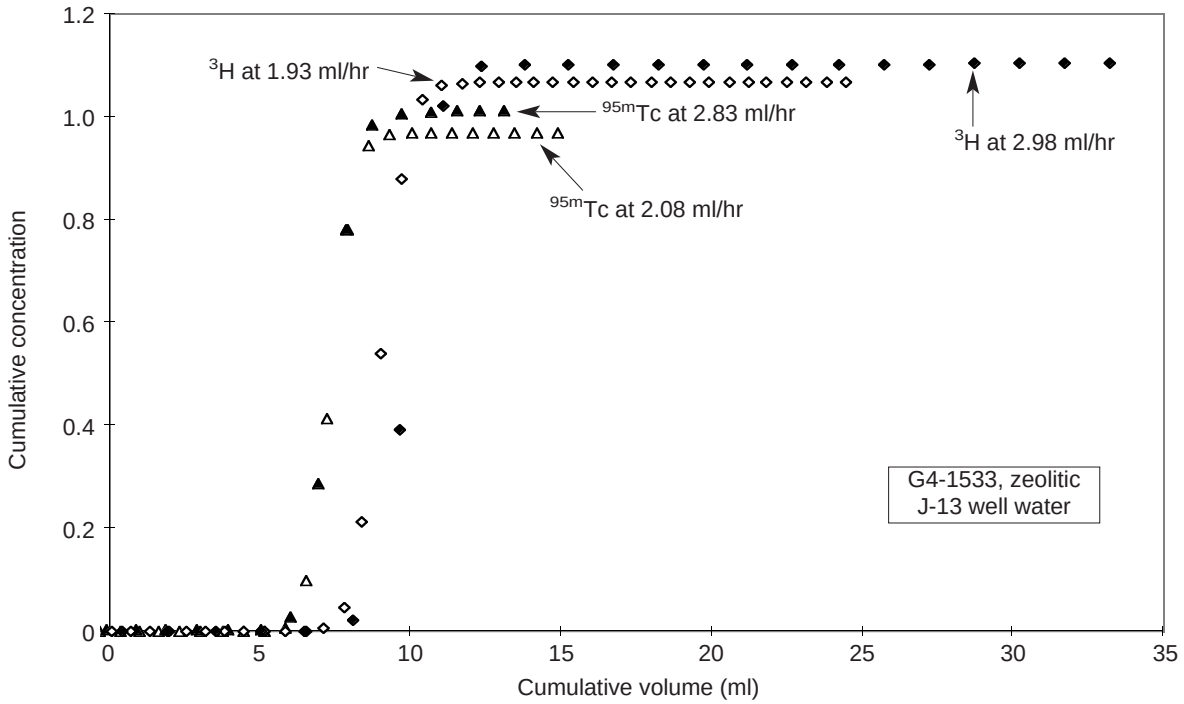

Figure 114. Technetium in Zeolitic Tuff. This plot shows the elution curves for tritium and technetium-95m at different flow rates with J-13 well water through zeolitic tuff sample G4-1533.

B. SOLID-ROCK COLUMNS

Direct measurements of transport parameters in actual subsurface materials under subsurface conditions are necessary for defensible modeling of contaminant transport in host rocks and engineered barriers surrounding nuclear and hazardous waste repositories. The hydraulic conductivity, K, and the retardation factor, R_f, along with the associated distribution coefficient, K_d, are poorly known transport parameters for real systems but are key input parameters to existing and developing contaminant release models. We experimentally determined unsaturated R_f and K for core samples of Yucca Mountain vitric-member tuff and zeolitic nonwelded tuff from G-Tunnel, Bed 5, with respect to J-13 well water with a selenium concentration (as selenite) of 1.31 mg/l (ppm) at 23ºC. Our intent was to demonstrate that a method in which flow is induced with an ultracentrifuge (the UFA™ method) could rapidly and directly measure R_f and K in whole-rock tuff cores and then to compare these directly measured unsaturated R_f values with those calculated from K_d values obtained through traditional batch tests on the same materials.

Methodology

Retardation

Retardation factors can be determined in flow experiments where R_f for a particular species is the ratio of the solution velocity to the species velocity. The retardation factor for that species is given by:

$$R_f = \frac{V_{gw}}{V_{sp}} = 1 + \rho_d \frac{K_d}{\epsilon} \quad , \qquad (89)$$

where V_{gw} is the velocity of carrier fluid, V_{sp} is the velocity of the species, ρ_d is the dry bulk density, ϵ is the porosity, and K_d is defined as the moles of the species per g of solid divided by the moles of the species per ml of solution. If none of a particular species is lost to the solid phase, then $K_d = 0$ and $R_f = 1$ for that species. In column experiments, a breakthrough curve is obtained for the particular species and R_f is determined as the pore volume at which the concentration of the species in the solution that has passed through the column is 50% of the initial concentration ($C/C_0 = 0.5$). It is now generally assumed that, for unsaturated systems, $\epsilon = \theta$, where θ is the volumetric water content (Bouwer 1991; Conca and Wright 1992a). The study described in this section experimentally addresses this concern under unsaturated conditions in whole rock and evaluates the use of data from batch experiments in determining R_f in whole rock.

We prepared solutions using J-13 well water with a selenite concentration of 1.31 ppm and determined the selenium concentrations with an inductively coupled, argon-plasma, atomic-emission spectrometer (Jarrell-Ash Model 976 Plasma Atomcomp). We used an ion chromatograph (Dionex Series 4000i) to determine the speciation of selenium in solution. All selenium in the starting and effluent solutions was found to exist as selenite.

Hydraulic conductivity

One way to drive fluid through rock is to use centripetal acceleration as the driving force. We used this approach with a new technology (UFA) to produce hydraulic steady-state, to control temperature, degree of saturation, and flow rates in all retardation experiments, and to measure the hydraulic conductivity. A specific advantage of this approach is that centripetal acceleration is a whole-body force similar to gravity that acts simultaneously over the entire system and independently of other driving forces, such as gravity or matrix suction. It has been shown that capillary bundle theory holds in the UFA method (Conca and Wright 1992a, 1992b).

The UFA instrument consists of an ultracentrifuge with a constant, ultralow flow-rate pump that provides fluid to the sample surface through a rotating seal assembly and microdispersal system (Fig. 115). Accelerations up to 20,000 g are attainable at temperatures from 220º to 150ºC and flow rates as low as 0.001 ml/hr. The effluent is collected in a transparent, volumetrically calibrated container at the bottom of the sample assembly. The effluent col-

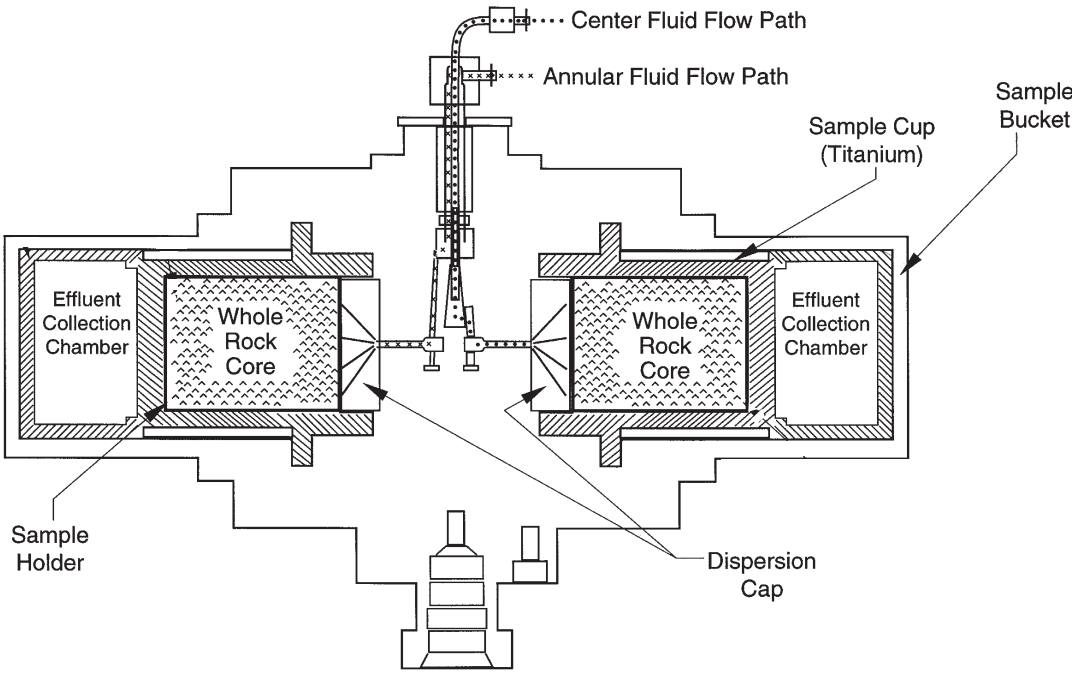

Figure 115. The UFA Method. This schematic of the UFA rotor is shown with paramagnetic seal and the large-sample options, a configuration that is optimal for adsorption and retardation studies.

lection chamber can be observed during centrifugation using a strobe light.

The current instrument has two different rotor sizes that hold up to 50 and 100 cm^3 of sample, respectively. Three different rotating-seal assemblies facilitate various applications and contaminant compatibilities; they are a face seal, a mechanical seal, and a paramagnetic seal. Figure 115 shows the large-sample option with the paramagnetic seal, a configuration that is optimal for adsorption and retardation studies.

Numerous studies have compared use of the UFA approach with traditional methods of doing this type of analysis in soils and clays, and the agreement is excellent (Conca and Wright 1992b; Nimmo et al. 1987). Good agreement is expected because the choice of driving force does not matter provided the system is Darcian (see next paragraph) and the sample is not adversely affected by a moderately high driving force ($\leq$ 1000 g for all samples run in these experiments); both of these provisions hold for most geologic systems. Additionally, all techniques for estimating hydraulic conductivity, $K(\theta)$, are extremely sensitive to the choice of the rock or soil residual water content, θ_r, and to the saturated hydraulic conductivity, K_s; minor variations in θ_r or K_s produce order-of-magnitude changes in $K(\theta)$ (Stephens and Rehfeldt 1985).

The UFA technology is effective because it allows the operator to set the variables in Darcy's Law, which can then be used to determine hydraulic conductivity. Under a centripetal acceleration in which water is driven by both the potential gradient, $d\psi/dr$, and the centrifugal force per unit volume, $\rho\omega^2 r$, Darcy's Law is

$$q = -K(\psi)\left[\frac{d\psi}{dr} - \rho\omega^2 r\right], \qquad (90)$$

where q is the flux density into the sample; K, the hydraulic conductivity, is a function of the matric

suction, ψ, and, therefore, of water content, θ; r is the radius from the axis of rotation; ρ is the fluid density; and ω is the rotation speed. When multicomponent and multiphase systems are present in the UFA instrument, each component reaches its own steady-state with respect to each phase, as occurs in the field. Appropriate values of rotation speed and flow rate into the sample are chosen to obtain desired values of flux density, water content, and hydraulic conductivity in the sample. Above speeds of about 300 rpm, depending upon the material and providing that sufficient flux density exists, $d\psi/dr \ll \rho\omega^2 r$. Under these conditions, Darcy's Law is given by $q = -K(\psi)\,[-\rho\omega^2 r]$. Rearranging the equation and expressing hydraulic conductivity as a function of water content, Darcy's Law becomes

$$K(\theta) = \frac{q}{\rho\omega^2 r} \quad . \qquad (91)$$

As an example, a whole-rock core of Topopah Spring Member tuff accelerated to 7500 rpm with a flow rate into the core of 2 ml/hr achieved hydraulic steady-state in 30 hours with a hydraulic conductivity of 8.3×10^{-9} cm/sec at a volumetric water content of 7.0%. Previous studies have verified the linear dependence of K on flux and the second-order dependence on rotation speed (Conca and Wright 1992a; Nimmo et al. 1987), and several comparisons between the UFA method and other techniques have shown excellent agreement (Conca and Wright 1992a, 1992b). Because the UFA method can directly and rapidly control the hydraulic conductivity, fluid content, temperature, and flow rates, other transport properties can then be measured as a function of fluid content by associated methods either inside or outside the UFA instrument during the overall run.

Fundamental physics issues involving flow in an acceleration field have been raised and successfully addressed by previous research and in numerous forums (Conca and Wright 1992a, 1992b; Nimmo et al. 1987; Nimmo and Akstin 1988; Nimmo and Mello 1991). These studies have shown, first, that compaction from acceleration is negligible for subsurface soils at or near their field densities. Bulk density in all samples remains constant because a whole-body acceleration does not produce high point pressures. A notable exception is surface soils, which can have unusually low bulk densities; special arrangements must be made to preserve their densities. Whole-rock cores are completely unaffected.

The studies have also shown that three-dimensional deviations of the driving force with position in the sample are less than a factor of 2, but moisture distribution is uniform to within 1% in homogeneous systems because water content depends only upon ψ, and unit gradient conditions are achieved in the UFA instrument in which $d\psi/dr = 0$. Hydraulic steady-state is not as sensitive to changes in rotation speed as to flux density. In heterogeneous samples or multicomponent systems such as rock, each component reaches its own hydraulic steady-state and water content, as occurs for such materials under natural conditions in the field. This last effect cannot be reproduced with pressure-driven techniques but only under a whole-body force field, such as with gravity columns or centrifugal methods. The ratio of flux to rotation speed is always kept high enough to maintain the condition of $d\psi/dr = 0$.

Results and Discussion for Vitric and Zeolitic Tuff

Column breakthrough test results

For these experiments, the rotation speed was set at 2,000 rpm with a flow rate into each sample of 0.2 ml/hr. The experiment was run for 9 days with an initial selenium concentration of 1.31 ppm. Figure 116 shows the breakthrough curves for selenite in the Yucca Mountain vitric member at 62.6% saturation and in the zeolitic nonwelded tuff at 52.8% saturation. The experiment was stopped before full breakthrough in the zeolitic nonwelded tuff, but the $C/C_o = 0.5$ point was reached. The retardation factor for each tuff sample is only 2.5, giving a K_d of 0.9 ml/g for the Yucca Mountain vitric-member tuff and 0.8 ml/g for the zeolitic nonwelded tuff.

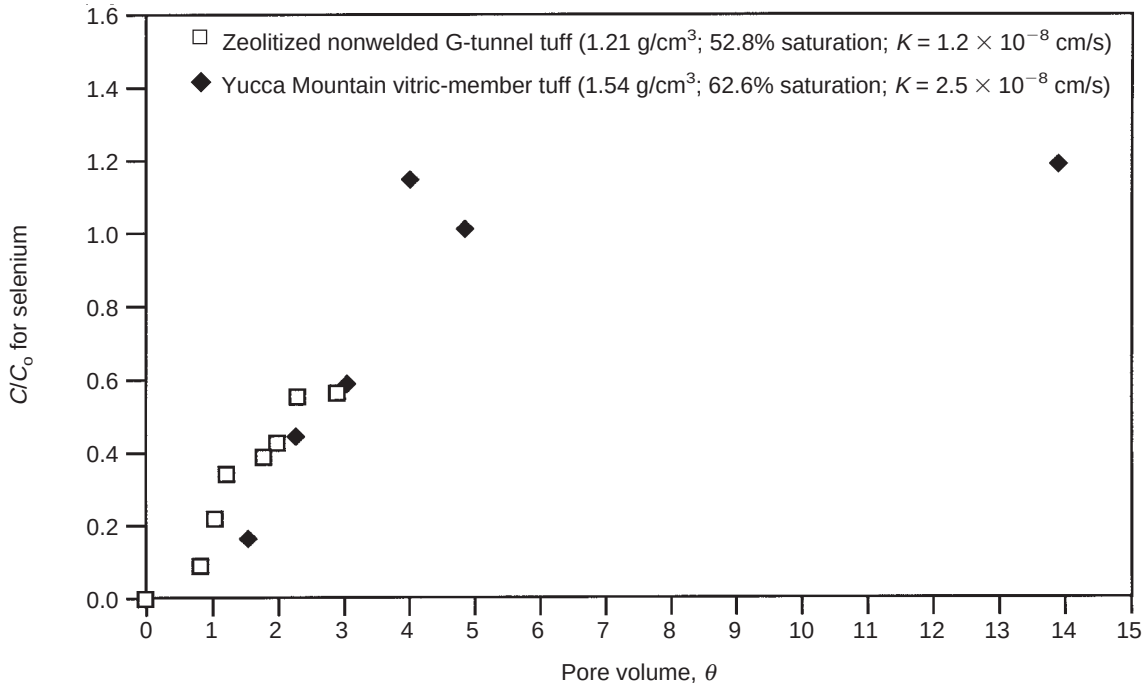

Figure 116. Breakthrough Curves. The UFA column data plotted here for a Yucca Mountain tuff retardation experiment show the breakthrough curves for selenium. The initial concentration, C_0, of selenium (as selenite) was 1.31 ppm in J-13 well water.

During these experiments, the unsaturated hydraulic conductivity, *K*, for each sample at these water contents was 2.5×10^{-8} cm/s for the Yucca Mountain vitric-member tuff and 1.2×10^{-8} cm/s for the zeolitic nonwelded tuff. Figure 117 gives the characteristic curves, $K(\theta)$, for these tuffs determined in separate experiments, as well as measurements for other tuffs and materials for comparison. As in most whole-rock cores studied (Conca and Wright 1992a, 1992b), the characteristic curves for the tuffs are steep, almost linear functions of the volumetric water content and are displaced according to the degree of welding and alteration.

Batch test results

We conducted batch-adsorption tests using the same J-13 well water with the slightly lower selenium concentration of 1.1 ppm and the same zeolitic nonwelded tuff from G-Tunnel, Bed 5, as in the UFA column breakthrough test. The batch-adsorption tests consist of crushing and wet-sieving the tuff, pretreating the tuff with J-13 water, placing the selenium solution in contact with the tuff, separating the phases by centrifugation, and determining the amount of selenium in each phase by difference using inductively coupled plasma mass spectrometry. Control samples were used to determine the sorption of selenium onto the walls of the sorption containers. The control procedure consisted of following the described batch-sorption procedure with a sample containing the selenium solution, except with no tuff added. The results of the control experiments indicate no loss of selenium due to precipitation or sorption onto the walls of the container during the batch-sorption experiment. The sorption distribution coefficients we obtained are given in Table 61. The Eh of all solutions, measured after the sorption experiments, varied from 140 to 150 mV.

The data presented in Table 61 and Fig. 117 indicate agreement between the column and the batch-

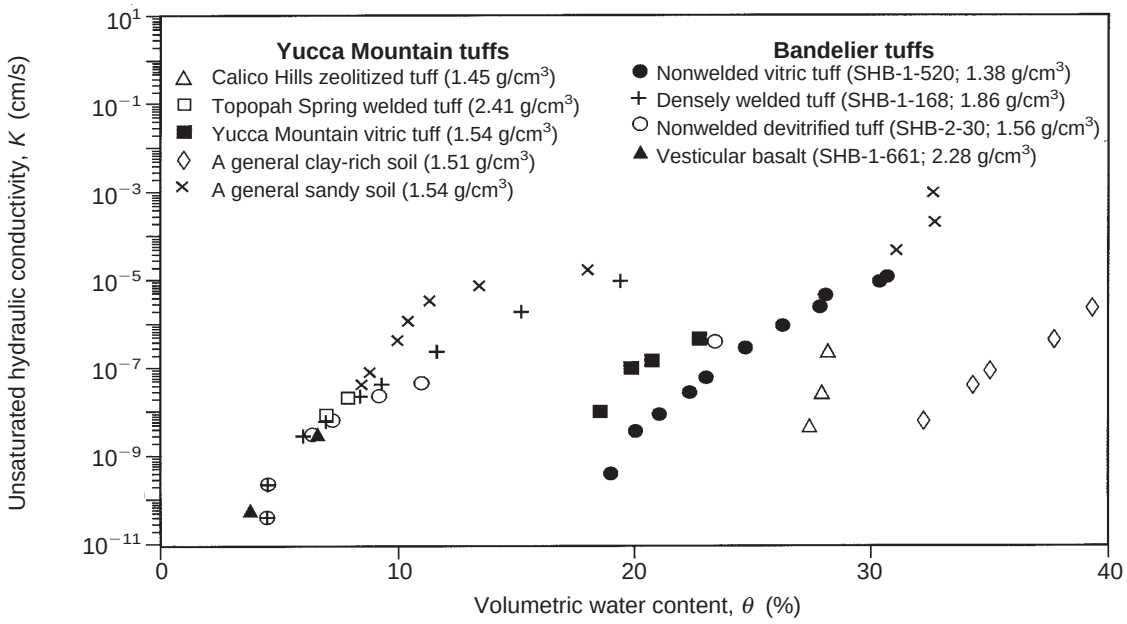

Figure 117. Unsaturated Hydraulic Conductivity. These UFA column data for various Yucca Mountain and Bandelier tuffs and other soil samples show the unsaturated hydraulic conductivity, *K*, as a function of volumetric water content, θ. The name and the density of each tuff is given in the legend.

sorption experiments. At a selenium concentration of ~1 ppm, no sorption of the selenium by the tuff is observed for the zeolitic tuff used in batch experiments, and minimal sorption (K_d of 0.8 ml/g) is observed for the zeolitic tuff used in the unsaturated column experiments. The method we used for the batch-sorption experiments to determine K_d values (by difference) involves subtracting the selenium concentration in solution after equilibration with the solid phase from the initial selenium concentration in solution. This method yields large scatter in the data when the batch-sorption distribution coefficient is small because two large numbers are subtracted to get a small number. Inspection of Table 61 also suggests that the kinetics of selenium sorption onto tuff are fast.

Table 61. Selenium Batch Adsorption on Nonwelded Zeolitic Tuff*

Pretreatment period (days)	Sorption period (days)	K_d (ml/g)
6.9	0.04	−0.2
6.9	0.04	0.3
6.8	13.9	0.0
6.8	13.9	0.2

*Experimental conditions: J-13 water; 20°C; 75-500 μm tuff particle sizes; 1.1 ppm initial selenium concentration; solution pH after sorption of 8.4; and samples from the same location in G-Tunnel, Bed-5, as the tuff used in the column experiments.

Conclusions

This study demonstrated the feasibility of using the UFA technology to rapidly and directly measure retardation factors and hydraulic conductivities in whole-rock cores of tuff under the unsaturated conditions that exist in the field. In UFA column breakthrough tests, the retardation factor for the selenite species was only 2.5 in both Yucca Mountain vitric member tuff at 62.6% saturation and zeolitic nonwelded tuff from G-tunnel at 52.8% saturation for a selenium concentration in

J-13 water of 1.31 ppm. In batch tests on the same material with an initial selenium concentration of 1.1 ppm, the average K_d was 0.08 $\pm$ 0.2 ml/g, which gives retardation factors that are slightly lower than those from the UFA column breakthrough experiments. This finding suggests that using batch-sorption coefficients to predict radionuclide transport through unsaturated tuff will yield conservative results.

Future experiments will use initial selenium concentrations smaller than the ones used in these experiments to further assess the validity of batch-sorption distribution coefficients to predict transport under unsaturated conditions. The unsaturated hydraulic conductivities during the experiments were 2.5×10^{-8} cm/s for the Yucca Mountain vitric-member tuff and 1.2×10^{-8} cm/s for the zeolitic nonwelded tuff.

C. RADIONUCLIDE TRANSPORT THROUGH FRACTURES

Yucca Mountain was chosen as a potential site for a high-level nuclear-waste repository because its geochemistry is believed to form both a physical as well as chemical barrier to radionuclide migration. However, the Yucca Mountain region has undergone significant deformation with the most recent tectonic activity occurring during the development of the Basin and Range geologic province and silicic volcanic activity. As a result of the tectonics and volcanism, many faults and fractures were produced within the tuffaceous units as well as the entire region. In addition, volcanic tuffs are often fractured as a result of cooling. The numerous fractures present at Yucca Mountain potentially represent a breach in the natural barrier, providing a fast pathway for contaminant migration.

Radionuclide transport calculations often assume that radionuclides can travel through fractures unimpeded; this assumption is too simplistic and leads to overconservative predictions of radionuclide releases to the accessible environment. The assumption ignores two main mechanisms by which retardation of radionuclides migrating through fractures can occur: diffusion of the radionuclides from the fractures into the rock matrix and sorption of radionuclides onto the minerals coating the fractures.

Minerals coating the fracture walls are generally different from the host-rock mineralogy due to a variety of factors ranging from precipitation of hydrothermal waters or meteoric waters to alteration of the pre-existing minerals. A review of the literature (Carlos 1985, 1987, 1989, 1990, 1994; Carlos et al. 1993) has provided a list of the minerals lining the fractures found at Yucca Mountain (Table 62; see the Appendix for detailed descriptions).

The transport of radionuclides through fractures from Yucca Mountain was examined to assess the retardation that can be provided by radionuclide diffusion into the matrix and sorption onto the minerals coating the Yucca Mountain fractures.

Experimental Procedures

Groundwaters

The groundwaters used for the experiments presented in this section were waters from Well J-13 (filtered through a 0.05-μm filter) and two sodium-bicarbonate buffers that simulated the water chemistry of the groundwaters from Wells J-13 and UE-25 p#1. We prepared the synthetic J-13 water by dissolving 0.03 g of Na_2CO_3 and 1.92 g of $NaHCO_3$ in 10 l of deionized water; the synthetic UE-25 p#1 water by dissolving 0.39 g of Na_2CO_3 and 8.90 g of $NaHCO_3$ in 10 l of deionized water. The reasons for having to use synthetic waters for the fracture-column experiments was the unavailability of water from Well UE-25 p#1 and the prevention of microbial activity in the columns.

Fractured-tuff samples

We used tuff samples with natural fractures from drill holes at Yucca Mountain chosen from the Yucca Mountain Project Sample Management Facility (SMF) in Mercury, Nevada. The tuff matrix of all samples consisted of devitrified tuff, and the minerals lining the fractures were stellerite, magnetite, hollandite, and romanechite. The sampling criteria were confined to 1) cores with natural fractures, determined by the presence of secondary mineral coatings, and 2) fractures with removable fracture walls that could be repositioned to their original orientation. Based on this criteria, we concluded that of the fractured-tuff cores selected (USW G1-1941, UE-25 UZ-16 919, USW G4-2981, and USW G4-2954) all consisted of natural fractures except G1-1941, the only core sample that did not have secondary minerals coating its fracture. The fracture in sample G1-1941 is apparently induced.

Radionuclide solutions

The radionuclide solutions used in the experiments (tritium, pertechnetate, and neptunium) were pre-

Table 62. Minerals Coating Fracture Walls in Yucca Mountain Tuffs

	Zeolites	
Heulandite ⟷ Clinoptilolite	$Ca_4Al_8Si_{28}O_{72}\cdot 24H_2O$ ⟷ $(Na, K)_6Al_6Si_{30}O_{72}\cdot 24H_2O$	
(range of compositions with arbitrary division of Si/Al $<$ 4.4 for heulandite and Si/Al $>$ 4.4 for clinoptilolite)		
Mordenite	$(Ca,Na_2,K_2)_4Al_8Si_{40}O_{96}\cdot 28H_2O$	
Analcime	$NaAlSi_2O_6\cdot H_2O$	
Chabazite	$CaAl_2Si_4O_{12}\cdot 6H_2O$	
Phillipsite	$(K_2,Na_2,Ca)Al_2Si_4O_{12}\cdot 4–5H_2O$	
Erionite	$(Ca,Na_2,K_2)_4Al_8Si_{28}O_{72}\cdot 27H_2O$	
Stellerite	$CaAl_2Si_7O_{18}\cdot 7H_2O$	
	Silica	
Quartz	SiO_2 — low-temperature polymorph of silica	
Tridymite	SiO_2 — high-temperature polymorph of silica	
Cristobalite	SiO_2 — highest-temperature polymorph of silica	
Opal	$SiO_2\cdot nH_2O$	
Feldspars		
Plagioclase (albite)	Solid solutions of albite ($NaAlSi_3O_8$) and anorthite ($CaAl_2Si_2O_8$)	
K-feldspar (sanidine)	Solid solutions of orthoclase ($KAlSi_3O_8$) and albite ($NaAlSi_3O_8$)	
	Clays	
Smectite family:		
Dioctahedral (montmorillonite)	$(Na,K,Mg_{0.5},Ca_{0.5},\text{possibly others})_{0.33}Al_{1.67}Mg_{0.33}Si_4O_{10}(OH)_2\cdot nH_2O$	
Trioctahedral (saponite)	$(Ca_{0.5},Na)_{0.33}(Mg,Fe)_3(Si_{3.67}Al_{0.33})O_{10}(OH)_2\cdot 4H_2O$	
Sepiolite	$Mg_4(Si_2O_5)_3(OH)_2\cdot 6H_2O$	
Palygorskite	$(Mg,Al)_2Si_4O_{10}(OH)\cdot 4H_2O$	
Illite	$(H_3O,K)_y(Al_4Fe_4Mg_4Mg_6)(Si_{8-y}Al_y)O_{20}(OH)_4$	
	Manganese oxides/hydroxides	
Pyrolusite	MnO_2	(1 $\times$ 1 tunnel structure)
Cryptomelane family:	$A_{0–2}(Mn^{4+},Mn^{3+})_8(O,OH)_{16}$	(2 $\times$ 2 tunnel structure)
Cryptomelane	A = K	
Hollandite	A = Ba	
Coronadite	A = Pb	
Romanechite	$(Ba,H_2O)_2Mn_5O_{10}$	(2 $\times$ 3 tunnel structure)
Todorokite	$(Na,Ca,Ba,Sr)_{0.3–0.7}(Mn,Mg,Al)_6O_{12}\cdot 3.2–4.5H_2O$	(3 $\times$ 3 tunnel structure)
Aurorite	$(Mn^{2+},Ag,Ca)Mn_3O_7\cdot 3H_2O$	
Lithiophorite	$m\{Al_{0.5}Li_{0.5}MnO_2(OH)_2\}\cdot n\{Al_{0.667}(Mn^{4+},Co,Ni,Mn^{2+})O_2(OH)_2\}\cdot pH_2O$	
Rancieite	$(Ca,Mn^{2+})(Mn^{4+})_4O_9\cdot 3H_2O$	
	Iron oxides/hydroxides	
Hematite	Fe_2O_3	
Magnetite	$(Fe,Mg)Fe_2O_4$	
	Carbonates	
Calcite	$CaCO_3$	
	Halides	
Fluorite	CaF_2	

pared in the same manner as for the crushed-tuff column experiments.

Fractured-column procedure

The experimental setup that we used for the fractured-tuff column is shown in Fig. 118 (the flow chart for the experiments is the same as for the crushed-tuff column experiments (Fig. 106), except the crushed-rock column is replaced with a fractured-tuff column). The fractured cores we chose for column experiments were cut with a rock saw perpendicular to the fracture to produce smooth ends. The fracture was secured with a hose clamp, and we measured and logged the dimensions of the fracture and the core for all samples.

We made round endcaps for the fracture columns from 1/2- to 1-inch flat Plexiglas™. The diameter of the endcaps was slightly larger than the core by approximately 1/8 inch to produce an overlip. We cored the endcaps within the overlip to a depth of 1/16 to 1/8 inch with the exact diameter of the rock core and then fitted them onto the core. We drew a trace of the fracture on the caps with a marking pen and, using a mill, cut 1/16-inch-deep troughs over the designated area. The purpose of the troughs was to induce equal dispersion of the tracer through the fracture at the time of the injection rather than creating a point injection. We also milled two areas (resembling opposing Ds) 1/8 inch outside both sides of the trough, 1/8 inch from the cored overlip, and with the same depth as the troughs.

Next, we drilled two 1/16-inch holes through the troughs of each endcap to act as the inlet and outlet flow ports for the columns. The top of each hole was redrilled to a depth of 1/4 inch and tapped to a 1/4-by-28 thread. We secured the endcaps to the fracture by placing a thin coating of Silastic™ within the overlip and the milled D-sections.

Silastic was also spread over all exposures of the rock core, including the fracture, and allowed to cure completely. We selected a tube of transparent Lucite™ with a diameter greater than that of the endcaps, and cut it to a length measured between the middle of both endcaps. A piece of Plexiglas, similar in thickness to the endcaps, was then cut in

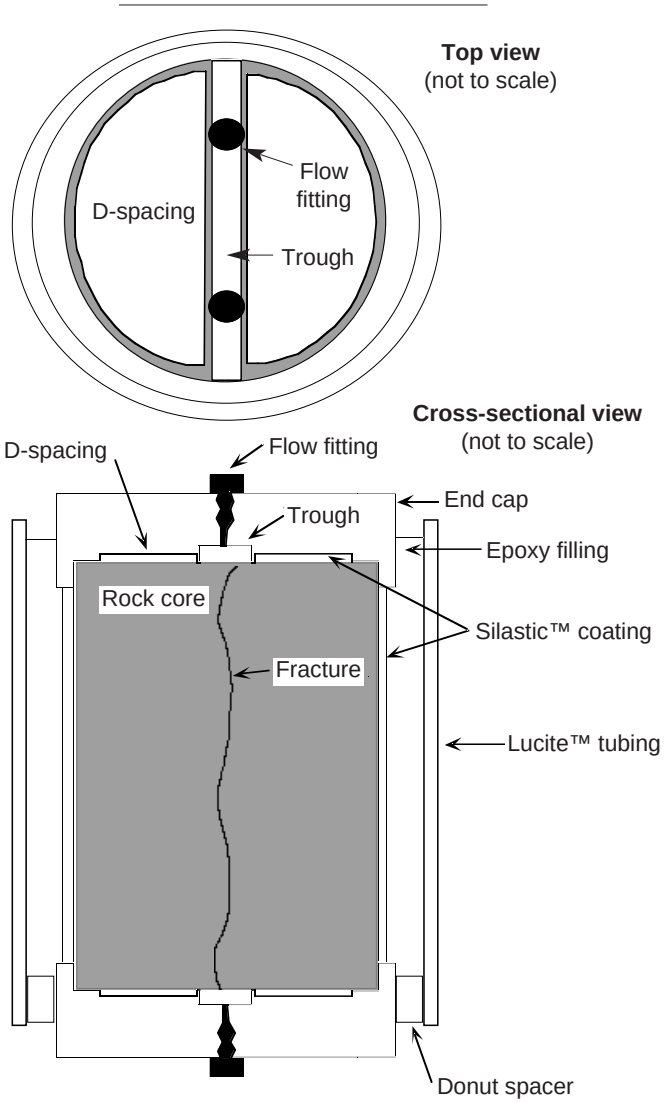

Figure 118. Fractured-column Setup. Top view (top) and cross-sectional view (bottom) of the column used in the fracture transport experiments.

donut form so that it would fit between the Lucite tube and the endcaps. The resulting donut spacer was then pressed and sealed with Silastic to one end of the fracture column. We poured epoxy into the top of the column through the gap from the Lucite tubing and the endcap until it almost overflowed the tube.

After all the epoxy cured, we flushed the column with carbon-dioxide gas for thirty minutes to facilitate removal of insoluble nitrogen gas. Then the column was submerged in a beaker containing either synthetic UE-25 p#1 or synthetic J-13 water. We subjected the beakers to a vacuum for a minimum of two weeks until all evacuating gas bubbles had ceased. After saturation, we connected the fracture columns, via one of the two outflow ports, to a syringe pump. The purpose of the second outflow port was to connect to a pressure transducer. We then set the columns onto ring stands so that tracer could be injected through the bottom. This setup was done so that if gas bubbles developed they would rest at the top of the column's trough and not against the fracture. A constant flow rate was established, and then we introduced a radionuclide tracer into the system through an injection valve. We collected the column elutions as a function of time and analyzed them, using our standard radiometric techniques, for the percentage of radionuclide tracer recovered. The aperture of the fractures has not yet been determined, but Table 63 gives the other characteristics of the four columns.

Batch-sorption experiments

For comparison with the fractured-column experiments, we conducted batch-sorption tests of neptu-

Table 63. Characteristics of Fractured Devitrified-tuff Columns

	Column #1	Column #2	Column #3	Column #4
Tuff type	G1-1941	UE-25 UZ-16 919	G4-2981	G4-2954
SMF number	N/A	0029365	0029366	0029368
Major minerals in tuff matrix	Alkali Feldspar and Quartz	Alkali Feldspar and Quartz	Alkali Feldspar and Opal CT	Alkali Feldspar and Opal CT
Minerals coating the fracture	None (apparent induced fracture)	Stellerite Magnetite	Hollandite Romanechite	Hollandite Romanechite
Water type	Synthetic J-13	Synthetic UE-25 p#1	Synthetic J-13	Synthetic J-13
pH	8.6	8.8	8.6	8.6
Concentration of ^{237}Np (M)	1.4×10^{-5}	4.8×10^{-6}	1.4×10^{-5}	1.4×10^{-5}
Length (cm)	12.6	6.1	6.0	To be determined
Diameter (cm)	6.1	5.2	5.2	To be determined
Fracture aperture	To be determined	To be determined	To be determined	To be determined
Porosity	To be determined	To be determined	To be determined	To be determined
Volumetric flow rate (ml/hr)	0.5	0.5	0.5	0.5

nium onto the fracture minerals stellerite, hollandite, romanechite, and magnetite. We did these tests under atmospheric conditions using J-13 well water with a Np(V) concentration of 6.7×10^{-7} M. The batch-sorption tests consisted of crushing and wet-sieving the minerals to a size of 75 to 500 μm, pretreating the minerals with J-13 water, placing the neptunium solution in contact with the minerals for a period of 3 days (using a solid to solution ratio of 1 g to 20 ml), separating the phases by centrifugation, and determining the amount of neptunium in each phase by difference using liquid scintillation counting. We used control samples to determine the sorption of neptunium onto the walls of the sorption containers. The control samples consisted of following the described batch-sorption procedure with a sample containing the neptunium solution only with no solid added. The results of the control experiments indicate no loss of neptunium due to precipitation or sorption onto the walls of the container during the batch-sorption experiment. The pH of the water in these experiments was approximately 8.5.

Results and Discussion

As discussed earlier, neptunium does not sorb onto devitrified tuff (for example, see Table 48, p. 126, or Triay et al. 1996a), which constitutes the matrix of all the fractures studied. Retardation during fracture flow occurs by diffusion of the radionuclides into the tuff matrix or by sorption of the radionuclides onto the minerals coating the fractures. Table 64 lists the results of batch-sorption experiments describing the sorption of neptunium onto natural minerals.

Although the extrapolation from these experiments to Yucca Mountain tuffs containing the same minerals is not immediate, the data of Table 64 show some important trends. Neptunium has a high affinity for hollandite and romanechite, whereas sorption onto the zeolite stellerite is not significant. If ion exchange is the main mechanism for neptunium sorption onto stellerite, changing the water from J-13 to UE-25 p#1 will only result in less sorption (due to the formation of a larger amount of the neptunyl carbonato complex and competitive effects as a result of the higher ionic strength in the UE-25 p#1 water). The sorption of neptunium onto magnetite does not appear to be significant either. As shown in Table 64, the magnetite sample we studied contains hematite and goethite, which could account for the entire observed sorption (Triay et al. 1996a).

Because no secondary minerals coating the fractures were observed for the G1-1941 fractured sample (column #1 of Table 63 and Fig. 119), it can be concluded that the retardation of neptunium observed for that column is due to diffusion into the matrix.

The total neptunium recovery of 70% in the UE-25 UZ-16 919 fractured sample (column #2 of Table 63 and Fig. 120) could be due to minimal sorption onto the stellerite and magnetite coating that fracture or due to diffusion into the matrix. It is important to note that in changing the water for this column from synthetic J-13 to synthetic UE-25 p#1, the speciation of neptunium changes from a mixture of neptunyl and carbonato complex to almost 100% carbonato complex (which can be excluded from tuff pores due to size and charge).

Neptunium seems to be significantly retarded even

Table 64. Batch-sorption Results for ^{237}Np in J-13 Well Water

Major mineral in solid phase	K_d (ml/g)	Solid-phase composition*
Stellerite	~ 0	N/A
Hollandite	700	100% Hollandite
Romanechite	600	N/A
Magnetite	7	85% Magnetite 12% Hematite 3% Goethite

*determined by x-ray-diffraction analysis

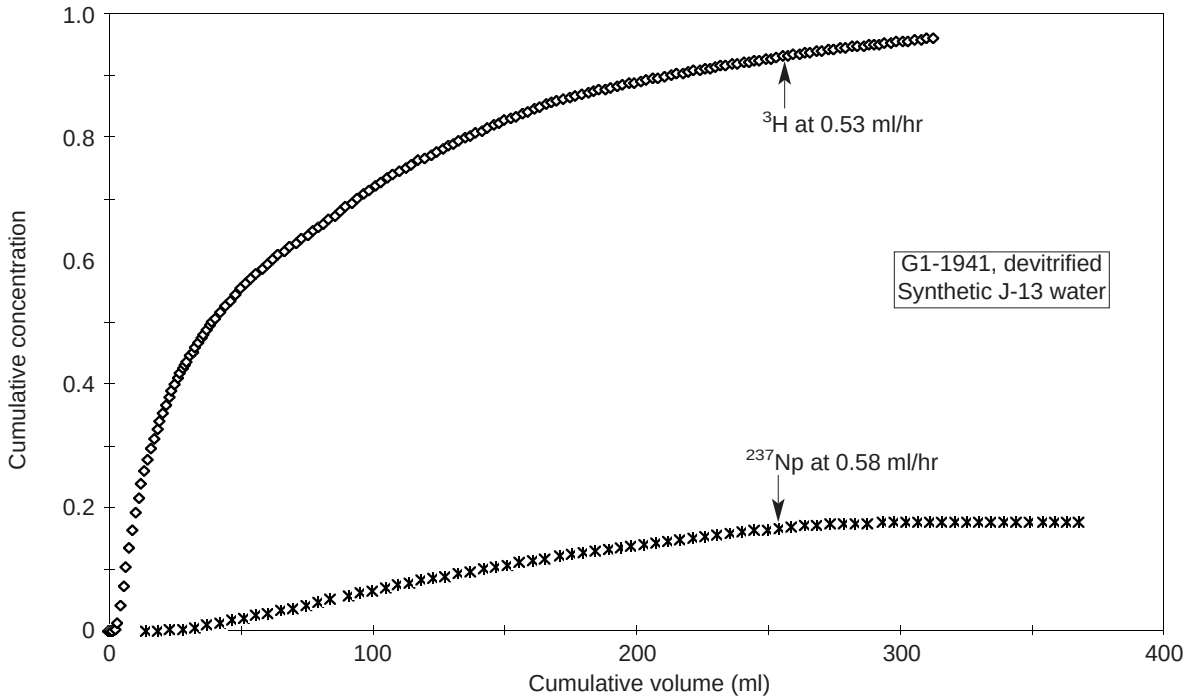

Figure 119. Neptunium in Fractured Tuff. This plot shows the elution curves for tritium and neptunium-237 in synthetic J-13 water through a fractured column of devitrified tuff sample G1-1941.

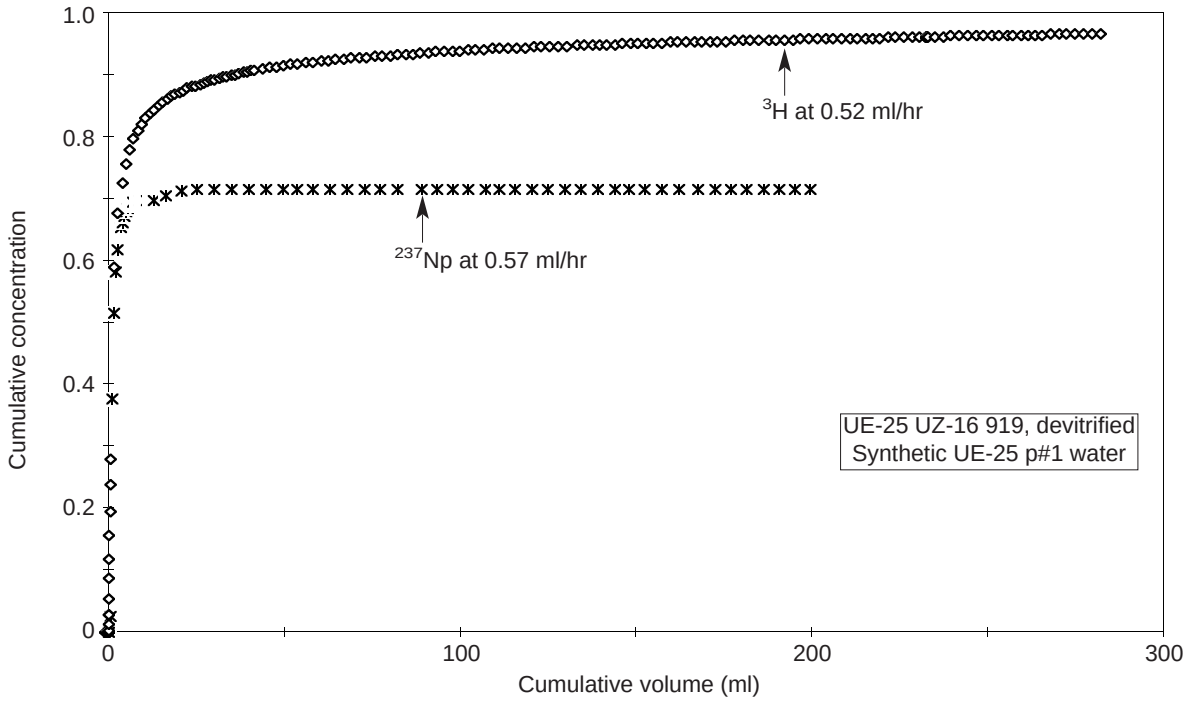

Figure 120. Neptunium in Fractured Tuff. This plot shows the elution curves for tritium and neptunium-237 in synthetic UE-25 p#1 water through a fractured column of devitrified tuff UE-25 UZ-16 919.

during fracture-flow in the G4-2981 fractured sample (Fig. 121) that is coated with hollandite and romanechite. The recovery of neptunium in this fracture is less than 10%, and its first appearance is delayed with respect to tritium and technetium.

Inspection of Figs. 121 and 122 (columns #3 and #4 of Table 63) indicates that diffusion from the fracture into the matrix has taken place because recovery of tritium was only 80% compared to 90% for technetium. This trend agrees with diffusion data that were previously obtained for ^{3}H and ^{95m}Tc in devitrified tuff and water from Well J-13. These data were fitted to the diffusion equation using the transport code TRACRN (Triay et al. 1993a), which yielded diffusion coefficients for saturated devitrified tuffs that were of the order of 10^{-6} cm^2/s for tritiated water and 10^{-7} cm^2/s for technetium. Thus, anion exclusion, in which the large pertechnetate anion is excluded from tuff pores due to its size and charge, has been previously observed.

Continuing with the explanation by de Marsily (1986, Chapter 10) of the fate of reactive and nonreactive solutes in porous and fractured media that we started in the earlier section on crushed-rock columns, we can expand the equation for a sorbing, nonreactive solute (Eqn. 85) to account for a solute that also undergoes radioactive decay:

$$\nabla \cdot (\mathbf{D}\,\nabla C - C\mathbf{U}) = \epsilon\left(\frac{\partial C}{\partial t} + \lambda C\right) + \rho_b\left(\frac{\partial F}{\partial t} + \lambda F\right), \qquad (92)$$

where λ is related to the half-life, $t_{1/2}$, of the decaying radionuclide by the relationship $\lambda = 0.693/t_{1/2}$.

As was pointed out earlier, the mechanism of sorption determines the relationship between F and C. If we substitute the linear, reversible, and instantaneous relationship for sorption, that is $F = K_d C$, then Eqn. 92 becomes

$$\nabla \cdot (\mathbf{D}\,\nabla C - C\mathbf{U}) = \epsilon\left(1 + \frac{\rho_b}{\epsilon}K_d\right)\left(\frac{\partial C}{\partial t} + \lambda C\right). \qquad (93)$$

The expression inside the first set of parentheses in Eqn. 93 is the retardation factor, R_f, which, of course, is only valid if sorption is linear, reversible, and instantaneous.

For radionuclide elution through fractures, two transport equations (like Eqn. 92) are considered, one for the porous medium and one for the fractured medium, each with its own Darcy's velocity and porosity (de Marsily 1986). The two transport equations for the porous and the fractured media can be coupled by a convection and a dispersion-exchange term.

The radionuclide elution data through fractured media was reduced and analyzed using the transport code FEHM and reported on by Robinson et al. (1995). Their analyses of neptunium-237 elution through fractured rock made it clear that the data are consistent with very large values of K_d, at least compared to the typical value of 2.5 for neptunium-237 on zeolitic tuff. They also felt it possible that minerals present in trace quantities in the bulk rock that appear to contribute insignificantly to sorption may be quite effective at retarding neptunium-237 transport when concentrated on fracture surfaces.

The most significant conclusion of the work presented here is that, contrary to previous assumptions about the role of fractures in radionuclide retardation, preliminary results from these experiments indicate that fracture flow does not necessarily result in a fast pathway for actinide migration through fractures. As can be seen in the experiments described above, the migration of actinides through fractures could be significantly retarded by sorption onto minerals coating the fractures and by diffusion into the tuff matrix.

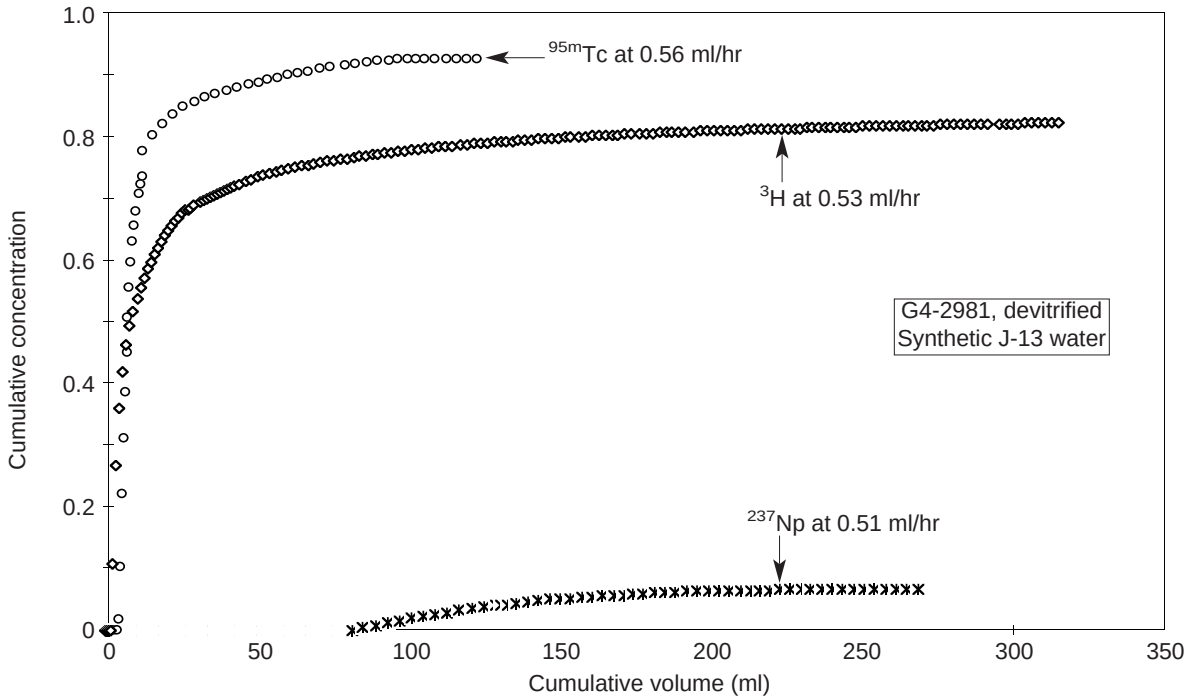

Figure 121. Neptunium and Technetium in Fractured Tuff. The plot shows elution curves for tritium, neptunium-237, and technetium-95m in synthetic J-13 water through a fractured column of tuff G4-2981.

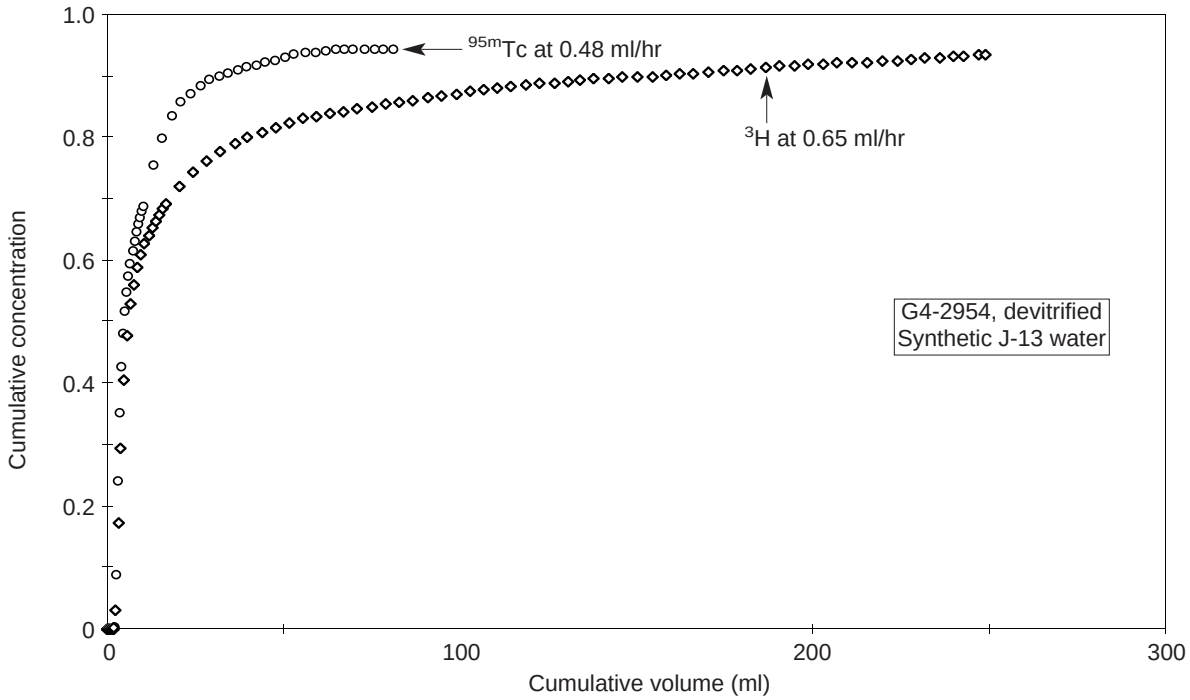

Figure 122. Technetium in Fractured Tuff. The plot shows elution curves for technetium-95m and tritium in synthetic J-13 water through a fractured column of devitrified tuff G4-2954.

D. COLLOID-FACILITATED RADIONUCLIDE TRANSPORT

The role of colloids in the transport of contaminants through the subsurface was reviewed by McCarthy and Zachara (1989). These authors concluded that the existing data suggest that colloidal species can enhance contaminant transport in the subsurface in the vadose and the saturated zones. McCarthy and Zachara also pointed out that the existing information is inadequate to assess the importance of colloid-facilitated transport or to develop a capability to predict contaminant migration that includes colloids. The work of McCarthy and Zachara identified several research needs: development of sampling techniques and predictive capabilities to determine the occurrence and properties of subsurface colloids, experiments and predictive transport models to assess the mobility of subsurface colloids, and data on the sorption of contaminants onto colloids to evaluate the implications of colloids for contaminant transport in the subsurface.

Ramsay (1988) reviewed the role of colloids in the release of radionuclides from a nuclear waste repository. He defines colloids as particles in the size range from 1 nm to 1 μm with large surface areas (on the order of 1000 m^2/g for the smallest particles). He points out that the role of colloids in migration involves many processes, such as enhancement of the source term by the leaching of the radionuclides in colloidal form from the waste form, degradation of the waste form (by bacterial action) to produce fine particulates, and sorption of radionuclides onto colloids present in the groundwater. Ramsay also points out that although it is clear that colloids exist, their significance in affecting radionuclide migration is not clear.

Ramsay's work describes three general cases for colloid-facilitated radionuclide migration based on colloidal charge. First, uncharged colloids (whose particle sizes are considerably smaller than the pore or fracture size of the medium) migrate without retardation. Second, charged colloids with the same sign as the surface charge of the medium are repelled by the medium walls, and there is a net increase in the flow velocity of the colloids. Third, the colloids and the medium surfaces have opposite charges, which can result in a slowing down of the colloids by their interaction with the medium.

There are two main categories of colloids in the subsurface in a nuclear waste repository: groundwater colloids and anthropogenic colloids. Groundwater colloids (Kim 1991) occur naturally in aquatic systems and consist of inorganic or organic molecular constituents or microorganisms. Anthropogenic colloids are colloids produced by physical, chemical, or biological processes acting on human-introduced materials. These include radioactive waste-derived colloids and colloids derived from other materials and activities related to waste isolation.

Radioactive waste-derived colloids include:

- degradation colloids generated directly from the waste form by disaggregation or spalling of actinide solid phases;
- precipitation colloids generated from solutions supersaturated with respect to actinide solid phases, including real actinide colloids produced by the agglomeration of hydrolyzed actinide ions, traditionally referred to as radiocolloids; and
- pseudocolloids generated by the attachment of radionuclides (in soluble or colloidal form) to other colloids (such as groundwater colloids).

The objectives of this section are to describe colloid transport models that can be used to assess the importance of colloid-facilitated radionuclide migration, summarize the observations of the existence of colloids from sampling studies and the evidence of colloid transport at the field scale, list the potential sources of colloids at Yucca Mountain, review the colloid transport experiments relevant to a potential nuclear waste repository at Yucca Mountain, and summarize the research questions that need to be answered to predict the role of

colloids in the release of radionuclides from a potential repository at Yucca Mountain.

Colloid Transport Calculations

The major processes that may occur during the migration of colloids in the subsurface are colloidal generation, sorption of radionuclides onto colloids in the groundwater, attachment/detachment of colloids, agglomeration of colloids in the groundwater, and exclusion of colloidal particles from pores due to size or surface-charge considerations. The limited applicability of filtration theory to describe particle transport through porous media has been discussed by McDowell-Boyer et al. (1986) who concluded that data were needed on particle retention, aggregate formation, permeability reduction, and the potential for erosion by changes in flow or solution chemistry before colloid transport through a natural aquifer could be predicted. Smith and Degueldre (1993) pointed out the limited applicability of filtration theory to describe colloid transport through fractured media in which colloid-wall interactions are important. Kessler and Hunt (1993) described the result of deposition and erosion of colloids in fractured media. They reported that colloids suspended in the water in fractures will deposit on fracture surfaces and partially or completely clog the fracture; the degree of clogging depends on whether deposited colloids can erode from the surfaces of the fractures. When the fracture remains only partially clogged, the unclogged portion becomes an open channel. Kessler and Hunt predict that for repository conditions (involving very low flow rates of $\sim$1 m/yr), erosion will not occur and the colloids will not travel very far because the fractures are expected to clog up completely with colloids.

The transport code CTCN (Colloid Transport Code–Nuclear) was developed within the Yucca Mountain Site Characterization Project for the study of colloid transport in porous and fractured media under unsaturated and saturated conditions (Jain 1991). The code was designed to solve both the unsteady-population-balance equations and the mass, energy, and momentum equations in up to four axes using the Method of Lines with Modified Gear Method to solve the population-balance equation. It is written in FORTRAN 77 and is capable of running on SUN, VAX, and CRAY systems. CTCN maintains a mass balance of the particles in the system and is capable of taking into account the likely colloid transport phenomena to describe migration of colloids through a natural medium. Most other colloid transport calculations (for example, Smith and Degueldre 1993) are performed with transport codes for soluble contaminant migration using parameters and boundary conditions that simulate the behavior of colloids.

Colloid-facilitated radionuclide transport was investigated in two dimensions for saturated and unsaturated fractures by Nuttall et al. (1991) using CTCN. A steady-state parabolic-flow-velocity profile was assumed for these calculations and a step input of colloids was used as a boundary condition to introduce particles into the fracture. The dynamic two-dimensional population-balance equation was solved numerically using CTCN. In the study by Nuttall et al., only the effects of capture and release mechanisms of the colloid transport model were studied. Agglomeration of colloids, pore size exclusion, particle growth, and size distributions were not taken into account in this work. The results of Nuttall et al. indicate that the diffusion rate of colloids in the direction perpendicular to the flow is an important parameter and the rate-controlling step for colloids diffusing to the fracture wall and being captured. The diffusion rate of colloids is approximately three orders of magnitude smaller than the diffusion rate for molecular species; consequently, colloids can transport long distances in fractures even with irreversible capture at the rock-water interface. Smaller particles are more likely to come in contact with the rock-water interface, but physical capture depends upon the electrokinetic and van der Waals forces. Nuttall et al. also report that for unsaturated conditions, hydrophobic colloids will preferentially collect at the air-water interface and transport at the highest water velocity.

Smith (1992) explored the influence of nonlinear sorption on colloid-facilitated radionuclide transport through fractured media. Smith and Degueldre (1993) also explored the result of different solute-colloid sorption mechanisms on radionuclide transport. Smith and Degueldre concluded that the assumption of fast, linear, and reversible radionuclide sorption onto colloids is nonconservative in the prediction of colloid-facilitated radionuclide transport. Smith and Degueldre's work suggests that the time for desorption (days or weeks) exceeds the time for sorption (seconds or minutes) in the radionuclide-colloid interactions. Consequently, it is important to determine the degree of completeness of desorption; irreversible sorption of the radionuclide onto the colloid may be present. If colloids migrate over long distances and are excluded from wall-rock pores due to their size, irreversible sorption would increase the rate of radionuclide transport in the subsurface. Smith and Degueldre concluded that for cases involving irreversible radionuclide-colloid sorption, the transport of radionuclides is strongly dependent on the extent of colloid interaction with the fractures.

Evidence of Colloids and Colloid Transport from Field Studies

Natural analog sites

Cigar Lake uranium deposit.

The colloids (< 1 μm) and particulate matter (> 1 μm) at the Cigar Lake uranium ore deposit in Canada were characterized by Vilks et al. (1988). The deposit is located at a depth of 400 m and has not been disturbed by mining operations or surface weathering. The ore is surrounded by a clay-rich zone containing iron hydroxides. The clay zone is surrounded by an altered sandstone separated from the surrounding unaltered sandstone by a silica-rich cap in which quartz has filled most of the fractures. Vilks et al. report that 1) the total particle concentration in groundwater at Cigar Lake ranges from 0.6 to 261 mg/l; 2) groundwater particles consist of clay minerals, iron-silicon precipitates, organics, rock particles, and drilling products; 3) the natural colloids and suspended particles in the groundwater at Cigar Lake contain significant amounts of uranium, thorium, and radium-226; 4) uranium dispersion has not been significant beyond the quartz cap; 5) there is no evidence of uranium migration away from the deposit; 6) radioactive colloid concentrations are low in the overlying sandstone and in the groundwater downgradient from the deposit; and 7) no significant migration of colloids and suspended particles away from the uranium ore deposit to the surrounding sandstone has occurred.

Koongarra uranium deposit.

Groundwater and particles from boreholes at the Koongarra uranium deposit in Northern Australia were characterized by Payne et al. (1992). The chemistry at Koongarra groundwaters is dominated by magnesium and bicarbonate, the pH is between 6 and 7.5, and the Eh ranges from 100 to 300 mV. The colloids (< 1 μm) and the particles (> 1 μm) in the Koongarra groundwaters include clay minerals and fine quartz grains. Iron was observed by Payne et al. as particle coating and as a separate colloidal form. They also report that 1) uranium migrates at Koongarra mostly as dissolved species; 2) thorium and actinium are mostly associated with immobile particles (> 1 μm); 3) of the small fraction of thorium that passes through a 1-μm filter, a large fraction is associated with colloids; 4) actinium appears to be more mobile than thorium and is associated with colloids to a greater extent, although in small concentrations; and 5) it is possible for trivalent and tetravalent actinides to migrate as colloids away from a nuclear waste repository.

Pocos de Caldas Plateau sites.

The characterization of suspended particles and colloids in waters from the Osamu Utsumi mine and Morro de Ferro analog sites at Pocos de Caldas, Brazil, was reported by Miekeley et al. (1991). These sites are located in the center of the Pocos de Calda Plateau. Uranium is mined by open-cast methods at Osamu Utsumi. Morro de Ferro is a thorium and rare-earth-element ore body that is 14 km from the Osamu Utsumi mine. The Morro de Ferro hill is 140 m above local stream

level and is in an advanced state of weathering.

The groundwaters at the Osamu Utsumi uranium mine are of the potassium-iron-sulfate type, oxidizing (values of Eh from 200 to 400 mV), and slightly acidic (values of pH from 5.4 to 6.1), the result of weathering of highly leached potassium-rich rocks. An upward groundwater flow gradient at the mine forces reducing water to ascend into more oxidizing environments. This process is responsible for the formation of ferric oxyhydrates in the suspended particles ($>$ 0.45 μm) and in the colloids (1.5 nm to 0.45 μm) in the groundwaters.

The Morro de Ferro ore body is in a much more advanced state of weathering than the mine. The ore body has very high concentrations of thorium and rare-earth elements in the soil and weathered rocks and a much lower concentration of uranium. Groundwater was sampled at several points downgradient from the ore body at Morro de Ferro. The gradient extends from strongly oxidizing (Eh from 450 to 650 mV) to a less oxidizing, unperturbed environment (Eh from 200 to 450 mV).

Concentrations of dissolved organic carbon in the groundwaters from the mine and the ore body range from 1 to 4 mg/l. In shallow waters (in the unsaturated zone) at the Morro de Ferro ore body, concentrations of 10 to 20 ppm of dissolved organic carbon were occasionally observed.

Miekeley et al. (1991) report that 1) a colloid concentration at the uranium mine and the ore body of less than 1 mg/l (consisting of Fe(III) oxyhydroxides and humic-like particles in the size range from 1.5 nm to 0.45 μm); 2) small amounts of uranium and other elements but significant amounts of thorium and rare-earth elements concentrated in the colloidal phases and suspended particles; 3) high concentrations of colloidal humic-like materials in surface and near-surface waters, which is the reason for the much higher concentrations and proportions of thorium and rare-earth elements in colloidal fractions of the organic-rich waters of Morro de Ferro; 4) solution and colloidal phases in equilibrium with respect to ^{234}U to ^{238}U isotopic ratios and identical rare-earth-element distribution patterns for these phases; 5) unfiltered groundwaters with low to moderate concentrations of suspended particles ($>$ 0.45 μm), that is, 0.2 to 0.4 mg/l for the mine and 1 to 5 mg/l for the ore body; and 6) no evidence of significant subsurface transport of suspended particles or colloids in either the Osamu Utsumi mine or the Morro de Ferro ore body.

Test sites and other areas

Gorleben area.

Colloids in groundwaters from the Gorleben area, the site for the future German repository, were characterized by Dearlove et al. (1991). The geohydrologic system at Gorleben comprises glacial sand-silt aquifers associated with a Zechstein salt diapir. Dearlove et al. report that 1) the colloid concentration in the Gorleben groundwaters is 10^{17} particles/l; 2) the bulk of the actinide and lanthanide elements in these groundwaters is associated with humic colloids; 3) the ^{234}U to ^{238}U ratio indicates that uranium in the colloidal fraction is not in equilibrium with the uranium in solution; 4) the colloids in the Gorleben aquifer are in the size range from 1.5 to 15 nm; and 5) the dissolved organic carbon in these groundwaters is composed of humic and fulvic acids. Kim (1991) reports that regardless of different redox fronts, plutonium and americium are always associated with colloids in the Gorleben groundwaters and that plutonium and americium pseudocolloids play an important role in the migration or retention of radionuclides in the subsurface.

Grimsel Test Site.

The characterization of colloids flowing in a fracture in the Grimsel Test Site was carried out by Degueldre et al. (1989a). The Grimsel Test Site is considered an example of a granitic-granodioritic far-field environment. The site is located in granite in the Swiss Alps about 1750 m above sea level and 450 m below land surface. A concentration of colloids of 10^{10} particles/l in the size range from 0.04 to 1 μm was found in the Grimsel Test Site groundwater. The particles are a mixture of silica

and organic material.

Whiteshell Research Area.
The Whiteshell Research Area is located in southern Manitoba, Canada, and is an example of fractured granite. Vilks et al. (1991) report that the upper 500 m of the geohydrologic systems at this site are connected by three major subhorizontal fracture zones partially interconnected at the surface by near-vertical fractures. At depths greater than 350 m, waters have a salinity between 1 and 15 g/l, a pH of 6.1 to 7.7, and are dominated by sodium, calcium, chloride, and sulfate. At shallower depths (50 to 350 m), the salinities of the waters range from 0.3 to 1.0 g/l, the pH ranges from 7.4 to 8.9, and the waters contain mainly sodium, bicarbonate, and to a lesser extent calcium. Both the shallow and deep waters are close to saturation with respect to calcite. Vilks et al. report that the average colloid concentration (in the size range from 10 nm to 0.45 μm) is 0.34 ± 0.34 mg/l and the suspended particle concentration is 1.3 ± 3.0 mg/l. Particles consist of aluminosilicates, carbonates, and iron oxides. Vilks et al. conclude that naturally occurring colloids (in the size range from 10 nm to 0.45 μm) will have a minimal effect on radionuclide transport, provided radionuclide sorption onto colloids is reversible. They point out that if radionuclide sorption onto colloids is irreversible, colloid-facilitated radionuclide transport may be important. If so, then information describing colloid concentrations, colloid stability, and the migration properties of colloids in granite fractures will become necessary.

El Berrocal site.
The El Berrocal experimental site is located 92 km southwest of Madrid (Gomez et al. 1992) in a fractured and weathered granitic formation. Uranium-bearing quartz dike/breccia intersects the excavated Berrocal site. Preliminary results indicate 1) the presence of particles in groundwaters at El Berrocal in the size range from 50 nm to 1 μm; 2) particles mainly consisting of silica, aluminosilicates, oxyhydroxides, and organic material; 3) dilute groundwaters that are slightly oxidizing to oxidizing (Eh of 4 to 379 mV); and 4) sulfide colloidal phases in the slightly oxidizing groundwaters.

Shallow aquifer in a semiarid region at Los Alamos.
Treated liquid wastes containing traces of plutonium and americium are released into Mortandad Canyon within Los Alamos National Laboratory boundaries (Penrose et al. 1990). The shallow alluvium of Mortandad Canyon is composed of sandy to silty clays formed by weathering of volcanic rocks. Penrose et al. observed detectable amounts of plutonium and americium in monitoring wells as far as 3390 m downgradient from the discharge even though Laboratory sorption studies predict that the movement of plutonium and americium will be limited to less than a few meters. Penrose et al. report that there is very strong evidence that plutonium and americium are associated with colloidal materials (in the size range from 25 nm to 0.45 μm) in a way that is effectively irreversible and that colloidal materials can be mobile for great distances.

Nevada Test Site and environs.
Kingston and Whitbeck (1991) characterized the colloids found in twenty-four springs and wells in central and southern Nevada in a region underlain by carbonate rocks. The majority of the sites are on or within 50 km of the Nevada Test Site; other sites are located near Hiko and Tonopah, Nevada.

Kingston and Whitbeck report particle concentrations in the following size ranges: 0.03 to 0.1 μm, 0.1 to 0.4 μm, 0.4 to 1 μm, and greater than 1 μm. They defined colloids as stable particles in suspension in the size range from 1 nm to 1 μm and then concluded the following: 1) Most of the groundwaters studied have colloid concentrations in the range from 0.28 to 1.35 mg/l. Three sites have high colloid concentrations that range from 6.48 to over 25 mg/l. 2) Colloid concentrations are similar regardless of hydrologic setting, aquifer lithology, or geographic location. 3) No obvious correlation exists between water chemistry and colloid concentrations in the waters studied. 4) Silica (but not

quartz) is present in all the colloids collected. Relatively small amounts of clay or zeolite are found in all samples. Calcite appeared in some samples but may be an artifact of the procedures used. The organic structures identified in the colloidal fractions are indicative of humic- or fulvic-acid coatings on the mineral colloid surfaces. 5) Their ubiquitous presence indicates that colloids travel successfully through the subsurface at the Nevada Test Site. Similar concentration distributions of sizes may indicate that groundwater flow at the Nevada Test Site is controlled by faults and fractures. 6) Silica colloids can sorb cesium, colbalt, and europium. Comparison of sorption distribution coefficients for colloids and tuff suggests that europium may preferentially sorb to the colloids rather than to the tuffaceous rocks of the Nevada Test Site.

Minai et al. (1992) isolated humic material from water from Well J-13. The carboxylate group concentration reported was 2.7 meq/g for the fulvic acid fraction and 4.6 meq/g for the humic acid fraction. Minai et al. report that their procedures to isolate the organic fraction were only able to recover 1 to 5 per cent of the total organic component in J-13 water. They based this information on work by other authors that report the total organic content in J-13 water to range from 0.15 to 0.54 ppm.

Field studies of radionuclide migration from underground nuclear tests at the Nevada Test Site have been carried out since 1974. Buddemeier and Hunt (1988) reported the transport of colloidal contaminants in groundwater away from the cavity of the Cheshire event, fired on February 14, 1976, with a yield in the 200 to 500 kiloton range. The Cheshire site is on Pahute Mesa. The nuclear test was performed at a depth of 1167 m in a formation consisting of fractured rhyolitic lavas. The pre-shot water level was at a depth of 630 m. Buddemeier and Hunt (1988) conducted filtration and ultrafiltration studies on groundwater samples from the seven-year old cavity of the Cheshire event and from the fractured lava and tuff formation 300 m downgradient from the cavity. Substantial concentrations of submicrometer colloids and significant radionuclide concentrations were found at both locations. A significant fraction of the radioactivity at both locations was associated with colloidal particles ranging in size down to 3 nm; lanthanide and transition-metal radionuclides were completely associated with particulates. Buddemeier and Hunt (1988) concluded that 1) a strong association exists between colloids and radionuclides and 2) both the dissolved and colloidal radionuclide species migrate through the interconnected fractures.

Detailed Colloid Analyses of J-13 Water at the Nevada Test Site

As pointed out earlier, Harrar et al. (1990) concluded that there is considerable justification for the use of Well J-13 water as a baseline, or reference, water for the Yucca Mountain Project investigations. Part of the justification is their conclusion that a major portion of the water produced by Well J-13 originates in the Topopah Spring Member of Paintbrush Tuff, the same stratigraphic unit as the one proposed for the repository. We used water from Well J-13 at the Nevada Test Site for particulate analysis. Comparison of the water chemistry data for Wells J-13 and UE-25 p#1 (Table 3 and Figs. 6 and 7 in Chapter I) indicates that determination of colloid concentration in water from Well J-13 would likely provide conservative estimates of the colloid concentration in Yucca Mountain groundwaters, given that colloid stability decreases with increasing groundwater ionic strength.

Water from Well J-13 has previously been used for particulate analysis, and the results have been reported by Ogard (1987). He diverted water from Well J-13 into a mobile laboratory at a rate of $\sim$1 l/min and used a prefilter to remove particles larger than 10 μm. He then filtered the water through a large stainless-steel filter assembly (One-Sevener Nucleopore Filter Assembly) loaded with seven 0.4-μm membrane filters mounted in parallel. Approximately half of the water filtered through this assembly subsequently passed through another filter system (Amicon Hollow Fiber Filter) that removed

particulates with diameters greater than ~5 nm. Thus, the particle size of the material caught by the 0.4-μm filter system should range from 0.4 to 10 μm, or 400 to 10,000 nm (large-size fraction), and the particle size of the material caught by the 5-nm filter system should range from 0.005 to 0.4 μm, or 5 to 400 nm (small-size fraction).

A filtration run conducted for 14 days yielded a sediment concentration for the large-size fraction of $\sim 2.7 \times 10^{-5}$ g/l, and a sediment concentration that was only 1 per cent of this value for the small-size fraction. The large-size particulate fraction was removed from the filter system with ultrasonic treatment, dissolved in acid, and analyzed for cation composition by emission spectroscopy. The weight percentages were silicon 60%, iron 20%, calcium 11%, and aluminum 4%. A similar analysis of the small-size particulate fraction, collected from the hollow-fiber system by backflushing with Nanopure water, yielded sodium 44%, silicon 42%, calcium 8%, and iron 4%. The iron-rich particulates are suspected to be the result of contamination from the steel piping and pumping systems used in the well.

Ogard (1987) assessed the importance of particulates in the transport of radionuclides at Yucca Mountain, basing his assessment on the particulate concentration in J-13 water that he reported ($\sim 2.7 \times 10^{-5}$ g/l for particles in the range from 0.4 to 10 μm) and reversible sorption of radionuclides onto colloidal species. Ogard concluded that the particulates in the J-13 well water would have to exhibit a sorption distribution coefficient greater than 4×10^{6} ml/g for a given radionuclide in order for pseudocolloids to contribute more than 10 per cent to the total amount of radionuclide migrating through Yucca Mountain. Ogard points out that sorption distribution coefficients of that magnitude have not been observed for the sorption of any radionuclide in the high-level waste onto tuff.

Particle size distribution in J-13 water

More recently, Los Alamos National Laboratory staff collected samples from Well J-13 to assess the particle size distribution in this water. The apparatus used for this effort (Fig. 123) incorporates serial filters of three different sizes to filter the water. Before and after each filtration (sample points A through D), water samples were obtained that ranged from unfiltered to highly filtered water (< 5 nm). The samples were collected in two different types of containers, borosilicate glass and Teflon™, and some were diluted with Nanopure water immediately after collection at a volume ratio of Nanopure water to J-13 well water of 3 to 1.

Collected samples were assigned bar codes SPC00503113 through SPC00503124 and sent to the Colloid Laboratory at the Paul Scherrer Institute (PSI) in Switzerland for analysis. All samples were collected in duplicate; upon receipt, one of each type of sample was acidified to a pH of 4. Sample traceability for this water collection is given in Yucca Mountain Project (YMP) Water Binder II, TWS-INC-11-93-08.

Colloid generation principles.

According to the theory of colloid generation, natural colloids are primarily generated by the physical fragmentation and erosion of components of the rock in contact with the water (Degueldre 1994). The colloid size distribution is continuous and may be described by a Pareto power law:

$$\frac{\mathrm{d}[coll]}{\mathrm{d}\phi} = A \cdot \phi^{-b} \ , \qquad (94)$$

where A and b are constants, ϕ is colloid size in terms of the unit size (here 1 nm), and $[coll]$ is the cumulative colloid concentration for size ϕ in particles/ml. When $b > 1$, the cumulative colloid concentration is given as follows for sizes ranging from $\phi_{\min}$, the smallest size analyzed, to $\phi_{\max}$, the largest size analyzed:

$$[coll] = \frac{A}{1-b}\left({\phi_{\min}}^{1-b} - {\phi_{\max}}^{1-b}\right). \quad (95)$$

Experimentally, an integrated colloid concentration, given by Eqn. 95, can be determined over a range from a low value of ϕ, such as the detection limit, to a maximum size, such as 1000 nm, above

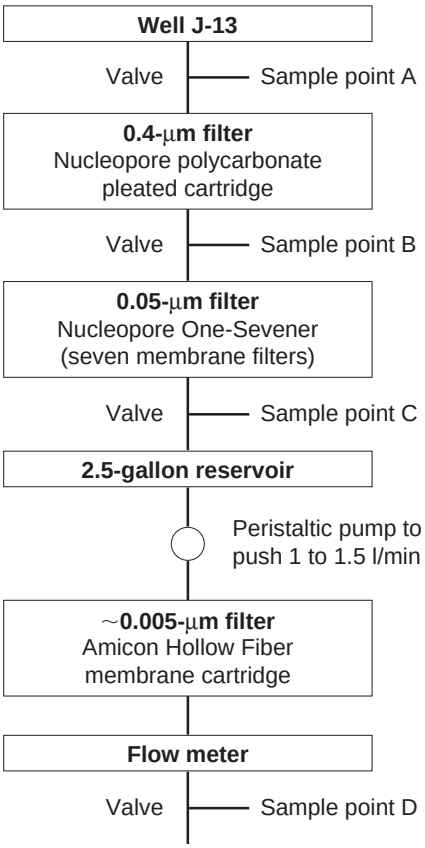

Figure 123. Colloid Sampling. Flow diagram of the colloid sampling apparatus at Well J-13.

---

which colloids are not found in significant concentrations. The integration constant is zero.

By assuming an average colloid density, ρ, and spherical colloids, determination of the colloid concentration (in terms of mass per unit volume) is possible using

$$\frac{\mathrm{d}\overline{[coll]}}{\mathrm{d}\phi} = \frac{\rho\pi\phi^3}{6} \cdot \frac{\mathrm{d}[coll]}{\mathrm{d}\phi} \quad , \qquad (96)$$

where $\overline{[coll]}$ may be expressed in μg/ml.

A surface-complexation capacity may be estimated assuming that the colloids are spherical. Two hypotheses for site distributions are suggested. One assumes that surface complexation occurs at the surface of the spherical colloids with an area site density, Δ, in sites/nm^2; the second considers the spherical colloids as nanoporous entities with a volume site density, Δ', in sites/nm^3. Both minimum and maximum capacities are evaluated using the following equations:

$$\left.\frac{\delta[site]}{\delta\phi}\right|_{\min} = \pi\phi^2\Delta\,\frac{\mathrm{d}[coll]}{\mathrm{d}\phi} \quad \text{and}$$
$$\left.\frac{\delta[site]}{\delta\phi}\right|_{\max} = \frac{\pi\phi^3}{6}\,\Delta'\,\frac{\mathrm{d}[coll]}{\mathrm{d}\phi} \quad . \qquad (97)$$

Analysis of colloid concentrations in J-13 water. At the Colloid Laboratory at the PSI, the colloid concentration in J-13 well water was determined by laser particle counting, a technique described previously (Degueldre 1994). After significant dilution in ultrapure water, the natural particles from the groundwater were counted with a 10-mW argon laser (Horiba PLC311) and analyzed with respect to size according to the intensity of scattered light that the particles produce in the unit laser beam. Information is displayed in a cumulative distribution:

$$[coll] = \int_{\phi_{\min}}^{\phi_{\max}} \frac{\mathrm{d}[coll]}{\mathrm{d}\phi}\mathrm{d}\phi \quad , \qquad (98)$$

where $\phi_{\min}$ and $\phi_{\max}$ are, respectively, the smallest and largest sizes analyzed.

To calculate the colloid concentration (either as particle concentration, $[coll]$, or as mass concentration, $\overline{[coll]}$) for a given size range and to calculate normal size distribution (either as $\mathrm{d}[coll]/\mathrm{d}\phi$ or as $\mathrm{d}\overline{[coll]}/\mathrm{d}\phi$), the results from these analyses were treated (by J. C. Loizeau at the University of Geneva) with the PSI code COLIAT (for colloid linear analytical treatment). Two COLIAT options, both based on Eqns. 94 to 96, are available. The first option considers A and b as constant over the size range; the second option considers A and b as a function of ϕ (although constant in the interval from ϕ to $\phi + \Delta\phi$). Both options assume that all colloids are spherical. Equation 96 relates the mass and particle concentrations of colloids for a size range

on the basis of colloid density. The resulting linear plot is conservative for the small colloids because, in principle, *b* decreases when colloid size decreases.

The following observations were made during the analysis of the J-13 well water:

- The concentration of colloids in the acidified samples was the same as the concentration of colloids in the unacidified samples. Thus, removing the water from the subsurface does not seem to cause precipitation of calcium carbonate or other solids that may change the amount of colloids measured in J-13 water.

- The concentration of colloids in samples placed in Teflon containers was smaller than in samples placed in glass containers, probably because of particle adsorption to the walls of the Teflon containers. Thus, a glass container seems to be better than a Teflon container for collecting water samples. A similar result was found during the Grimsel Colloid Exercise (Degueldre et al. 1990).

- The measured colloid concentration in the filtered samples was larger than in the unfiltered samples. Therefore, collecting water from the well itself without further filtration seems to be the best collection method because filters may add particles to the collected water.

Table 65 summarizes the concentration and characteristics of the colloids in the water from Well J-13 (assuming ρ = 2 g/ml). The Pareto power law (Eqn. 94) yields a value of 3.76 for *b* and a value of -3.2×10^{12} particles/ml for *A*. As suggested earlier by Degueldre (1994), when $b = 4$, colloids may have been generated by erosion, including, for example, rock multifragmentation. In natural media, however, specific attachment, nucleation, and aggregation may modify the values of *A* and *b*. In the case discussed earlier, when $b = 4$, no aggregation takes place; when $b < 4$, aggregation may have occurred.

There is good agreement between the earlier results obtained by Ogard and the results of this study. We found the concentration of colloids larger than 0.2 μm (200–1000 nm) to be 2.3×10^{-5} g/l, which agrees with Ogard's value of 2.7×10^{-5} g/l for the concentration of colloids larger than 0.4 μm.

Potential Sources of Colloids at Yucca Mountain

Moulin and Ouzounian (1992) pointed out that colloids and organic substances can affect the mobility of radionuclides as a result of complexation, sorption, and dissolution/precipitation. Radioactive waste-derived colloids are degradation colloids, precipitation colloids, and pseudocolloids.

Table 65. Concentration and Characteristics of Colloids in J-13 Well Water

Particle size (nm)	Number concentration (pt./ml)	Mass concentration (ng/ml)*	Minimum site concentration (nmoles/ml)**	Maximum site concentration (nmoles/ml)**
> 100	4.2×10^{6}	30.6	1.6×10^{-3}	7.6×10^{-2}
> 200	3.6×10^{5}	23.1	8.2×10^{-4}	5.8×10^{-2}
> 500	4.7×10^{4}	11.0	2.4×10^{-4}	2.7×10^{-2}

*The mass concentration was calculated for a size range of 100 to 1000, 200 to 1000, and 500 to 1000 nm, respectively, using an average colloid density of 2 g/ml.
**Site concentrations were calculated using site densities of 3 sites/nm^2 (minimum) and 3 sites/nm^3 (maximum).

Bates et al. (1993) studied the parameters that could affect the reactions of glass waste forms in an unsaturated environment with possible air exchange with adjacent biospheres (typical of what might be expected at Yucca Mountain). Buck et al. (1993) used analytical electron microscopy to study colloid generation from nuclear waste glass reactions. Buck et al. demonstrated that colloids are generated during waste glass dissolution and that the colloids generated often contain radioactive elements.

High-level waste glass in a nuclear waste repository may be contacted by water vapor, small amounts of sorbed liquid water, or flowing water (Bates et al. 1992). Bates et al. used a test method that involved dripping water onto a glass-metal assembly suspended in a vessel. Water collected in the bottom of the vessel was filtered to determine whether the actinides neptunium, plutonium, and americium were associated with particulates or dissolved in solution. They reported that 70 per cent of the neptunium passes through 1-nm filters and can be considered truly dissolved. Over 99 per cent of the plutonium and americium in the test groundwater is concentrated in colloidal particles that are fragments of a hydrated layer that spalls from the glass surface during aqueous alteration.

Feng et al. (1993) studied the colloids generated from the interaction of high-level nuclear waste glasses with groundwater at 90ºC. The tests consisted of immersing powder glass in water from Well J-13. The Teflon™ test vessel was then tightly sealed and placed in a 90ºC oven. After termination of a test, settling was allowed to occur at room temperature overnight. The resulting glass leachate was analyzed for colloids. Feng et al. concluded that waste glass contributes to the formation of colloids by 1) increasing ionic strength of the groundwater (which leads to nucleation), 2) releasing radionuclides that form pseudocolloids (by sorbing to groundwater colloids), and 3) spalling fragments of colloidal size from the surface layer of the reacted glass. They report that 1) the colloids found in the leachate are mainly silicon-rich smectites and uranium silicates; 2) colloids in the leachate agglomerate when the salt concentration is high but the agglomerated colloids can resuspend if dilution takes place; 3) colloids in the leachate agglomerate quickly after the leachate is cooled to room temperature, and most of the colloids settle out of the suspension after the leachate has been at ambient temperature for a few days; and 4) the colloids in the leachate are negatively charged between pH values of 1 and 10.5. Feng et al. inferred from these studies that 1) in a glass-reaction-dominated repository environment, where salt concentrations are likely to be high, the colloid concentration is likely to be low and the colloid transport of radionuclides will be minimal; 2) if a large amount of groundwater contacts the glass reaction site, the colloids that have settled out of suspension may resuspend and colloid transport may be important; and 3) at ambient temperatures, the colloids may agglomerate quickly and settle out of suspension in a short time.

Real Pu(IV) colloids, produced by the agglomeration of hydrolyzed Pu(IV) ions under acidic conditions have been reported by Hobart et al. (1989) and Triay et al. (1991a). Hobart et al. provided evidence that colloidal Pu(IV) is electrochemically reactive and structurally similar to plutonium oxide. Triay et al. reported stable Pu(IV) colloids under acidic conditions in the size range from ~1 nm to 0.4 μm. These Pu(IV) real colloids, generally referred to as Pu(IV) polymers, may not be stable at near-neutral pH values. In addition, the actinide colloids have a positive surface charge and would be expected to attach to tuffs at Yucca Mountain with negative surface charges. However, the formation of actinide pseudocolloids in groundwaters has been reported in numerous studies and reviewed by Kim (1991).

The existence and formation mechanisms of natural colloids at Yucca Mountain that may allow the generation of pseudocolloids at the potential repository have been studied by Levy (1992). Materials of potential interest include both gels that are still liquid-rich and former gels that have solidified and

crystallized. The materials studied by Levy include cores and sidewall samples from drill holes at Yucca Mountain and semitransparent fluid-gel samples from tunnel exposures at Rainier Mesa. Both Yucca Mountain and Rainier Mesa (40 km from Yucca Mountain) consist of ash-flow and bedded tuffs. Levy reports that diagenetic and hydrothermal alteration of volcanic glass are responsible for the genesis and deposition of gels at Yucca Mountain. The principal gel products at Yucca Mountain and Rainier Mesa were heulandite-clinoptilolite, silica minerals, and smectite. Given the heat generated by the potential repository (Buscheck and Nitao 1993) in devitrified Topopah Springs tuff, recharge water, or reflux water concentrated by the repository, Levy predicts that thermal effects may be sufficient to cause local alteration of glass in the underlying vitrophyre and colloid formation.

Kim (1991) pointed out the potential importance of microorganisms as colloids that can bind radionuclides and migrate through the subsurface. Bales et al. (1989) described the use of bacteriophage to study transport through sandy soil and fractured tuff. Bales et al. report that 1) virus particles can travel several meters in sandy aquifers, 2) the apparent exclusion from 35 to 40 per cent of the pore volume in a granular medium suggests that virus will travel 1.6 to 1.9 times faster than a conservative tracer, and 3) results from granular-medium and fractured-tuff experiments illustrate the inability of a soluble conservative tracer to provide estimates for the dispersion and effective porosity applicable to a colloid.

Choppin (1988) pointed out the importance of humic materials on metal-ion speciation and behavior in geologic systems at concentrations as low as 0.1 ppm. Minai et al. (1992) measured the binding constant of the humic- and fulvic-acid fractions in water from Well J-13 for Am(III); they report that these binding constants are similar to those of other aquatic materials. Based on a concentration in J-13 water of 0.01 to 0.1 ppm for total organic content, Minai et al. conclude that the americium-humate complex could be a significant species in J-13 water. Although Minai et al. did not measure any other actinide with the humic material from J-13 water, they extrapolated from other studies. Uranyl speciation would not be affected in J-13 water unless the total organic content is greater than 0.2 ppm. Minai et al. indicate that humic material at ppm levels reduces Pu(VI) and Pu(V) to Pu(IV); consequently, plutonium present in the V and VI oxidation states would be reduced to the IV state. If the Eh is low enough to allow formation of Pu(III), then plutonium speciation would be affected by humics in the same manner as Am(III).

Laboratory Experiments on Colloid Stability

To ascertain the conditions under which colloids would remain in suspension, we performed a series of laboratory aggregation experiments to determine the stability of colloids in synthetic and natural groundwaters as a function of groundwater chemistry. We used the results of our experiments to calculate particle-aggregation rate constants and to establish the stability of colloids. From the standpoint of colloid-facilitated transport to the accessible environment, only stable suspensions, suspensions that exhibit reversible aggregation, and suspensions that exhibit exponential aggregate growth at a comparable time scale as advective transport are of concern. Consequently, the stability of a particulate suspension is a question of the kinetics of aggregation as well as of the structure of the resulting aggregate.

For the stability investigations, we chose particles of kaolinite clay and amorphous silica because of their prevalence in the natural environment, their previous use in aggregation studies, and the requirement that particulate suspensions be made in a consistent and reproducible manner. Silica particles from the Nissan Chemical Co. were cleaned by repeated centrifugation, decanting, and resuspension in ultrafiltered deionized water until the conductivity of the particulate suspension was 40 μS/cm or less for three consecutive washings.

Kaolinite clay was acid washed and repeatedly cleaned (van Olphen 1977). The hydrodynamic mean diameter and particle-number concentration were 85 nm and 1.75×10^9 particles/ml, respectively, for the silica particles and was 200 nm and 1.59×10^9 particles/ml, respectively, for the kaolinite clay particles.

The chemical composition of the aqueous medium was designed to mimic groundwater compositions at Yucca Mountain (Kerrisk 1987). We prepared particle stock solutions by resuspending the sols in a carbonate-rich solution (0.368 mM Na_2CO_3 + 10.600 mM $NaHCO_3$) having a pH of 7.8. All experiments were performed at 27.5ºC. We induced aggregation by adding sufficient NaCl electrolyte solution to the prepared particulate suspensions to achieve a final NaCl concentration ranging from 100 to 800 mM. We ascribe observed differences in particle-aggregation rates to differences in solution chemistry (ionic strength) and particle composition.

We used autocorrelation photon spectroscopy (APS) to estimate the particle-aggregation rate constant for the early stages of the aggregation process. APS is sensitive to fluctuations in scattered intensity resulting from the Brownian motion of particles. The fluctuations in scattering intensity yield an intensity autocorrelation function in which the mean decay constant can be directly related to a mean diffusion coefficient (Ostrowsky 1988; Brown and Pusey 1975; and Amal et al. 1990). Particle size is related to the mean diffusion coefficient, D_{mean}, by the Stokes-Einstein relation:

$$D_{\text{mean}} = \frac{k_B T}{3\pi\eta\phi_{\text{mean}}} \quad , \qquad (99)$$

where k_B is Boltzmann's constant, T is the temperature in degrees Kelvin, η is the viscosity of the suspending liquid, and ϕ_{mean} is the hydrodynamic mean diameter of the particles. Because aggregate growth changes the particle size distribution over time, the rate of aggregation can be estimated using Eqn. 99 by determining the rate of decrease in the mean diffusion coefficient. The interpretation of diffusion coefficients, and consequently ϕ_{mean}, measured by APS is affected by polydispersivity, particle shape, and particle-particle interactions. In this study, we handled the effect of polydispersivity and particle shape on the autocorrelation function satisfactorily by preparing essentially monodispersed particle solutions, which allowed us to discard the higher-order terms of the cumulant method.

For a discrete particle size distribution, the generation of doublets by collisions of primary particles is represented by a second-order rate law (Stumm and Morgan 1981):

$$\frac{\partial[coll_I]}{\partial t} = -k_{II}[coll_I]^2 \quad , \qquad (100)$$

where k_{II} is the rate constant for doublet formation and $[coll_I]$ is the number concentration of primary particles. Aggregation rate constants, k_{II}, were calculated from the initial slope of a plot of ϕ_{mean} as a function of time, t, using

$$\phi_{\text{mean}} \cdot k_{II} = \frac{1}{F \cdot [coll_I]_{t=0}} \cdot \frac{\partial \phi_{\text{mean}}}{\partial t} \quad , \qquad (101)$$

where F is an optical factor and $[coll_I]_{t=0}$ is the initial number concentration of primary particles (Virden and Berg 1992). Because partial aggregation of the initial dispersion affects the analysis of the aggregation kinetics, we implemented a correction procedure to account for the initial size distribution of the aggregates. The correction was accomplished by projecting the slope of a plot of the function ϕ_{mean} to a time point where ϕ_{mean} corresponds to the initial (monodispersed) suspension.

APS measurements were made with a laser light-scattering system (Brookhaven Instruments) equipped with an argon laser (Innova 90) operating at λ = 514 nm and 0.5 to 1.0 W. Sampling times are dependent on particle concentration and ionic strength of the medium. Experimental run times for the aggregation experiments were typically 60 minutes (longer run times are necessary for highly stable colloids). Measurements of the hydrodynamic diameter, ϕ_{mean}, were made every minute

using a sampling duration of 30 seconds. All measurements were made at a scattering angle of 90°.

The experimental results (Figs 124 and 125) characterize the aggregation process of silica and kaolinite clay. Aggregation of silica particles and kaolinite clay particles decreased dramatically for an electrolyte concentration, C_{NaCl}, below 300 mM and 200 mM, respectively.

However, it is possible that reversible aggregation occurs in this concentration range if a secondary minimum, distinguished by the absence of a potential barrier in the potential curve, is present (Overbeek 1952). However, the duration of the current set of experiments was too short to resolve aggregate growth at this level of detail (Cametti et al. 1989). When the concentration of electrolyte is increased to induce aggregation, aggregate growth proceeds at an exponential rate, is irreversible, and the rate of aggregation increases with increasing electrolyte strength. The relationship between electrolyte strength and growth rate is evident for kaolinite clay particles at C_{NaCl} between 100 and 300 mM (as shown in Fig. 125). At high electrolyte concentrations, the rate of aggregation slows down abruptly after the initial rapid growth phase. The first stage of exponential growth is characterized by reaction-limited aggregation (RLA), and the second stage of the growth curve is characterized by diffusion-limited aggregation (DLA). The rapid and slow regimes of aggregation have been observed in various particulate systems, such as polystyrene, gold, and silica colloids (Cametti et al. 1989).

Aggregation rates are readily expressed in terms of stability, W, defined as the ratio between the Smoluchowski rate constant, k_{smol}, and the experimentally attained rate constant:

$$W = \frac{k_{smol}}{k_{II}} \quad , \qquad (102)$$

where W is a dimensionless parameter and k_{smol} is obtained from the Smoluchowski equation for doublet formation:

$$k_{smol} = \frac{8k_B T}{3\mu} \quad , \qquad (103)$$

where T is absolute temperature and μ is the dynamic suspension viscosity (Stumm and Morgan 1981). The effect of varying electrolyte concentration is shown in Fig. 126.

Kaolinite clay particles are destabilized at a lower electrolyte concentration than are silica particles. Also evident is the gradual increase in stability of the clay particles, compared with the abrupt transition from unstable to stable behavior exhibited by the silica particles. Kaolinite clay is characterized by the negative surface charge on the clay face, which is a result of isomorphic substitution and the electronegative character of the oxygen atoms, and by a positive charge on the mineral edges, which is a result of exposed cations. Thus, when the clay minerals are suspended in waters with low electrolyte concentration, collisions may produce aggregates having an open and porous structure. At higher electrolyte concentrations, the repulsive forces may be suppressed to allow aggregation into denser structures.

For slow aggregation processes, the time scale for aggregate rearrangement and consolidation is long compared with the time scale of collision, whereas for rapid or irreversible aggregation, rearrangement is less probable. If consolidation does take place, then aggregates having a uniform surface-charge distribution could form more compact and dense clusters during slow aggregation and more open clusters under fast aggregation. Consequently, colloid stability is a function of particle charge, surface-charge distribution, and aggregation kinetics (Lips and Duckworth 1988). The experimentally determined particle-aggregation constants may be used in transport models to assess the mobility of subsurface colloids along given flow paths as a function of groundwater chemistry.

Thompson (1989) studied the retardation of Pu(IV) real colloid (polymer) and Am(III) through columns made of crushed tuff from Yucca Mountain (in the grain size range from 75 to 500 μm).

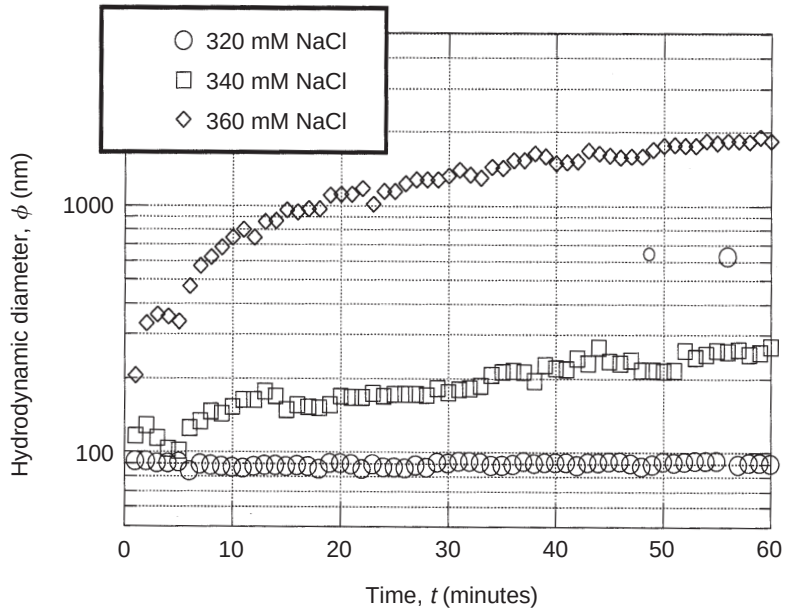

Figure 124. Aggregate Growth for Silica Particles. Here, ϕ_{mean} = 85 nm at t = 0, and the pH is 7.8. The flatness of the bottom curve (C_{NaCl} = 320 mM) indicates a steady-state condition with no aggregation; the middle curve (C_{NaCl} = 340 mM) shows reaction-limited aggregation (RLA); and the upper curve (C_{NaCl} = 360 mM) shows reaction-limited aggregation initially and diffusion-limited aggregation (DLA) later.

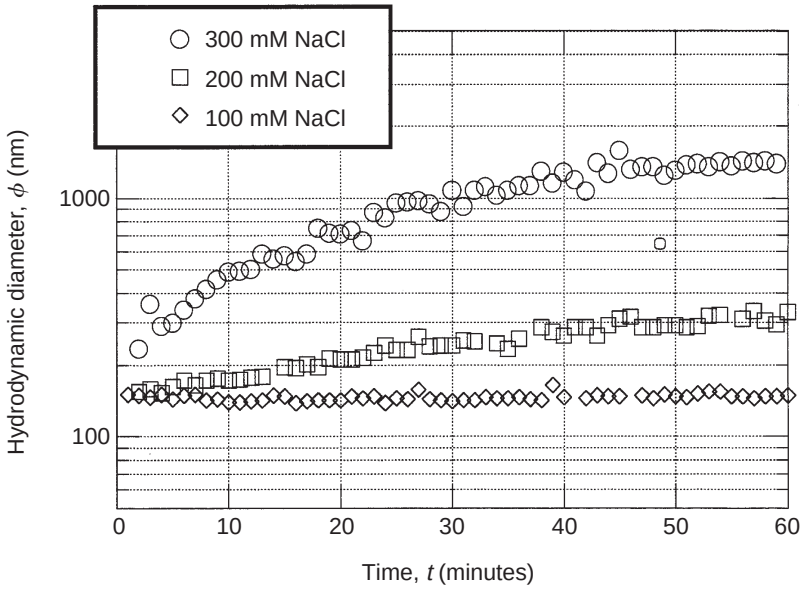

Figure 125. Aggregate Growth for Kaolinite Clay Particles. Here, $\phi_{mean} \sim$ 200 nm at t = 0, and the pH is 7.8. The lowest curve (C_{NaCl} = 100 mM) suggests a steady-state condition with no aggregation; the middle curve (C_{NaCl} = 200 mM) shows reaction-limited aggregation (RLA); and the upper curve (C_{NaCl} = 300 mM) shows reaction-limited aggregation initially and diffusion-limited aggregation (DLA) later.

The columns used for the study were 5 cm long and 0.45 cm in diameter with a porosity of 0.5 to 0.6. The interstitial velocity used for these studies was 150 m/yr. The Pu(IV) real colloid used by Thompson for these experiments ranged in size from 50 nm to 0.4 μm. Thompson reports that Pu(IV) real colloid and Am(III) are largely retained by the tuff, with a small fraction of the injected material moving through the columns faster than the tritiated water (used as the conservative tracer).

Rundberg et al. (1989) measured the migration of colloidal polystyrene tracers through a saturated fractured-tuff column. The fractured-tuff sample was an outcropping from Fran Ridge (near Yucca Mountain). The fractures in this sample were originally filled with calcite; after the fractured-tuff sample was encapsulated for tracer elution, the calcite was leached with dilute hydrochloric acid. Transport in this fracture sample was not describable using the cubic-law aperture determined from the fracture permeability. To fit the elution data for a conservative tracer, adjustment of the fracture aperture was required. Rundberg et al. (1989) report that polystyrene colloids with a ~1-μm diameter were found to have the lowest filtration coefficient, which is in qualitative agreement with the filtration model considered by Rundberg et al.

The relevance of these column studies for the prediction of colloid-facilitated radionuclide transport at Yucca Mountain is difficult to assess. Thompson's experiments were conducted with crushed tuff. The work of Rundberg et al. was conducted both by using fractures that were severely altered by the addition of dilute hydrochloric acid to dissolve the calcite fillings and by using colloids (such as polystyrene spheres) that are not representative of those at Yucca Mountain. The small scale of both sets of column experiments is

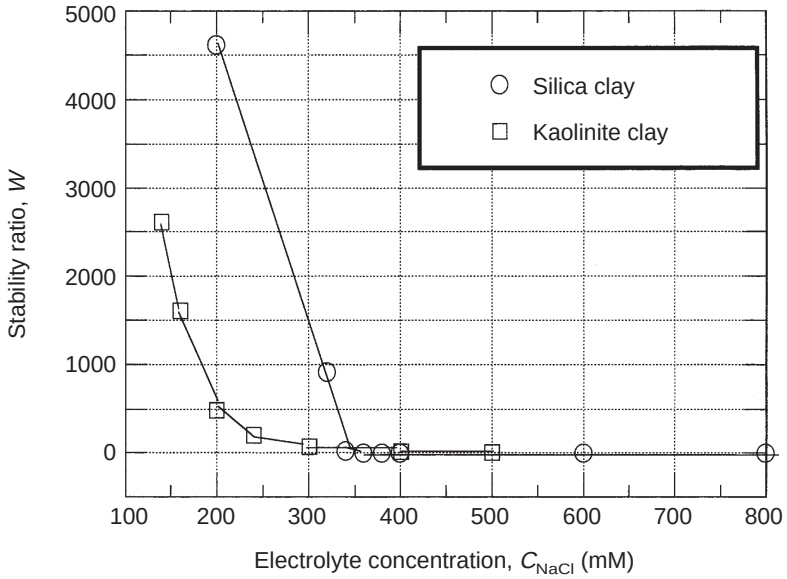

Figure 126. Stability Curves. The stability ratio, *W*, is shown for silica and kaolinite clay particles in synthetic groundwater at a pH of 7.8 as a function of sodium chloride electrolyte concentration, C_{NaCl}. The k_{smol} factor in the stability ratio ($W = k_{smol}/k_{II}$) remains constant with changing electrolyte concentration, but k_{II}, the kinetic rate factor for doublet formation, varies and, in fact, approaches k_{smol} in value as the electrolyte concentration increases. As a result, *W* approaches a minimum value of 1 at high electrolyte concentrations.

not comparable to the large scales available for colloid filtration at Yucca Mountain.

Future Direction of Colloid Studies in the Yucca Mountain Site Characterization Project

Degueldre (1993) presented a strategy to study the importance of colloid-facilitated radionuclide transport in granitic systems. This strategy was carefully considered in the development of the colloid strategy to assess the importance of colloid-facilitated radionuclide transport at Yucca Mountain. The strategy consists of asking the following:

1) Will radioactive waste-derived colloids be present at the potential repository?

2) Will these colloids be stable in the likely groundwaters?

3) Can these colloids migrate over field-scale distances?

Will radioactive waste-derived colloids be present at the potential repository?
In regard to first question, laboratory experiments similar to the ones being performed by Bates et al. (1992, 1993) will address the generation of degradation colloids from high-level waste glass forms. This type of study will provide a degradation-colloid concentration source term for the performance-assessment calculations for the potential repository that will include the actinide content of the degradation colloids.

The formation of colloids by natural glass alteration in a repository hydrothermal environment will be addressed by natural analog studies at Yucca Mountain. The natural hydrothermal alteration that occurred in the cooling pyroclastic deposits 12 to 13 million years ago may be a useful analog to a waste repository environment. Relict colloidal material has been identified among the alteration products in the glassy rocks below the potential repository.

The surface charge of radiocolloids (such as plutonium colloids) is positive; consequently, radiocolloids will attach to Yucca Mountain tuff, which has a negative surface charge at near-neutral pH values, and become immobilized. However, the formation of pseudocolloids from the sorption of real actinide colloids onto groundwater colloids is of concern. The generation and properties of real actinide colloids will be studied using the methods presented by Hobart et al. (1989) and Triay et al. (1991a).

Understanding the formation of pseudocolloids requires knowledge of the groundwater colloids at Yucca Mountain. To address the generation of groundwater colloids at Yucca Mountain, we will collect samples at selected sites in the vicinity of the potential repository block in an attempt to determine the types and amounts of inorganic colloids, high- and low-molecular-weight dissolved organic carbon compounds, and selected microorganisms present in saturated-zone groundwaters. Limitations on uses of the data derived from the samples will be a function of the extent to which samples represent the medium from which they are extracted. This point raises fundamental concerns about sample representativity and integrity.

We will collect samples from discrete intervals isolated by pneumatic packers, generally in uncased boreholes. Interval lengths likely will range between 2 and 20 m and will be selected based on borehole televiewer and caliper data. Borehole wall rugosity and fracture distribution and orientation will be primary factors used to determine packer locations. Rates of withdrawal from different intervals will range from about 0.5 to 2.0 l/min and will be selected to minimize horizontal shear velocities at the borehole wall in order to preclude or minimize detachment and entrainment of nonsuspended particles. Preliminary determination of velocity constraints will begin with information reported by Hunt (1982), Hubbe (1985a, 1985b), and Ryan (1988). We will construct the pump and isolation equipment within the borehole (packers, screens, and adjacent tubing) from stainless steel,

and the tubing used to transport samples up-hole to the mobile laboratory at the well head will be either nylon, polypropylene, or Teflon™. Our preparation will include efforts to preclude, minimize, or identify sampling-system effects on microbiologic samples.

Sample integrity will be influenced by the means used to collect and store raw samples and by the means used to isolate or concentrate colloidal phases. For example, microbiologic samples will be collected using aseptic procedures. The perceived options include centrifugation, filtration, and sedimentation, and it is assumed that pumping and isolation equipment do not deleteriously influence sample quality.

However, knowing that filtration methods can induce data artifacts (Rees 1990), we can use isolated-sequential filtration similar to that carried out by Ogard (1987) to preclude atmospheric influences and enable maintenance of sufficient pressure to satisfactorily prevent carbon-dioxide degassing with its attendant pH change. This method also is conducive to accumulating relative large masses of particles.

Tangential-flow filtration is a closed-system method that also can be used to process large volumes and yield particle concentration increases of at least two orders of magnitude. It is conceivable, however, that the recirculating tangential technique can disaggregate natural particles. An alternative to isolated sampling is an adaptation of the method developed by Degueldre and Thomi (1986) for pulsed diaultrafiltration under a controlled mixed-gas atmosphere, the carbon-dioxide partial pressure of which is determined using any of several geochemical codes.

We will measure particle properties quantitatively or qualitatively, as deemed appropriate, using one technique or a combination of several techniques. If feasible, either absolute inorganic colloid concentrations or size-range concentrations will be determined on site at selected intervals during pumping to provide transient information relative to representativity and to final representative concentration data. If this is not possible, periodic samples will be collected during pumping for subsequent separation and analysis. Particles as small as 1 nm can be filtered from discrete aliquots, counted, and size distributions measured using scanning (Degueldre et al. 1989a, 1989b) or transmission electron microscopy (Gschwend and Reynolds 1987; Ryan and Gschwend 1990) and attendant energy-dispersive spectroscopy or atomic-force microscopy (Emch et al. 1992; Zenhausern et al. 1992). Phases can also be identified by determination of bulk chemistry of filtered material and perhaps by x-ray diffraction analysis of particles of sufficient size.

We will measure the types and amounts of dissolved organic carbon contents of groundwaters, and the attendant high- and low-molecular-weight carbon fractions, represented generally as humic and fulvic acids.

We will study the sorption behavior of the actinides (plutonium, americium, uranium, and neptunium) onto the groundwater colloids to form pseudocolloids (Vilks and Degueldre 1991) to determine radionuclide distributions between the colloids and the groundwaters and to assess the reversibility of the sorption mechanism of radionuclides onto colloids. Spectroscopy studies will provide supplemental information by identifying the mechanisms of radionuclide sorption onto colloids. We will also study the formation of humic or fulvic pseudocolloids with the actinides in the organic fractions isolated from the saturated-zone colloidal fraction to assess the importance of actinide-humate or actinide-fulvate species. These various studies will yield groundwater colloid concentrations and the capacity of the colloids to carry radionuclides.

Will radioactive waste-derived colloids be stable in the likely groundwaters?

In regard to this second question, given the thermal loads being considered for the potential repository, elevated temperatures are expected in the

near field (Buscheck and Nitao 1993); consequently, colloids in the near field will not be stable. We will study the stability of degradation colloids as a function of temperature and likely water chemistries in the unsaturated zone using the colloids generated in the laboratory experiments to address colloid formation at the potential repository (Bates et al. 1992, 1993). We will study the stability of radiocolloids, groundwater colloids (silica, zeolites, and clays), and pseudocolloids as a function of unsaturated- and saturated-zone water chemistry and temperature. The studies will incorporate a range of calcium concentrations representative of the Yucca Mountain vicinity. Degueldre (1993) was able to correlate the concentrations of colloids in different granitic systems with the calcium concentration of the groundwater at those sites. Even though Kingston and Whitbeck (1991) did not find any correlation of the colloid concentrations at the Nevada Test Site with the groundwater chemistry, it is possible that the correlation exists and that the data of Kingston and Whitbeck is the result of particulate contamination during sampling.

Can radioactive waste-derived colloids migrate over field-scale distances without being removed by filtration?

We will address the mobility of the colloids through the medium at Yucca Mountain by conducting transport experiments. Laboratory-scale column experiments that involve the elution of well-characterized colloids (such as polystyrene spheres), degradation colloids, radiocolloids, and pseudocolloids through porous and fractured-tuff columns will be used to validate a transport code capable of describing colloid transport (such as the FEHM or CTCN codes). These studies will yield attachment/detachment parameters for colloids migrating through tuff that can be used in performance-assessment calculations.

We will perform experiments in which colloids are eluted through a large lysimeter filled with porous media and blocks ($\sim$1 m^3) of fractured tuff. Such experiments will address the gap between laboratory and field scales.

We will study field-scale colloid transport in unsaturated, fractured tuff (Hunt 1993). Hunt's proposal for such a study involves weapons tests at the Nevada Test Site, which could provide a worst-case scenario by evaluating whether or not radionuclides have leached beneath a weapons test that was fired above the water table. Hunt points out that a nuclear weapons test is similar to a high-level nuclear waste repository. A weapons test emplaces long-lived radionuclides within a fractured formation and within molten glass. The heat gradually diffuses away, and water enters the test cavity (first as a vapor and then as a condensed liquid partially coating the surfaces). This water would promote glass and mineral weathering. The weapons test can also produce a surface crater that will act as a collection point for precipitation and accelerate infiltration. Hunt proposes the use of a test site in which 1) the weapons cavity is at least 100 m above the water table (so that enough unsaturated-zone space exists beneath the cavity to carry out an adequate study), 2) the nuclear weapons test has produced a surface depression that would accelerate and concentrate water infiltration, and 3) the test should have occurred at least 10 years ago to allow for heat dissipation and water infiltration. Sampling the rock around and beneath this test would provide data that represents a worst-case scenario for Yucca Mountain—that is, an unpackaged waste-containing glass subjected to water and infiltration through partially saturated freshly-fractured tuff.

We will study field-scale colloid transport in the saturated zone by injecting polystyrene microspheres during cross-hole hydraulic testing at a well complex at Yucca Mountain (C-Wells). This effort will provide an opportunity to study colloid transport through saturated, fractured tuff and will simulate a scenario involving formation of pseudocolloids that reach the groundwater table at Yucca Mountain. The idea of the C-Wells field experiments is to inject various tracers (including well-characterized colloids) into the saturated zone via

an injection well and then observe the appearance of these tracers in sampling wells at downgradient locations.

The field experiments will allow the validation of a transport code to predict colloid transport through fractured tuff at large scales. If validation results are satisfactory, this code can then be used to perform sensitivity analyses that would identify the information that needs to be considered in a performance assessment to address the importance of colloid-facilitated radionuclide transport from the potential repository at Yucca Mountain.

In summary, the currently available information on colloid transport is not sufficient to conclude that colloids will not be able to carry radionuclides from a repository to the accessible environment at Yucca Mountain. In order for colloids to facilitate radionuclide transport at Yucca Mountain, they must be present in stable suspensions in sufficient quantities, the radionuclides must be associated with the colloids, and the colloids must be transported over field-scale distances. Consequently, the strategy developed above addresses these three main issues, which are critical to assessing the importance of colloid-facilitated radionuclide transport at a nuclear waste repository.

Conclusions and Summary of Data Needs for Colloid Investigations

A sensitivity analysis study to assess important parameters for colloid-facilitated radionuclide transport can be performed. The following assumptions could be made for this calculation.

1) The colloids generated are clays, silica, and iron oxides.

2) The amount of total organic carbon (TOC) in groundwaters is negligible.

3) The stability ratio of the colloids can be estimated on the basis of the data observed for model colloids.

4) The sorption of radionuclides onto colloids (K_p) can be calculated on the basis of available values of sorption distribution coefficients (K_d) (or on the basis of K_p values from the literature: $\sim 3 \times 10^4$ ml/g for the trivalent and tetravalent actinide species).

5) Irreversible sorption of radionuclides onto colloids occurs.

6) No attachment of colloids onto fracture walls occurs.

7) Colloids are excluded from tuff pores by their size and charge.

Depending on what parameters are the most important in controlling colloid-facilitated radionuclide transport, the following data needs may exist:

- experimental determination of type of colloids generated from spent fuel (to address assumption 1);

- study of Yucca Mountain as its own analog (to address assumption 1);

- experimental determination of total organic carbon (TOC) in groundwaters on-line (to address assumption 2);

- experimental determination of colloid population and size distributions in groundwaters using off-line particle-counting techniques (to address assumptions 3 and 5, because K_p depends on particle size);

- experimental determination of selected K_p values for clay and silica using likely groundwaters (to address assumption 5);

- experimental determination of the degree of colloid attachment to fracture walls using fractured-tuff columns (to address assumption 6);

- transport field experiment (under saturated

conditions) in the C Wells (to address assumption 7); and

- transport field experiment (under unsaturated conditions) using a nuclear test at the Nevada Test Site as a source term (to address assumption 7).

VI. DIFFUSION STUDIES

A model for matrix and fracture flow regimes in unsaturated, fractured porous media at Yucca Mountain was developed by Nitao (1991). This model provides a framework for assessment of the importance of matrix diffusion at Yucca Mountain. Solute transport in fractured rock in a potential radionuclide waste repository has been discussed by Neretnieks (1990) who concluded that most rocks (even dense rocks such as granites) have small fissures between the crystals that interconnect the pore system containing water. Small molecules of radioactive materials can diffuse in and out of this pore system. The inner surfaces in the rock matrix are much larger than the surfaces in the fractures on which the water flows. The volume of water in the microfissures is much larger than the volume in fractures. Therefore, over a long time scale, diffusion can play an important role in radionuclide retardation.

The objective of our diffusion experiments was to provide diffusion information for nonsorbing neutral molecules and anions and sorbing radionuclides. Because the uptake of radionuclides by tuff is measured as a function of time, the experiments also yield information on kinetics of sorption.

A. ROCK-BEAKER EXPERIMENTS

Experimental Procedure

The experimental technique we used involved fabricating rock beakers of tuff. The beaker sits inside a Plexiglas™ container surrounded by groundwater (Fig. 127). A stopper is used to prevent evaporation. The cavity in the rock beaker has a radius of approximately 1.4 cm and a length of 2.5 cm. The beaker itself has a length of approximately 5 cm and a radius of 3.1 cm.

The radionuclides we used in these experiments were ^{3}H, ^{95m}Tc, ^{237}Np, ^{241}Am, ^{85}Sr, ^{137}Cs, and ^{133}Ba. We placed a solution (prepared with groundwater from Well J-13) containing the radionuclide of interest in the rock cavity and then analyzed aliquots of the solution from the beaker for the remaining radionuclide concentration as a function of time. We also performed batch-sorption experiments with J-13 water and the tuffs under study using the batch-sorption procedures described in the first section of Chapter IV.

Data Analysis

The results of the rock-beaker experiments were modeled using TRACRN, a three-dimensional geochemical/geophysical-model transport code (Travis and Birdsell 1991). Because the geometry of the rock beaker is complex, an analytical solution is not available for this system. The concentration

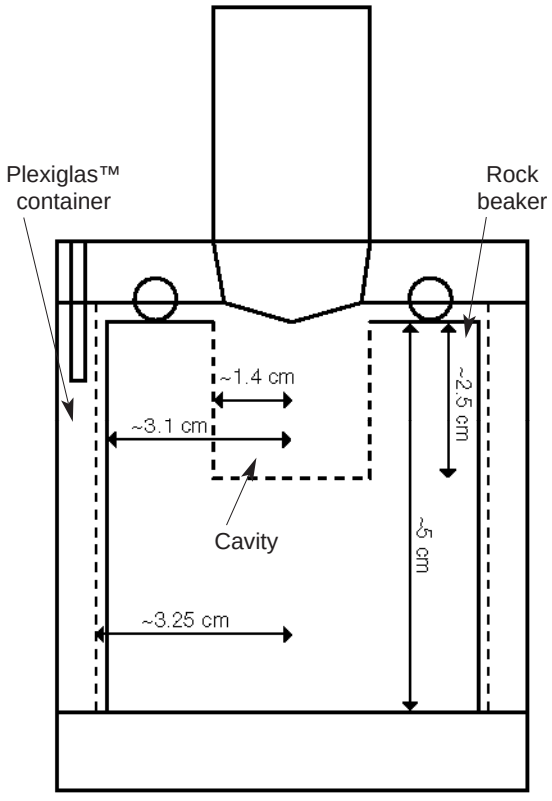

Figure 127. Rock Beaker. This cross section shows the beaker of tuff and surrounding container used in the rock-beaker diffusion experiments.

profiles of the diffusing tracer are fitted to the transport equation (de Marsily 1986, Chapter 10):

$$\nabla \cdot (\epsilon\, d\, \nabla C) = \epsilon\, \frac{\partial C}{\partial t} + Q \ , \qquad (104)$$

where ϵ is the total porosity of the tuff, d is the diffusion coefficient through the tuff, C is the concentration of the diffusing tracer in solution, and the source term, Q, is zero for a nonreactive tracer but for a sorbing solute

$$Q = \rho_b\, \frac{\partial F}{\partial t} \ , \qquad (105)$$

where F is the amount of tracer sorbed per unit mass of solid and ρ_b is the bulk tuff density ($\rho_b = (1 - \epsilon)\rho_s$, where ρ_s is the density of the solid particles). (Equation 84 in Chapter V reduces to the above equations for the case of no hydrodynamic dispersion, that is, the filtration velocity, **U,** is zero and the dispersion tensor, **D**, only includes molecular diffusion.)

As discussed in previous chapters, the mechanism of sorption determines the relationship between F and C. When sorption is linear, reversible, and instantaneous, the relationship between F and C is given by the sorption distribution coefficient

$$K_d = \frac{F}{C} \ . \qquad (106)$$

Substitution of this equation and Eqn. 105 into Eqn. 104 yields

$$\nabla \cdot (\epsilon\, d\, \nabla C) = \epsilon\, R_f\, \frac{\partial C}{\partial t} \ , \qquad (107)$$

where, once again, the retardation factor, R_f, is given by

$$R_f = 1 + \frac{\rho_b}{\epsilon}\, K_d \ . \qquad (108)$$

Equation 108 provides a means of comparing results for sorption coefficients obtained under diffusive conditions with sorption coefficients obtained from batch-sorption experiments and is valid only if sorption is linear, reversible, and instantaneous (the Langmuir and the Freundlich isotherms are examples of nonlinear relationships between F and C).

Consequently, we can determine the diffusion coefficient by fitting concentration profiles for the nonsorbing tracers, and we can determine sorption parameters, such as K_d, by fitting concentration profiles for the sorbing tracers.

Results and Discussion

Figure 128 shows an example of a set of diffusion data for a rock-beaker experiment in which we used the feldspar-rich tuff G4-737 and solutions of tracers in J-13 water. The concentration of tracer, C, remaining in the solution inside the cavity of the rock beaker divided by the initial concentration, C_o, is plotted as a function of elapsed time.

The solid lines in Fig. 129 are a fit of these same data to the diffusion equation (Eqn. 104) using the TRACRN transport code for the two nonsorbing radionuclides, tritium and technetium-95m. The diffusion coefficients obtained in this manner for these radionuclides for all the tuff samples studied (Table 66) agree well with previous results (Rundberg et al. 1987). These two tracers diffuse essentially as tritiated water and the pertechnetate anion, TcO_4^-. Large anions are excluded from tuff pores because of their size and charge, which can account for the lower diffusivity of TcO_4^-.

If sorption is linear, reversible, and instantaneous, then F/C is equal to a sorption coefficient, K_d. To test this assumption, we determined values of K_d in batch-sorption experiments using the tuffs under study (Table 67). We then calculated an expected diffusion curve using, for each tuff, the diffusion coefficient measured for tritiated water and the batch-sorption coefficient measured for each sorbing radionuclide. Figure 130 shows these calculated diffusion curves for devitrified tuff G4-737. Comparison of the calculated curves with the actual measured data (see the example in Fig. 131) shows that the concentration of the sorbing radionuclides remaining in the rock beaker drops

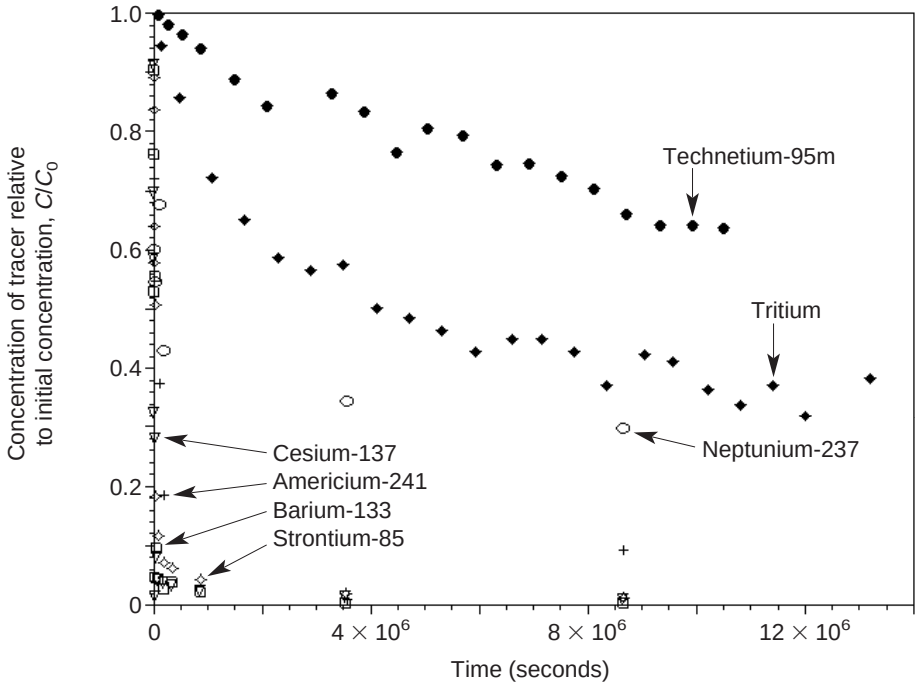

Figure 128. Diffusion Data. These data for diffusion of tracers in J-13 water and in rock beakers made of tuff G4-737 show the concentration, C, of tracer (relative to the initial concentration, C_0) remaining in the beaker as a function of elapsed time.

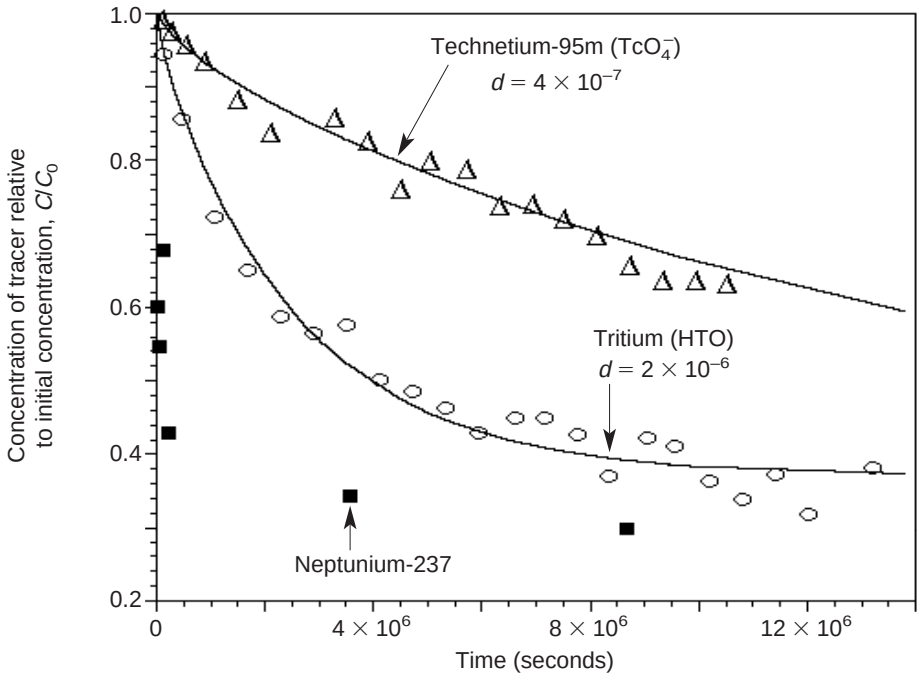

Figure 129. Diffusion Data Curve Fits. The solid curves are fits to the diffusion data by the TRACRN code for the nonsorbing tracers tritium and technetium in the rock-beaker experiments with tuff G4-737.

Table 66. Rock-beaker Diffusion Results for Nonsorbing Radioisotopes and Devitrified Tuffs

Tuff sample	Major minerals	Porosity	Diffusion coefficient, d (cm^2/s)	
			HTO	TcO_4^-
G4-737	Alkali feldspar 68% Cristobalite 28%	0.07	2.2×10^{-6}	3.9×10^{-7}
GU3-304 #1 GU3-304 #2	Alkali feldspar 75% Cristobalite 25%	0.06	1.5×10^{-6} 1.6×10^{-6}	3.0×10^{-7} 3.0×10^{-7}
GU3-433	Alkali feldspar 76% Cristobalite 15%	0.10	3.5×10^{-6}	
GU3-1119	Alkali feldspar 70% Quartz 19%	0.10	2.0×10^{-6}	4.9×10^{-7}
Topopah outcrop	Alkali feldspar 59% Cristobalite 23% Quartz 12%	0.07	1.0×10^{-6}	1.0×10^{-7}

Table 67. Batch-sorption Diffusion Coefficients for Devitrified Tuffs

Tuff sample	Major minerals	Diffusion coefficient, K_d (ml/g)				
		Neptunium	Americium	Cesium	Strontium	Barium
G4-737	Alkali feldspar 68% Cristobalite 28%	8	134	532	52	28
GU3-304	Alkali feldspar 75% Cristobalite 25%	8		342	18	19
GU3-433	Alkali feldspar 76% Cristobalite 15%	9	154	1264	20	61
GU3-1119	Alkali feldspar 70% Quartz 19%	8	136	494	42	27
Topopah outcrop	Alkali feldspar 59% Cristobalite 23% Quartz 12%	9		465	20	25

faster than predicted on the basis of a linear K_d. This result indicates that the diffusion of the sorbing radionuclides could not be fitted by assuming reversible, instantaneous, and linear sorption. These results also indicate that transport calculations using a batch-sorption K_d value and the diffusion coefficient measured for tritiated water will result in conservative predictions for the transport of sorbing radionuclides.

The results obtained from rock-beaker experiments agree with previous results (Rundberg

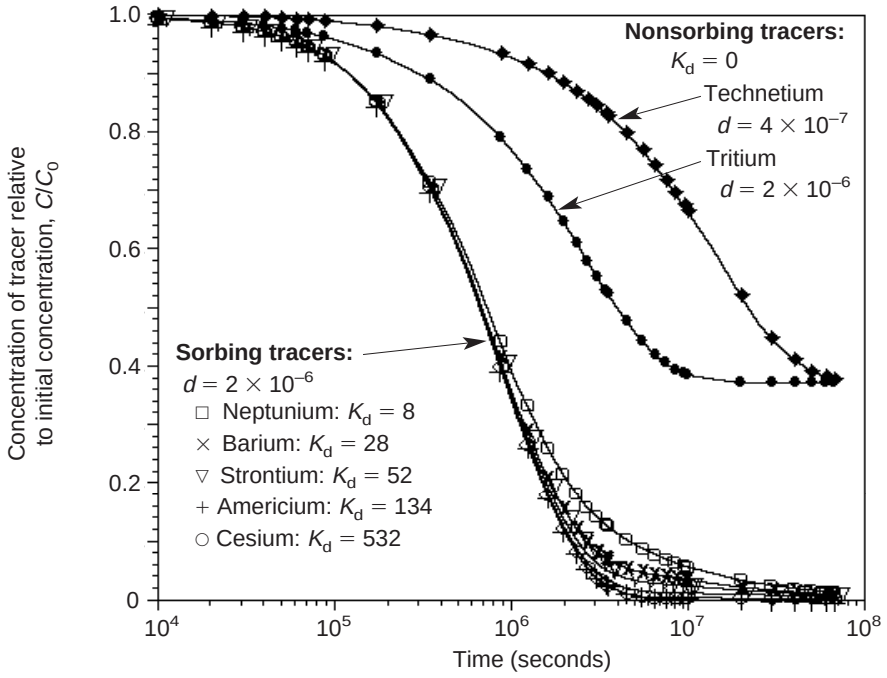

Figure 130. Calculated Diffusion Curves. These curves were calculated for tuff G4-737 using the diffusion coefficient, *d*, measured for tritiated water and the batch-sorption coefficients, K_d, measured for the sorbing radionuclides (given in Table 67). The diffusion curves for tritium and technetium are also shown.

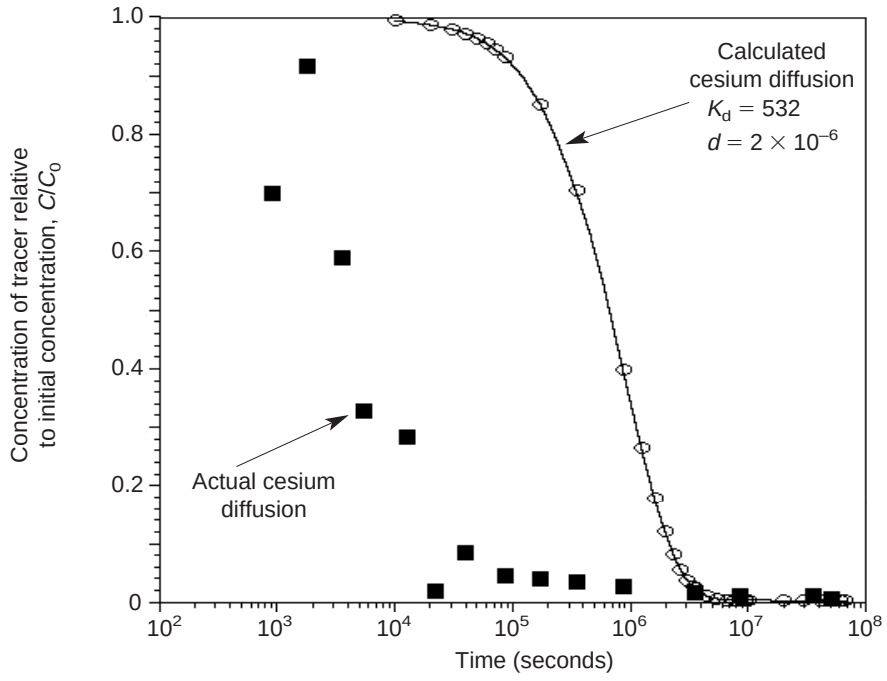

Figure 131. Comparison of Calculated and Actual Diffusion Data. The solid curve is the diffusion curve calculated for cesium using a K_d value and the diffusion coefficient for tritium (Fig. 130); the squares are the actual diffusion data for cesium with tuff G4-737 (Fig. 128).

1987). We performed experiments on the uptake of sorbing radionuclides by tuff and found that rate constants for uptake of the sorbing cations from solution onto tuff were consistent with a diffusion-limited model in which diffusion occurs in two stages. In the first stage, the cations diffuse into rock through water-filled pores; in the second stage, they diffuse into narrower intracrystalline channels. This diffusion model yielded sorption coefficients for cesium, strontium, and barium that agree well with the sorption coefficients determined by batch techniques.

B. DIFFUSION-CELL EXPERIMENTS

Experimental Procedures and Data Analysis

We constructed diffusion cells with two chambers containing groundwater separated by a slab of tuff. After radioactive tracers were added to one of the chambers, we periodically monitored the untraced chamber for the presence of radioactivity by taking an aliquot of the solution in the chamber and then replenishing that chamber with groundwater. The dimensions of the diffusion cells we used are given in Table 68.

Table 68. Dimensions of Diffusion Cells

Diameter of tuff slab	6 cm
Length of tuff slab	1 cm
Volume of traced chamber	750 cm^3
Volume of untraced chamber	80 cm^3

The only driving force in this experimental setup is the chemical concentration gradient; thus, the solute flux is purely diffusive. The apparent time of arrival depends on the porosity, the heterogeneity of the pore structure, the retardation factor for a given radionuclide, and the sensitivity of radionuclide measurements. The rate of concentration increase in the untraced chamber depends on the ionic diffusivity, the tuff porosity, and the tuff tortuosity/constrictivity factor. Thus, by measuring the movement of sorbing and nonsorbing tracers through tuff slabs as a function of time, we can measure the rock-dependent diffusion parameters.

The two major rock types used for the diffusion-cell experiments were zeolitic (UE-25 1362) and devitrified (G4-287). The zeolitic tuff has a porosity of 0.4 and a bulk density of 1.5 g/ml. The devitrified tuff has a porosity of 0.2 and a bulk density of 2.3 g/ml. The major component of the zeolitic tuff is clinoptilolite; the major component of the devitrified tuff is alkali feldspar.

The solutions used for the diffusion-cell experiments were prepared by taking an aliquot of a ^{3}H, ^{95m}Tc, natural U(VI), $^{237}Np(V)$, or $^{239}Pu(V)$ acidic stock and diluting it in the water being studied. The actinide concentration of the solutions used for the diffusion experiments was very close to the solubility limit of the actinides in the groundwaters. The experimentally determined solubilities (Nitsche et al. 1993a, 1994) of plutonium range from 2×10^{-7} (J-13 water at a pH of 7) to 1×10^{-6} M (UE-25 p#1 water at a pH of 8.5) and of neptunium range from 7×10^{-6} (UE-25 p#1 water at a pH of 8.5) to 5×10^{-3} M (J-13 water at a pH of 6). Table 47 in Chapter IV summarizes the solubilities and speciation of neptunium in these groundwaters.

The experimental setup for the diffusion cells can be described by a one-dimensional diffusion model. Thus, Eqn. 107 in the section on rock-beaker experiments can be rewritten as

$$D_e \frac{\partial^2 C}{\partial x^2} = \alpha \frac{\partial C}{\partial t} \quad , \qquad (109)$$

where x is the the axis along the direction of tracer diffusion, D_e is the effective diffusivity ($= \epsilon d$), and α is the rock-capacity factor ($= \epsilon R_f$). This equation yields an analytic solution to diffusion through a slab.

Bradbury et al. (1986) solved Eqn. 109 for a porous rock. For our experimental setup, the boundary conditions can be taken to be:

- at $x = 0$, a constant source concentration, C_o, is maintained and
- at $x = \ell$, where ℓ is the tuff-slab thickness, the concentration measured at the initially untraced cell, C_t, is much smaller than the source concentration ($C_t \ll C_o$).

For these conditions, the total quantity, Q_t, diffused through a tuff slab of area A after a time t is given

by the equation

$$\frac{Q_t}{A\,\ell\,C_o} = \frac{D_e\,t}{\ell^2} - \frac{\alpha}{6} - \frac{2\alpha}{\pi^2}\sum_{n=1}^{\infty}\frac{(-1)^n}{n^2}e^{-\left(\frac{D_e n^2 \pi^2 t}{\ell^2 \alpha}\right)}. \quad (110)$$

As $t \rightarrow \infty$, the asymptotic solution becomes

$$Q_t = \frac{A\,C_o\,D_e}{\ell}\,t - \frac{A\,C_o\,\ell\,\alpha}{6}\ . \quad (111)$$

Consequently, a plot of Q_t versus t yields the effective diffusivity, D_e, from the slope and the rock-capacity factor, α, from the intercept on the time axis of the extrapolated linear region. For a non-sorbing species, $K_d = 0$, $R_f = 1$, and $\alpha = \epsilon$; for a sorbing species, K_d may be calculated from the value of α.

The diffusion coefficient, d, can be calculated from the effective diffusivity ($D_e = \epsilon\, d$). The difference between the diffusion coefficient, d_s, for a tracer diffusing in the solution phase and the diffusion coefficient, d, for a tracer passing through tuff pores is given by

$$d = \frac{\delta}{\tau^2}\,d_s\ , \quad (112)$$

where δ is the constrictivity and τ is the tortuosity of the tuff pore structure.

Results and Discussion

We studied the diffusion of ^{3}H, ^{95m}Tc, natural U(VI), ^{237}Np(V), and ^{239}Pu(V) through devitrified and zeolitic tuffs using water from Well J-13 and synthetic UE-25 p#1 water. The radionuclides ^{3}H, natural U(VI), and ^{239}Pu(V) were studied together in four diffusion cells (devitrified and vitric tuff cells, each with both types of water). Likewise, the radionuclides ^{95m}Tc and ^{237}Np(V) were studied together in another four diffusion cells. Typical results for these experiments are shown in Figs. 132 through 134.

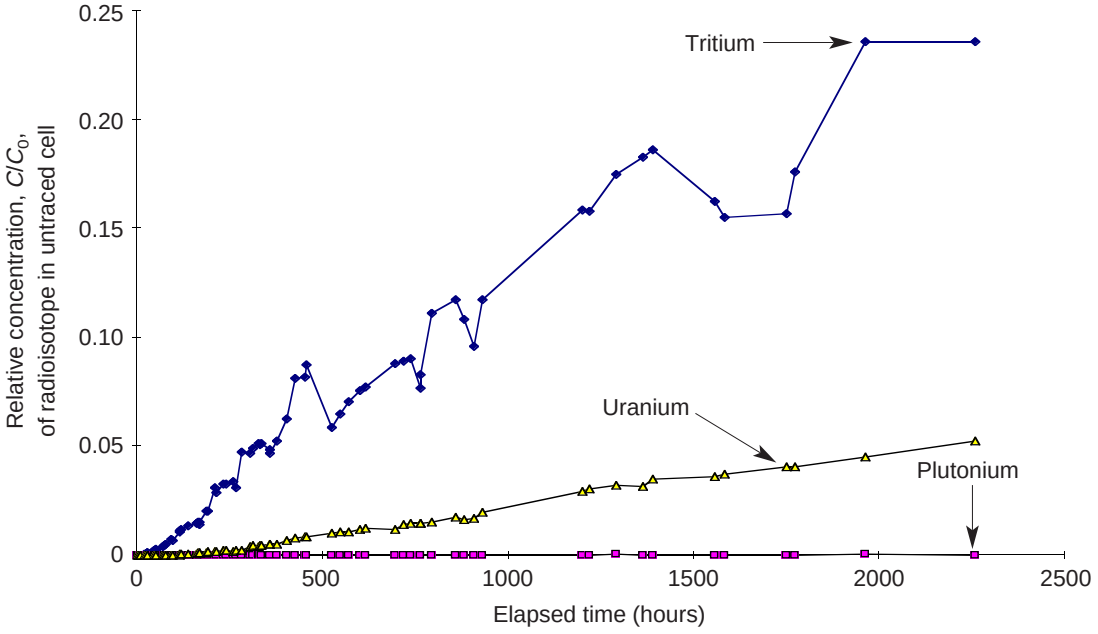

Figure 132. Tritium, Plutonium, and Uranium Diffusion through Devitrified Tuff. The data show the concentration in synthetic UE-25 p#1 water of ^{3}H, ^{239}Pu(V), and natural U(VI) (relative to the concentration in the traced cell, C/C_0) diffusing through devitrified tuff G4-287 into the untraced cell as a function of time.

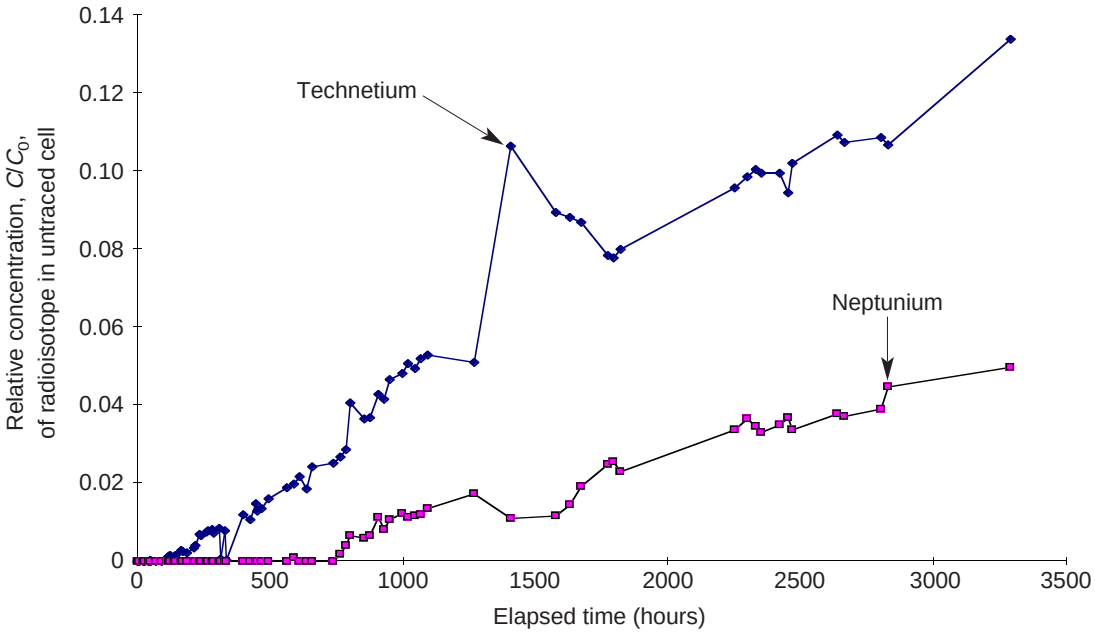

Figure 133. Technetium and Neptunium Diffusion through Devitrified Tuff. The data show the concentration in synthetic UE-25 p#1 water of ^{95m}Tc and ^{237}Np (relative to the concentration in the traced cell, C/C_0) diffusing through devitrified tuff G4-287 into the untraced cell as a function of time.

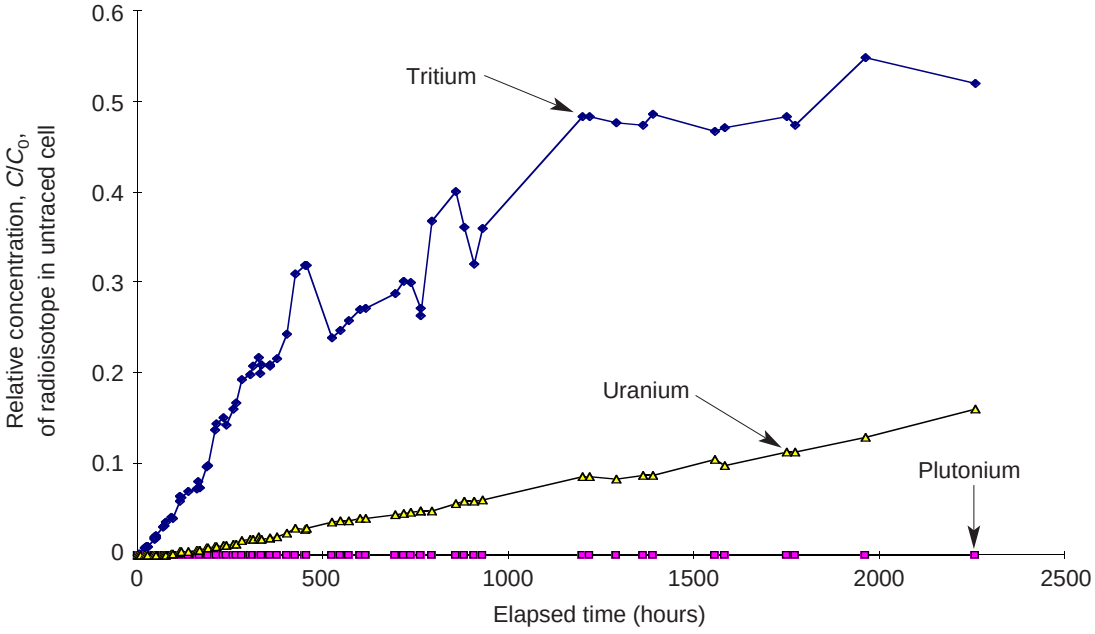

Figure 134. Tritium, Plutonium, and Uranium Diffusion through Zeolitic Tuff. The data show the concentration in synthetic UE-25 p#1 water of ^{3}H, ^{239}Pu(V), and natural U(VI) (relative to the concentration in the traced cell, C/C_0) diffusing through zeolitic tuff UE-25 1362 into the untraced cell as a function of time.

Our results indicate that the diffusion of nonsorbing radionuclides into saturated tuff (illustrated by the diffusion of tritiated water in Figs. 132 and 134) is slower in devitrified tuffs than in zeolitic tuffs. Large anions such as pertechnetate (which are excluded from the tuff pores by size and charge) diffuse slower through the pores than tritium regardless of the groundwater or tuff type (as also observed in the rock-beaker experiments). The migration of plutonium through tuff under diffusive conditions is dominated by sorption (as shown by Figs. 132 and 134). The migration of Np(V) and U(VI) through tuff depends on tuff type and water chemistry. In cases, such as tuff G4-287, for which the reported sorption of neptunium is essentially zero (Triay et al. 1996a, 1996b), the diffusion of neptunium through the tuff is slower than the diffusion of tritium but comparable to the diffusion of a nonsorbing, large anion, such as pertechnetate (Fig. 133).

The analysis of data described in the “Experimental Procedures and Data Analysis” section of this chapter has some problems with respect to the assumptions required to find an analytical solution. The assumptions do not allow for a changing concentration in the traced chamber, for a concentration in the untraced chamber that is not much smaller than the initial concentration in the traced chamber, and for the addition of groundwater to the untraced chamber each time an aliquot was taken.

Therefore, future analysis of these data will involve fitting the diffusion profiles using a transport code (such as the TRACRN code used in the rock-beaker diffusion experiments) to obtain diffusion coefficients. The concentration profiles of the diffusing radionuclides would be fitted to the same equation as Eqn. 109 but using the algebraic form given in the section on rock-beaker experiments (Eqns. 104 through 106).

C. DIFFUSION THROUGH UNSATURATED TUFF

Direct and indirect techniques have been used during the last fifty years to measure or calculate diffusion coefficients in most porous media (Kemper 1986). Both techniques employ steady-state and transient-state methods of analysis. Fick's first law forms the basis for evaluating steady-state experiments, and Fick's second law, modified to account for the properties of porous media, is used for transient-state experiments. Diffusion coefficients in geologic media have traditionally been measured by tracer half-cell diffusion methods that monitor the transient diffusion front of a tracer species through the material of interest.

Unsaturated diffusion experiments involving blocks of tuff have also been proposed for the study of diffusion in Yucca Mountain tuff (Yucca Mountain Project study plan 8.3.1.3.6.2). A block of tuff is machined to prescribed dimensions, and a narrow hole is drilled to the center of the block. The porosity is determined by measuring the difference in weight between dry and saturated samples. After initial saturation, the block is allowed to dry until the desired moisture content is achieved. The block is then sealed in an airtight container and placed in a constant-temperature bath to allow the moisture distribution to equilibrate. It takes many months for the water to distribute evenly through the block because the permeability of Yucca Mountain tuff is low. The appropriate time for equilibration to occur could be calculated using a transport code. After equilibration, a solution containing radionuclides is placed in the bottom of the injection hole. The tracers are allowed to diffuse for a fixed period of time, then the block is frozen, sectioned, and each section analyzed. The distribution of radionuclides in the tuff matrix is fitted to a diffusion equation using a transport code, and diffusion coefficients as a function of saturation are determined.

Unsaturated conditions, or saturated conditions with very low water content, present unique experimental problems. Diffusive fluxes through low-water-content materials require longer time periods to collect sufficient data from transient-state experiments. For diffusion coefficients less than 10^{-8} cm^2/s, the time period can be months to years. For direct steady-state techniques, maintaining proper boundary conditions under unsaturated conditions over long time periods is extremely difficult and has not yet been satisfactorily demonstrated.

Therefore, an indirect method is needed that provides reliable diffusion coefficients. The most widely used indirect method is the measurement of electrical conductivity in a potentiostatic or galvanostatic mode, coupled with the Nernst-Einstein relationship, which provides reliable diffusion coefficients in electrolyte solutions (Miller 1972; Robinson and Stokes 1959). Fortunately, water-wet geologic materials are ideal for this method because the geologic media consists of an electrolyte solution dispersed throughout a nonconductive porous solid. Diffusion is completely dominated by the aqueous solution. Electrical conductivity is related to the migration of ions in the aqueous solution because the ease with which ionic species can migrate through an aqueous solution is exactly analogous to the ease with which the aqueous species can align their dipoles along the electric field vector, as long as the frequency is appropriate.

Soil scientists have developed multi-electrode methods for measuring electrical conductivity and salinity of porous media in the field and laboratory (Rhoades and Oster 1986; Gupta and Hanks 1972). The proven method of obtaining conductivity data is the use of a fixed excitation frequency conductivity bridge, based on its tested design, direct resistance and conductivity readouts, ease of operation, and availability.

A variation of the two-electrode method is ideal for the study of geologic media (Geddes et al. 1971). The electrical conductivity cells designed for this study have two stainless-steel cap electrodes in contact with the whole-rock cores. Although platinized electrodes are usually considered ideal for

typical conductivity measurements, they are not recommended for solutions of low conductivity or with geologic materials (ASTM 1982). Stainless-steel electrodes have been shown to be appropriate for the low water contents and the current densities ($\leq$ 1 mA/cm^2) used in this experimental setup (Geddes et al. 1971; Scott et al. 1967).

Electrical conductivity measurements of aqueous solutions actually measure the impedance (the AC analog of DC resistance) at the impressed frequency, which is a complex variable vector sum of the real in-phase (resistive) and the imaginary out-of-phase (reactive) components of the system response. For conductivity (the reciprocal of resistivity) measurements using AC excitation, it is the in-phase component of impedance that is a measure of the true solution resistivity (or conductivity) and that can be used to represent the migration of ions in solution in geologic materials. Therefore, the impedance must be totally resistive, that is, no capacitive elements, for the Nernst-Einstein relationship to be applicable. This restriction has been verified for saturated and unsaturated geologic systems with a 1 kHz conductivity bridge using electrochemical impedance spectroscopy, which gives direct information about the real and imaginary components of impedance as a function of excitation frequency (Conca and Wright 1990). The impedance in geologic systems is a constant, frequency-independent quantity in the 600 to 7,000 Hz region and is totally resistive in the 400 to 10,000 Hz region. Thus, the measured impedance at 1 kHz on geologic systems is a good measure of the true system resistance and its reciprocal, conductivity, and this parameter will give reliable values for diffusion coefficients calculated from the Nernst-Einstein equation. In addition, Wright (1990) determined diffusion coefficient values as a function of water content on the same soils using the electrical conductivity method and using Kemper's empirically derived relationship (Bresler et al. 1982), and the agreement was excellent ($R^2 = 0.99$). Once electrical conductivity measurements are made, they can be related to the diffusion coefficient through the Nernst-Einstein equation (Jurinak et al. 1987; Conca and Wright 1990):

$$d_i = \frac{R\,T}{F^2} \cdot \frac{\Theta\,G\,t_i}{Z_i\,C_i} \quad , \qquad (113)$$

where d_i is the diffusion coefficient of the ith ion (cm^2/s), R is the gas constant (J/deg mole), T is the absolute temperature (Kelvin), F is Faraday's constant (coul/mole), Θ is the cell constant for the conductivity cell sample holder (cm^{-1}), G is the measured conductance on the conductivity bridge (mhos), t_i is the transport, or transference, number of the ith ion ($t_{K^+} = 0.4898$ at 0.1 M; $t_{Na^+} = 0.3854$ at 0.1 M), Z_i is the charge number on the ith ion, and C_i is the molar concentration of the ith ion. The diffusion coefficients are corrected for solution nonideality using the extended Debye-Hückel approximation (Stumm and Morgan 1981). Effluent is monitored to correct for possible water/substrate interactions that can change the solution electrolyte concentrations.

The most effective way to determine diffusion coefficients under various degrees of saturation is to use the centripetal-acceleration UFA method (described in the "Solid-rock Columns" section of Chapter V) to achieve hydraulic steady-state in the samples at target water contents using an appropriate electrolyte solution, for example, KCl or NaCl solutions in equilibrium with the tuff (Conca and Wright 1992b). Once steady-state has been achieved, the electrical conductivity is measured, and the Nernst-Einstein equation is used to determine the simple diffusion coefficient for that sample at that water content. The UFA method is then used to achieve another water content, and the diffusion coefficient is determined again. Simple diffusion coefficients in aqueous solution at 25ºC for almost all chemical species, including organics, are between 0.5×10^{-5} cm^2/s and 2.1×10^{-5} cm^2/s (Conca and Wright 1992b; Oelkers 1991; Robinson and Stokes 1959). Therefore, simple diffusion coefficients in porous media that are less than 10^{-6} cm^2/s at 25ºC result from mechanisms or conditions other than the inherent mobility differences between the ions themselves. The variable d repre-

sents a generic simple diffusion coefficient at infinite dilution that is a bulk property of the system and refers to the various combined physical effects of the porous media. The variable, thus, differs from the apparent diffusion coefficient, d_a, which includes retardation and other transient chemical effects and is specific for each species, medium, and fluid composition. Numerical models using $d(q)$ as an input parameter require the simple diffusion coefficient. Once breakthrough has occurred for a particular species, retardation ceases and the diffusion coefficient attains the simple value, which can be orders of magnitude higher than the apparent diffusion coefficients for many species in materials such as zeolitized tuff. The point at which breakthrough occurs is determined by the capacity of the flow paths in the media for that species under appropriate conditions.

VII. SUMMARY

The following is a summary of the state of knowledge with respect to the different elements of the natural barrier for radionuclide transport at Yucca Mountain: groundwater chemistry, radionuclide solubility, sorption, and diffusion. We also include a summary of material from the related Yucca Mountain Site Characterization Project milestone #3663, "Summary and Synthesis of Biological Sorption and Transport."

A. BIOLOGICAL SORPTION AND TRANSPORT (MILESTONE #3363)

The results of research performed as part of the Biological Sorption and Transport Task of the Yucca Mountain Site Characterization Project have been presented in a report on milestone #3663 (Hersman 1996). These studies reveal that microorganisms can affect transport in several ways.

- Based only on the relative concentration of microorganisms in the two studies (laboratory and field), it is tempting to predict that the effect of the indigenous population on the sorption of ^{239}Pu(IV) would be negligible and to conclude that the indigenous population will do little to retard the transport of plutonium by biosorption. However, the design of the laboratory experiment represents only a static, small location within the mountain. As the waste plume moves from one sorption location to the next, a continuum of sorption is occurring with each site sorbing 0.075 times as much more as it would if it were sterile, that is, by a factor of 1.075. Therefore, the effects of microbial sorption would enhance the sorption characteristics of the mountain by 7.5 per cent.

- Estimates suggest that the indigenous population of microorganisms is capable of producing enough chelating agents (for example, siderophores) to chelate 0.2 g/l of ^{239}Pu in the subsurface pore water. Because this amount exceeds the solubility of plutonium, there is a significant potential for siderophores to increase the transport of actinide elements.

- Based on the results of laboratory studies, microorganisms increased significantly the rate of colloidal agglomeration. The field studies suggest that there are enough microorganisms present to affect similarly the agglomeration of individual colloids, indicating that the indigenous population should reduce the colloidal transport of radioactive wastes.

- Field and isotopic analyses indicate that the elevated subsurface carbon-dioxide concentrations are the result of biogenic activity. Elevated carbon-dioxide levels will affect transport by lowering the pH of the pore water, thereby increasing the solubility of most actinide elements. Also, lowering the pH will promote the dissolution of minerals, such as calcite, that are important in the retardation of actinides.

- Samples collected along the Exploratory Study Facility (ESF) contain a small population of microorganisms that is metabolically active and responsible for the production of the elevated levels of subsurface carbon dioxide. Analysis also revealed that this population was significantly affected by anthropogenic disturbances, increasing nearly four fold from the time of initial sampling. It is important, therefore, that the population within the ESF be monitored routinely to assess the effects of construction activities on their numbers and types.

- It is not possible to quantify the overall potential for the indigenous population to affect transport. However, a cautious and qualitative interpretation of this work indicates that there is a strong potential for the subsurface popula-

tion to promote the transport of radionuclide wastes, based on the dominant potential for chelation and carbon-dioxide production to accelerate transport. However, more work is needed before these results can be quantified.

B. GROUNDWATER CHEMISTRY (CHAPTER II)

The chemical compositions of pore waters, perched waters, and saturated-zone groundwaters suggest there are basically two types of waters in Yucca Mountain.

- Type-1 water occurs as pore waters in hydrologic units mainly above, but also below, Tuff of Calico Hills. This water type generally has higher ionic strength than type-2 waters and is strongly influenced by soil-zone processes such as the precipitation of calcite, gypsum, and silica.

- Type-2 water occurs as perched waters and saturated-zone groundwaters. This water type is more dilute and is strongly influenced by hydrolysis reactions involving carbonic acid.

- Pore waters in Tuff of Calico Hills appear to be mixtures of the two basic water types, that is, pore waters from the overlying Topopah Spring Tuff and perched waters.

- The chemical data indicate that the equilibration of pore waters and perched or groundwaters is a very slow process.

- Future compositional variations in water chemistry under ambient conditions are likely to be of minor magnitude.

- The compositions of the J-13 and UE-25 p#1 waters appear to bound most of the compositional variations to be expected in the ambient flow system at Yucca Mountain in the future. The main parameters not entirely bounded by these compositions are pH, Eh, and chloride concentrations.

- The uncertainty in the identity of alteration phases that control the type-2 water compositions and the lack of experimental data on the kinetics of formation of possible alteration phases preclude the development of realistic quantitative models of water chemistry in Yucca Mountain.

C. RADIONUCLIDE SOLUBILITY STUDIES (CHAPTER III)

- The carbonate anion is an exceptionally strong complexing agent for actinide ions and is present in significant concentrations in waters characteristic of the Yucca Mountain region.

- The ability of some actinide cations to hydrolyze water requires that any aqueous model of actinides in Yucca Mountain groundwaters include thermodynamic descriptions of hydroxo, carbonato, and mixed hydroxo-carbonato complexes.

- The solubility of neptunium, plutonium, and americium will depend on solution speciation (especially with OH^- and CO_3^{2-}) and the solubility-limiting solid.

- Bulk solubility experiments can provide empirical data directly, but because they are long-term experiments, only a limited number of data points can be collected over a limited range of conditions. To determine solubility for general conditions, the system must be modeled thermodynamically.

- Bulk solubility of neptunium in J-13 water ranges from 6×10^{-6} M to 10^{-3} M; the solubility-limiting solid was predominately (but not exclusively) Np_2O_5.

- For water conditions expected at Yucca

Mountain, the data for Np(V) solutions is consistent, and modeling with the EQ3/6 code suggests a combination of NpO_2^+ and $NpO_2CO_3^-$ as the dominate species.

- Recent modeling work at Los Alamos indicates Np(IV) solids may form in Yucca Mountain waters, depending on which solid-state numbers are used. The importance of this observation is that Np(IV) solids may be much less soluble than the Np(V) currently considered in performance-assessment calculations.

- Bulk solubility of plutonium in J-13 water extends over a relatively narrow range from 4×10^{-9} to 5×10^{-8} M; the predominate solubility-limiting solid is Pu(IV)-oxide polymer at 25ºC, aging to more crystalline PuO_2(s) at 90ºC.

- In the model, plutonium speciation is calculated to be dominated by $Pu(OH)_5^-$ in J-13 water, and the solids PuO_2(s) and $Pu(OH)_4$(s) are calculated to be supersaturated to saturated.

- The bulk solubility of americium ranges from 3×10^{-10} to 4×10^{-6} M; the solubility limiting solid was reported to be a mixture of hexagonal and orthorhombic forms of $AmOHCO_3$, but this assertion is controversial and more work would need to be done to confirm or reject the statement.

- Only preliminary modeling of americium has been done. The predominate solution species was calculated to be $AmCO_3^+$ in J-13 water except at 90ºC and a pH of 8, in which case the dominant species was calculated to be $Am(CO_3)_2^-$. Furthermore, the hydroxo solids $Am(OH)_3$ and $Am(OH)_3$(amorphous) were calculated to be significantly below saturation throughout the experimental conditions for the bulk solubility study. The only solid to approach saturation in the calculations was $AmOHCO_3$.

D. SORPTION (CHAPTER IV)

- The elements niobium, tin, thorium, and zirconium show strong sorption onto surfaces available in Yucca Mountain rock units. In addition, these elements form solid oxides and hydroxides that have very low solubilities in Yucca Mountain groundwaters. In near-neutral solutions, they are fully hydrolyzed. A minimum sorption-coefficient value of 100 ml/g is appropriate in performance-assessment calculations for all these elements under essentially all conditions expected within the Yucca Mountain flow system.

- The elements actinium, americium, and samarium also sorb strongly to surfaces in Yucca Mountain rock units. These elements tend to form carbonates, phosphates, and mixed hydroxycarbonate compounds that are very sparingly soluble. A minimum sorption-coefficient value of 100 ml/g is appropriate for each of these elements.

- Plutonium's solution and sorption behavior are the most complex of all the elements of interest. The groundwater compositional parameter most critical to this element in the Yucca Mountain flow system is the redox potential, Eh. The available sorption data suggest that this element should sorb strongly to Yucca Mountain tuffs under most of the expected conditions. However, because in the experiments to date, the redox potential was not controlled, additional controlled experiments should be carried out. The recommendation is to bias the redox potential to a high level in a series of sorption experiments using several rock types and a water composition representative of the unsaturated zone. If the sorption coefficients obtained in these experiments are consistent with earlier results, plutonium can be classified with the strong sorbers and a minimum sorption-coefficient value of 100 ml/g could be used in performance-assessment calculations. On the other

hand, if the sorption coefficients are decreased by the elevated redox potential imposed, then additional experiments will need to be carried out to better define the appropriate range of the sorption coefficient to be used in the calculations.

- Cesium and radium have high affinities for most Yucca Mountain rock samples, particularly zeolitic samples. A minimum sorption-coefficient value of 100 ml/g could be used for these elements assuming that cesium concentrations in solution stay below 10^{-5} M. For strontium, the situation is more complex. Although this element has a high affinity for zeolitic samples, it is not strongly sorbed by devitrified and vitric tuffs. Because the zeolitic tuffs will be a strong barrier for this element, the small sorption-coefficient values obtained to date for this element could be used for devitrified and vitric units.

- The sorption coefficient data available for the elements nickel and lead are limited to a dozen or so experiments on nickel. In the surficial environment, lead appears to be less mobile than nickel. Therefore, the nickel sorption coefficients can be used as default values for lead. In devitrified and zeolitic zones, a minimum sorption-coefficient value of 100 ml/g is appropriate for nickel. In vitric zones, sorption coefficients will be in the range from 0 to 50 ml/g. For vitric zones, it is recommended that performance-assessment calculations use a random sampling technique to derive nickel and lead sorption coefficients from a normal distribution ranging from 0 to 50 ml/g.

- The group that includes the elements neptunium, protactinium, selenium, and uranium is the most difficult to deal with because the sorption affinities for this group are generally small. Neptunium appears to sorb primarily by surface-complexation and surface-precipitation mechanisms. The carbonate content of the rocks used in experiments with neptunium appear to have a large impact on sorption behavior. The presence of ferrous iron on surfaces in the tuffs may also be a factor. The recommendation is to oxidize the samples prior to use in sorption experiments to passify any ferrous iron that may be present on surfaces. If this procedure does not affect the sorption coefficient for the rock, a very weak acid leach should be used to remove potential carbonate minerals. If this additional procedure also has minimal effect, then the presently available sorption-coefficient data could be used for performance-assessment calculations. If either of these procedures results in the lowering of the sorption affinity, additional steps will have to be taken to derive appropriate sorption coefficients.

- Protactinium appears to be very insoluble in near-neutral solutions, but its sorption behavior is more complicated. At high pH, protactinium appears to sorb strongly, whereas just below neutral pH, it sorbs poorly. Because only lower-range pH experiments have been conducted with Yucca Mountain samples to date, the recommendation is to carry out several experiments in the higher pH range.

- Selenium will be present as an anion in Yucca Mountain flow systems and will have low sorption affinity. The main unresolved issue is the effect of elevated levels of calcium and magnesium on its sorption behavior. The recommendation is to carry out several additional sorption experiments with selenium using a water with relatively high amounts of calcium and magnesium.

- Uranium sorption appears to be controlled by pH, alkalinity, and the concentrations of alkaline-earth ions. Its affinity for Yucca Mountain rock samples is generally low with the highest sorption coefficients observed in zeolitic tuffs. The main gap in the available data is for sorption coefficients on zeolitic and

devitrified samples in contact with water enriched in calcium and magnesium at pH values from 6.5 to 8.0. The recommendation is to carry out two sets of experiments: one with a water high in calcium and magnesium but low in alkalinity; the other with a water high in calcium, magnesium, and alkalinity (for example, UE-25 p#l water). Both a zeolitic and a devitrified sample should be tested.

- The final group includes the elements carbon, chlorine, iodine, and technetium. These elements have little or no sorption affinity under the oxidizing conditions expected within the Yucca Mountain flow system. Any retardation of these will involve processes other than sorption.

- In a batch-sorption study of the effect of naturally occurring organic materials on the sorption of cadmium and neptunium on oxides and tuff surfaces, the model sorbents were synthetic goethite, boehmite, amorphous silicon oxides, and a crushed tuff material from Yucca Mountain, Nevada. An amino acid, 3-(3,4-dihydroxyphenyl)-DL-alanine (DOPA), and an aquatic-originated fulvic material, Nordic aquatic fulvic acid (NAFA), were used as model organic chemicals. DOPA and NAFA have little effect on neptunium sorption on all sorbents selected for study.

E. TRANSPORT AND DIFFUSION (CHAPTERS V AND VI)

Batch-sorption techniques yield sorption coefficients that appear to predict radionuclide transport under saturated and unsaturated conditions (at the laboratory scale) conservatively. These techniques need to be supplemented with dynamic transport and diffusion experiments.

- The Unsaturated Flow Apparatus (UFA) is a useful technique to assess the validity of batch-sorption coefficients. However, it would be practically impossible to measure all the necessary K_d values using the UFA approach because of the amount of time required for such an effort (as a result of the extremely low conductivities of the Yucca Mountain tuffs).

- The exclusion of anions such as pertechnetate in the vitric, devitrified, and zeolitic crushed tuffs we studied is almost negligible except in the case of zeolitic tuffs in J-13 water. In this case, the anion exclusion of pertechnetate in zeolitic tuffs is small but measurable.

To assess colloid-facilitated radionuclide transport in groundwaters at the potential nuclear waste repository at Yucca Mountain, it is very important to understand the generation and stability of colloids, including naturally occurring colloids.

- The colloid concentration in waters from Well J-13 was measured to be on the order of 10^6 particles/ml (for particle sizes larger than 100 nm). At this low particle loading, the sorption of radionuclides to colloids would have to be extremely high before the colloids could carry a significant amount of radionuclides from the repository to the accessible environment.

Diffusion is one of the most important retardation mechanisms in fractured media.

- The diffusion of nonsorbing radionuclides into saturated devitrified tuff is slower than diffusion into saturated zeolitic tuffs. The diffusion of tritiated water through saturated devitrified tuffs is on the order of 10^{-6} cm^2/s.

- Large anions, such as the neptunyl-carbonato complex or pertechnetate, are excluded from the tuff pores because of their size and charge. The diffusion coefficients for pertechnetate in saturated tuffs are on the order of 10^{-7} cm^2/s.

- The use of the Unsaturated Flow Apparatus is

the most efficient and cost effective way of studying diffusion as a function of saturation in Yucca Mountain tuffs.

Calculations of radionuclide transport often include assumptions about fast pathways, such as fractures, that are too simplistic. This approach leads to overconservative predictions of radionuclide releases to the environment.

- Our results indicate that diffusion from the fracture into the matrix can take place even at relatively fast flow rates.

- Neptunium can be significantly retarded, even during a fracture-flow scenario. Neptunium retardation in fractures could be due to both diffusion into the matrix and sorption onto the minerals lining the fracture walls

REFERENCES

Aagaard, P. 1974. Rare earth elements adsorption on clay minerals. *Bull. Groupe Fr. Argiles* 26: 193–199.

Åberg, M. 1978. The crystal structure of hexa-aqua-tri-μ-hydroxo-μ_3-oxo-triuranyl(VI) nitrate tetrahydrate, $[(UO_2)_3O(OH)_3(H_2O)_6]NO_3 \cdot 4H_2O$. *Acta Chemica Scandinavica A* 32: 101–107.

Åberg, M., D. Ferri, J. Glaser, and I. Grenthe. 1983a. Structure of the hydrated dioxo-uranium(VI) ion in aqueous solution: An x-ray diffraction and ^1H NMR study. *Inorganic Chemistry* 22: 3986–3989.

Åberg, M., D. Ferri, J. Glaser, and I. Grenthe. 1983b. Studies of metal carbonate equilibria: 8. Structure of the hexakis (carbonato) tris [dioxo-uranate(VI)] ion in aqueous solution: An x-ray diffraction and ^{13}C NMR study. *Inorganic Chemistry* 22: 3981.

Adamson, A. W. 1982. *Physical Chemistry of Surfaces*, p. 372. New York: John Wiley & Sons.

Allard, B. 1982. Sorption of actinides in granitic rock. SKBF Teknisk Rapport 82-21 (Stockholm: Svensk Karnbransleforsojning AB/Avdelning KBS).

Allard, B., and G. W. Beall. 1979. Sorption of americium on geologic media. *Journal of Environmental Health* A6: 507–518.

Allard, B., U. Olofsson, B. Torstenfelt, H. Kipatsi, and K. Andersson. 1982. Sorption of actinides in well-defined oxidation states on geologic media. In *Scientific Basis for Radioactive Waste Management V*, pp. 775–782. Pittsburgh, Pennsylvania: Materials Research Society.

Allard, B., U. Olofsson, B. Torstenfelt, and H. Kipatsi. 1983. Sorption behavior of well-defined oxidation states. INIS report SKBF-KBS-TR-83-61, 31 pp. Available from INIS Atomindex 1984, 15(9).

Allen, P. G., J. J. Bucher, D. L. Clark, N. M. Edelstein, S. A. Ekberg, J. W. Gohdes, E. A. Hudson, N. Kaltsoyannis, W. W. Lukens, M. N. Neu, P. D. Palmer, T. Reich, D. K. Shuh, C. D. Tait, and B. D. Zwick. 1995. Multinuclear NMR, raman, EXAFS, and x-ray diffraction studies of uranyl carbonate complexes in near-neutral aqueous solution: X-ray Structure of $[C(NH_2)_3]_6[(UO_2)_3(CO_3)_6] \cdot 6.5H_2O$. *Inorganic Chemistry* 34: 4797–4807.

Amal, R., J. R. Coury, J. A. Raper, W. P. Walsh, and T. D. Waite. 1990. Structure and kinetics of aggregating colloidal hematite. *Colloids and Surfaces* 46: 1.

Ames, L. L., J. E. McGarrah, and B. A. Walker. 1983. Sorption of trace constituents from aqueous solutions onto secondary minerals: 1. Uranium. *Clays and Clay Minerals* 31: 321–334.

Andersson, K. 1988. SKI Project-90: Chemical data. Swedish Nuclear Power Inspectorate report SKI TR 91:21 (Stockholm, Sweden).

ASTM. 1982. Standard test methods for electrical conductivity and resistivity of water. In *Annual Book of ASTM Standards*, 11.01 Water (1): 143–150. Philadelphia, Pennsylvania: American Society for Testing and Materials.

Baes, C. F., Jr., and R. E. Mesmer. 1976. *The Hydrolysis of Cations*. Wiley-Interscience.

Baeyens, B., and M. H. Bradbury. 1995a. A quantitative mechanistic description of Ni, Zn, and Ca sorption on Na-montmorillonite: Part I. Physico-chemical characterization and titration measurements. Paul Scherrer Institute report PSI Bericht Nr. 95-10 (Villigen, Switzerland).

Baeyens, B., and M. H. Bradbury. 1995b. A quantitative mechanistic description of Ni, Zn, and Ca sorption on Na-montmorillonite: Part II. Sorption measurements. Paul Scherrer Institute report PSI Bericht Nr. 95-11 (Villigen, Switzerland).

Bales, R. C., C. P. Gerba, G. H. Grondin, and S. L. Jensen. 1989. Bacteriophage transport in sandy soil and fractured tuff. *Applied and Environmental Microbiology* 55(8): 2061–2067. (YMP accession number NNA.930607.0065.)

Balistrieri, L. S., and T. T. Chao. 1987. Selenium adsorption by goethite. *Soil Science Society of America Journal* 51: 1145–1151.

Balistrieri, L. S., and J. W. Murray. 1982. The adsorption of Cu, Pb, Zn, and Cd on goethite from major ion seawater. *Geochimica et Cosmochimica Acta* 46: 1253–1265.

Banfield, J. F., and R. A. Eggleton. 1989. Apatite replacement and rare-earth mobilization, fractionation, and fixation during weathering. *Clays and Clay Minerals* 37: 113–127.

Bányai, I., J. Glaser, K. Micskei, I. Tóth, and L. Zékány. 1995. Kinetic behavior of carbonate ligands with different coordination modes: Equilibrium dynamics for uranyl(2+) carbonato complexes in aqueous solution: A ^{13}C and ^{17}O NMR study. *Inorganic Chemistry* 34: 3785–3796.

Barnard, R. W., M. L. Wilson, H. A. Dockery, J. H. Gauthier, P. G. Kaplin, R. R. Eaton, F. W. Binghan, and T. H. Robey. 1992. TSPA-1991: An initial total-system performance assessment for Yucca Mountain. Sandia National Laboratories report SAND91-2795 (Albuquerque, NM).

Barrer, R. M., and J. Klinowski. 1972. Ion exchange involving several groups of homogeneous sites. *Journal of the Chemical Society: Faraday Transactions I* 68: 73–87.

Barrer, R. M., and B. M. Munday. 1971. Cation exchange in the synthetic zeolite K-F. *Journal of the Chemical Society A* 1971: 2914–2921.

Barrer, R. M., and R. P. Townsend. 1976. Transition metal ion exchange in zeolites: Part 1. Thermodynamics of exchange of hydrated Mn^{2+}, Co^{2+}, Ni^{2+}, Cu^{2+}, and Zn^{2+} ions in ammonium mordenite. *Journal of the Chemical Society: Faraday Transactions I* 72: 661–673.

Barrese, E., C. Giampaolo, O. Grubessi, and A. Mottana. 1986. Rancieite from Mazzano Romano (Latium, Italy). *Mineralogical Magazine* 50 (March): 111–118.

Bar-Yosef, B., and D. Meek. 1987. Selenium sorption by kaolinite and montmorillonite. *Soil Science* 144: 11–19.

Basile, L. J., J. R. Ferraro, M. L. Mitchell, and J. C. Sullivan. 1978. The raman scattering of actinide(VI) ions in carbonate media. *Applied Spectroscopy* 32(6): 535–7.

Bates, J. K., B. S. Tani, E. Veleckis, and D. J. Wronkiewicz. 1990. Identification of secondary phases formed during reaction of UO_2 with EJ-13 water. *Materials Research Society Symposium Proceedings* 176: 499–506.

Bates, J. K., J. P. Bardley, A. Teetsov, C. R. Bradley, and M. Buchholtz ten Brink. 1992. Colloid formation during waste form reaction: Implications for nuclear waste disposal. *Science* 256: 649–651. (YMP accession number NNA.920416.0050.)

Bates, J. K., W. L. Bourcier, C. R. Bradley, E. C. Buck, J. C. Cunnane, N. L. Dietz, W. L. Ebert, J. W. Emery, R. C. Ewing, X. Feng, T. J. Gerding, M. Gong, J. C. Hoh, H. Li, J. J. Mazer, L. E. Morgan, L. Newton, J. K. Nielsen, B. L. Phillips, M. Tomozawa, L. Wang, and D. J. Wronkiewicz. 1993. ANL technical support program for DOE Environmental Restoration and Waste Management. *Annual Report: October 1991–September*

1992. Argonne National Laboratory report ANL-93/13. (YMP accession number NNA.930907.0056.)

Becraft, K., D. Hobart, P. Torretto, T. Prussin, H. Nitsche, K. Roberts, and S. A. Carpenter. 1994. Solubilities and speciation from oversaturation experiments of neptunium, plutonium, and americium in a neutral electrolyte with a total carbonate similar to UE-25 p#1 well water from the Yucca Mountain region. Lawrence Berkeley Laboratory report LA-LBL-TIP-94-002 on YMP milestone 3411 (under contract to Los Alamos National Laboratory).

Data for this milestone are in YMP notebooks:

TWS-LBL-01-93-02, pp. 81–302;
TWS-LBL-01-93-03, pp. 39–67;
TWS-LBL-01-93-04, pp. 1–241;
TWS-LBL-12-93-02, pp. 1–151.

Benjamin, M. M. 1983. Adsorption and surface precipitation of metals on amorphous iron oxyhydroxide. *Environmental Science and Technology* 17: 686–692.

Bennett, D. A., D. Hoffman, H. Nitsche, R. E. Russo, R. A. Torres, P. A. Baisden, J. E. Andrews, C. E. A. Palmer, and R. J. Silva. 1992. Hydrolysis and carbonate complexation of dioxoplutonium(V). *Radiochimica Acta* 56(1): 15–19.

Benson, L. V. 1976. Mass transport in vitric tuffs of Rainier Mesa, Nye County, Nevada. Water Resources Center report NVO-1253-10 (Desert Research Institute). (YMP accession number NNA.900117.0159.)

Bernkopf, M., and J. I. Kim. 1984. Hydrolysis reactions and carbonate complexation of americium(III) in natural aquatic systems. RCM 02884, Institute für Radiochemie, Technische Universität München. (Referenced in Kim (1986), Table 3, p. 428.)

Bidoglio, G. 1982. Characterization of americium(III) complexes with bicarbonate and carbonate ions at groundwater concentration levels. *Radiochemical and Radioanalytical Letters* 53(1): 45–60.

Bidoglio, G., G. Tanet, and A. Chatt. 1985. Studies on neptunium(V) carbonate complexes under geologic repository conditions. *Radiochimica Acta* 38(1): 21–6.

Bidoglio, G., P. Cavalli, I. Grenthe, N. Omenetto, P. Qi, and G. Tanet. 1991. Studies on metal carbonate equilibria: Part 21. Study of the U(VI)-H_2O-CO_2(g) system by thermal lensing spectrophotometry. *Talanta* 38: 433–437.

Bish, D. L., and S. J. Chipera. 1989. Revised mineralogic summary of Yucca Mountain, Nevada. Los Alamos National Laboratory report LA-11497-MS (March).

Bish, D. L., and J. E. Post. 1989. Thermal behavior of complex, tunnel-structure manganese oxides. *American Mineralogist* 74: 177–186.

Bish, D. L., and D. T. Vaniman. 1985. Mineralogic summary of Yucca Mountain, Nevada. Los Alamos National Laboratory report LA-10543-MS (October).

Bish, D. L., D. T. Vaniman, R. S. Rundberg, K. Wolfsberg, W. R. Daniels, and D. E. Broxton. 1983. Natural sorptive barriers in Yucca Mountain, Nevada, for long-term isolation of high-level waste. In *Radioactive Waste Management: Proceedings of the IAEA International Conference on Radioactive Waste Management, Seattle, Washington, 16–20 May 1983*, IAEA-CN-43/461, pp. 415–432. Vienna, Austria: International Atomic Energy Agency.

Bish, D. L., J. W. Carey, B. A. Carlos, S. J. Chipera, G. D. Guthrie, Jr., S. S. Levy, D. T. Vaniman, and G. WoldeGabriel. 1996a. Summary and synthesis report on mineralogy and petrology studies for the Yucca Mountain Site Characterization Project: Volume I. Introduction. Los Alamos National Laboratory Geology and Geochemistry

Group report on milestone 3665.

Bish, D. L., J. W. Carey, S. S. Levy, and S. J. Chipera. 1996b. Mineralogy-petrology contribution to the near-field environment report. Los Alamos National Laboratory report on milestone LA3368 (March).

Blanchard, G., M. Maunaye, and G. Martin. 1984. Removal of heavy metals from waters by means of natural zeolites. *Water Research* 18: 1501–1507.

Bolt, G. H., and M. G. M. Bruggenwert. 1976. *Soil Chemistry Basic Elements*. Amsterdam: Elsevier.

Bonnot-Courtois, C., and N. Jaffiezic-Renault. 1982. Etude des echanges entre terres rares et cations interfoliares de deux argiles. *Clays and Clay Minerals* 17: 409–420.

Borovec, Z. 1981. The adsorption of uranyl species by fine clay. *Chemical Geology* 32: 45–58.

Bourges, J. Y., B. Guillaume, G. Koehly, D. E. Hobart, and J. R. Peterson. 1983. Coexistence of americium in four oxidation states in sodium carbonate-sodium bicarbonate medium. *Inorganic Chemistry* 22(8): 1179–84.

Bouwer, H. 1991. Simple derivation of the retardation equation and application to preferential flow and macrodispersion. *Ground Water* 29: 41.

Bowman, R. S., and G. A. O'Connor. 1982. Control of nickel and strontium sorption by free metal ion activity. *Soil Science Society of America Journal* 46: 933–936.

Bradbury, M. H., and B. Baeyens. 1995. A quantitative mechanistic description of Ni, Zn, and Ca sorption on Na-montmorillonite: Part III. Modelling. Paul Scherrer Institute report PSI Bericht Nr. 95-12 (Villigen, Switzerland).

Bradbury, M. H., A. Green, D. Lever, and I. G. Stephen. 1986. Diffusion and permeability-based sorption measurements in sandstone, anhydrite, and upper magnesian limestone samples. Harwell report AERER 11995 (Oxfordshire, England, March).

Breck, D. W. 1974. *Zeolite Molecular Sieves: Structure, Chemistry, and Use*. New York: John Wiley & Sons.

Bresler, E., B. L. McNeal, and D. L. Carter. 1982. *Saline and Sodic Soils*. New York: Springer-Verlag.

Britten, J. A., B. J. Travis, and L. F. Brown. 1983. Calculation of surface site-energy distributions from adsorption isotherms and temperature-programmed desorption data. Los Alamos National Laboratory report LA-UR-83-1654.

Brookins, D. G. 1983. Migration and retention of elements at the Oklo natural reactor. *Environmental Geol*ogy 4: 201–208.

Brookins, D. G. 1988. *Eh-pH Diagrams for Geochemistry*. New York: Springer-Verlag.

Brouwer, E., B. Baeyens, A. Maes, and A. Cremers. 1983. Cesium and rubidium ion equilibria in illite clay. *Journal of Physical Chemistry* 87: 1213–1219

Brown, J. C., and P. N. Pusey. 1975. Photon correlation study of polydisperse samples of polystyrene in cyclohexane. *Journal of Chemical Physics* 62(3): 1136.

Brown, R. E., H. M. Parker, and J. M. Smith. 1956. Disposal of liquid wastes to the ground. In *Proceedings of the International Conference on the Peaceful Uses of Atomic Energy, Geneva, August 8–20, 1955, Reactor Technology and Chemical Processing, Vol. 9*, pp. 669–675.

Brown, P. L., J. Ellis, and R. N. Sylva. 1983. The hydrolysis of metal ions: Part 5. Thorium(IV). *Journal of the Chemical Society: Dalton*

Transactions (1983): 31–34.

Broxton, D. E., R. G. Warren, R. C. Hagan, and G. Luedemann. 1986. Chemistry of diagenetically altered tuffs at a potential nuclear waste repository, Yucca Mountain, Nye County, Nevada. Los Alamos National Laboratory report LA-10802-MS (October).

Bruno, J. 1990. The influence of dissolved carbon-dioxide on trace-metal speciation in seawater. *Marine Chemistry* 30: 231–240.

Bruno, J., I. Casas, I. Grenthe, and B. Lagerman. 1987. Studies on metal carbonate complexes: 19. Complex formation in the Th(IV)-H_2O-CO_2(g) system. *Inorganica Chimica Acta* 140: 299.

Bruno, J., I. Grenthe, and P. Robouch. 1989. Studies of metal carbonate equilibria: 20. Formation of tetra(carbonato) uranium(IV) ion, $U(CO_3)_4^{4-}$, in hydrogen carbonate solutions. *Inorganica Chimica Acta* 158: 221–226.

Bruque, S., T. Mozas, and A. Rodriguez. 1980. Factors influencing retention of lanthanide ions by montmorillonite. *Clays and Clay Minerals* 15: 413–420.

Bruton, C. J. 1990. Solubility controls on radionuclide concentrations in solution: Preliminary results for U, Np, Pu, and Am. Lawrence Livermore National Laboratory draft report.

Bruton, C. J. 1991. Equilibrium controls of radionuclide concentrations in Nevada Test Site waters: Preliminary results for Th, U, Np, Pu, Am, Sr, Ra, and Pb. Appendix D in Sandia National Laboratories report SAND91-0170 - UC-902 (Chu, M. S. Y., and E. A. Bernard. Waste inventory and preliminary source term model for the greater confinement disposal site at the Nevada Test Site.).

Buck, E. C., J. K. Bates, J. C. Cunnane, W. L. Ebert, X. Feng, and D. J. Wronkiewicz. 1993. Analytical electron microscopy study of colloids from nuclear waste glass. *Materials Research Society Symposium Proceedings* 294: 199–206. (YMP accession number NNA.930907.0053.)

Buddemeier, R. W., and J. R. Hunt. 1988. Transport of colloidal contaminants in groundwater. *Applied Geochemistry* 3(5): 535–548. (YMP accession number NNA.930701.0051.)

Buesseler, K. O., and E. R. Sholkovitz. 1987. The geochemistry of fallout plutonium in the North Atlantic: I. A pore water study in shelf, slope, and deep-sea sediments. *Geochimica et Cosmochimica Acta* 51: 2605–2622.

Buscheck, T. A., and J. J. Nitao. 1993. The analysis of repository-heat-driven hydrothermal flow at Yucca Mountain. In *High-Level Waste Management: Proceedings of the Fourth Annual International Conference, Las Vegas, Nevada, April 26–30, 1993*. (YMP accession number NNA.930315.0012.)

Butler, J. P., J. A. Reeds, and S. V. Dawson. 1981. Estimating solutions of first-kind integral equations with nonnegative constraints and optimal smoothing. *SIAM Journal on Numerical Analysis* 18: 381–397.

Byrne, R. H., and K. Kim. 1993. Rare-earth precipitation and coprecipitation behavior: The limiting role of PO_4^{3+} on dissolved rare-earth concentrations in seawater. *Geochimica et Cosmochimica Acta* 57: 519–526.

Cametti, C. P., P. Codastefano, and P. Tartaglia. 1989. Aggregation kinetics in model colloidal systems: A light scattering study. *Journal of Colloid and Interface Science* 131(2): 409–422.

Canepa, J. A., I. R. Triay, P. S. Z. Rogers, M. E. Hawley, and G. A. Zyvoloski. 1994. The Yucca Mountain Site Characterization Project: Site-specific research and development on the chemistry and migration of actinides. In *Chemistry and Migration Behavior of Actinides and Fission Products in the Geosphere: Proceedings of the*

Fourth International Conference, Charleston, South Carolina, USA, December 12–17, 1993, pp. 813–820.

Cann, J. R. 1970. Rb, Sr, Y, Zr, and Nb in some ocean floor basaltic rocks. *Earth and Planetary Science Lett*ers 10: 7–11.

Carey, J. W., D. L. Bish, and S. J. Chipera. 1996. Summary and synthesis report on mineralogy and petrology studies for the Yucca Mountain Site Characterization Project: Volume III. Kinetics and thermodynamics of mineral evolution at Yucca Mountain. Los Alamos National Laboratory Earth and Environmental Sciences division report on milestone 3665.

Carlos, B. A. 1985. Minerals in fractures of the unsaturated zone from drill core USW G-4, Yucca Mountain, Nye County, Nevada. Los Alamos National Laboratory report LA-10415-MS (May).

Carlos, B. A. 1987. Minerals in fractures of the saturated zone from drill core USW G-4, Yucca Mountain, Nye County, Nevada. Los Alamos National Laboratory report LA-10927-MS (April).

Carlos, B. A. 1989. Fracture-coating minerals in the Topopah Spring Member and Upper Tuff of Calico Hills from drill hole J-13. Los Alamos National Laboratory report LA-l1504-MS (February).

Carlos, B. A. 1990. Manganese-oxide minerals in fractures of the Crater Flat Tuff in drill core USW G-4, Yucca Mountain, Nevada. Los Alamos National Laboratory report LA-11787-MS (July).

Carlos, B. A. 1994. Field guide to fracture-lining minerals at Yucca Mountain, Nevada. Los Alamos National Laboratory report LA-12803-MS.

Carlos, B. A., D. L. Bish, and S. J. Chipera. 1990. Manganese-oxide minerals in fractures of the Crater Flat Tuff in drill core USW G-4, Yucca Mountain, Nevada. Los Alamos National Laboratory report LA-11787-MS (July).

Carlos, B. A., S. J. Chipera, D. L Bish, and S. J. Craven. 1993. Fracture-lining manganese oxide minerals in silicic tuff, Yucca Mountain, Nevada, USA. *Chemical Geology* 107: 47–69.

Carpenter, R., T. M. Beasley, D. Zahnle, and B. L. K. Somayalulu. 1987. Cycling of fallout (Pu, ^{241}Am, ^{137}Cs) and natural (U, Th, ^{210}Pb) radionuclides in Washington continental slope sediments. *Geochimica et Cosmochimica Acta* 51: 1897–1921.

Carr, W. J., F. M. Byers, Jr., and P. P. Orkild. 1986. Stratigraphic and volcano-tectonic relations of Crater Flat tuff and some older volcanic units, Nye County, Nevada. U.S. Geological Survey professional paper 1323.

Cassol, A., L. Magon, R. Portanova, and E. Tondello. 1972. Hydrolysis of plutonium(VI): Acidity. *Radiochimica Acta* 17(1): 28–32.

Chadwick, O. A., D. M. Hendricks, and W. D. Nettleton. 1987. Silica in duric soils: I. A depositional model. *Soil Science Society of America Journal* 51: 975–982.

Chipera, S. J., and D. L. Bish. 1989. Quantitative x-ray diffraction analyses of samples used for sorption studies by the Isotope and Nuclear Chemistry Division, Los Alamos National Laboratory. Los Alamos National Laboratory report LA-11669-MS (September).

Chipera, S. J., and D. L. Bish. 1994. Quantitative x-ray diffraction results for samples used for the sorption task. Letter report LA-EES-1-05-94-001, EES-1, Los Alamos National Laboratory (May).

Choppin, G. R. 1988. Humics and radionuclide migration. *Radiochimica Acta* 44/45: 23–28. (YMP accession number NNA.930607.0066.)

Choppin, G. R. 1992. The role of natural organics in radionuclide migration in natural aquifer systems. *Radiochimica Acta* 58/59: 113–120.

Choppin, G. R., and L. F. Rao. 1984. Complexation of pentavalent and hexavalent actinides by fluoride. *Radiochimica Acta* 37: 143–146.

Christ, C. L., J. R. Clark, and H. T. Evans, Jr. 1955. Crystal structure of rutherfordine. *Science* 121: 472.

Chukhrov, F. V., A. I. Gorshkov, A. V. Sivtsov, and V. V. Berezovskaya. 1985a. The nature and genesis of lithiophorite. *International Geology Review* 27: 348–361.

Chukhrov, F. V., A. I. Gorshkov, V. A. Drits, and Yu. P. Dikov. 1985b. Structural varieties of todorokite. *International Geology Review* 27: 1481–1491.

Chukhrov, F. V., A. I. Gorshkov, and V. A. Drits. 1987. Advances in the crystal chemistry of manganese oxides. *International Geology Review* 29: 435–444.

Ciavatta, L., D. Ferri, M. Grimaldi, R. Palombari, and F. Salvatore. 1979. Dioxouranium(VI) carbonate complexes in acid solution. *Journal of Inorganic and Nuclear Chemistry* 41: 1175–1182.

Ciavatta, L., D. Ferri, I. Grenthe, and F. Salvatore. 1981. The first acidification step of the tris(carbonato)dioxouranate(VI) ion, $UO_2(CO_3)_3^{4-}$. *Inorganic Chemistry* 20: 463–467.

Ciavatta, L., D. Ferri, I. Grenthe, F. Salvatore, and K. Spahiu. 1983. Studies on metal carbonate equilibria: 4. Reduction of the tris(carbonato)dioxourante(VI) ion, $UO_2(CO_3)_3^{4-}$, in hydrogen carbonate solutions. *Inorganic Chemistry* 22: 2088.

Clark, D. L. 1994. Letter report on the status of Pu(IV) colloid studies. Los Alamos National Laboratory YMP milestone 4026 (September 30, 1994).

Clark, D. L., and P. D. Palmer. 1994. ^{17}O and ^{13}C NMR studies of uranyl and neptunyl carbonate complexes in near-neutral solution. In *Chemistry and Migration Behavior of Actinides and Fission Products in the Geosphere: Proceedings of the Fourth International Conference, Charleston, SC, USA, December 12–17, 1993*, p. 32.

Clark, D. L., S. A. Ekberg, D. E. Morris, P. D. Palmer, and C. D. Tait. 1994. Actinide(IV) and actinide(VI) carbonate speciation studies by PAS and NMR spectroscopies: YMP milestone 3031. Los Alamos National Laboratory report LA-12820-MS. (YMP accession number NNA.931015.0074.)

Clark, D. L., Hobart, D. E., and M. P. Neu. 1995a. Actinide carbonate complexes and their role in actinide environmental chemistry. *Chemical Reviews* 95: 25.

Clark, D. L., C. D. Tait, M. P. Neu, P. D. Palmer, S. A. Ekberg, N. J. Hess, and S. D. Conradson. 1995b. Structural studies of pentavalent neptunium and plutonium in carbonate solutions using multinuclear NMR, raman, EXAFS, and single-crystal XRD techniques. Abstract for *Inorganic Chemistry Division, 1995 International Chemical Congress of Pacific Basin Societies (PACIFICHEM 95), Honolulu, HI, December 17–22, 1995*.

Clark, D. L., T. W. Newton, P. D. Palmer, and B. D. Zwick. 1995c. ^{13}C and ^{17}O binding constant studies of uranyl carbonate complexes in near-neutral aqueous solution: YMP milestone 3351. Los Alamos National Laboratory report LA-12897-MS. (YMP accession number NNA.931021.0073.)

Combes, J. M., C. J. Chisholm-Brause, G. E. Brown, Jr., G. A. Parks, S. D. Conradson, P. G. Eller, I. R. Triay, D. E. Hobart, and A. Meijer. 1992. EXAFS spectroscopic study of neptunium(V) sorption at the α-FeOOH/water interface. *Environmental Science and Technology* 26: 376–382.

Conca, J. L., and I. R. Triay. 1994. Selenite transport in unsaturated tuff from Yucca Mountain. In *High Level Radioactive Waste Management: Proceedings of the Fifth Annual International*

Conference, Las Vegas, Nevada, May 22–26, 1994, pp. 2175–2182. LaGrange Park, Illinois: American Nuclear Society.

Conca, J. L., and J. Wright. 1990. Diffusion coefficients in gravel under unsaturated conditions. *Water Resources Research* 26: 1055–1066.

Conca, J. L., and J. V. Wright. 1992a. A new technology for direct measurements of unsaturated transport. In *Proceedings of the Nuclear and Hazardous Waste Management Spectrum '92 Meeting, Vol. 2*, p. 1546. La Grange Park, Illinois: American Nuclear Society.

Conca, J. L., and J. V. Wright. 1992b. Flow and diffusion in unsaturated gravel, soils, and whole rock. *Applied Hydrogeology* 1: 5–24.

Cotton, F. A., and G. Wilkinson. 1988. *Advanced Inorganic Chemistry*, fifth edition. New York: John Wiley & Sons.

Cramer, J. J., and F. P. Sargent. 1994. The Cigar Lake analog study: An international R&D project. In *High Level Radioactive Waste Management: Proceedings of the Fifth Annual International Conference, Las Vegas, Nevada, May 22–26, 1994*, pp. 2237–2242. LaGrange Park, Illinois: American Nuclear Society.

Cremers, A. 1977. In *Molecular Sieves - II,* edited by J. R. Katzer, p. 179. Washington, D.C.: American Chemical Society.

Curtis, D. E., and J. Fabryka-Martin. 1988. Report on trip to Alligator River analogue project. Workshop held in Tucson, Arizona, November 21–22, 1988.

Daniels, W. R., K. Wolfsberg, R. S. Rundberg, A. E. Ogard, J. F. Kerrisk, C. J. Duffy, et al. 1982. Summary report on the geochemistry of Yucca Mountain and environs. Los Alamos National Laboratory report LA-9328-MS (December).

Davis, J. A., R. O. James, and J. O Leckie. 1978. Surface ionization and complexation at the oxide-water interface. *Journal of Colloid and Interface Science* 63(3): 480–499.

Davydov, Y. P., and I. G. Toropov. 1992. Hydrolysis of Th^{4+} cations with formation of polynuclear hydroxo complexes in solutions. *Doklady Akademii Nauk Belarusi* 36: 229–233.

Dearlove, J. P. L., G. Longworth, M. Ivanovich, J. I. Kim, B. Delakowitz, and P. Zeh. 1991. A study of groundwater colloids and their geochemical interactions with natural radionuclides in Gorleben aquifer systems. *Radiochimica Acta* 52/53: 83–89. (YMP accession number NNA.830607.0067.)

Decarreau, A. 1985. Partitioning of divalent transition metals between octahedral sheets of trioctahedral smectites and water. *Geochimica et Cosmochimica Acta* 49: 1537–1544.

Deer, W. A., R. A. Howie, and J. Zussman. 1966. *An Introduction to the Rock-forming Minerals*. London: Longman Group Limited.

Degueldre, C. 1993. Colloid properties in granitic groundwater systems, with emphasis on the impact on safety assessment of a radioactive waste repository. In *Materials Research Symposium Proceedings, November 30–December 4, 1992*, p. 294. Pittsburgh, Pennsylvania: Materials Research Society. (YMP accession number NNA.830807.0069.)

Degueldre, C. 1994. Colloid properties in groundwaters from crystalline formations. PSI/NAGRA report NTB-92-05 (Paul Scherrer Institute, Villigen, Switzerland).

Degueldre, C., and H. Thomi. 1986. Réalisation d'une cellule de diaultrafiltration a injection pulsée. Paul Scherrer Institute technical memo TM-42-86-37 (Villigen, Switzerland). (YMP accession number NNA.931005.0017.)

Degueldre, C., B. Baeyens, W. Goerlich, J. Riga, J. Verbist, and P. Stadelmann. 1989a. Colloids in water from a subsurface fracture in granitic rock, Grimsel Test Site, Switzerland. *Geochimica et Cosmochimica Acta* 53: 603–610. (YMP accession number NNA.930607.0068.)

Degueldre, C., G. Longworth, V. Moulin, P. Vilks, C. Ross, G. Bidoglio, A. Cremers, J. Kim, J. Pieri, J. Ramsay, B. Salibu, and U. Vuorinen. 1989b. Grimsel Colloid Exercise: An international intercomparison exercise on the sampling and characterization of groundwater colloids. Paul Scherrer Institute internal report TM-36 (Villigen, Switzerland). (YMP accession number NNA.930625.0034.)

Degueldre, C., G. Longworth, V. Moulin, and P. Vilks. 1990. Grimsel Colloid Exercise: An international intercomparison exercise on the sampling and characterization of groundwater colloids. PSI/NAGRA/CEDRA/CISRA technical report 90-01 (January 1990; Paul Scherrer Institute, Villigen, Switzerland).

De Laeter, J. R., J. K. R. Rosman, and C. L. Smith. 1980. The Oklo natural reactor: Cumulative fission yields and retentivity of the symmetric mass region fission products. *Earth and Planetary Science Lett*ers 50: 238–246.

de Marsily, G. 1986. *Quantitative Hydrogeology: Groundwater Hydrology for Engineers*. Academic Press, Inc.

Désiré, B., M. Hussonnois, and R. Guillaumont. 1969. Détermination de la premiere constante d'hydrolyse de l'americium, du curium, du berkelium et du californium. *Comptes Rendus des Séances de L'académie des Sciences, Série C: Sciences Chimiques* 269: 448–451.

DOE. 1988. Site Characterization Plan, Yucca Mountain Site, Nevada Research and Development Area, Nevada. U.S. Department of Energy report DOE/RW-199. Washington, D.C.: Office of Civilian Radioactive Waste Management.

Doi, K., S. Hirono, and Y. Sakamaki. 1975. Uranium mineralization by groundwater in sedimentary rocks, Japan. *Economic Geology* 70: 628–646.

Dozol, M., and R. Hagemann. 1993. Radionuclide migration in groundwaters: Review of the behaviour of actinides. *Pure and Applied Chemistry* 65: 1081.

Drever, J. I. 1988. *The Geochemistry of Natural Waters*, p. 437. New Jersey: Prentice Hall.

Drever, J. I., and C. L. Smith. 1978. Cyclic wetting and drying of the soil zone as an influence on the chemistry of groundwater in arid terrains. *American Journal of Science* 278: 1448–1454.

Duddy, I. R. 1980. Redistribution and fractionation of rare-earth and other elements in a weathering profile. *Chemical Geology* 30: 363–381.

Duffy, C. J. 1985. Preliminary conceptual model for mineral evolution in Yucca Mountain. Los Alamos report on YMP milestone R359. (YMP accession number NNA.900117.0152.)

Dzombak, D. A., and F. M. M. Morel. 1990. *Surface Complexation Modeling Hydrous Ferric Oxide*, Chapter 10. New York: John Wiley & Sons.

Efurd, D. W., W. Runde, J. C. Banar, F. R. Roensch, D. L. Clark, P. D. Palmer, and C. D. Tait. 1996. Measured solubilities and speciation of neptunium and plutonium in J-13 groundwater. Los Alamos National Laboratory report on YMP milestone 3411(in preparation).
Data for this milestone are in YMP notebook: LA-CST-NBK-95-010, pp. 1–156.

Eisenbud, M., K. Krauskopf, E. P. Franca, W. Lei, R. Ballad, P. Linsalata, and K. Fijimori. 1984. Natural analogues for the transuranic actinide elements: An investigation in Minas Gerais, Brazil. *Environmental Geology and Water Sciences* 6: 1–9.

Ellinger, F. H., and W. H. Zachariasen. 1954. The crystal structure of $KPuO_2CO_3$, $NH_4PuO_2CO_3$, and $RbAmO_2CO_3$. *Journal of Physical Chemistry* 58: 405.

Emch, R., F. Zenhausern, M. Jobin, M. Taborelli, and P. Descouts. 1992. Morphological difference between fibronectin sprayed on mica and on PMMA. In *Ultramicroscopy 1992, Proceedings of the Sixth International Conference on Scanning Tunneling Microscopy and Related Techniques*. (YMP accession number NNA.931103.0021.)

Engkvist, I., and Y. Albinsson. 1992. Hydrolysis studies of thorium using solvent-extraction technique. *Radiochimica Acta* 58/59(pt. 1): 109–112.

EPA. 1982. Radiation protection, subpart B, environmental standards for disposal. *Code of Federal Regulations*, 40 CFR 191. Washington, D.C.: Environmental Protection Agency.

Essington, E. H., E. B. Fowler, R. O. Gilbert, and L. L. Eberhardt. 1978. Plutonium, americium, and uranium concentrations in Nevada Test Site soil profiles. In *Transuranium Nuclides in the Environment* (IAEA publication SM-199/87), pp. 157–173. Vienna, Austria: International Atomic Energy Agency.

Fabryka-Martin, J. T., P. R. Dixon, S. Levy, B. Lui, H. J. Turin, and A. V. Wolfsberg. 1996. Summary report of Cl^{36} studies: Systematic sampling for chlorine-36 in the Exploratory Shaft Facility. Los Alamos National Laboratory milestone report (April).

Felmy, A. R., D. Rai, and R. W. Fulton. 1990. The solubility of americium hydroxide carbonate ($AmOHCO_3$(c)) and the aqueous thermodynamics of the system sodium(1+)-americium(3+)-bicarbonate-carbonate-hydroxide-water. *Radiochimica Acta* 50(4): 193–204.

Feng, X., E. C. Buck, C. Mertz, J. K. Bates, and J. C. Cunnane. 1993. Study on the colloids generated from testing of high-level nuclear waste glasses. In *Proceedings of the Symposium on Waste Management, Tucson, Arizona, February 28–March 4, 1993, Vol. 2*, pp. 1015–1021. (YMP accession number NNA.930907.0054.)

Ferri, D., I. Grenthe, and F. Salvatore. 1983. Studies on metal carbonate equilibriums: 7. Reduction of the tris(carbonato)dioxouranate(VI) ion, $UO_2(CO_3)_3^{4-}$, in carbonate solutions. *Inorganic Chemistry* 22(21): 3162–3165.

Ferri, D., J. Glaser, and I. Grenthe. 1988. Confirmation of the structure of $(UO_2)_3(CO_3)_6^{6-}$ by ^{17}O NMR. *Inorganica Chimica Acta* 148: 133–34.

Flexser, S., and H. A. Wollenberg. 1992. Radioelements and their occurrence with secondary minerals in heated and unheated tuff at the Nevada test site. In *High Level Radioactive Waste Management: Proceedings of the Third Annual International Conference, Las Vegas, Nevada, April 12–16, 1992*, pp. 1593–1598. LaGrange Park, Illinois: American Nuclear Society.

Flint, A. L., and L. E. Flint. 1994. Spatial distribution of potential near-surface moisture flux at Yucca Mountain. In *High Level Radioactive Waste Management: Proceedings of the Fifth Annual International Conference, Las Vegas, Nevada, May 22–26, 1994*, pp. 2352–2358. La Grange Park, Illinois: American Nuclear Society.

Freeze, A., and J. Cherry. 1980. *Groundwater*. New York: Prentice-Hall.

Frysinger, G. R., and H. C. Thomas. 1960. Adsorption studies on clay minerals: VII. Yttrium-cesium and cerium(III)-cesium on montmorillonite. *Journal of Physical Chemistry* 64: 224–228.

Fuger, J. 1992. Thermodynamic properties of actinide aqueous species relevant to geochemical problems. *Radiochimica Acta* 59(pt. 1): 81–91.

Gaines, G. L., Jr., and H. C. Thomas. 1953. Adsorption studies on clay minerals: II. A formulation of the thermodynamics of exchange adsorption. *Journal of Chemical Physics* 21: 714.

GCX. 1994. Groundwater compositional parameters most critical to the sorption behavior of radionuclides-of-concern to the Yucca Mountain Project. GCX (P.O. Box 82427, Albuquerque, NM).

Geddes, L. A., C. P. DaCosta, and G. Wise. 1971. The impedance of stainless-steel electrodes. *Medical and Biological Engineering* 9: 511–521.

George-Aniel, B., J. L. Leroy, and B. Poty. 1991. Volcanogenic uranium mineralizations in the Sierra Peña Blanca District, Chihuahua, Mexico: Three genetic models. *Economic Geology* 86: 233–248.

Giffaut, E., and P. Vitorge. 1993. Evidence of radiolytic oxidation of ^{241}Am in $Na^+/Cl^-/HCO_3^-/CO_3^{2-}$ media. *Materials Research Society Symposium Proceedings (Scientific Basis for Nuclear Waste Management XVI)* 294: 747–751.

Gifford, R. O., and D. M. Frugoli. 1964. Silica source in soil solutions. *Science* 145: 386–388.

Gilbin, A. M., and A. A. Snelling. 1983. Application of hydrogeochemistry to uranium exploration in the Pine Creek geosyncline, Northern Territory, Australia. *Journal of Geochemical Exploration* 19: 33–55.

Gislason, S. R., and H. P. Eugster. 1987. Meteoric water-basalt interactions: I. A laboratory study. *Geochimica et Cosmochimica Acta* 51: 2827–2840.

Goldschmidt, V. M. 1958. *Geochemistry*. Oxford: Clarendon Press.

Gomez, P., M. J. Turrero, V. Moulin, and M. C. Magonthier. 1992. Characterization of natural colloids in groundwaters of El Berrocal, Spain. In *Water-Rock Interaction*, edited by Kharaka and Maest, pp. 797–800. Balkema, Rotterdam. (YMP accession number NNA.830607.0071.)

Goodwin, B. W., J. J. Cramer, and D. B. McConnell. 1989. The Cigar Lake uranium deposit: An analogue for nuclear fuel waste disposal. Appendix B in *Natural Analogues in Performance Assessments for the Disposal of Long-Lived Radioactive Wastes*, IAEA technical reports series No. 304, pp. 37–50. Vienna, Austria: International Atomic Energy Agency.

Grambow, B. 1992. Geochemical approach to glass dissolution. In *Corrosion of Glass, Ceramics, and Ceramic Superconductors*, edited by D. E. Clark and B. K. Zoitos, pp. 124–152. Park Ridge, New Jersey: Noyes Publications.

Greenland, D. J., and M. H. B. Hayes. 1978. *The Chemistry of Soil Constituents.* New York: John Wiley & Sons.

Grenthe, I., and B. Lagerman. 1991a. Studies on metal carbonate equilibria: 22. A coulometric study of the uranium(VI)-carbonate system, the composition of the mixed hydroxide carbonate species. *Acta Chemica Scandinavica* 45: 122–128.

Grenthe, I., and B. Lagerman. 1991b. Studies on metal carbonate equilibria: 23. Complex formation in the thorium (IV)-water-carbon dioxide(g) system. *Acta Chemica Scandinavica* 45(3): 231–8.

Grenthe, I., D. Ferri, F. Salvatore, and G. Riccio. 1984. Studies on metal carbonate equilibria: Part 10. A solubility study of the complex formation in the uranium(VI)-water-carbon dioxide(g) system at 25ºC. *Journal of the Chemical Society: Dalton Transactions* (1984): 2439–2443.

Grenthe, I., C. Riglet, and P. Vitorge. 1986a. Studies of metal-carbonate complexes: 14. Composition and equilibria of trinuclear neptunium(VI)- and plutonium(VI)-carbonate complexes. *Inorganic Chemistry* 25(10): 1679–1684.

Grenthe, I., P. Robouch, and P. Vitorge. 1986b.

Chemical equilibria in actinide carbonate systems. *Journal of the Less-common Metals* 122: 225–231.

Grenthe, I., J. Fuger, R. J. M. Konigs, R. J. Lemire, A. B. Muller, C. Nguyen-Trung, and H. Wanner. 1992. *Chemical Thermodynamics of Uranium*. New York: Elsevier Science Publishing Company.

Grimaldi, F. S., and I. A. Berger. 1961. Niobium content of soils from West Africa. *Geochimica et Cosmochimica Acta* 25: 71–80.

Gschwend, P. M., and M. D. Reynolds. 1987. Monodisperse ferrous phosphate colloids in an anoxic groundwater plume. *Journal of Contaminant Hydrology* 113(1): 232–240. (YMP accession number NNA.931005.0018.)

Guiter, H. 1947. Hydrolyse du nitrate d'uranyl. *Bulletin de la Societe Chimique de France* (1947): 64–67.

Gupta, S. C., and R. J. Hanks. 1972. Influence of water content on electrical conductivity of the soil. *Soil Science Society of America Proceedings* 36: 855–857.

Harrar, J., J. Carley, W. Isherwood, and E. Raber. 1990. Report of the committee to review the use of J-13 well water in the Nevada nuclear waste storage investigations. Lawrence Livermore National Laboratory report UCID-21867.

Hayes, K. F., A. L. Roe, G. E. Brown, Jr., K. O. Hodgson, J. O. Leckie, and G. A. Parks. 1987. In-situ x-ray absorption study of surface complexes: Selenium oxyanions on α-FeOOH. *Science* 238: 783–786.

Hersman, L. E. 1996. Summary and synthesis report: Microbiological sorption and transport of radioactive wastes, Yucca Mountain, NV. Los Alamos National Laboratory report on milestone 3663.

Hevesi, J. A., A. L. Flint, and J. D. Istock. 1992. Precipitation estimation in mountainous terrain using multivariate geostatistics: Part II. Isohyetal maps. *Journal of Applied Meteorology*, 31: 677–688.

Hiester, N. K., and T. Vermeulen. 1952. Saturation performance of ion-exchange and adsorption columns. *Chemical Engineering Progress* 48(10): 505–516.

Hingston, F. J., A. M. Posner, and J. P. Quirk. 1971. Competitive adsorption of negatively charged ligands on oxide surfaces. *Discussions of the Faraday Society* 52: 334–351.

Hirose, K., and E. Tanoue. 1994. Thorium-particulate matter interaction: Thorium complexing capacity of oceanic particulate matter: Theory. *Geochimica et Cosmochimica Acta* 58: 1–7.

Ho, C. H., and N. H. Miller. 1986. Adsorption of uranyl species from bicarbonate solution onto hematite particles. *Journal of Colloid and Interface Science* 110: 165–171.

Hobart, D. E. 1990. Actinides in the environment. In *Fifty Years with Transuranium Elements: the Robert A. Welch Foundation Conference on Chemical Research, XXXIV, October 22–23, 1990, Houston, TX*, p. 379.

Hobart, D. E., K. Samhoun, J. R. Peterson. 1982. Spectroelectrochemical studies of the actinides: Stabilization of americium(IV) in aqueous carbonate solution. *Radiochimica Acta* 31: 139–145.

Hobart, D. E. , D. E. Morris, P. D. Palmer, and T. W. Newton. 1989. Formation, characterization, and stability of plutonium(IV) colloid: A progress report. In *Proceedings of the Nuclear Waste Isolation in the Unsaturated Zone, Focus '89 Conference, September 17–21, 1989, Las Vegas, Nevada*, pp. 118–124. La Grange Park, Illinois: American Nuclear Society. (YMP accession number NNA.890815.0254.)

Howard, J. H., III. 1977. Geochemistry of selenium: Formation of ferroselite and selenium behavior in the vicinity of oxidizing sulfide and uranium deposits. *Geochimica et Cosmochimica Acta* 41: 1665–1678.

Hsi, C. K. D., and D. Langmuir. 1985. Adsorption of uranyl onto ferric oxyhydroxides: Application of the surface complexation site-binding model. *Geochimica et Cosmochimica Acta* 49: 1931–1941.

Huang, C-P., and W. Stumm. 1973. Specific adsorption of cations on hydrous γ-Al_2O_3. *Journal of Colloid and Interface Science* 43(2): 409–420.

Hubbe, M. A. 1985a. Detachment of colloidal hydrous oxide spheres from flat solids exposed to flow: 1. Experimental system. *Colloids and Surfaces* 16: 227–248. (YMP accession number NNA.931005.0019.)

Hubbe, M. A. 1985b. Detachment of colloidal hydrous oxide spheres from flat solids exposed to flow: 2. Mechanisms of release. *Colloids and Surfaces* 16: 249–270. (YMP accession number NNA.930820.0005.)

Hunt, J. R. 1982. Particle dynamics in seawater: Implications for predicting the fate of discharged particles. *Environmental Science and Technology* 16: 303–309. (YMP accession number NNA.930920.0004.)

Hunt, J. R. 1993. Personal communication. (YMP accession number NNA.931026.0085.)

Hunter, K. A., D. J. Hawke, and L. K. Choo. 1988. Equilibrium adsorption of thorium by metal oxides in marine electrolytes. *Geochimica et Cosmochimica Acta* 52: 627–636.

Iler, R. K. 1973. Effect of adsorbed alumina on the solubility of amorphous silica in water. *Journal of Colloid and Interface Science* 43: 399–408.

Inoue, Y., and O. Tochiyama. 1985. Studies of the complexes of neptunium(V) with inorganic ligands by solvent extraction with thenoyltrifluoroacetone and 1,10-phenanthroline: I. Carbonato complexes. *Bulletin of the Chemical Society of Japan* 58(2): 588–91.

Itagaki, H., S. Nakayama, S. Tanaka, and M. Yamawaki. 1992. Effect of ionic strength on the solubility of neptunium(V) hydroxide. *Radiochimica Acta* 58/59: 61–66.

Jain, R. 1991. CTCN: A user's manual. M.S. thesis, Chemical and Nuclear Engineering Department, University of New Mexico, Albuquerque, New Mexico. (YMP accession number NNA.93071.0052.)

Janecky, D. R., C. J. Duffy, C. D. Tait, and D. Clark. 1994. Thermochemical data on actinides for modeling. Los Alamos National Laboratory YMP letter report 4025 (Group CST-7).

Janecky, D. R., J. Enter, C. Duffy, C. D. Tait. 1995. Modeled actinide solubilities and speciation. Los Alamos National Laboratory draft report on YMP milestone 3463 (Group CST-7).

Joâo, A., S. Bigot, and F. Fromage. 1987. Etude des carbonates complexes des éléments IVB: 1. Détermination de la constante de stabilité du pentacarbonatothorate(IV). *Bulletin de la Societe Chimique de France* (1987): 42–44.

Johnstone, J. K., and K. Wolfsberg, editors. 1980. Evaluation of tuff as a medium for a nuclear waste repository: Interim status report on the properties of tuff. Sandia National Laboratories report SAND 80-1464.

Johnstone, J. K., R. R. Peters, and P. F. Gnirk. 1984. Unit evaluation of Yucca Mountain, Nevada Test Site: Summary report and recommendations. Sandia National Laboratories report SAND83-0372 (Albuquerque, New Mexico).

Jonasson, R. G., G. M. Bancroft, and H. W. Nesbitt. 1985. Solubilities of some hydrous REE phosphates with implications for diagenesis and seawater concentrations. *Geochimica et Cosmochimica Acta* 49: 2133–2139.

Jurinak, J. J., S. S. Sandhu, and L. M. Dudley. 1987. Ionic diffusion coefficients as predicted by conductometric techniques. *Soil Science Society of American Journal* 51: 625–630.

Katz, J. J., G. T. Seaborg, and L. R. Morss. 1986. *The Chemistry of the Actinide Elements*. London: Chapman and Hall.

Keeney-Kennicutt, W. L., and J. W. Morse. 1985. The redox chemistry of $Pu(V)O_2^+$ interaction with common mineral surfaces in dilute solutions and seawater. *Geochimica et Cosmochimica Acta* 49: 2577–2588.

Kemper, W. D. 1986. Solute diffusivity. In *Methods of Soil Analysis: Part 1. Physical and Mineralogical Methods*, second edition, edited by A. Klute, pp. 1007–1024. Madison, Wisconsin: American Society of Agronomy and Soil Science Society of America.

Kent, D. B., V. S. Tripathi, N. B. Ball, J. O. Leckie, and M. D. Siegel. 1988. Surface-complexation modeling of radionuclide adsorption in subsurface environments. U.S. Nuclear Regulatory Commission report NUREG:CR-4807.

Kerrisk, J. F. 1984a. Solubility limits on radionuclide dissolution at a Yucca Mountain repository. Los Alamos National Laboratory report LA-9995-MS (May).

Kerrisk, J. F. 1984b. Americium thermodynamic data for the EQ3/6 database. Los Alamos National Laboratory report LA-10040-MS (July).

Kerrisk, J. F. 1985. Solubility experiments for the Nevada Nuclear Waste Storage Investigations Project. Los Alamos National Laboratory report LA-10560-MS.

Kerrisk, J. F. 1987. Groundwater chemistry at Yucca Mountain, Nevada, and vicinity. Los Alamos National Laboratory report LA-10929-MS.

Kessler, J. H., and J. R. Hunt. 1993. Open channels in fractures maintained by deposition and erosion of colloids. In *High Level Waste Management: Proceedings of the Fourth Annual International Conference, Las Vegas, Nevada, April 26–30, 1993*. La Grange Park, Illinois: American Nuclear Society. (YMP accession number NNA.930607.0072.)

Kim, J. I. 1986. Chemical behaviour of transuranic elements in natural aquatic systems. In *Handbook on the Chemistry and Physics of the Actinides, Volume 4*, edited by A. J. Freeman, and C. Keller, Chapter 8, pp. 413–455. North Holland.

Kim, J. I. 1991. Actinide colloid generation in groundwater. *Radiochimica Acta* 52/53: 71–81. (YMP accession number NNA.930625.0030.)

Kim, J. I. 1993. The chemical behavior of transuranium elements and barrier functions in natural aquifer systems. *Materials Research Society Symposium Proceedings (Scientific Basis for Nuclear Waste Management XVI)* 294: 3–21.

Kim, J. I., and B. Kanellakopulos. 1989. Solubility products of plutonium(IV) oxide and hydroxide. *Radiochimica Acta* 48: 145–150.

Kim, J. I., and T. Sekine. 1991. Complexation of neptunium(V) with humic acid. *Radiochimica Acta* 55: 187–192.

Kim, J. I., M. Bernkopf, C. Lierse, and F. Koppold. 1984. In *Geochemical Behavior of Disposed Radioactive Waste: ACS Symposium Series 246*. Washington, D.C.: American Chemical Society.

Kim, J. I., G. Buckau, E. Bryant, and R. Klenze. 1989. Complexation of americium(III) with humic

acid. *Radiochimica Acta* 48: 135–143.

Kingston, W. L., and M. Whitbeck. 1991. Characterization of colloids found in various groundwater environments in central and southern Nevada. Water Resources Center publication #45083 (July). (YMP accession number NNA.930607.0073.)

Kinniburgh, D. G., M. L. Jackson, and J. K. Syers. 1976. Adsorption of alkaline-earth, transition, and heavy-metal cations by hydrous oxide gels of iron and aluminum. *Soil Science Society of America Journal* 40: 796–799.

Kinniburgh, D. G., J. A. Barker, and M. J. Whitfield. 1983. A comparison of some simple adsorption isotherms for describing divalent-cation adsorption by ferrihydrite. *Journal of Colloid and Interface Science* 95: 370–384.

Klein, C., and C. S. Hurlbut, Jr. 1985. *Manual of Mineralogy (after James D. Dana)*. New York: John Wiley & Sons.

Knauss, K., and D. Peifer. 1986. Reaction of vitric Topopah Spring tuff and J-13 groundwater under hydrothermal conditions using Dickson-type, gold-bag rocking autoclaves. Lawrence Livermore National Laboratory report UCRL-53795 (November).

Knight, S. D., and F. O. Lawrence. 1988. Sorption of nickel and neptunium in tuff using groundwaters of various compositions. Los Alamos National Laboratory letter report on Nevada Nuclear Waste Storage Investigations milestone R505.

Knight, S. D., and K. W. Thomas. 1987. Sorption of radionuclides using different groundwater compositions. Los Alamos National Laboratory letter report on Nevada Nuclear Waste Storage Investigations milestone M316.

Koeppenkastrop, D., and E. H. De Carlo. 1992. Sorption of rare-earth elements from seawater onto synthetic mineral particles: An experimental approach. *Chemical Geology* 95: 251–263.

Koeppenkastrop, D., and E. H. De Carlo. 1993. Uptake of rare-earth elements from solution by metal oxides. *Environmental Science and Technology* 27: 1796–1802.

Kraus, K. A., and J. R. Dam. 1949. Hydrolytic behavior of plutonium(III): Acid-base titrations of plutonium(III). In *The Transuranium Elements*, edited by G. T. Seaborg, J. J. Katz, and W. M. Manning, pp. 466–477. New York: McGraw-Hill.

Kraus, K. A., and F. Nelson. 1948. The hydrolytic behavior of uranium and the transuranic elements. United States Atomic Energy Comission report no. AECD-1864.

Krevinskaia, Y. Y., V. D. Nikol'skii, B. G. Pozharskii, and Y. Y. Zastenker. 1959. *Soviet Radiochemistry* 1: 238.

Krishnaswami, S., W. C. Graustein, and K. K. Turekian. 1982. Radium, thorium, and radioactive lead isotopes in groundwaters: Application to the in-situ determination of adsorption-desorption rate constants and retardation factors. *Water Resources Research* 18: 1633–1675.

Kung, K. S., and M. B. McBride. 1989a. Adsorption of para-substituted benzoates on iron oxides. *Soil Science Society of America Journal* 53: 1673–1678.

Kung, K. S., and M. B. McBride. 1989b. Coordination-complexes of para-hydroxybenzoate on iron oxides. *Clays and Clay Minerals* 37: 333–340.

Kung, K. S., and M. B. McBride. 1991. Bonding of chlorophenols on iron and aluminum oxides. *Environmental Science and Technology* 25: 702–709.

Kunze, G. W., and J. B. Dixon. 1986. Pretreatment for mineralogical analysis. In *Method of Soil Analysis*, edited by A. Klute. Wisconsin: Soil

Science Society of America.

LaFlamme, B. D., and J. W. Murray. 1987. Solid/solution interaction: The effect of carbonate alkalinity on adsorbed thorium. *Geochimica et Cosmochimica Acta* 51: 243–250.

Langmuir, D., and J. S. Herman. 1980. The mobility of thorium in natural waters at low temperatures. *Geochimica et Cosmochimica Acta* 44: 1753–1766.

Levy, S. S. 1984. Petrology of samples from drill holes USW H-3, H-4, and H-5, Yucca Mountain, Nevada. Los Alamos National Laboratory report LA-9706-MS (June).

Levy, S. S. 1992. Natural gels in the Yucca Mountain area, Nevada, USA. *Applied Clay Science* 7: 79–85. (YMP accession number NNA.830607.0074.)

Levy, S. S., D. T. Vaniman, D. L. Bish, G. WoldeGabriel, S. J. Chipera, J. W. Carey, P. Dixon, S. J. Goldstein, and M. T. Murrell. 1996. Summary and synthesis report on mineralogy and petrology studies for the Yucca Mountain Site Characterization Project: Volume II. History and mineralogic and geochemical alteration of Yucca Mountain. Los Alamos National Laboratory Earth and Environmental Sciences and Chemical Science and Technology divisions report on milestone 3665.

Lierse, C. 1985. Ph.D. dissertation, Technische Universität München. (Referenced in Kim (1986), Table 3, p. 428.)

Lierse, C. 1986. RCM 02286, Institut für Radiochemie, Technische Universität München.

Lierse, C., W. Treiber, and J. I. Kim. 1985. Hydrolysis reactions of neptunium(V). *Radiochimica Acta* 38: 27–28.

Lieser, K. H., and R. Hill. 1992. Chemistry of thorium in the hydrosphere and in the geosphere. *Radiochimica Acta* 56: 141–151.

Lindberg, R. D., and D. D. Runnells. 1984. Groundwater redox reactions: An analysis of equilibrium state applied to Eh measurements and geochemical modeling. *Science* 225: 925–927.

Lindsay, W.L. 1979. *Chemical Equilibria in Soils*. New York: John Wiley & Sons. (YMP accession number NNA.900214.0215.)

Lips, A., and R. M. Duckworth. 1988. Combined study of coagulation kinetics and close-range aggregate structure. *Journal of the Chemical Society, Faraday Transactions I* 84(4): 1223–1242.

Loubet, M., and C. J. Allegre. 1977. Behavior of the rare-earth elements in the Oklo natural reactor. *Geochimica et Cosmochimica Acta* 41: 1539–1548.

Lundqvist, R. 1982. Hydrophilic complexes of the actinides: I. Carbonates of trivalent americium and europium. *Acta Chemica Scandinavica A* 36: 741–750.

Madic, C., D. E. Hobart, and G. M. Begun. 1983. Raman spectrometric studies of actinide(V) and (VI) complexes in aqueous sodium carbonate solution and of solid sodium actinide(V) carbonate compounds. *Inorganic Chemistry* 22(10): 1494–1503.

Maldonado, F., and S. L. Koether. 1983. Stratigraphy, structure, and some petrographic features of tertiary volcanic rocks at the USW G-2 drill hole, Yucca Mountain, Nye County, Nevada. U.S. Geological Survey report USGS-OFR-83-732.

Mariano, A. N. 1989. Economic geology of the rare-earth elements. In *Rare Earth Elements*, pp. 309–337. Washington, D.C.: Mineralogical Society of America Publications.

Maya, L. 1982a. Sorbed uranium(VI) species on hydrous titania, zirconia, and silica gel. *Radiochimica Acta* 31: 147–151.

Maya, L. 1982b. Hydrolysis and carbonate complexation of dioxouranium(VI) in the neutral-pH range at 25ºC. *Inorganic Chemistry* 21: 2895–2898.

Maya, L. 1983. Hydrolysis and carbonate complexation of dioxoneptunium(V) in 1.0 M sodium perchlorate at 25ºC. *Inorganic Chemistry* 22(14): 2093–2095.

Maya, L. 1984. Carbonate complexation of dioxoneptunium(VI) at 25ºC: Its effect on the Np(V)/Np(VI) potential. *Inorganic Chemistry* 23(24): 3926–3930.

McBride, M. B. 1994. *Environmental Chemistry of Soils*, pp. 71–72. New York: Oxford University Press.

McBride, M. B., and B. Wesselink. 1988. Chemisorption of catechol on gibbsite, boehmite, and noncrystalline alumina surfaces. *Environmental Science and Technology* 22: 703–708.

McCarthy, J. F., and J. M. Zachara. 1989. Subsurface transport of contaminants. *Environmental Science and Technology* 22(5): 496–502. (YMP accession number NNA.830625.0032.)

McDowell-Boyer, L. M., J. R. Hunt, and N. Sitar. 1986. Particle transport through porous media. *Water Resources and Research* 22(13): 1901–1921. (YMP accession number NNA.900302.0036.)

McKinley, P. W, and T. A. Oliver. 1994. Meteorological, stream-discharge, and water-quality data for 1986–1991 from two small basins in central Nevada. U.S. Geological Survey report USGS-OFR-93-651.

McKinley, P. W., and T. A. Oliver. 1995. Meteorological, stream-discharge, and water-quality data for 1992 from two small basins in central Nevada. U.S. Geological Survey report USGS-OFR-94-456.

McKinley, P. W., M. P. Long, and L. V. Benson. 1991. Chemical analysis of water from selected wells and springs in the Yucca Mountain area, Nevada and southeastern California. U.S. Geological Survey report USGS-OFR-90-355.

Means, J. L., D. A. Crerar, and M. P. Borcsik. 1978. Adsorption of Co and selected actinides by Mn and Fe oxides in soils and sediments. *Geochimica et Cosmochimica Acta* 42: 1763–1773.

Meece, D. E., and J. K. Benninger. 1993. The coprecipitation of plutonium and other radionuclides with calcium carbonate. *Geochimica et Cosmochimica Acta* 57(7): 1447–1458.

Meier, W. M., and D. H. Olson. 1992. *Atlas of Zeolite Structure Types*. London: Butterworth-Heinemann.

Meijer, A. 1990. Yucca Mountain Project far-field sorption studies and data needs. Los Alamos National Laboratory report LA-11671-MS (September).

Meijer, A. 1992. A strategy for the derivation and use of sorption coefficients in performance assessment calculations for the Yucca Mountain Site. In *Proceedings of the DOE/Yucca Mountain Site Characterization Project Radionuclide Adsorption Workshop at Los Alamos National Laboratory, September 11–12, 1990*, pp. 9–40. Los Alamos National Laboratory report LA-12325-C (August). (YMP accession number NNA.920819.0077).

Meijer, A. 1993. Far-field transport of carbon dioxide: Retardation mechanisms and possible validation experiments. In *Proceedings of the Topical Meeting on Site Characterization and Model Validation, Focus '93, September 26–29, 1993, Las Vegas, Nevada*. La Grange Park, Illinois: American Nuclear Society.

Meijer, A. 1995. Modeling and experimental results on saturated-zone water chemistry. Los Alamos National Laboratory report on milestone LA3387 (September).

Meijer, A. 1996. To be published.

Meijer, A., I. Triay, S. Knight, and M. Cisneros. 1989. Sorption of radionuclides on Yucca Mountain tuffs. In *Proceedings of the Topical Meeting on Nuclear Waste in the Unsaturated Zone, Focus '89: September 17–21, 1989, Las Vegas, Nevada*, pp. 113–117. La Grange Park, Illinois: American Nuclear Society.

Meinrath, G., and J. I. Kim. 1991a. The carbonate complexation of the americium (III) ion. *Radiochimica Acta* 53(pt. 1): 29–34.

Meinrath, G., and J. I. Kim. 1991b. Solubility products of different americium(III) and neodymium(III) carbonates. *European Journal of Solid State and Inorganic Chemistry* 28(suppl.): 383–8.

Miekeley, N., H. Coutinho de Jesus, C. L. Porto da Silveira, and C. Degueldre. 1991. Chemical and physical characterization of suspended particles and colloids in waters from the Osamu Utsumi and Morro de Ferro analog study sites, Pocos de Caldas, Brazil. SKB technical report 90-18, Stockholm, Sweden (January). (YMP accession number NNA.930625.0033.)

Milic, N. B., and T. M. Suranji. 1982. Hydrolysis of the thorium(IV) ion in sodium nitrate medium. *Canadian Journal of Chemistry* 60: 1298–1303.

Miller, D. G. 1972. Estimation of tracer diffusion coefficients of ions in aqueous solution. Lawrence Livermore National Laboratory report UCRL-53319.

Minai, Y., G. R. Choppin, and D. H. Sisson. 1992. Humic material in well water from the Nevada Test Site. *Radiochimica Acta* 56: 195–199 (and references therein). (YMP accession number NNA.930607.0076.)

Montazer, P., and W. E. Wilson. 1984. Conceptual hydrologic model of flow in the unsaturated zone, Yucca Mountain, Nevada. U.S. Geological Survey water-resources report 84-4345.

Moon, H. 1989. Equilibrium ultrafiltration of hydrolyzed thorium(IV) solutions. *Bulletin of the Korean Chemical Society* 10: 270–272.

Moore, R. M., and K. A. Hunter. 1985. Thorium adsorption in the ocean: Reversibility and distribution amongst particle size. *Geochimica et Cosmochimica Acta* 49: 2253–2257.

Moriyama, H., M. I. Pratopo, and K. Higashi. 1989. The solubility and colloidal behaviour of Np(IV) hydrous oxide solubility under reducing and carbonate conditions. *The Science of the Total Environment* 83: 227.

Moskvin, A. I. 1971a. Complex formation of neptunium(IV, V, VI) in carbonate solutions. *Soviet Radiochemistry* 13: 694–699.

Moskvin, A. I. 1971b. Hydrolytic behavior of neptunium(IV, V, VI). *Soviet Radiochemistry* 13: 700.

Moskvin, A. I., and V. P. Zaitseva. 1962. Hydrolytic behavior of plutonyl in aqueous solution. *Soviet Radiochemistry* 4: 63–70 (*Radiokhimiya* 4: 73–81).

Moulin, V., and G. Ouzounian. 1992. Role of colloids and humic substances in the transport of radioelements through the geosphere. *Applied Geochemistry, Supplemental Issue No. 1*: 179–186. (YMP accession number NNA.930607.0077.)

Moulin, V., J. Tits, and G. Ouzounian. 1992. Actinide speciation in the presence of humic. *Radiochimica Acta* 59(pt. 1): 179–90.

Murphy, W. M. 1992. Natural analog studies for geologic disposal of nuclear waste. *Technology Today* (June), pp. 16–21. San Antonio, Texas: Southwest Research Institute.

Murphy, J. B., and A. J. Hynes. 1986. Contrasting

secondary mobility of Ti, P, Zr, Nb, and Y in two metabasaltic suites in the Appalachians. *Canadian Journal of Earth Sciences* 23: 1138–1144.

Musante, Y., and M. Porthault. 1973. Contribution a l'etude des formes hydroxylees de l'ion plutonyle. *Radiochemical and Radioanalytical Letters* 15: 299–306.

Nagasaki, S., S. Tanaka, and Y. Takahashi. 1988. Speciation and solubility of neptunium in underground environments by paper electrophoresis. *Journal of Radioanalytical and Nuclear Chemistry* 124(2): 383–395.

Nair, G. M., K. Chander, and J. K. Joshi. 1982. Hydrolysis constants of plutonium (III) and americium(III). *Radiochimica Acta* 30(1): 37–40.

Nakayama, S., H. Arimoto, Y. Yamada, H. Moriyama, and K. Higashi. 1988. Column experiments on migration behavior of neptunium(V). *Radiochimica Acta* 44/45: 179.

Neal, R. H., G. Sposito, K. M. Holtzclaw, and S. J. Traina. 1987. Selenite adsorption on alluvial soils: I. Soil composition and pH effects. *Soil Science Society of America Journal* 51: 1161–1165.

Neck, V., J. I. Kim, and B. Kanellakopulos. 1992. Solubility and hydrolysis behavior of neptunium(V). *Radiochimica Acta* 56: 25.

Neck, V., W. Runde, J. I. Kim, and B. Kanellakopulos. 1994. Solid-liquid equilibrium reactions of neptunium(V) in carbonate solution at different ionic strength. *Radiochimica Acta* 65: 29–37.

Neretnieks, I. 1990. Solute transport in fractured rock: Applications to radionuclide waste repositories. SKB technical report 90-38, Stockholm, Sweden (December). (YMP accession number NNA.910502.0149.)

Neu, M. P., D. L. Clark, W. Runde, P. D. Palmer, C. D. Tait, and S. A. Ekberg. 1995. Structural studies of actinyl(VI) carbonato complexes using multinuclear NMR, raman, EXAFS, and single-crystal XRD techniques. Abstract for *Inorganic Chemistry Division, International Chemical Congress of Pacific Basin Societies (PACIFICHEM '95), Honolulu, HI, December 17–22, 1995*.

Newton, T. W. 1975. The kinetics of the oxidation-reduction reactions of uranium, neptunium, plutonium, and americium in aqueous solutions. Oak Ridge, TN, report (available as TID-26506: ERDA Critical Review Series, ERDA Technical Information Center).

Newton, T. W., and J. C. Sullivan. 1985. Actinide carbonate complexes in aqueous solution. In *Handbook on the Physics and Chemistry of the Actinides, Volume 3*, edited by A. J. Freeman and C. Keller, Chapter 10, pp. 387–406. North Holland.

Newton, T. W., D. E. Hobart, and P. D. Palmer. 1986. The formation of plutonium(IV)-colloid by the alpha-reduction of Pu(V) or Pu(VI) in aqueous solutions. *Radiochimica Acta* 39: 139–147.

Nguyen-Trung, C., G. M. Begun, and D. A. Palmer. 1992. Aqueous uranium complexes: 2. Raman spectroscopic study of the complex formation of the dioxouranium(VI) ion with a variety of inorganic and organic ligands. *Inorganic Chemistry* 31: 5280–5287.

Nielsen, A. E. 1964. *Kinetics of Precipitation*. Oxford: Pergamon Press.

Nimmo, J. R., and K. C. Akstin. 1988. Hydraulic conductivity of a sandy soil at low water content after compaction by various methods. *Soil Science Society of America Journal* 52: 303.

Nimmo, J. R., and K. A. Mello. 1991. Centrifugal techniques for measuring saturated hydraulic conductivity. *Water Resources Research* 27: 1263.

Nimmo, J. R., J. Rubin, and D. P. Hammermeister.

1987. Unsaturated flow in a centrifugal field: Measurement of hydraulic conductivity and testing of Darcy's Law. *Water Resources Research* 23: 124–134.

Nitao, J. J. 1991. Theory of matrix and fracture flow regimes in unsaturated, fractured porous media. In *High Level Radioactive Waste Management: Proceedings of the Second Annual International Conference, Las Vegas, Nevada, April 28–May 3, 1991*. La Grange Park, Illinois: American Nuclear Society. (YMP accession number NNA.930405.0073.)

Nitao, J. J., and T. A. Buscheck. 1989. On the infiltration of a liquid front in an unsaturated, fractured porous medium. In *Proceedings of the Topical Meeting on Nuclear Waste in the Unsaturated Zone, Focus '89, September 17–21, 1989, Las Vegas, Nevada*, pp. 381–397. La Grange Park, IL: American Nuclear Society.

Nitsche, H. 1987. Effects of temperature on the solubility and speciation of selected actinides in near-neutral solution. *Inorganica Chimica Acta* 127(1): 121–128.

Nitsche, H. 1991a. Basic research for assessment of geologic nuclear waste repositories: What solubility and speciation studies of transuranium elements can tell us. *Materials Research Society Symposium Proceedings* (*Scientific Basis of Nuclear Waste Management XIV*) 212: 517–529.

Nitsche, H. 1991b. Solubility and speciation studies for nuclear repository performance assessment. In *Proceedings of Technical Workshop on Near-field Performance Assessment for High-level Waste Storage*, pp. 67–77, SKB technical report 16-59.

Nitsche, H. 1992. The importance of transuranium solids in solubility studies for nuclear waste repositories. *Materials Research Society Symposium Proceedings* (*Scientific Basis of Nuclear Waste Management XV*) 257: 289–298.

Nitsche, H., and N. M. Edelstein. 1985. Solubilities and speciation of selected transuranium ions: A comparison of a noncomplexing solution with a groundwater from the Nevada Test Site. *Radiochimica Acta* 39(1): 23–33.

Nitsche, H., E. M. Standifer, and R. J. Silva. 1989. Americium(III) carbonate complexation in aqueous perchlorate solution. *Radiochimica Acta* 46(4): 185–189.

Nitsche, H., E. M. Standifer, and R. J. Silva. 1990. Neptunium(V) complexation with carbonate. *Lanthanide and Actinide Research* 3: 203–211.

Nitsche, H., R. C. Gatti, E. M. Standifer, S. C. Lee, A. Muller, T. Prussin, H. Deinhammer, H. Mauer, K. Becraft, S. Leung, and S. A. Carpenter. 1992a. Measured solubilities and speciations of neptunium, plutonium, and americium in a typical groundwater (J-13) from the Yucca Mountain Region: Milestone report 3010. Lawrence Berkeley Laboratory report 30958.

Nitsche, H., A. Muller, E. M. Standifer, R. S. Deinhammer, K. Becraft, T. Prussin, and R. C. Gatti. 1992b. Dependence of actinide solubility and speciation on carbonate concentration and ionic strength in groundwater. *Radiochimica Acta* 58/59(pt. 1): 27–32.

Nitsche, H., R. C. Gatti, E. M. Standifer, S. C. Lee, A. Müller, T. Prussin, R. S. Deinhammer, H. Maurer, K. Becraft, S. Leung, and S. A. Carpenter. 1993a. Measured solubilities and speciations of neptunium, plutonium, and americium in a typical groundwater (J-13) from the Yucca Mountain region: Milestone report 3010-WBS 1.2.3.4.1.3.1. Los Alamos National Laboratory report LA-12562-MS (July).

Nitsche, H., K. Roberts, T. Prussin, D. Keeney, S. A. Carpenter, K. Becraft, and R. C. Gatti. 1993b. Radionuclide solubility and speciation studies for the Yucca Mountain Site Characterization Project. In *High Level Radioactive Waste Management: Proceeding of the Fourth Annual International*

Conference, Las Vegas, Nevada, April 26–30, 1993, Vol. 2, pp. 1490–1495. La Grange Park, IL: American Nuclear Society; New York: American Society of Civil Engineers.

Nitsche, H., K. Roberts, T. Prussin, A. Muller, K. Becraft, D. Keeney, S. A. Carpenter, and R. C. Gatti. 1994. Measured solubilities and speciations from oversaturation experiments of neptunium, plutonium, and americium in UE-25 p#1 well water from the Yucca Mountain Region: Milestone Report 3329 - WBS1.2.3.4.1.3.1. Los Alamos National Laboratory report LA-12563-MS (April).

NRC. 1983. Disposal of high-level radioactive wastes in geologic repositories, technical criteria. *Code of Federal Regulations*, 10 CFR 60. Washington, D.C.: U.S. Nuclear Regulatory Commission.

NRC. 1984. Determination of radionuclide solubility in groundwater for assessment of high-level waste isolation. NRC technical position paper. Washington, D.C.: U.S. Nuclear Regulatory Commission.

NRC. 1987. Determination of radionuclide sorption for high-level nuclear waste repositories. NRC technical position paper. Washington, D.C.: U.S. Nuclear Regulatory Commission.

Nuttall, H. E., R. Jain, and Y. Fertelli. 1991. Radiocolloid transport in saturated and unsaturated fractures. In *High Level Radioactive Waste Management: Proceedings of the Second Annual International Conference, Las Vegas, Nevada, April 28–May 3, 1991*, pp. 189–196. La Grange Park, Illinois: American Nuclear Society. (YMP accession number NNA.930625.0031.)

Obeng, L. A., M. J. T. Carrondo, R. Perry, and J. N. Lester. 1981. The influence of zeolite type A on metal concentrations in water and waste water. *Journal American Oil Chemistry Society* 58: 81–85.

Oelkers, E. H. 1991. Calculation of diffusion coefficients for aqueous organic species. *Geochimica et Cosmochimica Acta* 55: 3515–3529.

Ogard, A. E. 1987. Importance of radionuclide transport by particulates entrained in flowing groundwaters. Appendix B in Los Alamos National Laboratory report LA-10929-MS (Kerrisk, J. F. Groundwater chemistry at Yucca Mountain, Nevada, and vicinity.), pp. 114–118. (YMP accession number NNA.830607.0078.)

Ogard, A. E., and J. F. Kerrisk. 1984. Groundwater chemistry along flow paths between a proposed repository site and the accessible environment. Los Alamos National Laboratory report LA-10188-MS (November).

Ogard, A. E., and D. T. Vaniman, compilers. 1985. Research and development related to the Nevada nuclear waste storage investigations: July 1–September 30, 1984. Los Alamos National Laboratory report LA-10299-PR (May).

Okajima, S., and D. T. Reed. 1993. Initial hydrolysis of plutonium(VI). *Radiochimica Acta* 60: 173–184.

Östhols, E., J. Bruno, and I. Grenthe. 1994. On the influence of carbonate on mineral dissolution: III. The solubility of microcrystalline ThO_2 in CO_2-H_2O media. *Geochimica et Cosmochimica Acta* 58(2): 613–623.

Ostrowsky, N. 1988. Particle characterization by photon correlation spectroscopy. In *Proceedings of the Sixth Particle Size Analysis Conference, April 19–20, 1988*. Guildford, U.K.: University of Surrey.

Overbeek, J. T. G. 1952. Stability of hydrophobic colloids and emulsions. In *Colloid Science: Vol. 1, Irreversible Systems*, edited by H. R. Kruyt. Elsevier Publishing Co.

Oversby, V. M. 1987. Important radionuclides in high-level nuclear waste disposal: Determination using a comparison of the U.S. EPA and NRC reg-

ulations. *Nuclear Chemistry Waste Management* 7: 149–161.

Pabalan, R. T. 1994. Thermodynamics of ion exchange between clinoptilolite and aqueous solutions of Na^+/K^+ and Na^+/Ca^{2+}. *Geochimica et Cosmochimica Acta* 58: 4573–4590.

Paces, T., S. A. Mahan, K. R. Ludwig, L. M. Kwak, L. A. Neymark, K. R. Simmons, L. D. Nealey, B. D. Marshall, and A. Walker. 1995. Progress report on dating Quaternary surficial deposits. U.S. Geological Survey milestone report 3GCH510M.

Palache, C., H. M. Berman, and C. Frandel. 1944. *Dana's System of Mineralogy.* New York: John Wiley & Sons.

Palmer, D. A., and R. Van Eldik. 1983. The chemistry of metal carbonato and carbon dioxide complexes. *Chemical Reviews* 83: 651–731.

Pashalidis, I., J. I. Kim, C. Leirse, and J. C. Sullivan. 1993. The hydrolysis of Pu(VI) and time-dependent polynucleation reactions. *Radiochimica Acta* 61(1): 29–34.

Pashalidis, I., J. I. Kim, T. Ashida, and I. Grenthe. 1995. Spectroscopic study of the hydrolysis of PuO_2^{2+} in aqueous solution. *Radiochimica Acta* 68: 99–104.

Payne, T. E., J. A. Davis, and T. D. Waite. 1991. Modeling of uranium sorption to substrates from the weathered zone in the vicinity of the Koongarra ore body. In *Alligators Rivers Analogue Project, First Annual Report, 1988–89*, pp. 39–46. Menai, Australia: Australian Nuclear Science and Technology Organization.

Payne, T. E., R. Edis, and T. Seo. 1992. Radionuclide transport by groundwater colloids at the Koongarra uranium deposit. *Materials Research Society Symposium Proceedings* 257: 481–488. (YMP accession number NNA.930607.0079.)

Pazukhin, E. M., and S. M. Kochergin. 1989. Stability constants of hydrolysed forms of americium(III) and solubility product of its hydroxide. *Soviet Radiochemistry* 31: 430–436 (Radiokhimiya 31: 72–78).

Pazukhin, E. M., and E. G. Kudryavtsev. 1990. Stability constants of hydrolyzed forms of Pu(IV) and solubility product of its hydroxide. *Soviet Radiochemistry* 32(4): 318–324 (*Radiokhimiya* 32(4): 18–25).

Pei-Lin Tien, M. D. Siegel, C. D. Updegraf, K. K. Wahi, and R. V. Guzowski. 1985. Repository site data report for unsaturated tuff, Yucca Mountain, NV. U.S. Nuclear Regulatory Commission report NUREG/CR-4110 (Washington, D.C.).

Penrose, W. R., W. L. Polzer, E. H. Essington, D. M. Nelson, and K. A. Orlandini. 1990. Mobility of plutonium and americium through a shallow aquifer in a semiarid region. *Environmental Science and Technology* 24: 228–234. (YMP accession number NNA.830607.0058.)

Perrin, D. D. 1982. *Ionisation Constants of Inorganic Acids and Bases in Aqueous Solution.* Oxford: Pergamon Press.

Polzer, W. L., and H. R. Fuentes. 1988. The use of a heterogeneity-based isotherm to interpret the transport of reactive radionuclides in volcanic tuff media. *Radiochimica Acta* 44/45: 361–365.

Polzer, W. L., E. H. Essington, and E. B. Fowler. 1983. Influence of soil chemistry on the mobility of PuEDTA. Los Alamos National Laboratory report LA-UR-83-3367 (May 1985).

Pratopo, M. I., H. Moriyama, and K. Higashi. 1990. Carbonate complexation of neptunium(IV) and analogous complexation of groundwater uranium. *Radiochimica Acta* 51: 27.

Price, E. H., and L. L. Ames. 1978. Characteristics of actinide-bearing sediments underlying liquid

waste disposal facilities at Hanford. In *Transuranium Nuclides in the Environment* (IAEA publication SM-199/87), pp. 191–211. Vienna, Austria: International Atomic Energy Agency.

Prout, W. E. 1959. Adsorption of radioactive waste by Savannah River plant soil. *Soil Science* 86: 13–17.

Radtke, A. S., C. M. Taylor, and D. F. Hewett. 1967. Aurorite, argentian todorokite, and hydrous silver-bearing lead manganese oxide. *Economic Geology* 62: 186–206.

Rai, D., and J. L. Ryan. 1985. Neptunium(IV) hydrous oxide solubility under reducing and carbonate conditions. *Inorganic Chemistry* 24(3): 247–251.

Rai, D., and J. M. Zachara. 1984. Chemical attenuation rates, coefficients, and constants in leachate migration: Volume 1. A critical review. Electric Power Research Institute report EA-3356 (Palo Alto, California).

Rai, D., R. J. Serne, and D. A. Moore. 1980. Solubility of plutonium compounds and their behavior in soils. *Soil Science Society of America Journal* 44: 490–495.

Rai, D., A. R. Felmy, and J. L. Ryan. 1990. Uranium(IV) hydrolysis constants and solubility product of $UO_2 \cdot xH_2O$(am). *Inorganic Chemistry* 29: 260–264.

Ramsay, J. D. F. 1988. The role of colloids in the release of radionuclides from nuclear waste. *Radiochimica Acta* 44/45: 165–170. (YMP accession number NNA.930701.0050.)

Rancon, D. 1973. The behavior in underground environments of uranium and thorium discharged by the nuclear industry. In *Environmental Behavior of Radionuclides Released in the Nuclear Industry* (IAEA report IAEA-SM-172/55, in French), pp. 333–346. Vienna, Austria: International Atomic Energy Agency.

Rees, T. F. 1990. Comparison of photon correlation spectroscopy with photosedimentation analysis for the determination of aqueous colloid size distributions. *Water Resources Research* 26(11): 2777–2781. (YMP accession number NNA.931102.0061.)

Reheis, M. C. 1995. Dust deposition in southern Nevada and California, 1984–1989: Relations to climate, source area, and source lithology. *Journal of Geophysical Research* 100: 8893–8918.

Relyea, J. F. 1982. Theoretical and experimental considerations for the use of the column method for determining retardation factors. *Radioactive Waste Management and the Nuclear Fuel Cycle* *3*(2): 151–166.

Rhoades, J. D., and J. D. Oster. 1986. Solute content. In *Methods of Soil Analysis: Part 1, Physical and Mineralogical Methods*, second edition, edited by A. Klute, pp. 985–1006. Madison, Wisconsin: American Society of Agronomy and Soil Science Society of America.

Rhodes, D. W. 1957. Adsorption of plutonium by soil. *Soil Science* 84: 465–469.

Richmond, W. E., and M. Fleischer. 1943. Cryptomelane, a new name for the commonest of the “psilomelane” minerals. *American Mineralogist* 28: 607–610.

Riglet, C. 1990. Chimie du neptunium et des autres actinies en milieu carbonate. Ph.D. dissertation, Centre d’Etudes Necléaires de Fontenay-aux-Roses.

Rimstidt, J. D., and H. L. Barnes. 1980. The kinetics of silica-water reactions. *Geochimica et Cosmochimica Acta* 44: 1683–1699.

Robinson, R. A., and R. H. Stokes. 1955. *Electrolyte solutions: The Measurement and*

Interpretation of Conductance, Chemical Potential, and Diffusion in Solutions of Simple Electrolytes. London: Butterworths Scientific Publications.

Robinson, R. A., and R. H. Stokes. 1959. *Electrolyte Solutions*, second edition. London: Butterworths Scientific Publications.

Robinson, B. A., A. V. Wolfsberg, G. A. Zyvoloski, and C. W. Gable. 1995. Milestone 3468: An unsaturated zone flow and transport model of Yucca Mountain. Los Alamos National Laboratory draft report for the Yucca Mountain Site Characterization Project (November; Group EES-5).

Robouch, P. 1989. Contribution a la prévision du comportement de l'américium, du plutonium et du neptunium dans la géosphere; données chimiques. Ph.D. thesis (no. CEA-R-5473), Commissariat á l'Energie Atomique, Gif-sur-Yvette, France, 216 pp.

Robouch, P., and P. Vitorge. 1987. Solubility of plutonium oxide carbonate ($PuO_2(CO_3)$). *Inorganica Chimica Acta* 140(1-2): 239–242.

Rogers, P. S. Z., and S. Chipera. 1994. Sorption characteristics of Yucca Mountain tuffs as a function of sample particle size, surface area, and water composition. Los Alamos National Laboratory report LA-12805-MS.

Rösch, F., M. Milanov, T. K. Hung, R. Ludwig, G. V. Buklanov, and V. A. Khalkin. 1987. Electromigration of carrier-free radionuclides: 6. Ion mobilities and hydrolysis of Np(V) in aqueous perchlorate solutions. *Radiochimica Acta* 42: 43–46.

Rose, A. W., H. E. Hawkes, and J. S. Webb. 1979. *Geochemistry in Mineral Exploration*, second edition. New York: Academic Press, Inc.

Rosholt, J. N., Prijana, and D. C. Noble. 1971. Mobility of uranium and thorium in glassy and crystallized silicic volcanic rocks. *Economic Geology* 66: 1061–1069.

Rundberg, R. S. 1987. Assessment report on the kinetics of radionuclide adsorption on Yucca Mountain Tuff. Los Alamos National Laboratory report LA-11026-MS (July). (YMP accession number NNA.930405.0075.)

Rundberg, R. S., A. E. Ogard, and D. T. Vaniman, compilers. 1985. Research and development related to the Nevada nuclear waste storage investigations, April 1–June 30, 1984. Los Alamos National Laboratory report LA-10297-PR (May).

Rundberg, R. S., I. Partom, M. A. Ott, A. J. Mitchell, and K. Birdsell. 1987. Diffusion of nonsorbing tracers in Yucca Mountain tuff. YMP report on milestone R524 (November). (YMP accession number NNA.930405.0074.)

Rundberg, R. S., A. J. Mitchell, I. R. Triay, and N. B. Torstenfelt. 1988. Size and density of a ^{242}Pu colloid. *Materials Research Society Symposium Proceedings (Scientific Basis for Nuclear Waste Management XI)* 112: 243–248.

Rundberg, R. S., A. J. Mitchell, M. A. Ott, J. L. Thompson, and I. R. Triay. 1989. Laboratory studies of radionuclide migration in tuff. In *Proceedings of Nuclear Waste Isolation in the Unsaturated Zone, FOCUS '89, September 17–21, 1989, Las Vegas, Nevada*, pp. 248–255. (YMP accession number NNA.891207.0090.)

Runde, W., and J. I. Kim. 1994. Untersuchung der Übertragbarkeit von Labordaten auf natürliche Verhältnisse: Chemisches Verhalten von drei- und fünfwertigem Americium in salinen NaCl-Lösungen. Institut für Radiochemie report RCM-01094 (TU München).

Ryan, J. J., Jr. 1988. Groundwater colloids in two Atlantic Coastal Plain aquifers: Colloid formation and stability. Master's thesis, Massachusetts Institute of Technology. (YMP accession number NNA.9301014.0027.)

Ryan, J. J., Jr., and P. M. Geschwend. 1990.

Colloid mobilization in two Atlantic Coastal Plain aquifers. *Water Resources Research* 26(2): 307–322. (YMP accession number NNA.930920.0006.)

Ryan, J. L., and D. Rai. 1987. Thorium(IV) hydrous oxide solubility. *Inorganic Chemistry* 26: 4140–4142.

Sakanoue, M. 1987. Transuranium nuclides in the environment. *Radiochimica Acta* 42: 103–112.

Sanchez, A. L., J. W. Murray, and T. H. Sibley. 1985. The adsorption of plutonium IV and V on goethite. *Geochimica et Cosmochimica Acta* 49: 2297–2307.

Scalon, B. R. 1991. Evaluation of moisture flux from chloride data in desert soils. *Journal of Hydrology* 128: 137–156.

Schindler, P. W. 1985. Grenzflächenchemie oxidischer mineralien. *Österreichische Chemie Zeitschrift* 86: 141–146.

Schmidt, K. H., S. Gordon, R. C. Thompson, and J. C. Sullivan. 1980. A pulse radiolysis study of the reduction of neptunium(V) by the hydrated electron. *Journal of Inorganic and Nuclear Chemistry* 42: 611.

Schmidt, K. H., S. Gordon, M. Thompson, J. C. Sullivan, and W. A. Mulac. 1983. The hydrolysis of neptunium(VI) and plutonium(VI) studied by the pulse radiolysis transient conductivity technique. *Radiation Physics and Chemistry* 21(3): 321–328.

Scott, R. B., and M. Castellanos. 1984. Stratigraphic and structural relations of volcanic rocks in drill holes USW GU-3 and USW G-3, Yucca Mountain, Nye County, Nevada. U.S. Geological Survey report USGS-OFR-84-491.

Scott, J. H., R. D. Carroll, and D. R. Cunningham. 1967. Dielectric constant and electrical conductivity measurements of moist rock: A new laboratory method. *Journal of Geophysical Research* 72: 5101–5115.

Scott, R. B., R. W. Spengler, S. Diehl, A. R. Lappin, and M. P. Chornack. 1983. Geologic character of tuffs in the unsaturated zone at Yucca Mountain, southern Nevada. In *Role of the Unsaturated Zone in Radioactive Hazardous Waste Disposal*, edited by J. W. Mercer, P. S. L. Rao, and I. W. Irvine, pp. 289–335. Ann Arbor, Michigan: Ann Arbor Scientific Publications.

Seaborg, G. T., and W. D. Loveland. 1990. *The Elements Beyond Uranium*. New York: Wiley Interscience.

Serne, R. J., and J. F. Relyea. 1983. The status of radionuclide sorption: Desorption studies performed by the WRIT program. In *The Technology of High-level Nuclear Waste Disposal, Volume 1*, Department of Energy report DOE/TIC-261 (Technical Information Center, DOE, Washington D.C.).

Sevost'yanova, E. P., and G. V. Khalturin. 1976. Hydrolytic behavior of neptunium(V). *Soviet Radiochemistry* 18: 738–743 (*Radiokhimiya* 6: 870–876).

Shannon, R. D. 1976. Revised effective ionic radii and systematic studies of interatomic distances in halides and chalcogenides. *Acta Crystallographica A* 32: 751–767.

Sholkovitz, E. R. 1983. The geochemistry of plutonium in fresh and marine water environments. *Earth-Science Reviews* 19: 95–161.

Siegel, M. D., P. L. Hopkins, R. J. Glass, and D. B. Ward. 1992. Design of an intermediate-scale experiment to validate unsaturated-zone transport models. In *High Level Radioactive Waste Management: Proceedings of the Third International Conference, Las Vegas, Nevada, April 12–16, 1992*. La Grange Park, Illinois: American Nuclear Society.

Siegel, M. D., D. B. Ward, W. C. Chang, C. Bryant,

C. S. Chocas, and C. G. Reynolds. 1993. Preliminary characterization of materials for reactive transport model validation experiment. In *High Level Radioactive Waste Management: Proceeding of the Fourth Annual International Conference, Las Vegas, Nevada, April 26–30, 1993, Vol. 1*, pp 348–358. La Grange Park, IL: American Nuclear Society; New York: American Society of Civil Engineers.

Sillen, L. G., and A. E. Martell. 1964. *Stability Constants of Metal-ion Complexes*. Special publication No. 17. London: The Chemical Society.

Sillen, L. G., and A. E. Martell. 1971. *Stability Constants of Metal-ion Complexes*. Special publication No. 25, supplement No. 1. London: The Chemical Society.

Silva, R. J. 1982. Thermodynamic properties of chemical species in nuclear waste: Topical report: The solubilities of crystalline neodynium and americium trihydroxides. Lawrence Berkeley Laboratory report LBL-15055, 57 pp.

Silva, R. J. 1985. Carbonate complexation of Pu(IV) in aqueous solution. Abstract for *Division of Nuclear Chemistry and Technology, 189th American Chemical Society Meeting, Miami Beach, FL*.

Silva, R. J., G. Bidoglio, M. H. Rand, P. B. Robouch, H. Wanner, and I. Puigdomenech. 1995. *Chemical Thermodynamics of Americium*. Elsevier Science Publishers.

Sinnock, S., Y. T. Lin, and J. P. Brannen. 1984. Preliminary bounds on the expected postclosure performance of the Yucca Mountain repository site, southern Nevada. Sandia National Laboratories report 84-1492.

Smith, P. A. 1992. The influence of nonlinear sorption on colloid-facilitated radionuclide transport through fractured media. In *Proceedings of the 1992 Material Research Society Fall Meeting, November 30–December 4, 1992, Boston, Massachusetts*. (YMP accession number NNA.930607.0059.)

Smith, P. A., and C. Degueldre. 1993. Colloid-facilitated transport of radionuclides through fractured media. *Journal of Contaminant Hydrology* 13: 143–166. (YMP accession number NNA.930607.0064.)

Snelling, A. A. 1980. Uraninite and its alteration products: Koongarra uranium deposit. In *Uranium in the Pine Creek Geosyncline*, edited by J. Ferguson and A. B. Goleby, pp. 487–498. Vienna, Austria: International Atomic Energy Agency.

Snelling, A. A., and B. L. Dickson. 1979. Uranium-daughter disequilibrium in the Koongarra uranium deposit, Australia. *Mineralium Deposita* 14: 109–118.

Snodgrass, W. J. 1980. Distribution and behavior of nickel in the aquatic environment. In *Nickel in the Environment*, edited by J. O. Nriagu, pp. 203–274. New York: John Wiley & Sons.

Spaulding, W. G. 1985. Vegetation and climates of the last 45,000 years in the vicinity of the Nevada Test Site, south central Nevada. U.S. Geological Survey professional paper 1329.

Spengler, R. W., and M. P. Chornack. 1984. Stratigraphic and structural characteristics of volcanic rocks in core hole USW G-4, Yucca Mountain, Nye County, Nevada. U.S. Geological Survey report USGS-OFR-84-789.

Spengler, R. W., D. C. Muller, and R. B. Livermore. 1979. Preliminary report on the geology and geophysics of drill hole UE25a-1, Yucca Mountain, Nevada. U.S. Geological Survey report USGS-OFR-79-1244.

Spengler, R. W., F. M. Byers, Jr., and J. B. Warner. 1981. Stratigraphy and structure of volcanic rocks in drill hole USW G1, Yucca Mountain, Nye

County, Nevada. U.S. Geological Survey report USGS-OFR-81-1349.

Spitsyn, V. I., V. D. Balukova, A. F. Naumova, V. V. Gromov, F. M. Spiridonov, E. M. Vetrov, and G. I. Grafov. 1958. A study of the migration of radioelements in soils. In *Proceedings of the Second United Nations Conference on the Peaceful Uses of Atomic Energy: Waste Treatment and Environmental Aspects of Atomic Energy, Volume 18, pp.* 439–448. Geneva: United Nations.

Sposito, G. 1979. Derivation of the Langmuir equation for ion exchange reactions in soils. *Soil Science Society of America Journal* 43: 197–198.

Sposito, G. 1980. Derivation of the Freundlich equation for ion exchange reactions in soils. *Soil Science Society of America Journal* 44: 652–654.

Sposito, G. 1984. *The Surface Chemistry of Soils*, Chapter 4. New York: Oxford University Press.

Sposito, G. 1989. *The Chemistry of Soils*, p. 277. New York: Oxford University Press.

Stadler, S., and J. I. Kim. 1988. Hydrolysis Reactions of Am(III) and Am(V). *Radiochimica Acta* 44/45: 39–44.

Stammose, D., and J. M. Dolo. 1990. Sorption of americium at trace levels on a clay mineral. *Radiochimica Acta* 51: 189–193.

Stephens, D. B., and K. R. Rehfeldt. 1985. Evaluation of closed-form analytical models to calculate conductivity in a fine sand. *Soil Science Society of America Journal* 49: 12–19.

Stezenbach K. 1992. Fingerprinting of groundwater by ICP-MS. Harry Reid Center for Environmental Studies progress report, October 1, 1992–December 31, 1992, DOE Cooperative Agreement No. DE-FC 08-90NV10872 (Las Vegas, Nevada).

Stumm, W. 1992. *Chemistry of the Solid-Water Interface*, p. 65. New York: John Wiley & Sons.

Stumm, W., and J. J. Morgan. 1981. *Aquatic Chemistry*, second edition. New York: John Wiley & Sons.

Sullivan, J. C., and J. C. Hindman. 1959. The hydrolysis of neptunium(IV). *Journal of Physical Chemistry* 63: 1332–1333.

Sullivan, J. C., M. Woods, P. A. Bertrand, and G. R. Choppin. 1982. Thermodynamics of plutonium(VI) interaction with bicarbonate. *Radiochimica Acta* 31: 45–50.

Sullivan, J. C., G. R. Choppin, and L. F. Rao. 1991. Calorimetric studies of NpO_2^+ hydrolysis. *Radiochemica Acta* 54: 17–20.

Tait, D. C. 1996. Specific-ion interaction theory studies. Los Alamos YMP report on milestone 3792M (August).

Tait, C. D., S. A. Ekberg, P. D. Palmer, and D. E. Morris. 1995a. Plutonium carbonate speciation changes as measured in dilute solutions with photoacoustic spectroscopy. Los Alamos National Laboratory report LA-12886-MS (YMP milestone 3350 and YMP data tracking numbers LA 000 000 000 076.001 and LA 000 000 000 076.002).

Tait, C. D., P. D. Palmer, S. A. Ekberg, and D. L. Clark. 1995b. Report on neptunium speciation by NMR and optical spectroscopies. Los Alamos National Laboratory report LA-13012-MS (YMP milestone 3413 and YMP data tracking numbers MOL.19951005.0058 and LA 000 000 000 105.001).

Tait, C. D., S. A. Ekberg, D. L. Clark, and P. D. Palmer. 1996. Temperature-dependent Pu(VI)-hydrolysis complexation. Los Alamos National Laboratory YMP letter report 4091.

Data in this report are contained in the following YMP notebooks:

LA-CST-NBK-94-003, pp. 155–159;

LA-CST-NBK-95-008, pp. 4–78;
LA-CST-NBK-95-021, pp. 76–139.

Taylor, E. M. 1986. Impact of time and climate on Quaternary soils in the Yucca Mountain area of the Nevada Test Site. M.Sc. thesis, University of Colorado, Boulder, Colorado.

Taylor, S. R., and S. M. McLennan. 1988. The significance of the rare earths in geochemistry and cosmochemistry. In *Handbook on the Physics and Chemistry of Rare Earths, 11*, edited by K. A. Gschneider and L. Eyring, pp. 2485–2580. Amsterdam: Elsevier Scientific Publications, North Holland Physics Publication Division.

Theis, T. L., and R. O. Richter. 1980. Adsorption reactions of nickel species at oxide surfaces. In *Advances in Chemistry Series 189*, pp. 73–96. Washington, D.C.: American Chemical Society.

Thiyagarajan, P., H. Diamond, L. Soderholm, E. P. Horwitz, L. M. Toth, and L. K. Felker. 1990. Plutonium(IV) polymers in aqueous and organic media. *Inorganic Chemistry* 29(10): 1902–7.

Thomas, K. W. 1987. Summary of sorption measurements performed with Yucca Mountain, Nevada, tuff samples and water from the Well J-13. Los Alamos National Laboratory report LA-10960-MS (December).

Thomas, K. W., compiler. 1988. Research and development related to the Nevada nuclear waste storage investigations, October 1–December 31, 1984. Los Alamos National Laboratory report LA-11443-PR (November).

Thompson, L. C. 1979. Complexes. In *Handbook on the Physics and Chemistry of Rare Earths, 4*, edited by K. A. Gschneider and L. Eyring, pp. 209–295. Amsterdam: Elsevier Scientific Publications, North Holland Physics Publication Division.

Thompson, J. L. 1989. Actinide behavior on crushed-rock columns. *Journal of Radioanalytical and Nuclear Chemistry* 130(2): 353–364. (YMP accession number NNA.920131.0401.)

Thorstenson, D. C., E. P. Weeks, H. H. Haas, and J. C. Woodward. 1989. Physical and chemical characteristics of topographically affected airflow in an open borehole at Yucca Mountain. In *Proceedings of the Topical Meeting on the Unsaturated Zone, Focus '89, September 17–21, 1989, Las Vegas, Nevada*., pp. 256–270. La Grange Park, Illinois: American Nuclear Society.

Torstenfelt, B., R. S. Rundberg, and A. J. Mitchell. 1988. Actinide sorption on granites and minerals as a function of pH and colloids/pseudocolloids. *Radiochimica Acta* 44/45: 111–117.

Travis, B. J. 1996. Personal communication.

Travis, B. J., and K. H. Birdsell. 1991. TRACR3D: A model of flow and transport in porous media. Los Alamos National Laboratory report LA-11798-M (April). (YMP accession number NNA.910515.0163.)

Triay, I. R., and R. S. Rundberg. 1987. Determination of selectivity coefficient distributions by deconvolution of ion-exchange isotherms. *Journal of Physical Chemistry* 91(20): 5269–5274.

Triay, I. R., and R. S. Rundberg. 1989a. Application of deconvolution to the analysis of univalent ion-exchange isotherms in zeolites X and Y. *Zeolites* 9: 217–223.

Triay, I. R., and R. S. Rundberg. 1989b. Deconvolution of multivalent cation-exchange isotherms. *Journal of Physical Chemistry* 93: 5617–5623.

Triay, I. R., D. E. Hobart, A. J. Mitchell, T. W. Newton, M. A. Ott, P. D. Palmer, R. S. Rundberg, and J. L. Thompson. 1991a. Size determinations of plutonium colloids using autocorrelation photon spectroscopy. *Radiochimica Acta* 52/53: 127–131. (YMP accession number NNA.930607.0060.)

Triay, I. R., A. Meijer, M. R. Cisneros, G. G. Miller, A. J. Mitchell, M. A. Ott, D. E. Hobart, P. D. Palmer, R. E. Perrin, and R. D. Aguilar. 1991b. Sorption of americium in tuff and pure minerals using synthetic and natural groundwaters. *Radiochimica Acta* 52/53: 141–145.

Triay, I. R., A. J. Mitchell, and M. A. Ott. 1991c. Radionuclide migration as a function of mineralogy. In *High-Level Radioactive Waste Management: Proceedings of the Second Annual International Conference, Las Vegas, Nevada, April 28–May 3, 1991*, pp. 494–498. LaGrange Park, IL: American Nuclear Society.

Triay, I. R., K. H. Birdsell, A. J. Mitchell, and M. A. Ott. 1993a. Diffusion of sorbing and nonsorbing radionuclides in tuff. In *High Level Radioactive Waste Management: Proceeding of the Fourth Annual International Conference, Las Vegas, Nevada, April 26–30, 1993*, vol. 2, pp. 1527–1532. La Grange Park, IL: American Nuclear Society.

Triay, I. R., B. A. Robinson, R. M. Lopez, A. J. Mitchell, and C. M. Overly. 1993b. Neptunium retardation with tuffs and groundwaters from Yucca Mountain. In *High-Level Radioactive Waste Management: Proceedings of the Fourth Annual International Conference, Las Vegas, Nevada, April 26–30, 1993*, pp. 1504–1508. LaGrange Park, IL: American Nuclear Society.

Triay, I. R., C. R. Cotter, and P. Harrigan. 1995a. Interim report: sorption isotherms: Milestone 3339. To be published as a Los Alamos National Laboratory report.

Triay I. R., A. Simmons, S. Levy, S. Nelson, H. Nuttall, B. Robinson, W. Steinkampf, and B. Viani. 1995b. Colloid-facilitated radionuclide transport at Yucca Mountain. Los Alamos National Laboratory report LA-12779-MS (April).

Triay, I. R., C. R. Cotter, M. H. Huddleston, D. E. Leonard, S. C. Weaver, S. J. Chipera, D. L. Bish, A. Meijer, and J. A. Canepa. 1996a. Batch sorption results for neptunium transport through Yucca Mountain tuffs: Yucca Mountain Site Characterization Program milestone 3349. Los Alamos National Laboratory report LA-12961-MS (September).

Triay, I. R., C. R. Cotter, S. M. Kraus, M. H. Huddleston, S. J. Chipera, and D. L. Bish. 1996b. Radionuclide sorption in Yucca Mountain tuffs with J-13 well water: neptunium, uranium, and plutonium: Yucca Mountain Site Characterization Program Milestone 3338. Los Alamos National Laboratory report LA-12956-MS (August).

Triay, I. R., A. Furlano, and B. Strietelmeier. 1996c. Comparison of neptunium sorption results using batch and column techniques: Yucca Mountain Site Characterization Program Milestone 3041. Los Alamos National Laboratory report LA-12958-MS (August).

Tsuji, M., and S. Komarneni. 1993. Selectivity study of alkaline-earth and divalent transition metal ions on $[Al^{3+}+Na^{+}]$-substitued tobermorites. *Separation Science and Technology* 28: 2061–2071.

Tsunashima, A., G. W. Brindley, and M. Bastovanov. 1981. Adsorption of uranium from solutions by montmorillonite: Compositions and properties of uranyl montmorillonites. *Clays and Clay Minerals* 29: 10–16.

Ullman, W. J., and F. Schreiner. 1988. Calorimetric determination of the enthalpies of the carbonate complexes of uranium(VI), neptunium(VI), and plutonium(VI) in aqueous solution at 25ºC. *Radiochimica Acta* 43(1): 37–44.

van den Hul, H. J., and J. J. Lyklema. 1968. Determination of specific surface areas of dispersed materials: Comparison of the negative adsorption method with some other methods. *Journal of the American Chemical Society* 90(12): 3010–3015.

Vaniman, D. T., and S. J. Chipera. 1996. Geochemical stratigraphy of secondary calcites in the tuffs of Yucca Mountain, Nevada. *Geochimica et Cosmochimica Acta* (in press).

Vaniman, D. T., S. J. Chipera, and D. L. Bish. 1995. Petrography, mineralogy, and chemistry of calcite-silica deposits at Exile Hill, Nevada, compared with local spring deposits. Los Alamos National Laboratory report LA-13096-MS (December).

van Olphen, H. 1977. *An Introduction to Clay Colloid Chemistry*, second edition. New York: John Wiley & Sons.

Viani, B. E., and C. J. Bruton. 1992. Modeling ion exchange in clinoptilolite using the EQ3/6 geochemical modeling code. In *Proceedings of the 7th International Symposium on Water-Rock Interaction-WRI-7/Park City/Utah/USA/13–18 July 1992*, pp. 73–77. Rotterdam: Balkema.

Vilks, P., and C. Degueldre. 1991. Sorption behavior of ^{85}Sr, ^{131}I, and ^{137}Cs on colloids and suspended particles from the Grimsel Test Site, Switzerland. *Applied Geochemistry* 6: 553–563. (YMP accession number NNA.930607.0063.)

Vilks, P., J. J. Cramer, T. A. Shewchuk, and J. P. A. Larocque. 1988. Colloid and particulate-matter studies in the Cigar Lake natural-analog program. *Radiochimica Acta* 44/45: 305–310. (YMP accession number NNA.930607.0061.)

Vilks, P., H. G. Miller, and D. C. Doern. 1991. Natural colloids and suspended particles in the Whiteshell Research Area and their potential effect on radiocolloid formation. *Applied Geochemistry* 6: 565–574. (YMP accession number NNA.930607.0062.)

Virden, J. W., and J. C. Berg. 1992. The use of photon correlation spectroscopy for estimating the rate constant for doublet formation in an aggregating colloidal suspension. *Journal of Colloid and Interface Science* 141(2): 528–535.

Vitorge, P. 1995. Neptunium in reducing concentrated solutions: Bibliography for OECD-NEA-TDB. Commissariat á l'Energie Atomique, France, report no. CEA-BIB-246.

Waddell, R. K., J. H. Robison, and R. K. Blankennagel. 1984. Hydrology of Yucca Mountain and vicinity, Nevada-California: Investigative results through mid-1983. U.S. Geological Survey water-resources investigations report 84-4267.

Wagner, G. H., and K. F. Steele. 1989. Na^+/Cl^- ratios in rain across the USA, 1982–1986. *Tellus* 41B: 444–451.

Wanner, H., and I. Forest. 1992. *Vol. 1: Chemical Thermodynamics of Uranium*. The Netherlands: North-Holland Elsevier Science Publishers.

Waters, R. L. 1983. Aquatic chemistry of plutonium. In *Plutonium Chemistry, ACS Symposium Series No. 216*, edited by W. T. Carnall and G. R. Choppin. Washington, D.C.: American Chemical Society.

Watson, A. 1992. Desert soils. In *Weathering, Soils, and Paleosols*, edited by I. P. Martini and W. Chesworth, pp. 225–260. New York: Elsevier Publishers.

White, A. F., H. C. Claasen, and L. V. Benson. 1980. The effect of dissolution of volcanic glass on the water chemistry in a tuffaceous aquifer, Rainier Mesa, Nevada. U.S. Geological Survey water-supply paper 1535-Q.

White, A. F., S. M. Benson, A. W. Yee, H. A. Wollenberg, Jr., and S. Flexser. 1991. Groundwater contamination at the Kesterson Reservoir, California 2: Geochemical parameters influencing selenium mobility. *Water Resources Research* 27: 1085–1098.

Wieland, E. 1988. Die Verwitterung schwerlöslicher Mineralien - ein koordinationschemischer Ansatz zur Beschreibung der Auflösungskinetik.

Ph.D. thesis, ETH Zurich, Switzerland.

Wilson, C. N. 1990a. Results from NNWSI Series 2 bare fuel dissolution tests. Pacific Northwest Laboratory report PNL-7169 (Richland, Washington).

Wilson, C. N. 1990b. Results from NNWSI Series 3 bare fuel dissolution tests. Pacific Northwest Laboratory report PNL-7170 (Richland, Washington).

Wilson, M., J. H. Gauthier, R. W. Barnard, G. E. Barr, and H. A. Dockery. 1994. Total-system performance assessment for Yucca Mountain. Sandia National Laboratories report SAND93-2675, second iteration (TSPA-1993).

Winograd, I. J., and W. Thordarson. 1975. Hydrologic and hydrochemical framework, south-central Great Basin, Nevada-California, with special reference to the Nevada Test Site. U.S. Geological Survey professional paper 712-C.

Wolery, T. J. 1983. EQ3NR, a computer program for geochemical aqueous speciation-solubility calculations: User's guide and documentation. Lawrence Livermore National Laboratory report UCRL-53414 (April).

Wolfsberg, K., and D. T. Vaniman, compilers. 1984. Research and development related to the Nevada nuclear waste storage investigations, October 1–December 31, 1983. Los Alamos National Laboratory report LA-10032-PR (August).

Wolfsberg, K., B. P. Bayhurst, B. M. Crowe, W. R. Daniels, B. R. Erdal, F. O. Lawrence, A. E. Norris, and J. R. Smyth. 1979. Sorption-desorption studies on tuff: I. Initial studies with samples from the J-13 drill site, Jackass Flats, Nevada. Los Alamos National Laboratory report LA-7480-MS (April).

Wood, S. A. 1990. The aqueous geochemistry of the rare-earth elements and yttrium: 1. Review of available low-temperature data for inorganic complexes and the inorganic REE speciation of natural waters. *Chemical Geology* 82: 159–186.

Wright, J. 1990. Diffusion coefficients and hydraulic conductivity in unsaturated Hanford soils and sediments. In *High-Level Radioactive Waste Management: Proceedings of the First Annual International Topical Meeting, April 8–12, 1990,* vol. 1, pp. 835–842. La Grange Park, IL: American Nuclear Society.

Yamaguchi, T., Y. Sakamoto, and T. Ohnuki. 1994. Effect of complexation on solubility of Pu(IV) in aqueous carbonate system. In *Chemistry and Migration Behavior of Actinides and Fission Products in the Geosphere: Proceedings of the Fourth International Conference, Charleston, SC, USA, December 12–17, 1993,* abstract no. A1-2.

Yang, I. C., A. K. Turner, T. M. Sayre, and P. Montazer. 1988. Triaxial-compression extraction of pore water from unsaturated tuff, Yucca Mountain, Nevada. U.S. Geological Survey water resources investigation report 88-4189. (YMP accession number NNA.890309.0161.)

Yang, I. C., G. S. Davis, and T. M. Sayre. 1990. Comparison of pore-water extraction by triaxial compression methods and high-speed centrifugation methods. In *Proceedings of Conference on Minimizing Risk to the Environment, 1990,* pp. 250–259. American Institute of Hydrology.

Yang, I. C., G. W. Rattray, and P. Yu. 1996. Chemical and isotopic data and interpretations, unsaturated-zone boreholes, Yucca Mountain, Nevada. Draft of U.S. Geological Survey water resources investigation report: Interagency Agreement # DE-AI08-92NV10874.

Zenhausern, F., M. Adrian, R. Emch, M. Taborelli, J. Jobin, and D. Descouts. 1992. Scanning-force microscopy and cryo-electron microscopy of tobacco mosaic virus as a test specimen. In *Ultramicroscopy 1992, Proceedings of the Sixth*

International Conference on Scanning Tunneling Microscopy and Related Techniques. (YMP accession number NNA.931124.0007.)

Zielinski, R. A. 1980. Uranium in secondary silica: A possible exploration guide. *Economic Geology* 75: 592–602.

Zielinski, R. A., R. W. Bush, R. W. Spengler, and B. J. Szabo. 1986. Rock-water interaction in ash-flow tuffs, Yucca Mountain, Nevada: The record from uranium studies. *Uranium* 2: 361–386.

APPENDIX: DESCRIPTIONS OF MINERALS COATING THE FRACTURES OF YUCCA MOUNTAIN TUFFS

Zeolites

Zeolites describe a group of minerals characterized by an open framework of aluminosilicate tetrahedra. They are known as good sorbers because of the exchangeable cations within the channels of the framework structures. The common exchangeable cations in zeolites are sodium, calcium, and potassium (Deer et al. 1966).

Most zeolites are generally white but may be brown, red, pink, yellow, green, and blue. Their specific gravity is low (2.0–2.5) as a result of their open framework, and their hardness is moderate (3–5). Zeolites occur in regimes of low temperature and pressure. They are commonly found as secondary minerals resulting from alteration of volcanic rocks and as authigenic minerals within sedimentary units (Klein and Hurlbut 1985).

- **Analcime** is commonly white with some gray, green, red, and in rare cases, blue samples. It is an isometric mineral, usually found as trapezohedral crystals. Crystals tend to be anonymously biaxial with birefringent lamellar twinning. The hardness is 5.5 with a specific gravity of 2.7. The crystalline framework is comprised of combinations of 4- and 6-member rings of aluminosilicate tetrahedra. The channels have a minimum diameter of 2.2 Å (Deer et al. 1966). Analcime has a higher metamorphic-rock gradient than the other zeolites and is associated with the feldspathoids. In some references, it is not classified as a zeolite.

- **Chabazite** is commonly white with some yellow, pink, and red samples. It is a hexagonal mineral usually found as rhombohedrons with nearly cubic angles. The hardness ranges from 4 to 5, and the specific gravity from 2.05 to 2.15. The framework structure contains 4-, 6-, and 8-member rings of aluminosilicate tetrahedra. The channels have a minimum diameter of 3.8 Å (Meier and Olson 1992).

- **Erionite** is part of the chabazite group. It is a hexagonal, commonly acicular, fibrous mineral. It is one of the more siliceous zeolites. The crystalline framework is comprised of combinations of 4-, 6-, and 8-member rings of aluminosilicate tetrahedra. The channels have a minimum diameter of 3.6 Å (Meier and Olson 1992).

- **Heulandite** is commonly white with some samples being yellow and red. It is a monoclinic mineral, but crystals often display orthorhombic symmetry. Crystals are typically tabular. The hardness ranges from 3.5 to 4, and the specific gravity from 2.18 to 2.2. The framework is comprised of combinations of 5-, 6-, and 8-member rings of aluminosilicate tetrahedra. The channels have a minimum diameter of 3.3 Å (Meier and Olson 1992). Heulandite has low bond strength in one direction and therefore loses structural integrity with dehydration (Breck 1974).

- **Clinoptilolite** is part of the heulandite group. It is monoclinic with typically tabular to platy crystals. In contrast to heulandite, clinoptilolite is stable under dehydration. The crystalline framework is similar to heulandite (Breck 1974).

- **Stellerite** is the calcium end member of the stilbite solid solution, which is part of the heulandite group. It is usually transparent to white and rarely yellow, brown, or red. The crystal system is monoclinic, typically in platy, sheetlike aggregates, which may also form cruciform penetration twins. The hardness ranges from 3.5 to 4, and the specific gravity is 2.2. The framework is comprised of combinations of 4-, 8-, and 10-member rings

of aluminosilicate tetrahedra. The channels have a minimum diameter of 2.7 Å (Meier and Olson 1992).

- **Mordenite** is usually transparent to white with a distinctive waxy luster. It is an orthorhombic mineral, typically in laths or fibrous crystals. It is a high-silica zeolite. The framework is comprised of combinations of 5-, 8-, and 12-member rings of aluminosilicate tetrahedra. The channels have a minimum diameter of 2.6 Å (Meier and Olson 1992).

- **Phillipsite** is an orthorhombic mineral commonly displaying cruciform penetration twins. Its hardness ranges from 4 to 4.5. The framework is comprised of combinations of 4- and 8-member rings of aluminosilicate tetrahedra. The channels have a minimum diameter of 3.0 Å (Meier and Olson 1992).

Silica

The silica minerals are part of a mineral group referred to as tectosilicates, of which zeolites are also a member. Tectosilicates define a mineral classification in which all four oxygen atoms of a silica tetrahedron (SiO_4) are shared with other neighboring silica tetrahedra. These minerals are generally very strong, stable structures with a silicon-to-oxygen ratio of 1 to 2 (Klein and Hurlbut 1985).

- **Quartz** is one of the most abundant of all minerals. It is generally transparent to white, but it comes in a host of different colors, varieties, and names. Quartz is hexagonal with enantiomorphous crystals in the trigonal trapezohedral class of the rhombohedral subsystem. Striations occur perpendicular to the long axis. The hardness is 7, and the specific gravity is 2.65. Of the nine known polymorphs of SiO_2, α-quartz, or low quartz, is the polymorph that is stable below 574ºC and one atmosphere pressure (Klein and Hurlbut 1985).

- **Tridymite** is one of the high-temperature polymorphs of silica. The mineral is stable between 870 and 1470ºC. It is commonly found in vugs and cavities of siliceous volcanic rocks as tabular crystals or scales. The lower-temperature α-tridymite is in the orthorhombic crystal system, whereas the higher-temperature β-tridymite is hexagonal (Klein and Hurlbut 1985).

- **Cristobalite** is the highest-temperature polymorph of silica. It is commonly formed as a devitrification product of siliceous volcanic glass. Similarly to tridymite, cristobalite is found in vugs and cavities of siliceous volcanic rocks but usually as white octahedrons. The lower-temperature α-cristobalite is in the tetragonal crystal system, whereas the higher-temperature β-cristobalite is isometric (Klein and Hurlbut 1985).

- **Opal** is actually not a mineral but a mineraloid, because it lacks a crystalline structure. It is usually white but can be found in any color. Opal is best known for its property of opalescence. It is comprised of packed spheres of silica and water molecules that can range in content from 3 to 20 per cent. The hardness varies from 5.5 to 6.5, and the specific gravity varies from 2.0 to 2.2 (Klein and Hurlbut 1985).

- **Feldspars** are the most abundant and widespread of the minerals, constituting 60 per cent of the earth's crust. They are usually white but can be pink, orange, blue, and green. The mineral is comprised of a framework of aluminosilicate tetrahedra with large voids that house the large cations of potassium, calcium, and sodium. Feldspars are generally classified into two groups: **K-feldspars** and **plagioclase**. The K-feldspars have identical chemical constituents but differ in structural states, defined as order or disorder, that are a result of their cooling history. Rapidly cooled K-feldspars produce **sanidines,** where-

as slow cooling creates **orthoclase** and **microcline**. Plagioclase nomenclature is based on chemical variances of a solid-solution series. The sodic end member is **albite**; the calcic end member is **anorthite**; other compositions have various names. The feldspars all have a hardness of 6 and a specific gravity that ranges from 2.55 to 2.76 (Klein and Hurlbut 1985).

Clays

The term "clays" is somewhat ambiguous. Clays are described as finely crystalline or amorphous hydrous silicates with metacolloidal properties (Deer et al. 1966). They are loosely classified as phyllosilicates that have a platy habit due to a prominent single cleavage. They commonly have low specific gravity and flexible elasticity. Their structure consists of composite layers built from components with tetrahedrally and octahedrally coordinated cations (Klein and Hurlbut 1985). The phyllosilicates are grouped into two major divisions: **dioctahedral** and **trioctahedral**. In dioctahedral clays, only two-thirds of the sites in the octahedral sheets are occupied, whereas in trioctahedral clays, all are occupied (Deer et al. 1966). Clays are ordinarily produced as an alteration or weathering product from primary minerals. The primary interest in clays is both their ability to absorb water and their ionic exchange.

- **Smectite** is a general name for the group of swelling clays. They are a three-layer mineral comprised of two silica tetrahedral sheets and a central alumina octahedral sheet. Charge deficiencies exist between octahedral and tetrahedral sheets, which are balanced by exchangeable cations. The unique, reversible swelling property of smectites is a result of infiltration of water and other polar molecules into the region between the sheets, causing expansion (Deer et al. 1966).

- **Sepiolite** and **palygorskite** are rarer than other clays and have a hornblende-like chain structure of silica tetrahedra. They are able to absorb and retain water, a capability that derives from a structure consisting of inverted linked ribbons of silica tetrahedra that form elongate rectangular boxes. Water is able to fill the channels produced on the elongated sides of the boxes. Furthermore, in this structure, the octahedral sheets are discontinuous and contain cations, generally Mg^{2+}, at the edges. These cations, besides being susceptible to cation exchange, are also able to hold water molecules. This structure tends to give the minerals a fibrous, fuzzy appearance in hand-samples (Deer et al. 1966).

- **Illite** is a commonly used description of non-expanding phyllosilicates with a basal d-spacing of 10 Å. Approximately 15 per cent of the silicon atoms from the silica tetrahedra are replaced by aluminum atoms, a change that results in a charge deficit that is balanced by potassium cations between the illite sheets. The potassium ions are stacked, allowing no potential for expansion (Klein and Hurlbut 1985).

Oxides and Hydroxides

The oxide minerals are naturally occurring compounds in which one or more metals is bonded with oxygen. (We have listed quartz and its polymorphs, the most common of all oxides, separately because their structures are more appropriately associated with other silica-oxide compounds.) The oxide minerals are generally simple in composition and structure (Palache et al. 1944); however, some varieties of manganese oxide (MnO) have complex tunnel-structures, such as todorokite, romanechite, and coronadite/hollandite (Bish and Post 1989; Chukhrov et al. 1985b, 1987). Most of the manganese-oxide minerals appear as amorphous to fine-grained black coatings that cannot be distinguished from one another except by x-ray diffraction, electron microdiffraction, or energy-dispersive analysis. Oxides generally have strong ionic bonds, giving them a hard, dense, and often

refractory characteristic. They are often found as residual-detritus grains in sediments, commonly from igneous or metamorphic paragenesis (Klein and Hurlbut 1985). The hydroxides, as opposed to the oxides, are generally found as secondary minerals with low hardness and density. They are bonded to either hydroxyls or water molecules, which tends to create a weaker structure than that of the oxides (Palache et al. 1944).

Manganese oxides

- **Aurorite** generally occurs as an irregular mass but is also found as platy or scaly grains, commonly with black calcite. Large grains of aurorite are generally less then 8 μm (Radtke et al. 1967).

- **Cryptomelane** is commonly found as a fine-grained mass with prominent conchoidal fractures. Botryoidal as well as radial fibrous habits with prominent cleavage are known but are uncommon. The color of the mineral is black with a brownish-black streak. The hardness is 6 to 6.5; however, the hardness of the masses may be as low as 1 (Richmond and Fleischer 1943).

- **Hollandite** is a black tetragonal mineral, usually found as a fine-grained mass. The habit, although generally massive, can also be found as short prismatic crystals terminated by a flat pyramid and as fibrous crystals. Cleavage is prismatic and distinct. The mineral has a black streak and a hardness of 6 on the crystal faces. The hardness can be significantly less from exposures of the fracture (Palache et al. 1944).

- **Coronadite** is isostructural with hollandite. It is a black mineral with a habit generally found as a fine-grained mass; however, botryoidal crusts or fibrous structures are also known. The mineral has a brownish-black streak and a hardness of 4.5 to 5 (Palache et al. 1944).

- **Lithiophorite** is generally found as a shiny to dull-black mineral. Its name was derived from the belief that it contained lithium as one of its key components; however, now it is known that the mineral can have varieties that are virtually lithium free and that cobalt and nickel play a more essential role in its make-up. The structure of the mineral is analogous to gibbsite (Chukhrov et al. 1985a).

- **Rancieite** is a soft, reddish-black to black mineral. The structure contains disordered stacking of MnO_6 hexagonal layers or octahedra of $Mn(OH)_6$ with a cation, typically Ca^{2+}, located between the layers (Barrese et al. 1986).

- **Romanechite** is generally found as a dull iron-black orthorhombic mineral. Its habit is commonly fined-grain masses, but it can also be found as botryoidal or reniform structures. The streak is shiny brownish-black to black and has a hardness of 5 to 6 (Palache et al. 1944).

- **Todorokite** is generally found as a metallic-black monoclinic or orthorhombic mineral. It generally occurs as spongy banded and reniform aggregates of small lath-like crystals (Palache et al. 1944).

- **Pyrolusite** is the most common of the manganese-oxide minerals. Its best field characteristic is its sooty-black streak. The mineral is tetragonal but is generally found as massive structures. It is also commonly found as fibrous, acicular, radial, or dendritic growths on fracture exposures. The hardness is 6 to 6.5 with a perfect cleavage in one direction (Klein and Hurlbut 1985).

Iron oxides

- **Hematite** is a common iron oxide and can range from a metallic steel-gray to an earthy brownish-red. The hardness ranges from 5 to 6, and the specific gravity from 4.9 to 5.3. The fracture is uneven to splintery. The crystal system is hexagonal with many common forms, such as tabular-striated growths, gran-

ular, radiated, reniform, compact, micaceous, botryoidal, and earthy. It can be identified by its red streak and hardness (Klein and Hurlbut 1985).

- **Magnetite** is generally a metallic iron-black mineral with a dark black streak. The hardness ranges from 5.5 to 6.5, and the specific gravity ranges from 4.9 to 5.2. The fracture is uneven to subconchoidal. The crystal system is isometric, usually found as octahedrons or striated dodecahedrons. The field characteristics of magnetite include its dark black streak and magnetic property (Klein and Hurlbut 1985).

Carbonates

The carbonates contain an anionic CO_3^{2-} structural unit in which the three oxygen atoms form an equilateral triangle with the carbon atom at the center. Covalent bonds describe the oxygen-carbon unity, whereas bonds to this group are generally ionic (Klein and Hurlbut 1985).

- **Calcite** is the most common of all the carbonate group. It is generally white to transparent but can come in all the hues of the rainbow. It has perfect cleavage in three directions, giving it a common rhombohedral shape. The crystal system is hexagonal. Calcite has a hardness of 3 and a specific gravity is 2.7. It is best identified by its rhombohedron shape and by its vigorous effervescent effect when exposed to acid (Klein and Hurlbut 1985).

Halides

The halides represent a group in which a halogen is the dominant anionic component.

- Fluorite occurs in any color. It has a hardness of 4 with perfect cleavage in four directions. The specific gravity is 3.0 to 3.2. The crystal system is isometric, commonly found as cubes, octahedra, and sometimes as dodecahedra. Calcite is easily identified by its crystal shape, hardness, fluorescent properties, and waxy luster (Klein and Hurlbut 1985).

Los Alamos
NATIONAL LABORATORY
Los Alamos, New Mexico 87545